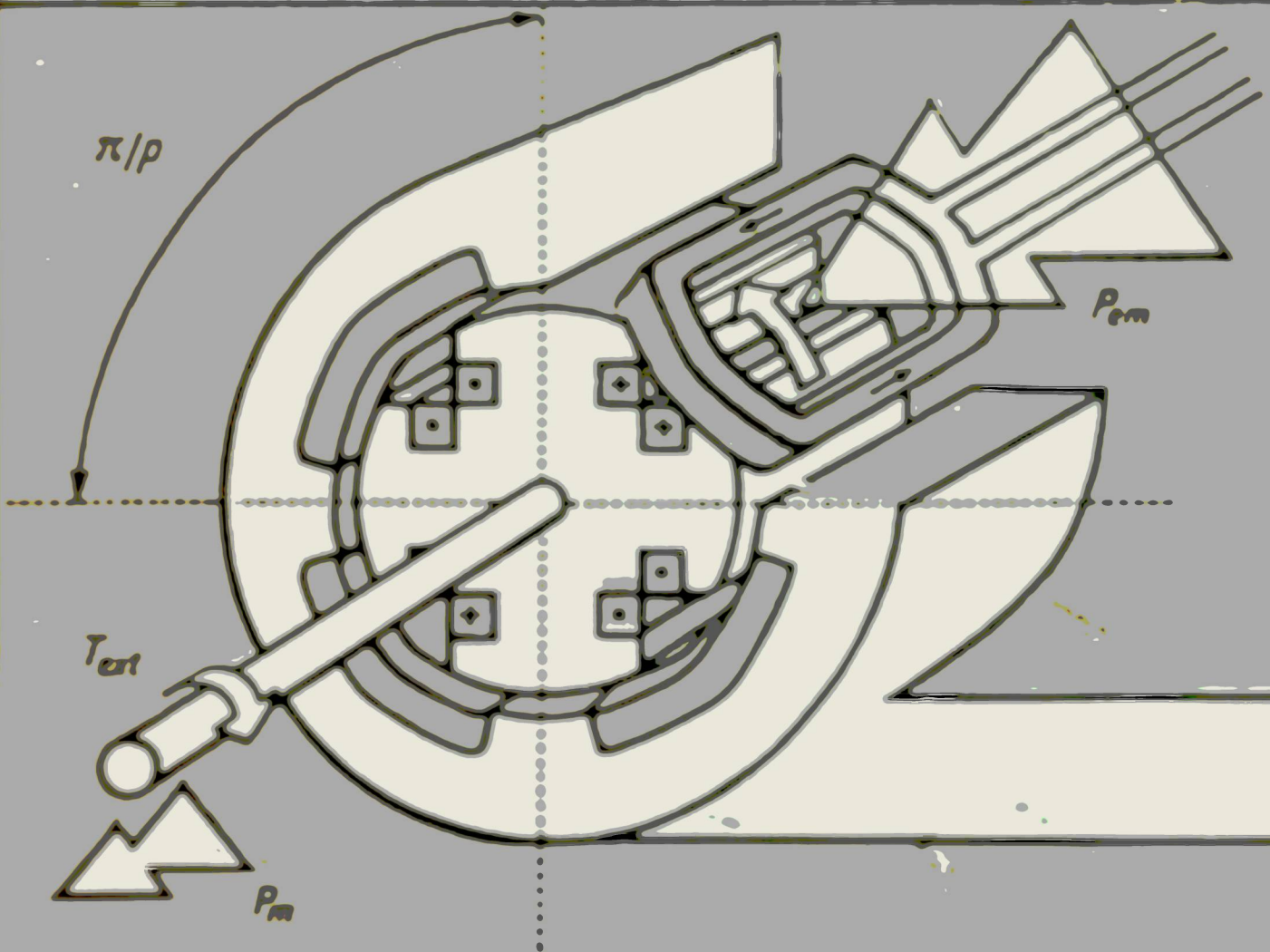


# ELECTRICAL MACHINES

A. IVANOV-SMOLENSKY

2

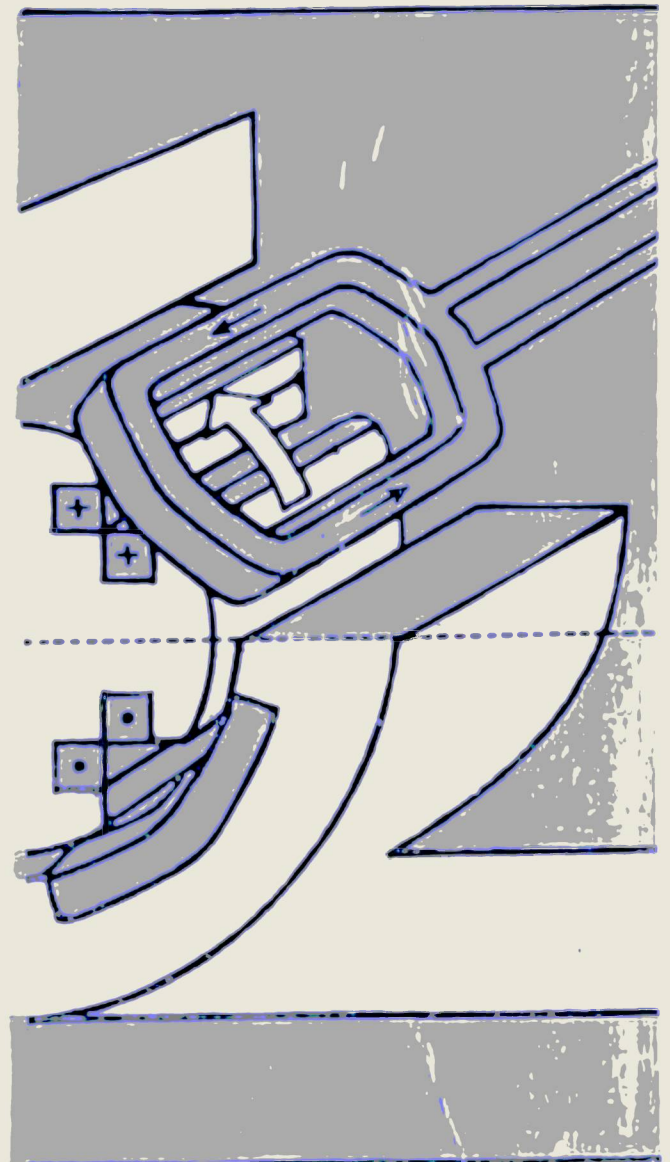


MIR Publishers

Moscow

#### ABOUT THE AUTHOR

Professor Alexei V. IVANOV-SMOLENSKY, D. Sc. (Tech.), is a leading Soviet authority in his field. Currently, he is with the Moscow Power Institute. He has written (individually and as a coauthor) six books on electricity including the present one.





## ABOUT THE BOOK

The book is in three volumes as follows.

### Volume I:

Preface. Introduction. Transformers. A General Theory of Electrical Machines.

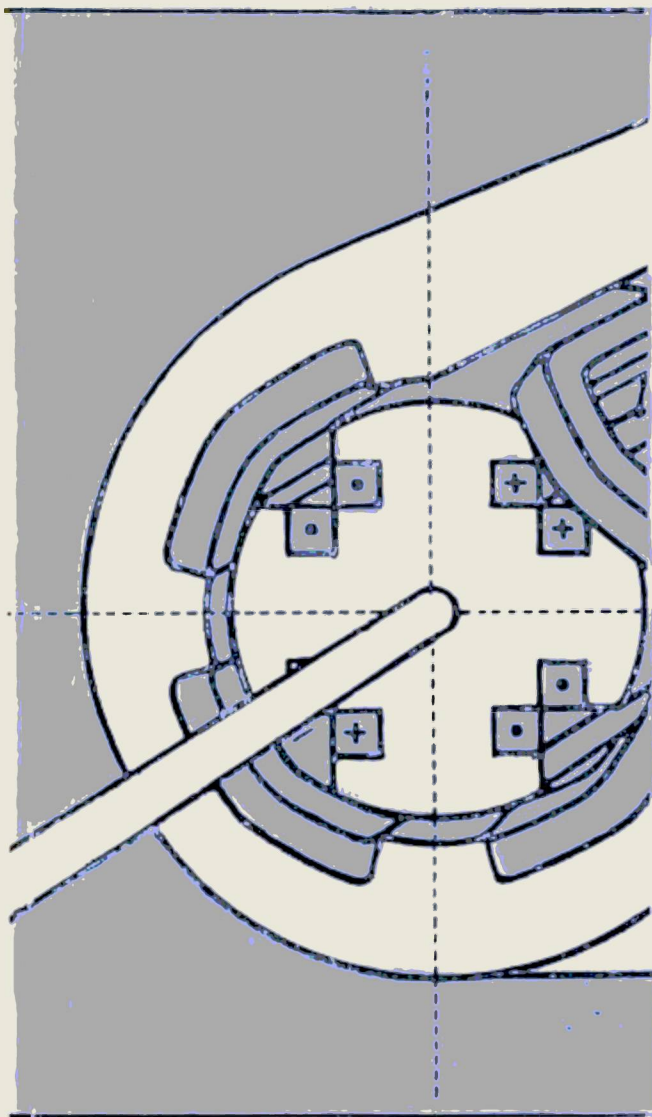
### Volume II:

Classification of Electrical Machines. Mechanical, Hydraulic and Thermal Analysis and Design. Induction Machines. Synchronous Machines.

### Volume III:

D.C. and Commutator Machines. Transients in Electrical Machines.

The book is intended for college and university students majoring in electrical-machine theory and design. It will also be useful to electrical power engineers.



# ELECTRICAL<sup>vol. 2</sup> MACHINES

---

A. IVANOV-SMOLENSKY

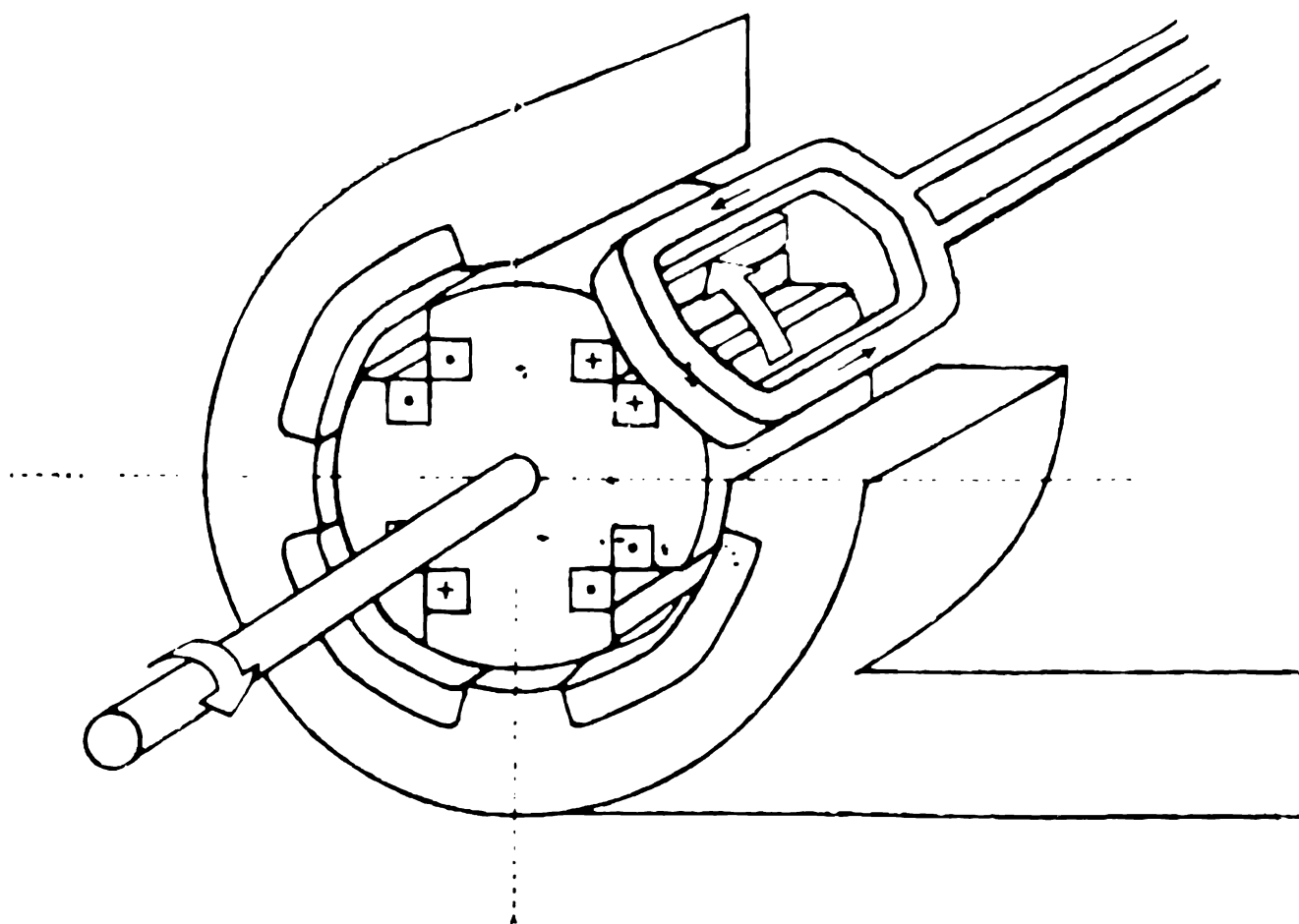




**Mir Publishers Moscow**



А. В. Иванов-Смоленский  
ЭЛЕКТРИЧЕСКИЕ МАШИНЫ



Издательство «Энергия» Москва

# ELECTRICAL MACHINES

A. IVANOV—SMOLENSKY

Vol.

2

Translated from Russian  
by BORIS V. KUZNETSOV

MIR Publishers      Moscow

First published 1982  
Revised from the 1980 Russian edition

*На английском языке*

© Издательство «Энергия», 1980 г.

© English translation, Mir Publishers, 1982

# Contents

---

## 3

### **Classification of Electrical Machines. Mechanical, Hydraulic and Thermal Analysis and Design**

---

<b>Chapter 32 Basic Construction of Electrical Machines</b>	<b>11</b>
32-1 Parts of an Electrical Machine and Their Functions	11
32-2 General Requirements for the Construction of Electrical Machines	15
<b>Chapter 33 Construction Types of Electrical Machines</b>	<b>17</b>
33-1 Type and Direction of Mounting. Type of Shaft	17
33-2 Types of Enclosure	18
33-3 Cooling Arrangements	21
33-4 Noise Level (Quietness) Classification	23
33-5 Some of the Soviet Standards Covering Electrical Machines	24
<b>Chapter 34 Mechanical Design of Electrical Machines</b>	<b>25</b>
34-1 Parts Transmitting Mechanical Power	25
34-2 Analysis of the Rotor Elements for Security of Attachment	27
34-3 Shaft Analysis for the Effect of the Rotor Self-Weight and Magnetic Attraction	29
<b>Chapter 35 Thermal Analysis of the Cooling System</b>	<b>32</b>
35-1 Basic Arrangement of the Cooling System in an Electrical Machine	32
35-2 Transfer of Heat from a Hot Body to the Surroundings	34
35-3 Heating and Cooling of Solid	36
35-4 Steady-State Temperature Analysis	39
<b>Chapter 36 Hydraulic Analysis and Design of the Cooling System</b>	<b>41</b>
36-1 The Choice of a Coolant. Determination of Flow Rate	41
36-2 The Resistances of Series or Parallel Paths of the Hydraulic Circuit	44
36-3 Analysis and Design of a Multipath Hydraulic Circuit	46
<b>Chapter 37 The Size of an Electrical Machine</b>	
37-1 Size and Performance of a Machine	47



- 37-2 Relation Between the Principal Dimensions and Electromagnetic Loading 49
- 37-3 Power Output, Power Losses and Mass of Geometrically Similar Machines 51

# 4

## Induction Machines

<b>Chapter 38 A General Outline of Induction Machines</b>	<b>53</b>
38-1 Definitions. Applications	53
38-2 An Historical Outline of the Induction Motor	56
<b>Chapter 39 Construction of Induction Machines</b>	<b>57</b>
39-1 The Squirrel-Cage Induction Motor	57
39-2 Construction of the Slip-Ring Induction Motor	61
<b>Chapter 40 Electromagnetic Processes in the Electric and Magnetic Circuits of an Induction Machine at No-Load</b>	<b>64</b>
40-1 The Ideal No-Load Condition	64
40-2 Analysis of the Magnetic Circuit at No-Load	65
40-3 Calculation of No-Load Current	71
40-4 Calculation of the Main Stator Winding Impedance	72
<b>Chapter 41 Electromagnetic Processes in Induction Machines on Load</b>	<b>73</b>
41-1 Basic Definitions and Assumptions	73
41-2 The Stator Voltage Equation. Stator MMF	75
41-3 The Rotor Voltage Equation. Rotor MMF	78
41-4 Analysis and Design of the Squirrel-Cage Winding	81
41-5 MMF Equation. Magnetizing Current. Mutual Field	84
41-6 Voltage and Current Phasor Diagrams for an Induction Machine	86
41-7 Energy Conversion by an Induction Machine. Power Losses. Efficiency	87
<b>Chapter 42 Application of Transformer Theory to the Induction Machine</b>	<b>91</b>
42-1 The Rotor at Standstill	91
42-2 Transferring the Rotor Quantities to the Stator Winding	95
42-3 Basic Equations and the Space-Time Vector Diagram of an Induction Machine	96
42-4 Equivalent Circuits of an Induction Machine	98
<b>Chapter 43 Analytical and Graphical Determination of Electro-mechanical Characteristics of Induction Machines</b>	<b>103</b>
43-1 Modes of Operation	103
43-2 Currents in the Stator and Rotor Windings	109

43-3	Electromagnetic Torque	110
43-4	Active and Reactive Power	113
43-5	Stray Electromagnetic Torques	115
43-6	The Circle Diagram of an Induction Machine	125
<b>Chapter 44</b>	<b>Starting of Induction Motors</b>	<b>131</b>
44-1	Starting of Squirrel-Cage Motors	131
44-2	Phase-Wound Induction Motors	133
44-3	Squirrel-Cage Induction Motors with Improved Starting Performance	135
<b>Chapter 45</b>	<b>Steady-State Performance of Induction Motors. Speed Control</b>	<b>139</b>
45-1	Loading Conditions. Stability	139
45-2	Performance Characteristics of an Induction Motor	141
45-3	Methods of Speed Control	143
45-4	Speed Control by Change of Field Velocity	144
45-5	Speed Control without Slip Power Recovery	148
45-6	Speed Control with Slip Power Recovery	150
<b>Chapter 46</b>	<b>Unbalanced Operation of Induction Machines</b>	<b>155</b>
46-1	Unbalanced Operation due to Unbalanced Primary Voltages	155
46-2	Unbalanced Impedances in the Rotor <del>Winding</del> Phases	159
<b>Chapter 47</b>	<b>Single-Phase Induction Motors</b>	<b>163</b>
47-1	Field of Application. General Arrangement and Principle of Operation	163
47-2	Basic Equations and Equivalent <del>Circuit of the</del> Single-Phase Induction Motor	167
47-3	The Split-Phase Induction Motor	170
47-4	Capacitor Motors	174
47-5	The Shaded-Pole Motor	177
<b>Chapter 48</b>	<b>Special-Purpose Induction Machines</b>	<b>179</b>
48-1	The Induction Generator	179
48-2	Induction Frequency Converters	180
48-3	An Induction Machine in the Transformer Mode of Operation	182
48-4	The Solid-Rotor Induction Motor	186
48-5	The Nonmagnetic Drag-Cup Motor	188
48-6	Electromagnetic Induction Pumps	189
48-7	Linear and Limited-Rotation Induction Motors	192
<b>Chapter 49</b>	<b>Induction Machines for Automatic Control Applications</b>	<b>195</b>
49-1	Induction Control Motors and Tacho-generators	195
49-2	Induction Resolvers	200
49-3	Synchros	204
<b>Chapter 50</b>	<b>Practical Induction Motors</b>	<b>207</b>
50-1	General	207
50-2	Modifications of the Basic Models	208

# 5

## Synchronous Machines

<b>Chapter 51</b>	<b>A General Outline of Synchronous Machines</b>	<b>210</b>
51-1	Purpose and Field of Application	210
51-2	A Brief Historical Outline of Synchronous Machines	214
51-3	Construction of Salient-Pole Synchronous Machines	217
51-4	Construction of Nonsalient-Pole Synchronous Machines	226
<b>Chapter 52</b>	<b>Excitation Systems for Synchronous Machines</b>	<b>230</b>
52-1	Arrangement of and Requirements for an Excitation System	230
52-2	Classification of Excitation Systems	234
<b>Chapter 53</b>	<b>Electromagnetic Processes in a Synchronous Machine</b>	<b>236</b>
53-1	Voltage and Magnetic Field Waveforms on Open Circuit	236
53-2	Calculation of the Magnetic Circuit of a Salient-Pole Machine on Open Circuit	242
53-3	Calculation of the Magnetic Circuit for a Nonsalient-Pole Machine on Open Circuit	250
<b>Chapter 54</b>	<b>MMF, Magnetic Field, EMF and Parameters of the Armature Winding</b>	<b>254</b>
54-1	Armature MMF and Its Direct-Axis and Quadrature-Axis Components	254
54-2	The Armature MMF at Various Loads in the Generator Mode	257
54-3	Mutual Field and EMF due to the Armature Currents	260
54-4	Equivalent Armature MMF in an Unsaturated Machine	263
54-5	Parameters of the Armature Winding (for Positive Sequence Currents)	265
<b>Chapter 55</b>	<b>Electromagnetic Processes in a Synchronous Machine on Load</b>	<b>271</b>
55-1	Electromagnetic Processes in a Nonsalient-Pole Machine (Neglecting Saturation)	271
55-2	Electromagnetic Processes in a Salient-Pole Synchronous Machine (Neglecting Saturation)	275
55-3	Electromagnetic Processes in a Nonsalient-Pole Synchronous Machine (with Saturation)	279
55-4	Electromagnetic Processes in a Salient-Pole Synchronous Machine with Allowance for Saturation	284

<b>Chapter 56</b>	<b>Energy Conversion by a Synchronous Machine</b>	<b>293</b>
56-1	Energy Conversion in the Generator Mode of Operation. Losses and Efficiency	293
56-2	Electromagnetic Power and Electromagnetic Torque	296
<b>Chapter 57</b>	<b>Characteristics of a Synchronous Generator Supplying an Isolated Load</b>	<b>301</b>
57-1	Operation of a Synchronous Generator into an Isolated Load	301
57-2	Excitation Characteristic of a Synchronous Generator	302
57-3	External Characteristics	306
57-4	Short-Circuit Characteristic	309
57-5	Load Characteristics	313
57-6	Self-Excitation of a Synchronous Generator Operating into a Capacitive Load	316
<b>Chapter 58</b>	<b>Parallel Operation of Synchronous Machines</b>	<b>323</b>
58-1	Parallel Operation of Synchronous Generators in an Electric System	323
58-2	Bringing in a Generator for Parallel Operation	326
58-3	Control of Load on a Synchronous Generator Connected to an Infinite Bus	329
58-4	Active and Reactive Power of a Synchronous Machine Connected to an Infinite Bus	331
58-5	Electromagnetic Power and Electromagnetic Torque of a Synchronous Machine Connected to an Infinite Bus	335
58-6	Control of Active Power at Constant $V$ and $I_f$ . Power Angle Characteristic	337
58-7	Stability in Parallel Operation	340
58-8	Reactive Power- $\theta$ Characteristic of a Synchronous Machine	345
58-9	Control of Reactive Power in Parallel Operation. "V" Curves	346
58-10	Synchronous Motors	350
58-11	Synchronous Condensers	355
<b>Chapter 59</b>	<b>Synchronization Methods</b>	<b>358</b>
59-1	Exact Synchronization	358
59-2	Self-Synchronization. Conditions for Pulling into Synchronization	361
59-3	Synchronizing by Frequency Control	366
59-4	Induction Starting	369
59-5	Induction Running of Synchronous Machines. Resynchronization	373
<b>Chapter 60</b>	<b>Instability of Synchronous Machines in Parallel Operation</b>	<b>376</b>
60-1	Free Oscillations of the Rotor Following a Sudden Change in External Torque	376
60-2	Forced Oscillations of the Rotor	383



<b>Chapter 61 Unbalanced Operation of Synchronous Machines</b>	<b>387</b>
61-1 An Outline of Unbalanced Operation	387
61-2 Positive-Sequence Impedance of the Armature Winding	387
61-3 Negative-Sequence Impedance of the Armature Winding	389
61-4 Zero-Sequence Impedance of the Armature Winding	396
61-5 Unbalanced Operation of a Synchronous Machine	397
61-6 Parallel Operation with an Unbalanced System	399
61-7 Operation of a Synchronous Generator into an Isolated Unbalanced Load	401
61-8 Unbalanced Steady-State Short-Circuits	402
<b>Chapter 62 Synchronous Machines of Soviet Manufacture</b>	<b>405</b>
62-1 Turbogenerators	405
62-2 Hydrogenerators and Engine-Driven Synchronous Generators	415
62-3 Synchronous Motors and Synchronous Condensers	422
<b>Chapter 63 Special-Purpose Synchronous Machines</b>	<b>424</b>
63-1 Electromagnetically Excited Single-Phase Synchronous Generators	424
63-2 Reluctance Synchronous Motors	425
63-3 Claw-Pole Synchronous Machines	429
63-4 Inductor Machines	431
63-5 Rolling-Rotor and Flexible Wave-Rotor Motors	438
63-6 Permanent-Magnet Synchronous Machines	444
63-7 Hysteresis Motors	448
63-8 Stepper Motors	452
63-9 Doubly-Fed Synchronous Machines	453
<b>Bibliography</b>	<b>459</b>
<b>Index</b>	<b>462</b>

---

# Classification of Electrical Machines. Mechanical, Hydraulic and Thermal Analysis and Design

---

3

## 32 Basic Construction of Electrical Machines

### 32-1 Parts of an Electrical Machine and Their Functions

In an electrical machine, energy is converted within a space taken up by an electromagnetic field. The parts that serve to establish and confine the field may be called *active* (or *electrical*) as they directly contribute to energy conversion. These are the cores, conductors (coils), and air gaps.

In addition, there are parts which do not contribute to energy conversion directly, but are essential to the operation of a machine. They may be called *structural* (or *mechanical*) parts. Among other things, they

- (a) hold the stator and rotor in their designated relative position and ensure (or limit) the desired degrees of freedom;
- (b) transfer electric energy between the cores and coils, on the one hand, and external lines, on the other;
- (c) transfer mechanical energy between the prime mover and the driven machine;
- (d) provide cooling;
- (e) insulate the coil turns from one another, from mechanical parts, and from the cores electrically;
- (f) protect the cores and coils against exposure to external factors (moisture, harmful gases or fumes, and the like) and prevent ingress of foreign objects inside the machine;
- (g) ensure safety to attending personnel by limiting (or preventing) access to and contact with rotating or live parts;
- (h) facilitate the installation of a machine at its permanent location.

The typical parts of an electrical machine are illustrated in Fig. 32-1 which shows a salient-pole synchronous machine. The arrangement shown will be found in most electrical machines in general.

The active parts are stator winding 1, rotor winding 7, stator core 2, and rotor core which consists of poles 3 and

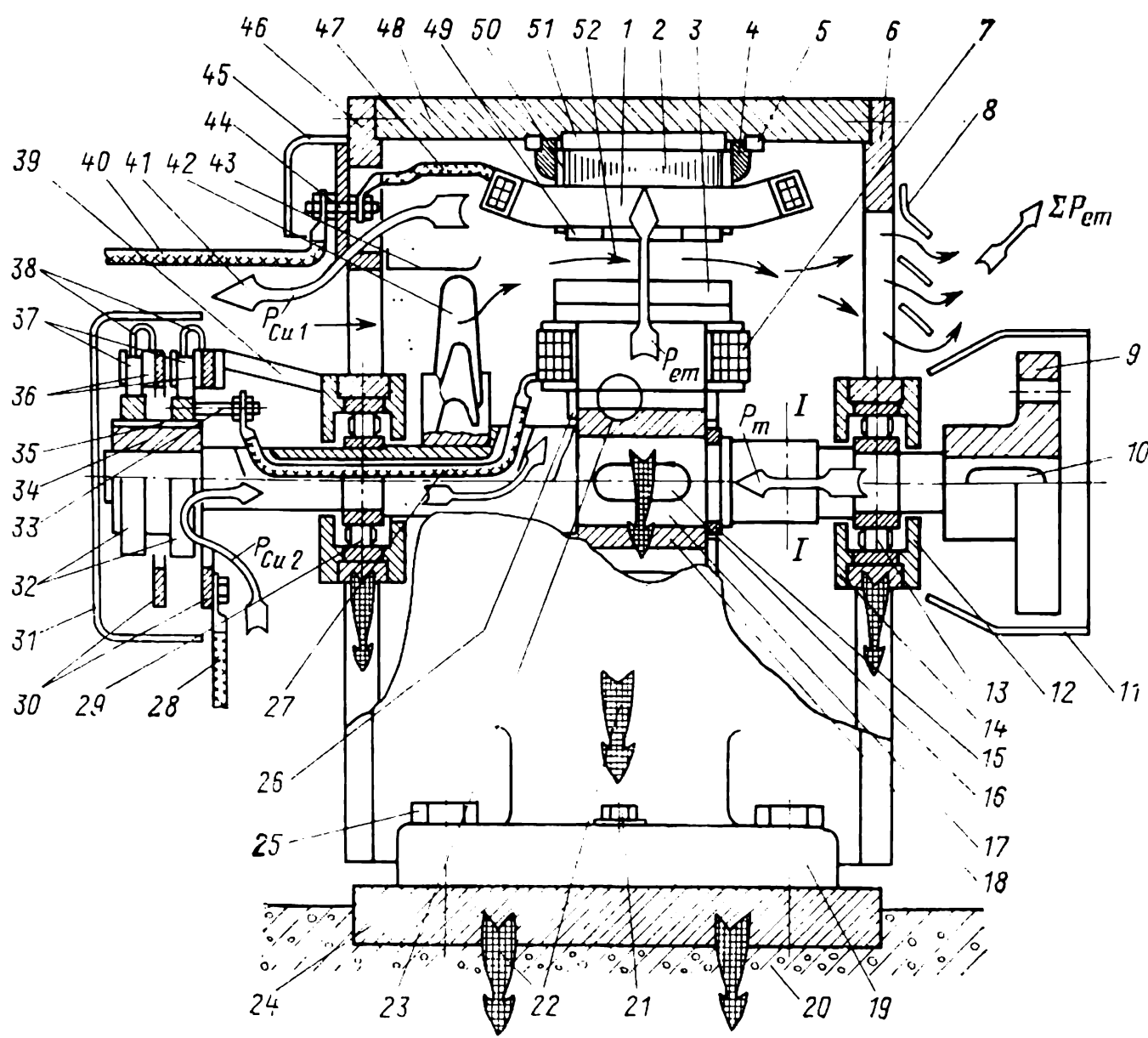


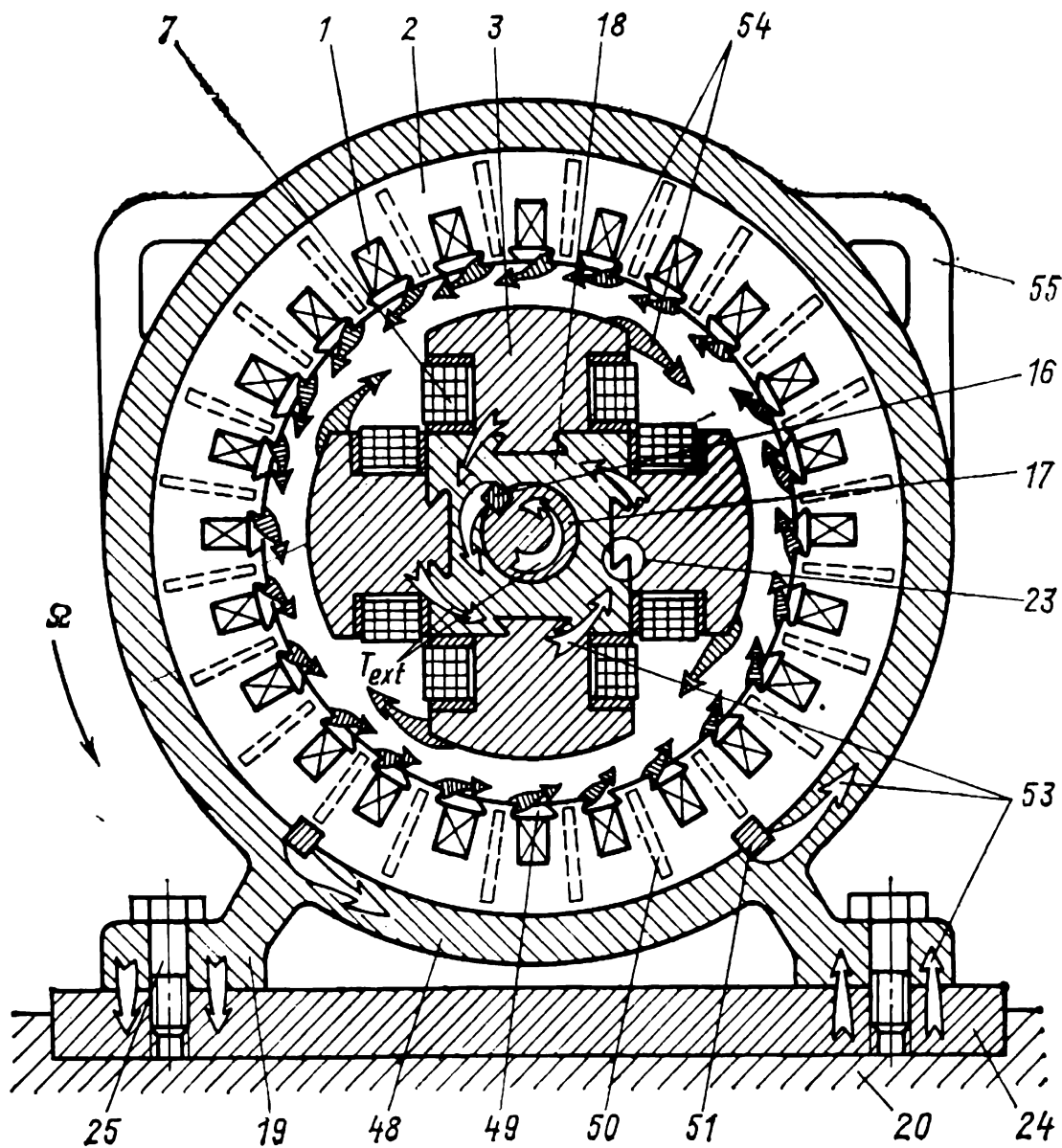
Fig. 32-1 General arrangement of an electrical machine

yoke 18. In the arrangement shown, the magnetic field in the poles and yoke of the rotor is constant in magnitude and direction. This implies that these parts are not subject to cyclic magnetization, so they may be fabricated of solid (one piece) steel forgings.

In the stator core, the magnetic field varies periodically at the supply frequency. To minimize hysteresis and eddy-current losses (see Sec. 31-3), it is built up of insulated electrical-sheet steel laminations 2 clamped together by

clamps 50, pressure blocks 4, and keys 5 inserted in annular recesses in frame 48.

The tangential electromagnetic forces acting on the stator are mainly applied to the stator teeth (see Sec. 29-3). These forces are, in the final analysis, transmitted to and absorbed by the foundation. Their path is from the stator teeth and



yoke, through keys 51, frame 48, frame feet 19, anchor bolts 25, baseplate 24, to foundation 20. (The electromagnetic forces and the forces transmitting external torque via fixed parts are shown by arrows 53 and 54, respectively, in Fig. 32-1).

Appreciable electromagnetic forces (especially during transients) are acting on the coil conductors as well. To counteract them, the active conductors are anchored to slots by wedges 49, whereas the coil ends (over-



hangs) are held in place by tape or clamps.

The tangential electromagnetic forces acting on the rotor are mainly applied to the pole-shoes. On the shaft acted upon by the external torque that balances the torque due to the tangential electromagnetic forces, the poles are held by a combination of dovetail joint 23, rotor yoke 18, and key 16.

Axially, the rotor parts are additionally locked by straps 26 that prevent the poles from moving in the dovetail joints, and also annular key 15. The rotor is held in its designated position and permitted to rotate relative to the stator by axial and radial bearings. The radial bearings in the design shown in Fig. 32-1 are of the roller type, 13 and 29, held in end shields 6 and 46 by caps 14 and 12.

The weight of the rotor is transmitted to the foundation via end shields 6 and 46, and frame 48 to which the end shields are fastened by means of flanges. To the rotor weight is added the weight of the stator (the respective forces are shown in Fig. 32-1 by arrows 22).

The flow of electromagnetic power,  $P_{em}$ , across the air gap separating the cores is shown by arrow 41. For the adopted sense of rotor rotation,  $\Omega$ , the directions of torques, forces, and energy fluxes are those existing in the generator mode of operation.

Mechanical power,  $P_m$  (the direction of its flow is shown by arrow 41), is transmitted from the associated prime mover to the rotor via a chain of mechanically strained rotating parts. Starting at half-coupling 9, the mechanical power is transmitted via key 10, through shaft 17 and key 16 to the rotor, whence it is directed to rotor yoke 18, dovetail joint 23, and poles 3 which are acted upon by the bulk of the electromagnetic forces (see Sec. 29-3) shown in the cross-sectional view by arrows 53.

Electric power is conveyed from the stator coils laid in stator slots by leads 47 to terminals 44 and cables 40.

To the rotor coils, electric power is conveyed over cables, via conducting segments 30, pig-tails 38, brushes 37 which are free to move in brush-holders 36, slip-rings 32, slip-ring leads 33, and leads 27 passing through an opening in the shaft. Segments 30 are attached over insulating parts to rocker-arm 39; the slip-rings are press-fitted on sleeve 34 insulated by cylinder 35.

The total power losses,  $\sum P$ , are dissipated in the machine as heat which is abstracted by cooling air flowing in the direction shown by arrows 52. The static pressure required to circulate cooling air is produced by axial-flow fan 42. Air enters the machine by openings in end shield 46, is directed by baffles 43, scooped by the fan and, on passing through ventilating ducts in the cores, is expelled from the machine through openings in end shield 6 and louvres 8. Many of the baffles, ducts and enclosures (8, 45, 31, and 11) serve a two-fold function in the machine: they prevent ingress of foreign objects and water drops and also keep attending personnel from direct contact with the rotating and bare live parts.

As a further safety measure, the frame of the machine must reliably be grounded. To this end, it has grounding bolt 21. This will prevent an electric shock upon contact with the machine, should its insulation be damaged.

To facilitate installation at its permanent location, the machine is fitted with lifting lugs or eyes (at 55 in Fig. 32-1).

As already noted, the arrangement illustrated in Fig. 32-1 is basically common to all rotating electrical machines. Whatever variations there may be, they will mainly concern the core shape and the winding circuits. (Various designs and types will be examined in separate sections and chapters.)

The arrangement and size of the active and mechanical parts vary with the form of cooling used (see Chap. 37), the type of enclosure adopted, the type of shaft, and some other features (see Chap. 33).

### **32-2 General Requirements for the Construction of Electrical Machines**

The active and mechanical parts of a machine must be designed, detailed and manufactured so as to meet the requirements of relevant standards, and so that the machine could perform its designated function adequately.

Among other things, appropriate standards or codes require that a machine should reliably operate under nominal service conditions. In the Soviet Union, the limiting service conditions are taken to be an ambient temperature of  $+40^{\circ}\text{C}$  and an altitude of not over 1 000 m above sea level. Also, a machine should remain fully serviceable under conditions

of overcurrents, overvoltages, excessive rpms, and starting currents, voltages and electromagnetic torque (in the case of motors) to the extent likewise specified in applicable standards or codes.

The choice of materials and dimensions for the active and mechanical components is decided upon and checked at the time of electromagnetic design and analysis, insulation design, stress-strain analysis (Chap. 34), hydraulic design (Chap. 36), and thermal analysis (Chap. 35). The turn insulation must be designed to withstand the interturn voltage, and the ground insulation must be able to stand up to the voltage between the conductors and the grounded core.

The type and form of insulation (insulating and impregnating materials, clearances, radii of curvature and bends, and the like) must be chosen such that the electric field strength in the insulation at the highest operating voltage will not exceed the safe limit and the insulation will retain its electrical strength for a long time. The insulation must also be checked and tested for its ability to withstand repeated application of atmospheric and switching surges. The electric strength and insulation resistance of a machine should be checked at the time of testing the ground and turn insulation [13]. The insulation is required to pass these tests without any damage or impairment in quality.

The winding insulation must have ample mechanical strength so as to withstand all kinds of mechanical forces during erection and in service (static, impact, vibrational, etc.). The requirements for the mechanical strength of insulation are not very stringent, because the electromagnetic forces transferred from the conductors to the slot sides in a tangential direction are insignificant (see Sec. 29-3). The prevailing factor is the pulsational forces arising from the interaction of currents with the leakage field, which drive the conductors against the slot bottom.

The maximum temperature at which a given type of insulation retains its electrical and mechanical strength and durability (the ability to preserve its properties for a period of 15 to 30 years without noticeable changes) serves as a basis for dividing all insulating materials into several classes, such as listed in Table 32-1. In more detail, this matter is discussed in [13].

The insulation classes listed in Table 32-1 are as follows.  
Class A. Cotton, silk, paper, and similar organic materials

Table 32-1 Temperature Limits and Insulation Classes

Temperature, °C	Insulation class				
	A	E	B	F	H
Temperature limit for insula- tion	105	120	130	155	180
Safe operating temperature for winding	100	115	120	140	165

when either impregnated or immersed in a liquid dielectric.

Class E. Some synthetic films.

Class B. Materials or combinations of materials such as mica, asbestos, glass fibre, etc., with suitable organic bonding, impregnating or coating substances.

Class F. Materials or combinations of materials such as mica, asbestos, glass fibre, etc., with suitable synthetic bonding, impregnating or coating substances.

Class H. Materials such as silicone elastomer and combinations of materials such as mica, asbestos, glass fibre, etc., with suitable bonding, impregnating or coating substances such as appropriate silicone resins.

In designing an electrical machine, it is customary to use standard insulation arrangements, each adapted to a particular voltage level, rather than to do analysis and design work each time.

☆ 33 Construction Types  
of Electrical Machines\*

33-1 Type and Direction of Mounting.  
Type of Shaft

The tables that follow apply to the classifications for Soviet-made machines. Similar classifications are in use in the CMEA countries.

\* As in Volume One, the material marked with a starlet is optional.

The most commonly used designs of electrical machines as regards type and direction of mounting, and type of shaft are illustrated in Fig. 33-1.

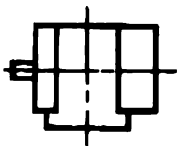
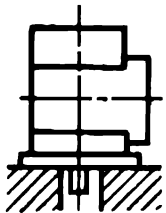
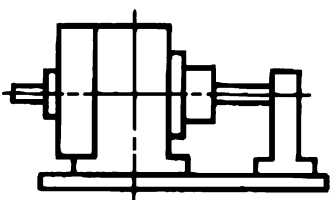
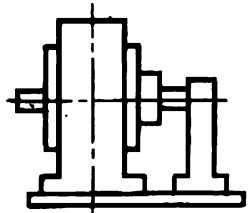
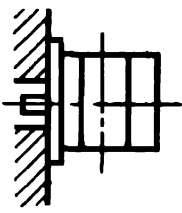
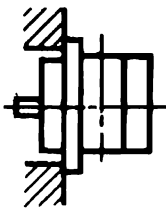
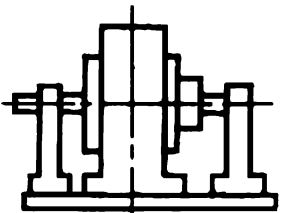
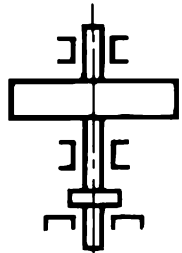
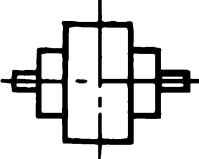
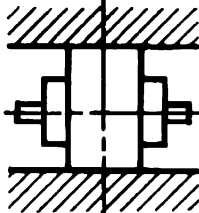
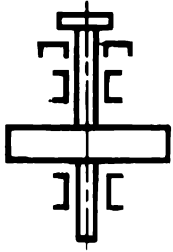
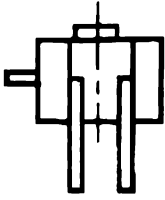
<i>IM 1001</i>	<i>IM 2011</i>	<i>IM 6211</i>	<i>IM 7011</i>
			
<i>IM 3001</i>	<i>IM 4001</i>	<i>IM 7211</i>	<i>IM 8221</i>
			
<i>IM 5002</i>	<i>IM 5102</i>	<i>IM 8421</i>	<i>IM 9401</i>
			

Fig. 33-1 Various forms of mounting, shaft position, and bearing design for electrical machines

**33-2     Types of Enclosure**

Quite a number of machine designs exist, using different degrees of enclosure and protection to the operating parts and windings. The most commonly encountered standard types are defined below.

1. An open machine is one having ventilating openings which permit passage of external cooling air over and around the windings of the machine.

2. A guarded machine is an open machine in which all openings giving direct access to live or rotating parts are limited in size by the design of the structural parts or by screens, grills, expanded metal, and the like, so as to prevent accidental contact with such parts and ingress of foreign objects.

Table 33-1 Type and Direction of Mounting

Code de- signa- tion	Description
IM1	Foot-mounted, end-shield type
IM2	Foot-mounted, end-shield, with a flange on an end-shield(s)
IM3	Flange-mounted, end-shield type, with a flange on one side
IM4	Flange-mounted, end-shield type, with a flange on the frame
IM5	Non-bearing type
IM6	End-shield, pedestal-bearing type
IM7	Pedestal-bearing type (no end-shields)
IM8	Vertical-shaft type (other than in Groups IM1 to IM4)
IM9	Special-purpose machines

3. A drip-proof machine is an open machine in which the ventilating openings are so constructed that drops of liquid or solid particles cannot enter the machine either directly or by striking and running along a horizontal or inwardly inclined surface of the machine.

4. A splash-proof machine is an open machine in which the ventilating openings are so constructed that splashes of liquid or solid particles falling on the machine or coming towards it in a straight line cannot enter the machine either directly or by striking and running along a surface of the machine.

Table 33-2 Type of Shaft

Code de- signa- tion	Description
0	No shaft extension
1	One cylindrical shaft extension
2	Two cylindrical shaft extensions
3	One tapered shaft extension
4	Two tapered shaft extensions
5	One flanged shaft extension
6	Two flanged shaft extensions
7	Flanged shaft extension on the drive end, and a cylindrical shaft extension on the opposite side
8	All other shaft arrangements

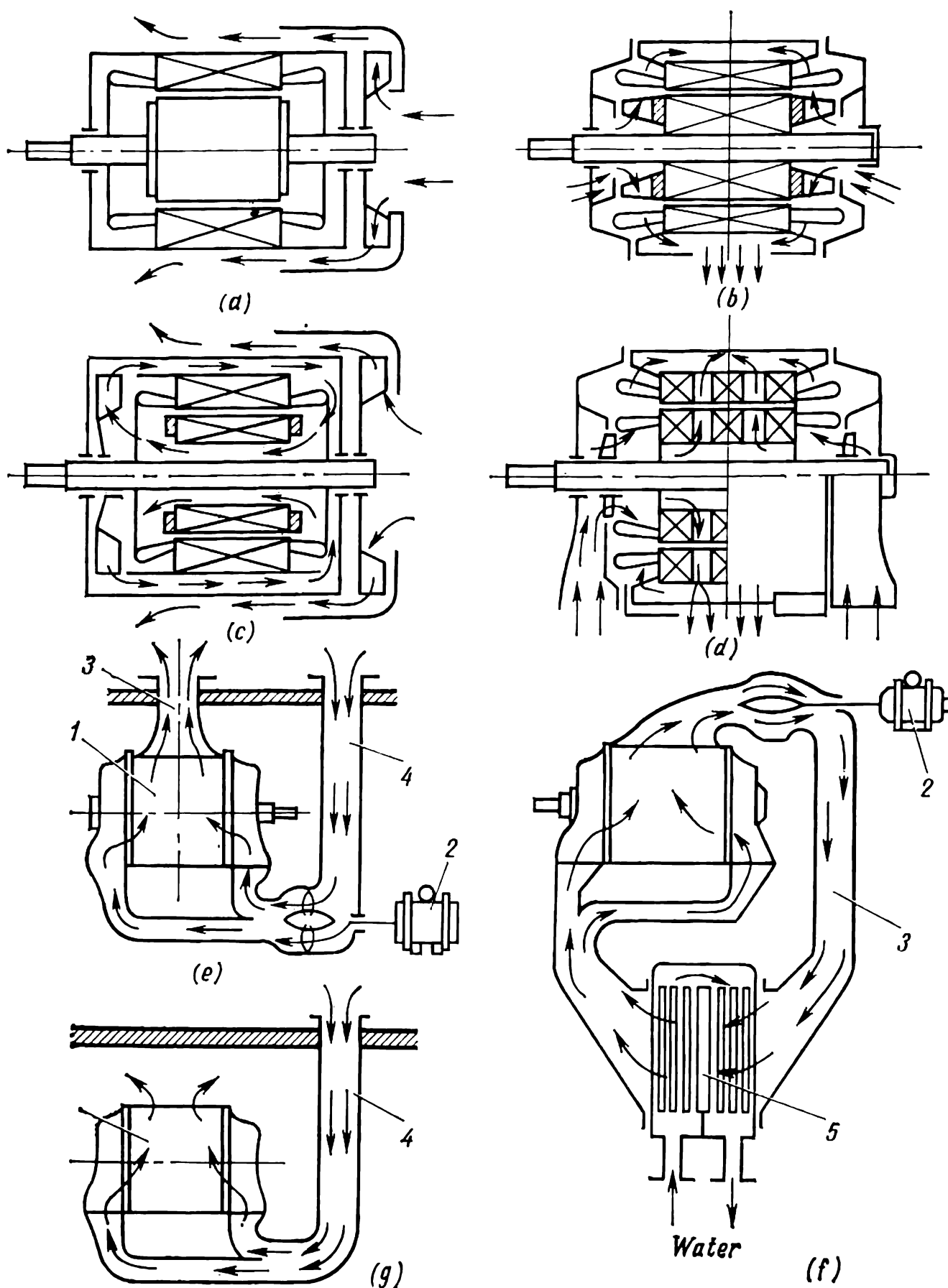


**Fig. 33-2** Ventilation and cooling systems used on electrical machines:  
 1 - machine being cooled; 2 - external-fan motor; 3 - hot air (gas) pipe conduit;  
 4 - cold-air (gas) pipe conduit; 5 - water-cooled heat-exchanger

5. A water-proof machine is a totally enclosed machine so constructed that it will exclude water applied in the form of a stream from a hose, and also solid particles and foreign objects.

6. A sea-proof machine is a totally enclosed machine so constructed that, when installed on the deck of a sea-going vessel, it will exclude water in the form of waves, and also prevent contact with running or live parts, ingress of foreign objects, and deposit of conducting or abrasive dust.

7. A short-time submersible machine is a totally enclosed machine which permits a short stay underwater.

8. A long-time submersible machine is a totally enclosed machine so constructed that it can be held underwater for an unlimited span of time.

9. An explosion-proof machine is a totally enclosed machine whose enclosure is designed and constructed so as not to cause the ignition or explosion of an ambient atmosphere of the specific dust and also not to cause the ignition of the dust on or around the machine.

10. A weather-protected machine is an open machine or a totally enclosed machine designed for service at elevated relative humidity.

11. A frost-proof machine is a totally enclosed machine designed and constructed so as to be able to operate with hoar-frost forming on the enclosure.

12. A chemical-proof machine is a totally enclosed machine designed and constructed so as to be able to operate in the presence of chemically active substances.

13. A tropicalized machine is a machine capable of operating under conditions of likely fungous growth.

### **33-3 Cooling Arrangements**

Any one of several cooling arrangements can be used in electrical machines. For example, they may or may not use a fan (or a blower) to supply cooling. In the latter case, they are classed as naturally air-cooled. In them, cooling air is made to circulate by the rotating parts of the machine and by convection. This form of cooling is ordinarily limited to open machines.

Another major class includes forced-cooled machines.

Forced-cooled machines may further be subdivided into self-ventilated, if a fan is mounted on the shaft inside the



machine (which is usually the case with guarded and totally enclosed machines, Fig. 33-2*a*, *d*, and *g*), and separately ventilated, if the fan is driven by a separate motor (which is usually the case with totally enclosed machines, Fig. 33-2*e* and *f*).

Another distinction with forced-cooled machines is the manner in which the coolant is applied. Some of them have a blower (Fig. 33-2*a*) that forces cooling air over the machine often fitted with fins to give a larger cooling area. This form of cooling is applied to enclosed machines. In others (Fig. 33-2*b*, *d* and *g*), mostly enclosed or guarded, cooling is accomplished by forcing air through ducts so that it blows over the hot parts (coils and cores) and is discharged into the atmosphere.

In medium-rated enclosed machines using blowers and intended for operation in a dust-laden air, it is usual to add a built-in fan for better air circulation inside the machine and for better heat transport from the hotter to the colder parts (cooled by a blower).

In self-ventilated machines, the cooling air may be caused to flow axially (as in Fig. 33-2*c*), radially (as in Fig. 33-2*b*), or both axially and radially (as in Fig. 33-2*d*).

The cooling system may be either open-circuit or closed-circuit. Open-circuit ventilation is ordinarily used in guarded or partially enclosed machines, with the coolant scooped or drawn in from inside or outside the hall or room where the machine is installed, and the outgoing coolant is either discharged inside the room or carried outside, as the case may be.

For small- and medium-rated machines installed in spacious rooms with a clean atmosphere, the coolant may be both drawn in from and expelled into the room, as in Fig. 33-2*b* and *d*.

For enclosed machines installed in rooms with a polluted atmosphere, cooling air is scooped from the outside and guided by a pipe or pipes into the machine from which the hot air is expelled outside likewise by a pipe or pipes (pipe-ventilated machines, as in Fig. 33-2*g*).

For large machines, it is preferable to scoop cooling air from the rooms where they are installed, and to discharge the foul air by a pipe outside so as to avoid heating the atmosphere indoors. If a large machine (such as a water-wheel turboalternator) is installed in a locality with a clean

atmosphere, the best scheme is when cooling air is drawn in from and discharged into the atmosphere so as to avoid both excessive heating and high-velocity air currents indoors (see Fig. 33-2e).

Closed-circuit ventilation is preferable for large machines of the totally enclosed type. After the ventilating medium (air or, frequently, hydrogen), held at a constant volume, has been heated by circulating through the various parts of the machine, it is cooled by passing it through a fin-tube cooler in which cooling water is circulated (as in Fig. 33-2f). Sometimes, the cooler may be built into the machine.

The coolant may be air, hydrogen, oil, or water. Sometimes, a combination of several coolants may be used in the same machine (say, hydrogen to cool the rotor and oil to cool the stator of a turboalternator). In some cases, cooling is provided by causing a coolant to evaporate. Quite aptly, this is referred to as evaporative cooling.

The windings of a machine may likewise be cooled in any one of several ways. For example, the coolant may or may not come in direct contact with the conductors. This respectively is direct and indirect cooling. In the case of direct cooling, machines ordinarily have ventilating ducts to guide the coolant as appropriate. The ducts take the form of thin-walled, nonmagnetic conduits given a thin layer of insulation and built into the windings. Such an arrangement is employed in heavy-duty, large-power machines, such as large-size steam-turbine and water-wheel alternators, and super-heavy squirrel-cage induction motors (see Sec. 62-1).

### 33-4 Noise Level (Quietness) Classification

According to the noise level ( $D$  in decibels) they produce when running, all electrical machines in the USSR are divided into the following classes:

- noiseless machines with  $D < 35$  dB on scale A;
- low-noise machines with  $D$  ranging between 35 and 55 dB;
- normal machines with  $D$  ranging from 55 to 75 dB.

The noise produced by an electrical machine comes from several sources, namely:

- (1) Windage noise due to the turbulent coolant flow produced by the rotor and fan.

(2) Humming produced by the vibrating stator and rotor under the action of electromagnetic forces.

(3) Mechanical noise coming from the vibration of the bearings, baseplate, and other structural parts.

The noise level is found by the following equation

$$D = 10 \log_{10} (I/I_0) = 20 \log_{10} (p/p_0)$$

where  $I$  = noise intensity

$p$  = sound pressure

$I_0 = 10^{-12} \text{ Wm}^{-2}$  = noise intensity corresponding to the threshold of sensitivity of the human ear

$p_0 = 2 \times 10^{-5} \text{ Pa}$  = sound pressure corresponding to the threshold of sensitivity of the human ear

### **33-5 Some of the Soviet Standards Covering Electrical Machines**

The objectives of the standards covering commercially available electrical machines in the USSR are to make the machines interchangeable as regards mounting dimensions, lead and terminal designation, power ratings, voltage ratings, and speed ratings.

Mounting dimensions are covered by USSR State Standards GOST 12126-71, GOST 8592-71, GOST 13267-73, GOST 12080-66, and GOST 12081-72.

Lead and terminal designations are given in GOST 183-74.

Power ratings up to 10 MW are subject to GOST 12139-74. Speed ratings are given in GOST 10683-73.

The principal requirements to be complied with by electrical machines of any type and design are given in the Soviet standards listed below.

GOST 183-74. Electrical machines. General requirements.

GOST 12139-74. Electrical machines. Power ratings up to 10 MW.

GOST 10683-73. Electrical machines. Speed ratings and tolerances.

GOST 12126-71. Electrical machines, low-power. Mounting dimensions. Mounting arrangements.

GOST 8592-71. Electrical machines. Tolerances on mounting dimensions.

GOST 12327-66. Electrical machines. Residual rotor disbalance. Limits and methods of measurements.

GOST 13267-73. Electrical machines and direct-coupled nonelectrical machines. Axial heights and dimensions.

GOST 2479-65. Electrical machines. Enclosures and type designations.

GOST 4541-70. Electrical machines. Designations---Overall and mounting dimensions.

GOST 12080-66. Shaft extensions, cylindrical.

GOST 12081-72. Shaft extensions, tapered.

GOST 16372-70. Electrical machines, rotating. Noise level limits.

CMEA ST 169-75. Electrical machines. Forms, terms and definitions.

## 34 Mechanical Design of Electrical Machines

### 34-1 Parts Transmitting Mechanical Power

An electrical machine must be designed so that all of its members have ample mechanical strength and rigidity to carry all likely forces within the specified limits of deformation.

The elements are checked for strength and rigidity as a part of the mechanical analysis and design of a machine, which reduces to determining the stresses and strains that may be induced by the various forces and moments (mechanical and electromagnetic).

To begin with, consider the mechanical analysis of the members transmitting mechanical power.

In the generating mode of operation, input mechanical power is conveyed to the conversion assembly where it is turned into electric power (see Fig. 32-1) by a chain of elements which include a half-coupling (9), the shaft (17), the rotor yoke (18), and the poles (3).

Let us take a closer look at how mechanical power is transmitted along the shaft of the machine. In a steady state, the shaft is acted upon by mutually balancing torques, namely an external torque,  $T_{\text{ext}}$  (arrows 53 in the figure)

applied to the right-hand side and directed in the sense of rotation, and an electromagnetic torque,  $T_{em}$  (arrows 54) transmitted via the rotor yoke and directed in the opposite

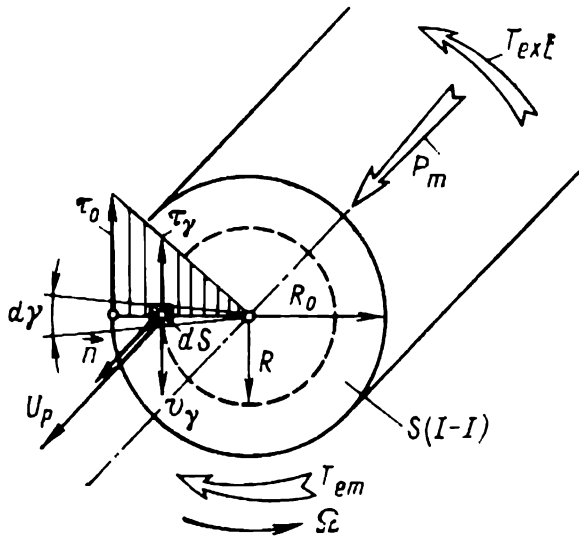


Fig. 34-1 Mechanical power transferred by a rotating shaft

sense. An enlarged shaft detail at section  $I-I$  is shown in Fig. 34-1.

The two torques stress the shaft. The part of the shaft to the left of section  $I-I$  transmits the torque to the right-hand part of the shaft by virtue of the tangential stresses  $\tau_\gamma$  induced in the elements  $dS$  of that section. The stresses are proportional to the distance  $R$  of the element  $dS = (Rd\gamma)dR$  from the shaft centre line and are a maximum,  $\tau_0$ , at the outer surface of the shaft

$$\tau_\gamma = -\tau_0 R/R_0$$

The sum of the elementary torques

$$dT_{em} = R |\tau_\gamma dS|$$

must be equal to the total electromagnetic torque

$$T_{em} = \int_{S_{I-I}} dT_{em} = \frac{\tau_0}{R_0} \int_0^{2\pi} d\gamma \int_0^{R_0} R^3 dR = \tau_0 \left| \frac{\pi R_0^3}{2} \right|$$

Hence, the tangential stress at the outer surface of the shaft is

$$\tau_0 = T_{em}/(\pi R_0^3/2) \quad (34-1)$$

where  $\pi R_0^3/2$  is the moment of resistance in torsion.

Under rated conditions, it should not exceed the limit set for the shaft material. In practice, it ranges from 40 to 100 MPa according to service conditions and the grade of steel used.

The flow of mechanical power per unit area of a section passed through a rotating body (say, section  $I-I$  across the shaft) is given by the projection of the Umov vector on an outward normal to that surface, or mathematically

$$U_p = -v_\gamma \tau_\gamma = 2R^2 \Omega T_{em}/\pi R_0^4$$

where  $\tau_v =$  tangential stress at a given surface element  $dS$   
 $v_v = R\Omega =$  tangential linear velocity of the surface element

The total flow of mechanical power,  $P_m$ , through the surface  $S$  separating one part of the rotating body from the other is obtained by adding together the elementary power flows  $U_p dS$  over the entire surface  $S$ .

It is an easy matter to see that the total power flow through the shaft section is equal to the mechanical power,  $T_{ext}\Omega$ , transmitted along the shaft:

$$P_m = \int_S U_p dS = \int_0^{2\pi} d\gamma \int_0^{R_p} U_p R^3 dR = T_{em}\Omega$$

### 34-2 Analysis of the Rotor Elements for Security of Attachment

When a machine is running, the rotor elements (poles, core teeth, coils) are acted upon by radial centrifugal forces

$$C = mR\Omega^2 \quad (34-2)$$

where  $m =$  mass of the element

$R =$  distance from the axis of rotation to the centroid

$\Omega =$  angular velocity of the rotor

The joints of the rotor elements must be designed to resist without damage the centrifugal force induced at an elevated rotational speed,  $n_e$ . In Eq. (34-2),

$$\Omega = 2\pi n_e/60$$

Among other things, the cross-sectional area,  $b_z l_z$ , of a tooth where it joins the yoke (Fig. 34-2) must be chosen such that the tensile stress

$$\sigma_z = C_z/b_z l_z$$

due to the centrifugal force  $C_z$  acting on and transmitted from the coil to the tooth could not exceed the safe limit. For solid teeth, this limit is half the yield strength of the material.

The rotor yoke is acted upon by a centrifugal force due to the yoke itself

$$C_a = m_a R_a \Omega^2$$

and the sum of the centrifugal forces due to the teeth

$$\sum C_z = ZC_z = Zm_z R_z \Omega^2$$

where  $m_a$  = mass of the yoke

$m_z$  = mass of a tooth

$R_a$  = distance from the axis of rotation to the centroid of the yoke element

$R_z$  = distance from the axis of rotation to the centroid of a tooth

$Z$  = number of teeth on the rotor

Let us isolate the rotor element shown by solid lines in Fig. 34-2 and consider the equilibrium equation for the centrifugal forces  $C_a$  and  $ZC_z$  uniformly distributed around the

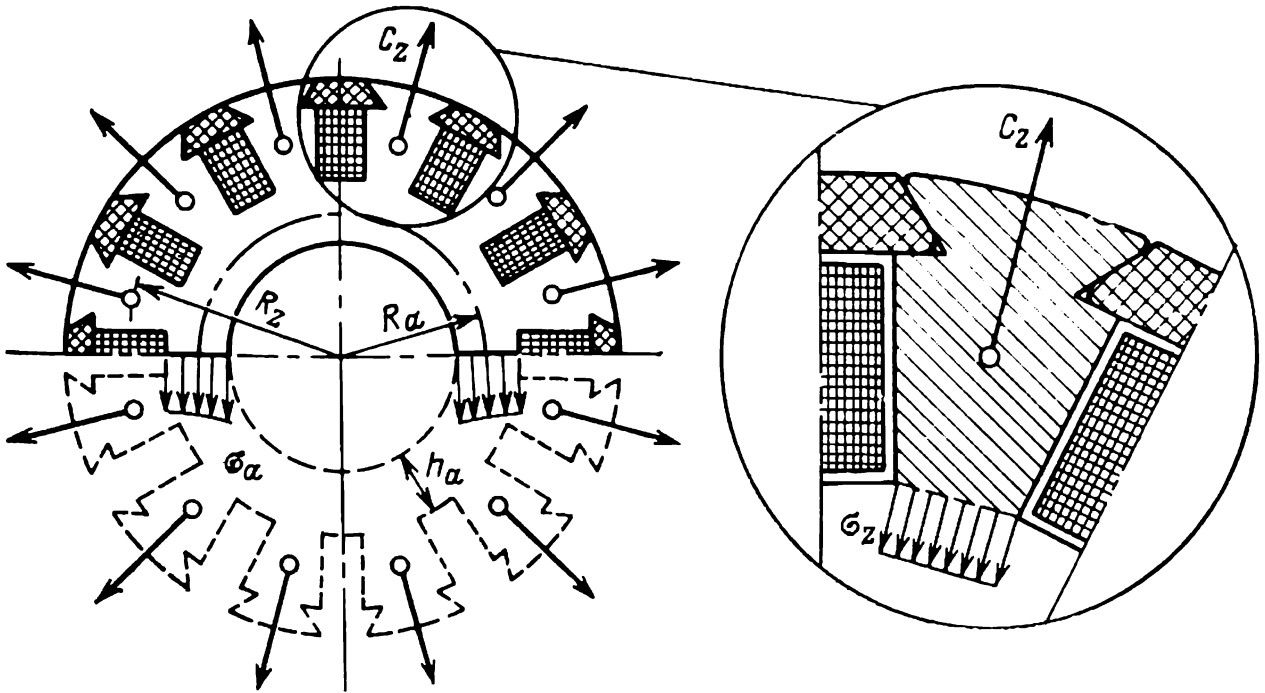


Fig. 34-2 Stresses in the rotor elements due to centrifugal forces

periphery of the rotor, and also the tensile forces  $2\sigma_a h_a l_a$  existing in the rotor part shown by dashed lines. The centrifugal force acting on a yoke element within an angle  $d\gamma$  is given by

$$\frac{C_a + ZC_z}{2\pi} d\gamma$$

Its projection on the vertical axis is

$$\frac{C_a + ZC_z}{2\pi} \cos \gamma d\gamma$$

On combining the projections of elementary centrifugal forces within the top part of the rotor, we get

$$\int_{-\pi/2}^{+\pi/2} \frac{C_a + ZC_z}{2\pi} \cos \gamma d\gamma = 2\sigma_a h_a l_a$$

$$\sigma_a = \frac{C_a + ZC_z}{2\pi h_a l_a}$$





nal to the specific magnetic tensile force (see Sec. 29-3)

$$T_n = B^2/2\mu_0 \quad (34-4)$$

where  $B$  = air-gap magnetic flux density at the rotor surface  
 $\mu_0 = 4\pi \times 10^{-7} \text{ H m}^{-1}$  = permeability

When the rotor is arranged concentrically with the stator and both are separated by a uniform air gap  $\delta$ , the magnetic tensile forces applied at diametrically opposite points on the rotor balance one another (for a periodic field, the flux density at diametrically opposite points is the same).

When the rotor is arranged eccentrically relative to the stator, so that its axis is displaced by a distance  $e_0$  from that of the stator, and the air gap varies from  $\delta_{\max} = \delta + e_0$  to  $\delta_{\min} = \delta - e_0$  (Fig. 34-3), the flux density at diametrically opposite points is different. The winding mmf waveform remains periodic as before, but the peak value of flux density is inversely proportional to the gap

$$B_{\max} = \frac{F_1 \mu_0}{(\delta - e_0) k_\delta}$$

$$B_{\min} = \frac{F_1 \mu_0}{(\delta + e_0) k_\delta}$$

The distribution of magnetic flux density in the air gap of an eight-pole machine is shown in Fig. 34-3 which also gives the specific magnetic tensile force  $T_n$ .

As is seen, the specific magnetic tensile force acting on the lower half of the rotor exceeds that acting on the top half. When the two forces are combined, the rotor is acted upon by a radial force of magnetic attraction from one side only

$$N_0 = K_0 e_0 \quad (34-5)$$

where  $K_0 = (\pi/2) (B_\delta^2/2\mu_0) (Dl/\delta) = 3 \times 10^5 (Dl_\delta/\delta)$  = specific force of one-sided magnetic attraction at an average air gap flux density amplitude of about 0.7 T

$D$  = rotor diameter

$l_\delta$  = design core length (axial gap length)

$\delta$  = mean air gap

In the worst case, when the rotor is displaced vertically downwards, the force of magnetic attraction,  $N_0$ , acts in the same direction as the rotor self-weight,  $G$ . The force of one-sided magnetic attraction tends to displace the rotor

still more downward, the eccentricity is increased, and so is the force of one-sided attraction. Finally, the force of one-sided attraction reaches a value

$$N = K_0 (e_0 + y)$$

and the shaft sags by an amount  $y$  such that this force and the self-weight are balanced by the reaction of the deformed shaft,  $yK$  [see Eq. (34-3)]

$$N + G = yK$$

$$K_0 (e_0 + y) + G = yK$$

Solving the above equation for the steady-state sag of the shaft, we get

$$y = \frac{K_0 e_0 + G}{K - K_0} \quad (34-6)$$

The shaft must be proportioned so that it has a sufficient rigidity  $K$ , and its sag is not more than 10% of the air gap ( $y \leq 0.1 \delta$ ). The initial eccentricity due to inaccuracies in assembly and the wear of bearings is taken equal to 10% of the air gap.

Also, the shaft must be analyzed for its ability to resist the bending moment due to  $N = K_0 (e_0 + y)$  and  $G$ . The stress induced in the shaft by this moment is

$$\sigma = \frac{(N + G) l}{4W_e} \quad (34-7)$$

where  $W_e = \pi R_0^3/4$  is the equatorial moment of resistance.

As the shaft rotates, this stress varies cyclically at the speed of the shaft. Therefore, the limit stress must be adopted with allowance for fatigue effects and ought not to exceed  $80 \times 10^6$  Pa for high-carbon steel (which is about half the fatigue strength in tension).

In the design and analysis of the shaft, it is important to determine what is called the *critical angular velocity of the shaft*,  $\Omega_c$ . It is the same as the angular frequency of transverse (bending) vibration of the shaft, and it is the frequency at which resonance takes place.

The natural frequency of transverse vibration of the shaft increases with increasing stiffness,  $K$ , and decreases with increasing mass of the rotor,  $m$ . An increase in the one-sided magnetic attraction brings down this frequency. As is shown in [7], the natural frequency of transverse vibration

of the shaft is a function of the sag under the self-weight of the shaft and magnetic attraction\*

$$f_c = \frac{1}{2\pi} \sqrt{g/y}$$

This frequency is the same as the rotational frequency corresponding to the critical angular velocity

$$\Omega_c = 2\pi f_c = \sqrt{g/y} \quad (34-8)$$

The resonant vibrations that occur at this frequency may be prohibitively large in amplitude. Therefore, the shaft stiffness,  $K$ , must be chosen such that the critical rotational frequency differs from the rated one by at least 30%.

In more detail, the mechanical analysis and design of electrical machines is discussed in [39, 40].

## 35 Thermal Analysis of the Cooling System

### 35-1 Basic Arrangement of the Cooling System in an Electrical Machine

Energy conversion by an electrical machine inevitably involves the loss of some power dissipated as heat in the coils, cores, and structural parts. To avoid overheating and damage to the machine, this heat must be abstracted and discarded outside the machine. This purpose is served by a cooling system and a cooling agent (which may be a gas or a liquid) which is made to circulate through the system continuously.

Ordinarily, the cooling system of an electrical machine consists of ducts inside the machine to guide the coolant, and a fan or pump to build up the static pressure necessary to circulate the coolant. Closed-circuit cooling systems use a constant quantity of coolant which, on being heated, is made to pass through a cooler where it gives up its heat to, say, water, and this discards the heat to the surroundings.

A typical arrangement of a cooling system is shown in Fig. 35-1. A cold gas (mostly air) at inlet temperature  $\Theta_1$  enters the machine at the left end, flows axially in the air

---

\* This equation applies to both horizontal and vertical machines.

gap between the stator and rotor, and ventilating ducts 6. Inside the machine, the coolant bathes the hot parts (the conductors in windings 1 and 2, and cores 3 and 4), is gradually raised in temperature by the heat it absorbs from the hot parts (the heat flows are shown by arrows 8, 9, 10, etc.).

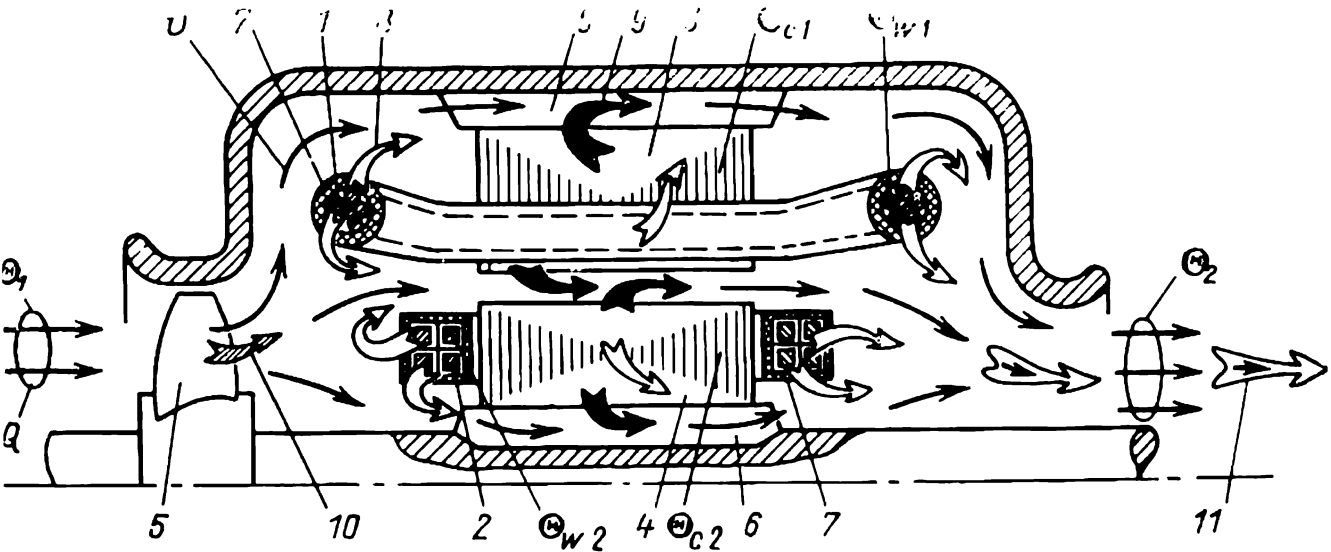


**Fig. 35-1** Cooling system of an electrical machine:  
1—stator winding conductor; 2—rotor winding conductor; 3—stator core; 4—rotor core; 5—fan to force cooling air (gas) through machine; 6—ventilating ducts; 7—stator and rotor winding ground insulation; 8—copper losses dissipated as heat (unfilled arrows); 9—core losses dissipated as heat (filled arrows); 10—friction and windage losses (cross-hatched arrows); 11—losses with expelled cooling gas;  $Q$ —flow rate of cooling gas;  $\Theta_1$  and  $\Theta_2$ —inlet and outlet temperatures of cooling gas;  $\Theta_{w1}$ ,  $\Theta_{w2}$ ,  $\Theta_{c1}$ ,  $\Theta_{c2}$ —temperatures of the stator and rotor windings and of the stator and rotor cores;  $u$ — speed and direction of flow of cooling gas

The heating of the coolant on its passage through the cooling system may be expressed in terms of the flow rate of the coolant,  $Q$ , and its specific heat capacity per unit volume,  $c_v$

$$\Theta_2 - \Theta_1 = \sum P_i / c_v Q$$

where  $\sum P_i$  is the total mean heat abstracted by the coolant. The specific heat capacities per unit volume and densities of the most frequently used coolants are listed in Table 35-1.

**Table 35-1** Specific Heat Capacities per Unit Volume and Densities of Some Coolants

Coolant	$c_v$ , J/(m <sup>3</sup> °C)	$\gamma$ , kg m <sup>-3</sup>
Air (0°C, 10 <sup>5</sup> Pa)	$1.1 \times 10^3$	1.29
Hydrogen (0°C, 10 <sup>5</sup> Pa)	$1.1 \times 10^3$	0.0898
Water (15°C)	$4.14 \times 10^6$	999
Transformer oil (15°C)	$1.54 \times 10^6$	850

The static pressure required to circulate the coolant is built up by fan 5 which may be mounted on the shaft of the machine. In a steady state, the temperatures ( $\Theta_{w1}$ ,  $\Theta_{w2}$ ,  $\Theta_{c1}$ , and  $\Theta_{c2}$  in Fig. 35-1) of the hot parts are so high above that of the coolant that all of the heat dissipated in them is transferred to the coolant and withdrawn from the machine.

The temperatures of the hot machine parts (coils and cores) are found by the *thermal analysis of the machine*.

### ☆ 35-2 Transfer of Heat from a Hot Body to the Surroundings

The thermal analysis of an electrical machine is based on the laws of thermodynamics.

Let the temperature of a given body be  $\Theta$ , and that of the coolant,  $\Theta_0$ . Then the temperature rise of the body will be

$$\Delta\Theta = \Theta - \Theta_0$$

Experiments have shown that the *time rate of heat flow* (that is, the quantity of thermal energy transferred from a body to the medium per unit time) is proportional to the *temperature rise* of the body and inversely proportional to the *thermal resistance*  $R$  ( $^{\circ}\text{C}/\text{W}$ ) between the body and the coolant

$$P_R = \Delta\Theta/R \quad (35-1)$$

If heat is transferred by conduction through the wall enclosing the body (which may be a solid, a liquid, or a gas), then the thermal resistance of the wall is given by

$$R_\lambda = \delta/S\lambda \quad (35-2)$$

where  $\lambda$  = thermal conductivity of the wall material

$S$  = surface area of the wall through which the heat flow is transported

$\delta$  = wall thickness in the direction of the heat flow.

The thermal resistance of a multilayer wall is found as the sum of the thermal resistances of the individual layers

$$R_\lambda = R_{\lambda_1} + R_{\lambda_2} + \dots = \delta_1/S_1\lambda_1 + \delta_2/S_2\lambda_2 + \dots$$

The thermal resistance of the wall ranges between broad limits, depending on the thermal conductivity of its material. Referring to Table 35-2, it is seen that the thermal conduc-

Table 35-2 Thermal Conductivity of Some Materials

Material	$\lambda, \text{W m}^{-1} \text{ }^\circ\text{C}^{-1}$	Material	$\lambda, \text{W m}^{-1} \text{ }^\circ\text{C}^{-1}$
Copper	385	Asbestos	0.2
Aluminium	200	Electric-grade pressboard	0.17
Electrical-sheet steel (along laminations)	20-45	Glass	0.11
Electrical-sheet steel, varnished (across laminations)	1.2-1.5	Slot insulation (class B)	0.16
Mica	0.36	Transformer oil	0.12-0.17
		Thin film of stagnant air	0.025
		Thin film of stagnant hydrogen	0.017

tivity of metals is substantially higher than that of insulating materials .The value of thermal conductivity is especially low for thin sheets of stagnant gases.

The thermal resistance to the transfer of heat from the wall of a hot body to a coolant fluid

$$R_{\alpha} = 1/\alpha_v S \tag{35-3}$$

is inversely proportional to the coefficient of heat transfer  $\alpha_v$  and the area  $S$  of the cooling surface.

The coefficient of heat transfer  $\alpha_v$  depends on the density and viscosity of the coolant, the velocity  $u$  of the medium and the pattern of flow in the passage adjacent to the wall.

For liquids, the coefficient of heat transfer is substantially higher than it is for gases. As the velocity of the coolant is raised, the coefficient increases, the increase being especially noticeable when a laminar flow gives way to a turbulent flow.

For use in tentative thermal analysis and design, the coefficient of heat transfer for air-cooled electrical machines may be taken as given by

$$\alpha_v = \alpha (1 + k \sqrt{u}) \tag{35-4}$$

where  $\alpha$  is the coefficient of heat transfer by radiation and convection in a quiet air ( $u = 0$ ), in  $\text{W m}^{-2} \text{ }^\circ\text{C}^{-1}$ , which varies with the properties of the surface being cooled. For varnished surfaces, it ranges between 12 and 16  $\text{W m}^{-2} \text{ }^\circ\text{C}^{-1}$ , whereas for bare metal surfaces it is anywhere between 8 and 11  $\text{W m}^{-2} \text{ }^\circ\text{C}^{-1}$ . The velocity of air,  $u$ , is taken in  $\text{m s}^{-1}$ .

The blowing rate factor  $k$  varies with the geometry of the surface being cooled, the efficiency of blowing, etc. For electrical machines, it usually equals 0.8.

When the coolant is hydrogen rather than air, the coefficient of heat transfer can be raised by a factor of 1.35. When the coolant is distilled water, it increases 30 to 60 times.

The overall thermal resistance to heat transfer between a hot body and a coolant is the sum of the thermal resistance of the wall,  $R_\lambda$ , and the thermal resistance between the wall and the coolant,  $R_\alpha$ :

$$R = R_\lambda + R_\alpha \quad (35-5)$$

### ☆ 35-3 Heating and Cooling of a Solid

From a thermodynamic point of view, an electrical machine is a complex combination of solids and sources of heat. For proper insight into what happens in a machine, we shall

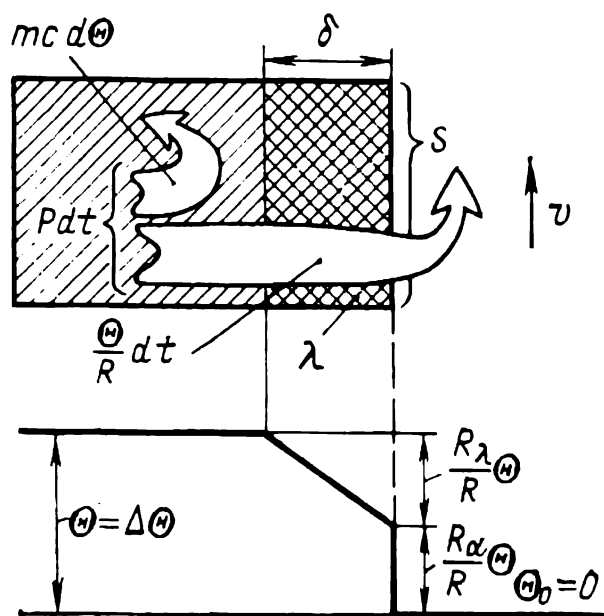


Fig. 35-2 Heating of a solid

first take a closer look at the heating of a homogeneous solid specimen which dissipates an amount of heat equal to  $P$ .

If we assume that the thermal conductivity of the specimen is infinitely large ( $\lambda_s = \infty$ ), then all points on its surface will be at the same temperature and have the same temperature rise,  $\Delta\Theta = \Theta - \Theta_0 = \Theta$ . (For simplicity, we assume that the coolant has a zero temperature,  $\Theta_0 = 0$ .)

Consider the heat balance around the specimen (Fig. 35-2).

The heat energy generated in the specimen over a time  $dt$  and equal to  $P dt$  is partly accumulated in the specimen as its temperature rises by  $d\Theta$ , and partly transferred to the coolant against a thermal resistance

$$R = R_\lambda + R_\alpha = \delta / S\lambda + 1 / \alpha_r S$$

If the specimen has a mass  $m$  and a specific heat capacity  $c$  (see Table 35-3), then it will take an amount of heat equal to

Table 35-3 Specific Heat Capacity of Some Materials

Material	$c, \text{ J kg}^{-1} \text{ }^\circ\text{C}^{-1}$	Material	$c, \text{ J kg}^{-1} \text{ }^\circ\text{C}^{-1}$
Copper	390	Asbestos	840
Aluminium	240	Transformer	
Steel	480	oil	1750
Micanite	925	Glass	850

$mc \, d\Theta$  in order to raise its temperature by  $d\Theta$ . If the temperature of the specimen rises above that of the coolant, the amount of heat transferred to the coolant over a time  $dt$  will be given by

$$P_R dt = (\Theta/R) \, dt$$

On writing the equation of conservation of energy, we obtain a differential equation describing the heating of the specimen

$$P dt = mc \, d\Theta + (\Theta/R) \, dt \tag{35-6}$$

To begin with, let us find the steady-state temperature rise,  $\Theta = \Theta_\infty$ , at which all of the heat dissipated in the specimen is transferred against the resistance  $R$  and there is no further rise in its temperature,  $d\Theta = 0$ . (Theoretically, this temperature can be attained over a very long time,  $t = \infty$ .) Under such conditions, we obtain from Eq. (35-6)

$$\Theta_\infty = PR \tag{35-7}$$

This implies that the steady-state temperature rise increases with an increase in power loss and with a decrease in heat transfer (that is, with an increase in the thermal resistance  $R$ ).

Multiplying both sides of Eq. (35-6) by  $R$  and using Eq. (35-7), we get

$$\Theta_\infty \, dt = T \, d\Theta + \Theta \, dt \tag{35-8}$$

Here

$$T = mcR = mc\Theta_\infty/P \tag{35-9}$$

has the units of time

$$\text{kg (J/kg }^\circ\text{C)} \times (^\circ\text{C/W)} = \text{s}$$

and is called the *time constant of heating*. It increases in value with an increase in the heat capacity,  $mc$ , of the speci-



men and with an increase in  $R$ . In Eq. (35-9), the numerator  $mc\Theta_\infty$  is the heat stored by the specimen as it rises in temperature towards  $\Theta_\infty$ . Therefore, the time constant  $T$  may, in accord with Eq. (35-9), be construed as the time during which the specimen might have reached the steady-state value  $\Theta_\infty$ , if all of the heat dissipated,  $P$ , had been spent to heat the specimen, and no heat had been transferred to the coolant.

Now, let us see how a solid specimen is being heated. Suppose that at  $t = 0$  its initial temperature rise is  $\Theta = \Theta_1$ . On dividing the variables in Eq. (35-8) and rewriting it as

$$dt/T = d\Theta/(\Theta_\infty - \Theta)$$

we obtain, upon integration,

$$t/T = -\ln(\Theta_\infty - \Theta) + K \quad (35-10)$$

On recalling the initial condition

$$\Theta = \Theta_1 \text{ at } t = 0$$

we get

$$K = \ln(\Theta_\infty - \Theta_1)$$

On substituting  $K$  in Eq. (35-10), we obtain an expression for the temperature rise as a function of time

$$\Theta = \Theta_\infty (1 - e^{-t/T}) + \Theta_1 e^{-t/T} \quad (35-11)$$

Consider two important cases. Figure 35-3a gives a plot of  $\Theta$  as a function of time for  $\Theta_h = 0$ , when the equation of heating has the form

$$\Theta = \Theta_\infty (1 - e^{-t/T})$$

Figure 35-3b shows the cooling curve for a specimen which dissipates no heat,  $P = 0$  and  $\Theta_\infty = 0$ , and in which the temperature rise at  $t = 0$  is  $\Theta = \Theta_h$ . Now, the equation of cooling has the form

$$\Theta = \Theta_h e^{-t/T}$$

It is seen from Eq. (35-11) that in the general case the temperature rise is the sum of two terms one of which contains  $\Theta_\infty$ , and the other,  $\Theta_h$ . If the heat dissipated in a specimen is such that  $\Theta_\infty > \Theta_h$ , the specimen will rise in temperature (Fig. 35-3c). If  $\Theta_\infty < \Theta_h$ , it will fall in temperature (Fig. 35-3d).

Analysis of temperature variations with time is essential for electrical machines intended for short-time and intermittent duties [13]. In the case of machines intended for long-

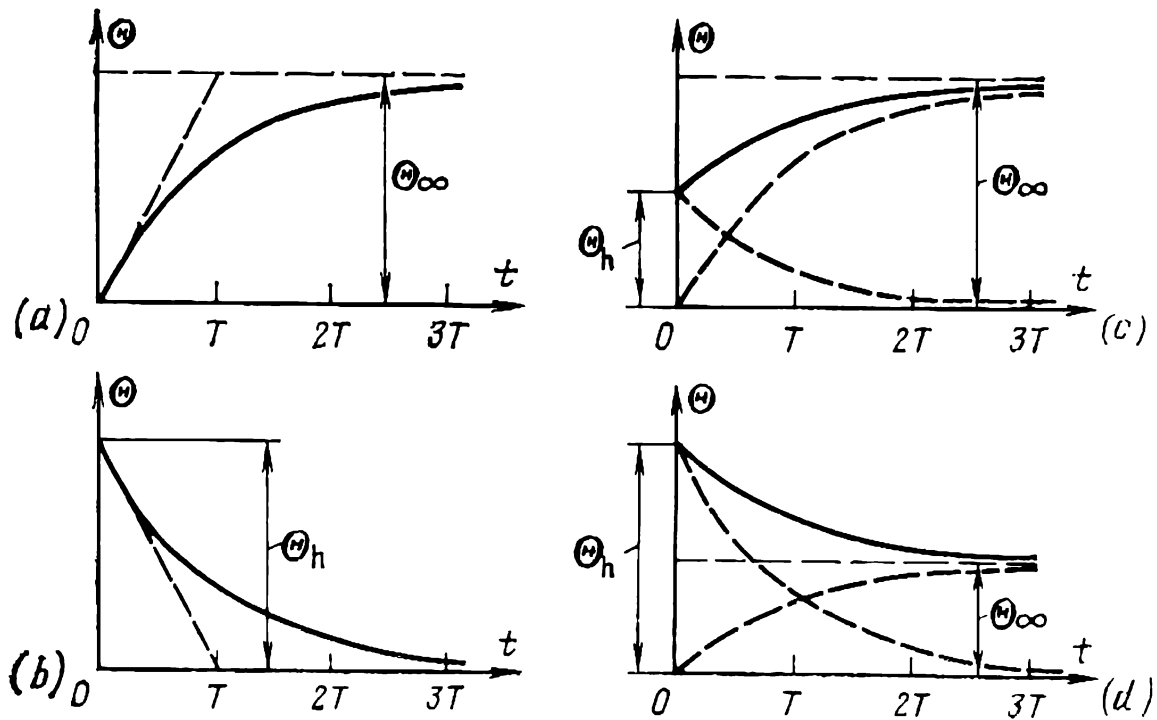


Fig. 35-3 Heating and cooling curves of a solid

time duty, analysis may be limited to operation at *steady-state temperatures*.

### 35-4 Steady-State Temperature Analysis

This form of analysis uses a set of heat transfer equations similar to Eq. (35-7), written with allowance for the likely paths of heat flow from the hot parts to the coolant.

In the analysis, the quantities assumed to be known in advance are the heat dissipated in the machine, the thermal resistances presented by the likely paths of heat transport, the flow rate of coolant,  $Q$  (see above), the velocity  $u$  of the coolant around the parts being cooled, and the respective coefficients of heat transfer  $\alpha_v$ . The inlet temperature of the coolant must also be specified in advance. (For general-purpose machines [13], it is set at 40°C.)

A convenient way to determine steady-state temperatures is to set up a *thermal resistance network*. It is composed of the heat sources and thermal resistances through which heat is transported in a machine from hot parts to the coolant.

A thermal resistance network is set up by analogy with electric networks and is described by Eq. (35-7) which is

analogous to Ohm's voltage equation. More specifically, the thermal resistances are treated as the analogs of electrical resistances, the power of heat flows as the analogue of electric current, and the steady-state temperature rise as the analogue of voltage.

As an example, let us develop a thermal resistance network for the machine in Fig. 35-1 and find the steady-state tem-

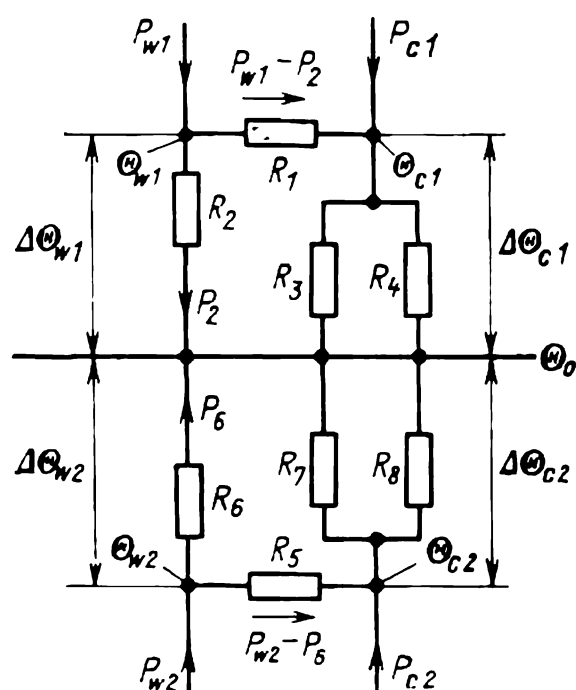


**Fig. 35-4** Thermal analog circuit of an electrical machine

peratures of the coils and cores. The network appears in Fig. 35-4. The heat flows from the stator are plotted at the top, and the heat flows from the rotor, at the bottom. The thermal potential at the centre line  $\Theta_0$  is equal to the average temperature of the coolant.

$$\Theta_0 = \frac{\Theta_1 + \Theta_2}{2} = \Theta_1 + \sum P_i / 2c_v Q \quad (35-12)$$

The notation used in the network is as follows.  $P_{w1}$  and  $P_{c1}$  stand for the copper (winding) and core losses in the stator,  $P_{w2}$  and  $P_{c2}$  for the copper (winding) and core losses in the

rotor,  $R_1$  is the thermal resistance presented by the insulation between the stator winding and the stator core [see Eq. (35-2)],  $R_2$  is the thermal resistance presented by the stator overhangs to the coolant, with allowance for the insulation resistance of the overhangs [see Eqs. (35-2), (35-3)],  $R_3$  is the thermal resistance that the heat flow experiences in transfer from the stator teeth to the coolant in the direction of the air gap,  $R_4$  is the thermal resistance that the heat flow experiences in transfer from the outer surface of the stator yoke to the coolant.  $R_5$ ,  $R_6$ ,  $R_7$ , and  $R_8$  are the thermal resistances in the rotor which respectively correspond to  $R_1$ ,  $R_2$ ,  $R_3$ , and  $R_4$  in the stator.

The temperature-rise equations are written in the same manner as the voltage equations for an electric network (the

temperature plays the part of electric potential):

$$\begin{aligned}\Delta\Theta_{w1} &= \Theta_{w1} - \Theta_0 = R_2 P_2 \\ \Delta\Theta_{c1} &= \Theta_{c1} - \Theta_0 = R_{34} (P_{c1} + P_{w1} - P_2) \quad (35-13) \\ \Theta_{w1} - \Theta_{c1} &= \Delta\Theta_{w1} - \Delta\Theta_{c1} = R_1 (P_{w1} - P_2)\end{aligned}$$

where  $R_{34} = R_{34} \parallel R_4$ ;

$$\begin{aligned}\Delta\Theta_{w2} &= \Theta_{w2} - \Theta_0 = R_6 P_6 \\ \Delta\Theta_{c2} &= \Theta_{c2} - \Theta_0 = R_{78} (P_{c2} + P_{w2} - P_6) \quad (35-14) \\ \Theta_{w2} - \Theta_{c2} &= \Delta\Theta_{w2} - \Delta\Theta_{c2} = R_5 (P_{w2} - P_6)\end{aligned}$$

where  $R_{78} = R_7 \parallel R_8$ .

Equations (35-13) for the stator and Eqs. (35-14) for the rotor can be solved independently. For example, the temperature rise of the stator winding is

$$\Delta\Theta_{w1} = \frac{R_{34}P_{c1} + (R_1 + R_{34})P_{w1}}{R_2 + R_{34} + R_1} R_2 \quad (35-15)$$

The temperature rise of the stator core is

$$\Delta\Theta_{c1} = \frac{(R_1 + R_2)P_{c1} + R_2P_{w1}}{R_2 + R_{34} + R_1} R_{34} \quad (35-16)$$

The temperature of the stator winding is given by

$$\Theta_{w1} = \Theta_0 + \Delta\Theta_{w1} = \Theta_1 + (\sum P_i / 2c_v Q) + \Delta\Theta_{w1} \quad (35-17)$$

The temperature of the stator core is given by

$$\Theta_{c1} = \Theta_0 + \Delta\Theta_{c1} = \Theta_1 + (\sum P_i / 2c_v Q) + \Delta\Theta_{c1} \quad (35-18)$$

For the rotor, similar temperature equations can be written.

## 36 Hydraulic Analysis and Design of the Cooling System

### 36-1 The Choice of a Coolant. Determination of Flow Rate

As has been shown in the previous chapter, for proper functioning of the cooling system it is essential that the coolant be circulated at a sufficient rate and in a sufficient quantity. In other words, the total flow rate  $Q$  of the coolant and its

velocity in the ducts,  $u$ , must be such that the temperature rise of the cores and coils does not exceed the safe limit.

The primary objective in hydraulic analysis and design of the cooling system is to find the static pressure  $h$  that will maintain the desired flow rate  $Q$  and velocity  $u$  of the coolant in the various parts of the system. Another objective is to determine the dimensions of the pressure elements of pumps (fans) that would give the desired circulation.

The coolant and also the shape, position and size of the ducts in which it will travel are chosen according to the design of the machine. The choice is carried out so as to optimize the machine itself in terms of manufacturing costs and service life. For most machines, the best choice is *indirect cooling for the windings*, in which case the coils enclosed in ground insulation are bathed in the coolant coming in contact with their outer surface.

With such an arrangement, the coolant is a gas nearly always (mostly, air). In high-speed, high-power machines (rated at 25 MW and higher) and also in synchronous condensers, the coolant is hydrogen at atmospheric or a gauge pressure of up to  $5 \times 10^5$  Pa. Very seldom, an indirectly cooled machine may be filled with water, kerosene, or transformer oil.

To prevent the ducts in a directly cooled machine from clogging, the coolant must be of an especially high purity. It is usually distilled water or highly refined transformer oil.

Once the coolant has been selected, the next step is to determine its required flow rate. This is done from the known power losses,  $\sum P_i$ , in the machine, the recommended temperature rise of the coolant as it travels round the hydraulic system (it usually ranges anywhere between 20 and 30 degrees C), and its specific heat capacity per unit volume,  $c_v$  (see Table 35-1):

$$Q = \frac{\sum P_i}{c_v (\Theta_1 - \Theta_2)} \quad (36-1)$$

where  $\Theta_1$  and  $\Theta_2$  are the inlet and outlet temperatures of the coolant.

The cooling ducts must be arranged so that all the parts capable of dissipating heat are bathed in an ample quantity of coolant and that the cooling surfaces have a sufficient area. To maintain the thermal resistances in a machine at an acceptable level, the coolant must travel in the ducts at a sufficiently high velocity [see Eqs. (35-3) and

(35-4)]:

$$u_i = Q_i/q_i \tag{36-2}$$

As is seen, this can be done by adopting suitable cross-sections  $q_i$  for the cooling ducts.

It is important to remember that the hydraulic (cooling) system of a machine ordinarily has several paths operating

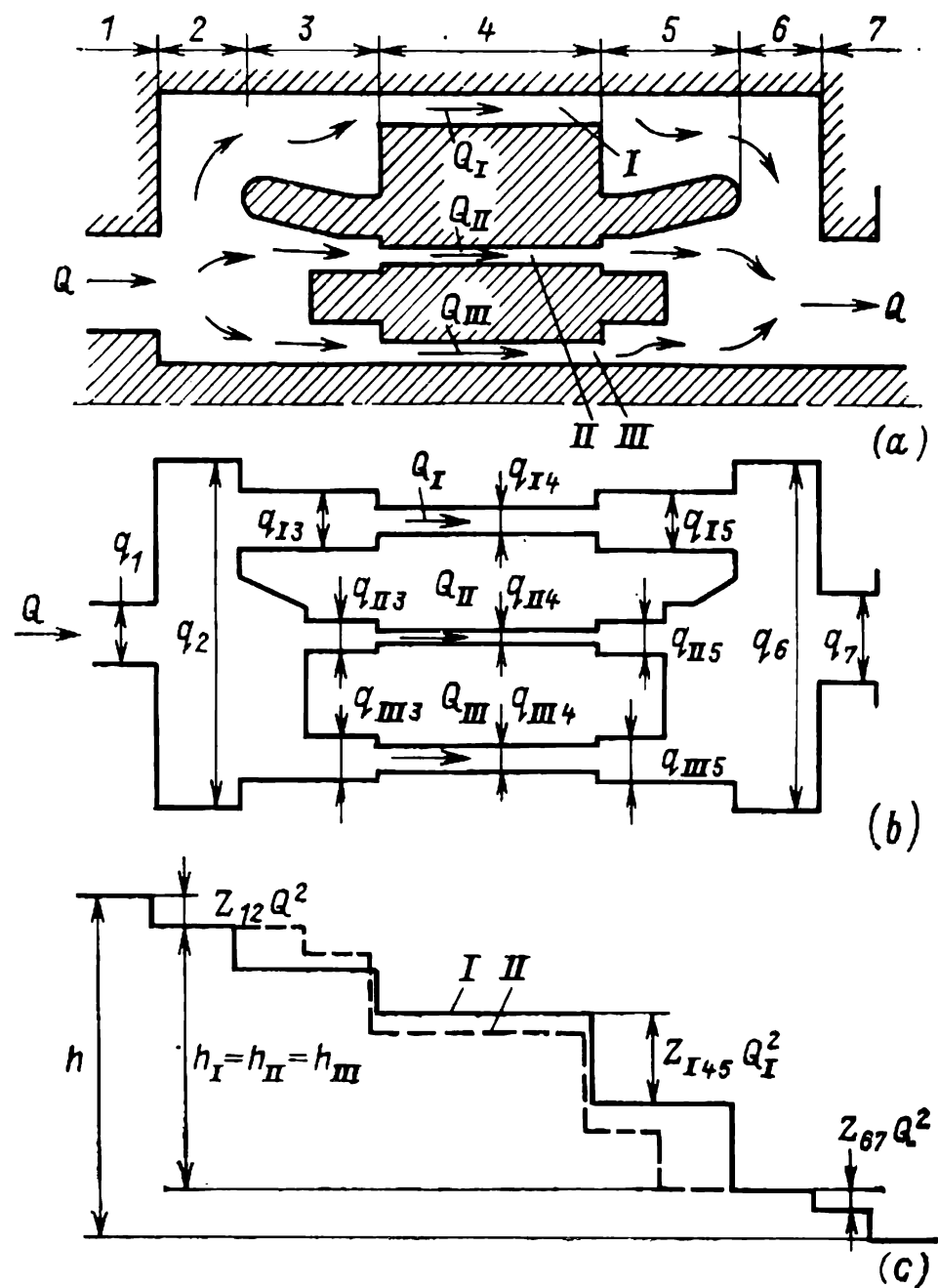


Fig. 36-1 Hydraulic circuit of an electrical machine

in parallel. Therefore, the flow rate in the  $i$ th path,  $Q_i$ , is a fraction of the total flow rate,  $Q$ . As an example, the liquid cooling system of the machine shown in Fig. 35-1 consists, as is seen from Fig. 36-1, of three parallel paths, namely, the annular space between the stator core and the frame (at  $I$  in Fig. 36-1), the annular clearance between the stator and rotor cores (at  $II$  in the same figure), and the annular space

between the rotor core and the shaft (at *III* in the same figure)\*.

In carrying out the hydraulic and thermal design, the parallel passages must be detailed and proportioned so that the flow rate in each particular path,  $Q_i$ , is proportional to the heat transferred to the coolant in that path whereas the sum of the flow rates is equal to the total flow rate,  $Q$ .

### 36-2 The Resistances of Series or Parallel Paths of the Hydraulic Circuit

The static pressure,  $h$ , required to force the coolant around the hydraulic circuit of an electrical machine is equal to the sum of the pressure losses in the series elements of the ducts (say, elements 1 through 7 in Fig. 36-1).

As experiments show, a loss of pressure occurs each time the cross-sectional area  $q$  of a duct changes. This is illustrated in Fig. 36-1c. As is seen, when the cross-section changes from, say,  $q_1$  (within element 1) to  $q_2$  (within element 2) or from  $q_{I4}$  (within element 4 of path *I*) to  $q_{I5}$  (within element 5 of path *I*), there occurs a loss of pressure. This is also true when a duct undergoes a change in direction. For long and narrow passages, one has to allow for the loss of pressure owing to friction against the walls.

In most cases, the coolant in the ducts of an electrical machine produces a turbulent flow. In the circumstances, the pressure loss is proportional to the square of the flow rate and can be found by the equation

$$h_{12} = Z_{12}Q^2 \quad (36-3)$$

Here,  $Z_{12}$  is the *local hydraulic resistance* from section 1 to section 2:

$$Z_{12} = \zeta\gamma/2q_2^2 \quad (36-4)$$

where  $\gamma$  = density of the coolant, Eq. (35-1)

$q_2$  = cross-sectional area of the duct downstream from the local resistance or (when  $q_1 = q_2$ ) in the region of the local resistance\*\*

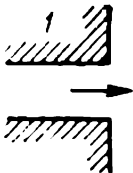
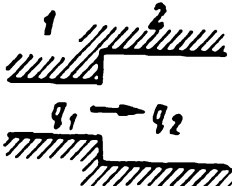
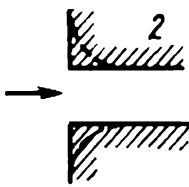
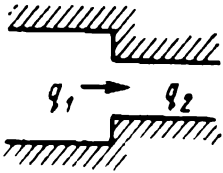
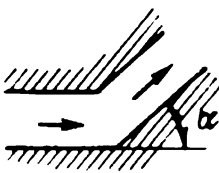
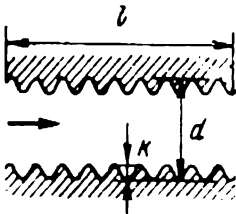
---

\* In calculating the cross-sectional areas of these passages, deduction must be made for the vent fingers.

\*\* Where the coolant is discharged from a duct into a free space and  $q_2 \gg q_1$  ( $q_2 = \infty$ ), one replaces  $q_2$  with  $q_1$ , the cross-sectional area of the duct upstream of the local resistance,

$\zeta$  = coefficient of local hydraulic resistance (see Table 36-1)

Table 36-1    Coefficients of Local Hydraulic Resistances

Description	Sketch	Coefficient $\zeta$												
Duct exit, $q_2 \gg q_1$		1.0												
Duct expansion, $q_2 > q_1$		$(q_2/q_1 - 1)^2$												
Duct inlet, $q_1 \gg q_2$		0.5 (or 0.1 for a gradual change in cross section)												
Duct contrac- tion, $q_1 > q_2$		<table><tr><td><math>q_2/q_1</math></td><td>0</td><td>0.2</td><td>0.4</td><td>0.6</td><td>0.8</td></tr><tr><td><math>\zeta</math></td><td>.5</td><td>.35</td><td>.3</td><td>.2</td><td>.1</td></tr></table>	$q_2/q_1$	0	0.2	0.4	0.6	0.8	$\zeta$	.5	.35	.3	.2	.1
$q_2/q_1$	0	0.2	0.4	0.6	0.8									
$\zeta$	.5	.35	.3	.2	.1									
Duct bend		<table><tr><td><math>\alpha</math></td><td>20</td><td>40</td><td>60</td><td>80</td><td>90</td></tr><tr><td><math>\zeta</math></td><td>.05</td><td>.14</td><td>.35</td><td>.75</td><td>1.0</td></tr></table>	$\alpha$	20	40	60	80	90	$\zeta$	.05	.14	.35	.75	1.0
$\alpha$	20	40	60	80	90									
$\zeta$	.05	.14	.35	.75	1.0									
Friction in duct		$\zeta = \lambda (l/d)$ where $\lambda = \frac{1}{1.74 + 2 \log_{10} \frac{d}{2k}}$												

The pressure losses in series local hydraulic resistances are added together, so the hydraulic resistance of a chain of several such resistances is equal to their sum. For example,



the hydraulic resistance of path  $I$  in Fig. 36-1 is

$$Z_I = Z_{2(I3)} + Z_{I34} + Z_{I45} + Z_{I5(6)} \quad (36-5)$$

where

$$Z_{I34} = \xi\gamma/2q_{I4}^2$$

is the hydraulic resistance from section  $q_{I3}$  to section  $q_{I4}$ , etc.

Because the pressure loss in parallel paths is the same (say,  $h_I = h_{II} = h_{III}$  in Fig. 36-1), and the total flow rate  $Q$  is the sum of the flow rates in the parallel paths,

$$Q = Q_I + Q_{II} + Q_{III}$$

we may conclude that the hydraulic resistance of the parallel paths,  $Z_{I-II-III}$ , is connected to the resistances by a relation of the form

$$Z_{I-II-III} = (1/\sqrt{Z_I} + 1/\sqrt{Z_{II}} + 1/\sqrt{Z_{III}})^{-2} \quad (36-6)$$

The total resistance of the hydraulic circuit in Fig. 36-1 is

$$Z = Z_{12} + Z_{I-II-III} + Z_{67} + Z_7$$

where  $Z_7 = \xi\gamma/2q_7^2 = \gamma/2q_7^2$  is the resistance at the outlet of the hydraulic circuit.

The static pressure required to produce the desired flow rate is given by

$$h = ZQ^2 \quad (36-7)$$

The loss of pressure in the parallel paths is

$$h_I = h_{II} = h_{III} = Z_{I-II-III}Q^2$$

The flow rates in the parallel paths are given by

$$Q_I = \sqrt{h_I/Z_I}; \quad Q_{II} = \sqrt{h_{II}/Z_{II}}; \quad Q_{III} = \sqrt{h_{III}/Z_{III}}$$

The velocity of the coolant in the ducts is given by Eq. (36-2).

### 36-3 Analysis and Design of a Multipath Hydraulic Circuit

For a more elaborate hydraulic circuit, one has to set up static-pressure equations for the loops (or meshes) of the circuit and flow-rate equations for the nodes of the circuit. This is done by analogy with Kirchhoff's electric circuit equations. Taking the system in Fig. 36-1 as an example, we

may write a set of four equations as follows:

$$\begin{aligned}Z_I Q_I^2 - Z_{II} Q_{II}^2 &= 0 \\Z_I Q_I^2 - Z_{III} Q_{III}^2 &= 0 \\(Z_{12} + Z_{67} + Z_7) Q^2 + Z_I Q_I^2 &= h \\Q_I + Q_{II} + Q_{III} &= Q\end{aligned}$$

Solving the above set of equations yields the static pressure  $h$ , and the flow rates  $Q_I$ ,  $Q_{II}$ , and  $Q_{III}$  in the individual paths.

The power  $P_f$  required to drive a fan or a pump so as to keep the coolant circulating around the system is found with allowance for its efficiency

$$P_f = Qh/\eta_f \quad (36-8)$$

where  $\eta_f$  ranges anywhere between 0.5 and 0.6.

## 37 The Size of an Electrical Machine

### 37-1 Size and Performance of a Machine

Given the desired power output and speed, the best approach for the designer to follow would seem to build a machine that would take up as little space as practicable, have a small mass, and be inexpensive to make. Unfortunately, as a machine decreases in size, its power loss per unit weight goes up, and this leads to higher operating costs. It is usual, therefore, to trade off size and design for a minimum total cost (the sum of manufacturing and operating costs) and a minimum power loss. The trade-off also presumes that the materials and dimensions for the electrical and structural parts are chosen such that the electric intensity in the insulation, stresses and strains, and—especially—temperature are within the prescribed limits.

Temperature affects many physical properties of materials. For one thing, an increase in temperature leads to a higher resistivity of conductors and to a lower permeability of ferromagnetic materials. At the Curie point ( $770^\circ\text{C}$ ), the permeability undergoes a sudden change and approaches that of a free space. At over  $600^\circ\text{--}700^\circ\text{C}$ , the mechanical properties of magnetic materials and conductors

deteriorate to a dangerous proportion. One must also reckon with the increase in the size of the machine parts with temperature (especially in large units) and with a build-up of stresses, because mating parts made of different materials change in size differently.

Fortunately, a machine is never allowed to run that hot, so the effect of temperature on the magnetic and mechanical properties of machine materials may be neglected almost always. The point is that for each class of insulation there is a limiting temperature. For the most commonly used classes of insulation, this temperature is anywhere between  $105^{\circ}$  and  $180^{\circ}\text{C}$ .

The temperature of a machine part is found by thermal analysis, following the selection of the size and material(s) for a particular part and finding the associated power loss (dissipated as heat in the part concerned).

The temperature rise of a part is related to the specific power loss of a given material, the volume of the part, and the thermal resistance from the part to the coolant. The hottest parts of any machine are its conductors. In indirectly cooled (blown) machines, heat is abstracted from the outer surface of the coil insulation bathed in the coolant (which may be air or hydrogen). With this form of cooling, the heat flow traverses the insulation, so the primary factor is the thermal resistance of the insulation. Because of this, it is important to minimize the thickness of the insulation and to make its thermal conductivity as high as practicable. One way to minimize thermal resistance and to raise current density in the conductors of large machines is to use direct cooling (ventilation). With this arrangement, the coolant flows in suitably arranged ducts and comes in direct contact with the parts to be cooled. Obviously, the thermal resistance of the insulation is no longer important. In fact, the current density in the conductors can be substantially increased and the size of the coils and, as a result, of the entire machine can be decreased without exceeding the specified temperature limit.

### 37-2 Relation Between the Principal Dimensions and Electromagnetic Loading

The first step in the design of an electrical machine is to select the dimensions of and the materials for its parts. The dimensions of primary importance are the diameter  $D$  and the design length  $l_\delta$  of the armature\*. Then come an electromagnetic analysis (see Parts 4 through 6), mechanical analysis, thermal and hydraulic calculations. If necessary, the figures thus found are adjusted or other materials are taken. These steps are repeated until the design alternative meets the specified objectives.

The amount of work involved in design optimization depends on the correct choice of the principal dimensions. Therefore, it is important to trace the relation between them and the machine's power output and electromagnetic loading (the rated gap flux density  $B_{\delta,R}$  and the armature electric loading,  $A = 2m_1w_1I_R/\pi D$ ).

For a.c. machines,  $I_R$  in the equation for the design power

$$S_d = m_1 E_R I_R$$

must be expressed in terms of the armature electric loading, the resultant mutual emf under rated conditions in terms of the mutual flux

$$\Phi_m = E_R / 4k_B f w_1 k_{w1}$$

and in terms of the rated gap flux density

$$B_{\delta,R} = \Phi_m / \alpha_\delta \tau l_\delta$$

Because  $\tau = \pi D / 2p$  and  $f = p\Omega / 2\pi$ , we can derive an equation for the *machine constant* which connects the design power  $S_d$ , the principal dimensions, and electromagnetic loading:

$$C_A = D^2 l_\delta \Omega / S_d = 2 / \pi \alpha_\delta k_B k_{w1} B_{\delta,R} A \approx 1 / B_{\delta,R} A \quad (37-1)$$

Here,

$k_B$  = shape factor of the flux density waveform (for a harmonic field,  $k_B \approx \pi/2\sqrt{2} = 1.11$ )

---

\* The member of an electrical machine in which an alternating current is generated by virtue of relative motion to a magnetic flux field. It may be a rotor or a stator, depending on type of machine.—*Translator's note.*

$\alpha_\delta$  = pole enclosure (= pole arc  $\div$  pole pitch), usually from 0.6 to 0.75

$k_{w1}$  = winding factor for the fundamental component of the magnetic field (in most cases, 0.92 to 0.96)

$\Omega = 2\pi n/60$  = synchronous angular velocity ( $n$  = synchronous speed, rpm)\*

For a.c. machines,

$$S_d = m_1 E_R I_R = k_E S_R$$

where

$S_R = m_1 V_R I_R$  = total rated power

$k_E = E_R/V_R$  = a coefficient (equal to 0.95-0.98 for induction machines, and 1.07-1.15 for synchronous machines)

For d.c. machines,

$$S_d = k_E V_R I_R$$

where  $k_E$  is 1.05 for generators, and 0.95 for motors.

Given a particular electromagnetic loading, the machine constant remains unchanged. An increase in electromagnetic loading leads to a decrease in the machine constant. The magnitude of electromagnetic loading depends on the properties of the materials that go to make the coils and cores, and also the arrangement of the cooling system.

The rated gap density,  $B_{\delta, R}$ , is limited by the saturation of the armature core teeth, and its value usually lies between 0.7 T and 0.95 T. An increase in the gap flux density and, as a consequence, in the tooth flux density leads to an increase in the core loss,  $P_{Cu} \sim B_{\delta, R}^2$ .

In geometrically similar machines, the electric loading is proportional to the conductor size and current density:

$$A = Q_{Cu} J / \tau \sim l$$

where  $Q_{Cu} \sim l^2$  is the total cross-sectional area of the conductors occupying one pole pitch, and  $\tau = \pi D/2p \sim l$ , where  $l$  is the base (or reference) dimension of the machine. Therefore, the copper loss in the armature winding is proportional to the base dimension and the square of the electric loading

$$P_{Cu} \sim l^3 J^2 \sim l A^2$$

---

\* Synchronous speed (velocity) is that which corresponds to the frequency of the a.c. supply.—*Translator's note.*

The temperature rise of the armature insulation is proportional to the square of the electric loading

$$\Theta_{\text{insul}} \sim P_{\text{Cu}} \delta_{\text{insul}} / \lambda_{\text{insul}} l^2 \sim l^2 J^2 \sim A^2$$

where  $\delta_{\text{insul}} \sim l$  is the insulation thickness, and  $\lambda_{\text{insul}}$  is the thermal conductivity of the insulation (see Chap. 35). The temperature rise of the insulation surface in the case of indirect cooling (by a blower) is proportional to the square of the electric loading and inversely proportional to the machine size

$$\Theta_{\alpha} \sim P_{\text{Cu}} / \alpha l^2 \sim l J^2 \sim A^2 / l$$

where  $\alpha$  is the coefficient of heat transfer (see Chap. 35).

The electric loading is a function of power output, rpm, and method of cooling, and can vary between fairly broad limits (from  $2 \times 10^4$  to  $2 \times 10^5$  A m<sup>-1</sup>). From past experience, the electric loading should preferably be chosen such that the total temperature rise (finalized by thermal analysis and equal to  $\Theta_{\text{insul}} + \Theta_{\alpha}$  in the case of indirect cooling and to  $\Theta_{\alpha}$  in the case of direct cooling) does not exceed the temperature limit for the class of insulation used.

As is seen from Eq. (37-1), the product  $D^2 l_{\delta}$ , and also the volume, mass and cost of a machine, which depend on that product, are inversely proportional to the rated gap density,  $B_{\delta, R}$ , and the electric loading,  $A$ . Obviously, the size, mass and cost of a machine can be minimized by maximizing the gap density and the electric loading. However, their maximum values ought not to exceed the specified limits.

### 37-3 Power Output, Power Losses and Mass of Geometrically Similar Machines

Consider a range of geometrically similar machines designed for the same frequency  $f$  and the same synchronous angular velocity  $\Omega = 2\pi f/p$  (which also implies that all the machines have the same number of pole pairs,  $p$ ).

Suppose that the rated gap density has been chosen the same for all the machines,  $B_{\delta, R} = \text{constant}$ , and so has the current density,  $J = \text{constant}$ . As has been shown, the electric loading for such machines increases in direct proportion to the physical dimensions, that is,

$$A \sim J l$$

Taking the design core length as the base (reference) dimension,  $l = l_\delta$ , and noting that the core diameter is likewise proportional to the base dimension,  $D \sim l$ , we can derive from Eq. (37-1) a very important relation

$$S_d \sim l^4 \quad (37-2)$$

As follows from Eq. (37-2), the power of geometrically similar machines manufactured so that  $B_{\delta, R} = \text{constant}$  and  $J = \text{constant}$  is proportional to the base dimension raised to the fourth power.

In other words, electrical machines fully obey the relationship deduced in Sec. 9-1 for transformers. Therefore, we may extend to electrical machines the relations derived in Secs. 9-1 and 9-2 for the relative mass and the relative loss. As in transformers, the mass of active parts per unit of design power in electrical machines is inversely proportional to their dimensions:

$$m/S_d \sim l^3/l^4 \sim 1/l \sim 1/\sqrt[4]{S_d}$$

The sum of electrical and magnetic (copper and core) losses per unit of design power is likewise inversely proportional to the base dimension:

$$\sum P/S_d \sim l^3/l^4 \sim 1/l \sim 1/\sqrt[4]{S_d}$$

Accordingly, the manufacturing and operating costs per unit power go down as the power rating of machines goes up. This explains why the present-day tendency is to build ever bigger machines especially generators for electric power stations.

An electric power station will be less expensive to build and operate, if it uses generators having the largest attainable power output. On the other hand, an increase in power output entails an increase in the power losses per unit area of the cooling surface

$$\sum P/l^2 \sim l^3/l^2 \sim l \sim \sqrt[4]{S_d}$$

In order to bring down the temperature of the coils and cores in high-power machines, one has to increase the cooling surface area by artificial means, such as ducts in the cores and coils, to use better coolants (such as hydrogen or transformer oil), and to replace indirect cooling (blowers, ordinarily used on smaller machines) by direct (internal) cooling (ventilation).

## 38 A General Outline of Induction Machines

### 38-1 Definitions. Applications

An induction machine is an a.c. two-winding unit in which only one (primary, usually the stator) winding is supplied with an alternating current at a constant frequency  $\omega_1$  from an external source. In the other (secondary, usually the rotor) winding, currents arise from induction. The fact that the rotor currents are produced by induction is the basis for the name of this class of machines. The frequency  $\omega_2$  of the rotor currents is a function of the rotor mechanical speed  $\Omega$ , and the rotor rpm depends on the torque applied to the shaft.

Induction machines are also called “asynchronous” because their operating speed is slightly less than synchronous in the motor mode and slightly higher than synchronous in the generator mode.

Induction machines are rarely used as generators, but are very popular as motors. In fact, of all electric motors, they are the most commonly used ones.

More often than not, induction machines have a three-phase, symmetrical (balanced), heteropolar winding on the stator (see Chap. 22) and a three (or poly-) phase, symmetrical (balanced), heteropolar winding on the rotor.

The rotor winding is either of the squirrel-cage or the phase-wound type. The squirrel-cage rotor (Fig. 39-1) consists of metal bars pushed through the rotor slots and shorted at both ends by rings. In a phase-wound rotor, the terminal of each phase is brought out to a collector or slip ring. Squirrel-cage motors are less expensive to make, are more reliable in service and have, therefore, found a wider field



of application than wound-rotor motors. They have a flat torque-speed characteristic—as load is varied from no-load to full load, the rpm drops by 2% to 5% at most. A further advantage is a larger starting torque than in the case of a phase-wound motor. Their disadvantages are as follows.

(a) The power factor is low.

(b) The starting current is high (five to seven times the rated current).

(c) The speed is not easily varied, except by an elaborate design.

Phase-wound (or slip-ring) induction motors (see Fig. 39-6) are free from the above limitations. Unfortunately, they are more elaborate in design and, as a consequence, more expensive to build. Because of this, they are only preferable under adverse starting conditions and where a broader speed control is essential.

Slip-ring motors are sometimes used in cascade with other machines. Cascade connection extends the range of speed control and improves the power factor, but such an arrangement is far more expensive, and this limits its field of application.

As already noted, the terminal of each phase in a wound-rotor motor is connected to a slip or collector ring. The slip rings are held in contact with brushes by means of which an additional impedance may be brought in the rotor circuit or an additional emf injected so as to modify the starting or running performance of the machine (see Chap. 45). Also, the brushes can be used to short-circuit the rotor winding.

In most cases, an additional resistance is brought in the rotor circuit only at starting. This serves to increase the starting torque, to bring down the starting current, and to make the starting easier. When an induction motor is running on load, the starting rheostat must be fully brought out, and the rotor winding must be short-circuited. Sometimes, induction motors are fitted with a device which shorts together the slip-rings at the end of the starting time and lifts the brushes clear of the slip-rings. Such motors have a better efficiency because they are free from the losses due to friction between the slip-rings and brushes, and also from the brush-drop loss.

Each type of induction motor is designed to operate under particular service conditions [13]. These conditions, or

ratings, are usually listed on the nameplate of the machine. They are:—

mechanical power,  $P_R = P_{2,R}$

supply frequency,  $f_1$

line stator voltage,  $V_{1, \text{line}}$

line stator current,  $I_{1, \text{line}}$

rotor rpm,  $n_R$

power factor,  $\cos \varphi_{1, R}$

efficiency,  $\eta_R$ .

If the stator has a three-phase winding with the start and finish of each phase brought out, and the winding may be star- or delta-connected, the nameplate gives the currents and voltages for all the likely connections (a star or a delta) as a fraction,  $V_{1 \text{ line, Y}}/V_{1 \text{ line, } \Delta}$  and  $I_{1 \text{ line, Y}}/I_{1 \text{ line, } \Delta}$ .

For a slip-ring motor, the nameplate also gives the locked-rotor voltage, with the slip-rings open-circuited and the line rotor current at its rated value.

Induction motors are available in a wide range of ratings. For example, the rated power may extend from a fraction of a watt to tens of megawatts. The rated synchronous speed may be from 3 000 to 500 rpm or less for a supply frequency of 50 Hz and from 100 000 rpm upwards at higher supply frequencies. (The rated rpm of the rotor is ordinarily 2% to 5% below the synchronous one; in fractional-horsepower motors, it is 5% to 20% below the synchronous speed.) The rated voltage may extend from 24 V to 10 kV (the higher values applying to higher power ratings).

The rated efficiency of induction motors increases with rising power and frequency. At power ratings in excess of 0.5 kW, it is 0.65 to 0.95. For fractional-horsepower motors, it is 0.2 to 0.65.

The power factor defined as the ratio of the active power to the total power drawn from the supply line

$$\cos \varphi_1 = P_1 / \sqrt{P_1^2 + Q_1^2}$$

likewise increases with rising power and rpm. At over 1 kW, it is 0.7 to 0.9. For fractional-horsepower motors, it is 0.3 to 0.7.

## ☆ 38-2 An Historical Outline of the Induction Motor

The principle by which the present-day induction motor operates may in fact be traced back to the rotational magnetism first discovered by Arago in 1824 and explained by Faraday in 1831. In Arago's experiments, however, a copper disc was driven by a rotating magnet rather than a rotating magnetic field established by a fixed device, or stator, as this is done in present-day machines.

Arago's discovery had remained an academic curiosity until 1879 when Baily came out with a device in which the magnetic field was caused to move in space by a fixed arrangement made up of four electromagnets placed an equal distance from the axis of rotation of a copper disc. The electromagnets were supplied with d.c. pulses of appropriate magnitude and polarity via commutator.

The rotating (or revolving) magnetic field, as it is understood today, was discovered in 1888 independently by Ferraris, and Nikola Tesla. In their experiments, the rotating magnetic field was produced by two coils set at right angles to each other and supplied with two identical sinusoidal currents in quadrature. At the intersection of the coil axes, the flux vector was found to be rotating at a uniform speed, with its peak value remaining unchanged.

Unfortunately, Ferraris' two-phase motor which had an open magnetic circuit and a copper-disc rotor could develop an output power of as little as 3 W. Also, reasoning that his motor could advantageously be used at maximum power only, Ferraris did not believe it could have an efficiency of more than 50%. Quite naturally, this did not serve to stimulate commercial interest in his invention and the otherwise sound engineering idea had practically been rejected.

Tesla's two-phase induction motors used concentrated windings on both the stator and rotor. This impaired the starting performance of the machine and made the starting torque dependent on the initial position of the rotor. This was the reason why Tesla's motor later gave way to the three-phase construction.

A major breakthrough came with the invention of the three-phase induction motor, largely developed by Dobrowolsky of Russia. In 1889, he proposed the squirrel-cage structure

for the rotor and a distributed three-phase drum winding for the stator. Later, he proposed the use of a phase-wound rotor and also, in 1890, a starting rheostat to be brought in the rotor circuit at starting. They are all the basic features of the present-day induction motor.

## 39 Construction of Induction Machines

### 39-1 The Squirrel-Cage Induction Motor

The basic arrangement of a squirrel-cage induction motor is shown in Fig. 39-1. As is seen, it is about the same as that of the rotating electrical machine examined in Sec. 32-1 (see Fig. 32-1).

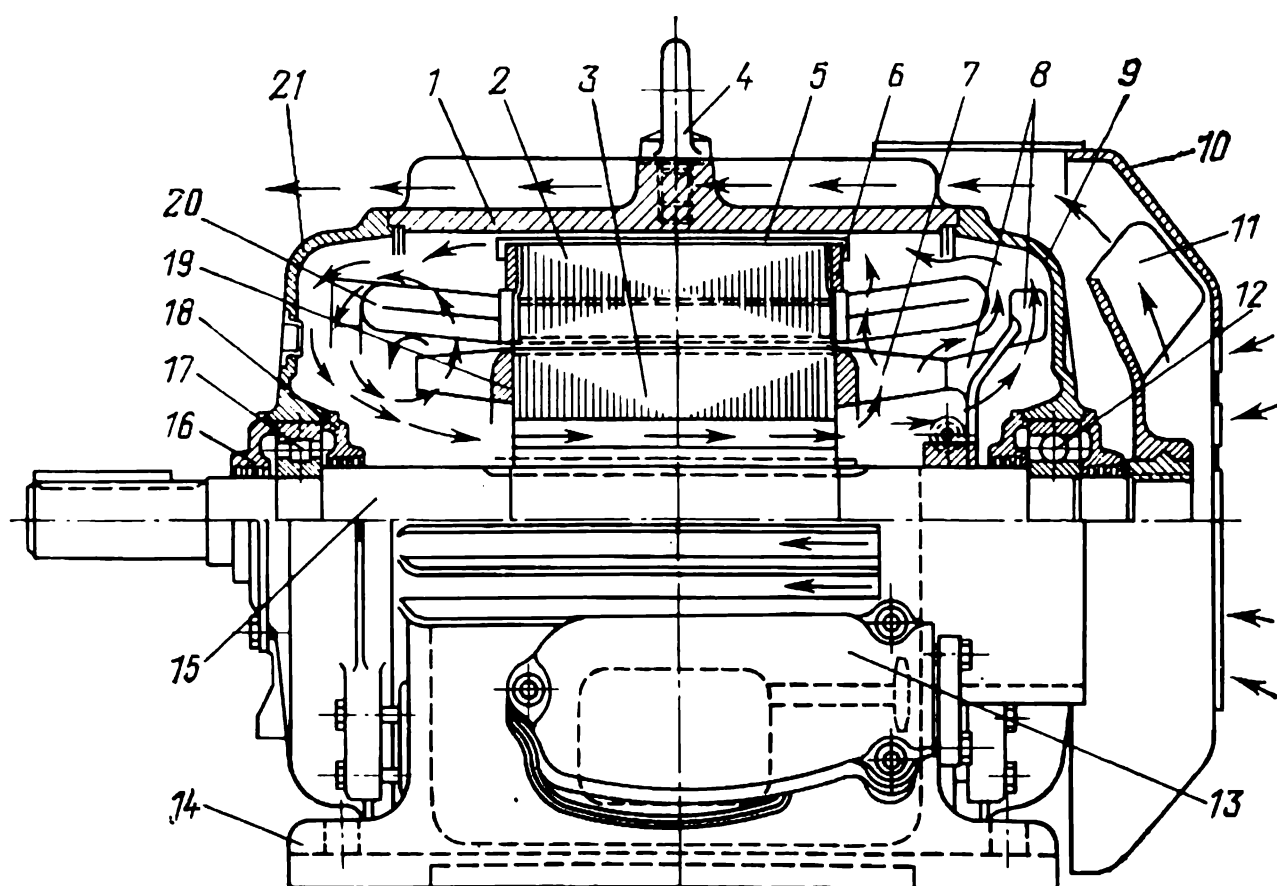


Fig. 39-1 A 55-kW, 1500-rpm, 50-Hz, totally enclosed, blower-cooled squirrel-cage induction motor

The *stator* consists of a core 2, a three-phase heteropolar winding 20 in which each phase is taken via a terminal box 13 to the respective phase of a supply line, and a frame 1.

The core and coils produce a rotating (revolving) magnetic field. The frame serves as a mechanical support for the active (electrical) parts and is made fast to a foundation by feet 14.

The stator core is built up of electrical-sheet steel laminations usually 0.5 mm thick, insulated by a coat of varnish on either side\*. For cores with an outside diameter of less than 1 m (which is true of all induction motors except the largest ones), the laminations are made in one piece, with suitable slots on their inner periphery (Fig. 39-2*b*).

The core may or may not be divided into blocks by means of vent fingers. In the former case (see Fig. 39-1), the laminations are stacked up and clamped together on a suitable mandrel outside the frame, so that no radial vent ducts are formed. The complete stack is held compressed by end plates 6 and clamps 5, and is installed in the frame after the coils have been put in place.

In a core divided into blocks, the blocks are separated from each other by radial vent ducts. Such a core is ordinarily assembled inside the frame. An unwound stator of this type is shown in Fig. 39-3. Radially, the laminations 1 are held in place by the ribs of the frame 2; axially, they are clamped and held in place by end plates 3 and keys 4 welded on after the core has been clamped. The ducts are formed by means of vent fingers 5.

For cores with an outside diameter of over 1 m, the laminations consist each of several segments, and the stator has the same construction as that of a large synchronous machine (see Sec. 51-3).

The stator winding uses single- or double-layer multiturn coils mush-wound with insulated circular wire (at 1 in Fig. 39-4*a*). The term "mush" refers to the fact that the conductors are laid in slots at a time. The slots are of the semi-closed type (see Fig. 39-4) so as to minimize the ripple in the magnetic field and the additional loss due to the core saliency\*\*.

Insulation on the coils for the stator (armature) winding consists of strand insulation if the conductors are stranded, conductor or turn insulation, coil or ground insulation, and

---

\* The selection of the thickness and material for core laminations has been discussed in Sec. 31-3.

\*\* Large induction machines use either preformed-coil or bar-type windings and open slots (see Sec. 51-3).

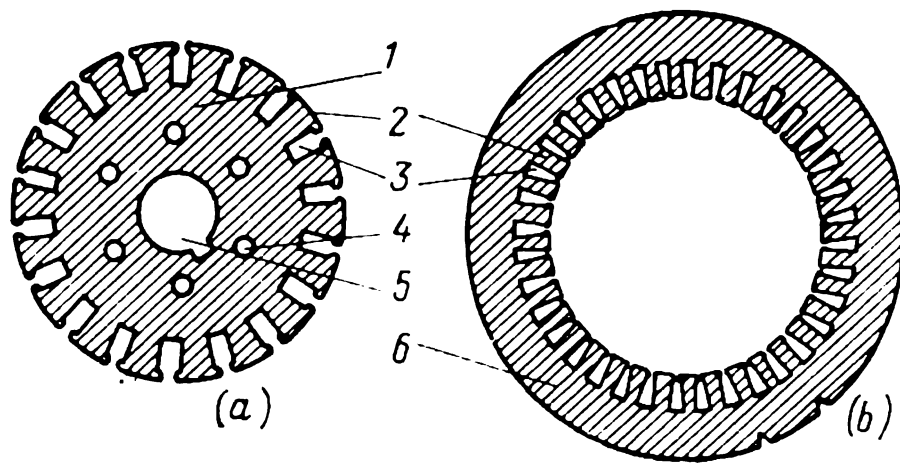


**Fig. 39-2** Ring-shaped stampings for (a) rotor core and (b) stator core:

1 - rotor yoke; 2 - tooth; 3 - slot; 4 - axial venting duct; 5 - shaft opening; 6 - stator yoke

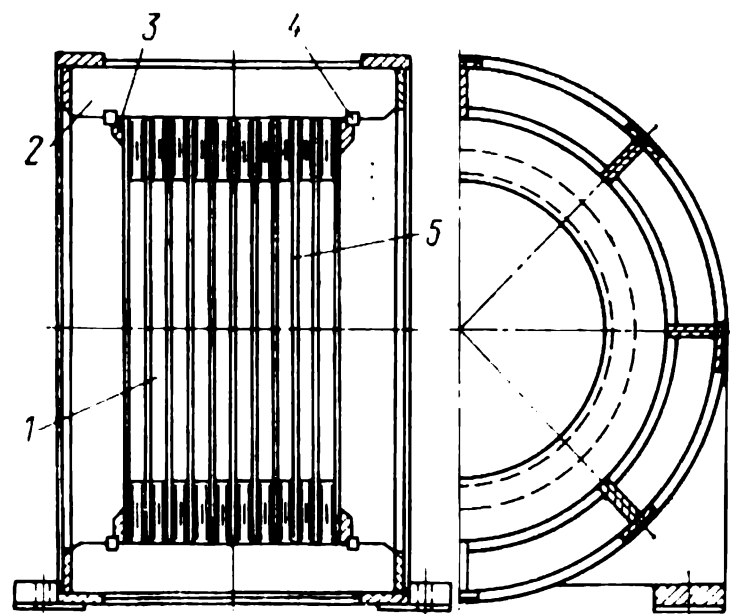


**Fig. 39-3** Radial-duct stator core built up of one-piece laminations and mounted in the frame

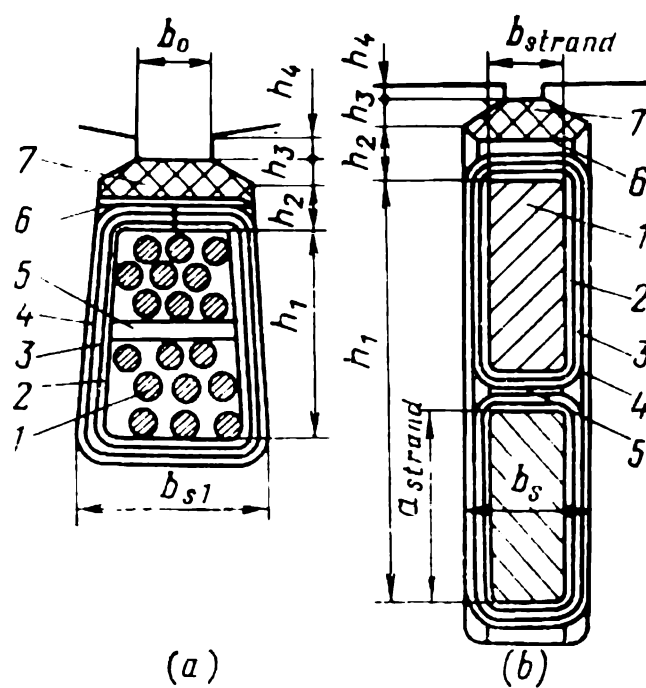


**Fig. 39-4** Slots:

(a) for the double-layer mush stator winding of an induction machine; (b) for the three-phase, double-layer, bar-type, wave rotor winding of a wound-rotor induction machine

the slot liner or cell. The slot liner or cell is usually made up of two or more layers of insulating material; it is placed in each slot prior to placing the coils. In the slots, the coils are anchored by top insulation plates 6 and slot wedges 7. In a double-layer winding, the layers are separated by inter-layer 5 (or, simply, layer) insulation. No such insulation is needed in a single-layer winding.

The *rotor* consists of a core 3 (see Fig. 39-1) with slots on its outer periphery, a polyphase winding 19, integrally cast

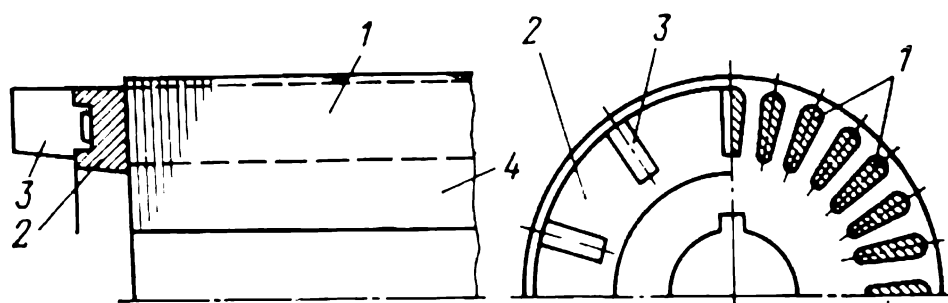


**Fig. 39-5** The core of a cast-aluminium squirrel-cage induction motor

cooling blades 7, a shaft 15, and two fans, 8 and 11. Only the core and the winding contribute to energy conversion: the remaining parts serve various structural or mechanical functions. For example, the shaft transmits mechanical energy to the associated driven machine, the fans make the coolant circulate inside the machine, etc.

In more detail, the construction of the core and winding is shown in Fig. 39-5. The core, 4, is built up of one-piece electrical-sheet steel laminations 0.5 mm thick. On the outer periphery, the laminations are punched with slots of a suitable shape (closed in Fig. 39-5, and partly closed in Fig. 39-2a).

The rotor core laminations are stacked up on a mandrel, clamped, and held compressed so long as the rotor winding is fabricated. The rotor winding consists merely of identical copper or cast-aluminium bars solidly connected to a conducting (short-circuiting) end ring at each end (at 2 in Fig. 39-5), thus forming a short-circuited squirrel-cage structure. The end rings are cast integral with fan blades 3.

Apart from serving as the secondary winding, the squirrel-cage structure holds together the rotor laminations upon removal from the mandrel. With this arrangement, there is no need to use separate axial clamps.

The rotor is mounted on the shaft (at 15 in Fig. 39-1) which is carried in two ball or roller bearings (12 and 17).

The bearings are press-fitted in end shields or end frames (9 and 21) with caps (16 and 18) by which they are attached to the frame.

Ball bearing 12 centres the rotor both radially and axially and takes up radial and axial (thrust) forces. The bearings are lubricated with grease which is packed under the bearing caps and can last for several years of service.

Because the clearance (air gap) between the rotor and stator cores is very small (0.3 to 1 mm for machines rated at 0.5 kW and higher and 0.02 to 0.3 mm for fractional-horsepower machines), it is important that the shaft should have ample stiffness (see Sec. 34-3), and the structural parts ensuring the correct position of the shaft in space should be machined to a very high level of accuracy.

Figure 39-1 shows a totally enclosed, externally blown machine (see Sec. 33-2). Cooling is provided by an external blower, and protection to attending personnel is given by an enclosure (10) which also serves to guide cooling air towards the ribbed surface of the frame. Inside the machine, air is forced by the integrally cast fan and fan blades (the direction of air flow is indicated by arrowheads).

Wherever necessary, the motor can be lifted and moved about by means of a lifting ring (at 4 in Fig. 39-1).

### 39-2 Construction of the Slip-Ring Induction Motor

The general arrangement of a slip-ring (wound-rotor) induction motor is shown in Fig. 39-6. From the squirrel-cage machine, it only differs in the construction of the rotor.

The *stator* may be built along the same lines as for a squirrel-cage machine. The stator of the motor in Fig. 39-6 (with the core divided into blocks by vent ducts) is almost identical with that in Fig. 39-3 (see Sec. 39-1). The stator consists of a frame 1 in which end washers 5 and keys 7 hold the stator core blocks built up of ring-shaped laminations 2. The vent ducts between the core blocks are formed by vent fingers 4. The slots on the inner periphery of the stator core receive a two-layer winding made up of coils 30 joined by end connections (or overhangs) 8. The terminals of the stator winding are brought out via a terminal box 23. Attachment of the frame to its foundation is by feet 22. To facilitate



handling in transit or during erection, the frame has a lifting ring 6.

The *rotor* consists of a shaft 26 on which end plates 24, a key 21, and a split key 20 hold the compressed core blocks built up of ring-shaped laminations 3 (see Fig. 39-2a). The radial vent ducts are formed by vent fingers placed within each pole pitch. The partially closed slots made on the outer periphery of the rotor core (shown in the sectional

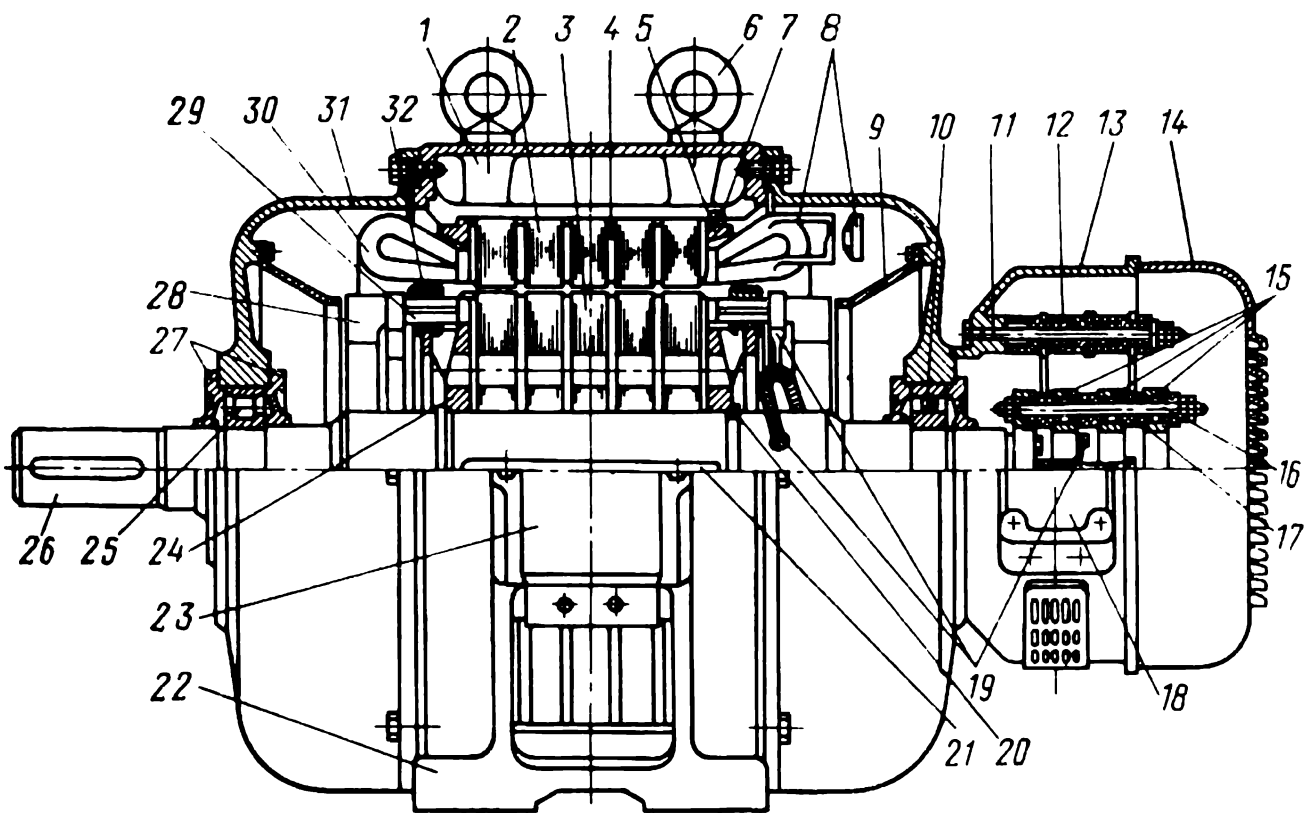


Fig. 39-6 A 250-kW, 3000-rpm, 50-Hz, totally-enclosed, internally blown wound-rotor induction motor

view of Fig. 39-4b) receive a three-phase, double-layer (usually star-connected) wave winding 29 made up of preformed bars. The three terminal leads are brought out by means of cables 19 passing through a hole in the shaft to slip rings 15 mounted on the shaft.

The winding bars (at 1 in Fig. 39-4b), preformed at one end and with the turn insulation (2 and 3) already applied, are pushed from one end of the core through the slots already insulated with slot liners or cells 4. The bars are anchored in the radial direction and also the turn and ground insulation is augmented with plates 5 and 6. The centrifugal force acting on the overhangs is resisted by slot wedges 7.

The coil and connections (overhangs) are supported by end plates 24 (Fig. 39-6) which also double as coil clamps. On

the outside, the overhangs are taped with bands 32 to resist centrifugal forces.

Electrical connection of the rotor winding to external (nonrotating) circuits is by means of slip rings to which the coil terminal leads are brought out, and a brush assembly connected to the external circuits directly. It is usual to make the slip rings as an integral assembly. The rings (at 15 in the figure) may be made of steel or brass alloy and are separated from one another and from ground by insulating spacers 17. The assembly is held together by insulated studs 16 and joined to the shaft end by a flange. The slip rings make sliding contact with carbon or copper-carbon brushes electrically connected to the conductors 12 of the brush yoke (or rocker arm). Figure 39-6 also shows the brush-yoke studs 11 and insulating parts, the brushgear enclosure 13 and cover 14; the brushes and brush-holders are not shown.

The necessary contact between the brushes and slip-rings is maintained by brush-holders mounted on the brush yoke (for more detail, see Sec. 51-3). Connection of the brush-yoke conductors to the starting rheostat is made inside the slip-ring terminal box 18.

The rotor is held in a proper position relative to the stator and made free to rotate by the same parts as are used in a squirrel-cage motor. These are a roller bearing 25, a ball bearing 10, end shields (or frames) 31, and bearing caps 27.

The motor shown in Fig. 39-6 is of ventilated, drip-proof construction (see Sec. 33-2). Inside the machine, cooling air follows both radial and axial paths. Atmospheric air enters the machine by openings in the end shields and is directed by baffles 9 towards the cooling blades 28, between the overhangs of the rotor winding, and towards the axial ducts in the rotor core. From the axial ducts, the air enters the radial ducts in the rotor and stator cores. The air driven by the cooling blades past the rotor overhangs bathes the stator overhangs. The hot air then enters the clearance between the stator yoke and the frame whence it is discharged through side openings in the frame into the atmosphere. The static pressure required to drive cooling air inside the machine is produced by the radial ducts in the rotor, which act as centrifugal fans.

## 40 Electromagnetic Processes in the Electric and Magnetic Circuits of an Induction Machine at No-Load

### 40-1 The Ideal No-load Condition

It is convenient to begin our study of the induction machine with the ideal no-load condition. In this condition, the electromagnetic processes involved are less elaborate than they are on load.

In the ideal no-load condition, the external torque applied to the shaft is zero,  $T_{\text{ext}} = 0$ . It is also assumed that the friction torque is likewise zero. The rotor is spinning at the same angular velocity as the rotating (or revolving) field ( $\Omega = \Omega_1$ ), the slip (defined as the quotient of the difference between the synchronous speed and the actual speed of the rotor, divided by the synchronous speed) is zero ( $s = 0$ ), no emf or current is induced in the rotor winding ( $I_2 = 0$ ), and the electromagnetic torque required to balance the external torque and the friction torque is zero ( $T_{\text{em}} = 0$ ).

At no-load, an induction motor closely resembles a transformer (see Part 1). In either case, there is only a current in the primary winding,  $I_1 \neq 0$ , and no current in the secondary  $I_2 = 0$ ; the magnetic field is established solely by the primary current, for which reason we may call it the magnetizing current ( $I_1 = I_0$ ). In contrast to a transformer, however, the set of magnetizing currents in the phases of the polyphase stator winding establishes a rotating (or revolving) magnetic field.

By analogy with a transformer, the voltage equation at no-load is only needed for one phase of the stator (that is, primary) winding:

$$\dot{V}_1 = -\dot{E}_1 + (R_1 + jX_1) \dot{I}_0$$

where  $\dot{E}_1$  = emf induced in the phase by a rotating magnetic flux  $\dot{\Phi}_m$

$\dot{V}_1$  = primary phase voltage

$R_1$  = primary phase leakage resistance (to be explained later)

$X_1$  = primary phase leakage inductance (to be explained later)

Because the inductive and resistive drops,  $X_1 I_0$  and  $R_1 I_0$ , are negligible,  $\dot{V}_1$  is almost completely balanced by  $\dot{E}_1$ , that is

$$\dot{V}_1 = -\dot{E}_1$$

## 40-2 Analysis of the Magnetic Circuit at No-Load

The magnetic circuit needs to be analyzed at no-load in order to determine the stator magnetizing current  $I_0$  (or the stator mmf  $F_0$ ) which produces the rotating magnetic flux  $\Phi_m$  that will induce the desired emf,  $E_1$ , in the stator.

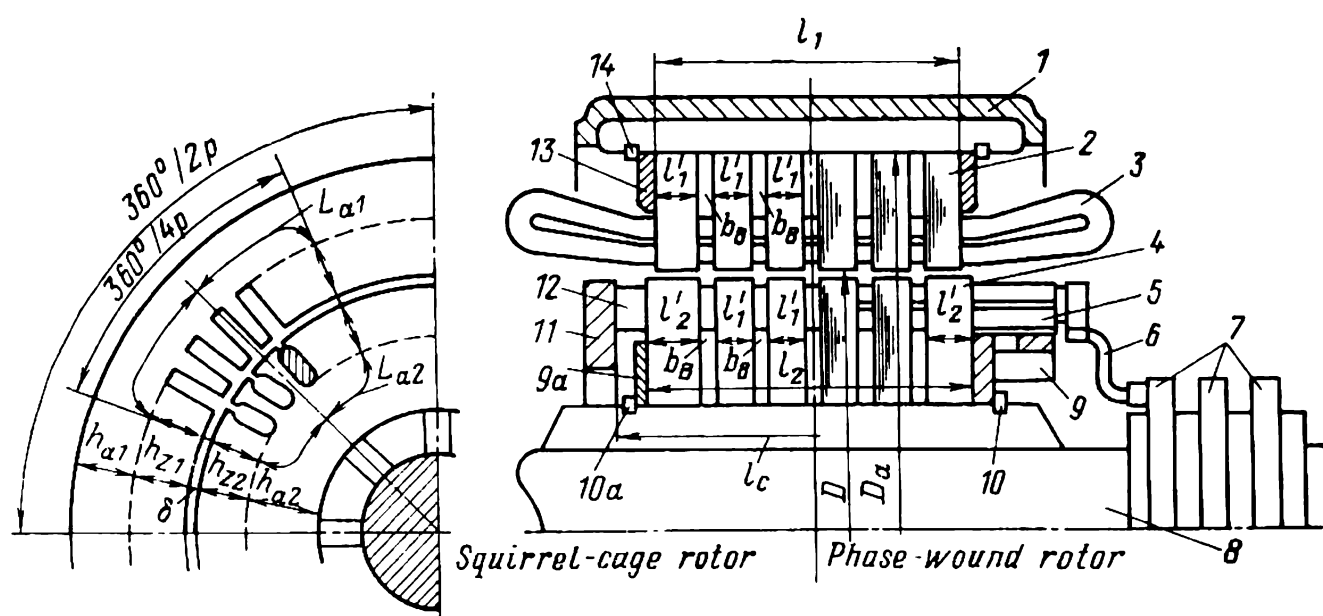


**Fig. 40-1** To calculation of the magnetic circuit for an induction machine:

1—frame (stator yoke); 2—stator core block; 3—stator winding; 4—rotor core block; 5—insulated, three-phase rotor winding in a wound-rotor motor; 6—rotor-winding terminal lead; 7—slip rings; 8—shaft; 9, 9a—pressure plate; 10, 10a—key; 11—end ring of a squirrel-cage rotor; 12—squirrel-cage bar; 13—pressure plate; 14—key

Two sectional views (transverse and axial) of the magnetic circuit in an induction machine are shown in Fig. 40-1. The cross-sectional view shows one half-cycle of change in the field, occupying a sector spanning the angle  $360^\circ/2p$ . The figure also shows the mean line of the mutual magnetic field.

So long as it is unsaturated, the iron parts of the magnetic circuit have an insignificant reluctance, and the air gap field is mainly controlled by the gap reluctance. Therefore, the gap flux density follows the sine-wave distribution of the fundamental mmf, Eq. (25-18). In Fig. 40-1, the gap flux density and mmf are maximal at the start and end of a half-cycle and vanish at the middle of the half-cycle. As the mmf builds up in magnitude, the stator and rotor teeth are saturated increasingly more, their reluctances go up, and the relation between the mmf and flux density ceases to be linear (the mmf rises at a higher rate than the flux density). However, the teeth are saturated only within the regions of high mmfs (at the edges of the half-cycle in Fig. 40-1), and are not where the mmf is low (at the middle of the half-cycle). Because of this, tooth saturation distorts the sine-wave gap flux distribution, and the flux waveform in the region of high mmfs is "flattened".

Since the rms value of emf,  $E_1$ , is mainly controlled by the fundamental flux density, the magnetic flux in the case of a nonsinusoidal flux distribution has to be calculated by the equation

$$\Phi_m = E_1 / 4k_B f_1 w_1 k_{w1} \quad (40-1)$$

where  $k_B$  is the shape factor of the flux density waveform.

In an unsaturated machine, when the magnetizing forces in the stator and rotor teeth are low in comparison with the air gap magnetizing force,

$$F_{z1} + F_{z2} \ll F_\delta$$

the flux density waveform is nearly sinusoidal, and

$$k_B = \pi/2 \sqrt{2} = 1.11$$

As the teeth are saturated in the region of high mmfs more and more, the magnetizing forces in the teeth,  $F_{z1} + F_{z2}$ , become comparable with the air gap magnetizing force,  $F_\delta$ , the flux density waveform is flattened, and  $k_B$  somewhat decreases in value

$$k_B = (\pi/2 \sqrt{2}) \xi_B$$

Here,  $\xi_B$  is a correction factor. It can be found from the plot in Fig. 40-2 where it is shown as a function of the tooth saturation factor

$$k_z = (F_\delta + F_{z1} + F_{z2}) / F_\delta$$

For each specified value of  $E_1$ , the values of  $k_z$  and  $k_B$  are found by the method of successive approximation (to be described later). To a first approximation, we may deem that  $k_z = 1$ .

The mmf  $F_0$  that produces the magnetic flux  $\Phi_m$  is found by applying Ampere's circuital law to the mean magnetic line composed of the segments  $L_{a1}$ ,  $h_{z1}$ ,  $\delta$ ,  $h_{z2}$ , and  $L_{a2}$  (see Fig. 40-1):

$$\frac{1}{2} \oint H \, dl = F_0$$

where  $H$  is the magnetic intensity at  $\Phi_m$ , and  $dl$  is an element of length of the mean magnetic line.

To facilitate calculations, the line integral is replaced by a sum of mmfs within the characteristic segments of the mean magnetic line, assuming that within each segment the magnetic intensity is constant:

$$\frac{1}{2} \oint H \, dl = F_\delta + F_{z1} + F_{z2} + F_{a1} + F_{a2} = F_0 \quad (40-2)$$

The *air gap mmf* is given by

$$F_\delta = H_\delta \delta k_\delta = B_m \delta k_\delta / \mu_0 \quad (40-3)$$

where  $k_\delta = k_{\delta 1} k_{\delta 2}$  = air gap factor defined in Eq. (24-10), which accounts for the effect of the stator and rotor saliency on the air gap reluctance

$B_m = \Phi_m / \alpha_\delta \tau l_\delta$  = maximum air gap flux density

$l_\delta$  = design core length (axial gap length) as given by Eq. (23-10).

The value of  $\alpha_\delta$  depends on the saturation of the stator and rotor teeth, in turn given by  $k_z$ . At low saturation, when the gap flux density waveform is sinusoidal,  $\alpha_\delta = 2/\pi$  [see Eq. (27-2)]. At saturation,  $\alpha_\delta$  goes up; now it is  $\alpha_\delta = 2\xi_\alpha/\pi$ . The correction factor  $\xi_\alpha$  (usually greater than unity) can be found from the plot of Fig. 40-2. The values of  $k_z$  and  $\alpha_\delta$  are found for each specified value of  $E_1$  by the method of successive approximation.

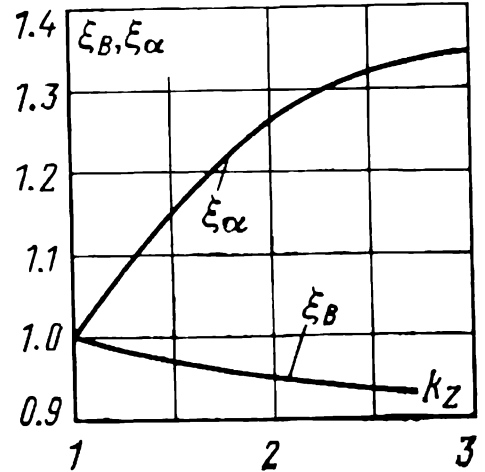


Fig. 40-2 Plots of  $\xi_\alpha = f(k_z)$  and  $\xi_B = f(k_z)$

The *mmf in the stator teeth*

$$F_{z1} = H_{z1}h_{z1} \quad (40-4)$$

is found from the field intensity in the tooth section which is  $h_{z1}$  distant from the narrowest section (that is, the tooth tip). The active surface area of iron at that section is

$$A_{z1} = b_{z1}l_{c1}k_f$$

where

$$\begin{aligned} b_{z1} &= \text{tooth width at the section} \\ l_{c1} &= l'_1 (n_v + 1) = \text{total length of the stator core,} \\ &\quad \text{that is, lamination blocks in} \\ &\quad \text{the stator of Fig. 40-1 (here,} \\ &\quad n_v \text{ is the number of radial vent} \\ &\quad \text{ducts)} \\ k_f &= \text{block fill factor (= 0.93 for} \\ &\quad \text{varnished laminations 0.5 mm} \\ &\quad \text{thick)} \end{aligned}$$

The tooth flux density is found, assuming that the magnetic field is continuous and that the flux is conserved at all the sections within the tooth pitch. At a moderate tooth saturation, which is true when the tooth flux density is  $B_{z1} \ll 1.8 \text{ T}$ , it is legitimate to deem that the tooth-pitch flux, as found from the air gap flux density,

$$\Phi_\delta = t_{z1}l_\delta B_m$$

is concentrated solely within the tooth laminations and does not extend into the slots and nonmagnetic clearances between them (the radial vent ducts and insulation between the tooth punchings). On this assumption, the tooth flux

$$\Phi_z = B_{z1}b_{z1}l_{c1}k_f$$

does not differ from the air gap flux

$$\Phi_z = \Phi_\delta$$

Hence,

$$B_{z1} = B_m \frac{l_\delta t_{z1}}{k_f l_{c1} b_{z1}} \quad (40-5)$$

When  $B_{z1} \leq 1.8 \text{ T}$ , the tooth magnetic intensity  $H_{z1}$  can be found from the main magnetization curve,  $H = f(B)$ . Such curves plotted for several grades of electrical-sheet steels may be found, for example, in [13].

If Eq. (40-5) gives  $B_{z1} > 1.8 \text{ T}$  and, as a consequence, the assumption made does not hold, the calculation must

be refined by allowing for the flux branching into the slot and nonmagnetic clearances

$$\Phi_s = B_{s1} A_{s1}$$

where

$$A_{s1} = l_1 b_{s1} + (1 - k_f) l_{c1} b_{z1} + b_v n_v b_{z1}$$

is the cross-sectional area of the slot and nonmagnetic clearances per slot pitch,  $B_{s1}$  is the flux density in the slot and nonmagnetic clearances,  $b_{s1}$  is the slot width at the section which is  $h_{z1}/3$  distant from the tooth tip,  $l_1$  is the total length of the stator core, and  $b_v$  is the width of a vent duct. In the circumstances,

$$\Phi_z = \Phi_\delta - \Phi_s$$

Let us divide the right- and left-hand sides of the equation by the active cross-sectional area of the tooth,  $A_{z1}$ , and take into account the fact that when two paths with flux density  $B_{z1}$  and  $B_{s1}$  are arranged in parallel, the magnetic intensity in them will be the same

$$H_{s1} = B_{s1}/\mu_0 = H_{z1} = f(B_{z1})$$

Then we get

$$B_{z1} = B'_{z1} - \mu_0 k_s H_{z1}$$

where  $B_{z1} = \Phi_z/A_{z1}$  is the actual tooth flux density,  $B'_{z1}$  is the tooth flux density as found by Eq. (40-5) on the assumption made originally,  $H_{z1}$  is the tooth field intensity corresponding to  $B_{z1}$  on the main magnetization curve, and  $k_s = A_{s1}/A_{z1}$  is the coefficient allowing for the effect of nonmagnetic clearances.

The sought flux density  $B_{z1}$  is found by simultaneously solving the above equation, where  $B_{z1}$  is a linear function of  $H_{z1}$ , and the equation describing the main magnetization curve  $H_{z1} = f(B_{z1})$  for the core material used. As a rule, the solution is obtained graphically at the intersection of the straight line  $B_{z1} = B'_{z1} - \mu_0 k_s H_{z1}$ , passing through point  $B'_{z1}$ , with the curve  $H_{z1} = f(B_{z1})$ . The procedure can be facilitated by using magnetization curves  $H_{z1} = f(B_{z1})$  plotted in advance for several values of  $k_s$ .

*The mmf in the rotor teeth*

$$F_{z2} = H_{z2} h_{z2} \quad (40-6)$$



is found in the same manner as for the stator teeth. At moderate saturation, when  $B_{z2} \leq 1.8 \text{ T}$ , the flux density is calculated on the assumption that all of the tooth-pitch flux is concentrated within the tooth iron

$$B_{z2} = B_m \frac{l_{\delta} t_{z2}}{k_f l_{C2} b_{z2}} \quad (40-7)$$

where  $b_{z2}$  is the tooth width at the section which is  $h_{z2}/3$  distant from its base, and  $l_{C2} = l'_1 (n_v - 1) + 2l'_2$  is the total length of the rotor core shown in Fig. 40-1.

If  $B_{z2}$  as found by Eq. (40-7) exceeds 1.8 T, the next step is to refine its value by allowing for the fraction of the total magnetic flux crowded out of the teeth into the slots and nonmagnetic materials. This is done in the same manner as for the stator teeth.

After  $F_{\delta}$ ,  $F_{z1}$  and  $F_{z2}$  have been found, it is important to verify the value of  $k_z$ . Should it differ from the specified value by more than 5%, the mmfs must be re-calculated, adopting the refined value of  $k_z$ .

*The mmf in the stator yoke*

$$F_{a1} = H_{a1} L_{a1} \xi \quad (40-8)$$

is found from the maximum yoke field intensity corresponding to

$$B_{a1} = \Phi_m / 2h_{a1} l_{C1} k_f \quad (40-9)$$

on the main magnetization curve [13]. The coefficient  $\xi$  accounts for variations in the magnetic intensity along the length  $L_{a1}$ , and is taken for  $B_a = B_{a1}$  from the table that follows.

$B_a, \text{ T}$	1.0	1.1	1.2	1.3	1.4	1.5
$\xi$	0.57	0.54	0.5	0.46	0.4	0.33

*The mmf in the rotor yoke*

$$F_{a2} = H_{a2} L_{a2} \xi \quad (40-10)$$

is found in a similar way from the maximum flux density in the rotor yoke

$$B_{a2} = \Phi_m / 2h_{a2} l_{C2} k_f \quad (40-11)$$

The peak value of  $F_0$  which establishes the mutual flux  $\Phi_m$  is calculated by Eq. (40-2). At low saturation,  $F_0$  does not practically differ from the air gap mmf,  $F_\delta$ . In the general case, it is  $k_s$  times the value of  $F_\delta$ :

$$F_{0m} = k_s F_\delta = F_\delta + F_{z1} + F_{z2} + F_{a1} + F_{a2} \quad (40-12)$$

where  $k_s$  is the saturation coefficient of the magnetic circuit.

### 40-3 Calculation of No-Load Current

The reactive component of no-load current, responsible for  $F_0$ , is found from Eq. (25-9):

$$I_{0r} = \frac{\pi p F_{0m}}{\sqrt{2} m_1 w_1 k_{w1}} \quad (40-13)$$

In addition to  $\dot{I}_{0r}$  which is in quadrature leading with  $\dot{E}_1$ , the stator winding in the ideal no-load condition carries the active component,  $\dot{I}_{0a}$ , which, given the flux  $\Phi_m$  and the emf  $E_1$ , is proportional to the core loss,  $P_c$ :

$$I_{0a} = P_c / m_1 E_1 \quad (40-14)$$

At no-load, the core loss only occurs in the stator whose teeth and yoke are cyclically magnetized by a rotating (revolving) field at frequency  $f_1$ . At no-load, the rotor is revolving at the field frequency, so it suffers no core loss. This is because the rotor elements stationary relative to the field are not magnetized cyclically. (Under rated conditions, when the slip and the frequency of cyclic magnetization are low, the rotor core loss is negligible.)

The core loss at no-load is assumed equal to the main core loss in the stator teeth and yoke and is found by Eqs. (31-11), (31-12), and (31-9) for  $f_1$ ,  $B_{z1}$ ,  $B_{a1}$ ,  $m_{z1}$ , and  $m_{a1}$ :

$$P_c = (k_{adz} B_{z1}^2 m_{z1} + k_{ad,a} B_{a1}^2 m_{a1}) p_{1.0/50} (f_1/50)^{1.3} \quad (40-15)$$

where  $k_{adz} = 1.7$  and  $k_{ad,a} = 1.4$ .

In induction machines, the active component of no-load current is a small fraction of the reactive component. Therefore, the no-load current does not practically differ from the reactive component

$$I_0 = \sqrt{I_{0r}^2 + I_{0a}^2} \approx I_{0r} \quad (40-16)$$

The phase angle  $\beta'_0$  between  $\dot{I}_0$  and  $-\dot{E}_1$  (see Fig. 2-8) does not differ from the angle between  $\dot{I}_0$  and  $I_{0a}$ , and may be written

$$\beta'_0 = \arccos (I_{0a}/I_0)$$

Accordingly, we may define the active and reactive components of the no-load current as

$$I_{0a} = I_0 \cos \beta'_0$$

and

$$I_{0r} = I_0 \sin \beta_0$$

By the same token, the active and reactive components of  $-\dot{E}_1$  may be written as  $E_1 \cos \beta'_0$  and  $E_1 \sin \beta'_0$ .

At  $V_1 = V_{1,R}$ , the no-load current in an induction machine accounts for a larger proportion of the rated current than in a transformer. This is because the stator and rotor cores are always separated by a nonmagnetic clearance which presents a considerable opposition to the magnetic flux, whereas in transformers the cores are usually of the closed construction.

The relative no-load current,  $I_0/I_{1,R}$ , increases with decreasing power output and rpm. For motors rated anywhere between 1 and 100 kW, it ranges from 0.5 to 0.25. For fractional-horsepower motors, it ranges from 0.5 to 1.0.

By finding  $I_0$  for several values of  $E_1$  (or  $\Phi_m$ ), we can plot the relations  $E_1 = f(I_0)$  and  $\Phi_m = f(I_0)$ . The former is known as the *no-load characteristic of a machine*, and the latter, the *magnetization curve (or characteristic) of the machine*. The two relations are linear only at  $E_1 \ll V_{1,R}$ . At  $E_1 > V_{1,R}$  when the magnetic circuit of a machine is usually saturated, the relations are strongly nonlinear.

#### 40-4 Calculation of the Main Stator Winding Impedance

Once the magnetic circuit has been designed and analyzed and the no-load current found, the next step is to determine the *main stator winding impedance* with allowance for the saturation of the magnetic circuit

$$Z_0 = R_0 + jX_0 = -\dot{E}_1/\dot{I}_0 \quad (40-17)$$

where  $R_0 = E_1 \cos \beta'_0 / I_0 =$  main resistance  
 $X_0 = E_1 \sin \beta'_0 / I_0 =$  main reactance

$\beta'_0 = \arctan (I_{0r} / I_{0a}) =$  angle between  $-\dot{E}_1$  and  $\dot{I}_0$   
 (see above).

The power dissipated in  $R_0$  represents the actual core loss,  $P_c$ . Therefore, we may express  $R_0$  in terms of  $P_c$ :

$$R_0 = \frac{E_1 \cos \beta'_0}{I_0} \frac{m_1 I_0}{m_1 I_0} = P_c / m_1 I_0^2 \quad (40-18)$$

The reactive power,  $Q_0$ , stored by  $X_0$  at  $I_0$  represents the reactive power stored by the main reactive impedance due to self-inductance  $X_{11} = 2\pi f_1 L_{11m} = E_1 / I_{0r}$  at  $I_{0r}$ . Therefore,

$$Q_0 = m_1 X_0 I_0^2 = m_1 X_{11} I_{0r}^2$$

Hence,

$$X_0 = X_{11} (I_{0r}^2 / I_0^2) = X_{11} \sin^2 \beta'_0 \quad (40-19)$$

where

$$\sin \beta'_0 = I_{0r} / I_0 = \frac{X_0}{\sqrt{X_0^2 + R_0^2}} \approx \frac{X_{11}}{\sqrt{X_{11}^2 + R_0^2}}$$

In most cases, it will be sufficiently accurate to take  $\sin \beta'_0 \approx 1$ .

In an unsaturated machine,  $L_{11m}$  is found by Eq. (28-4). In a saturated machine, it should be reduced by a factor of  $k_s$ . The relative magnitudes of  $R_0$  and  $X_0$  for the stator winding are dependent on the core saturation which in turn varies with  $E_1$  or  $\Phi_m$ .

## 41 Electromagnetic Processes in Induction Machines on Load

### 41-1 Basic Definitions and Assumptions

Our discussion will be limited to the steady-state electromagnetic processes in a loaded induction machine whose stator winding carries a balanced polyphase system of sinusoidal voltages.

An induction machine is capable of energy conversion in any condition, except at no-load (open-circuit) and a short-circuit. At no-load (an open-circuit), the mechanical power developed by the rotor,  $P_m = T_{em} \Omega$ , is zero, because the rotor is revolving at the same angular velocity as the field,  $\Omega = \Omega_1$ , and  $T_{em} = 0$ . In the case of a short-circuit, the

mechanical power is zero, because the rotor is at standstill,  $\Omega = 0$ .

Given  $V_1$  and  $f_1$ , the electromagnetic processes in an induction machine depend on the external torque,  $T_{\text{ext}}$ , applied to the shaft, and its direction. If the external torque opposes the rotation of the field, the machine will be operating as a motor. Should the applied torque be increased, the mechanical power output will also increase,

$$P_2 = T_{\text{ext}}\Omega$$

At the same time, the angular velocity  $\Omega$  of the rotor will go down ( $\Omega < \Omega_1$ ), and the slip  $s$  will increase:

$$s = \frac{\Omega_1 - \Omega}{\Omega_1} > 0$$

Conversely, should the external torque be in the direction of the revolving field, the machine will be operating as a generator. Now, an increase in

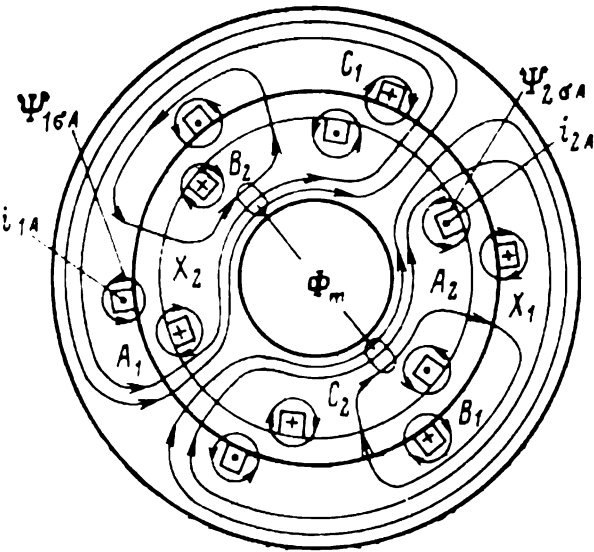


Fig. 41-1 Mutual and leakage fields in an induction machine

the torque will lead to an increased amount of active electric power delivered to the receiving line,

$$P_2 = T_{\text{ext}}\Omega$$

At the same time, the angular velocity of the rotor will increase ( $\Omega > \Omega_1$ ), but the slip will take on a negative value:

$$s = \frac{\Omega_1 - \Omega}{\Omega_1} < 0$$

In order to establish quantitative relations between the external torque  $T_{\text{ext}}$ , the angular velocity  $\Omega$ , and the electric quantities associated with the polyphase stator and rotor circuits (voltages, currents, active and reactive power), we need a set of equations describing the electromagnetic processes in those circuits.

Because all quantities associated with the stator and rotor circuits vary in time practically sinusoidally, it is convenient to write the above set of equations in complex notation. Also, the analysis can best be done, using a two-pole model (see Sec. 30-2), such as shown in Fig. 41-1.

Within a pitch pole, a two-pole model retains all the basic dimensions of the prototype machine (air gap length, slot width and depth, number of effective turns per slot, slot currents, turn voltages, magnetic flux densities, and magnetic fluxes). The angles between any elements within a pole pitch are multiplied by  $p$  (where  $p$  is the number of pole pairs in the prototype machine). The angular velocity of the field,  $\Omega_1$ , and the angular velocity of the rotor,  $\Omega$ , are each multiplied by  $p$  to become respectively

$$\Omega_1 p = (\omega_1/p) p = \omega_1$$

and

$$\omega = \Omega p$$

The slip and the stator and rotor current frequencies,  $f_1$  and  $f_2$ , remain unchanged.

To simplify matters, the two-pole model shown in all the subsequent drawings has a smooth stator and a smooth rotor.

#### 41-2 The Stator Voltage Equation. Stator MMF

A three-phase stator winding (see Chap. 22) may be star or delta connected. When energized with a balanced set of phase currents  $I_1$ , it establishes a rotating (revolving) field with  $2p$  poles. The phase currents are induced by a balanced set of supply voltages  $V_1$ . The frequency  $f_1$  of these currents is the same as the supply frequency. The peak value of the  $2p$ -pole (fundamental) stator mmf

$$F_{1m} = (\sqrt{2}/\pi) m_1 \frac{I_1 w_1 k_{w1}}{p} \quad (41-1)$$

is proportional to  $I_1$ , the number  $w_1$  of series phase conductors, and the winding factor for the fundamental component,  $k_{w1}$  [see Eq. (25-9)].

The stator mmf  $F_{1m}$  and the mutual flux density  $B_m$  which, in addition to the stator mmf, are produced by the rotor mmf,  $F_{2m}$ , rotate at an angular velocity given by

$$\Omega_1 = 2\pi f_1/p = \omega_1/p$$

In the diagram of a two-pole model shown in Fig. 41-2a, the electric quantities  $\dot{V}_1$  and  $\dot{I}_1$ , and also the space-distrib-

buted quantities  $\dot{F}_{1m}$  and  $\dot{B}_m$  are depicted as complex amplitudes rotating at an electrical angular velocity  $\omega_1$ .

The projections of the complex functions representing the rms phase quantities ( $\dot{V}_1 e^{j\omega_1 t}$ ,  $\dot{I}_1 e^{j\omega_1 t}$ , and so on) on the stator phase axes  $A_1$ ,  $B_1$  and  $C_1$  are equal to  $1/\sqrt{2}$  of the corresponding instantaneous phase quantities. The

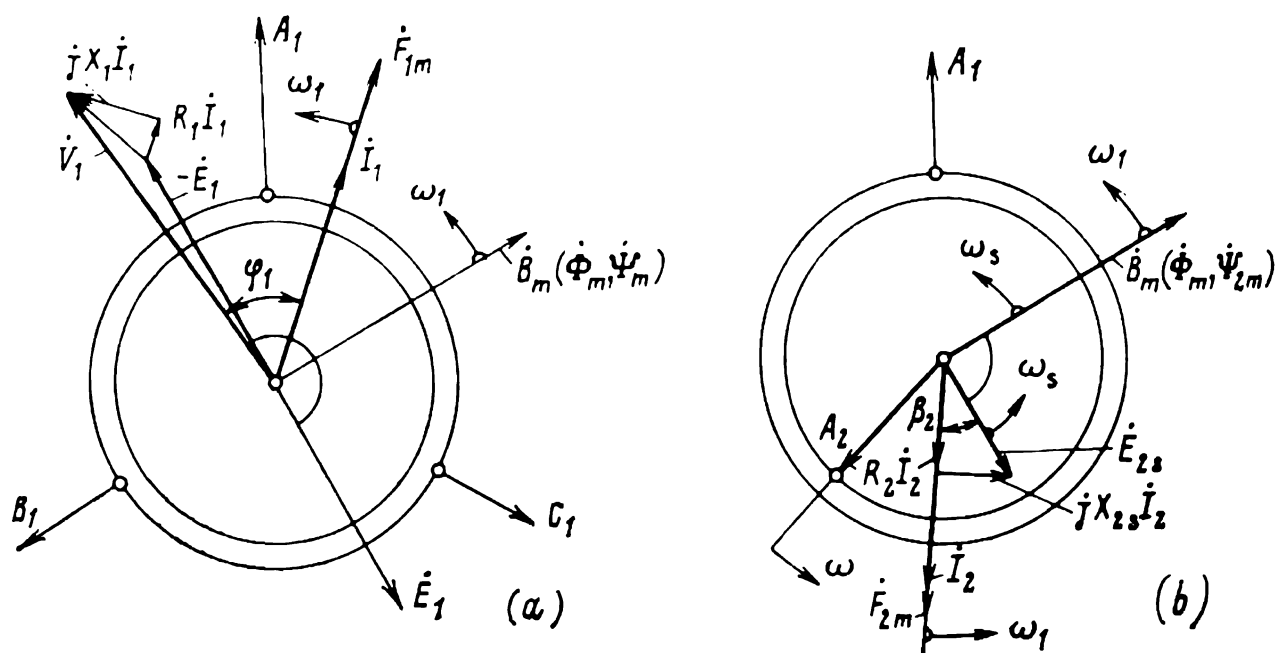


**Fig. 41-2** Phasor diagrams for (a) stator quantities and (b) rotor quantities of an induction machine (motor mode of operation,  $\omega < \omega_1$ ,  $s > 0$ )

projections, on an arbitrary direction, of the space-distributed complex functions representing the quantities sinusoidally distributed in the air gap give the instantaneous values of these quantities at a given point on the periphery of the air gap.

The rotating mutual field and the stator phase winding produce a flux linkage (see Sec. 27-5) whose peak value

$$\Psi_{1m} = w_1 k_{w1} \Phi_m$$

is proportional to the flux

$$\Phi_m = \frac{2}{\pi} \tau l_\delta B_m$$

and, in the final analysis, to the peak value of the gap flux density,  $B_m$ .\*

\* Here, the  $\Phi_m$  and  $E_1$  equations hold for an unsaturated machine with a sinusoidally distributed gap flux density. For a saturated machine, they are given in Chap. 40.

On the diagram  $\dot{B}_m$ ,  $\dot{\Phi}_m$ , and  $\dot{\Psi}_{1m}$  rotate all in the same direction (see Fig. 41-2). Variations in the flux linkage at  $\omega_1 = 2\pi f_1$  induce in each phase a mutual emf whose complex rms value is given by

$$\dot{E}_1 = -j\omega_1 \frac{\dot{\Psi}_{1m}}{\sqrt{2}} = -j \frac{2\pi}{\sqrt{2}} f_1 w_1 k_{w1} \dot{\Phi}_m \quad (41-2)$$

Also, the stator phase is linked by the leakage flux, giving rise to a leakage flux linkage  $\dot{\Psi}_{1\sigma}$  proportional to the phase current  $\dot{I}_1$  (the lines of mutual and leakage fields for phase  $A_1$  and the other stator phases are shown in Fig. 41-1).

The leakage emf  $E_{\sigma 1}$  induced in the stator phase by variations in the leakage flux linkage at  $\omega_1$  is usually expressed in terms of  $\dot{I}_1$  and  $X_1 = \omega_1 L_{\sigma 1}$ , the leakage inductive reactance of the stator (see Sec. 28-7):

$$\dot{E}_{1\sigma} = -j\omega_1 \dot{\Psi}_{1\sigma} / \sqrt{2} = -jX_1 \dot{I}_1 \quad (41-3)$$

The stator phase voltages, emfs, and currents must satisfy the voltage equation which, as written in complex notation, is the same as for the transformer primary (see Sec. 3-2)

$$\dot{V}_1 + \dot{E}_1 + \dot{E}_{1\sigma} = R_1 \dot{I}_1$$

where  $R_1$  is the stator phase resistance at  $f_1$  (see Sec. 31-2).

On expressing  $\dot{E}_{1\sigma}$  in terms of  $\dot{I}_1$  in accord with Eq. (41.3), we may introduce the stator phase impedance  $Z_1$ :

$$\dot{V}_1 = -\dot{E}_1 + Z_1 \dot{I}_1 \quad (41-4)$$

where  $Z_1 = R_1 + jX_1$  is the stator phase impedance.\*

Graphically, Eq. (41-4) is shown on the stator voltage phasor diagram plotted in Fig. 41-2a for motoring. In this diagram, the magnitude and direction of  $\dot{E}_1$  induced by the rotating  $\dot{B}_m$  field are chosen such that at the specified  $\dot{V}_1$  the machine could operate as a motor. For this to happen, it is required that the phase current

$$\dot{I}_1 = (\dot{V}_1 + \dot{E}_1) / Z_1$$

---

\*  $Z_1$  is determined without allowance for the mutual flux linkage.



should lag behind  $\dot{V}_1$  by  $\varphi_1 < \pi/2$  and that the active power should be

$$P_1 = m_1 V_1 I_1 \cos \varphi_1 > 0$$

(The power drawn from the supply line is assumed positive.)

### 41-3 The Rotor Voltage Equation. Rotor MMF

The rotor of an induction machine rotates at an angular velocity  $\Omega$  which is in the general case different from the angular velocity of the mutual field

$$\Omega_1 = 2\pi f_1 / p = \omega_1 p$$

Accordingly, in a two-pole model, as shown in Fig. 41-2, the electrical angular velocity of the rotor,  $\omega = \Omega p$ , is different from the electrical angular velocity of the field

$$\omega_1 = \Omega_1 p = 2\pi f_1$$

Relative to the rotor, the mutual field depicted in the diagram of Fig. 41-2b by  $\dot{B}_m$  rotates at an angular velocity

$$\Omega_s = \Omega_1 - \Omega$$

called the *angular slip velocity*. Accordingly, in the model the field rotates relative to the rotor at

$$\omega_s = \omega_1 - \omega$$

Recalling that the slip is defined as

$$s = \Omega_s / \Omega_1 = \omega_s / \omega_1 \quad (41-5)$$

we may express the angular slip velocity in terms of the angular field velocity as

$$\Omega_s = \Omega_1 - \Omega = s\Omega_1$$

or

$$\omega_s = \omega_1 - \omega = s\omega_1 \quad (41-6)$$

In the motor mode of operation to which the diagram in Fig. 41-2 applies, both  $s$  and  $\Omega_s$  are positive. This implies that in motoring the  $B_m$  field is rotating relative to the rotor in the same direction as it does relative to the stator ( $\omega_s$  is in the same direction as  $\omega_1$ ).

The rotating mutual field and the rotor phase winding produce a flux linkage (see Sec. 27-5) whose peak value

is

$$\Psi_{2m} = w_2 k_{w2} \Phi_m \quad (41-7)$$

where  $\omega_2 =$  rotor phase turns

$k_{w2} =$  rotor phase winding factor for the fundamental ( $2p$ -pole) component of magnetic flux density

In Eq. (41-7), the mutual flux  $\Phi_m$  is the same as in Eq. (41.2). Both  $\dot{\Phi}_m$  and  $\dot{\Psi}_{2m}$  are acting in the same direction as  $\dot{B}_m$ . As they vary at  $\omega_s$ , the rotor phase flux linkages give rise to the mutual emf  $E_{2s}$ . The frequency  $f_2$  of the mutual emf, currents and other quantities in the rotor phases is a function of the angular field velocity relative to the rotor

$$f_2 = \omega_s / 2\pi = \omega_1 s / 2\pi = f_1 s \quad (41-8)$$

The complex emf  $\dot{E}_{2s}$  lags behind the complex flux linkage by  $\pi/2$ , and the rms value of the emf at slip  $s$  is given by

$$\dot{E}_{2s} = -j\omega_s \dot{\Psi}_{2m} / \sqrt{2} = -j(2\pi / \sqrt{2}) f_2 w_2 k_{w2} \dot{\Phi}_m \quad (41-9)$$

The rotor phase mutual emf,  $E_{2s}$ , may be expressed in terms of the mutual emf,  $E_2$ , that would be induced by the same field in the rotor at standstill, when  $\omega = 0$ ,  $\omega_s = \omega_1 - \omega = \omega_1$ ,  $s = 1$ , and  $f_2 = f_1 s = f_1$ .

As follows from Eq. (41-8),

$$E_{2s} = E_2 s \quad (41-10)$$

where  $E_2 = \omega_1 \Psi_{2m} / \sqrt{2}$ .

The rotor phase is also linked by the leakage flux. This produces a leakage flux linkage,  $\Psi_{2\sigma}$ , proportional to  $I_2$  (the lines of the mutual and leakage fields for phase  $A_2$  and the other rotor phases are shown in Fig. 41-1).

The leakage emf,  $\dot{E}_{2\sigma s}$ , induced in a rotor phase by variations in the phase flux linkage at

$$\omega_s = 2\pi f_2 = s\omega_1$$

is usually expressed in terms of  $\dot{I}_2$  and the rotor leakage inductive reactance at slip  $s$ , given by

$$X_{2s} = 2\pi f_2 L_{\sigma 2} = 2\pi s f_1 L_{\sigma 2} = sX_2 \quad (41-11)$$

where

$$X_2 = 2\pi f L_{\sigma 2}$$

is the leakage inductive reactance of the rotor at standstill, when  $s = 1$  and  $f_2 = f_1$  (see Sec. 28-7).

The rms value of the rotor leakage emf is

$$\dot{E}_{2\sigma s} = -jX_{2s}\dot{I}_2 \quad (41-12)$$

The rotor phase emfs and currents must satisfy the voltage equation which, as written in complex notation, is the same as for the transformer primary (see Sec. 3-2):

$$\dot{E}_{2s} + \dot{E}_{2\sigma s} = R_2\dot{I}_2$$

where  $R_2$  is the rotor phase resistance at

$$f_2 = sf_1$$

On expressing  $\dot{E}_{2\sigma s}$  in terms of  $\dot{I}_2$  in accord with Eq. (41-12), we may introduce in the voltage equation the rotor phase impedance ( $R_2 + jX_{2s}$ ):

$$\dot{E}_{2s} = (R_2 + jX_{2s})\dot{I}_2 \quad (41-13)$$

The action of  $\dot{E}_{2s}$  is such that the rotor phases carry a current

$$\dot{I}_2 = \frac{\dot{E}_{2s}}{R_2 + jX_{2s}} \quad (41-14)$$

which lags behind  $\dot{E}_{2s}$  by angle  $\beta_2$  (see Fig. 41-2b):

$$\beta_2 = \arctan (X_{2s}/R_2) \quad (41-15)$$

The current  $I_2$  induced in the rotor phases varies at the same frequency as  $E_{2s}$ , that is  $f_2 = sf_1$ .

Graphically, Eq. (41-13) is illustrated in the rotor voltage phasor diagram plotted in Fig. 41-2b. The rotor phase quantities are obtained by projecting the respective complex quantities on the rotor phase axes  $A_2$ ,  $B_2$ , and  $C_2$  which rotate together with the rotor at an electrical angular velocity  $\omega$ . Because the complex quantities representing the rotor phase quantities rotate relative to the rotor at

$$\omega_s = \omega_1 - \omega$$

their projections vary at  $f_2 = \omega_s/2\pi$ .

The balanced set of currents  $I_2$  in the  $m_2$ -phase rotor winding, displaced from each other by an angle  $2\pi/m_2$ , establishes in the rotor a  $2p$ -pole (fundamental) mmf whose

peak value (see Sec. 25-9) is given by

$$F_{2m} = (\sqrt{2}/\pi) m_2 \frac{I_2 w_2 k_{w2}}{p} \quad (41-16)$$

Relative to the rotor,  $F_{2m}$  rotates at  $\omega_s = 2\pi f_2$  in the two-pole model, and at  $\Omega_s = \omega_s/p$  in the prototype machine. In doing so,  $\dot{F}_{2m}$  is acting in the same direction as  $\dot{I}_2$ . Since the rotor velocity is  $\omega = \Omega p$  in the two-pole model and  $\Omega$  in the prototype machine, it is an easy matter to see that relative to the stator  $\dot{F}_{2m}$  rotates at

$$\omega + \omega_s = \omega_1$$

in the model, and at

$$\Omega + \Omega_s = \Omega_1$$

in the prototype machine.

To sum up, the rotor mmf,  $\dot{F}_{2m}$ , rotates in space at the same velocity as the stator mmf,  $F_{1m}$ .

#### ☆ 41-4 Analysis and Design of the Squirrel-Cage Winding

A squirrel-cage rotor consists of  $Z_2$  bars cast or pushed through the rotor slots and connected at both ends by end rings so that the cage is permanently shorted.

Each phase of a squirrel-cage winding is in effect a single-turn loop composed of two adjacent bars and the intervening end-ring segments. For example, phase loop 1 consists of bars 1 and 2 and the respective segments of the end rings. The bars carry each a current  $I_{b1}$ ,  $I_{b2}$ ,  $I_{b3}$ , . . . , and the end-ring segments carry each a current  $I_{er1}$  between bars 1 and 2,  $I_{er2}$  between bars 2 and 3, and so on (Fig. 41-3).

Obviously, the number of phases in a squirrel-cage rotor is equal to the number of bars (or loops):

$$m_2 = Z_2$$

As already noted, each phase is a single-turn loop:

$$w_2 = 1$$

The phase winding factor is equal to the pitch factor:

$$k_{w2} = k_{p2} = \sin (\pi y/2\tau) = \sin (\pi p/Z_2) \quad (41-17)$$

where  $y = 1$  = phase loop pitch (in slot or tooth pitches)  
 $\tau = Z_2/2p$  = half-pole pitch (or half-cycle) of the  
 fundamental component of the rotating  
 field (also in slot or tooth pitches)

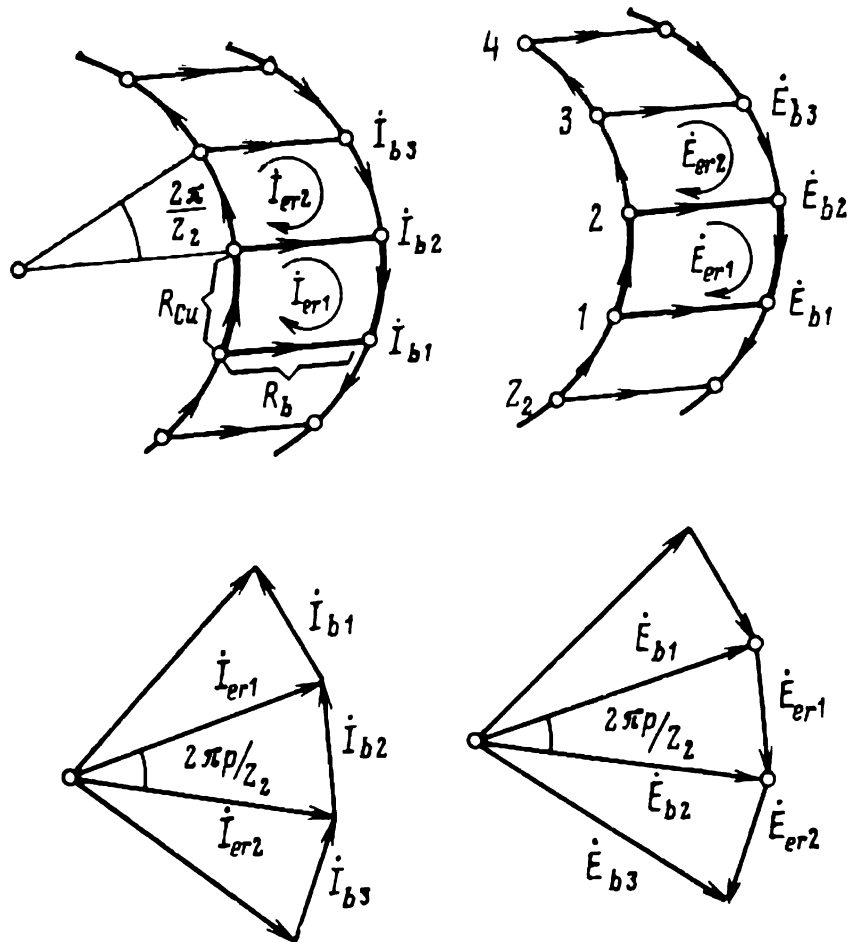


Fig. 41-3 Currents and emfs in the loops and bars of a squirrel-cage structure

A phase current refers to the loop current in turn equal to the current in the respective end-ring segments:

$$\dot{I}_{2(1)} = \dot{I}_{er1}, \quad \dot{I}_{2(2)} = \dot{I}_{er2}, \text{ etc.}$$

Each bar actually belongs to two adjacent phases. Therefore, the current in a bar is equal to the difference in currents between these two adjacent phases (or loops):

$$\dot{I}_{b2} = \dot{I}_{er1} - \dot{I}_{er2} \quad (41-18)$$

Owing to the symmetry of the squirrel-cage structure, the currents induced in the phases by a  $2p$ -pole rotating field are the same:

$$I_2 = I_{er} = I_{er1} = I_{er2} = \dots$$

On a phasor diagram, the complex phase currents form a symmetrical star in which the currents of adjacent phases

spaced an angle  $2\pi p/Z_2$  apart. (The loops of adjacent phases are displaced from one another by an angle  $2\pi/Z_2$ .)

The bar currents are the sides of a polygon constructed on the loop-current star. The rms value of a bar current is given by

$$I_b = 2I_2 \sin (\pi p/Z_2) \quad (41-19)$$

(Hint: to derive the above equation, consider the triangle of currents  $I_{er1}$ ,  $I_{er2}$ ,  $I_{b2}$  in Fig. 41-3.)

The phase emf

$$E_{2s} = E_{er} = E_{er1} = E_{er2} = \dots$$

may be regarded as the difference in emf between the bars forming a loop. For example,

$$\dot{E}_{er1} = \dot{E}_{b2} - \dot{E}_{b1} \quad (41-20)$$

The rms value of a bar emf

$$E_b = E_{b1} = E_{b2} = \dots$$

is found from the triangle of vectors  $E_{b1}$ ,  $E_{b2}$ ,  $E_{er1}$ :

$$E_b = \frac{E_{2s}}{2 \sin (\pi p/Z_2)} \quad (41-21)$$

The equivalent resistance,  $R_2$ , and the equivalent reactance,  $X_2$ , of a squirrel-cage winding is found from power considerations. The sum of copper losses in the phases

$$Z_2 R_2 I_2^2$$

must be equal to the sum of losses in the bars,  $Z_2 R_b I_b^2$  and in the end-ring segments between adjacent bars,  $2Z_2 R_{er} I_{er}^2$ . (Here,  $I_{er} = I_2$ ,  $R_b$  is the resistance of a bar, and  $R_{er}$  is the resistance of the end-ring segment between adjacent bars (see Fig. 41-3).) Upon rearrangement, we get

$$R_2 = 2R_{er} + R_b (I_b/I_2)^2 \quad (41-22)$$

Similarly,

$$X_2 = 2X_{er} + X_b (I_b/I_2)^2 \quad (41-23)$$

where  $X_b$  is the leakage inductive impedance of a bar, and  $X_{er}$  is the leakage inductive impedance of an end-ring segment.

$$(I_b/I_2)^2 = 4 \left( \sin \frac{\pi p}{Z_2} \right)^2$$

(see Eq. (41-19)).

### 41-5 MMF Equation. Magnetizing Current. Mutual Field

As has been shown in Sec. 41-3, the rotor mmf,  $F_{2m}$ , rotates at the same velocity as the stator mmf,  $F_{1m}$ . Either mmf rotates at an angular velocity  $\Omega_1$  relative to the stator and an angular slip velocity  $\Omega_s$  relative to the rotor. In the model, this occurs at an electrical angular velocity  $\omega_1$  and an electrical angular slip velocity  $\omega_s$ , respectively.

The relative position of the stator and rotor mmfs shown in the model by the complex amplitudes  $\dot{F}_{1m}$  and  $\dot{F}_{2m}$  remains unchanged so long as the machine is in a steady state (see Fig. 41-4). Therefore, the resultant mmf,  $\dot{F}_{0m}$ , has

a certain definite peak value in either condition (at no-load and on load), rotates at  $\Omega_1$  relative to the stator (at  $\omega_1$  in the model), and is given by

$$\dot{F}_{0m} = \dot{F}_{1m} + \dot{F}_{2m} \quad (41-24)$$

Accordingly, the mutual field set up by the resultant mmf,  $\dot{F}_{0m}$ , has a certain definite peak flux density  $\dot{B}_m$  in either condition (at no-load and on load), and rotates relative to the stator at the same velocities.

On load, the mutual flux  $\Phi_m$  can be found from the magnetic-circuit analysis carried

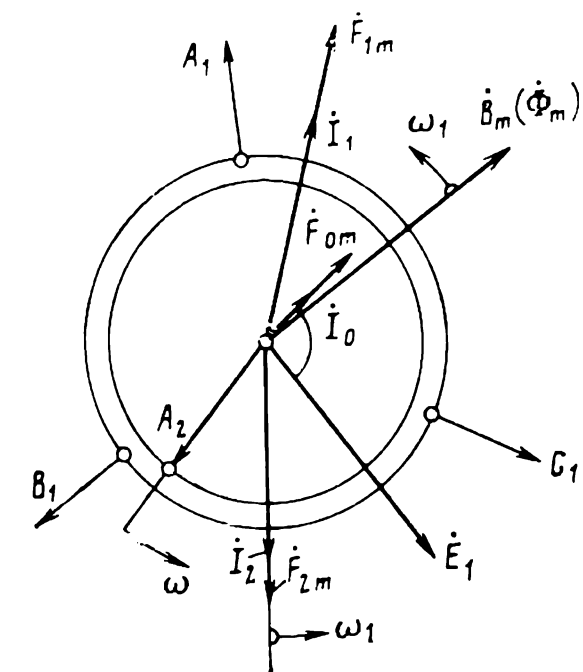


Fig. 41-4 Phasor diagram of mmfs and currents in an induction machine (motor mode of operation,  $\omega < \omega_1$ ,  $s > 0$ )

out for the no-load condition by Eq. (40-2). In doing so, it is legitimate to use the magnetization curve  $\Phi_m = f(F_{0m})$ , assuming that  $F_{0m}$  is the resultant mmf on load. If the resultant mmf,  $F_{0m}$  has the same value at no-load and on load, the mutual flux will likewise be the same in either case.

Extending the no-load analogy to the generation of the mutual field, we may introduce the concept of *magnetizing current*,  $I_0$ . It will refer to the stator current which produces an mmf equal to the resultant mmf,  $F_{0m}$ . In the diagram

of Fig. 41-4, the magnetizing current is plotted as a complex quantity

$$\dot{I}_0 = \frac{\dot{F}_{0m}\pi p}{\sqrt{2} m_1 \omega_1 k_{w1}} \quad (41-25)$$

which, on the complex plane, is in line with  $\dot{F}_{0m}$ . At the same time,  $F_{2m}$  may be imagined as being produced by a current  $I'_2$  traversing the stator winding. It is called the rotor current referred (or transferred) to the stator winding and is written

$$\dot{I}'_2 = \frac{\dot{F}_{2m}\pi p}{\sqrt{2} m_1 \omega_1 k_{w1}} - k_I \dot{I}_2 \quad (41-26)$$

where

$$k_I = \frac{m_2 \omega_2 k_{w2}}{m_1 \omega_1 k_{w1}}$$

is the referring coefficient for the rotor current.

It is to be noted that the phase currents  $I_0$  and  $I'_2$  are balanced sets of stator currents varying at a frequency  $f_1$  and producing rotating mmfs with amplitudes  $F_{0m}$  and  $F_{2m}$ , respectively.

On introducing  $\dot{I}_0$  and  $\dot{I}'_2$ , we may express  $\dot{F}_{0m}$ ,  $\dot{F}_{2m}$  and  $\dot{F}_{1m}$  in Eq. (41-24) in terms of the respective currents by use of Eqs. (41-25) and (41-26). Then, dividing the equation through by  $\sqrt{2} m_1 \omega_1 k_{w1} / \pi p$ , we obtain an alternate form of the mmf equation

$$\dot{I}_0 = \dot{I}_1 + \dot{I}'_2 \quad (41-27)$$

Quite appropriately, it is called the current equation. The magnetizing current  $\dot{I}_0$  given by this equation sets up the same mutual field as the no-load current  $\dot{I}_0$  equal in magnitude. By the same token, the on-load stator mutual emf  $E_1$  is the same as it is at no-load and at current  $I_0$ . Quite naturally, the equation connecting the mutual emf  $E_1$  and the magnetizing current  $I_0$  on load turns out to be the same as at no-load (see Eq. 40-17):

$$\dot{E}_1 = -Z_0 \dot{I}_0 \quad (41-28)$$



where

$$Z_0 = R_0 + jX_0$$

is the main impedance of the stator winding.

The complex flux density,  $\dot{B}_m$ , and the complex flux,  $\dot{\Phi}_m$ , lead the complex emf  $\dot{E}_1$  by  $\pi/2$ . The relationship between  $E_1$ , on the one hand, and  $B_m$  and  $\Phi_m$ , on the other, remains the same as at no-load [see Eq. (40-1) and also Eq. (40-3) with allowance for saturation and Eq. (41-2) without allowance for saturation].

The mmf and current phasor diagrams corresponding to Eqs. (41-24) and (41-27) appear in Fig. 41-4.

#### 41-6 Voltage and Current Phasor Diagrams for an Induction Machine

The voltage and current phasor diagram of an induction machine shown in Fig. 41-5 gives a graphical interpretation of the equations that describe the processes in the stator and rotor electric circuits: (41-4), (41-13), (41-27), and (41-28).

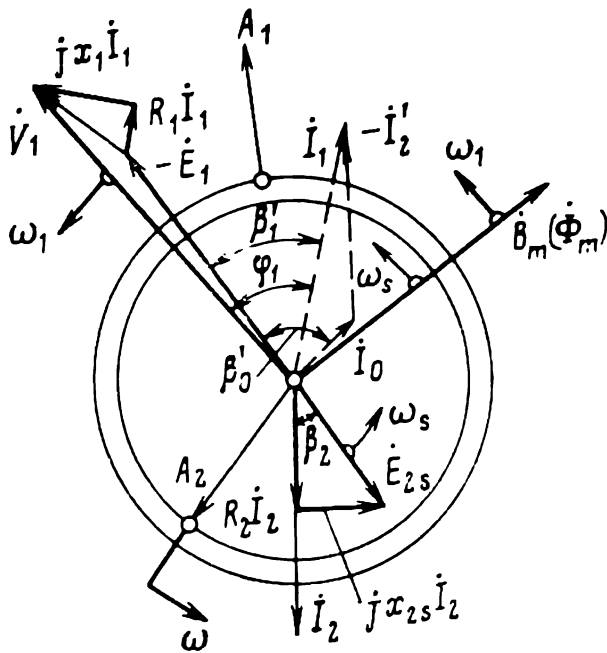


Fig. 41-5 Phasor diagram of an induction machine (motor mode of operation,  $\omega < \omega_1$ ,  $s > 0$ )

The diagram is constructed on the space complex plane of a two-pole model and combines in effect the partial diagrams appearing in Figs. 41-2 and 41-4. All complex quantities shown in the diagram rotate at  $\omega_1 = 2\pi f_1$ ; the rotor and its phase axes rotate at an electrical angular velocity  $\omega = \Omega p$ ; the stator and its phase axes are assumed to be at standstill. The stator phase quantities are the projections

of the respective complex quantities ( $\dot{V}_1$ ,  $\dot{E}_1$ ,  $\dot{I}_1$ , etc.) on the stator phase axes. The rotor phase quantities are the projections of the respective complex quantities ( $\dot{E}_{2s}$ ,  $\dot{I}_2$ , etc.) on the rotor phase axes relative to which they rotate at  $\omega_1 - \omega = \omega_s$ .

The space-distributed quantities are obtained by projecting  $\dot{B}_m$ ,  $\dot{F}_{1m}$ ,  $\dot{F}_{2m}$ , and  $\dot{F}_{0m}$  on the radii originating at a given point in the air gap.

It is convenient to begin the construction of the diagram by plotting  $\dot{B}_m$ , because it is in line with  $\dot{\Phi}_m$ ,  $\dot{\Psi}_{1m}$ , and  $\dot{\Psi}_{2m}$ . In addition to the value of  $B_m$ , the quantities assumed to be specified in advance are the stator current frequency  $f_1$ , the rotor angular velocity  $\Omega$ , the circuit parameters  $X_0$ ,  $R_0$ ,  $R_1$ ,  $R_2$ ,  $X_1$  and  $X_{2s}$  and the magnetization curves. All the other quantities associated with the stator and rotor electric circuits ( $E_{2s}$ ,  $I_2$ ,  $I_0$ ,  $I_1$ ,  $E_1$ ,  $V_1$ , and so on) are found in the course of construction.

The diagram shown in Fig. 41-5 holds for the motor mode of operation ( $0 < \Omega < \Omega_1$ ,  $1 > s > 0$ ). The sequence of steps is as follows.

1. Choose an arbitrary position for  $\dot{B}_m$ .
2. Plot  $\dot{\Phi}_m$ ,  $\dot{\Psi}_{1m}$ , and  $\dot{\Psi}_{2m}$  so that they are in line with  $\dot{B}_m$ . Calculate  $\Phi_m$  by Eq. (41-2) or Eq. (40-3), with allowance for the flattening of the flux density curve.
3. Plot  $\dot{E}_1$  as found by Eq. (40-1) or (41-2) and  $\dot{E}_{2s}$  as found by Eq. (41-9), so that they lag behind  $\dot{\Phi}_m$  by  $\pi/2$ .
4. Using Eq. (41-14), find  $\dot{I}_2$  lagging behind  $\dot{E}_{2s}$  by an angle  $\beta_2$ , and construct the rotor voltage diagram.
5. Using Eq. (41-26), find the rotor current referred to the stator,  $\dot{I}'_2$ .
6. Using Eq. (41-28), find  $\dot{I}_0$ .
7. Using Eq. (41-27), find  $\dot{I}_1$ .
8. Using Eq. (41-4), construct the stator voltage diagram and determine the supply voltage  $\dot{V}_1$  and the phase angle  $\varphi_1$  between  $\dot{V}_1$  and  $\dot{I}_1$ .

#### 41-7 Energy Conversion by an Induction Machine. Power Losses. Efficiency

For better insight into the electromagnetic processes that take place in an induction machine, it is useful to trace the various steps in the energy conversion that it implements.

In the motor mode of operation (Fig. 41-6), the mechanical angular velocity of the rotor does not exceed that of the field ( $0 < \Omega < \Omega_1$ ), and the machine draws active power from the supply line

$$P_1 = m_1 V_1 I_1 \cos \varphi_1 \quad (41-29)$$

where  $\varphi_1$  is the phase angle between the stator voltage and current, shown in the diagram of Fig. 41-5. It is taken positive when the current is lagging behind the voltage. In the

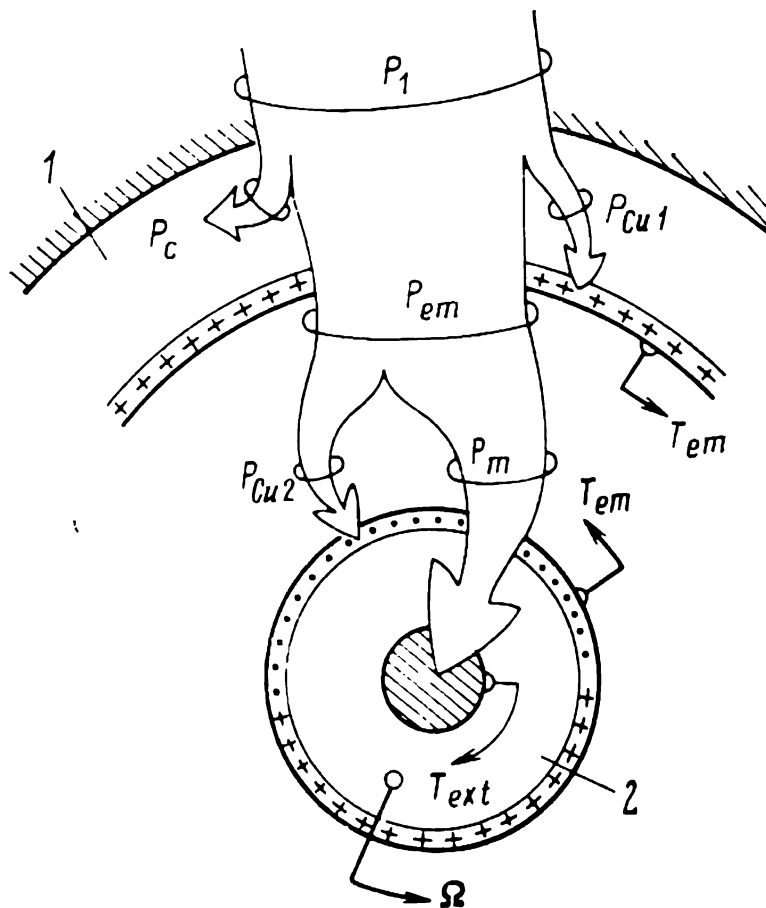


**Fig. 41-6** Energy conversion by an induction machine (motor mode of operation): 1—stator; 2—rotor

motor mode of operation, it lies in the interval  $\pi/2 > \varphi_0 > \varphi_1 > 0$ , and  $P_1$  is positive.

On expressing the active stator voltage  $V_1 \cos \varphi_1$  as the sum of  $R_1 I_1$  and  $E_1 \cos \beta'_1$  and writing

$$P_1 = m_1 I_1 (V_1 \cos \varphi_1) = m_1 I_1 E_1 \cos \beta'_1 + m_1 R_1 I_1^2$$

we can see that the second term represents the copper loss

$$m_1 R_1 I_1^2 = P_{Cu1}$$

that is the power dissipated as heat in the stator winding (Fig. 41-6).

On expressing the active stator current  $I_1 \cos \beta'_1$  as the sum of the active magnetizing current  $I_0 \cos \beta'_0 = I_{0a}$  and the active component of the secondary referred current,  $I'_2 \cos \beta_2$

$$m_1 E_1 (I_1 \cos \beta'_1) = m_1 E_1 I_0 \cos \beta'_0 + m_1 E_1 I'_2 \cos \beta_2$$

we can see that the second term represents the core loss

$$m_1 E_1 I_0 \cos \beta'_0 = P_c$$

that is the power dissipated as heat in the stator core (see Sec. 40-3).

The remaining power,

$$P_{em} = P_1 - P_{Cu1} - P_c = m_1 E_1 I'_2 \cos \beta_2 \quad (41-30)$$

is transferred electromagnetically across the air gap from the stator to the rotor. Quite aptly, it is called *electromagnetic power*,  $P_{em}$  (see Sec. 30-1).

Taking the mutual emf as defined by Eq. (41-2) and noting that the electromagnetic torque acting on the stator may, in accord with Eq. (29-13), be written as

$$T_{em} = (pm_1/\sqrt{2}) \Psi_{1m} I'_2 \cos \beta_2 \quad (41-31)$$

where  $\beta_2$  is the phase angle between  $\dot{E}_1$  and  $\dot{I}'_2$ , we find that the electromagnetic power is proportional to the electromagnetic torque and the angular velocity of the field:

$$P_{em} = m_1 E_1 I'_2 \cos \beta_2 = T_{em} \Omega_1 \quad (41-32)$$

Going back (see Eq. (41-10)) to  $E_2$ , the emf induced in a phase of the rotor at standstill, and expressing the referred rotor current  $I'_2$  in terms of the rotor current  $I_2$ , we may write the electromagnetic power in terms of the rotor quantities as follows:

$$P_{em} = m_2 E_2 I_2 \cos \beta_2 = T_{em} \Omega_1 \quad (41-33)$$

where

$$T_{em} = (pm_2/\sqrt{2}) \Psi_{2m} I_2 \cos \beta_2$$

is the electromagnetic torque acting on the rotor. It is equal to the electromagnetic torque given by Eq. (41-31) and acting on the stator.

The conversion of the electromagnetic power,  $P_{em}$ , coming into the rotor across the air gap was examined in Sec. 30-1. In an induction machine, the total angular velo-

city  $\Omega$  of the surface rotor current  $A_2$  is the sum of the mechanical (rotational) angular speed of the rotor

$$\Omega = \Omega_1 (1 - s)$$

and the angular velocity of the surface current relative to the rotor

$$\Omega_s = s\Omega_1$$

which is a function of the frequency of the rotor current,

$$f_2 = sf_1$$

Accordingly,  $P_{em} = T_{em}\Omega_1$  may be written as the sum of two power components

$$P_{em} = T_{em}\Omega_1 = T_{em}\Omega_s + T_{em}\Omega \quad (41-34)$$

The term  $T_{em}\Omega_s = T_{em}\Omega_1 s$  represents the electrical or rotor copper loss,  $P_{e2} = P_{Cu2}$ . This can be proved by writing the torque in terms of the rotor quantities and noting that  $E_{2s}\cos\beta_2 = R_2 I_2$  (see Fig. 41-5):

$$\begin{aligned} T_{em}\Omega_s &= (pm_2/\sqrt{2}) \Psi_{2m} I_2 \cos\beta_2 \Omega_s \\ &= m_2 (\omega_s \Psi_{2m}/\sqrt{2}) I_2 \cos\beta_2 = m_2 I_2 (E_{2s} \cos\beta_2) \\ &= m_2 R_2 I_2^2 = P_{Cu2} \end{aligned} \quad (41-35)$$

Accordingly, the term  $T_{em}\Omega = T_{em}\Omega_1 (1 - s)$  is the mechanical power developed by the electromagnetic torque  $T_{em}$  as the rotor rotates at the angular velocity  $\Omega$ :

$$T_{em}\Omega = P_m = P'_2$$

Thus,

$$P_{em} = P_{Cu2} + P_m = P_{e2} + P'_2$$

It is an easy matter to show that the relation between  $P_{e2}$  and  $P'_2$  (or  $P_{Cu2}$  and  $P_m$ ) and the electromagnetic power depends on the rotor slip  $s$ :

$$\left. \begin{aligned} P_{e2} &= sP_{em} \\ P_m &= P'_2 = (1 - s) P_{em} \end{aligned} \right\} \quad (41-36)$$

The useful mechanical power transmitted by the shaft to the associated driven machine is less than the mechanical power  $P'_2$  applied to the rotor by an amount equal to the friction and windage losses,  $P_{f/w}$ , and the additional (or stray) losses,  $P_{ad}$ , in the windings and cores, associated

with the higher-harmonic currents and fields,

$$P_2 = P'_2 - P_{f/w} - P_{ad} \quad (41-37)$$

The efficiency of an induction machine operating as a motor is defined as the ratio of the useful mechanical power  $P_2$  to the active power drawn from the supply line,  $P_1$ :

$$\eta = P_2/P_1 = 1 - \Sigma P/P_1 \quad (41-38)$$

where

$$\Sigma P = P_c + P_{Cu1} + P_{Cu2} + P_{f/w} + P_{ad}$$

is the total power loss in the machine.

## 42 Application of Transformer Theory to the Induction Machine

### 42-1 The Rotor at Standstill

The equations derived in Chap. 41 to describe the electric circuits of an induction machine give an adequate insight into the associated processes. Unfortunately, they are inconvenient to use, because the rotor circuit quantities vary at a frequency different from that of the stator circuit quantities. This stands in the way of explaining the performance of induction machines by transformer theory, where the primary and secondary quantities vary at the same frequency.

Fortunately, the stator voltage equation, (41-4), written at  $f_1$  is the same as the primary voltage equation of the transformer. Therefore, we need only to re-arrange the rotor voltage equation in such a way that the rotor quantities vary at the same frequency as the stator quantities, that is,  $f_1$ .

As follows from the foregoing (see Chap. 41), this can be done by replacing the rotor rotating at  $\Omega$  by a rotor at standstill, because then  $s = 1$ , and  $f_2 = sf_1 = f_1$ . In doing so, the circuit parameters of the rotor at standstill must be chosen such that the replacement could not affect energy conversion in the machine. It is an easy matter to show that with the rotor at standstill the rotating mutual

field, the electromagnetic torque and all the stator quantities will remain unchanged, if the rotor current  $I_2$  and the rotor mmf  $E_{2m}$  remain the same as before in both magnitude and phase.

A model of an induction motor, with the rotor rotating at  $\omega = \omega_1 (1 - s) < \omega_1$  is shown on the left of Fig. 42-1. In the figure the resultant rotating field is represented by  $\dot{B}_m$  rotating at  $\omega_1 = 2\pi f_1$  relative to the stator and at  $\omega_s = s\omega_1$  relative to the rotor. The emf  $\dot{E}_{2s}$  induced in the

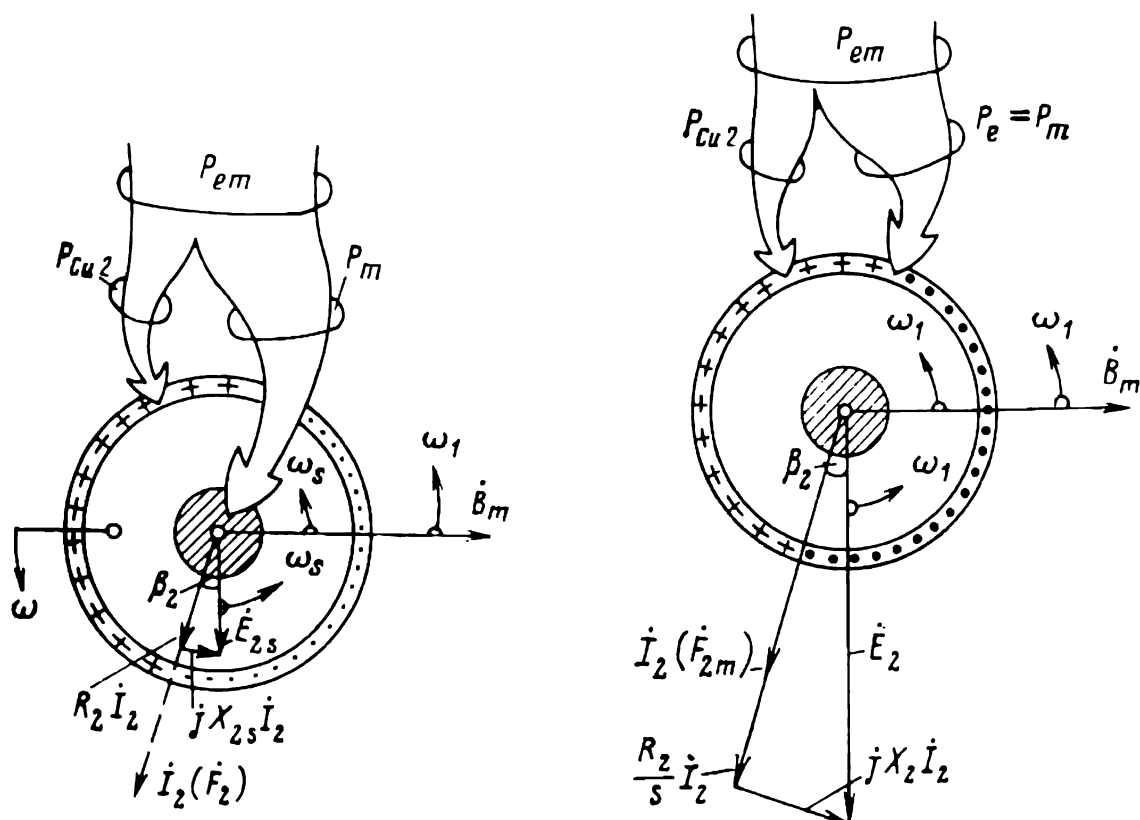


Fig. 42-1 An equivalent rotor at standstill as a model of a rotating rotor

rotor and defined by Eq. (41-9) lags behind the flux density vector by  $\pi/2$ . The rotor current  $I_2$  given by Eq. (41-14) lags behind  $\dot{E}_{2s}$  by an angle  $\beta_2$  as given by Eq. (41-15).

Let us see how we should adjust the rotor phase impedance at standstill so that its current remains unchanged. Because the mutual field remains as it was before, and its velocity relative to the rotor (on the right of Fig. 42-1) is increased  $\omega_1/\omega_s = 1/s$  times, the rotor mutual emf ( $E_2$  on the right of Fig. 42-1 instead of  $E_{2s} = sE_2$  on the left of the same figure) and its frequency will be multiplied by the same factor.

Obviously, for the rotor current to retain its magnitude and its phase relative to the emf, the resistive and reactive

components of the impedance must be multiplied by  $1/s$ , that is, in proportion to the change in  $E_{2s}$ . The resistance  $R_2$  must be replaced by  $R_2/s$ , and the leakage inductive reactance of the rotating rotor,  $X_{2s} = 2\pi f_2 L_{\sigma 2}$ , must be replaced by  $X_2 = X_{2s}/s = 2\pi f_1 L_{\sigma 2}$  which is the phase leakage inductive impedance of the rotor at standstill at  $f_1$  [see Eq. (41-11)]. Then, the rotor phase currents at standstill, defined as

$$I_2 = \frac{E_2}{\sqrt{(R_2/s)^2 + jX_2^2}} \quad (42-1)$$

will be the same as it is when the rotor is rotating.

The standstill rotor current will lag behind  $E_2$  by the same angle

$$\beta_2 = \arctan \frac{X_2}{R_2/s} \quad (42-2)$$

as when the rotor is rotating [see Eq. (41-15)]. The voltage triangle on the standstill rotor diagram (on the right of Fig. 42-1), answering the voltage equation of the equivalent standstill rotor,

$$\dot{E}_2 = (R_2/s) \dot{I}_2 + jX_2 \dot{I}_2 \quad (42-3)$$

is multiplied by  $1/s$  as compared with the voltage triangle on the diagram of the rotating rotor (on the left of Fig. 42-1).

The voltage equation of the rotating rotor, Eq. (41-13), can also be transformed into the voltage equation of an equivalent standstill rotor by multiplying it by  $1/s$ . However, in order to be able to reproduce in the rotor at standstill the processes that occur when the rotor is rotating, an additional resistance must be included in the rotor phase

$$R_m = R_2/s - R_2 = R_2 \frac{1-s}{s}$$

which, when combined with the intrinsic rotor resistance  $R_2$ , gives the required resistance  $R_2/s$ . The inductive impedance,  $X_2 = 2\pi f_1 L_{\sigma 2}$ , is reproduced automatically as the frequency in the rotor at standstill is increased  $1/s$  times, because the rotor leakage inductance,  $L_{\sigma 2}$ , remains unchanged.

As follows from Fig. 42-1, so long as  $\dot{I}_2$  retains its magnitude and phase,  $\dot{F}_{2m}$  remains unchanged as well—with



the rotor at standstill, it will have the same peak value, the same phase relative to  $\dot{B}_m$ , and the same angular velocity relative to the stator,  $\omega_1$ , as when the rotor is rotating. As a consequence, there will be no change in the mutual flux field  $B_m$  established by the stator and rotor mmfs, the stator and rotor flux linkages  $\Psi_{1m}$  and  $\Psi_{2m}$ , the electromagnetic torque  $T_{em}$ , and the electromagnetic power  $P_{em}$ . However, there will be a change in the manner of energy conversion within the rotor itself. In a running machine (on the left of Fig. 42-1), the input electromagnetic power is converted to a mechanical power

$$P_m = T_{em}\Omega_1 (1 - s) = P_{Cu2} (1 - s)/s$$

and to an electrical power or the rotor copper loss

$$P_{e2} = P_{Cu2} = T_{em}\Omega_1 s = m_2 R_2 I_2^2$$

In a machine with its rotor at standstill (on the right of Fig. 42-1), no electromechanical energy conversion takes place, and all of the input electromagnetic power,  $P_{em}$ , is converted to electric power dissipated as heat in  $R_2/s$ . In the resistance added to the phases of the standstill rotor,  $R_m = R_2 (1 - s)/s$ , the heat dissipated is the power

$$m_2 R_2 \frac{1-s}{s} I_2^2 = P_{e2} (1 - s)/s$$

equal to the mechanical power

$$P_m = P_{e2} (1 - s)/s$$

developed by the rotor. The remainder

$$P_{em} - P_m = P_{e2} = P_{Cu2} = m_2 R_2 I_2^2$$

is dissipated as heat in the rotor winding.

In conclusion, it should be noted that energy conversion in an induction machine with its rotor at standstill and with  $R_m$  added to its phases does not differ from energy conversion in a transformer loaded into  $R_m$ .

An induction machine with its rotor at standstill in which all the circuit quantities vary at frequency  $f_1$  is in effect a rotating-field transformer.

The rotor voltage equation for such a machine does not differ from that for the transformer secondary

$$\dot{E}_2 = R_2 \dot{I}_2 + jX_2 \dot{I}_2 + \dot{V}_2 \quad (42-4)$$

where  $\dot{V}_2 = R_m \dot{I}_2$  is the voltage developed across the equivalent load.

## 42-2 Transferring the Rotor Quantities to the Stator Winding

To obtain a complete mathematical description for what happens in a rotating-field transformer, one more change is needed: the rotor winding with  $m_2$  phases and  $w_2$  turns per phase must be replaced by a referred (or transferred) winding which has the same number  $m_1$  of phases and the same number  $w_1$  of turns per phase as the stator. This referring (or transferring) procedure leads to  $I'_2$ ,  $E'_2$ ,  $R'_2$ , and  $X'_2$  which are called the *referred* (or *transferred*) *quantities*. They must be chosen such that the transferring procedure does not affect the magnetic field in the machine or the associated energy conversion processes. A referred (or transferred) quantity will be designated by the same symbol with a prime.

The referred rotor current

$$\dot{I}'_2 = k_I \dot{I}_2 \quad (42-5)$$

and the referring coefficient for the rotor current

$$k_I = \frac{m_2 w_2 k_{w2}}{m_1 w_1 k_{w1}} \quad (42-6)$$

have already been derived in Chap. 41 [see Eq. (41-26)], subject to the requirement that the mmf in the rotor with a referred winding should remain the same as it was before, that is,

$$\dot{F}'_{2m} = \dot{F}_{2m}$$

The referring coefficient for rotor voltage is defined as the ratio of the emfs (or flux linkages) in the referred and unreferred rotor windings, with the mutual flux  $\Phi_m$  remaining unchanged,

$$E'_2/E_2 = \Psi'_{2m}/\Psi_{2m} = \frac{w_1 k_{w1} \Phi_m}{w_2 k_{w2} \Phi_m} = \frac{w_1 k_{w1}}{w_2 k_{w2}} = k_V$$

Both  $E'_2$  and  $\Psi'_{2m}$  are the same as the respective stator quantities:

$$\dot{E}'_2 = \dot{E}_1, \quad \dot{\Psi}'_{2m} = \dot{\Psi}_{1m} \quad (42-7)$$

The rotor phase resistance is transferred in such a way that the copper loss (electrical power) remains unaffected:

$$mR'_2 (I'_2)^2 = m_2 R_2 I_2^2 = P_{e2} = P_{Cu2}$$

Hence, the referring coefficient for resistances may be written

$$R'_2/R_2 = (m_2/m_1) (I_2/I'_2)^2 = \frac{m_1 (w_1 k_{w1})^2}{m_2 (w_2 k_{w2})^2} = k_V/k_I = k_Z \quad (42-8)$$

The same relation must apply to the phase leakage inductive reactance of the referred and unreferred rotors

$$X'_2/X_2 = k_Z$$

because it is only then that the rotor current will retain its phase given by the angle

$$\beta_2 = \arctan (X_2 s/R_2) = \arctan (X'_2 s/R'_2)$$

and there will be no change in the electromagnetic torque  $T_{em}$  acting on the rotor carrying the referred winding

$$T_{em} = (pm_1/\sqrt{2}) \Psi'_{2m} I'_2 \cos \beta_2 = (pm_2/\sqrt{2}) \Psi_{2m} I_2 \cos \beta_2 \quad (42-9)$$

The voltage equation for the referred rotor winding may alternatively be derived by multiplying Eq. (42-4) by  $k_V$ :

$$k_V \dot{E}_2 = (R_2 + jX_2) (k_V/k_I) (k_I \dot{I}_2) + R_m (k_V/k_I) (k_I \dot{I}_2) \quad (42-10)$$

and, finally,

$$\dot{E}'_2 = \dot{E}_1 = Z'_2 \dot{I}'_2 + R'_m \dot{I}'_2$$

where

$$\dot{E}'_2 = \dot{E}_1 = -j (w_1 k_{w1} \dot{\Phi}_m) \omega_1 / \sqrt{2}$$

$$R'_m = R'_2 (1 - s)/s = \text{referred additional resistance in a rotor phase at standstill}$$

$$Z'_2 = R'_2 + jX'_2 = \text{referred impedance of the rotor at standstill}$$

### 42-3 Basic Equations and the Space-Time Vector Diagram of an Induction Machine

Taken together, Eqs. (41-4), (41-27), (41-28) and (42-10) derived in Chapters 41 and 42 for an induction machine treated as a transformer, give an exhaustive description

of the associated electromagnetic processes. Arranged in a logic sequence, this set of equations is as follows.

1. The stator voltage equation

$$\dot{V}_1 = -\dot{E}_1 + Z_1 \dot{I}_1 \quad (42-11a)$$

2. The standstill rotor voltage equation

$$\dot{E}'_2 = \dot{E}_1 = Z'_2 \dot{I}'_2 + R'_m \dot{I}'_2 \quad (42-11b)$$

3. The emf equation

$$\dot{E}'_2 = \dot{E}_1 = -Z_0 \dot{I}_0 \quad (42-11c)$$

4. The current equation

$$\dot{I}_1 + \dot{I}'_2 = \dot{I}_0 \quad (42-11d)$$

In appearance, the above equations do not differ from the set of equations describing a referred transformer loaded into  $R'_m$ :

Graphically, Eqs. (42-11a) through (42-11d) are shown in the phasor diagram plotted in Fig. 42-2 for an induction machine interpreted as a transformer. In appearance, it does not differ from the phasor diagram of a transformer, but it has a different physical meaning. For an induction machine, this diagram is plotted on the complex plane of its two-pole model, with the rotor at a standstill in an arbitrary position relative to the stator. To go over from the complex quantities rotating at  $\omega_1 = 2\pi f_1$  to the phase quantities, the complex stator quantities must be projected onto the stator phase axes ( $A_1$ ,  $B_1$ , and  $C_1$ ), and the complex rotor quantities must be projected on the stationary and arbitrarily oriented rotor phase axes ( $A_2$ ,  $B_2$ , and  $C_2$ ).

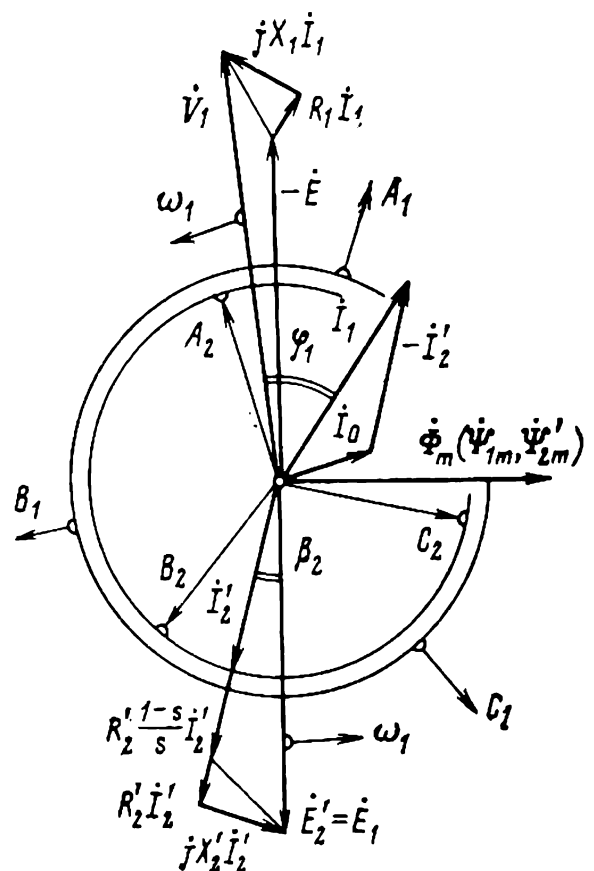


Fig. 42-2 Phasor diagram of an induction machine modelled as a transformer (motor mode of operation,  $1 > s > 0$ )

In some cases, the diagram may be used to solve the set of equations graphically. For example, suppose that the operating conditions are specified by giving the mutual emf  $\dot{E}_1 = \dot{E}'_2$  and the slip  $s = (\Omega_1 - \Omega)/\Omega_1$ . Then, to find the currents, voltages and phase angles, the procedure should be as follows.

- (1) Using Eq. (42-11b), find  $I'_2$  and  $\beta_2$ .
- (2) Plot  $\dot{I}'_2$  and the rotor voltage diagram  $(\dot{E}'_2, R'_2\dot{I}'_2, R'_m\dot{I}'_2, jX'_2\dot{I}'_2)$ .
- (3) Using Eq. (42-11c), calculate and plot  $\dot{I}_0$ .
- (4) Using Eq. (42-11d), construct the current triangle and determine  $\dot{I}_1$ .
- (5) Using Eq. (42-11a), construct the stator voltage diagram and find  $\dot{V}_1$ .

In other cases, such as when the operating conditions are specified by giving the stator voltage  $V_1$  and the slip  $s$ , the diagram cannot be used to solve the set of equations graphically and to find the currents  $I_1$  and  $I'_2$ , and the phase angles. Instead, Eqs. (42-11) must be solved analytically, and the diagram may only serve to facilitate an interpretation of the solution obtained and to determine the stator and rotor phase quantities graphically.

Once the diagram is constructed, it is an easy matter, using Eq. (42-9), to calculate the electromagnetic torque

$$T_{em} = (pm_1/\sqrt{2}) \Psi'_{2m} I'_2 \cos \beta_2$$

and also the active and reactive powers of the machine.

#### 42-4 Equivalent Circuits of an Induction Machine

By analogy, the mathematical description of an induction machine treated as a transformer may be based on the equivalent circuit for the transformer (see Sec. 3-5). For an induction machine with its rotor at standstill, the equivalent circuit will be shown in Fig. 42-3a. The additional resistance

$$R'_m = R'_2 (1 - s)/s$$

may be regarded as the load resistance of a transformer whose secondary is referred to the primary side. The voltage

across that resistance is the referred secondary voltage of the equivalent transformer

$$\dot{V}'_2 = R'_m \dot{I}'_2$$

The power dissipated in that resistance is numerically equal to the mechanical power developed by the induction machine

$$P_m = m R'_m (I'_2)^2$$

The equivalent circuit fully answers Eqs. (42-11), and is called the equivalent T-circuit of an induction machine. Using it, we can develop (see Chap. 43) the exact design

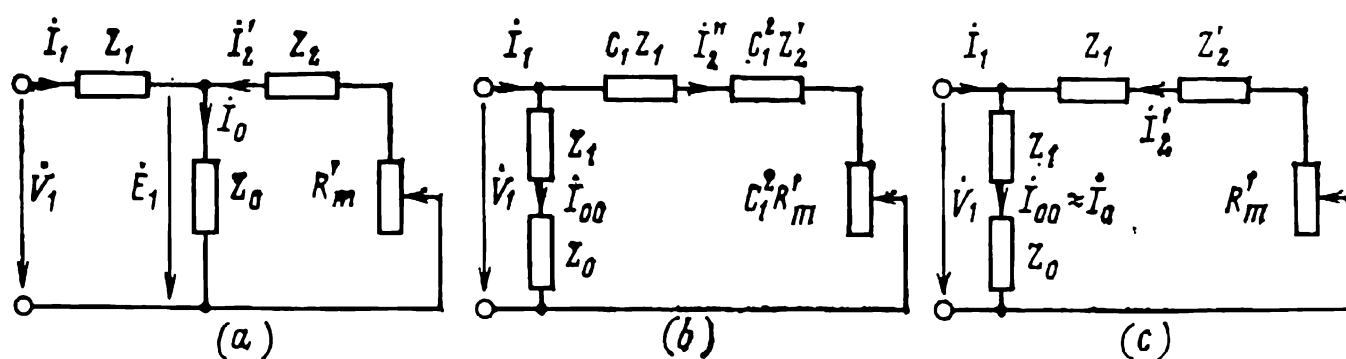


Fig. 42-3 Equivalent circuits of an induction machine

equations for all the quantities characterizing the electromagnetic processes in the machine (for example,  $I_1$ ,  $I'_2$ ,  $I_0$ ,  $E_1 = E'_2$ ,  $P_{em}$ ,  $P_m$ , etc.). In some cases, however, such as when it is required to construct the circle diagram (see Chap. 44), the equivalent T-circuit should preferably be transformed into an equivalent L-circuit, such as shown in Fig. 42-3b. It differs from the T-circuit in that the magnetizing arm is brought out to the terminals and connected to receive  $\dot{V}_1$ . The impedance of the magnetizing arm in the L-circuit is taken equal to  $Z_0 + Z_1$ , and it is assumed to carry a fictitious magnetizing current

$$\dot{I}_{00} = \dot{V}_1 / (Z_1 + Z_0)$$

which is the same as the actual magnetizing current  $\dot{I}_0$  in the T-circuit under ideal no-load conditions, when  $s = 0$  and  $R'_m = \infty$ .

The current  $I'_2$  in the right-hand arm of the L-circuit (the rotor arm) may be found subject to the requirement that

the primary current  $\dot{I}_1$  should remain unchanged in the L-circuit. Obviously,

$$\dot{I}_2'' = \dot{I}_1 - \dot{I}_{00}$$

and, because  $\dot{I}_{00} \neq \dot{I}_0$ , we have

$$\dot{I}_2'' \neq -\dot{I}_2' = \dot{I}_1 - \dot{I}_0$$

Using Eq. (42-11) and the equivalent T-circuit, let us first find the currents in the primary and secondary windings

$$\begin{aligned} \dot{I}_1 &= \dot{V}_1 \frac{Z_0 + Z_{2eq}'}{Z_1 Z_0 + Z_0 Z_{2eq}' + Z_1 Z_{2eq}'} = \dot{V}_1 \frac{1 + Y_0 Z_{2eq}'}{Z_1 + C_1 Z_{2eq}'} \\ -\dot{I}_2' &= \dot{V}_1 \frac{Z_0}{Z_1 Z_0 + Z_0 Z_{2eq}' + Z_1 Z_{2eq}'} = \dot{V}_1 \frac{1}{Z_1 + C_1 Z_{2eq}'} \end{aligned} \quad (42-12)$$

where

$$Z_{2eq}' = R_2'/s + jX_2'$$

and

$$Y_0 = 1/Z_0$$

The complex coefficient,  $C_1 = (Z_1 + Z_0)/Z_0$ , used here and elsewhere, is the sum of a real and an imaginary part

$$C_1 = (Z_0 + Z_1)/Z_0 = c' + c''j \quad (42-13)$$

where

$$c' = [(R_0 + R_1) R_0 + (X_0 + X_1) X_0] / (R_0^2 + X_0^2)$$

$$c'' = [(X_0 + X_1) R_0 - (R_0 + R_1) X_0] / (R_0^2 + X_0^2)$$

Now we can determine  $\dot{I}_2''$ , the current in the right-hand arm of the equivalent L-circuit:

$$\begin{aligned} \dot{I}_2'' &= \dot{I}_1 - \dot{I}_{00} = \dot{V}_1 \frac{1 + Y Z_{2eq}'}{Z_1 + C_1 Z_{2eq}'} - \frac{\dot{V}_1}{Z_1 + Z_0} \\ &= \frac{\dot{V}_1}{C_1 (Z_1 + C_1 Z_{2eq}')} = -\dot{I}_2' / C_1 \end{aligned} \quad (42-14)$$

It is connected to  $\dot{I}_2'$  by a simple relation—it is  $1/C_1$  times the value of  $-\dot{I}_2'$ .

From the expression for  $\dot{I}_2''$  it is seen that the impedance of the rotor arm in the equivalent L-circuit is

$$C_1 (Z_1 + C_1 Z_{2eq}') = C_1 Z_1 + C_1^2 Z_2' + C_1^2 R_m'$$

In practical engineering calculations, the equivalent T-circuit can sometimes be replaced by the simplified L-circuit shown in Fig. 42-3c. The simplification is based on the relations between the parameters of the equivalent T-circuit. To begin with, let us express the parameters of the equivalent T-circuit on a per-unit basis, taking the stator impedance as the base (or reference) quantity

$$Z_{1,b} = V_{1,R}/I_{1,R}$$

For the most commonly used commercial induction motors rated from 3 to 100 kW, the per-unit parameters are

$$X_{*0} = X_0/Z_{1,b} = 2.5 \text{ to } 3.5$$

$$X_{*1} = X'_{*2} = 0.07 \text{ to } 0.15$$

$$R_{*1} = R'_{*2} = 0.02 \text{ to } 0.06$$

$$R_{*0} = 0.1 \text{ to } 0.4$$

The lower values apply to motors of higher ratings.

The parameters of induction machines are such that the replacement of the equivalent T-circuit by a simplified L-circuit in which the magnetizing current ( $I_0$ ) arm is brought out to the stator winding terminals does not lead to an appreciable error. To minimize it still more, the magnetizing current arm of the L-circuit is extended to include  $Z_1$  in addition to  $Z_0$ .

The simplified L-circuit is fairly accurate only under the ideal no-load conditions, when  $s = 0$ ,  $R'_m = R'_2(1-s)/s = \infty$  and  $I'_2 = 0$ . In these conditions, the stator current

$$\dot{I}_1 = \dot{I}_0 = \dot{V}_1/(Z_1 + Z_0)$$

does not differ from the current found from the equivalent T-circuit. At  $V_{*1} = V_{*1,R} = 1$ , the per-unit no-load current is

$$I_{*0} = \frac{V_{*1}}{Z_{*1} + Z_{*0}} \approx 0.3 \text{ to } 0.4$$

Under rated conditions, when  $I_{*1} = I_{*1,R} = 1$  and  $V_{*1} = V_{*1,R} = 1$ , the voltage drop across the impedance

$$Z_1 = \sqrt{R_1^2 + X_1^2}$$

of the T-circuit is on the average 0.1, whereas at no-load it is about 0.035. Taking the approximate phase angles of



currents, we find that under rated conditions,  $E_{*1} \approx 0.915$ , whereas at no-load it is about 0.965.

Using the equivalent T-circuit, we find that in going from no-load to full load the magnetizing current decreases by about

$$[(0.965 - 0.915)/0.965] \times 100 = 5\%$$

In calculations on the basis of the L-circuit, changes in load (the slip,  $R'_m$ , and  $I'_2$ ) do not affect the magnetizing current. As a consequence, under rated conditions (at full load) it is exaggerated by about 5%. As found from the L-circuit,  $I'_2$  is exaggerated by about 0.5% because of the underrated voltage drop across  $Z_1$  which carries  $I'_2$  instead of  $I_1$ . The error in the primary current

$$\dot{I}_1 = \dot{I}_0 - \dot{I}'_2$$

arising from inaccuracies in the calculation of  $I_0$  and  $I'_2$  from the simplified L-circuit does not exceed +1% or +2%.

In the third typical condition, a short-circuit, when the rotor is at standstill ( $\Omega = 0$ ), the slip is unity, and  $R'_m = R'_2(1 - s)/s = 0$ , and the winding of the equivalent standstill rotor is short-circuited, the value of  $I_0$  as found from the T-circuit is about half the no-load current (because  $X_1 \approx X'_2$  and  $R_1 \approx R'_2$ ). In calculations from the L-circuit, the magnetizing current at a short-circuit remains about the same as it is at no-load. In other words, it is exaggerated by the current which is half the no-load current and equal (on a per-unit basis) to 0.175.

However, the referred rotor current at a short-circuit and at  $V_{*1} = V_{*1,R} = 1$  is several times the rated stator current

$$I'_{*2} = V_1 / |Z_1 + Z_2| \approx 1/0.2 = 5$$

and the error in the stator current

$$\dot{I}_1 = \dot{I}_0 - \dot{I}'_2$$

does not exceed

$$0.175 \div 5 \times 100 = +3.5\%$$

The errors in the currents, power losses, active and reactive powers found from the simplified L-circuit for all the other operating conditions of an induction machine will likewise be insignificant.

## 43 Analytical and Graphical Determination of Electromechanical Characteristics of Induction Machines

### 43-1 Modes of Operation

An induction machine can operate in any one of three modes, namely:

- as a motor, when  $0 < s < 1$  and  $\Omega_1 > \Omega > 0$ ;
- as a generator, when  $s < 0$  and  $\Omega > \Omega_1$ ;
- as a brake, when  $s > 1$  and  $\Omega < 0$ .

In all of these modes, the machine converts mechanical energy to electrical or back. There are two more conditions in which no energy conversion takes place. These are an open-circuit (ideal no-load) and a short-circuit. In the former,  $s = 0$  and  $\Omega = \Omega_1$ . In the latter,  $s = 1$  and  $\Omega = 0$ .

In  $\nabla$ motoring (region  $M$  in the plot of Fig. 43-2), the electromagnetic torque  $T_{em} > 0$ , which is in the direction of the field, causes the rotor to rotate with the field at a velocity less than the field velocity ( $\Omega_1 > \Omega > 0$  and  $0 < s < 1$ ). In the circumstances,

$$P_{em} = T_{em}\Omega_1 = P_{Cu2}/s > 0$$

$$P_m = T_{em}\Omega = P_{Cu2} (1 - s)/s > 0$$

The input electric power

$$P_1 = P_{em} + P_c + P_{Cu1} > 0$$

is converted to mechanical power

$$P_2 = P_m - P_{ad} - P_{f/w} > 0$$

which is transmitted by the shaft to the associated driven machine.

The events occurring in the motor mode of operation are illustrated in Fig. 43-1a. Here, the active rotor current  $i_{2a}$  acts in the same direction as the emf induced in the rotor. The direction of the electromagnetic torque,  $T_{em}$ , is decided by  $B_m i_{2a}$  acting on  $i_{2a}$  (see Fig. I-3, vol. 1).

The useful (output) power,  $P_2$ , is less than the power drawn from the supply line (input power) by an amount

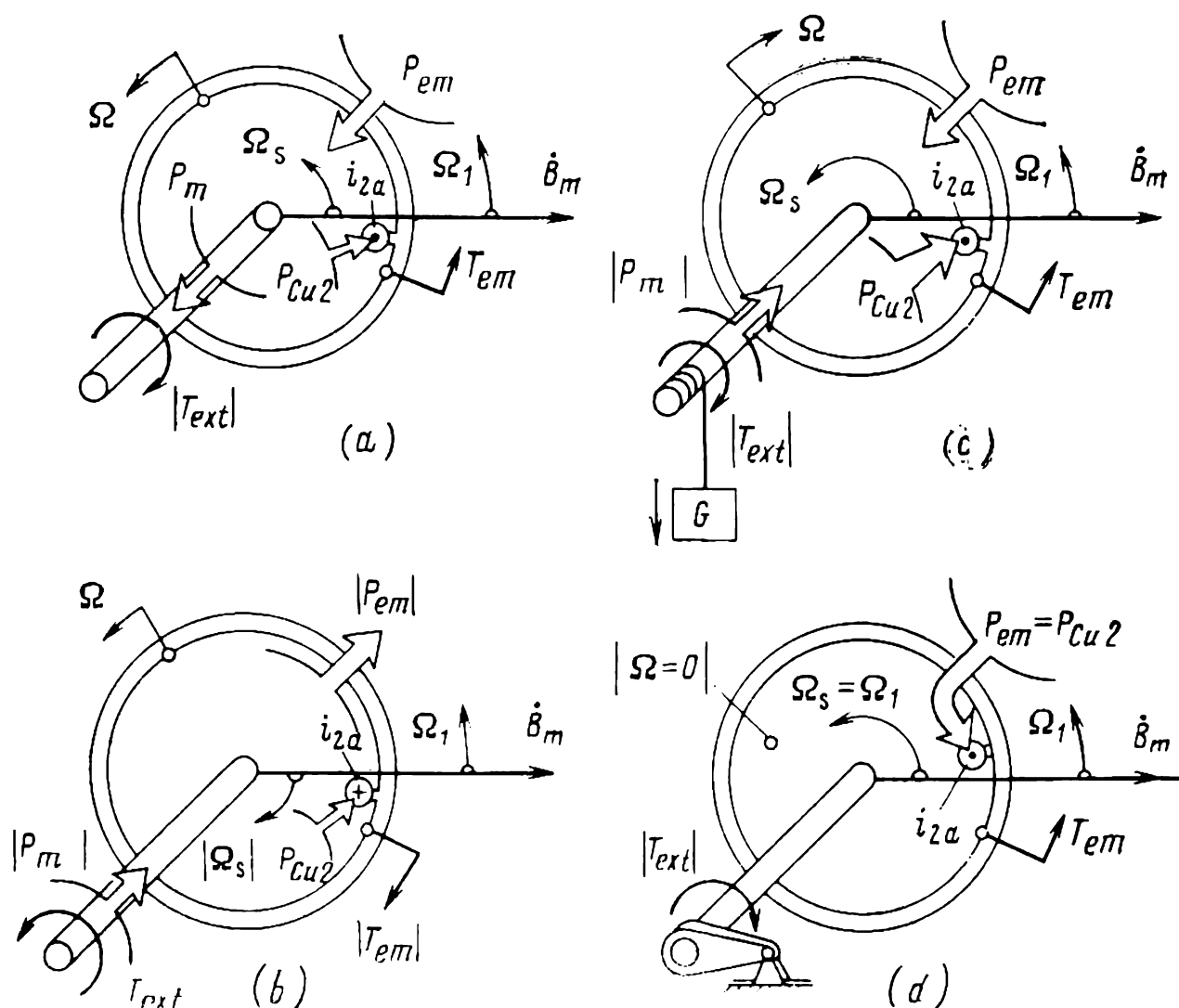


**Fig. 43-1** Operating modes of an induction machine:

(a) motoring; (b) generating; (c) braking; (d) transformer (or short-circuit)

equal to the total power loss,  $\Sigma P$ :

$$P_2 = P_1 - \Sigma P = P_1 - (P_{Cu1} + P_c + P_{Cu2} + P_{ad} + P_{f/w})$$

So the efficiency of the motor is given by

$$\eta = P_2/P_1 = 1 - \Sigma P/P_1 = f(s) \quad (43-1)$$

In the generator mode of operation (region  $G$  in Fig. 43-2) the external torque,  $T_{ext} > 0$ , acting in the direction of the field (see Fig. 43-1b) causes the rotor to rotate at a speed exceeding the field velocity ( $\Omega > \Omega_s$ ,  $s < 0$ ). In this mode, the field is travelling relative to the rotor in the opposite direction, and the active rotor current  $i_{2a}$  is also reversed (in comparison with the motor action). Therefore, the electro-

magnetic torque

$$T_{em} = B_m i_{2a}$$

balancing the external torque acts against the field and is assumed to be negative ( $T_{em} < 0$ ). The electromagnetic

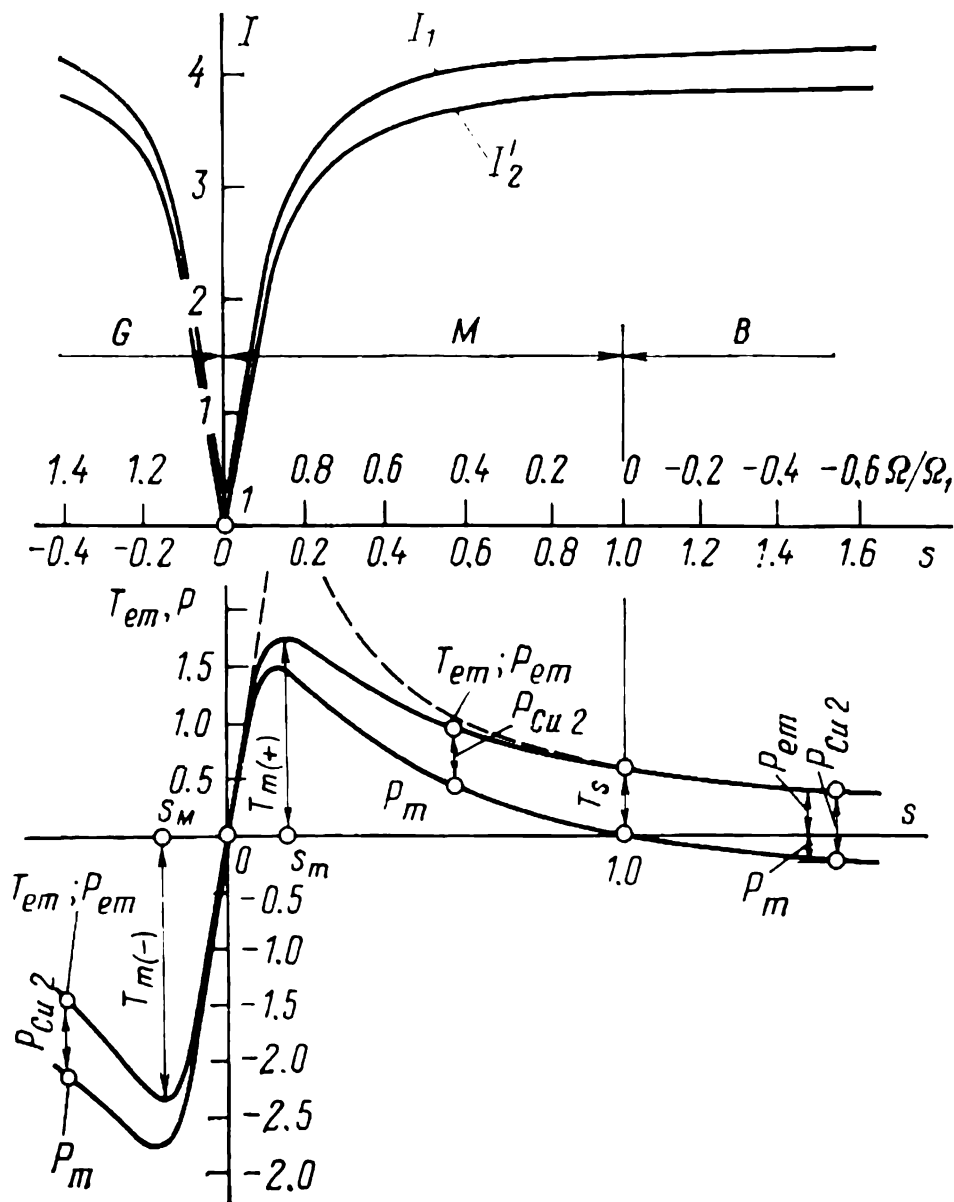


Fig. 43-2 Performance characteristics of an induction machine (on a per-unit basis), with  $V_1 = 1$ ,  $I_0 = 0.364$ ,  $\cos \varphi_0 = 0.185$ ,  $X_1 = X'_2 = 0.125$ ,  $R_1 = 0.0375$ ,  $R'_2 = 0.0425$

power,  $P_{em}$ , and the mechanical power,  $P_m$ , are likewise taken to be negative:

$$P_{em} = T_{em} \Omega = P_{Cu2}/s < 0$$
$$P_m = T_{em} \Omega = P_{Cu2} (1 - s)/s < 0$$

The direction of energy conversion is likewise reversed: the mechanical power  $P_2$  applied to the shaft (input power) is converted to electric power  $P_1$  supplied to the external

line (output power). Because the power loss is always positive (in any mode of operation, it is always dissipated as heat), the mechanical power

$$P_m = P_{em} - P_{Cu2} < 0 \text{ at } s < 0$$

is greater in absolute value than the electromagnetic power (Fig. 43-2):

$$|P_m| = |P_{em}| + P_{Cu2}$$

By the same token, the input mechanical power

$$P_2 = P_1 - \sum P < 0$$

is greater in absolute value than the electric power delivered to the using line

$$|P_2| = |P_1| + \sum P$$

and the efficiency of the generator is

$$\eta = |P_1|/|P_2| = 1 - \sum P/|P_2| \quad (43-2)$$

In the braking mode of operation (region *B* in Fig. 43-2), the external torque,  $T_{ext} < 0$ , acting against the field (see Fig. 43-1c), causes the rotor to run in the direction opposite to the field ( $\Omega < 0$ ,  $s = \frac{\Omega_1 - \Omega}{\Omega_1} > 1$ ). In this mode, the electromagnetic torque,  $T_{em}$ , balancing the external torque, acts in the direction of the field, as it does in the motor mode of operation (the field is rotating relative to the rotor in the same direction), and it is taken to be positive,  $T_{em} > 0$ . However, because  $\Omega < 0$ , the mechanical power is negative:

$$P_m = T_{em}\Omega = P_{Cu2} (1 - s)/s < 0$$

This implies that it is consumed by the machine. The electromagnetic power in this mode is positive:

$$P_{em} = T_{em}\Omega_1 = P_{Cu2}/s > 0$$

Therefore, the machine draws it from the supply line.

The powers applied to the rotor from the supply line,  $|P_{em}|$ , and via the shaft,  $|P_m|$ , are dissipated as heat,  $P_{Cu2}$ , in the rotor resistance,  $R'_2$  (see Fig. 43-2):

$$\begin{aligned} |P_m| + |P_{em}| &= P_{Cu2} (s - 1)/s + P_{Cu2}/s = P_{Cu2} \\ &= m_1 R'_2 (I'_2)^2 \end{aligned}$$

In operation as a brake, an induction machine can be used to slow down the lowering of a load by a lifting crane. Then

$$|P_m| = |T_{em}\Omega|$$

is delivered to the rotor of the machine (see Fig. 43-1).

In the ideal no-load condition, the external torque  $T_{ext}$ , the friction and windage torque  $T_{f/w} = P_{f/w}/\Omega$ , and the torque associated with additional (stray) losses,  $T_{ad} = P_{ad}/\Omega$ , are zero. The rotor is spinning at the field velocity ( $\Omega = \Omega_1$ ,  $s = 0$ ), and does not develop any useful mechanical power ( $T_{em} = 0$ ,  $P_m = T_{em}\Omega = 0$ ). This condition has been examined in detail in Chap. 40.

At no-load (the open-circuit condition),

$$R'_m = R'_2 (1 - s)/s = \infty \text{ and } I'_2 = 0$$

Therefore, the equivalent circuit shown in Fig. 42-3 contains only one arm,  $Z_1 + Z_0$ . (Now the T- and the L-circuits are the same.)

At a short-circuit, the external torque  $T_{ext}$  balancing the electromagnetic torque  $T_{em}$  holds the rotor at a standstill ( $\Omega = 0$ ,  $s = 1$ ), and no useful mechanical work is done ( $P_m = T_{em}\Omega = 0$ ). Both  $i_{2a}$  and  $T_{em}$  are in the same direction as they are in the motor mode of operation, and  $T_{em} > 0$  (see Fig. 43-1d). The electromagnetic power is positive:

$$P_{em} = T_{em}\Omega_1 > 0$$

—it is transferred from the stator to the rotor where it is dissipated as heat

$$P_{em} = P_{Cu2}$$

In this mode, an induction machine is operating as a transformer short-circuited on the secondary side, the only difference being that instead of a pulsating mutual field there exists a rotating mutual field.

At a short-circuit,

$$R'_m = R'_2 (1 - s)/s = 0$$

and the equivalent circuit in Fig. 42-3 has an impedance given by the parallel combinations of  $Z_1 + Z_0$  and  $Z_1 + Z'_2$ . Noting that

$$|Z_1 + Z'_2| \ll |Z_1 + Z_0|$$

(see Chap. 42), we may discard the arm  $Z_1 + Z_0$  and take the impedance of the equivalent circuit in the case of a short-circuit equal to

$$Z_{sc} = Z_1 + Z'_2 = R_{sc} + jX_{sc} \quad (43-3)$$

where

$$R_{sc} = R_1 + R'_2$$

$$X_{sc} = X_1 + X'_2$$

If we connect to the rotor of an induction machine at standstill a balanced set of additional impedances

$$R_{2,ad} + jX_{2,ad}$$

it will operate as a transformer converting the electric energy drawn from the primary supply line into an electric energy having other parameters and expended by  $(R_{2,ad} + jX_{2,ad})$ . This is the reason why at  $s = 1$  the mode of operation is termed the transformer action.

The mode of operation or the slip in a given mode of an induction machine (at  $V_1 = \text{const.}$ , and  $f_1 = \text{const.}$ ) can be changed only by varying the external torque,  $T_{ext}$ , applied to the machine shaft. At  $T_{ext} = 0^*$ , the rotor is travelling at the field velocity ( $\Omega = \Omega_1$ , and  $s = 0$ ), and the machine performs no useful energy conversion. If the external torque  $T_{ext}$  applied to the shaft is in opposition to the field rotation, the rotor will slow down until there appears an electromagnetic torque,  $T_{em} = f(s)$ , which balances the external torque. When this happens, the machine changes to operating as a motor

$$s = (\Omega_1 - \Omega)/\Omega_1 > 0$$

Conversely, when the external torque is in the direction of the field, the rotor speed exceeds the field velocity, and the machine changes to operating as a generator

$$s = (\Omega_1 - \Omega)/\Omega_1 < 0$$

Finally, the braking action can be obtained by causing the machine to cease operating as a motor. This is done by varying the external torque in such a way that the rotor first comes to a standstill, then begins rotating in the direction opposite to that of the field rotation.

---

\* We neglect the friction torque and the torque associated with additional losses.

### 43-2 Currents in the Stator and Rotor Windings

The events taking place in an induction machine are functions of the stator voltage  $V_1$ , the supply frequency  $f_1$ , and the rotor slip  $s$ .

Given a constant stator voltage and a constant supply frequency, the dependence of the quantities associated with the operation of an induction machine on the slip is graphically represented by performance characteristic curves. The equations describing the quantities involved can be derived by means of the equivalent T- or L-circuit (see Fig. 42-3).

The stator and rotor currents are found by reference to the equivalent L-circuit in Fig. 42-3b.

The magnetizing current is given by

$$I_{00} = \frac{V_1}{\sqrt{(R_1 + R_0)^2 + (X_1 + X_0)^2}} \quad (43-4)$$

The active component of the no-load current is given by

$$I_{00a} = I_{00} \cos \varphi_{00} = \frac{V_1 (R_1 + R_0)}{(R_1 + R_0)^2 + (X_1 + X_0)^2}$$

where  $\varphi_{00}$  is the phase angle between  $\dot{V}_1$  and  $\dot{I}_{00}$ , and

$$\cos \varphi_{00} = \frac{R_1 + R_0}{\sqrt{(R_1 + R_0)^2 + (X_1 + X_0)^2}}$$

The reactive component of the no-load current is

$$\dot{I}_{00r} = I_{00} \sin \varphi_{00} = \frac{V_1 (X_1 + X_0)}{(R_1 + R_0)^2 + (X_1 + X_0)^2}$$

where

$$\sin \varphi_{00} = \frac{X_1 + X_0}{\sqrt{(R_1 + R_0)^2 + (X_1 + X_0)^2}}$$

The current in the rotor arm of the equivalent L-circuit as defined by Eq. (42-14) is

$$\dot{I}_2'' = -\dot{I}_2'/C_1 = V_1/Z_s$$

where

$$Z_s = C_1 Z_1 + C_1^2 Z_{2eq}' = R_s + jX_s$$

is the impedance of the right-hand arm in the equivalent L-circuit;

$$R_s = c'R_1 + (c')^2 (R_2'/s) - c''X_1 - 2c'c''X_2'$$



is its resistive component, and

$$X_s = c'X_1 + (c')^2X_2' + c''R_1 + 2c'c''(R_2'/s)$$

is its reactive component.

The current in the rotor arm is given by

$$I_2'' = V_1 / \sqrt{R_s^2 + X_s^2} \quad (43-5)$$

The active component of the rotor arm current is

$$I_{2a}'' = I_2'' \cos \varphi_2 = V_1 R_s / (R_s^2 + X_s^2) \quad (43-6)$$

where  $\varphi_2$  is the phase angle between  $V_1$  and  $I_2''$  and

$$\cos \varphi_2 = R_s / \sqrt{R_s^2 + X_s^2}$$

The reactive component of the rotor arm current is

$$I_{2r}'' = I_2'' \sin \varphi_2 = V_1 X_s / (R_s^2 + X_s^2) \quad (43-7)$$

where

$$\sin \varphi_2 = X_s / \sqrt{R_s^2 + X_s^2}$$

From the current equation applying to the equivalent L-circuit

$$\dot{I}_1 = \dot{I}_{00} - \dot{I}_2' / C_1 = \dot{I}_{00} + \dot{I}_2'' \quad (43-8)$$

we can obtain both the active and reactive component of the stator current

$$I_{1a} = I_{00a} + I_{2a}'' \quad (43-9)$$

$$I_{1r} = I_{00r} + I_{2r}''$$

the stator current

$$I_1 = \sqrt{I_{1a}^2 + I_{1r}^2} \quad (43-10)$$

and the power factor relative to the primary supply line

$$\cos \varphi_1 = I_{1a} / I_1 \quad (43-11)$$

Plots of  $I_2' \approx I_2'' = f(s)$  and  $I_1 = f(s)$  for an induction machine with typical values found by Eq. (43-5) and (43-10) appear in Fig. 43-2.

### 43-3 Electromagnetic Torque

In deriving an equation for the electromagnetic torque as a function of slip, we shall proceed from the equation, (41-33), for electromagnetic power and from the relation between

that power and the copper loss in the rotor, as given by Eq. (41-36):

$$T_{em} = P_{em}/\Omega_1 = P_{Cu2}/s\Omega_1 = m_1 R'_2 (I'_2)^2/s\Omega_1$$

Using Eq. (42-12) for the rotor current, we can obtain an equation of electromagnetic torque as a function of slip

$$T_{em} = \frac{m_1 V_1^2 R'_2}{s\Omega_1 [(R + c' R'_2/s)^2 + (X + c'' R'_2/s)^2]} \quad (43-12)$$

where  $R = R_1 - c'' X'_2$  and  $X = X_1 + c' X'_2$ . In approximate calculations, it is safe to take  $c' = 1$  and  $c'' = 0$ , and  $X = X_{sc} = X_1 + X'_2$ .

A plot of  $T_{em} = f(s)$  at  $V_1, f_1$  and other circuit parameters held constant gives what is known as the *torque-slip characteristic* of a machine. The torque-slip characteristic for typical values of machine quantities is shown in Fig. 43-2.

At  $s = 0$ , when the angular velocity of the rotor,  $\Omega$ , is the same as that of the field,  $\Omega_1$ , the electromagnetic torque is zero,  $T_{em} = 0$ . At  $s > 0$ , the electromagnetic torque is positive (it is acting with the field). At  $s < 0$ , when  $\Omega > \Omega_1$ , the electromagnetic torque is negative,  $T_{em} < 0$ .

We take a closer look at the torque-slip characteristic,  $T_{em} = f(s)$ . To begin with, let us prove that at  $s \ll 1$ , the torque-slip characteristic is linear very closely. We shall do this by considering the denominator of the torque expression. On setting  $c' = 1$  and  $c'' = 0$  and neglecting  $R_1$ , in comparison with  $R'_2/s$ , and  $X_{sc}^2$  in comparison with  $(R'_2/s)^2$ , we get

$$T_{em} = m_1 V_1^2 s / R'_2 \Omega_1$$

With torque plotted against slip, the above equation yields a straight line (shown by the dashed line in Fig. 43-2). Conversely, if the slip is close to unity, then

$$R'_2/s \approx R'_2$$

Hence, with an error tolerable for practical purposes, we may write

$$T_{em} = \frac{m_1 R'_2 V_1^2}{s\Omega_1 (X_{sc}^2 + R_{sc}^2)}$$

The above equation describes a hyperbola (it is shown by a dashed line).

Let us determine what is known as the critical (or maximum) slip,  $s = s_m$ , at which the torque is at its maximum

(or breakdown) value,  $T_{em} = T_{em, m}$ . To simplify the matters, we shall determine  $s_m$  at which the variable part of the denominator in Eq. (43-12) is a minimum:

$$A(s) = s [(R + c' R'_2/s)^2 + (X + c'' R'_2/s)^2]$$

On equating the derivative to zero and solving the equation

$$dA(s)/ds = 0$$

we obtain

$$s_m = \pm \frac{R'_2 |C_1|}{\sqrt{R^2 + X^2}} \approx \pm \frac{R'_2}{\sqrt{R_1^2 + X_{sc}^2}} \quad (43-13)$$

where  $R = R_1 - c'' X'_2$  and  $X = X_1 + c' X'_2$ . Neglecting  $R_1^2$  in comparison with  $X_{sc}^2$  introduces an error of about 1% in the critical slip.

As is seen, the torque-slip curve shows two peaks, one in the region of positive slips and the other in the region of negative slips, respectively corresponding to the “+” and “-” sign in Eq. (43-13) (see Fig. 43-2).

Practically, the critical slip is a function of only the rotor resistance  $R'_2$  and the leakage inductive reactances of the stator and rotor,  $X_1$  and  $X'_2$ . Therefore, the only way to control  $s_m$  is to insert a series impedance in the rotor circuit.

For general-purpose induction machines in sizes upwards of 3 kW, the critical slip usually ranges between 0.15 and 0.3. In special-purpose machines and also in cases where a series impedance is introduced in the rotor circuit, it may be higher.

The maximum torque is found by substituting  $s_m$  as defined by Eq. (43-13) for  $s$  in Eq. (43-12):

$$\begin{aligned} T_{em, m} &\approx \pm \frac{m_1 V_1^2}{2\Omega_1 C_1 [\sqrt{R^2 + X^2} \pm (c' R + c'' X)/C_1]} \\ &\approx \pm \frac{m_1 V_1^2}{2\Omega_1 (\sqrt{R_1^2 + X_{sc}^2} \pm R_1)} \end{aligned} \quad (43-14)$$

where the “+” sign applies to  $s_m > 0$ , when  $T_{em, m(+)} > 0$ , and the “-” sign applies to  $s_m < 0$ , when  $T_{em, m(-)} < 0$ .

In absolute value, the maximum torque at negative slip is substantially larger than the maximum torque at positive slip  $|T_{em, m(-)}| > |T_{em, m(+)}|$ . It is interesting to note that  $T_{em, m}$  is strongly dependent on the applied voltage

squared and the leakage inductive reactance  $X_{sc}$ , but is only slightly affected by the stator resistance  $R_1$ , and is independent of the rotor resistance  $R'_2$ . Variations in the latter only tell on the critical slip,  $s_m$  [see Eq. (43-13)]. As the rotor resistance is increased, the maximum torque,  $T_{em,m(+)}$ , shifts on the diagram to the right, but remains unchanged in magnitude.

An important point on the torque-slip characteristic is the point where  $s = 1$ . It corresponds to the instant when the rotor is at a standstill ( $\Omega = 0$ ,  $s = 1$ ) prior to starting. Accordingly, the torque corresponding to  $s = 1$  is called the *inherent* (or *static*) *starting torque*. An expression for it can be deduced from Eq. (43-12) on substituting  $s = 1$ :

$$T_{em,s} = \frac{m_1 R'_2 V_1^2}{\Omega_1 (R + c' R'_2)^2 + (X + c'' R'_2)^2} \approx \frac{m_1 R'_2 V_1^2}{\Omega_1 (R_{sc}^2 + X_{sc}^2)} \quad (43-15)$$

#### 43-4 Active and Reactive Power

The active power drawn from the supply line can be expressed in terms of the active stator current which is a function of slip, using Eq. (43-9):

$$P_1 = m_1 V_1 I_1 \cos \varphi_1 = m_1 V_1 I_{1a}$$

The electromagnetic power can be expressed in terms of the rotor copper loss or electromagnetic torque, using Eqs. (41-33), (41-36), and (43-12):

$$P_{em} = P_1 - P_{Cu1} - P_c = P_{Cu2}/s = T_{em} \Omega_1 \quad (43-16)$$

where  $P_c = m_1 R_0 I_0^2 =$  stator core loss  
 $P_{Cu1} = m_1 R_1 I_1^2 = f(s) =$  stator copper loss  
 $P_{Cu2} = m_1 R'_2 (I'_2)^2 = f(s) =$  rotor copper loss

If we take as a unit power the rated total power of a machine

$$S_{1,R} = m_1 V_{1,R} I_{1,R}$$

and as a unit torque

$$T_{em,1} = S_{1,R} / \Omega_1$$

we shall obtain identical per-unit expressions for both the electromagnetic power and the electromagnetic

torque:

$$\begin{aligned} T_{em,*} &= T_{em}/T_1 = \frac{R'_{*2} V_{*1}^2}{s [(R_* + c' R'_{*2}/s)^2 + (X_* + c'' R'_{*2}/s)^2]} \\ &= P_{em}/S_{1,R} = P_{*em} \end{aligned}$$

Therefore, the torque-slip and the power-slip characteristics plotted in Fig. 43-2 on a per-unit basis are identical.

The mechanical power developed by the rotor can be found from Eq. (41-36):

$$\begin{aligned} P_m &= (1-s) P_{em} = \frac{(1-s) m_1 R'_2 V_1^2}{s [(R + c' R'_2/s)^2 + (X + c'' R'_2/s)^2]} \\ &= T_{em} \Omega \end{aligned} \quad (43-17)$$

The power-slip curve crosses zero twice (see Fig. 43-2), namely at  $s = 0$  (when  $T_{em} = 0$ ) and at  $s = 1$  (when  $\Omega = 0$ ).

The useful mechanical power available at the shaft of a machine,  $P_2$ , is found by accounting for the additional (stray) losses  $P_{ad}$  and the friction and windage losses  $P_{f/w}$ , which should likewise be found as functions of slip:

$$P_2 = P_m - P_{ad} - P_{f/w} \quad (43-18)$$

Whatever the mode of operation and whatever the direction of energy conversion, an induction machine always draws from the supply line a reactive power required to set up the mutual rotating field and leakage fields. The reactive power drawn by an induction machine from the supply line is given by

$$Q_1 = m_1 V_1 I_1 \sin \varphi_1 = m_1 V_1 I_{1r} \quad (43-19)$$

where  $I_{1r} = f(s)$  is from Eq. (43-9).

The total reactive power is the sum of the reactive powers required to set up the mutual rotating field

$$Q_0 = m_1 X_0 I_0^2 \quad (43-20)$$

the stator leakage field

$$Q_{\sigma 1} = m_1 X_1 I_1^2 \quad (43-21)$$

and the rotor leakage field

$$Q_{\sigma 2} = m_1 X'_2 (I'_2)^2 \quad (43-22)$$

where  $I'_2 = f(s)$  is from Eq. (42-12).

### 43-5 Stray Electromagnetic Torques

Apart from the principal electromagnetic torque produced by the interaction of the fundamental mutual field with the currents induced in the rotor (see Sec. 43-3), the rotor of an induction machine is additionally acted upon by several minor or stray electromagnetic torques arising from various physical sources. In many cases, such torques have an appreciable effect on the torque-slip characteristic of the machine. Because the calculation of stray torques involves elaborate and widely varying techniques, we shall limit ourselves to a qualitative explanation of their origin.

**Induction stray torques.** In their origin, they are analogous to the principal electromagnetic torque and only differ in that they arise from the interaction of the higher harmonics of the stator field (and also the lower harmonics in the case of fractional-pitch windings) with the currents induced in the rotor winding. The most noticeable induction stray torques are those produced by the stator tooth (slot) harmonics of the order  $\nu = (Z_1/p) \pm 1$ . The peak value of the associated flux density,

$$B_{1\nu m} = \mu_0 F_{1\nu m} C_\nu / \delta k_{\delta 2}$$

is especially high not only because the winding factors in the mmf equation

$$F_{1\nu m} = \frac{\sqrt{2} m_1 I_1 w_1 k_{d\nu} k_{p\nu}}{\pi p \nu}$$

are close to unity and are the same as the winding factors for the fundamental field ( $k_{d\nu} = k_{d1}$  and  $k_{p\nu} = k_{p1}$ ), but also because these harmonic fields build up owing to the stator saliency (the slotting effect). For an open-slot stator, the saliency factor  $C_\nu$  may be as high as 3 or 4 (see Sec. 25-6).

As an example, let us consider a three-phase induction machine for which  $m_1 = 3$ ,  $q_1 = 1$ ,  $p = 2$ , and  $Z_1 = 2pm_1q_1 = 12$ . In this machine, the order of the tooth harmonics is

$$\nu = 12/2 \pm 1$$

that is,  $\nu = 5$  and  $\nu = 7$ . The 7th harmonic rotates in the same direction as the fundamental at  $\Omega_7 = \Omega_1/7$ . The 5th harmonic rotates in the opposite direction at  $\Omega_5 = -\Omega_1/5$ .

When the rotor is at standstill, the 7th harmonic travels relative to the rotor in the same direction as the fundamen-

tal and produces a torque,  $T_{em,7} > 0$ , which acts in the same direction as the principal torque (Fig. 43-3). As the angular speed of the rotor builds up, the slip

$$s_7 = (\Omega_7 - \Omega) / \Omega_7$$

relative to the rotor decreases until it reduces to zero at  $\Omega = \Omega_7$  and  $s = 6/7$ . Now the 7th harmonic is stationary

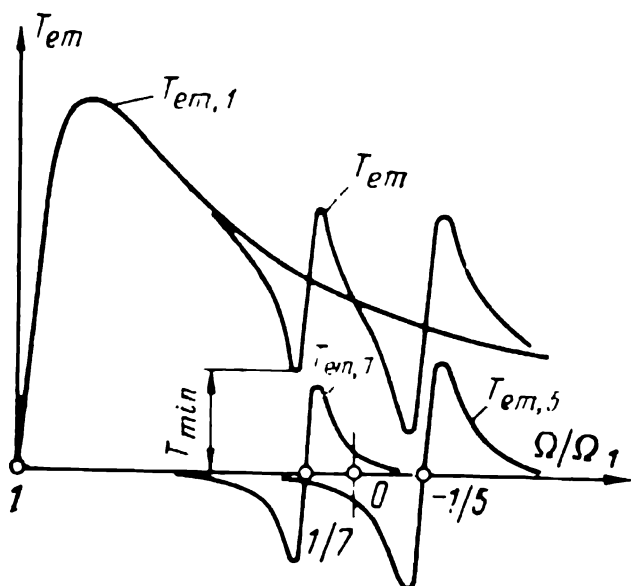


**Fig. 43-3** Stray induction torques associated with higher harmonics

relative to the rotor, no currents are induced, and  $T_{em,7} = 0$ . As the angular speed of the rotor relative to the 7th harmonic keeps rising,  $\Omega > \Omega_7$  ( $s_7 < 0$ ), the machine goes into the generator mode of operation, and the electromagnetic torque is reversed,  $T_{em,7} < 0$  (see Fig. 43-3). The 5th-harmonic torque,  $T_{em,5}$ , depends on the angular speed of the rotor in a similar manner, but now the slip

$$s_5 = (\Omega_5 - \Omega) / \Omega_5$$

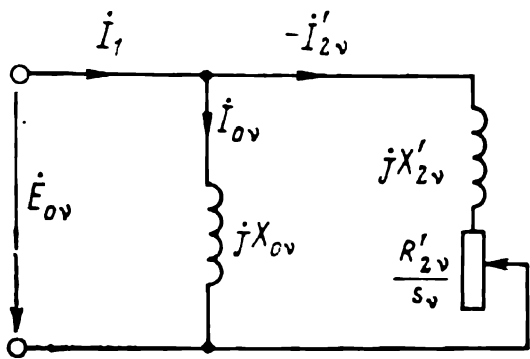


**Fig. 43-4** Equivalent circuit of an induction machine for the  $v$ th harmonic of the magnetic field

reduces to zero at  $\Omega = -\Omega_1/5$ , that is, in the region of braking action for the fundamental component, where  $s=6/5>1$ . The other harmonics of the stator field likewise produce stray induction torques, and the resultant electromagnetic torque is their sum

$$T_{em} = T_{em1} + T_{em5} + T_{em7} + T_{em11} + T_{em13} + \dots$$

The stray induction torques distort the waveform of the principal electromagnetic torque.

The distortion is most severe at low rotational speeds where the stray induction torques associated with the higher harmonics are maximal. The “dips” in the starting torque curve make the starting of the motor more difficult, and a condition, known as crawling, arises.

Quantitatively, the stray induction torque associated with the  $\nu$ th space harmonic field may be evaluated by reference to the equivalent circuit in Fig. 43-4. This equivalent circuit is developed by analogy with that for the fundamental in Fig. 42-3a. The stator current  $I_1$  is assumed to be fixed. At any angular rotor velocity, it depends on the processes associated with the fundamental space component and is found from Eq. (43-8). The angular rotor speed  $\Omega$  and the slip for the  $\nu$ th harmonic,  $s_\nu = (\Omega_\nu - \Omega)/\Omega_\nu$ , where  $\Omega_\nu = \pm \Omega_1/\nu$ , are also fixed.

From the equivalent circuit, the referred current  $I'_{2\nu}$  induced by the  $\nu$ th harmonic field in the rotor winding is:

$$-I'_{2\nu} = I_1 \frac{jX_{0\nu}}{R'_{2\nu}/s_\nu + j(X_{0\nu} + X'_{2\nu})}$$

As is seen,  $-I'_{2\nu}$  is a fraction of  $I_1$ , and is a function of both  $s_\nu$  and the resistance of the equivalent circuit.  $X_{0\nu}$  is the mutual inductive reactance of the stator associated with the  $\nu$ th harmonic field.  $X'_{2\nu}$  is the referred leakage inductive reactance of the rotor for the  $\nu$ th harmonic field.  $R'_{2\nu}$  is the referred rotor resistance for the  $\nu$ th harmonic field (with allowance for the current crawling at  $f_{2\nu} = f_1 s_\nu$ ).

At  $s_\nu = 0$ , when the rotor is travelling at a synchronous speed relative to the  $\nu$ th harmonic,  $I'_{2\nu} = 0$ , and the magnetizing current  $I_{0\nu}$  which produces the resultant  $\nu$ th harmonic field is the same as  $I_1$ . At  $s_\nu \neq 0$ , there appears in the rotor a current,  $I'_{2\nu}$ , which weakens the stator field, and the magnetizing current is reduced,

$$I_{0\nu} = I_1 - (-I'_{2\nu})$$

The stray induction torque due to the  $\nu$ th harmonics of the stator field can be found, using Eqs. (41-33) and (41-36):

$$T_{em, \nu} = P_{em, \nu}/\Omega_\nu = P_{Cu2, \nu}/s_\nu \Omega_\nu = \frac{m_1 R'_{2\nu} (I'_{2\nu})^2}{s_\nu \Omega_\nu}$$

As is seen from the equivalent circuit, given  $I_1$  and  $s_\nu$ , and assuming that all the other conditions are equal,  $I'_{2\nu}$  and  $T_{em, \nu}$  increase with a decrease in  $X'_{2\nu}$ . Therefore, in a wound-rotor machine displaying a very high leakage at any higher field harmonics,  $I'_{2\nu}$  and  $T_{em, \nu}$  are very small, and their distorting effect may be neglected. This can be



explained as follows. Firstly, a wound-rotor machine has very low winding factors for the tooth (slot) harmonics of the stator field, so that these harmonics induce very small emfs in the rotor winding. Secondly,  $I'_{2v}$  induced in a phase-wound rotor produces, in addition to the small  $v$ th harmonic field, a fairly strong fundamental field which acts as a leakage field with respect to the  $v$ th harmonic.

In contrast, in a squirrel-cage rotor,  $X'_{2v}$  is comparable in magnitude with  $X_{0v}$ , so  $I'_{2v}$  induced in the rotor winding and the stray induction torques present a real hazard. This is because a squirrel-cage structure consists of several elementary loops each of which is made up of two adjacent bars and the intervening end-ring segments. Such loops offer a low leakage inductive reactance,  $X'_{2v}$ , to the higher field harmonics. An increase in the number of bars,  $Z_2$ , and a decrease in loop width bring about a decrease in  $X'_{2v}$ , and an increase in "dips" in the torque-slip curve. This, too, might lead to crawling.

To avoid a noticeable distortion of the torque-slip characteristic, it is recommended that  $Z_2$  should be less than  $Z_1$ . The detrimental effect of the higher harmonics on the torque-slip characteristic of an induction machine can be reduced, if the rotor slots (bars) are skewed by one stator tooth (slot) pitch. In the case of a squirrel-cage rotor with insulated bars skewing substantially reduces the currents induced by the stator slot (tooth) ripples in the rotor winding and removes nearly all "dips" from the torque-slip curve.

In a squirrel-cage rotor with uninsulated bars, skewing is ineffective in minimizing the effect of the higher harmonics. This is because in such a case transverse induced currents would flow between adjacent bars via the rotor teeth and introduce further losses. This is why skewing by a tooth (slot) pitch is nearly never used, although skewing by a half-tooth pitch can be used in some exceptional cases.

**Synchronous stray torques.** These minor torques are produced under certain conditions due to the interaction of two higher harmonics of the same order  $v$ , one of which is produced by the stator current  $I_1$  at frequency  $f_1$  and the other by the rotor current  $I_2$  at frequency  $f_2 = sf_1$ . They are independent harmonics, because neither is induced by the other. They owe their origin to the stator and rotor currents,  $I_1$

and  $I_2$ , produced by mutual induction at the fundamental frequency of the field.

Proper insight into the matter can best be given by an example. Consider the case where a synchronous torque is produced by the most pronounced tooth (slot) harmonics. Suppose that the stator has  $m_1 = 3$ ,  $q_1 = 1$ ,  $2p = 6$ , and  $Z_1 = 18$ , whereas the phase-wound rotor has  $m_2 = 2$ ,  $q_2 = 2$ , and  $Z_2 = 24$ . Then the lowest tooth harmonics due to  $I_1$  will be of the order  $\nu_1 = Z_1/p \pm 1 = 18/3 \pm 1 = 7$  (for the harmonic travelling in the forward direction) and 5 (for the harmonic travelling backward).

The lowest tooth harmonics due to  $I_2$  are of the order  $\nu_2 = Z_2/p \pm 1 = 24/3 \pm 1 = 9$  and 7 (for the forward and the backward one, respectively).

As is seen, the forward stator harmonic and the backward rotor harmonic are of the same order,

$$\nu = \nu_1 = \nu_2 = 7$$

The forward stator harmonic with a peak flux density

$B_{1\nu m}$  rotates at  $\Omega_1/\nu$  (Fig. 43-5). The backward rotor harmonic with a peak flux density  $B_{2\nu m}$  rotates at

$$(-s\Omega_1)/\nu = -(\Omega_1 - \Omega)/\nu$$

relative to the rotor, and at

$$\Omega - (\Omega_1 - \Omega)/\nu$$

relative to the stator. Relative to the rotor harmonic, the stator harmonic is travelling at

$$\Omega_{12} = \Omega_1/\nu - \left( \Omega - \frac{\Omega_1 - \Omega}{\nu} \right)$$

Thus, in an arbitrary steady state, such that  $\Omega_{12} \neq 0$ , the stator and rotor harmonics are rotating out of synchro-

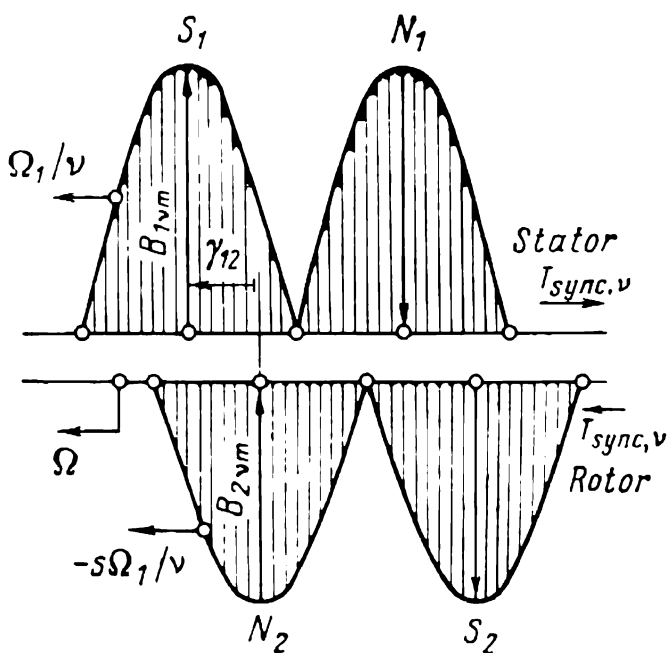


Fig. 43-5 Interaction of the independent  $\nu$ th stator and rotor harmonics developing stray synchronous torques

nism, and their relative position defined by the angle

$$\gamma_{12} = \Omega_{12}t$$

is changing continually. This gives rise to a continuous change in the electromagnetic torque  $T_{\text{sync}, v}$  produced by the interaction between the stator-harmonic poles  $N_1$  and  $S_1$ , on the one hand, and the rotor-harmonic poles  $N_2$  and  $S_2$ , on the other. This torque changes sign periodically, is a function of the electrical angle  $\alpha_{12v} = v p \gamma_{12}$  between the harmonics and varies as the sine of that angle

$$T_{\text{sync}, v} = T_{\text{sync}, v, m} \sin \alpha_{12v}$$

At  $\alpha_{12v}$  equal to zero or  $\pi$ , when the unlike or like poles are opposite one another,

$$T_{\text{sync}, v} = 0$$

At  $\alpha_{12v} = \pi/2$ , the torque on the rotor is a maximum

$$T_{\text{sync}, v} = T_{\text{sync}, v, m}$$

and is directed with the rotation. At  $\alpha_{12v} = -\pi/2$ , the electromagnetic torque has a negative peak value:

$$T_{\text{sync}, v} = -T_{\text{sync}, v, m}$$

The average value of  $T_{\text{sync}, v}$  alternating in magnitude and sign at  $\omega_{12v} = \gamma p \Omega_{12}$  is zero and has no effect on the rotation of the rotor because the latter has a large mechanical inertia.

The interaction of a stator and a rotor harmonic produces a synchronous torque only when they are stationary relative to each other. This occurs at a certain definite angular velocity of the rotor

$$\Omega_{\text{sync}, v} = 2\Omega_1/(v + 1) = 2\Omega_1/(7 + 1) = \Omega_1/4$$

which can be found on setting  $\Omega_{12} = 0$ . At this angular velocity of the rotor (Fig. 43-6), either a positive or a negative synchronous torque is produced, depending on the relative position of the stator and rotor harmonics. Its value lies in the range

$$-T_{\text{sync}, v, m} \leq T_{\text{sync}, v} \leq T_{\text{sync}, v, m}$$

A synchronous torque might cause the rotor to lock at starting or fail to come up to the normal speed (the crawling condition). In contrast to an induction torque which

exists over a relatively broad range of angular velocities, the effect of a synchronous locking torque is felt for a very short time at starting, as the motor passes  $\Omega_{\text{sync},v}$ , and it can be overcome by the kinetic energy stored by the rotating rotor. Because of this, synchronous torques are less

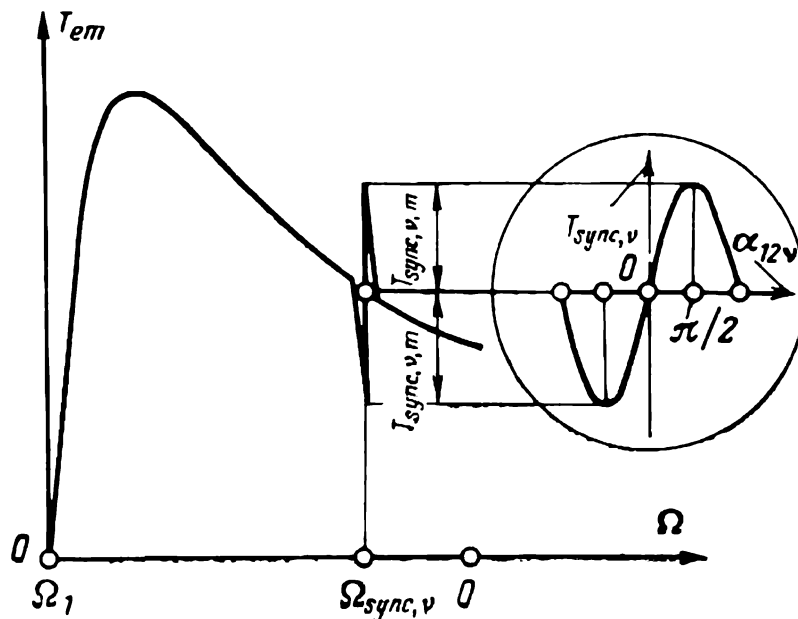


Fig. 43-6 Stray synchronous torque due to the  $v$ th stator and rotor harmonics

troublesome than induction torques, and they have to be reckoned with only when they are likely to be developed at  $\Omega_{\text{sync},v} = 0$ .

Synchronous stray torques are at their strongest when the lowest tooth (slot) harmonics of the stator and rotor are of the same order, that is, when

$$v_1 = Z_1/p \pm 1 = Z_2/p \pm 1 = v_2$$

This can occur with two combinations of stator and rotor tooth numbers. When  $Z_1 = Z_2$ , the stator and rotor harmonics travelling in the same direction will be of the same order. When  $Z_2 - Z_1 = \pm 2p$ , this is true of the stator and rotor harmonics travelling in the opposite directions. In the former case, the stator and rotor harmonics are travelling in synchronism with the rotor at standstill. Obviously, the rotor does not store any kinetic energy and should the synchronous torques exceed the fundamental starting torque, the rotor will fail to start rotating. The latter case has already been examined earlier.

As follows from the foregoing, in order to avoid substantial synchronous stray torques, it is essential that  $Z_1 \neq Z_2$  and  $Z_2 - Z_1 \neq \pm 2p$ . The detrimental effect of stray synchronous torques on the torque-slip (or torque-speed) characteristic of an induction machine can be minimized by skewing the rotor slots by a rotor tooth (slot) pitch.

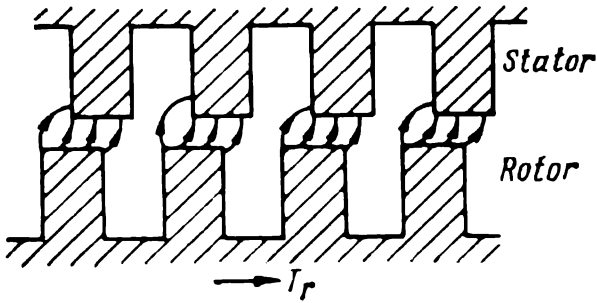


Fig. 43-7 Production of a reactive torque at  $Z_1 = Z_2$

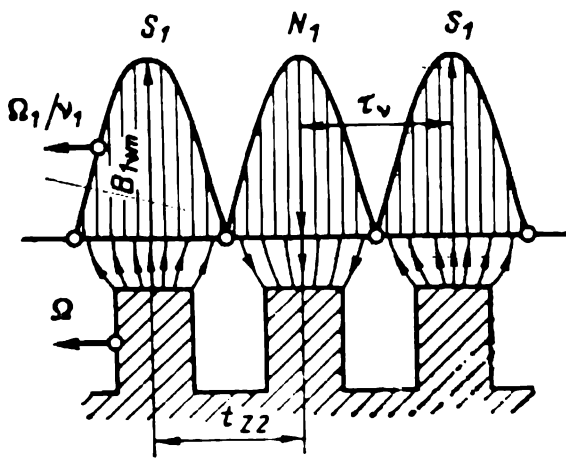


Fig. 43-8 Production of a reactive torque by a slot (tooth) harmonic of the magnetic field

stator and rotor teeth so that they oppose one another, that is, when the airgap has a maximum permeance. In this position, the stray reactive torque is zero,  $T_r = 0$ . When the rotor teeth move out of alignment with the stator teeth (Fig. 43-7), the rotor is acted upon by a reactive torque acting towards the position of a maximum permeance. Because of such stray reactive torques, the rotor of an induction motor with  $Z_1 = Z_2$  fails to start (this is known as sticking).

In the latter case (Fig. 43-8), the lowest tooth (slot) harmonic has a pole pitch

$$\tau_v = 2\pi R / 2pv_1 = \pi R / (Z_1 \pm p)$$

**Reactive stray torques.** The term 'reactive' refers to the stray torques acting on a ferromagnetic body in a magnetic field and tending to turn it in a position in which the magnetic circuit has a maximum permeance.

In an induction machine, stray reactive torques may be developed in two basically different cases, namely: (1) when the stator and rotor have the same number of teeth,  $Z_1 = Z_2$ ; and (2) when the lowest tooth (slot) harmonic of the stator field has as many poles as the rotor has teeth, that is,

$$2pv_1 = 2(Z_1 \pm p) = Z_2$$

In the former case, the mutual field tends to position the

which is the same as the tooth (slot) pitch of the rotor

$$t_{Z_2} = 2\pi R/Z_2$$

Therefore, the rotor teeth tend to take up a position opposite the poles of the lowest tooth (slot) harmonic of the stator field, that is, where the airgap has a maximum permeance for that harmonic. Thus, so long as the rotor is rotating at an angular velocity  $\Omega$  equal to that of the lowest slot harmonic,  $\Omega_v = \Omega_1/v_1$ , and the rotor teeth are positioned relative to the harmonic poles as shown in the figure, the stray reactive torque will be zero,  $T_r = 0$ . When the rotor teeth move out of alignment with the harmonic poles, the rotor is acted upon by a reactive torque,  $T_r$ , directed towards the position of a maximum permeance. This reactive torque is developed at a certain definite angular velocity,  $\Omega = \Omega_v$ , and affects the torque-slip (or torque-speed) characteristic of the machine in the same manner as the stray synchronous torque (see Fig. 43-6). For example, when  $m_1 = 3$ ,  $2p = 6$ ,  $q_1 = 1$ , and  $Z_1 = 18$ , the stray reactive torque will be developed at

$$Z_2 = 2 (Z_1 \pm p) = 2 (18 \pm 3) = 30 \text{ or } 42$$

and at a rotor speed equal to

$$\Omega = -\Omega_1/5 \text{ or } \Omega_1/7$$

**Eddy-current and hysteresis stray torques.** In contrast to synchronous and induction stray torques, those due to eddy currents and hysteresis are associated with the fundamental field rather than its higher harmonics.

Both eddy-current and hysteresis torques can be traced back to what happens when the rotor core is cyclically magnetized by the main magnetic field. The eddy-current torque,  $T_{ec}$ , is produced by the interaction of the eddy currents induced in the core with the main magnetic field. It differs from the principal electromagnetic torque only in that the induced currents that produce it are flowing in the core body rather than in the rotor winding.

The generation of hysteresis torque will be discussed in more detail in Sec. 63-7 concerned with hysteresis motors. This form of torque has its origin in the hysteresis of the rotor core material, owing to which the rotor is cyclically magnetized with a certain delay from the field travelling relative to the rotor. As a result, the fundamental stator and

rotor fields are displaced from each other by an angle  $\gamma_{12}$  which depends on the magnetic properties of the rotor core, and their relative position is the same as is shown in Fig. 43-5. This figure applies to the case where the rotor is travelling more slowly than the stator field, and the attraction of the unlike poles ( $S_1$  and  $N_2$  or  $N_1$  and  $S_2$ ) gives rise to a hysteresis torque,  $T_h = T_{hm} > 0$ , which acts in the direction of rotor rotation. When the rotor is travelling faster than the stator field the angle  $\gamma_{12}$  becomes negative, and the hysteresis torque acts in the opposite direction,  $T_h = -T_{hm} < 0$ .

When the rotor is travelling at synchronous speed, the angle between the axes of the stator and rotor fields may vary between  $\gamma_{12}$  and  $-\gamma_{12}$ , and the hysteresis torque between  $T_{hm}$  and  $-T_{hm}$ , depending on the direction of the external torque.

To see how the above torques vary with slip, let us assume that the mutual flux  $\Phi_m$  and, as a consequence, the mutual flux density in the rotor core remain unchanged as the slip varies. Then the hysteresis loss in the rotor,  $P_h$ , will be proportional to the frequency of cyclic magnetization,  $f_2 = sf_1$ , and the eddy-current loss,  $P_{ec}$ , will be proportional to  $f_2^2$ . Hence,

$$P_h = sP_{h,0}, \quad P_{ec} = s^2P_{ec,0}$$

where  $P_{h,0}$  and  $P_{ec,0}$  are the respective losses at  $s = 1$ . The electromagnetic powers  $P_{h,em}$  and  $P_{ec,em}$  bear the same relation to the respective losses  $P_h$  and  $P_{ec}$ , as  $P_{em}$  to  $P_{Cu2}$ , Eq. (41-36). Therefore,

$$P_{h,em} = P_h/s = P_{h,0}$$

$$P_{ec,em} = P_{ec}/s = sP_{ec,0}$$

Dividing the electromagnetic powers by the field angular velocity  $\Omega_1$  will give the hysteresis and eddy-current torques

$$T_h = P_{h,em}/\Omega_1 = pP_{h,0}/2\pi f_1$$

$$T_{ec} = P_{ec,em}/\Omega_1 = spP_{ec,0}/2\pi f_1$$

where  $p$  is the number of pole pairs.

As is seen from the equations derived above, the hysteresis torque is independent of the slip. In passing through a zero slip, it changes sign relative to the direction of rotor rotation. On the assumption that  $\Phi_m$  is constant, which is

equivalent to neglecting the reaction of eddy currents, the eddy-current torque is proportional to the slip.

Thus, the eddy-current and hysteresis torques aid the principal electromagnetic torque in both the motor and generator modes of operation, so they contribute to energy conversion. In ordinary induction motors, however, the rotor core is built up of laminations insulated from one another and punched from electrical-sheet steel which has low hysteresis losses. Because of this, both  $T_h$  and  $T_{ec}$  are small and may be neglected in determining the torque-slip (or torque-speed) characteristic.

### ☆ 43-6 The Circle Diagram of an Induction Machine

**The rationale of the circle diagram.** As the slip varies over the range  $\pm \infty$ , the primary current phasor,  $\dot{I}_1$ , will trace out a circular locus (Fig. 43-9), if the impedance parameters ( $R_1$ ,  $X_1$ ,  $R'_2$ ,  $X'_2$ ,  $R_0$ , and  $X_0$ ) and also  $V_1$  and  $f_1$  are assumed to remain constant. This circular locus, known as the *circle diagram*, offers a means for a speedy determination of a machine's performance.

Let us construct the circle diagram of an induction machine with reference to the equivalent circuit in Fig. 42-3c.

The voltage equation for the rotor arm of the equivalent circuit has the form

$$\dot{V}_1 = R_s \dot{I}_2'' + jX_{sc} \dot{I}_2''$$

where  $\dot{I}_2'' = -\dot{I}_2'$ .

Since we have assumed that

$$V_1 = \text{constant, and } X_{sc} = X_1 + X'_2 = \text{constant}$$

the current  $\dot{I}_2'$  will vary due to changes in

$$R_s = R_1 + R'_2/s$$

To prove that, as the slip varies, the locus of  $\dot{I}_2''$  will be a circle, let us divide the right- and left-hand sides of the last equation by  $jX_{sc}$

$$-j\dot{V}_1/X_{sc} = -j(R_s/X_{sc}) \dot{I}_2'' + \dot{I}_2''$$

On the right-hand side of the above equation, the current  $\dot{I}_2''$ , represented in the diagram of Fig. 43-9 by  $A_oA_s$ , is



combined with the current  $-j (R_s/X_{sc}) \dot{I}_2''$  which lags behind  $\dot{I}_2''$  by  $\pi/2$ . In the diagram,  $-j (R_s/X_{sc}) \dot{I}_2''$  is represented by  $A_s D$ . The sum of  $\dot{I}_2''$  and  $-j (R_s/X_{sc}) \dot{I}_2''$  is equal to an unvarying current,  $-j (\dot{V}_1/X_{sc})$ , shown in the diagram as  $A_0 D$ . (The current  $-j \dot{V}_1/X_{sc}$  lags behind  $\dot{V}_1$  by  $\pi/2$ .)

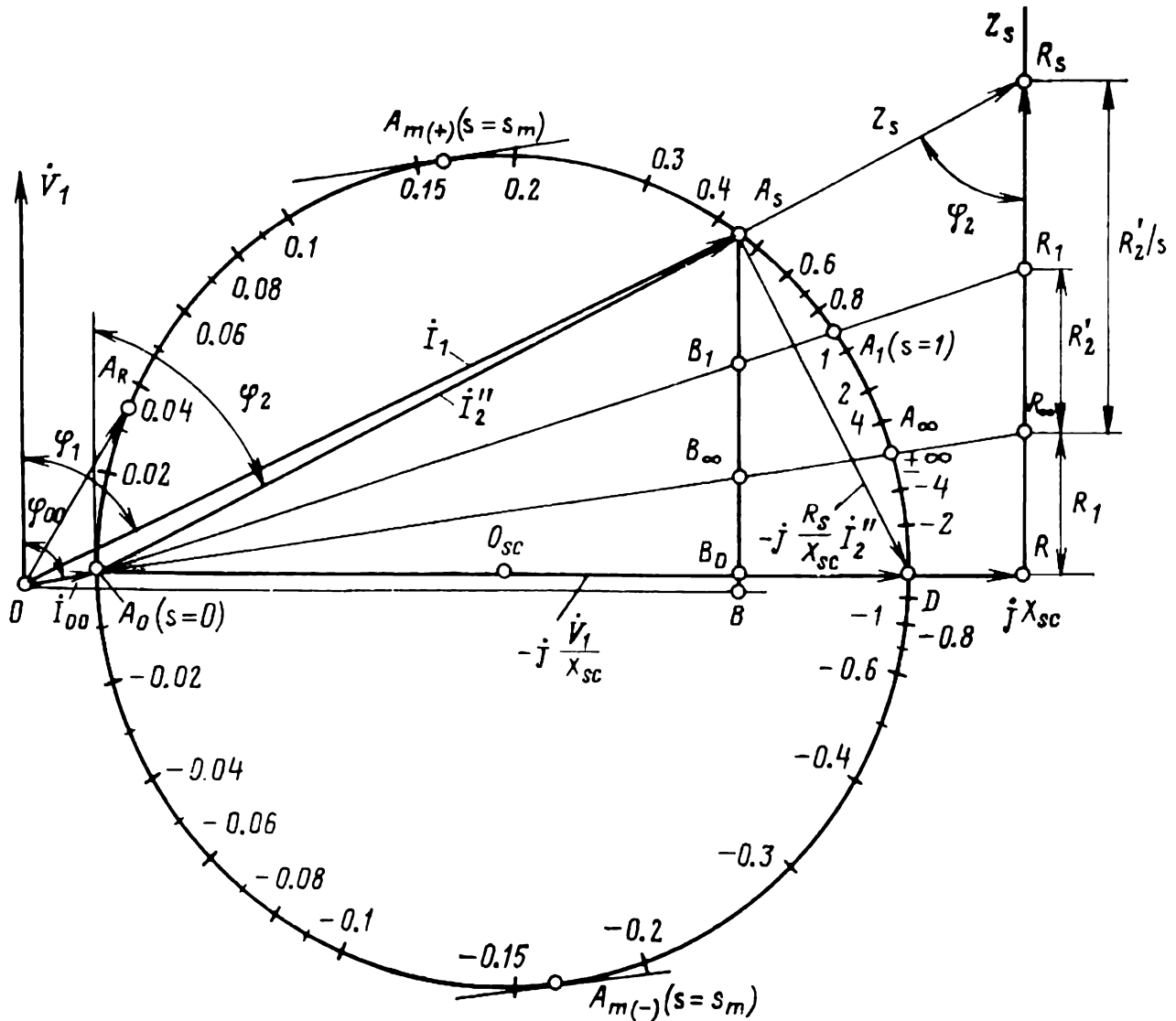


**Fig. 43-9** The circle diagram of an induction machine (on a per-unit basis), with  $V_1 = 1$ ,  $I_0 = 0.364$ ,  $\cos \varphi_{00} = 0.185$ ,  $X_1 = X_2' = 0.125$ ,  $R_1 = 0.0375$ ,  $R_2' = 0.0425$

The current phasors  $\dot{I}_2''$  and  $-j (R_s/X_{sc}) \dot{I}_2''$  are the legs of a right-angled triangle whose hypotenuse,  $-j \dot{V}_1/X_{sc}$ , remains unchanged. Hence, whatever the relative magnitudes of  $\dot{I}_2''$  and  $-j (R_s/X_{sc}) \dot{I}_2''$ , and whatever the values of  $R_s = R_1 + R_2'/s$ , the right-angle apex  $A_s$  will always lie on a circle with point  $O_{sc}$  as centre and with  $A_0 D$  as diameter. This circle is the locus of the current phasor  $\dot{I}_2''$  tip.

$A_s$ . To draw this circle, the current phasor  $-j\dot{V}_1/X_{sc}$ , corresponding to the circle diameter, is plotted as  $A_0D$  at right angles to  $\dot{V}_1$ . Choosing the length of  $A_0D$  as appropriate, we obtain a current scale, A/mm, given by

$$c_I = (V_1/X_{sc})/A_0D$$

where  $A_0D$  is the length in mm.

As the next step, the centre of  $A_0D$  is located at point  $O_{sc}$ , and the circle of constant  $\dot{I}_2''$  is drawn with  $O_{sc}A_0$  as radius.

Now we shall see how the position of  $A_s$  on the circle can be found if we know the slip.

The angle  $\varphi_2$  between  $V_1$  and  $I_2''$  is a function of the ratio  $R_s/X_{sc}$ . Let us draw a resistance triangle,  $A_0R_sR$ , to a certain scale. Its horizontal leg  $A_0R$  is proportional to  $jX_{sc}$ ; its vertical leg  $RR_s$  is proportional to the resistance  $R_s$  in the rotor arm; its hypotenuse  $A_0R_s$  is proportional to the impedance of that arm

$$Z_s = R_s + jX_{sc}$$

As  $s$  and  $R_s$  are varied, the tip of the phasor  $Z_s$  will trace out the resistance line  $RR_s$ . The angle between  $A_0R_s$  and  $RR_s$  is equal to the angle  $\varphi_2$  between  $V_1$  and  $I_2''$ , such that

$$\tan \varphi_2 = X_{sc}/R_s$$

Hence, the line drawn through points  $A_0$  and  $R_s$  will cut the circle at point  $A_s$  (the tip of the current phasor  $I_2''$ ). To locate point  $A_s$ , lay off  $RR_s$  proportional to  $R_s = R_1 + R_2'/s$  from point  $R$  on the impedance ( $Z_s$ ) line. To determine the stator current

$$\dot{I}_1 = \dot{I}_2'' + \dot{I}_{00}$$

add to  $\dot{I}_2''$  the no-load current  $\dot{I}_0$  which lags behind  $\dot{V}_1$  by the angle  $\varphi_{00}$  and is equal to  $\dot{V}_1/(Z_1 + Z_0)$ . The start of the current phasor  $\dot{I}_{00}$  will locate the origin  $O$  to which the voltage phasor may now be shifted. On joining the points  $O$  and  $A_s$ , we obtain the stator current phasor  $\dot{I}_1$  (the segment  $OA_s$ ), which lags behind the voltage by the angle  $\varphi_1$ .

Let us mark on the resistance line the points corresponding to the characteristic values of slip as follows.

(1)  $s = 1$  (the rotor is at standstill).  $R_s = R_1 + R'_2 = R_{sc}$ . For this case, the point on the resistance line gives  $R_1$  and the point on the current circle gives  $A_1$ .

(2)  $s = \pm \infty$  (the rotor is rotating with or against the field at an infinitely high speed). Accordingly,  $R_s = R_1$ , which is proportional to  $RR_\infty$ . The characteristic points are  $R_\infty$  and  $A_\infty$ .

(3)  $s = 0$  (an ideal no-load condition). Now,  $R_s = \infty$ , and the point  $R_s$ , on moving along the resistance line, tends to infinity. On the current circle, this condition is represented by point  $A_0$ .

Proceeding in the same way for any other values of slip, we shall scale off the circle in units of slip.

The characteristic points on the circle diagram mark the likely regions of operation for an induction machine. Within the arc  $A_0A_1$  where the slip varies from zero to unity, lies the motor region of operation. Within the arc  $A_1A_\infty$  where the slip varies from unity to  $+\infty$ , is the braking region of operation. Within the arc  $A_0A_\infty$ , where the slip varies from zero to  $-\infty$ , the machine is operating as a generator.

It is important to stress that the circle diagram gives an idealized locus of current in an induction machine, because it is constructed on assuming that  $X_{sc}$  is constant. Actually, the saturation of the magnetic circuit by leakage fields causes  $X_{sc}$  to decrease as the currents increase. As a consequence, the actual locus is other than a circle. Fortunately, this departure is negligible in the range from no-load to full-load current.

**Determination of currents, powers, losses and other quantities from the circle diagram.** In addition to  $I_1$  and  $I'_2 = I''_2$ , the circle diagram enables the analyst or designer to determine the powers, efficiency, and power factor of an induction machine as functions of slip. This is done by measuring appropriate line segments on the circle diagram.

The stator current is

$$I_1 = (OA_s) c_I$$

where  $c_I$  is the current scale factor.

The referred rotor current is

$$I'_2 = I''_2 = (A_0A_s) c_I$$

In order to determine powers, we need to carry out some additional constructions. Let us pass  $OB$  parallel to  $A_0D$ ,

which is the diameter of the circle, through point  $O$ , and also  $A_0A_1$  and  $A_0A_\infty$  through point  $A_0$ ; the latter two lines will cut the circle at the characteristic points  $A_1$  and  $A_\infty$ .

Jumping a little ahead, it is to be noted that  $A_0A_1$  is called the mechanical power ( $P_m$ ) line,  $A_0A_\infty$  is called the electromagnetic power ( $P_{em}$ ) line or electromagnetic torque ( $T_{em}$ ) line, and  $OB$  is the primary power ( $P_1$ ) line.

Drop a perpendicular  $A_sB_0$  from point  $A_s$  on the diameter  $A_0D$  and denote the points where the perpendicular cuts the characteristic lines as  $B_1$ ,  $B_\infty$ , and  $B$ .

Let us prove that the active power drawn from the supply line is represented, to scale, by  $A_sB$ :

$$P_1 = m_1 V_1 I_{1a} = m_1 V_1 c_I (A_s B) = c_P (A_s B)$$

where  $c_P = m_1 V_1 c_I$  is the power scale factor,  $W \text{ mm}^{-1}$ .

The electromagnetic power is represented by  $A_s B_\infty$ . From the similarity of the triangles,  $\triangle (A_0 A_s B_\infty)$  and  $\triangle (A_0 R_s R_\infty)$ , we get

$$A_s B_\infty = (R_s R_\infty) (A_0 A_s) / (A_0 R_s) = (R'_2/s) (A_0 A_s) / Z_s$$

Hence,

$$\begin{aligned} c_P (A_s B_\infty) &= m_1 (R'_2/s) (V_1/Z_s) (A_0 A_s) c_I \\ &= m_1 (R'_2/s) (I''_2)^2 = P_{Cu2}/s = P_{em} \end{aligned}$$

Now we will show that  $A_s B_1$  is proportional to the mechanical power. Since  $R_s R$  is parallel to  $A_s B$ , we may write

$$\begin{aligned} (A_s B_1)/(A_s B_\infty) &= (R_s R_1)/(R_s R_\infty) \\ &= (R'_2/s - R'_2)/(R'_2/s) = 1 - s \end{aligned}$$

Hence,

$$c_P (A_s B_1) = c_P (A_s B_\infty) (1 - s) = P_{em} (1 - s) = P_m$$

The sum of the magnetic (hysteresis and eddy-current) losses and the electric (copper) losses in the stator is proportional to  $B_\infty B$ :

$$P_c + P_{Cu1} = c_P (B_\infty B)$$

The rotor copper loss is proportional to  $B_1 B_\infty$ :

$$P_{Cu2} = P_{em} - P_m = c_P (B_1 B_\infty)$$

The electromagnetic torque is proportional to the electromagnetic power:

$$T_{em} = P_{em}/\Omega_1 = (c_P/\Omega_1) (A_s B_\infty)$$

The power factor,  $\cos \varphi_1$ , can be found from the ratio of the powers involved. The efficiency in motoring and generating can be found by Eqs. (43-1) and (43-2). The mechanical power at the shaft cannot be found directly from the circle diagram. Instead, it is deduced from the mechanical power on the rotor:

$$P_2 = P_m - P_{f/w} - P_{ad} \text{ in motoring}$$

$$|P_2| = |P_m| + P_{f/w} + P_{ad} \text{ in generating}$$

Using the circle diagram, we can also find  $I_{1,R}$ ,  $\cos \varphi_R$ ,  $s_R$ ,  $\eta_R$ ,  $T_{em,m}$ , and  $T_{em,s}$ . Under rated conditions, when the machine is operating as a motor, point  $A_s$  coincides with point  $A_R$  chosen from the specified rated power,  $P_R = P_{2,R}$ , such that

$$A_s B_1 = P_{m,R}/c_P$$

where  $A_s \rightarrow A_R$ ,  $P_{m,R} = P_{2,R} + P_{f/w} + P_{ad}$ , and  $A_s B_1$  is the intercept of the perpendicular  $A_s B$  on the diameter.

The electromagnetic torque is a maximum,  $T_{em, m(+)}$  or  $T_{em, m(-)}$ , when point  $A_s$  coincides with point  $A_{m(+)}$  in the case of a positive slip, or with point  $A_{m(-)}$  in the case of a negative slip. At those points, the length of  $A_s B_\infty$  perpendicular to the diameter and bounded between the circle and the electromagnetic power line,  $A_0 A_\infty$ , is a maximum:

$$T_{em, m(+)} = (c_P/\Omega_1) (A_s B_\infty), \text{ where } A_s \rightarrow A_{m(+)}$$

$$T_{em, m(-)} = (c_P/\Omega_1) (A_s B_\infty), \text{ where } A_s \rightarrow A_{m(-)}$$

When point  $A_s$  coincides with point  $A_1$ , the inherent (static) starting torque can be found from

$$T_s = (c_P/\Omega_1) (A_s B_\infty), \text{ where } A_s \rightarrow A_1$$

The circle diagram can be constructed from a no-load or a short-circuit test, as either can readily be applied to an induction machine. From the circle diagram thus obtained, it is an easy matter to determine all the intermediate conditions.



The torque-speed curve of the associated load is shown in Fig. 44-1 as the  $|T_{\text{ext}}| = f(\Omega)$  curve. The shape of the curve depends on the type of driven machine. As a rule,  $|T_{\text{ext}}|$  increases with rising speed (to a greater extent in the case of fans and pumps, and to a lesser degree in the case of metal-cutting machines).

If, with the rotor at standstill ( $\Omega = 0$ ), the inherent starting torque of the motor,  $T_s$ , exceeds the torque required to put the driven machine in motion,  $|T_{\text{ext}}|$ , then, in accord with the equation of motion

$$T_{\text{em}} + T_{\text{ext}} = J \, d\Omega/dt \quad (44-1)$$

(where  $J$  is the moment of inertia of rotating parts, referred to the rotor), a positive acceleration,  $d\Omega/dt > 0$ , will be applied to the rotor, and it will begin picking up speed. This will go on until the sum of  $T_{\text{em}}$  and  $T_{\text{ext}}$ , where  $T_{\text{em}} > 0$  and  $T_{\text{ext}} < 0$ , vanishes. This will occur at point  $I$  where the two curves,  $T_{\text{em}} = f(\Omega)$  and  $|T_{\text{ext}}| = f(\Omega)$ , intersect. From that instant on, the motor will keep running at the rated electromagnetic torque,  $T_{\text{em},R}$ , and at the rated angular speed  $\Omega_R^*$ .

The starting time,  $t_s$ , can be found by integrating Eq. (44-1) graphically

$$t_s = \int_0^{\Omega_R} \frac{J \, d\Omega}{T_{\text{em}} + T_{\text{ext}}}$$

As an alternative, Eq. (44-1) may be integrated numerically, using a computer.

The starting time is found to be proportional to the shaded area under the  $J/(T_{\text{em}} + T_{\text{ext}}) = f(\Omega)$  curve. From the equation it follows that the starting time is a function of the moment of inertia  $J$  of the rotating parts and of the sum of the torques,  $T_{\text{em}} + T_{\text{ext}}$  (or their difference,  $T_{\text{em}} - |T_{\text{ext}}|$ ). Although it lasts from a split second to several seconds, an important point to remember is that at starting the primary and secondary currents,  $I_1$  and  $I_2$ , are many times the rated (full-load) current. On a per-unit basis, the static starting current is

$$I_{*s} = I_s/I_{1,R} = 5 \text{ to } 7$$

---

\* It is not always that the point of intersection of the two curves corresponds to the rated operating condition.

As is seen from Fig. 43-2, it slowly goes down as the slip increases. Therefore, should the electromagnetic torque be insufficient (and the difference  $T_{em} - |T_{ext}|$  too small), the starting time may be stretched out so that the windings may be overheated.

According to relevant Soviet standards, the ratio  $T_{em,m}/T_{em,R}$  for general-purpose industrial induction motors must be anywhere between 1.7 and 2.2, and the ratio  $T_s/T_{em,R}$  should range between 0.7 and 2.0. Also, the ratio of  $T_{min}$  (Fig. 44-1) to the rated torque must be not less than from 0.6 to 1.0. Should the minimum torque be too small, the load torque-speed curve may cut the motor torque-speed curve at point *II*. At that point, the angular speed falls below the rated value, and the motor would fail to come up sufficiently close to the synchronous speed,  $\Omega_1$ .

When "direct-on-line" starting is used for large squirrel-cage motors, the power supply, especially one of low capacity, may be adversely affected. The voltage  $V_1$  may "dip" excessively, and other loads may suffer a malfunction. In such a case, the starting current may be brought down by inserting a reactor or an autotransformer between the motor and the supply line. It should however be remembered that a decrease in  $V_1$  at starting leads to a sizeable reduction in the starting torque because it is proportional to the voltage squared. This is the reason why "direct-on-line" starting is inapplicable to squirrel-cage motors operating under severe starting conditions (when  $|T_{ext}|$  is very large).

## 44-2 Phase-Wound Induction Motors

The starting performance of a phase-wound induction motor can be improved by inserting an external resistance in the rotor circuit at starting. The starting resistance  $R_{2s}$  is connected to the rotor resistance  $R_{2,R}$  by means of slip rings and brushes. The rotor phase resistance is the sum of these two values:

$$R_{2,R} + R_{2s} = R_2$$

At starting, it is essential to bring down the static starting current

$$I_s \approx \frac{V_1}{\sqrt{(R_1 + R'_2)^2 + X_{sc}^2}}$$



and to raise the static (inherent) starting torque, Eq. (43-15):

$$T_s = \frac{m_1 R'_2 V_1^2}{\Omega [(R_1 + R'_2)^2 + X_{sc}^2]}$$

The starting torque is a maximum when the critical (or maximum) slip is

$$s_m = \frac{R'_2}{\sqrt{R_1^2 + X_{sc}^2}} = 1$$

that is, when the rotor phase resistance is

$$R'_{2m} = \sqrt{R_1^2 + X_{sc}^2} \approx X_{sc}$$

As a rule,  $R'_{2R} < R'_{2m}$ , and the insertion of an external starting resistance with  $R'_{2s} < R'_{2m} - R'_{2R}$  in the rotor circuit leads to a higher starting torque (compare the starting torques for curves 1 and 2 in Fig. 44-2). When  $R'_{2s} = R'_{2m} - R'_{2R}$  the starting torque is a maximum (curve 3).

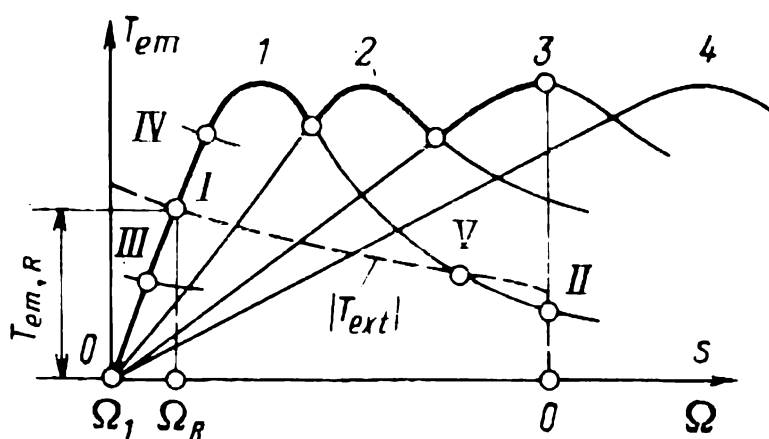


Fig. 44-2 Starting of a wound-rotor induction motor

A further increase in  $R_{2s}$  leads to a decrease in the starting torque again (curve 4). Physically, this occurs because in the range  $R'_2 < R'_{2m}$ , an increase in  $R'_2$  has a stronger effect on the electromagnetic torque than a decrease in the starting current

$$T_s \approx m_1 R'_2 I_s^2 / \Omega_1$$

If the external starting resistance can be set to several consecutive values,

$$R_{2R} = R_{2(1)} < R_{2(2)} < R_{2(3)} < R_{2(4)}$$

several torque-speed (or torque-slip) characteristics (curves 1, 2, 3) can be obtained, having all the same maximum torque, but differing in the critical slip (Fig. 44-2).

Curve 1 is the natural torque-speed characteristic. In this case, the starting resistance is brought out of circuit, and  $R_{2(1)} = R_{2R}$ . In the course of starting, the resistance is moved from step to step at the instants when the difference between the electromagnetic and load torques is a maximum.

Before a phase-wound motor is connected to a supply line, a resistance is inserted in its rotor circuit, so as to ensure a maximum starting torque (curve 3 for  $R_{2(3)}$ ). The motor begins to pick up speed, because  $T_{em} > |T_{ext}|$ . At the instant when curve 3 cuts curve 2, the starting resistance is set to  $R_{2(2)}$ , and the motor is picking up speed along curve 2. The transition to the natural torque-speed characteristic (curve 1) proceeds in a similar way. Under the steady state, the motor is running at a point on the natural torque-speed (torque-slip) curve, where  $T_{em,R}$  and  $\Omega_R$  exist.

Wound-rotor motors can be used under the more severe starting conditions than squirrel-cage machines. Unfortunately, they have to be fitted with slip-rings and brushes for the insertion of an external starting resistance, and this results in a higher manufacturing cost and a lower reliability in service.

### 44-3 Squirrel-Cage Induction Motors with Improved Starting Performance

At starting, no resistance can be inserted in a squirrel-cage rotor as this is done in wound-rotor machines. Yet, the starting performance of squirrel-cage motors can be improved in more than one way. One is to increase the effective resistance of the rotor winding by utilizing the skin effect in the bars of the squirrel-cage structure. This effect manifests itself at the beginning of starting, when the rotor current frequency,  $f_2 = sf_1$ , is close to the supply-line frequency  $f_1$ .

In order to increase the bar resistance at  $f_2 \approx 50$  Hz (see Sec. 31-2), the bar height  $h$  must substantially exceed the depth of penetration of the electromagnetic field

$$\Delta = \sqrt{2\rho/\omega_1\mu_0} = \sqrt{\rho/\pi f_1\mu_0}$$

At  $f = 50$  Hz, the penetration depth is about 10 mm for copper and 15 mm for aluminium. With  $h$  in excess of  $2\Delta$ , the effective bar resistance at  $f_2 = 50$  Hz is  $k_r = h/\Delta$  times its d.c. resistance.

**Deep-bar rotors.** For deep bars of aluminium, the height is usually chosen anywhere between 40 and 60 mm. This gives a three- or even four-fold increase in the effective a.c. resistance of the rotor winding at 50 Hz.

The leakage-flux paths for a deep-bar design are shown in Fig. 44-3. For convenience of analysis, we may think of each bar as consisting of several layers of equal cross-section with a d.c. resistance of  $R_{\text{layer}} = \rho l / q_{\text{layer}}$ . Since inductance is the number of flux linkages produced per ampere, it is obvious that the layers, or parts, of each bar extending deeper into the core have higher leakage inductances,

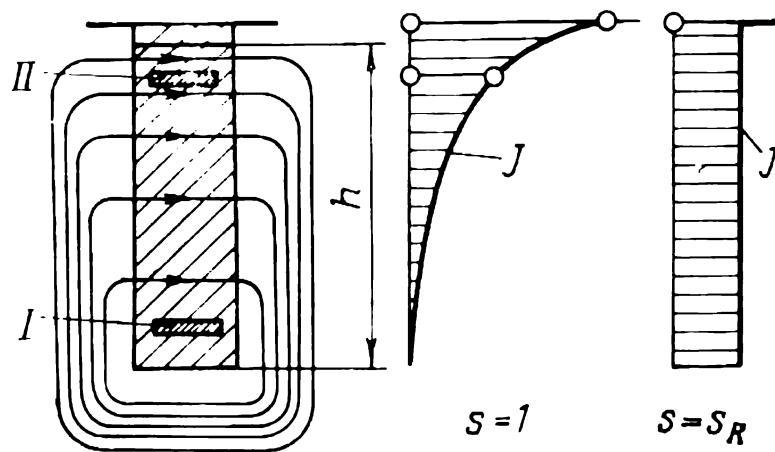


Fig. 44-3 Current density distribution in a bar of a deep-bar squirrel-cage structure

$L_{\text{layer}}$ , than the parts of the bar cross-section lying closer to the airgap. Referring to the figure, layer *I* nearer the slot bottom has a maximum  $L_{\text{layer}}$ ; layer *II* lying closer to the airgap has a minimum  $L_{\text{layer}}$ . On the other hand, the mutual field has the same flux linkage with each of the bar layers and induces in all of them the same mutual emf,  $sE_{\text{layer}}$ , where  $E_{\text{layer}}$  is the emf at  $s = 1$ . Therefore, the current density in each layer, or part, of the bar cross-section

$$J \approx \frac{sE_{\text{layer}}}{q_{\text{layer}} \sqrt{R_{\text{layer}}^2 + (2\pi s f_1 L_{\text{layer}})^2}}$$

depends on the position of a given bar layer in the slot and on the slip. At high slips ( $s \approx 1$ ),  $2\pi s f_1 L_{\text{layer}} > R_{\text{layer}}$ , and it plays an important part. In the parts near the air gap which have a lower reactance, the current density is therefore substantially higher (see the current density distribution at  $s = 1$ ). Conversely, at rated slip ( $s_R \ll 1$ ),

$$R_{\text{layer}} \gg 2\pi s f_1 L_{\text{layer}}$$

Therefore, the inductive reactance may be ignored and we may deem that the current density is the same in all the parts of the bar cross-section (see the curve for  $s = s_R$ ). At  $s_R$ , the current is uniformly distributed over the cross-section of the bar, and the effective a.c. resistance of the rotor,  $R_2$ , does not differ from its d.c. resistance,  $R_{2(1)}$ . At  $s = 1$ , the current occupies only a fraction of the total bar cross-section, and the effective resistance of the rotor rises to  $R_{2(2)}$ . The torque-slip characteristic of a deep-bar rotor machine is shown in Fig. 44-4. Curve 1 holds for a constant resistance,  $R_{2(1)}$ . Curve 2 applies to  $R_{2(2)}$  which exists at any slip. Curve 3 gives the actual torque-slip characteristic of a deep-bar motor in which the resistance of the rotor winding gradually rises from  $R_{2(1)}$  to  $R_{2(2)}$  as the slip is varied from  $s_R$  to  $s = 1$ . Most commercially available induction motors are built with deep-bar rotors.

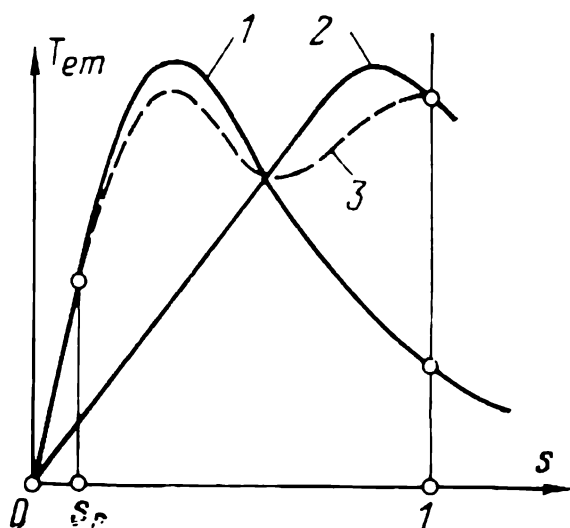


Fig. 44-4 Torque-slip characteristic of a deep-bar induction motor

**Double-cage rotors.** A double-cage rotor has two squirrel cages, with the bars of one cage lying, say, deeper in semi-closed slots than those of the other, and separated by a narrow neck (at 5 in Fig. 44-5).

A double-cage structure may be cast or brazed (welded or soldered). In the former case, the slots and necks are filled with molten aluminium, and the two cages form a single structure. In the latter case, the bars of the outer (starting) cage are usually made of a material having a high resistivity (brass or, though seldom, bronze), whereas the bars of the inner (running) cage are made of copper. Frequently, the bars in the starting cage have a smaller cross-sectional area than the bars in the running cage. This also serves to raise the effective a.c. resistance of the starting cage. The two cages may be connected to the same end rings, or there may be separate end rings for each cage.

At starting, the frequency of the current in the bars is that of the supply line and, for the same reasons as in a

deep-bar rotor, the bulk of the current is flowing in the starting cage which has a lower inductive reactance than the running cage. This leads to an increase in the effective resistance of the starting cage and, as a result, to a higher starting torque.

After the motor has come to the rated or nearly rated speed, the frequency of the rotor current falls (to a few hertz), the inductive reactance of the bars reduces to a fraction of their effective a.c. resistance, and the rotor current is shared between the two cages in inverse proportion

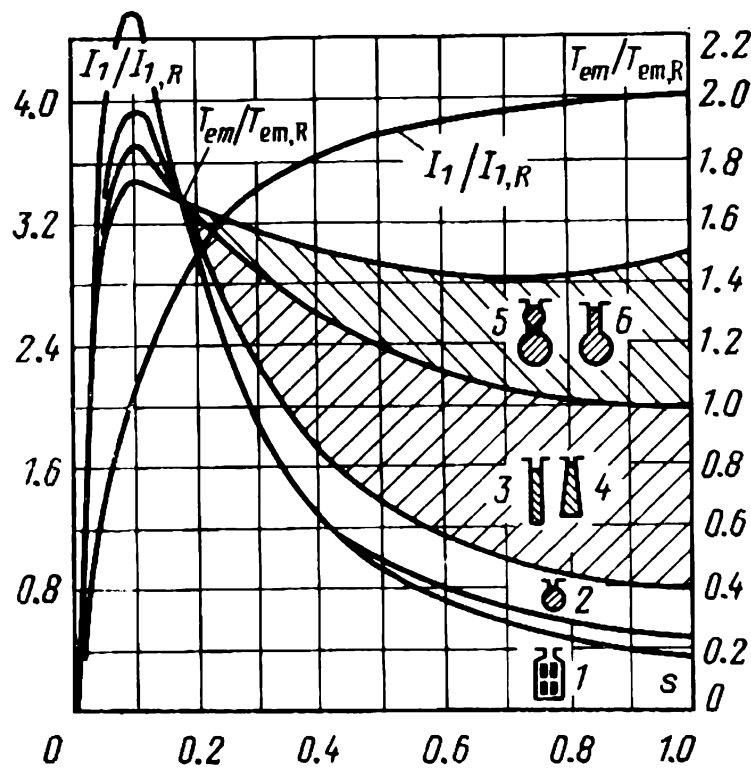


**Fig. 44-5** Torque-slip characteristics of squirrel-cage motors with improved starting performance:

1—wound-rotor motor; 2—round-bar squirrel-cage motor; 3—rectangular deep-bar squirrel-cage motor; 4—trapezoidal-bar squirrel-cage motor; 5—double-cage motor; 6—bulb-bar squirrel-cage motor

to their effective a.c. resistances. If the running cage has a lower resistance than the starting cage, the bulk of the current will be flowing in the running cage. In a cast double cage, the current density is distributed practically uniformly over the entire cross-section of the slot.

Apart from the deep-bar design (at 3 in Fig. 44-5) and the double-cage design (at 5 in the same figure), recent years have seen the advent of bell-shaped (6) and trapezoidal bars (4), especially for high-speed and high-power motors. At starting, the rotor current in copper bell-shaped bars is crowded into the narrower top part which has a higher

effective a.c. resistance, and this serves to raise the starting torque. As regards starting performance, bell-shaped-bar and double-cage rotors are about equal (see the shaded area 5-6 in Fig. 44-5). Motors with a trapezoidal-bar rotor (at 4 in Fig. 44-5) show about the same high starting performance as motors with a rectangular-bar rotor (see the shaded area 3-4).

Typical torque-slip and current-slip characteristics of motors using the various bar designs are shown in Fig. 44-5. All motors have the same power rating, the same inherent starting current, and the same rotor loss at full (rated) load. For comparison, the figure also shows the natural torque-slip characteristic (curve *I*) of a wound-rotor induction motor. The shaded areas give the ranges of improved starting performance for motors using the various bar designs. As is seen, the increase in starting torque due to the use of special bar designs is accompanied (owing to an increase in  $X_2$ , the leakage inductive reactance of the rotor) by a decrease of 15% to 25% in the maximum electromagnetic torque and a decrease of 4% to 6% in the power factor as compared with motors using a round-bar rotor.

## 45 Steady-State Performance of Induction Motors. Speed Control

### 45-1 Loading Conditions. Stability

When properly started (see Figs. 44-1 and 44-2), an induction motor must come up to a speed such that it will be running at rated (full) load (point *I*) or less than rated load (point *III* lying on the characteristic curve between the no-load point where  $T_{em} = 0$  and  $\Omega = \Omega_1$ , and the rated-torque point where  $T_{em} = T_{em,R}$  and  $\Omega = \Omega_R$ ).

For short intervals of time, the load may be such as exists at point *IV* which lies between points  $(T_{em,R}, \Omega_R)$  and  $(T_m, \Omega_m)$  at torques exceeding the rated value ( $T_{em} > T_{em,R}$ ), but lower than the maximum (breakdown or pull-out) torque ( $T_{em} < T_m$ ). How long a motor may be

allowed to run in such a condition depends on the amount of heat dissipated in the windings.

Long-term operation at the intersection of the motor and load torque-speed curves,  $T_{em} = f(\Omega)$  and  $T_{ext} = f(\Omega)$ , is permissible only if a chance departure of speed from the steady-state value produces a torque,  $T_{em} + T_{ext}$ , on the rotor which will restore the previous steady-state speed.

The condition for stable operation can be written in terms of changes in (or derivatives of) torques,  $|dT_{em}|$  and  $|dT_{ext}|$ , assuming the same departure of speed,  $d\Omega$ , from the value at the intersection of the two torque-speed curves, say, at point  $I$  in Fig. 44-1 or 44-2.

If

$$\begin{aligned} d|T_{ext}| &= \frac{d|T_{ext}|}{d\Omega} d\Omega > d|T_{em}| \\ &= \frac{d|T_{em}|}{d\Omega} d\Omega \end{aligned}$$

and, as a consequence,

$$\frac{d|T_{ext}|}{d\Omega} > \frac{d|T_{em}|}{d\Omega}$$

the operation is *stable*. If, however,

$$\frac{d|T_{ext}|}{d\Omega} < \frac{d|T_{em}|}{d\Omega}$$

the operation is *unstable*. For example, at point  $I$  where

$$\frac{d|T_{ext}|}{d\Omega} > \frac{d|T_{em}|}{d\Omega}$$

the operation is stable. Should, by any chance, the speed at point  $I$  rise to  $(\Omega_R + d\Omega)$ , the electromagnetic torque  $T_{em}$  would fall off, because

$$\frac{d|T_{em}|}{d\Omega} < 0$$

whereas the external (or load) torque  $T_{ext}$  would go up, because

$$\frac{d|T_{ext}|}{d\Omega} > 0$$

The rotor would be acted upon by a negative torque

$$T_{em} - |T_{ext}| = +d|T_{em}| - d|T_{ext}| < 0$$

and there would be a negative acceleration (deceleration) which would cause the rotor to slow down until it goes back to its previous speed,  $\Omega_R$ .

The operation will likewise be stable at point *III* or *IV* within the effective part of the torque-speed characteristic under the most commonly encountered load torques. Conversely, it can be shown that the operation at point *V* is unstable. This may happen when a sudden fall in supply voltage is followed by a sudden voltage recovery. At this point,

$$\frac{d|T_{\text{ext}}|}{d\Omega} < \frac{d|T_{\text{em}}|}{d\Omega}$$

A chance increase in speed,  $d\Omega > 0$ ,

$$T_{\text{em}} - |T_{\text{ext}}| = d|T_{\text{em}}| - d|T_{\text{ext}}| > 0$$

and there would be a positive acceleration

$$d\Omega/dt > 0$$

causing the rotor to pick up speed until a stable condition arises at point *IV* in Fig. 44-1 or at point *I* in Fig. 44-2. A chance decrease in speed,  $d\Omega < 0$ , the unstable condition at point *V* will change to a stable condition at point *II* in Fig. 44-1 or to a short-circuit ( $\Omega = 0$ ) in Fig. 44-2.

## 45-2 Performance Characteristics of an Induction Motor

An induction motor of a particular power rating may operate in actual service under loads varying from no-load to full load. Therefore, it is required that it should have a sufficiently high efficiency and power factor not only at rated load, but also at half the full load. An increase in efficiency leads to a decrease in the active power,  $P_1 = P_2/\eta$ , drawn by the motor. An improvement in the power factor cuts down the total power,  $S_1 = P_1/\cos \varphi_1$ , owing to a decrease in the reactive power,  $Q_1 = S_1 \sin \varphi_1 = P_1 \tan \varphi_1$ . In either case, there will be a decrease in the current drawn from the supply line

$$I_1 = S_1/m_1 V_1 = P_2/m_1 V_1 \eta \cos \varphi_1$$

in the capacity of the synchronous generators that must be installed at the supply power station, and in the losses



occurring in the transformers and networks conveying electricity to loads. In the final analysis, there will be a cut-down in the operating costs of the motor.

The efficiency and power factor of a motor can be improved in one of several ways. For example, we can use better magnetic materials (those with reduced specific loss

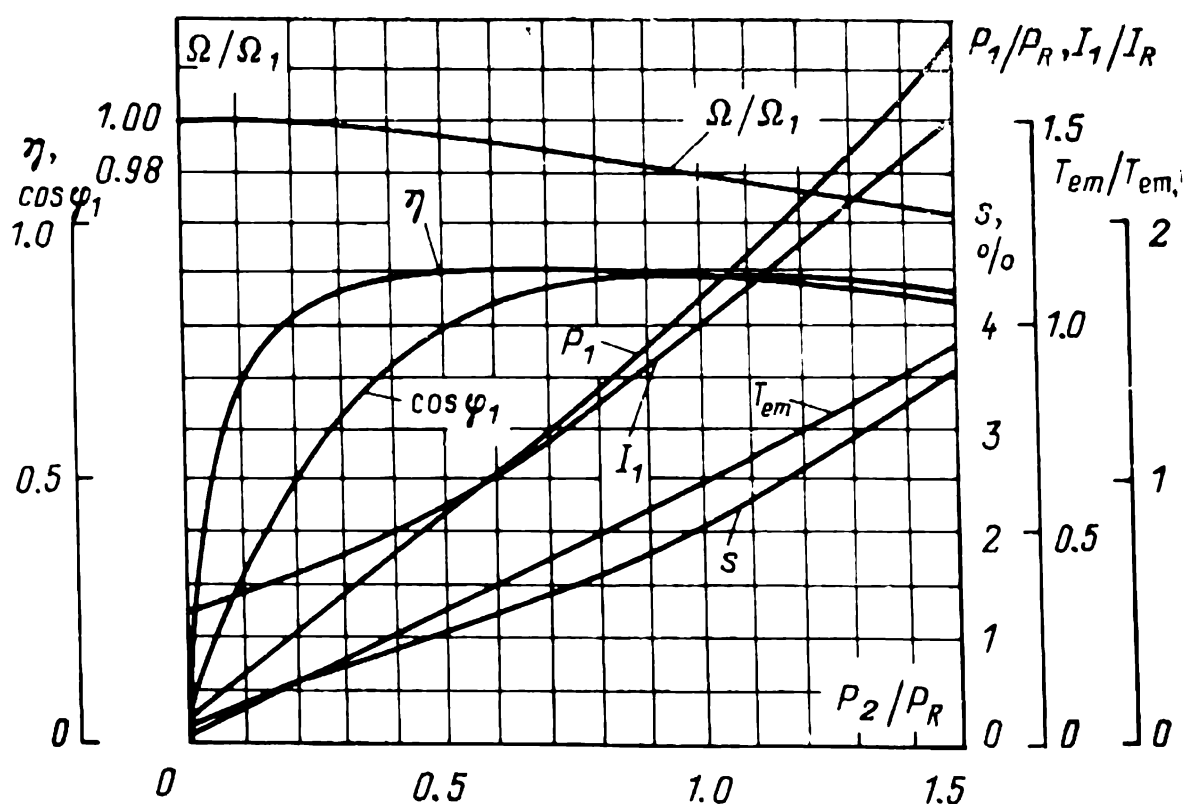


Fig. 45-1 Performance characteristics of an induction motor

and increased permeability), reduce the air gap between the stator and rotor to a permissible minimum (0.3-1.5 mm, depending on the power rating of the motor), or bring down the electromagnetic loading (current density in the windings and magnetic flux density) by scaling up the motor. Unfortunately, this would raise the manufacturing cost of the machine.

In designing an induction motor, its efficiency and power factor are most frequently adjusted through a suitable choice of materials so as to minimize the sum of the manufacturing and operating costs.

The performance of a motor under varying load conditions is usually presented in graphic form as plots of  $\eta$ ,  $\cos \varphi_1$ ,  $P_1$ ,  $T_{em}$ ,  $s$ , and  $n$  versus power output,  $P_2$ . Typical performance characteristics of an induction motor (plotted on a per-unit basis) are shown in Fig. 45-1.

The performance characteristics of a motor can be calculated, derived from the circle diagram (see Chap. 43), or obtained by experiment.

As is seen from the circle diagram (see Fig. 43-9), variations in load (represented by the mechanical power,  $P_2 \approx P_m$ ), are accompanied by variations in  $I_1$  and  $\varphi_1$ . As  $P_2$  increases, the power factor changes from  $\cos \varphi_0$  at  $I_0$  to its maximum value,  $\cos \varphi_{\max}$ , at  $I_1$  whose phasor is tangent to the circle. As a rule, the power factor is a maximum at a current close to rated (see Fig. 45-1). The rated power factor is anywhere between 0.7 and 0.9. As load goes down to about 50%, the power factor falls off by 0.1.

As in transformers (see Sec. 6-3), the efficiency is a maximum when the constant losses ( $P_c$ ,  $P_{f/w}$ ), which depend on load but little, are equal to the varying losses ( $P_{Cu1}$ ,  $P_{Cu2}$ , and  $P_{ad}$ ) which vary with load.

A motor is usually designed in such a way that the efficiency is a maximum when the actual load is less than the rated, or full, load (in Fig. 45-1,  $\eta = \eta_{\max}$  at  $P_2/P_{2,R} = 0.7$ ). If this requirement is met, the efficiency will remain nearly constant and equal for general-purpose industrial motors to 0.75-0.95 as the load varies from 50% to full.

Variations in load entail insignificant changes in the rpm of the motor, usually from  $n = n_1$  to  $n_R = n_1 (1 - s_R)$ , that is, by as few as several per cent. Such a motor is said to have a *flat* speed-power or speed-torque characteristic.

### 45-3 Methods of Speed Control

Speed control refers to a deliberate change in the rotor speed  $\Omega$  by the operator. It is presumed that speed control leaves the torque-speed or torque-slip characteristic unchanged. Because

$$\Omega = \Omega_1 (1 - s)$$

the speed can be controlled in any one of two ways, namely: (1) by varying the angular field velocity  $\Omega_1$  or (2) by varying the slip,  $s$ .

In turn, the angular field velocity defined as

$$\Omega_1 = 2\pi f_1/p$$

can be controlled by (1) change of the line frequency  $f_1$ ; (2) by change of the number of pole pairs  $p$ ; and (3) by cascade connection.

Slip control can be effected in several ways which may be classed into two groups as follows: (1) slip control by causing the slip power  $sP_{em}$  to be dissipated as heat in the rotor circuit (this can be done by varying  $V_1$ , by inserting a series resistance or series reactances in the rotor circuit), and (2) by recovering the greater part of slip power and letting only the smaller part,  $m_2 I_2^2 R_2$ , be dissipated as heat in the rotor circuit (by injecting an auxiliary slip emf into the rotor circuit by what is known as cascade connection).

#### 45-4 Speed Control by Change of Field Velocity

(a) **Speed control by change of the line frequency,  $f_1$ .** This form of speed control can be effected only if the motor draws its power from a supply with an independently controlled frequency. This purpose can be served by variable-speed synchronous generators, synchronous and induction frequency converters, gas-tube and semiconductor rectifiers.

If the motor is to retain a flat torque-slip (or torque-speed) characteristic and a sufficient overload capacity, it is essential to control both  $f_1$  and  $V_1$  so that the magnetic flux remains unchanged

$$\Phi \sim V_1/f_1 = \text{constant}$$

This requirement can be satisfied if the actual frequency is comparable in magnitude with the rated frequency.

Speed control by change of supply frequency is mostly employed for a group of identical squirrel-cage motors, such as used in roller-table drives. This form of speed control permits a wide range of change (from 10-to-1 to 12-to-1), but the cost of the scheme is relatively high.

(b) **Speed control by pole changing.** This form of speed control is effected in what are known as *multispeed induction motors*. To this end, a multispeed motor may have two stator (or rotor) windings arranged for different number of poles. As an alternative, it may have one winding with special connections, which can be reconnected simply to give two or even three different numbers of poles. The rotor is preferably of the squirrel-cage construction so that no connection change is required on the secondary.

Multispeed motors are used to drive machines where it is essential to change their speed in steps (hoists, winches, machine tools, etc.).

A single pole-changing winding is especially simple when it is arranged for the number of poles to be changed in the

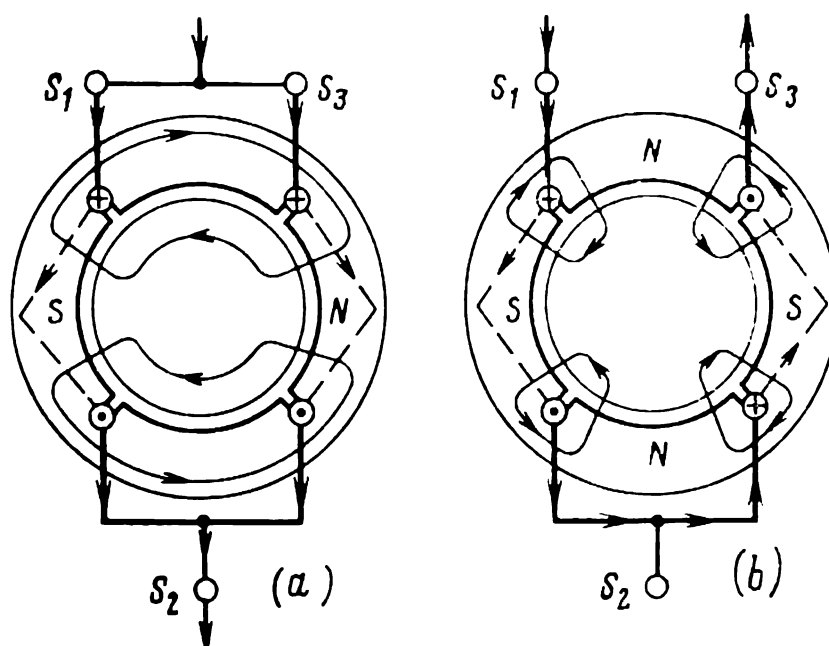


**Fig. 45-2** Pole-changing winding for two and four poles ( $2p_1 = 2$ ,  $2p_2 = 4$ )

proportion 2:1 (Fig. 45-2). The coil pitch is chosen such that with the lowest number of poles ( $2p_1$  equal to, say, 2) it is  $y = 0.5 \tau_1$ . Each phase of the winding is divided into two identical sections (Fig. 45-2 shows only one phase,  $A$ ). When the winding is switched to have the smaller number of poles ( $2p_1$ ), each phase has two parallel paths, and the adjacent coil groups in the two sections carry currents in the opposite directions (see Fig. 45-2a). When the winding is switched to have the greater number of poles ( $2p_2 = 4p_1$  equal to, say, 4), each phase has only one parallel path, and the adjacent coil groups in the two sections carry currents in the same direction (see Fig. 45-2b). The winding has a total of six phase terminal leads.

Balanced windings which can offer three, four or even two different speeds, but with the pole ratios other than 2-to-1 or 3-to-2, have a larger number of terminal leads and involve the use of more sophisticated pole-changing switches.

Although a multispeed motor has a larger size and is more expensive to make than an equivalent single-speed induction motor, speed control by pole changing is fairly wide-spread.

(c) **Cascade control.** A cascade connection of two induction machines, proposed independently by Görges and Steinmetz, is shown in Fig. 45-3.

As is seen, the cascade consists of two wound-rotor induction machines, 1 and 2, one having  $2p_1$  poles and the other,  $2p_2$  poles. The rotors of the two machines are mounted on a common shaft, and the rotor windings are interconnected

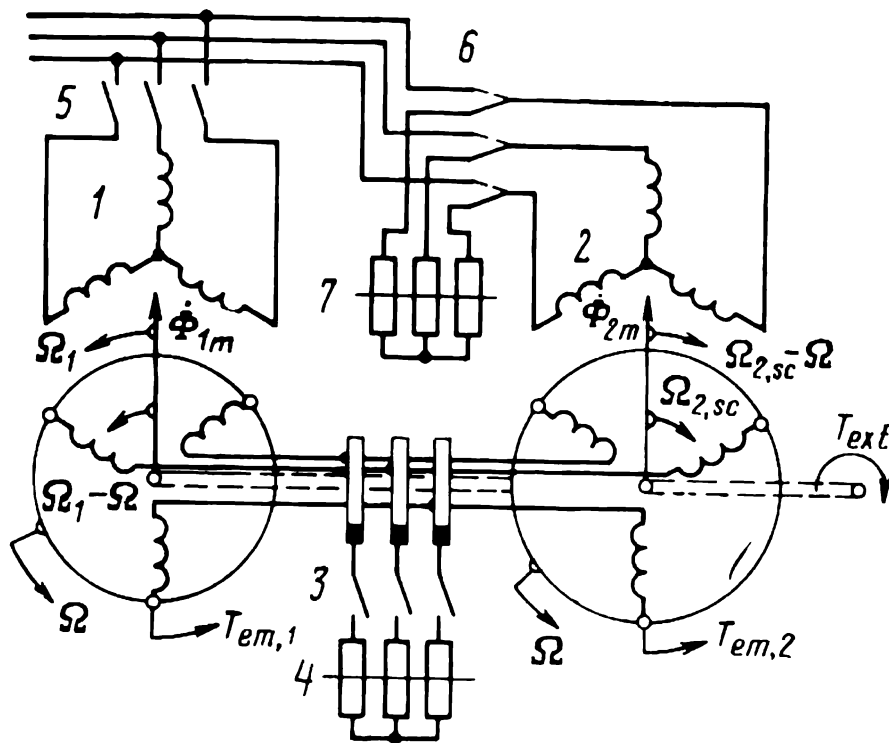


Fig. 45-3 Cascade connection of two induction machines

and brought out on slip-rings. The circuit has two contactors, 3 and 5. One serves to connect an external starting resistance 4 to the slip rings, and the other is used to connect the stator winding of motor 1 to the supply line. Using a switch 6, the operator can connect the stator winding of motor 2 to the supply line or to close it through another external resistance 7.

The scheme in Fig. 45-3 gives three different synchronous speeds of shaft rotation. When motor 1 is connected to the supply line and rheostat 4 is short-circuited upon starting, the shaft will rotate at a synchronous speed given by

$$\Omega_1 = 2\pi f_1/p_1$$

When motor 2 is connected to the supply line and rheostat 4 is shorted upon starting, the shaft will rotate at another synchronous speed given by

$$\Omega_2 = 2\pi f_1/p_2$$

(it is assumed that the external, or load, torque is zero.)

When both motors in the cascade are running at the same time, the shaft will be rotating at a synchronous speed  $\Omega_{12}$  which differs from both  $\Omega_1$  and  $\Omega_2$ . Now the stator winding of motor 1 is connected to the supply line, starting rheostat 4 is brought out of circuit, the rotor winding of motor 2 is energized from the rotor winding of motor 1, and the stator winding of motor 2 (which, in a cascade connection becomes its secondary) is shorted or closed through starting rheostat 7.

Let the shaft rotate at an angular velocity  $\Omega$ . Then the emf induced in the rotor of motor 1 will be  $E_2 s_1$  at frequency  $f_2 = s_1 f_1$ , where

$$s_1 = (\Omega_1 - \Omega)/\Omega_1$$

is the slip of the first motor, and

$$\Omega_1 = 2\pi f_1/p_1$$

is the angular velocity of the flux  $\Phi_1$  established by the stator winding of the first motor. The emf  $E_2 s_1$  gives rise to a current  $I_2$  which traverses the rotor winding of motor 2 and sets up a magnetic flux  $\Phi_2$  which rotates relative to the rotor of motor 2 at an angular velocity

$$\Omega_{2sc} = 2\pi f_2/p_2 = (\Omega_1 - \Omega) p_1/p_2$$

Since  $\Omega_{2sc}$  is directed in opposition to  $\Omega$ , the  $\Phi_2$  field rotates relative to the shorted stator winding of motor 2 at an angular velocity

$$\Omega_{2sc} - \Omega = s_2 \Omega_{2sc}$$

where  $s_2$  is the slip of the second motor.

If we investigate the last equation together with the equation for  $\Omega_{2sc}$ , the speed of the shaft in a cascade connection is found to be

$$\Omega = \frac{p_1 \Omega_1 (1 - s_2)}{p_2 + p_1 (1 - s_2)}$$

As  $T_{ext}$  is decreased,  $s_2$  goes down as well. At  $T_{ext} = 0$ , when both  $T_{em,1}$  and  $T_{em,2}$  vanish at the same time,  $s_2 = 0$ , and the shaft of the cascaded machines is rotating at a synchronous speed

$$\Omega_{12} = \Omega_{(s_2=0)} = \Omega_1 p_1 / (p_1 + p_2) = 2\pi f_1 / (p_1 + p_2)$$

In the circumstances,  $\Phi_2$  is stationary relative to stator of motor 2.

Neglecting the losses in the motors, it is an easy matter to find how the electromagnetic power

$$P_{em1} = T_{em,1}\Omega_1$$

transferred across the air gap from stator to rotor in the first motor is shared between the two motors. (Now  $s_2 = 0$ ,  $\Omega = \Omega_{12}$ , and  $s_1 = (\Omega_1 - \Omega_{12})/\Omega_1$ .)

Of the total power developed by the first motor, the fraction directly converted to mechanical power is given by

$$P_{m1} = T_{em,1}\Omega \approx T_{em,1}\Omega_{12} = P_{em1}\Omega_{12}/\Omega_1$$

The remainder, proportional to the slip of motor 1 and equal to

$$P_{em1} - P_{m1} \approx T_1 (\Omega_1 - \Omega_{12}) \approx s_1 P_{em1}$$

is transferred electrically to the rotor of motor 2 and converted to mechanical power

$$P_{m2} \approx T_{em,2}\Omega_{12} = s_1 P_{em1}$$

The electromagnetic torque of the two cascaded motors is

$$T_{em} = T_{em,1} + T_{em,2}$$

where

$$T_{em,1} = P_{em1}/\Omega_1$$

and

$$T_{em,2} = T_{em,1}s_1/(1 - s_1)$$

The reactive power required to magnetize the motors in cascade has to be drawn from the supply line. Because of this, the power factor of the cascade is reduced. Also, since the motor windings are connected in series, the short-circuit impedance of the combination is doubled, and its maximum (breakdown or pull-out) torque is reduced.

## 45-5 Speed Control without Slip Power Recovery

As we have seen, speed control in the case of squirrel-cage motors can only be based on variations in the amplitude or symmetry of the supply voltage  $V_1$  (see subsections “a” and “b” below). In the case of wound-rotor motors, speed control can also be effected by inserting additional resistances in the rotor circuit (see subsection “c” below). Speed control by slip control in cases where the slip power,  $sP_{em}$ , is not converted to mechanical power, but is dissipated as

heat in the rotor circuit, is wasteful of power and results in a low efficiency. At sufficiently large slips, the  $sP_{em}$  loss dominates the other losses in the machine, and its efficiency is

$$\eta = P_m/P_1 \approx (P_{em} - sP_{em})/P_{em} = 1 - s$$

**(a) Speed control by variation of the primary voltage.** The electromagnetic torque of an induction motor is proportional to the primary voltage squared:

$$T_{em} \sim V_1^2$$

(see Sec. 43-3). Therefore, a change in  $V_1$  brings about a marked change in the torque-slip characteristic of the motor. If we arrange so that the load torque remains unchanged, this will lead to a change in the slip. So long as the load torque remains constant, the slip will vary in inverse proportion to the primary voltage squared:

$$s \sim 1/V_1^2$$

Referring to Fig. 45-4, it is seen that  $V_{1R}$ ,  $0.85V_{1R}$  and  $0.7V_{1R}$  respectively correspond to  $s_1$ ,  $s_2$ , and  $s_3$ .

Unfortunately, speed control by primary voltage change suffers from several drawbacks, namely the overload capacity of the motor is reduced; as the slip is varied from  $s = 0$  to  $s = s_m$ , the speed can be controlled within narrow limits; the rotor copper loss,  $P_{cu2} = sP_{em} = sT_{em}\Omega_1$ , is increased. This form of speed control is mainly used on motors with a low power output and an increased maximum slip.

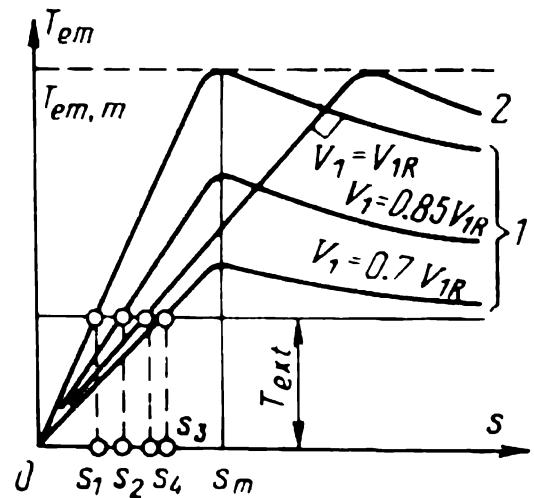


Fig. 45-4 Torque-slip characteristics with speed control: 1 — by change of  $V_1$ ; 2 — by insertion of resistance in the rotor circuit

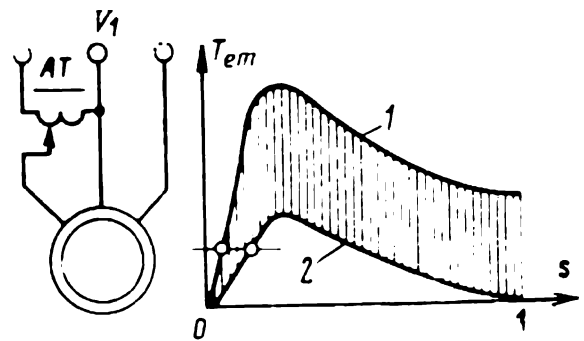


Fig. 45-5 Speed control of a three-phase induction motor by change of symmetry of the stator voltage:

1 — torque-slip characteristic with a balanced set of primary voltages; 2 — same with single-phase supply voltage



**(b) Speed control by change of symmetry of the primary voltage.** When the stator winding is supplied with an unbalanced set of voltages, the magnetic field in the motor may be visualized as consisting of two fields rotating at the same speed, but in opposite directions, and having, in the general case, different peak values. The total torque of the motor is determined by the difference in torques between the forward and reverse fields. The torque-slip characteristics of a three-phase induction motor supplied with an unbalanced set of primary voltages lie between the normal characteristic obtained when the supply is a balanced set of voltages, and the characteristic obtained with a single-phase supply (Fig. 45-5). A change in the relative magnitudes of the PPS and NPS voltages leads to a change in the torque-slip characteristic and, as a consequence, in the slip of the motor.

**(c) Speed control by change of resistance in the rotor circuit.** An increase in the rotor circuit resistance,  $R_2$ , brings about a change in the torque-slip characteristic of the motor. More specifically, the maximum slip  $s_m$  increases (see Sec. 43-3), whereas the maximum (breakdown or pull-out) torque remains unchanged; the net result is that the torque-slip characteristic is drooping rather than flat.

Referring to Fig. 45-4, it is seen that the insertion of an added resistance  $R_\Delta$  in the rotor circuit causes the torque-slip characteristic (curve 2) to change. At a constant electromagnetic torque, this causes the slip to rise from  $s_1$  to  $s_4$ .

In the case of speed control by change of resistance in the rotor circuit, the rotor circuit loss,  $sP_{em}$ , is shared between the motor and the adjusting rheostat in proportion to their resistances. At large slips when  $R_2 \approx R_\Delta$ , this loss is mainly dissipated in the rheostat (it is equal to  $sP_{em}R_\Delta/R_2$ ). If speed control is effected with  $T_{em}$  and  $I_2$  held constant, the loss in the rotor winding will remain constant.

## 45-6 Speed Control with Slip-Power Recovery

In this speed control scheme, an additional emf,  $E_\Delta$ , is injected into the rotor circuit via the slip rings. This injected emf has the same frequency,  $f_2 = sf_1$ , as the rotational emf,  $sE_2$ , in the rotor. The source of  $E_\Delta$  may be a rotary converter or an SCR circuit (see Sec. 68-4).

In the general case,  $\dot{E}_\Delta$  may be oriented relative to  $\dot{E}_2$  in any arbitrary manner, and it may be visualized as consisting of two terms

$$\dot{E}_\Delta = \dot{E}'_\Delta + \dot{E}''_\Delta = k'_\Delta \dot{E}_2 + jk''_\Delta \dot{E}_2$$

The magnitudes of the complex coefficients  $k'_\Delta$  and  $jk''_\Delta$  are the relative values of  $E'_\Delta$  and  $E''_\Delta$ ; their arguments define the phases of  $E'_\Delta$  and  $E''_\Delta$  relative to  $\dot{E}_2$ .

The injection, into the rotor circuit, of  $\dot{E}_\Delta = \dot{E}'_\Delta = k'_\Delta \dot{E}_2$  which is in phase with  $\dot{E}_2$  when  $k'_\Delta > 0$  and in anti-phase with  $\dot{E}_2$  when  $k'_\Delta < 0$ , offers an economical method of controlling the rotor speed gradually and over a wide range on either side of the synchronous speed. Suppose that prior to the injection of  $\dot{E}_\Delta$  in the rotor circuit, the slip was  $s_1 > 0$  and the emf induced in the rotor winding was  $s_1 \dot{E}_2$  (Fig. 45-6a). Assuming for simplicity that the slips are small and  $R_2 \gg sX_2$ , we may write

$$Z_2 = \sqrt{R_2^2 + (sX_2)^2} \approx R_2; \quad \tan \beta_2 = sX_2/R_2 \approx 0;$$

$$I_2 = s_1 E_2 / Z_2 = s_1 E_2 / R_2$$

and write the original electromagnetic torque given by Eq. (42-9) as

$$\begin{aligned} T_{\text{em}, 1} &= \frac{pm_2 w_2 k_{w2} \Phi_m}{\sqrt{2}} I_2 \cos \beta_2 \\ &= C_T \Phi_m s_1 E_2 / R_2 = C_T \Phi_m I_2 = T_{\text{ext}} \end{aligned}$$

After  $\dot{E}_\Delta$  has been injected, the electromagnetic torque can be expressed in terms of the resultant emf

$$s_2 \dot{E}_2 + \Delta \dot{E} = \dot{E}_2 (s_2 + k'_\Delta)$$

as

$$T_{\text{em}, 2} = C_T \Phi_m \frac{E_2 (s_2 + k'_\Delta)}{R_2} = C_T \Phi_m I_2$$

Also, if the load torque,  $T_{\text{ext}}$ , remains unchanged, the electromagnetic torque will likewise remain as it was before:

$$T_{\text{em}, 2} = T_{\text{em}, 1} = T_{\text{ext}}$$

The secondary current,  $I_2$ , will also remain unchanged, and a new operating condition will arise with

$$s_2 = s_1 - k'_\Delta$$

If  $s_1 > k'_\Delta > 0$ , the new slip will lie in the range

$$0 < s_2 < s_1$$

If  $k'_\Delta > s_1 > 0$ , the slip will become negative,  $s_2 < 0$

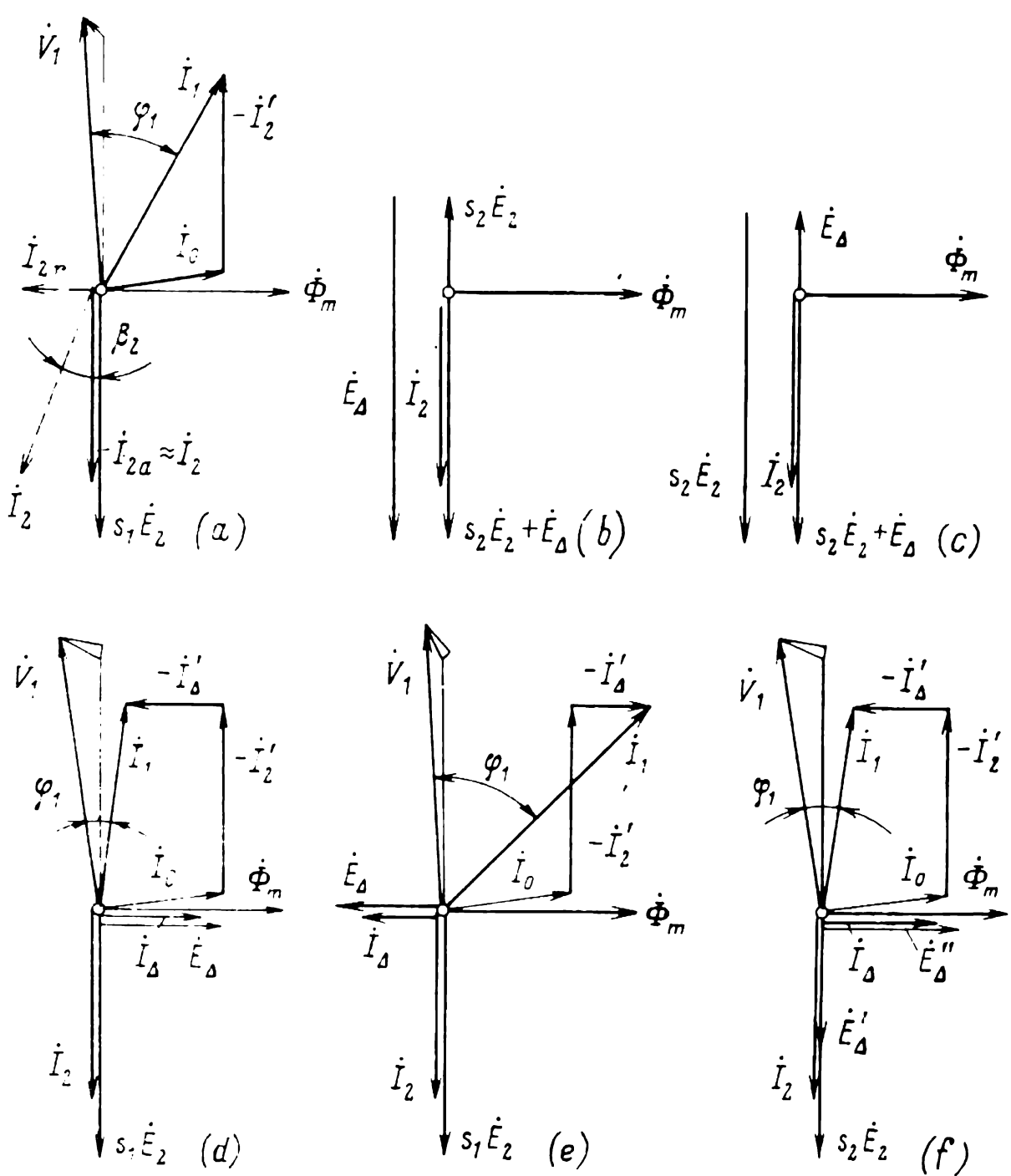


Fig. 45-6 The effect of an injected emf in the rotor circuit on slip and reactive currents

(Fig. 45-6b). Conversely, when  $k'_\Delta < 0$ , the slip will increase,  $s_2 > s_1 > 0$  (Fig. 45-6c).

The injection of  $\dot{E}_\Delta = \dot{E}_\Delta'' = jk_\Delta'' \dot{E}_2$ , which is turned through  $\pm\pi/2$  relative to  $\dot{E}_2$ , gives rise to an additional reactive current which can be found on the same assumptions:

$$\dot{I}_\Delta \approx \dot{E}_\Delta / R_2 = jk_\Delta'' (\dot{E}_2 / R_2)$$

When  $k_\Delta'' > 0$ ,  $\dot{I}_\Delta$  leads  $\dot{E}_2$  by  $\pi/2$  and contributes to  $\Phi$  as part of the magnetizing current  $\dot{I}_0$ . This results in a decrease in the reactive component of  $\dot{I}_1$  and in the phase angle  $\varphi_1$  (Fig. 45-6d). Conversely, when  $k_\Delta'' < 0$ ,  $\dot{I}_\Delta$  lags behind  $\dot{E}_2$ , and this results in an increase in the reactive component of  $\dot{I}_1$  and in the phase angle  $\varphi_1$  (Fig. 45-6e). If, at  $k_\Delta'' > 0$ , the current  $\dot{I}_\Delta'$  is equal to the magnetizing current  $\dot{I}_0$ , the rotating field will completely be set up by  $\dot{I}_\Delta$  flowing in the rotor winding, and there will be no magnetizing current flowing in the stator winding.

It is to be noted that at  $s < 1$  the reactive power required to set up the field on the rotor side,

$$P_{2r} = m_1 I_\Delta' E_2' s = m_1 I_0 E_1 s$$

is smaller than the reactive power required to set up the field on the stator side

$$P_{2r} \ll P_{1r} = m_1 I_0 E_1$$

Accordingly, a smaller reactive-power source will be required to excite the machine from the rotor than from the stator side.

If  $\dot{E}_\Delta$  contains both  $\dot{E}_\Delta' = k_\Delta' \dot{E}_2$  and  $\dot{E}_\Delta'' = jk_\Delta'' \dot{E}_2$ , then, on the assumptions made, each will act independently of the other. More specifically, at a constant torque,  $\dot{E}_\Delta'$  will cause a change in the slip, and  $\dot{E}_\Delta''$  in the angle  $\varphi_1$ . The phasor diagram applicable to the injection of such an emf,  $\dot{E}_\Delta$ , at  $s_1 > k_\Delta' > 0$  and  $k_\Delta'' > 0$  is shown in Fig. 45-6f.

If the injection of an emf is accompanied by a noticeable change in the rpm and the assumption that  $R_2 \gg sX_2$  cannot be adopted, then the rotor current in the initial

state and its active and reactive components will be

$$\begin{aligned}\dot{I}_{21} &= \dot{E}_2 s_1 / (R_2 + jX_2 s_1) \\ \dot{I}_{21a} &= \dot{E}_2 s_1 R_2 / (R_2^2 + s_1^2 X_2^2) \\ \dot{I}_{21r} &= -j \dot{E}_2 s_1^2 X_2^2 / (R_2^2 + s_1^2 X_2^2)\end{aligned}$$

Upon the injection of  $\dot{E}_\Delta = \dot{E}_2 (k'_\Delta + jk''_\Delta)$  will be

$$\begin{aligned}\dot{I}_{22} &= \dot{E}_2 [(s_2 + k'_\Delta) + jk''_\Delta] / (R_2 + jX_2 s_2) \\ \dot{I}_{22a} &= \dot{E}_2 [(s_2 + k'_\Delta) R_2 + k''_\Delta X_2 s_2] / (R_2^2 + s_2^2 X_2^2) \\ \dot{I}_{22r} &= j \dot{E}_2 [k''_\Delta R_2 - (s_2 + k'_\Delta) X_2 s_2] / (R_2^2 + s_2^2 X_2^2)\end{aligned}$$

Assuming, as we did in the approximate analysis, that the external torque and the electromagnetic torque remain unchanged

$$T_{\text{ext}} = T_{\text{em},1} = C_T \Phi_m I_{21a} = T_{\text{em},2} = C_T \Phi_m I_{22a}$$

we can see that the active components of current will also remain unchanged,  $\dot{I}_{21a} = \dot{I}_{22a}$ . On expressing the currents in terms of  $s_1$  and  $s_2$  and solving the equation thus obtained

$$a_\Delta s_2^2 - b_\Delta s_2 + c_\Delta = 0$$

we get

$$s_2 = \frac{+b_\Delta \pm \sqrt{b_\Delta^2 - 4a_\Delta c_\Delta}}{2a_\Delta}$$

where  $a_\Delta = s_1 \tan^2 \beta_2$

$$\tan \beta_2 = X_2 / R_2$$

$$b_\Delta = (1 + k''_\Delta \tan \beta_2) (1 + s_1^2 \tan^2 \beta_2)$$

$$c_\Delta = s_1 - k'_\Delta (1 + s_1^2 \tan^2 \beta_2)$$

At  $X_2 \ll R_2$  and  $\tan \beta_2 = 0$ , when  $a_\Delta = 0$ ,  $b_\Delta = 1$ , and  $c_\Delta = s_1 - k'_\Delta$ , the equation for  $s_2$  is the same as the approximate equation.

In the general case,  $s_2$  depends on both the active component of the injected emf,  $\dot{E}'_\Delta = k'_\Delta \dot{E}_2$ , and (though to a lesser degree) its reactive component,  $\dot{E}''_\Delta = jk''_\Delta \dot{E}_2$ . The added reactive component of current

$$\dot{I}_\Delta = \dot{I}_{22r} - \dot{I}_{21r}$$

is likewise, in the final analysis, dependent on  $\dot{E}''_\Delta$  and (although, to a lesser degree) on  $\dot{E}'_\Delta$ .

## ☆ 46 Unbalanced Operation of Induction Machines

### 46-1 Unbalanced Operation due to Unbalanced Primary Voltages

In unbalanced operation, the currents appearing in the stator or rotor phases of an induction machine are different in magnitude and displaced from one another by a different electrical angle. In the case of symmetrical polyphase windings on the rotor and stator, current unbalance may be caused by any one of two factors: (1) the primary voltage system applied to the machine is unbalanced or (2) the impedances closing the rotor winding are unbalanced.

We shall begin our discussion by considering first the unbalanced operation caused by an unbalanced system of primary voltages. We shall do this, using the method of symmetrical components.

If the star-connected neutral points of the stator winding are isolated, no ZPS currents or voltages will be produced, and the unbalanced system of primary voltages ( $\dot{V}_{A1}$ ,  $\dot{V}_{B1}$ ,  $\dot{V}_{C1}$ ) may be visualized as the sum of PPS voltages ( $\dot{V}_{A11}$ ,  $\dot{V}_{B11}$ ,  $\dot{V}_{C11}$ ) and of NPS voltages ( $\dot{V}_{A12}$ ,  $\dot{V}_{B12}$ ,  $\dot{V}_{C12}$ ) such that

$$\begin{aligned}\dot{V}_{A11} &= \dot{V}_{11} = (\dot{V}_{A1} + \dot{V}_{B1}a + \dot{V}_{C1}a^2)/3 \\ \dot{V}_{A12} &= \dot{V}_{12} = (\dot{V}_{A1} + \dot{V}_{B1}a^2 + \dot{V}_{C1}a)/3\end{aligned}$$

where

$$a = \exp(j2\pi/3)$$

Then the currents in the stator winding may be written as the sum of PPS currents ( $\dot{I}_{A11} = \dot{I}_{11}$ ,  $\dot{I}_{B11}$ ,  $\dot{I}_{C11}$ ) and of NPS currents ( $\dot{I}_{A12} = \dot{I}_{12}$ ,  $\dot{I}_{B12}$ ,  $\dot{I}_{C12}$ ), respectively produced by the balanced sets of PPS and NPS voltages.

The PPS current  $\dot{I}_{11}$  in the main stator phase (phase A) can be found by reference to the usual equivalent circuit of an induction machine (see Sec. 42-4). For convenience, it is repeated in Fig. 46-1a, with the notation adopted for the PPS quantities. The rotor slip relative to the PPS field

is given by

$$s_1 = (\Omega_1 - \Omega)/\Omega_1$$

where  $\Omega_1$  is the angular velocity of the PPS field, and  $\Omega$  is the angular velocity of the rotor. Therefore, the PPS current will be

$$\dot{I}_{11} = \dot{V}_{11}/Z_{11}$$

where

$$Z_{11} = (R_1 + jX_1) + (Z_0^{-1} + Z_{21}^{-1})^{-1}$$

is the impedance of the stator phase for the PPS currents (see Fig. 46-1a), and

$$Z_{21} = R'_2/s + jX'_2$$

is the impedance of the equivalent rotor at standstill for the PPS currents.

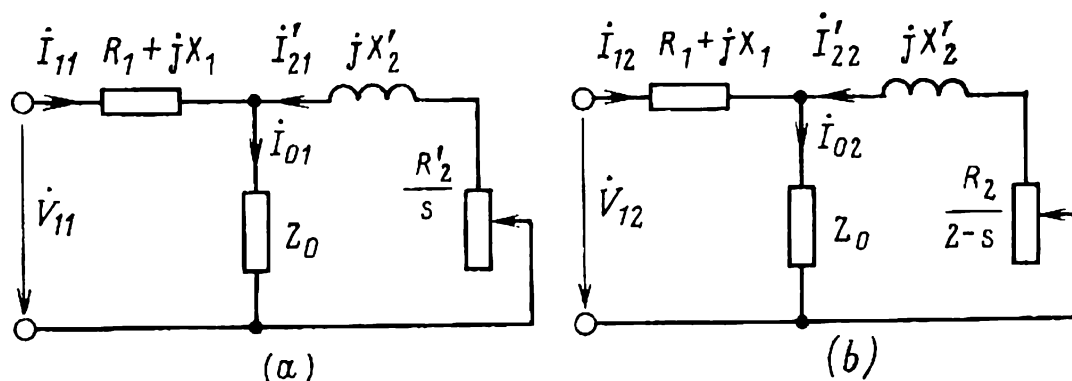


Fig. 46-1 Equivalent circuits of an induction machine for (a) positive sequence and (b) negative sequence voltages

The NPS current  $\dot{I}_{12}$  in the main stator phase can be found from the equivalent circuit shown in Fig. 46-1b, which differs from that for PPS currents only in that it is extended to include the rotor slip relative to the NPS field

$$s_2 = (-\Omega_1 - \Omega)/(-\Omega_1) = 2 - s$$

where  $(-\Omega_1)$  is the angular velocity of the NPS field, and  $\Omega = \Omega_1(1 - s)$  is the angular velocity of the rotor expressed in terms of the slip relative to the PPS field. Therefore, the NPS current is given by

$$\dot{I}_{12} = \dot{V}_{12}/Z_{12}$$

where

$$Z_{12} = (R_1 + jX_1) + (Z_0^{-1} + Z_{22}^{-1})^{-1}$$

is the impedance that the stator phase offers to the NPS currents (Fig. 46-1*b*), and

$$Z_{22} = R'_2/(2 - s) + jX'_2$$

is the impedance of the equivalent rotor at standstill to the NPS currents.

In calculating  $R'_2$  and  $X'_2$  for NPS currents in the rotor, it is important to remember that their frequency,  $f_{22} = (2 - s)f_1$ , is many times the frequency of PPS currents in the rotor,  $f_{21} = sf_1$ , and also to allow for the crowding of current in the rotor conductors (see Sec. 44-3).

Referring to the equivalent circuits of Fig. 46-1, we can find PPS and NPS currents  $\dot{I}_{11}$  and  $\dot{I}_{12}$  in phase *A* and also the total current in each stator phase:

$$\dot{I}_{A1} = \dot{I}_{11} + \dot{I}_{12}$$

$$\dot{I}_{B1} = \dot{I}_{11}a^2 + \dot{I}_{12}a$$

$$\dot{I}_{C1} = \dot{I}_{11}a + \dot{I}_{12}a^2$$

The current unbalance is caused by the injection of an NPS current. The degree of unbalance can be judged from the magnitude of the ratio  $I_{12}/I_{11}$ . If the voltage unbalance is insignificant ( $V_{12}/V_{11} \ll 1$ ), the PPS voltage is at its rated value ( $V_{11} = V_{1R}$ ), and the slip is small ( $|s| \ll 1$ ), which is typical of the generator or motor modes of operation at full load, the current unbalance,  $I_{12}/I_{11}$ , can readily be expressed in terms of the voltage unbalance,  $V_{12}/V_{11}$ . In the circumstances, the machine is operating in the braking region relative to the NPS field, because the rotor slip relative to that field,  $s_2 = 2 - s \approx 2$ , ranges anywhere between 1 and 2. At  $s_2 \approx 2$ , the equivalent circuit for NPS currents in Fig. 46-1*b* may be simplified in the same way as for operation on short-circuit, when  $s = 1$ . Since

$$|R'_2/2 + jX'_2| \ll |Z_0|$$

the resistive and reactive components of the impedance to the NPS current

$$Z_{12} = R_{12} + jX_{12}$$

may be written

$$X_{12} \approx X_1 + X'_2 \approx X_{sc}$$

$$R_{12} = R_1 + R'_2/s < R_{sc} \ll X_{sc}$$



In view of the foregoing, the NPS current at  $s \approx 2$  is given by

$$I_{12} = V_{12} / \sqrt{R_{12}^2 + X_{12}^2} \approx V_{12} / X_{sc}$$

Because  $X_{12} \approx X_{sc}$  is small,  $I_{12}$  may be very heavy even at a relatively small value of  $V_{12}$ .

Since the positive sequence impedance is substantially higher than the negative sequence impedance,

$$|Z_{11}| \gg |Z_{12}|$$

the current unbalance,  $I_{12}/I_{11}$ , is many times the voltage unbalance,  $V_{12}/V_{11}$ . For example, under the rated conditions for the positive sequence quantities, that is, at  $s = s_R$ ,  $V_{11} = V_{1R}$ ,  $I_{11} = I_{1R} = V_{1R}/|Z_{11R}|$ , the current unbalance is

$$\begin{aligned} I_{12}/I_{11} &= (V_{12}/|Z_{12}|) (|Z_{11R}|/V_{11}) \\ &\approx (V_{12} |Z_{11R}|)/V_{11} X_{sc} = V_{12}/V_{11} X_{*sc} \end{aligned}$$

where

$$X_{*sc} = X_{sc}/|Z_{11R}| = X_{sc} I_{1R}/V_{1R}$$

is the per-unit short-circuit reactance. Thus, the current unbalance is about  $1/X_{sc}$  times as great as the voltage unbalance. At the usually encountered value of  $X_{*sc} = 0.2$ , it is about five times as great.

Accordingly, supply lines for induction machines are to meet especially stringent requirements as regards voltage balance. If we take the temperature rise of the most loaded phase as a yardstick, the limit of current unbalance will be

$$I_{12}/I_{11} = 0.2$$

Then the per-unit current in one of the phases may be 1.2, and the losses may be 1.44, so that the limit of voltage unbalance will be

$$V_{12}/V_{11} = (I_{12}/I_{11}) X_{*sc} = 0.2 \times 0.2 = 0.04$$

Under voltage unbalance conditions, the total electromagnetic torque  $T_{em}$  is the sum of  $T_{em,1}$  due to the PPS voltage and  $T_{em,2}$  due to the NPS voltage, that is,

$$T_{em} = T_{em,1} + T_{em,2}$$

where

$$T_{em,1} = \frac{m_1 V_{11}^2 R_2'}{s \Omega_1 [(R_1 + R_2'/s)^2 + X_{sc}^2]}$$

and

$$T_{em,2} = \frac{m_1 V_{12}^2 R'_2}{(s-2) \Omega_1 \left[ \left( R_1 + \frac{R'_2}{2-s} \right)^2 + X_{sc}^2 \right]}$$

In the motor mode of operation, when  $0 < s < 1$ ,  $T_{em,1} > 0$  and  $T_{em,2} < 0$ . To retain the same resultant torque under voltage unbalance,  $T_{em,1}$  must be increased by  $|T_{em,2}|$ . This leads to an increase in the slip (about  $|T_{em,2}|/T_{em,1}$  times), increased losses, a higher temperature rise, and a reduced efficiency.

### ☆ 46-2 Unbalanced Impedances in the Rotor Winding Phases

The unbalance of impedances in the phases of a balanced rotor winding may arise under various service conditions. In slip-ring (wound-rotor) induction motors, this may be

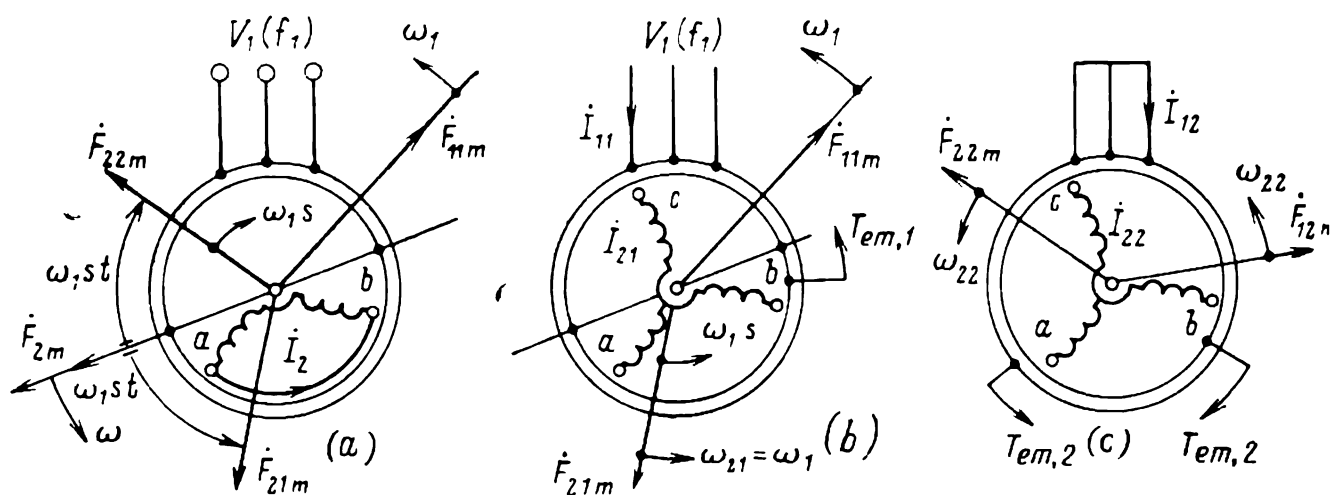


Fig. 46-2 MMFs in the case of an open-circuited rotor phase:

(a) pulsating rotor mmf and its resolution into forward and backward mmf waves; (b) stator and rotor mmfs setting up a positive-sequence field; (c) stator and rotor mmfs setting up a negative-sequence field

caused by the difference in starting resistance between the various phases. In squirrel-cage induction motors, impedance unbalance may arise from poor workmanship in, say, the squirrel-cage structure (the reduced cross-sectional area of some bars or a complete open-circuit due to poor casting).

Impedance unbalance is most noticeable when one of the phases is open-circuited (say, phase  $c$  in a star-connected three-phase winding). In such a case, the remaining phases,  $a$  and  $b$ , carrying a common current,  $\dot{I}_{a2} = -\dot{I}_{b2}$ , form in effect a single-phase winding (Fig. 46-2a).

In such a winding,  $\dot{I}_{a2}$  establishes a pulsating mmf,  $\dot{F}_2$ . The axis of this mmf is oriented relative to the winding as shown in the diagram, and rotates at the rotor angular velocity,  $\omega = \omega_1 (1 - s)$ . The frequency of the pulsating mmf is the same as that of  $\dot{I}_{a2}$ , and is equal to

$$f_2 = sf_1$$

where  $f_1$  is the frequency of the supply line to which the stator winding is connected.

The events taking place when phase  $c$  is open-circuited can best be analyzed, using the method of symmetrical components. Because the neutral point of the rotor winding is not brought out, there is no ZPS current flowing,  $\dot{I}_{20} = 0$ . Nor is there any current flowing in the open-circuited phase  $c$ :

$$\dot{I}_{c2} = \dot{I}_{c21} + \dot{I}_{c22} = 0$$

Hence, the positive and negative sequence currents in that phase are equal in magnitude, but opposite in direction

$$\dot{I}_{c21} = -\dot{I}_{c22}$$

where  $\dot{I}_{c21} = \dot{I}_{21}$  is the positive sequence current in the three-phase rotor winding, and  $\dot{I}_{c22} = \dot{I}_{22}$  is the negative sequence current in the same winding.

In terms of positive and negative sequence currents, the currents in phases  $a$  and  $b$  may be written

$$\begin{aligned}\dot{I}_{a2} &= \dot{I}_{a22} + \dot{I}_{a21} = +a\dot{I}_{22} + a^2\dot{I}_{21} \\ &= \dot{I}_{21} \sqrt{3} \exp(-j\pi/2) \\ \dot{I}_{b2} &= \dot{I}_{b22} + \dot{I}_{b21} = a^2\dot{I}_{22} + a\dot{I}_{21} \\ &= -\dot{I}_{21} \sqrt{3} \exp(-j\pi/2)\end{aligned}$$

As is seen, they are equal in magnitude, but opposite in direction (the positive direction of current flow is assumed to be from the finish to the start of the phase):

$$\dot{I}_2 = \dot{I}_{a2} = -\dot{I}_{b2}$$

The pulsating rotor mmf,  $\dot{F}_2$ , may be visualized as the sum of two rotating mmfs, namely  $\dot{F}_{21m}$  due to the positive sequence currents,  $\dot{I}_{21}$ , travelling with and relative to the rotor at an angular velocity  $\omega_1 s$ , and  $\dot{F}_{22m}$  due to the negative sequence currents, travelling at  $\omega_1 s$ , but against the rotor.

The magnetic field in the machine may be treated as the sum of the fields associated, respectively, with the positive and negative sequence currents in the rotor. The synchronous field rotating at synchronous velocity  $\omega_1$  is produced by the joint action of two mmfs, namely the stator mmf  $\dot{F}_{11m}$  which is associated with the stator currents  $\dot{I}_{11}$  at line frequency  $f_1$  and  $\dot{F}_{21m}$  associated with the positive sequence currents in the rotor and rotating relative to the stator at

$$\omega_{21} = \omega + \omega_1 s = \omega_1$$

The generation of the synchronous field is illustrated in Fig. 46-2b. At any slip, the total mmf,  $\dot{F}_{11m} + \dot{F}_{21m}$ , is such that the resultant flux is proportional to the primary (supply line) voltage,  $V_1$ . The interaction of this field with  $\dot{I}_{21}$  produces an electromagnetic torque,  $T_{em,1}$ , which, in motoring, acts on the rotor in the same direction as it rotates. The rotor mmf,  $\dot{F}_{22m}$ , due to  $\dot{I}_{22}$  travels relative to the stator at  $\omega_{22} = \omega - \omega_1 s = (1 - 2s) \omega_1$ .

The field set up by the rotor mmf induces in the stator winding an emf at

$$f_{22} = \omega_{22}/2\pi = f_1 (1 - 2s)$$

For this emf, the stator winding may be taken as closed by the infinitesimal resistance of the supply line. Therefore, the currents  $\dot{I}_{22}$  flowing in the rotor winding (which acts as the primary for them) give rise to currents  $\dot{I}_{12}$  at frequency  $f_{22}$  in the stator winding (acting as a secondary) connected across the supply line. These currents produce an mmf,  $\dot{F}_{12m}$ , which contributes to the production of a magnetic field revolving at  $\omega_{22}$ .

The production of the backward field rotating at  $\omega_{22}$  is illustrated in Fig. 46-2c. The interaction of this field with

$\dot{I}_{12}$  produces a torque,  $T_{em,2}$ , acting on the stator in the same direction as  $\dot{F}_{22m}$  rotates. A similar torque,  $T_{em,2}$ , acts on the rotor in the opposite direction.

The extent to which  $T_{em,2}$  can manifest itself depends on the value of slip. At  $1 \geq s > 0.5$ , the rotation of  $\dot{F}_{22m}$  is in the negative direction ( $\omega_{22} < 0$ ), and  $T_{em,2}$  aids in rotating the rotor much as  $T_{em,1}$  does. At  $0.5 > s > 0$ , the rotation of  $\dot{F}_{22m}$  is in the positive direction ( $\omega_{22} > 0$ ), and  $T_{em,2}$  opposes the rotation of the rotor. At  $s = 0.5$ ,  $\dot{F}_{22m}$  is stationary relative to the stator, the slip of the stator winding relative to this mmf reduces to zero, and  $\dot{I}_{12}$  no longer flows in the stator winding ( $\dot{I}_{12} = 0$ ). This is what may be treated as an ideal no-load condition for the negative sequence rotor currents  $\dot{I}_{22}$ . Because there is no

reaction from the stator,  $I_{22}$  are the same as the magnetizing current  $I_{220}$  required to set up the negative sequence field and take on the lowest possible value. At  $s = 0.5$ , the positive sequence currents, equal to the negative sequence currents,  $I_{21} = I_{22} = I_{220}$ , likewise fall in magnitude in the same proportion.

At  $s = 0$ , the condition is a short circuit for the synchronous field and the stator currents  $I_{11}$ , the rotor comes to a standstill relative to the synchronous field, and no currents are induced in it,  $I_{21} = I_{22} = 0$  and  $I_{11} = I_{110}$ .

The reduction in  $I_{21}$  and  $I_{22}$  at  $s = 0$  and  $s = 0.5$  leads to a proportionate decrease in  $T_{em,1}$  and  $T_{em,2}$  and in the resultant electromagnetic torque,  $T_{em} = T_{em,1} + T_{em,2}$ . As is seen from Fig. 46-3, at  $s = 0.5$ , when the angular velocity is equal to half the synchronous one,

$$\omega = \omega_1 (1 - s) = 0.5\omega_1$$

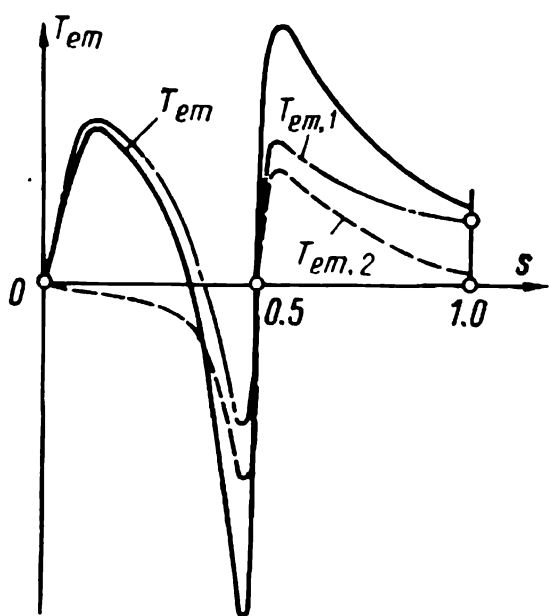


**Fig. 46-3** Torque-slip characteristics of an induction motor with a rotor phase open-circuited

the resultant torque may take on a negative value. This is the reason why a wound-rotor motor with one phase open-circuited would cease picking up any more speed on reaching half the synchronous speed. When run in such a condition on load, the motor would have a reduced power factor, an impaired efficiency, and increased stator and rotor currents, so that long-time operation would only be possible if the external torque is less than half its rated value,  $T_{\text{ext}} \leq 0.5T_{\text{em,R}}$ .

An open-circuited rotor phase also causes the stator currents to beat at a frequency equal to the difference in frequency between the stator current components,  $I_{11}$  and  $I_{12}$ , that is,

$$f = f_1 - f_{22} = 2f_1s$$

The distortion of the torque-slip characteristic caused by open-circuiting a rotor phase will usually decrease as the resistance in the rotor phases is increased.

## 47 Single-Phase Induction Motors

### 47-1 Field of Application. General Arrangement and Principle of Operation

Single-phase induction motors are inferior to three-phase units in performance, and their use is warranted where only a single-phase supply is available (mostly in household appliances, such as refrigerators, washing machines, and fans).

The primary is wound single-phase and is dropped in slots on the stator core. The rotor is of the squirrel-cage type. In fact, the primary may be treated as a two-phase winding in which one phase, say phase *A* (Fig. 47-1a) is open-circuited. The remaining phase *B* operates as a single-phase winding which occupies a half of the pole pitch and has a fairly high distribution factor

$$k_{d1} = 2\sqrt{2}/\pi = 0.9$$

The current in the single-phase winding

$$i_1 = \sqrt{2} I_1 \cos \omega_1 t$$

produces a pulsating mmf which can be resolved into two revolving waves, a forward wave,  $F_{11m} \exp(j\omega_1 t)$ , and a backward wave,  $F_{12m} \exp(-j\omega_1 t)$ . Their peak values are

$$F_{11m} = F_{12m} = F_{1m}/2 = \sqrt{2} I_1 w_1 k_{d1} k_{p1} / \pi p$$

The forward mmf wave rotates at  $\Omega_1 = \omega_1/p$  with the rotor. The backward wave does so at  $\Omega_2 = -\Omega_1$  in the opposite direction. Relative to the rotor, the forward wave travels with a slip equal to

$$s_1 = s = (\Omega_1 - \Omega) / \Omega_1$$

whereas the backward wave does so with a slip equal to

$$s_2 = (-\Omega_1 - \Omega) / (-\Omega_1) = 2 - s$$

The forward stator mmf induces in the rotor phases a set of currents,  $\dot{I}_{21}$ , which establish a forward mmf wave in the

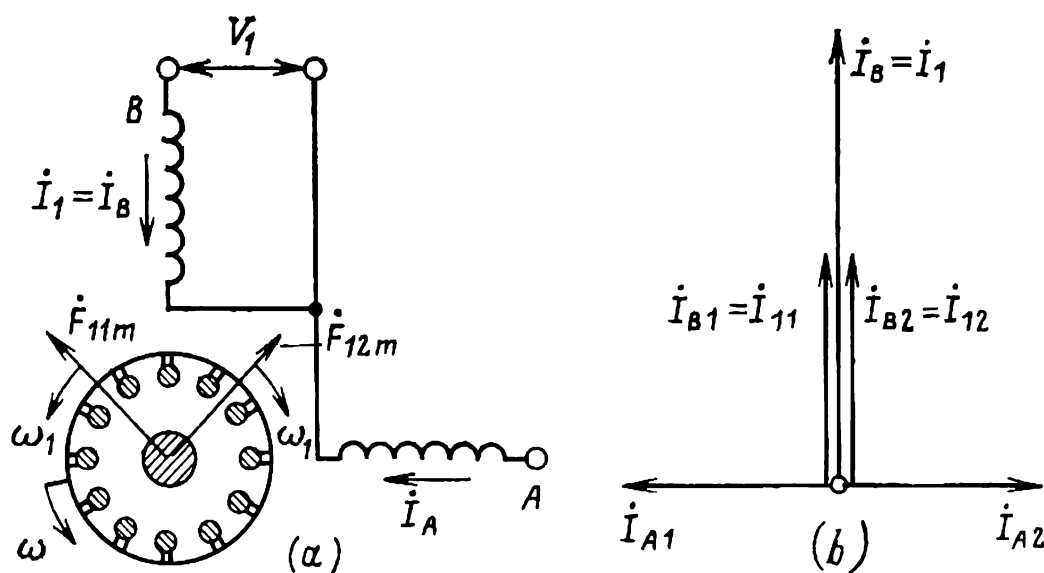


Fig. 47-1 Circuit of a single-phase motor derived from a two-phase unit by opening one of the phases

rotor,  $\dot{F}_{21m}$ . Since  $\dot{F}_{21m}$  produces a damping (retarding) effect, the resultant forward mmf is

$$\dot{F}_{01m} = \dot{F}_{11m} + \dot{F}_{21m}$$

The forward revolving field corresponding to the above mmf on the magnetizing curve has a peak value of  $B_{1m} \exp[j(\omega_1 t + \alpha_1)]$ .

Similarly, the backward stator mmf induces in the rotor phases a set of currents,  $\dot{I}_{22}$ , which establish a backward

mmf,  $\dot{F}_{22}$ . Since  $\dot{F}_{22m}$  has a damping effect, too, the resultant backward mmf is given by

$$\dot{F}_{02m} = \dot{F}_{12m} + \dot{F}_{22m}$$

and the corresponding revolving field has a peak flux density equal to  $B_{2m} \exp [-j(\omega_1 t + \alpha_2)]$ .

When the rotor is rotating with the forward field (in which case  $s_1 = s < 1$  and  $s_2 = 2 - s > 1$ ), the backward field is travelling relative to the rotor faster than the forward field is ( $s_2 \Omega_1 > s_1 \Omega_1$ ), and the rotor currents dampen it more heavily than the forward field.

As a result, the dominating component is the forward field

$$F_{01m} > F_{02m} \text{ and } B_{1m} > B_{2m}$$

The result is what is known as an *elliptical revolving field* whose flux density is given by

$$\tilde{B} = B_{1m} \exp [j(\omega_1 t + \alpha_1)]$$

$$+ B_{2m} \exp [-j(\omega_1 t + \alpha_2)]$$

The field owes its name “elliptical” to the fact that the locus of the flux density phasor is an ellipse (Fig. 47-2). Its semi-major axis,  $1-0$ , represents the maximum flux density of the field,

$$B_{\max} = B_{1m} + B_{2m}$$

whereas its semi-minor axis,  $2-0$ , represents the minimum flux density

$$B_{\min} = B_{1m} - B_{2m}$$

It is to be noted that at  $B_{2m} = 0$  the elliptical field becomes a circular one with a peak flux density  $B_{1m}$  (the circle is shown dashed in the figure). At  $B_{1m} = B_{2m}$ , we have a pulsating field with a peak flux density  $2B_{2m}$  (the ellipse contracts to a straight-line segment between points 5 and 6).

The torque of a single-phase motor is the sum of two torques

$$T_{em} = T_{em,1} + T_{em,2}$$

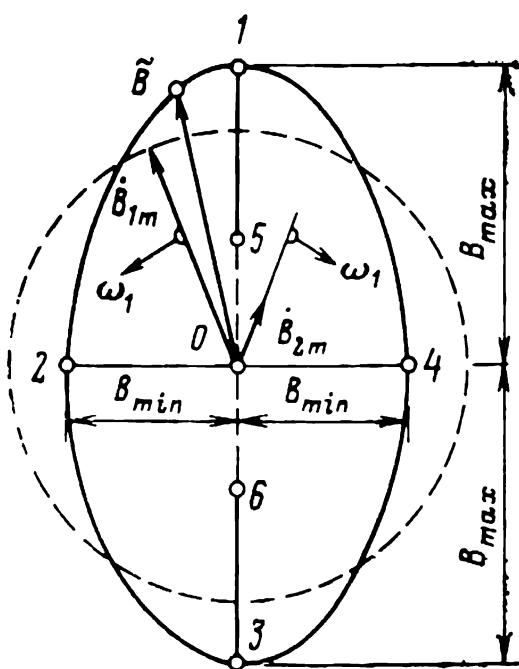
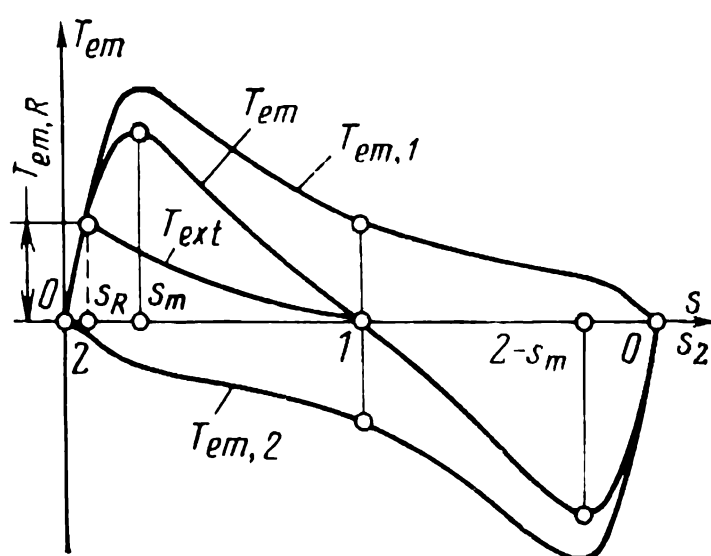


Fig. 47-2 Locus of the elliptical induction field phasor



where  $T_{em,1}$  is due to the forward component of the elliptical field, and  $T_{em,2}$  is due to the backward component of the same field. A plot of these torques as functions of slip appears in Fig. 47-3.

When the rotor is at standstill and  $s = s_2 = 1$ , the forward and backward fields are weakened by the rotor currents to the same degree, their peak flux densities are the same,  $B_{1m} = B_{2m}$ , and there appear two torques, equal in



**Fig. 47-3** Torque-slip characteristic of a single-phase motor ( $R'_2 = R_1 = 0.05$ ,  $X_1 = X'_2 = 0.1$ ,  $R_0 = 0$ ,  $X_0 = 3$ )

magnitude but opposite in direction,  $T_{em,2} = -T_{em,1}$ . Because of this, the starting torque of a single-phase motor is zero, and it needs some special arrangement to set it going.

With movement somehow initiated in any one direction, an elliptical field is set up, and the dominant torque will be one ( $T_{em,1}$  or  $T_{em,2}$ , as the case may be) associated with the field rotating in the direction in which the motor was started.

Referring to the torque-slip characteristic of a single-phase motor in Fig. 47-3, it is seen to consist of two equal parts, one corresponding to the forward and the other to the backward sense of rotation. At  $s = 1$ ,  $s = 0$ , and  $s = 2$ , the torque reduces to zero. At  $s \approx s_m$  and  $s \approx 2 - s_m$ , the torque is a maximum. Once the motor is set going by a starting arrangement in, say, the direction of rotation of the  $B_{1m}$  field and the electromagnetic torque exceeds the external torque, then, after all transients have died out, the motor will have settled to a steady-state operation with a

slip,  $s_R$ , corresponding to the intersection of the  $T_{em} = f(s)$  and  $T_{ext} = f(s)$  curves.

In a steady state with  $s = s_R$ , the resultant field in a single-phase motor is practically circular, as it is in a three-phase motor. However, the rotor currents in a single-phase motor weaken the backward component of the field, and this leads to increased losses and a poorer performance as compared with a three-phase unit. Therefore, size for size, a single-phase motor will have a power rating which is not more than 50% to 60% that of a three-phase motor, and its efficiency and power factor are lower.

Should any phase in the stator circuit of a three-phase motor be open-circuited (as a result of, say, the fuse in phase  $C$  blowing), the remaining two phases,  $A$  and  $B$ , will form a single-phase winding in which each phase belt occupies two-thirds of a pole pitch, and the motor will keep operating as a single-phase unit—a condition fraught with grave consequences. Since the transition to single-phase operation does not entail an appreciable change in the speed and external torque, the mechanical power developed by the motor remains unchanged as well:

$$P_3 = T_{em,3}\Omega_3 \approx T_{em,1}\Omega_1 = P_1$$

Hence, recalling that in three-phase operation

$$P_3 = \sqrt{3} V_{line} I_3 \eta_3 \cos \varphi_3$$

and in single-phase operation

$$P_1 = V_{line} I_1 \eta_1 \cos \varphi_1$$

we may conclude that the current in single-phase operation increases by factor of  $\sqrt{3} \eta_3 \cos \varphi_3 / \eta_1 \cos \varphi_1$ . If we add to this the reduction in the efficiency and power factor, the increase in current will be by factor of more than  $\sqrt{3}$ . At the same time, the copper loss in the stator phase will increase more than three-fold and, if the motor is not disconnected from the supply line, it may fail through overheating.

## 47-2 Basic Equations and Equivalent Circuit of the Single-Phase Induction Motor

We shall consider the operation of a single-phase induction motor as an unbalanced operation of a two-phase motor in which phase  $A$  is disconnected ( $I_A = 0$ ), and the remaining

phase  $B$  carrying a current  $\dot{I}_B = \dot{I}_1$  forms a single-phase winding connected for a supply voltage  $\dot{V}_1$  (see Fig. 47-1).

By analogy with a three-phase winding (see Sec. 46-1), an unbalanced set of currents in a two-phase winding may be visualized as the sum of positive and negative sequence currents:

$$\dot{I}_A = \dot{I}_{A1} + \dot{I}_{A2}, \quad \dot{I}_B = \dot{I}_{B1} + \dot{I}_{B2}$$

where

$$\dot{I}_{A1} = j\dot{I}_{B1}, \quad \dot{I}_{A2} = -j\dot{I}_{B2}$$

The positive sequence currents,  $\dot{I}_{B1} = \dot{I}_{11}$  and  $\dot{I}_{A1}$ , establish a forward mmf,  $\dot{F}_{11m}$ , and a forward rotating field. The negative sequence currents produce a backward mmf and a backward rotating field. Solving the above set of equations for the current components in phase  $B$ , with phase  $A$  disconnected, we get:

$$\dot{I}_{B1} = \dot{I}_{11} = (\dot{I}_B - j\dot{I}_A)/2 = \dot{I}_B/2$$

$$\dot{I}_{B2} = \dot{I}_{12} = (\dot{I}_B + j\dot{I}_A)/2 = \dot{I}_B/2$$

The current diagram answering the above equations appears in Fig. 47-1b.

The voltage across a single-phase winding may be visualized as the sum of positive and negative sequence components:

$$\dot{V}_1 = \dot{V}_B = \dot{V}_{B1} + \dot{V}_{B2}$$

On expressing  $\dot{V}_{B1}$  and  $\dot{V}_{B2}$  in terms of positive and negative sequence currents and impedances,

$$\dot{V}_{B1} = \dot{V}_{11} = \dot{I}_{11}Z_{11} = \dot{I}_1Z_{11}/2$$

and

$$\dot{V}_{B2} = \dot{V}_{12} = \dot{I}_{12}Z_{12} = \dot{I}_1Z_{12}/2$$

we obtain a voltage equation for a single-phase motor

$$\dot{V}_1 = I_1 (Z_{11}/2 + Z_{12}/2)$$

The terms  $Z_{11}$  and  $Z_{12}$  are the phase impedances of a two-phase winding to the positive and negative sequence currents (see the equivalent circuit in Fig. 46-1). To calculate

$Z_{11}$  and  $Z_{12}$ , we may use the equations given in Sec. 46-1, but it must be remembered that  $R'_2$  and  $X'_2$  should be construed as the impedances referred to a phase of the two-phase winding. Therefore, the impedance referring coefficient as given by Eq. (42-8) and used in

$$R'_2 = R_2 k_z$$

and

$$X'_2 = X_2 k_z$$

must be adjusted for the number of phases in the primary two-phase winding,  $m_1 = 2$ .

On the basis of the voltage equation, we may treat the current in a single-phase motor as one produced in a series combination of  $Z_{11}/2$  and  $Z_{12}/2$  due to  $V_1$ . Therefore, the equivalent circuit of a single-phase induction motor can be obtained by combining the equivalent circuits for positive and negative sequence currents appearing in Fig. 46-1a and b, with the resistances and reactances in those circuits all divided by two. The upper portion of the equivalent circuit thus derived applies to the positive-sequence quantities, and the lower portion to the negative-sequence quantities.

The torque of a single-phase motor can be written as the sum of two torques,  $T_{em,1}$  and  $T_{em,2}$ , respectively associated with the positive-sequence voltage,  $V_{11}$ , and the negative-sequence voltage,  $V_{12}$ :

$$T_{em} = T_{em,1} + T_{em,2}$$

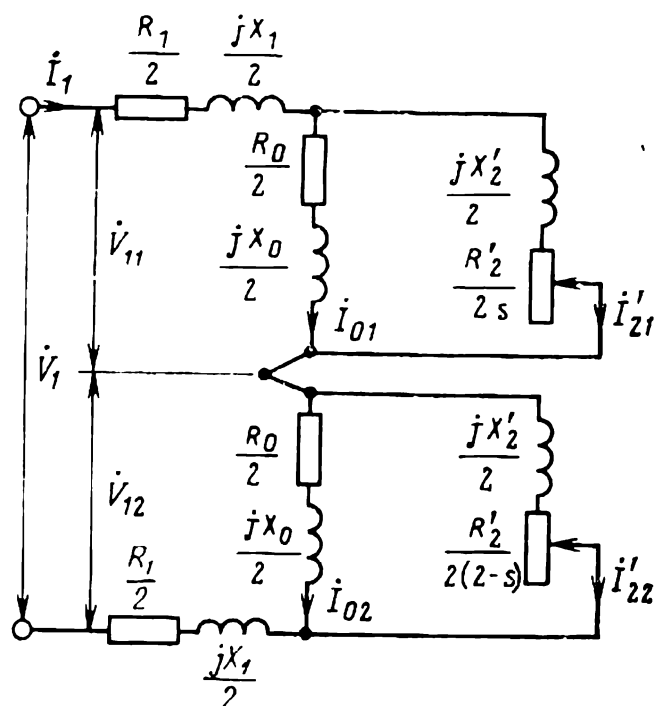


Fig. 47-4 Equivalent circuit of a single-phase motor

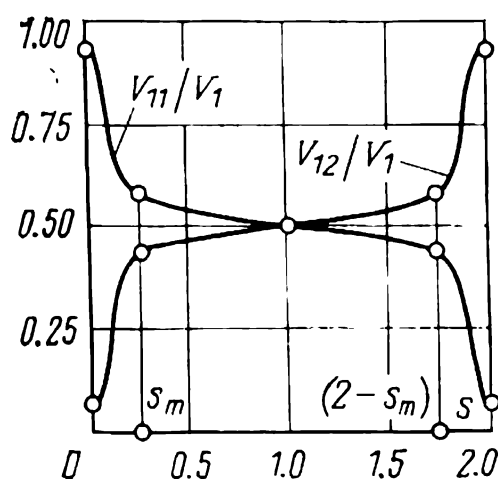


Fig. 47-5 Positive and negative sequence voltages of a single-phase motor as functions of slip ( $R'_2 = R_1 = 0.05$ ,  $X_1 = X'_2 = 0.1$ ,  $R_0 = 0$ ,  $X_0 = 3$ )

The equations for  $T_{em,1}$  and  $T_{em,2}$  (see Sec. 46-1) should be adjusted for  $m_1 = 2$  and extended to include the positive and negative sequence voltages as found from the equivalent circuits of Fig. 47-4:

$$\dot{V}_{11} = \dot{V}_1 \left| \frac{Z_{11}}{Z_{11} + Z_{12}} \right|$$

$$\dot{V}_{12} = \dot{V}_1 \left| \frac{Z_{12}}{Z_{11} + Z_{12}} \right|$$

Because, with  $V_1$  held constant,  $V_{11}$  and  $V_{12}$  vary with slip approximately as shown in Fig. 47-5, the plots of  $T_{em,1}$  and  $T_{em,2}$  as functions of slip differ from those obtained with  $V_{11}$  or  $V_{12}$  held constant, and have the form shown in Fig. 47-3.

### 47-3 The Split-Phase Induction Motor

A split-phase motor has two windings, one called the running (run or main) winding,  $RW$ , and an auxiliary, or starting winding,  $SW$ , displaced from the run winding by an electrical angle of  $\pi/2$  (Fig. 47-6a).

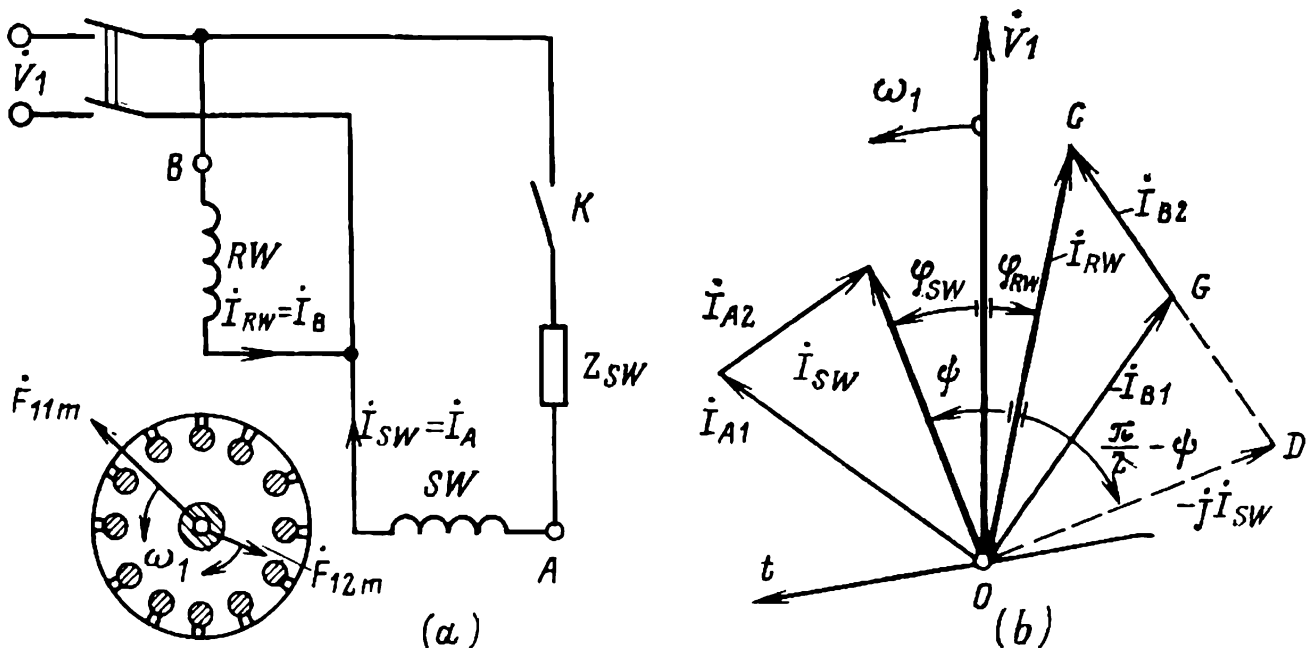


Fig. 47-6 Split-phase induction motor: (a) circuit and (b) phasor diagram

To simplify the matters, let us assume that the two windings are identical in their design ( $w_{SW} = w_{RW}$  and  $k_{w,SW} = k_{w,RW}$ ). The starting winding is connected to the supply line via a phase-shifting impedance,  $Z_{SW}$ , chosen such that the current in the starting winding,  $I_{SW}$ , leads the current

in the run winding,  $I_{RW}$ , by as large an angle (called the phase split) as practicable,

$$\psi = \varphi_{RW} - \varphi_{SW}$$

(Fig. 47-6b). Owing to this arrangement, the motor at starting behaves as a two-phase unit.

If, with  $Z_{SW} = -j/\omega C$  chosen such that  $\varphi_{SW} = \varphi_{RW} - \pi/2$ , the phase currents form a balanced set ( $I_{SW} = I_{RW}$  and  $\psi = \pi/2$ ), a circular rotating field will be established in the motor, and it will develop the largest possible starting torque. If, on the other hand, the phase currents form an unbalanced set ( $I_{SW} \neq I_{RW}$  and  $\psi \neq \pi/2$ ), what happens at starting can conveniently be analyzed by the method of symmetrical components.

To this end, let us identify the run winding with phase  $B$  and the starting winding with phase  $A$  of a two-phase motor. Then the unbalanced set of currents,  $\dot{I}_{RW} = \dot{I}_B$  and  $\dot{I}_{SW} = \dot{I}_A$ , shown in the diagram of Fig. 47-6b may be written as the sum of positive and negative sequence currents thus:

$$\dot{I}_{RW} = \dot{I}_B = \dot{I}_{B1} + \dot{I}_{B2}$$

$$\dot{I}_{SW} = \dot{I}_A = \dot{I}_{A1} + \dot{I}_{A2}$$

where

$$\dot{I}_{B1} = (\dot{I}_{RW} - j\dot{I}_{SW})/2$$

$$\dot{I}_{A1} = j\dot{I}_{B1}$$

$$\dot{I}_{B2} = (\dot{I}_{RW} + j\dot{I}_{SW})/2$$

$$\dot{I}_{A2} = -j\dot{I}_{B2}$$

Graphically,  $I_{B1} = I_{11}$  can be found as the median  $OG$  of triangle  $OCD$  or calculated from the equation

$$I_{11} = I_{B1} = (I_{RW}/2) \sqrt{1 + k^2 - 2k \cos(\pi/2 + \psi)}$$

Similarly,  $I_{B2} = I_{12}$  can be found graphically as half the side  $CD$  or calculated from the equation

$$I_{12} = I_{B2} = (I_{RW}/2) \sqrt{1 + k^2 - 2k \cos(\pi/2 - \psi)}$$

where  $k = I_{SW}/I_{RW}$  is the relative current in the starting winding.

The peak values of the forward and backward stator mmfs,

$F_{11m}$  and  $F_{12m}$ , are proportional to the corresponding currents,  $F_{11m} \sim I_{11}$ , and  $F_{12m} \sim I_{12}$ . The positions that their phasors take up in space (see Fig. 47-6a) correspond to those occupied by the respective current phasors (see Fig. 47-6b) in time (relative to the  $t$ -axis).

The ratio  $I_{12}/I_{11}$  varies with the phase split  $\psi$  and the relative current in the starting winding,  $k = I_{SW}/I_{RW}$ . As is seen from Fig. 47-7, where these dependences are shown

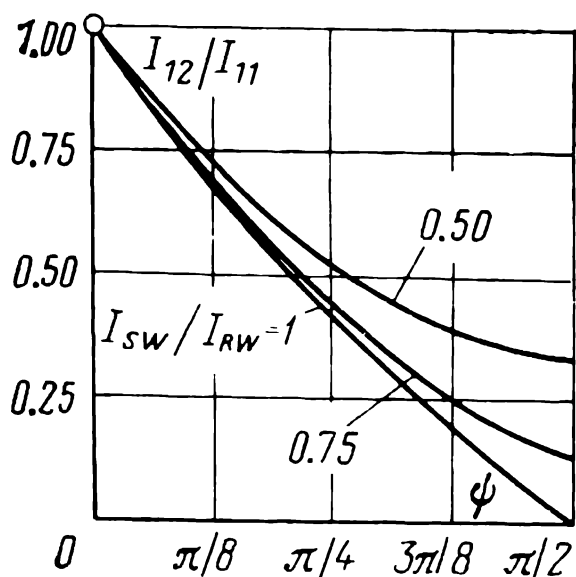


**Fig. 47-7** Effect of starting-winding current and its phase on the negative-sequence current (as compared with the positive-sequence current)

graphically,  $I_{12}$  reduces to zero and sets up a circular field only when  $k = 1$ ,  $I_{11} = I_{RW} = I_{SW}$  and  $\psi = \pi/2$ , which can be obtained by inserting in the starting-winding circuit a suitably chosen capacitive reactance (see above). In all other cases, where any other capacitive reactance or a resistance is inserted in the starting-winding circuit, the phase split for the starting current will be

$$\psi = \varphi_{RW} - \varphi_{SW} < \pi/2$$

and its relative magnitude will be  $k < 1$ . Then, in addition

to a forward mmf,  $F_{11m}$ , due to  $I_{11}$ , there will appear a backward mmf,  $F_{12m}$ , due to  $I_{12} < I_{11}$ . As a result, an elliptical field will be produced, and the starting torque will be reduced owing to the action of the backward field.

If we connect the starting winding to the supply line directly ( $Z_{SW} = 0$ ,  $\varphi_{SW} = \varphi_{RW}$ , and  $\psi = 0$ ), then  $I_{12}$  will be equal to  $I_{11}$ , a pulsating field will be produced, and there will be no starting torque.

Although the best starting conditions are obtained when a capacitance is inserted in the starting winding, this form of starting is used relatively seldom, when a very large starting torque is essential. More frequently, the necessary phase split is obtained by inserting a resistance, and the machine is usually called a resistance split-phase motor. As a way of reducing the value of the external resistance, the starting winding is made to have an increased resistance of its own (this is done by using a smaller size of wire and a

bifilar arrangement for some of the turns). Upon starting, the auxiliary winding in a resistance split-phase motor must be disconnected from the supply line, or else it might be overheated and the efficiency of the motor might be impaired. As a rule, the auxiliary winding is disconnected by a centrifugal switch, a time relay, a current relay, or by a manual switch (symbolized by  $K$  in Fig. 47-6a).

The torque-slip characteristic of a resistance split-phase motor is shown in Fig. 47-8. The auxiliary winding is disconnected at  $s = 0.3$ .

Where necessary, a three-phase induction motor can be operated as a resistance split-phase unit. Two of its phases form a main winding in which each phase belt occupies two-thirds of a pole pitch. The third phase serves as the starting winding in which each phase belt occupies one third of a pole pitch. The two windings are displaced from each other by  $\pi/2$ . The run winding has twice as many turns as the auxiliary one,  $w_{RW} = 2w_{SW}$ , and a fairly large distribution factor,  $k_{d,RW} = 3\sqrt{3}/2\pi = 0.826$ . A preferable connection of a three-phase motor to a single-phase supply is shown in Fig. 47-9. In performance, a three-phase motor connected as shown in the figure is equivalent to a specially designed split-phase unit. Its full-load power in single-phase operation will be no more than 50% to 60% of that in the case of three-phase supply. The desired phase split can be introduced by a resistance or a capacitive reactance, so chosen that the starting torque is a maximum (see below). Upon starting, it is usual to disconnect the auxiliary winding from the supply line.

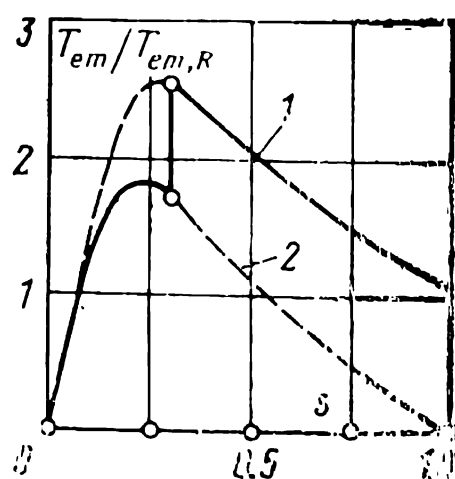


Fig. 47-8 Load-slip characteristic of a split-phase motor:

1 — with the starting winding brought in; 2 — with the starting winding disconnected

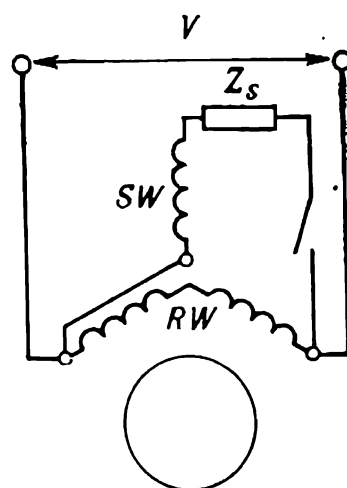


Fig. 47-9 Connection of a three-phase motor to a single-phase supply





same,

$$V_B = V'_A$$

$$I_B = I'_A$$

$$\varphi_B = \varphi_A$$

$$P_B = V_B I_B \cos \varphi_B = V'_A I'_A \cos \varphi_A = P_A$$

The phase  $A$  quantities at  $w'_A = w_B$  are primed and represented on the diagram of Fig. 47-10*b* by dashed lines. Also, since a balanced two-phase supply produces a circular field, the phase currents and voltages are shifted in time-phase by  $\pi/2$ , that is,  $\dot{I}'_A = j\dot{I}_B$  and  $\dot{V}'_A = j\dot{V}_B$ . It should be stressed, however, that such a voltage on phase  $A$  can only be obtained with a two-phase supply.

If, on the other hand, phase  $A$  having the same number of turns as phase  $B$  is energized from a single-phase supply, it will, in the general case, be impossible to adjust the value of  $C$  so that the phase  $A$  voltage is  $\dot{V}'_A = j\dot{V}_B$  which is essential for a circular field to be established. The situation is usually corrected by additionally adjusting the number of turns in winding  $A$ . The circular field will be retained if, in passing to a winding with  $w_A \neq w_B$ , the phase  $A$  mmf remains unchanged:

$$F_A = w_A I_A = w_B I'_A = F'_A = \text{constant}$$

Hence, the phase  $A$  current is

$$I_A = I'_A w_B / w_A = I_B w_B / w_A = I_B / n_{AB}$$

where  $n_{AB} = w_A / w_B$  is the turns ratio of a capacitor motor.

Since the circular field is retained, the phase  $A$  voltage changes in proportion to the turns ratio:

$$V_A = V'_A w_A / w_B = V_B n_{AB}$$

At the same time, the angle  $\varphi_A = \varphi_B$  and the phase  $A$  power remain unaffected:

$$P_A = V'_A I'_A \cos \varphi_A = V_A I_A \cos \varphi_B = \text{constant}$$

A change in  $w_A$  leads to a change in both  $V_A$  and  $I_A$ . The objective is to choose such a value of  $w_A$  that the voltage across the series circuit of phase  $A$  and capacitance  $C$  is the same as the supply voltage,  $\dot{V}$ , that is,

$$\dot{V}_A + \dot{V}_C = \dot{V}$$

and the voltage across the capacitance lags behind the phase  $A$  current by  $\pi/2$ , that is,

$$\dot{V}_C = -j\dot{I}_A/\omega C$$

As is seen from the phasor diagram in Fig. 47-10b, the desired phase  $A$  voltage is

$$V_A = V_B \tan \varphi_B$$

Hence,

$$n_{AB} = V_A/V_B = \tan \varphi_B$$

and the number of turns in winding  $A$  required to set up a circular field is

$$w_A = w_B n_{AB} = w_B \tan \varphi_B$$

The value of capacitance required for a circular field to exist is given by

$$C = I_B \cos \varphi_B / \omega V \tan \varphi_B$$

This capacitance draws a fairly large amount of reactive power

$$Q_C = V_C I_A = VI_B / \sin \varphi_B$$

In fact, it is the same as the total power taken by the motor in the case of a circular field:

$$S = VI = VI_B / \sin \varphi_B$$

It is to be noted that with the value of capacitance adjusted as explained above, the circular field will only exist at rated load. At any other load, the balance of mmfs will be upset, and in addition to the forward field there will be a backward component.

Sometimes, the backward field proves so strong that the starting torque obtained with the capacitance chosen to suit the rated condition is insufficient. This drawback can be rectified by placing an auxiliary capacitance,  $C_s$ , in parallel with the main capacitance  $C$  for the duration of starting (shown by the dashed line in Fig. 47-10a). This modification is usually known as the *two-value capacitor motor*.

A conventional three-phase induction motor can likewise be used as a capacitor motor. The capacitance required for connection to a single-phase supply line (see Fig. 47-9) may be found from the equation given earlier. In doing so, however, it is important to remember that the effective turns in the  $A$  phase containing a capacitor and those in

the phase  $B$  which contains no capacitor (see Fig. 47-9) cannot be varied at will,

$$w_A = w_1 k_{wA}, \quad w_B = 2w_1 k_{wB}$$

(where  $w_1$  is the number of turns per phase in a three-phase winding), so the turns ratio cannot be varied at will either:

$$n_{AB} = w_A/w_B = k_{wA}/2k_{wB} = 0.95 \div (2 \times 0.826) = 0.575$$

Therefore, when the value of capacitance is found from the equation

$$C = I_B \cos \varphi_B / \omega V \tan \varphi_B$$

a circular field can be obtained only when the load on the motor is such that

$$\tan \varphi_B = k_{AB} = 0.575$$

$$\varphi_B = 0.521 \approx 30^\circ$$

$$\cos \varphi_B = 0.866$$

In adjusting the value of capacitance for the rated operating conditions with a single-phase supply,  $V$  should be understood as the rated line voltage for a star connection,  $I_B$  as the rated phase current, and  $\varphi_B$  as the phase split between the phase current and voltage under the rated three-phase operating conditions. Also, if  $\varphi_B \neq 0.521$ , the field will contain both a forward and a backward component. As  $\varphi_B$  departs more from the value  $0.521 \approx 30^\circ$ , the backward component plays an increasingly greater role in the total field.

### 47-5 The Shaded-Pole Motor

In sketch form, the arrangement of a typical shaded-pole motor is shown in Fig. 47-11a. The motor has a squirrel-cage rotor, 2, and a concentrated single-phase stator winding 1 wound on salient stator poles. Parts of each salient stator pole, nearer to the trailing edge, are enclosed by heavy, shorted, single-turn copper coils, 3. These are called "shading coils".

Assuming that the magnetic circuit of the motor is linear and using the principle of superposition, let us examine the fields set up in the stator winding separately. The single-phase-winding current  $I_1$  establishes a pulsating flux,  $\dot{\Phi}_{1u}$

in the leading, or unshaded, part of each pole, and a pulsating flux,  $\dot{\Phi}_{1s}$ , in the trailing, or shaded part of the pole. In the shading coils,  $\dot{\Phi}_{1s}$  induces an emf,  $\dot{E}_{sc}$ , lagging behind the flux by  $\pi/2$ , and giving rise to a current,  $I_{sc}$  which lags behind  $\dot{E}_{sc}$  by an angle  $\varphi_{sc}$ . In turn,  $I_{sc}$  sets up a flux,  $\dot{\Phi}_{sc}$ , which has a shading effect on  $\dot{\Phi}_{1s}$  in the trailing (shaded)

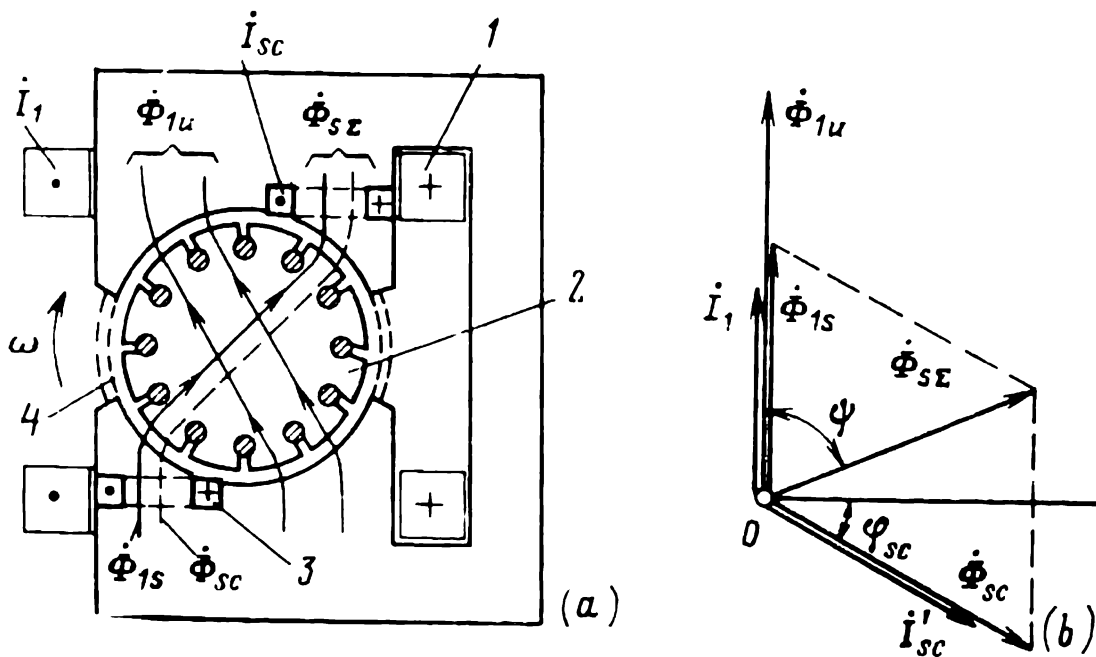


Fig. 47-11 Shaded-pole motor:  
(a) arrangement and (b) stator flux diagram

part of the salient stator pole. As a consequence, the resultant flux in the shaded part of the pole

$$\dot{\Phi}_{s\Sigma} = \dot{\Phi}_{1s} + \dot{\Phi}_{sc}$$

lags in time behind the flux in the leading (unshaded) part,  $\dot{\Phi}_{1u}$ , by an angle  $\psi$ . Because, the axes of  $\dot{\Phi}_{s\Sigma}$  and  $\dot{\Phi}_{1u}$  are additionally displaced from each other by a certain angle in space, there appears a rotating field travelling in the direction shown in the drawing. As  $\dot{\Phi}_{s\Sigma}$  and  $\dot{\Phi}_{1u}$  differ in magnitude and are shifted from each other in time and space by small angles, the rotating stator field is elliptical rather than circular. Yet, the shaded-pole motor develops a sufficiently large starting torque,  $T_{em,s} = 0.2T_{em,R}$  to  $0.5T_{em,R}$ .

The starting performance of a shaded-pole motor is adversely affected by the third space harmonic of the rotating field. Among other things, it brings about a sizeable drop

in the torque at the rotational speed one-third of the synchronous one (see Sec. 43-5). In motors rated at over 20 or 30 W, this effect can be minimized by placing magnetic shunts (at 4 in Fig. 47-11a) between the pole-pieces, or by increasing the air gap under the leading (unshaded) parts of the poles, or by winding the shading coils with two or three turns differing in width, instead of a single turn.

Because of the heavy losses in the shading coils, the efficiency of shaded-pole motors is rather low (25% to 40%). Commercially, they are built in sizes from a fraction of a watt to 300 W and are used in household fans, record players, tape recorders, etc.

## 48 Special-Purpose Induction Machines

### ☆ 48-1 The Induction Generator

If we connect an induction machine to a source of reactive power and make the rotor run at a speed exceeding that of the magnetic field ( $\Omega > \Omega_1$ ), the emf in the rotor winding will be reversed as compared with the motor mode of operation (see Chap. 43). As a consequence, the active components of  $I_2$  and  $I_1$  will also be reversed (in comparison with motoring), and the machine will deliver active power to an external circuit—this will be the generator mode of operation.

A major roadblock to a wider use of induction generators is that they cannot alone supply a power system, but must always operate in parallel with synchronous machines, thereby increasing the load.

In the circle diagram of an induction machine (see Fig. 43-9), the generator mode of operation corresponds to the lower half-circle of currents, lying between points  $A_0$  and  $R_\infty$ . The conditions under which an induction generator delivers active power to an external circuit are defined by points on the current circle lying below the line  $OB$ . The line  $A_0A_1$  represents the mechanical power  $P_m \approx P_2$  that must be applied to the generator by a prime mover.

Induction generators are mostly of the squirrel-cage type and have found a limited field of application, mostly at

small unattended hydroelectric stations, because they do not call for frequency or voltage control.

Instead of synchronous generators, the reactive power needed to set up a rotating magnetic field in an induction generator may be taken from a bank of capacitors arranged as shown in Fig. 48-1. In the case of a resistive-inductive load, the capacitors can additionally supply reactive power for the load as well.

With the reactive power supplied by a bank of capacitors, an induction generator operates by self-excitation, as it

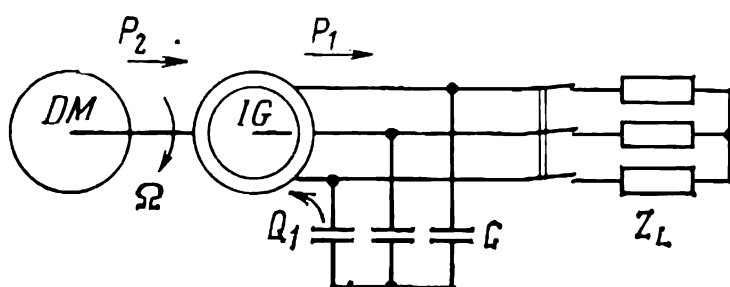


**Fig. 48-1** Connection of an induction generator using self-excitation: *IG* — induction generator; *DM* — drive motor; *C* — capacitors;  $Z_L$  — load impedance

utilizes the residual magnetization in the rotor. In the circumstances, the capacitors must of necessity be very large, so the entire unit is expensive. This is why capacitor-supplied induction generators are only used for special purposes.

## ☆ 48-2 Induction Frequency Converters

The frequency of the emf induced in the rotor of an induction machine is decided by the difference in velocity between the rotor and the magnetic field

$$f_2 = (\Omega_1 - \Omega) (p/2\pi) = sf_1$$

where  $\Omega > 0$  when the rotor is travelling with the field. A voltage at  $f_2$  can be picked off the slip-rings of a wound-rotor induction machine. In this way, it can be used as a frequency converter.

The output voltage of an induction frequency converter may be at a fixed or a variable frequency. In the former case, its rotor must rotate against the field if it is desired that  $f_2$  be higher than  $f_1$  ( $s > 1$ ), or with the field, if it is desired that  $f_2$  be lower than  $f_1$  ( $s < 1$ ).

When  $f_2 > f_1$ , an induction frequency converter is driven by an external motor,  $M$  (usually an induction or a synchronous one, see Fig. 48-2), which applies an amount of power,  $P_2$ , to the frequency converter; the latter operates as a brake, with  $s > 1$  (see Sec. 43-1). The directions of power flows in this case are shown in Fig. 48-2 by solid arrows.

When  $f_2 < f_1$ , the rotor of an induction frequency converter is braked by the electromagnetic torque from  $M$  which is now operating as a generator and delivers its output to the same system as the frequency converter. The directions of power flows in this case are shown in Fig. 48-2 by dashed arrows. The frequency converter is now operating as a motor.

Recalling that

$$\Omega_1 = 2\pi f_1 / p_{fc} = \Omega_{1,fc}$$

and

$$\Omega \approx \pm \Omega_{1,m} = \pm 2\pi f_1 / p_m$$

we obtain

$$f_2 = s f_1 = \frac{\Omega_1 - \Omega}{\Omega_1} f_1 = \frac{p_m \mp p_{fc}}{p_m} f_1$$

where the “+” and “−” signs apply respectively to the braking mode ( $f_2 > f_1$ ) and the motor mode ( $f_2 < f_1$ ) of operation,  $p_{fc}$  and  $p_m$  are the numbers of pole pairs in the frequency converter and motor, respectively. If the drive motor,  $M$ , is an induction machine, the above equation gives an approximate value of  $f_2$ , on neglecting the slip.

On neglecting losses, the active and reactive powers are given by

$$P_{\text{load}} = s P_1$$

$$Q_{\text{load}} = s Q_1$$

$$P_m = P_2 = (1 - 1/s) P_{\text{load}}$$

The value of  $f_2$  can be varied continuously by adjusting  $f_1$  or the rpm of the drive motor.

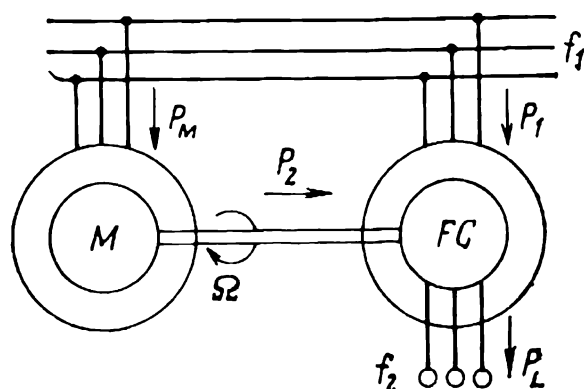


Fig. 48-2 Connection of an induction frequency converter:

$P_1$ —power drawn by converter from supply line;  $P_M$ —power drawn by motor from supply line;  $P_2$ —mechanical power transferred by shaft;  $P_L$ —load power;  $M$ —motor;  $FC$ —frequency converter



Induction frequency converters are mainly used to obtain an alternating voltage at 100-200 Hz ordinarily utilized to energize induction drives operating at speeds in excess of 3 000 rpm (electric saws and some other hand-held electric tools).

### ☆ 48-3 An Induction Machine in the Transformer Mode of Operation

(1) **Phase regulator.** If we restrain the rotor of an induction machine from rotating, the phase shift between  $\dot{E}_1$  and  $\dot{E}_2$  induced, respectively, in the stator and rotor windings,

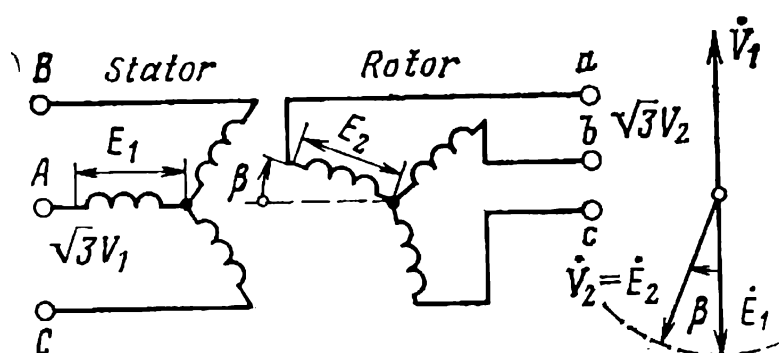


Fig. 48-3 The circuit and voltage/phasor diagram of a phase regulator

will be decided by the electrical angle  $\beta$  between the phase axes, because both emfs are induced by a common rotating magnetic field. A change in  $\beta$  will immediately lead to a change in the phase of  $E_2$ .

Such a form of phase control is utilized in the phase regulator shown in Fig. 48-3. Basically, it is a three-phase wound-rotor induction machine operated in the transformer mode, that is, with its rotor locked (see Sec. 43-1). The stator winding is connected to the supply line, and the rotor winding is connected via the slip-rings to a load. If we neglect the resistances and leakage inductive reactances of the stator and rotor windings, then

$$\dot{V}_1 = -\dot{E}_1 \quad \text{and} \quad \dot{V}_2 = \dot{E}_2$$

Furthermore, if the two windings are identical,

$$\begin{aligned} w_1 &= w_2 \\ k_{w1} &= k_{w2} \\ E_1 &= E_2 \end{aligned}$$



emf  $\dot{E}_1$  in the primary and another emf  $\dot{E}_2$  in the secondary. The phase voltage of the secondary, if we neglect its impedance, is the vectorial sum of the supply voltage  $\dot{V}_1$  and the secondary induced emf  $\dot{E}_2$ :

$$\dot{V}_2 = \dot{V}_1 + \dot{E}_2$$

The phase shift between the  $\dot{V}_1$  and  $\dot{E}_2$  vectors and, as a consequence, the value of  $V_2$  depend on the electrical angle between the phase axes of the stator and rotor windings. If we turn the rotor, the tips of the  $\dot{E}_2$  and  $\dot{V}_2$  vectors will move along a circle. The minimum and maximum values of  $V_2$  correspond to the angles  $\beta = 0^\circ$  and  $\beta = 180^\circ$ ,

$$V_{2\min} = V_1 - E_2$$

$$V_{2\max} = V_1 + E_2$$

If we ignore the resistance,  $R_1$ , and reactance,  $X_1$ , of the primary, then  $V_1 = E_1$ . The emfs induced in the primary and secondary are connected by a relation of the form

$$E_1/E_2 = w_1 k_{w1}/w_2 k_{w2}$$

The primary of an induction regulator may be star- or delta-connected. The rotor can be turned and locked in the desired position in much the same way as in a phase regulator.

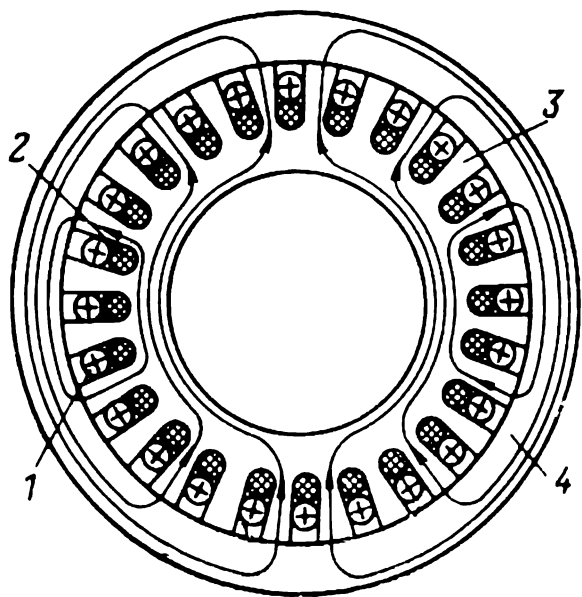


Fig. 48-5 Rotating-field transformer

(3) **Rotating-field transformer for frequency and phase conversion.** A still further use for an induction machine in which the rotor is restrained from rotation is phase and frequency conversion. Since the rotor need not move relative to the stator, no clearance, or air gap, need be provided between them. So, in order to reduce the magnetizing current, the outer core, 4, may be press-fitted on the inner core,

3 (Fig. 48-5). The primary, 1, and the secondary, 2, which remain stationary relative to each other, may, as a way of

reducing the leakage, be dropped in the slots of say, the inner core alone. Then the other core may be made slotless, as a smooth ring press-fitted on the inner core after the conductors have been placed in the inner-core slots. The primary of a rotating-field transformer does not differ in any way from the stator winding of an induction machine. More specifically, it is a heteropolar winding with  $p_1$  pole pairs,  $m_1 = 3$  phases, and  $w_1$  turns per phase. The primary is connected to an a.c. supply line with a phase voltage  $V_1$  at frequency  $f_1$ , and sets up a  $2p_1$ -pole rotating field whose lines are drawn in the figure. This field rotates at  $\Omega_1 = 2\pi f_1/p_1$ . The design of the secondary depends on the intended application of the rotating-field transformer. If it is intended for phase conversion, the secondary will have the same number of pole pairs as the primary,  $p_2 = p_1$ , and will only differ in the number of phases,  $m_2$ , and the number of turns per phase,  $w_2$ . The emfs induced in the phases of the secondary winding form a balanced  $m_2$ -phase set

$$E_2 = (w_2 k_{w2}/w_1 k_{w1}) E_1$$

The phase shift between  $\dot{E}_2$  and  $\dot{E}_1$  depends on the relative position of the phase axes in core slots. At no-load,

$$\dot{V}_1 = -\dot{E}_1 \quad \text{and} \quad \dot{V}_2 = \dot{E}_2$$

The on-load currents  $I_1$  and  $I_2$  and the on-load voltage  $V_2$  can be found in exactly the same manner as in the case of a phase regulator.

If a rotating-field transformer is intended for frequency conversion, it utilizes the distortion in the sinusoidal distribution of the rotating-field flux in the airgap owing to core saturation. As has been explained in Sec. 40-2, the tooth saturation in the region of high mmf "flattens" the rotating-field flux waveform, so that its Fourier expansion has, in addition to a  $2p_1$ -pole fundamental term, also a number of odd harmonics with  $6p_1$ ,  $10p_1$ ,  $14p_1$  poles etc. To accentuate this effect, a rotating-field transformer intended for frequency conversion is built with a heavily saturated magnetic circuit (with a maximum tooth flux of over 2 T), and has a secondary designed to respond only to one of the higher (usually, third) harmonic of the rotating field.

When the secondary responds to the third harmonic, a rotating-field transformer operates as a frequency trebler.

It has a three-phase winding ( $m_1 = 3$ ) which sets up a  $2p_1$ -pole “flattened” field rotating at an angular velocity  $\Omega_1 = 2\pi f_1/p_1$ . Because, in travelling, the field does not change in waveform, all of its harmonics travel at the same angular velocity,  $\Omega_1$ . To give a voltage at three times the original frequency, the secondary must be a single-phase one ( $m_2 = 1$ ) with  $p_2 = 3p_1$  pole pairs. In such a winding, the flattened field mainly induces the 3rd harmonic of emf with  $3p_1$  pole pairs, relative to which the secondary winding has a winding factor of close to unity. Its frequency is three times the primary frequency

$$f_2 = p_2\Omega_1/2\pi = 3f_1$$

The flux linkage of the secondary with the fundamental flux and also with the  $10p_1$ -,  $14p_1$ -,  $22p_1$ -pole and higher (but other than triplen) harmonics is zero, so they induce no emf in the secondary.

To prevent the generation of emfs and currents at three times the original frequency in the primary, it is chorded by one-third of a pole pitch. Then its winding factor relative to a field with  $p_2 = 3p_1$  reduces to zero.

#### 48-4 The Solid-Rotor Induction Motor

As its name implies, this type of motor has a solid rotor in the shape of a cylinder (Fig. 48-6), which acts as both a core and a current conductor.

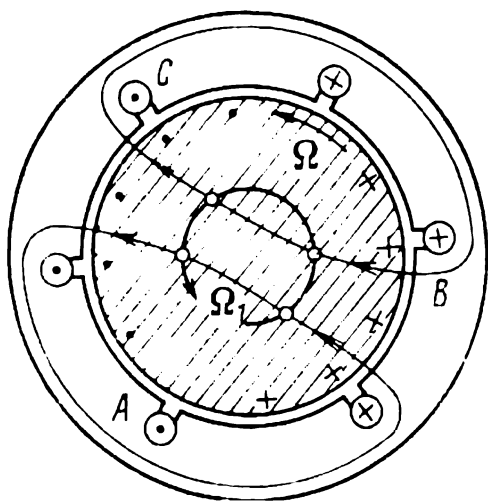


Fig. 48-6 Solid-rotor induction motor

The rotating magnetic field penetrates the rotor to a certain depth and induces eddy currents in it. The eddy currents interact with the magnetic field and produce an electromagnetic torque. Owing to the skin effect, the eddy currents are flowing in a relatively thin layer at the penetration depth. The equivalent penetration depth depends on the frequency of cyclic magnetization of the rotor. For a motor

designed to operate from a 50-Hz supply, the equivalent penetration depth at starting ( $s = 1$ ) is as little as 1 to 3 mm; at running ( $s = 0.05$ ), it is about 5 to 15 mm.

In a linear approximation, the penetration depth varies inversely as  $\sqrt{s}$ . This results in a change in the cross-section of the layer in which eddy currents can flow, in the effective rotor resistance

$$R'_2 \approx R'_{20} \sqrt{s}$$

where  $R'_{20}$  is the referred effective resistance at  $s = 1$ , and in the leakage inductive reactance  $X'_2$  of the rotor. Therefore, at starting  $R'_2$  is large, whereas  $X'_2$  is small; as the slip decreases,  $R'_2$  goes down and  $X'_2$  goes up. As a result, a solid-rotor induction motor has a relatively large starting torque

$$T_{\text{em},s}/T_{\text{em},R} = \text{from } 1.5 \text{ to } 2.0$$

In fact, it is inferior to a squirrel-cage motor only in terms of efficiency and power factor. This is because at rated load and at  $s = 0.02$  to  $0.1$ , the penetration depth is still small, whereas the resistance to current and the reluctance to flux are high, so the electric loss in the rotor and the magnetizing current are also high.

The performance of a solid-rotor motor can sometimes be improved by fastening copper short-circuiting rings to the ends of the solid rotor. The copper rings have a substantially smaller resistivity than the steel rotor and serve the same purpose as the end rings on the squirrel-cage structure. As a result, the effective resistance of the solid rotor is brought down owing to an increase in the conductance of the rotor ends. The same purpose can be served by applying a thin coat of copper (0.1 to 0.3 mm thick) to the outer surface of the rotor. Also, the performance of the motor can be improved by using a material for the rotor that would have an optimal combination of conductance and permeance. Recently, alloys have been developed with a higher conductance and a lower permeance than steel. They substantially increase the penetration of the field and improve the performance of the motor.

Solid rotor motors are mostly used in automatic control systems. Since the rotor is very robust mechanically, machines in this class can be built for very high rotational speeds (10 000-100 000 rpm and more). Such motors are intended for operation from a supply at 400 to 1 500 Hz and higher, and are used in special-purpose drives, for example in gyroscopic systems.

Although they are relatively simple to build, solid-rotor

motors have not yet been used in general-purpose industrial drives. The main cause is their low efficiency in operation.

In what may be looked upon as a modification of the above type of motor, the rotor is made hollow, of a ferromagnetic material so as to reduce the mass and moment of inertia of the rotor, or the drag cup, as it is usually called. The wall thickness of the drag cup is chosen to be equal to the penetration depth under operating conditions. At 400-1000 Hz, it is 0.3-0.5 mm, whereas at 50 Hz it rises to 1-3 mm.

Because the magnetic flux has its path closed through the walls of the drag cup, this type of motor requires no inner stator. In this respect, it compares favourably with motors in which the drag cup is fabricated of a nonmagnetic material (see the next section). Unfortunately, the magnetic drag cup has a low efficiency, a low power factor, and some other important drawbacks. Because of this, its use is limited.

#### 48-5 The Nonmagnetic Drag-Cup Motor

In this form of motor, the rotor (see Fig. 48-7) is a thin-walled, hollow cylinder, or cup, 3, fabricated from a conducting, nonmagnetic material (usually, an aluminium alloy).

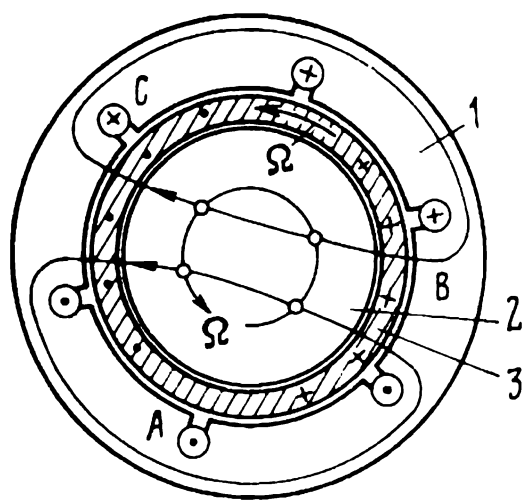


Fig. 48-7 Nonmagnetic drag-cup motor

The drag cup rotates in the air gap between an outer, 1, and an inner, 2, stator core. One of the stators (in our case, this is the outer core) carries a single- or polyphase winding. The electromagnetic torque acting on the drag cup is produced by the interaction of the rotating field with the eddy currents induced in the drag cup.

Nonmagnetic drag-cup induction motors are mainly used as control or servo motors in various automatic control systems. Their popularity is in part owing to a very valuable property—the extremely low moment of inertia of the drag cup. Drag-cup motors come in sizes from a fraction of a watt to several hundred watts for 50, 200, 400, 500, and 1 000 Hz.

In contrast to the solid rotor, the wall thickness of the

drag cup is a small fraction of the penetration depth even at starting. Therefore, eddy currents are uniformly distributed across the wall thickness at any slip, and the referred effective resistance of the drag cup,  $R'_2$ , is independent of the slip. Also, the leakage inductive reactance,  $X'_2$ , of the drag cup is so small that it may be neglected in calculations. The value of  $R'_2$  can readily be found, if we ignore the resistance of the ends and imagine that it consists of  $Z_2$  elementary bars. The resistance of such a bar is

$$R_b = \rho l / t_{Z_2} \Delta$$

where  $l$  is the rotor length,  $\Delta$  is the wall thickness of the drag cup, and  $t_{Z_2} = 2\pi R / Z_2$  is the extent of the bar in a tangential direction. Then, using Eqs. (41-22) and (42-8), we get

$$R'_2 = 2\rho l m_1 (w_1 k_{w1})^2 / \pi R \Delta$$

where  $R$  = radius of the drag cup

$m_1$  = number of phases in the stator winding

$w_1$  = number of turns in the stator winding

$k_{w1}$  = winding factor of the stator winding

Although the walls of the drag cup are made as thin as practicable (0.1 to 1.0 mm), the nonmagnetic gap between the two stators is fairly large (0.4 to 1.5 mm). Therefore, the magnetizing current in a drag-cup motor is markedly higher than it is in a squirrel-cage motor, being 0.8 to 0.9 of the rated (full-load) current. This leads to a reduction in the power factor ( $\cos \phi_R = 0.2$  to  $0.4$ ), increased stator copper losses, and a decrease in efficiency to 0.2-0.4 (under rated operating conditions).

#### 48-6 Electromagnetic Induction Pumps

Electromagnetic induction pumps for liquid metals are a modification of a.c. MHD machines. In such pumps, the movable member is the liquid metal being pumped. It is set in motion by a travelling or a rotating magnetic field established by a three-phase a.c. winding.

According to the shape of the liquid-metal conduit inside the magnetic field, such pumps are classed into helical (spiral) and linear.

**Helical (spiral) induction pump.** This type of induction pump (Fig. 48-8) is arranged similarly to a drag-cup induction motor. It, too, has two stators, outer 1 and inner 2.



The slots in the external core accommodate a three-phase winding connected to a supply line (sometimes, the three-phase winding may be arranged on both the outer and inner core). The air gap between the stators is occupied by a flat nonmagnetic-steel conduit 4, to guide the liquid metal 3.

In Fig. 48-8, the liquid-metal conduit completes one turn around the inner core and has a cross-sectional area equal

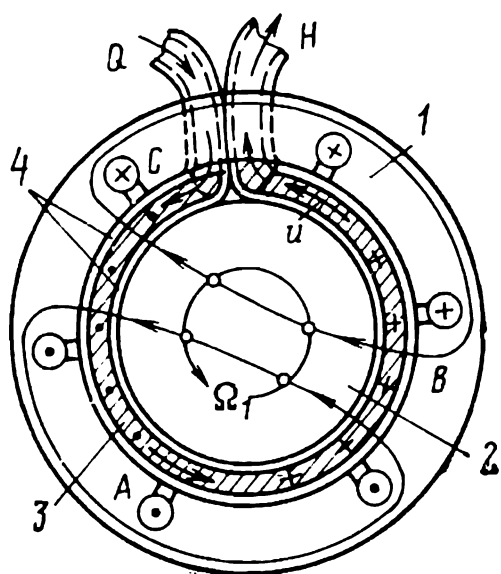


Fig. 48-8 Helical (spiral) induction pump

to  $\Delta l$ , where  $\Delta$  is the radial thickness of liquid metal, and  $l$  is the length of the core and liquid-metal conduit in the axial direction. More often than not, the liquid-metal conduit has several turns wound around the stator.

The currents flowing in the stator winding set up a rotating field which induces eddy currents in the liquid metal. The interaction of the eddy currents with the field gives rise to electromagnetic forces that drive the liquid metal at a

linear speed  $u$  in the direction of field rotation.

Energy conversion in a single-turn helical electromagnetic pump can be described by the equations and equivalent circuit applicable to the drag-cup induction motor, except that the leakage inductive reactance of the "rotor" is set equal to zero (see above). Then the electromagnetic power transferred from the stator to the liquid metal is, in accord with Eq. (41-32), given by

$$P_{em} = m_1 E_1 I'_2 = p s u_1^2 B_m^2 l \tau \Delta / \rho$$

where  $E_1 = 2 \sqrt{2} f_1 w_1 k_{w1} \tau l B_m$  = mutual emf in the stator winding

$I'_2 = E_1 s / R'_2$  = referred current in the liquid metal

$R'_2$  = referred resistance of the liquid metal (to be found as for the drag cup, see above)

$p$  = pole pairs of the field

$u_1 = 2\pi f_1 R \Omega_1 = R \Omega_1$  = linear speed of the field

$\tau$  = pole pitch

$\rho$  = resistivity of the liquid metal

$B_m$  = peak flux density

$s = (u_1 - u)/u_1$  = slip of the liquid metal relative to the field

The electromagnetic force exerted on the liquid metal is given by

$$N = T_{em}/R = P_{em}/\Omega_1 R = P_{em}/u_1 = psu_1 B_m^2 \tau l \Delta / \rho$$

and the pressure built up by the pump is

$$H = N/l\Delta = psu_1 B_m^2 \tau / \rho$$

The mechanical power of the pump is given by

$$P_m = Nu = (N/l\Delta) (ul\Delta) = HQ$$

where

$$Q = ul\Delta$$

is the volumetric flow rate through (delivery of) the pump.

When the liquid-metal conduit makes  $n$  turns around the inner stator, the pressure developed by the pump,  $H$ , is as many times greater, but the flow rate (or, rather, delivery of the pump) is decreased by the same factor.

**Flat linear induction pump.** This form of pump (Fig. 48-9) resembles a linear induction machine (see Sec. 48-7). It

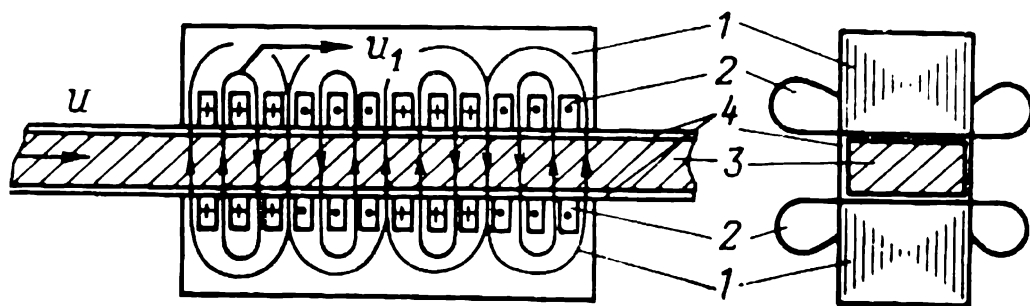


Fig. 48-9 Flat linear induction pump

consists of two flat stators or inductors, 1. The slots made in the inductors carry three-phase multipole windings, 2. The air gap between the inductors is taken up by a flat conduit, 4. Its rectangular cross-section is filled by the liquid metal being handled. The interaction of the travelling field in the inductors with the eddy currents induced in the liquid metal 3 gives rise to electromagnetic forces. When combined, the electromagnetic forces acting on the metal particles build up a pressure causing the liquid metal to flow in the direction of the field with a certain slip.

**Annular linear induction pump.** In this form of pump (Fig. 48-10), the electromagnetic forces acting on the liquid metal are produced by a travelling field. The liquid-metal duct 4 is circular in cross-section. Inside the conduit there is an unwound core, 2, and outside there is an inductor, 1, enclosing the conduit. The annular slots in the inductor carry the coils of a three-phase winding 5.

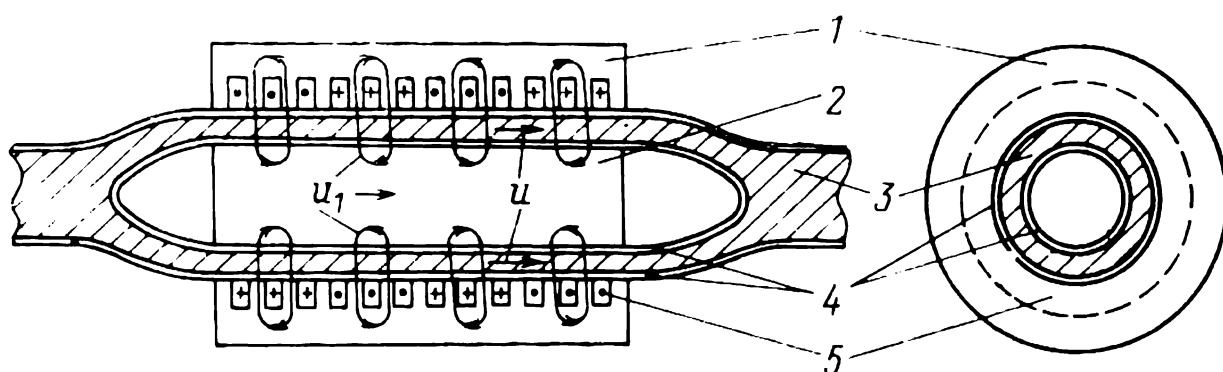


Fig. 48-10 Annular linear induction pump

An important field of application for induction pumps is in fast reactors where they handle liquid-metal coolants (sodium, potassium, and sodium-potassium).

#### 48-7 Linear and Limited-Rotation Induction Motors

In sketch form, the general arrangement of a linear and a limited-rotation induction motor is shown in Fig. 48-11a and b, respectively.

The stator 1 of a linear motor has the shape of a parallelepiped, and that of a limited-rotation motor, the shape of a sector of an arc. In a linear motor, the heteropolar, three-phase primary winding 2 is arranged in slots on a face of the parallelepiped. In a limited-rotation motor, it is placed in slots on the inner (or outer) surface of the sector.

The movable member in a linear motor is in a reciprocating motion. Its core, 4, like that of the stator, has the shape of a parallelepiped (see Fig. 48-11a). The slots made on the surface of the movable core facing the stator accommodate a short-circuited winding, 3. In a limited-rotation motor, the movable member is free to rotate within a certain sector. As in a conventional motor, it is called the rotor and has the shape of a hollow cylinder (at 4 in Fig. 48-11b). The slots on its outer surface hold a short-circuited winding,

3. In a linear and a limited-rotation motor, the movable member may be fabricated from a single piece of a magnetic material, in which case there will be no need for a short-circuited winding. Sometimes, some massive part of the driven machine may serve as the rotor.

Depending on the design of the movable member, the performance of the machine will be like that of a squirrel-cage unit or of a solid-rotor unit (see Sec. 48-4). The efficiency

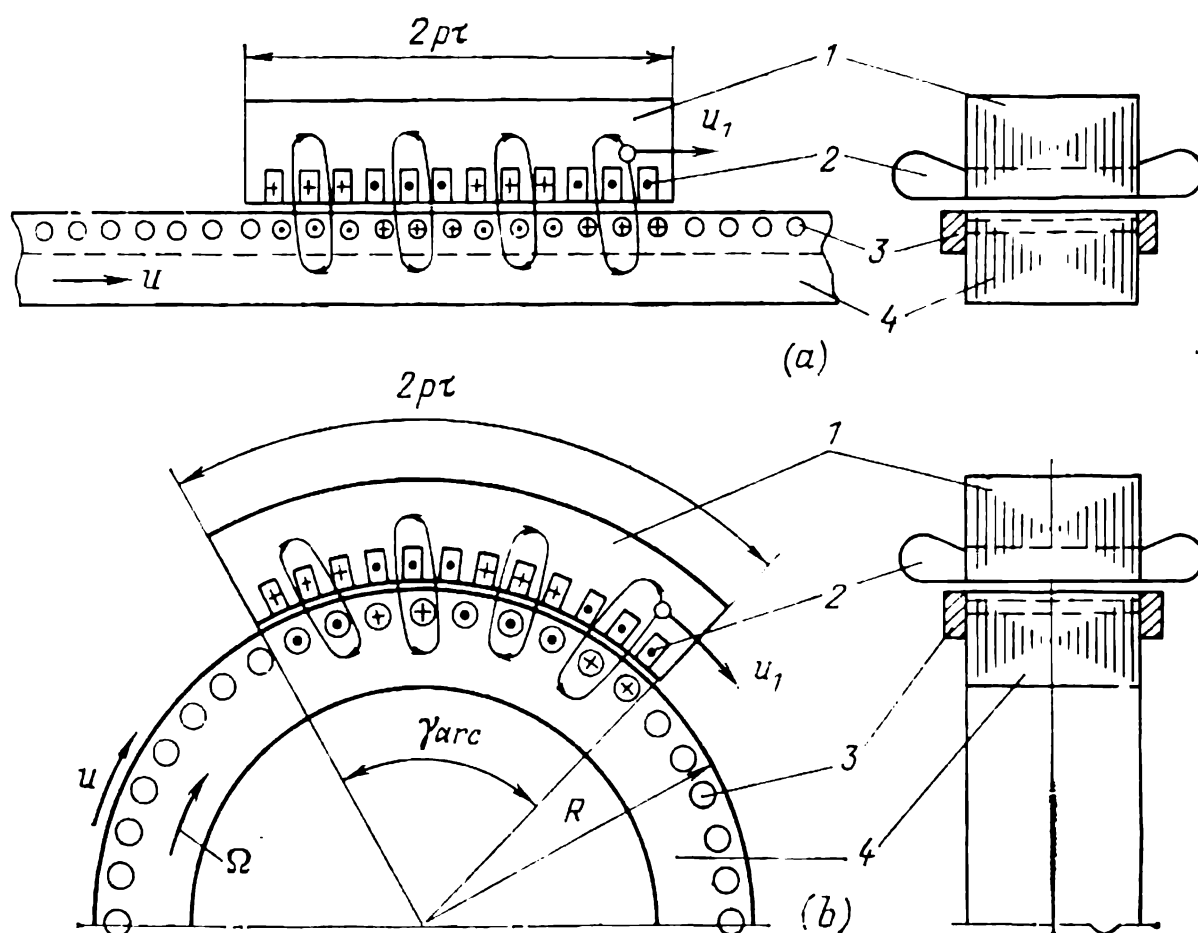


Fig. 48-11 (a) Linear and (b) limited-rotation induction motor

and power factor of linear and limited-rotation motors are usually inferior to those of units with a circular stator. This is because their stators do not form a complete circle, and there appear edge effects.

The slip in linear and limited-rotation motors is defined as the ratio of the linear slip velocity,  $u_1 - u$ , to the synchronous linear velocity of the travelling field,  $u_1 = 2\tau f_1$ . Under rated conditions,  $u$  is very close to  $u_1$ , so  $s = (u_1 - u)/u_1$  is as small as it is in conventional induction machines.

Linear induction machines can be used to give reciprocating motion by periodically reversing the phases of the stator winding, such as in metal-cutting machine tools. In such an application, the movable part must be longer than the

stationary one by the displacement desired. Because of a sizeable increase in the mass of the movable part and the energy wasted during acceleration and deceleration, such linear motors have not found any appreciable use. There is a better outlook for them in electric traction, especially where high speed is involved.

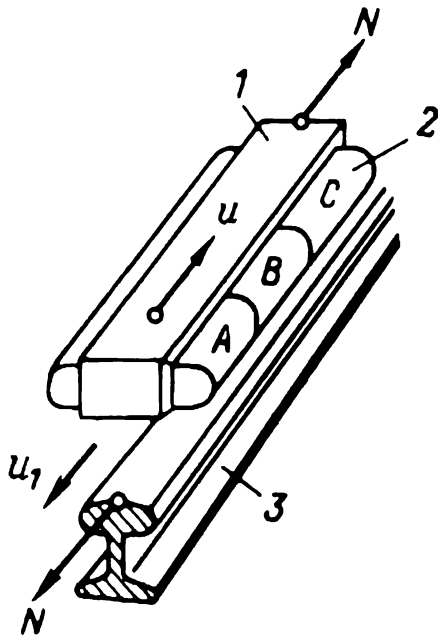


Fig. 48-12 Linear traction motor

Figure 48-12 gives a sketch explaining the likely use of a linear induction motor on railways. The stator core 1 and a polyphase winding 2 are mounted on an electric locomotive and draw their power from an a.c. supply line. The travelling field thus produced interacts with the rail, 3, and tends to pull it along. Since, however, the rail is anchored to the ground, motion at speed  $u$  is imparted to the stator and, hence, the electric locomotive.

Limited-rotation induction motors are used in cases where the rotor is to travel at a relatively low angular velocity.

To demonstrate, the stator of a limited-rotation machine having  $p$  pole pairs and spanning a sector with a central angle  $\gamma_{\text{arc}}$  (Fig. 48-11b) sets up on the radius  $R$  a field which rotates at a linear velocity

$$u_1 = 2\tau f_1 = \gamma_{\text{arc}} R f_1 / p$$

where  $\tau = \gamma_{\text{arc}} R / 2p$  is its pole pitch. In the circumstances, the synchronous angular velocity of the rotor

$$\Omega_1 = u_1 / R = \gamma_{\text{arc}} f_1 / p$$

is by a factor of  $2\pi/\gamma_{\text{arc}}$  lower than it is for a circular rotor having the same number of pole pairs.

Limited-rotation induction motors are especially attractive where some massive part of the associated driven machine can serve as its rotor.

## 49 Induction Machines for Automatic Control Applications

### 49-1 Induction Control Motors and Tacho-generators

**Induction control motors.** Induction control (or servo) motors are used in automatic control as devices that convert the amplitude or phase of a control voltage into the angular displacement or angular velocity of the output shaft (the final control element).

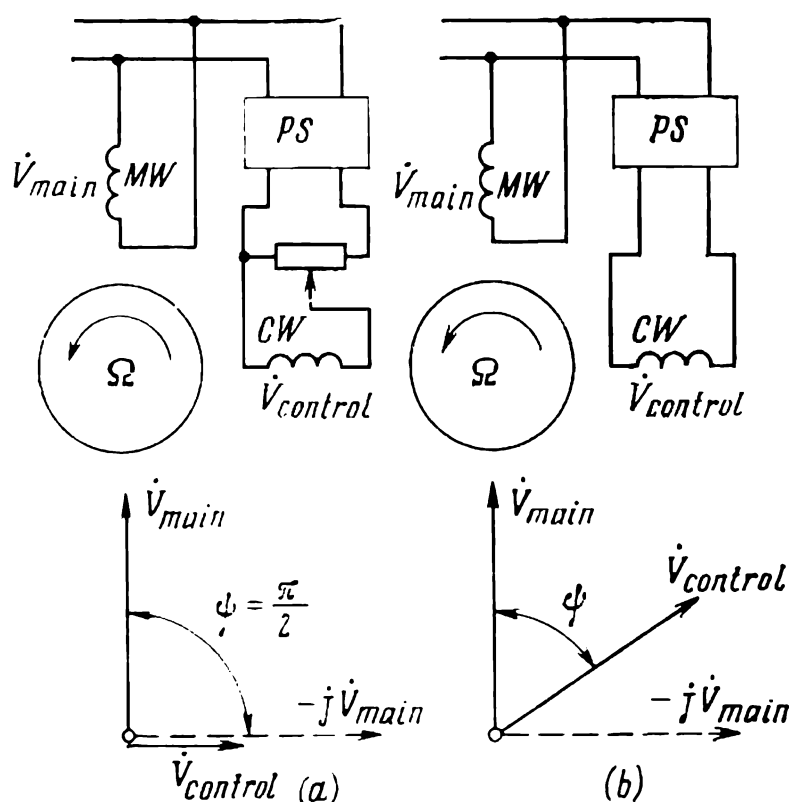


**Fig. 49-1** Induction control (servo) motor:  
(a) amplitude-controlled and (b) phase-controlled

They are small (0.1 to 300 W) squirrel-cage induction motors with a stator carrying two distributed windings displaced from each other by an electrical angle of  $90^\circ$  (Fig. 49-1). To simplify matters, let the two windings be identical. One, called the main or field winding, is always energized with  $\dot{V}_{main} = \text{constant}$ . The other, called the control winding, is supplied with  $\dot{V}_{control}$ , which varies in accord with the control signal.

For a torque to be produced,  $\dot{V}_{\text{control}}$  must be out of phase with  $\dot{V}_{\text{main}}$ , that is,  $\psi \neq 0$  and  $V_{\text{control}} \neq 0$ . At  $\psi = 0$  or  $\dot{V}_{\text{control}} = 0$ , there is no torque produced. At  $\psi = 90^\circ$ ,  $\dot{V}_{\text{control}} = V_{\text{main}}$  or  $\dot{V}_{\text{control}} = -j\dot{V}_{\text{main}}$  (this case is shown by dashed lines in Fig. 49-1), the torque is a maximum.

Control (or servo) motors can be controlled by varying the amplitude or the phase of the control (error) voltage. In the former case (Fig. 49-1a), the amplitude of  $\dot{V}_{\text{control}}$  is varied, whereas its phase,  $\psi$ , remains constant. The desired phase shift,  $\psi = 90^\circ$ , is produced by a suitable phase-shifter, *PS*. In the latter case (Fig. 49-1b), the phase  $\psi$  of  $\dot{V}_{\text{control}}$  is varied, whereas its amplitude remains constant. The phase of the control voltage is varied by a phase shifter, *PS*.

Control motors are required to have some special characteristics necessary for their use in automatic control. For example, in the case of amplitude control, these requirements are as follows.

(1) The angular speed must be controllable over a wide range as the amplitude of the control voltage is varied.

(2) The torque-speed characteristic,  $T_{\text{em}} = f(\Omega)$ , at a constant  $V_{\text{control}}$ , and the control characteristic,  $\Omega = f(V_{\text{control}})$  at a constant  $T_{\text{em}}$ , must be as linear as practicable.

(3) The moment of inertia of the rotor must be a minimum (so as to give a high speed of response).

(4) The starting torque must be sufficiently large.

(5) The breakaway voltage should be low (and the friction torque small).

(6) Control power must be negligible.

(7) As the control voltage falls to zero, the motor ought not to run of its own accord.

To meet the above requirements (especially those in 1, 2, and 7), the rotor resistance is chosen such that

$$s_m = R'_2/X_{sc}$$

is 3 or 4. Then in the motor mode of operation the torque-speed characteristic will be practically linear and the motor will not run of its own accord at zero control voltage. This

can readily be proved by comparing the directions of the torques at  $V_{\text{control}} \neq 0$  and  $V_{\text{control}} = 0$ .

At  $V_{\text{control}} \neq 0$  (Fig. 49-2a) and  $\Omega = 0$ , the torque  $T_{\text{em},1}$  due to the positive sequence voltages  $V_1$  exceeds the torque  $T_{\text{em},2}$  due to the negative sequence voltages, because  $V_2 < V_1$ . Since  $T_{\text{em},1} > T_{\text{em},2}$ , the resultant torque is positive:

$$T_{\text{em}} = T_{\text{em},1} - T_{\text{em},2} > 0$$

and the machine runs in the forward direction at  $\Omega > 0$ . When the control voltage is removed,  $V_{\text{control}} = 0$ , and  $V_1 = V_2$  (see Fig. 49-2b),  $T_{\text{em},1}$  and  $T_{\text{em},2}$  at  $\Omega = 0$  balance each other, whereas at  $\Omega > 0$  the resultant torque is negative:

$$T_{\text{em}} = T_{\text{em},1} - T_{\text{em},2} < 0$$

and the motor comes to a stop.

A motor designed to meet the above requirements has a low efficiency and a low power factor. But this has to be reconciled with.

Two-phase control (or servo) induction motors usually come in any one of three modifications, namely the squirrel cage, the nonmagnetic drag cup (see Sec. 48-5), and the ferromagnetic drag cup (see Sec. 48-4), the first two types being most common. The squirrel cage is preferable for the smaller control motors, and the nonmagnetic drag cup for the larger control motors.

As compared with conventional squirrel-cage motors, the squirrel-cage control motor differs in the following.

(1) The length-to-diameter ratio of the rotor is anywhere from 1.5 to 2.0, so that the moment of inertia is kept to an acceptable level.

(2) The air gap between the stator and rotor is kept to a minimum value of 30 to 50  $\mu\text{m}$  so as to minimize the magnetizing current.

(3) There is a relatively large number of pole pairs (usually

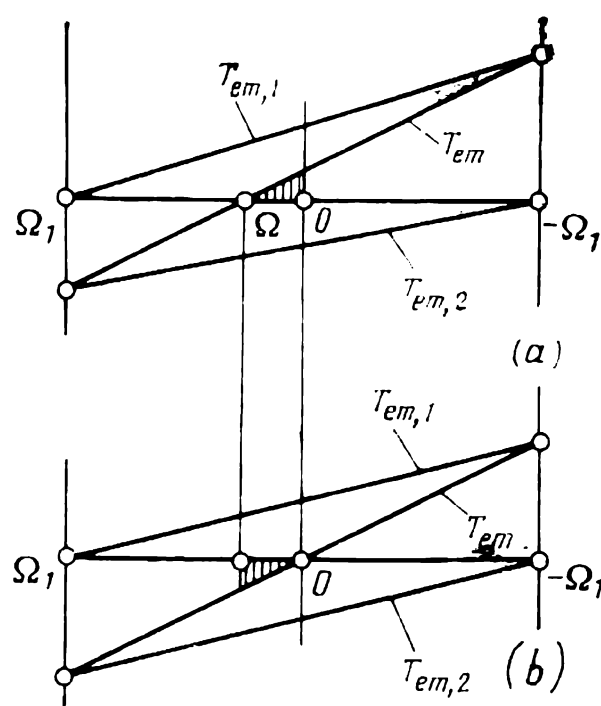


Fig. 49-2 Torque-speed characteristics of a control motor:

- (a) at  $V_{\text{control}} \neq 0$ ;  
(b) at  $V_{\text{control}} = 0$



from four to eight), so as to enhance the speed of response.

(4) Resort is made to skewing by one tooth pitch as a way of minimizing the stray torques (see Sec. 43-5).

Also, control motors usually have built-in electromagnetic dampers to give an effective braking action upon removal of the control signal. The dampers come in a variety of designs and differ in the principle of operation. The simplest

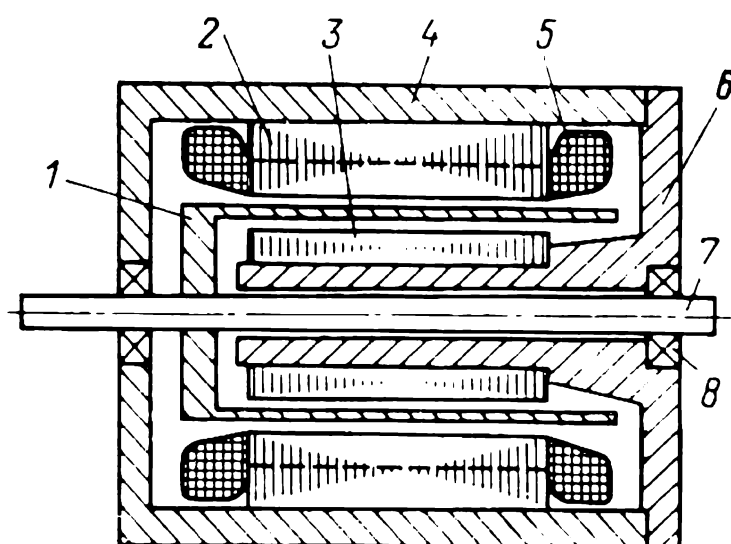


Fig. 49-3 Sketch of a drag-cup control motor

of all is an eddy-current damper in which the braking torque is produced by an aluminium drag cup rotating in the field set up by permanent magnets.

The salient features of the drag-cup motor have been examined in Sec. 48-5. It is important to add that this form of motor is free from both stray synchronous and reactive torques. Among its major advantages is the low moment of inertia of the rotor. In sketch form, a drag-cup control motor is shown in Fig. 49-3. The drag cup 1 rotates in the air gap between an outer stator 2 and an inner stator 3. The slots on the outer stator which is press-fit in a frame 4 accommodate the control and main windings, 5. The inner core is mounted on a hub which is made integral with the cover 6. The shaft 7 mounting the drag cup is carried by bearings 8.

Ferromagnetic drag-cup motors are inferior in several aspects to squirrel-cage and nonmagnetic drag-cup control motors. Naturally, this limits their application.

In some control applications, the rotor of a control motor needs only to turn through a limited angle proportional to the torque of the motor and the control voltage. Quite aptly, they are called *torque motors*.

**Induction tacho-generators.** A nonmagnetic drag-cup motor may well serve as a *tachometer generator* (or, simply, a *tacho-generator*), if its shaft is coupled to that of the machine whose rpm is to be measured.

The circuit of a tacho-generator is shown in Fig. 49-4. As in a control (or servo) motor, the main winding,  $MW$ , is connected to a supply of  $V_{main}$  at frequency  $f$ . The voltage waveform must be as close to sinusoidal as possible, and its amplitude and frequency stabilized. In the main winding, the applied voltage gives rise to a current and a magnetic flux,  $\Phi_{main}$ , partly contributed by the transformer currents induced in the rotor as well. Because the transformer emf and currents in the rotor are independent of the rotational speed,  $\Phi_{main}$  remains the same at any rpm.

The main flux does not link with the signal winding,  $SW$ , because it is in electrical quadrature with the axis of the flux. Therefore, at standstill ( $\Omega = 0$ ), no other currents, except the transformer currents, are induced in the rotor, and the voltage across the signal winding is  $V_s = 0$ .

When the rotor is running at  $\Omega$ , the emfs induced in it include transformer emf and also rotational emfs proportional to  $\Omega$ . Under their action, rotational currents,  $i_{2\Omega}$  (shown in the diagram) appear in the drag cup. Their amplitudes and also the amplitude of the magnetic flux,  $\Phi_{sm}$ , they set up are likewise proportional to  $\Omega$ , so long as the core is unsaturated.  $\Phi_s$  is pulsating at the frequency  $f$  of the main voltage and induces in the signal winding an emf whose rms value,  $E_s$ , is likewise proportional to  $\Omega$ . The signal winding is connected to an indicator or a final control element. Their impedance,  $Z_{load}$ , is chosen so high that the current in the signal winding does not produce any noticeable voltage drop, and  $V_s \approx E_s$ . Thus, only the rms value of emf,  $E_s$ , is varying in an induction tacho-generator, whereas its frequency remains unchanged. Because of this, induction tachogenerators are used more frequently than

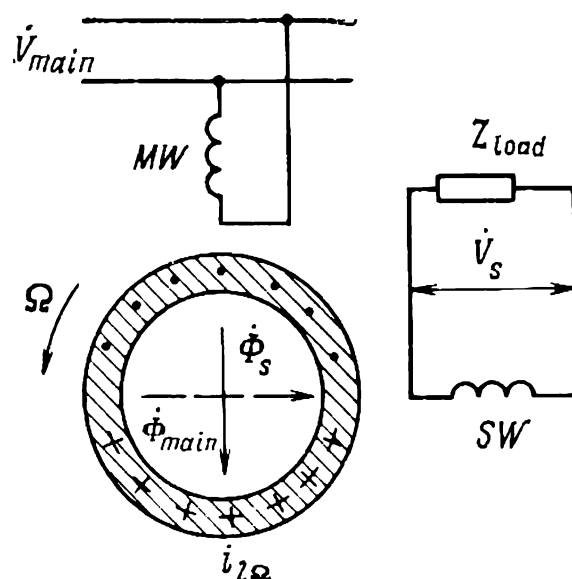


Fig. 49-4 Circuit of an induction tachometer-generator

synchronous units in which both the rms value and frequency of the signal emf are varying.

## 49-2 Induction Resolvers

Induction resolvers are used in various automatic control and computer circuits to convert an angular displacement (shaft position) to an alternating voltage whose peak value follows the angular position in a predetermined manner.

Most frequently, induction resolvers have two or more poles, two stator windings in electrical quadrature with

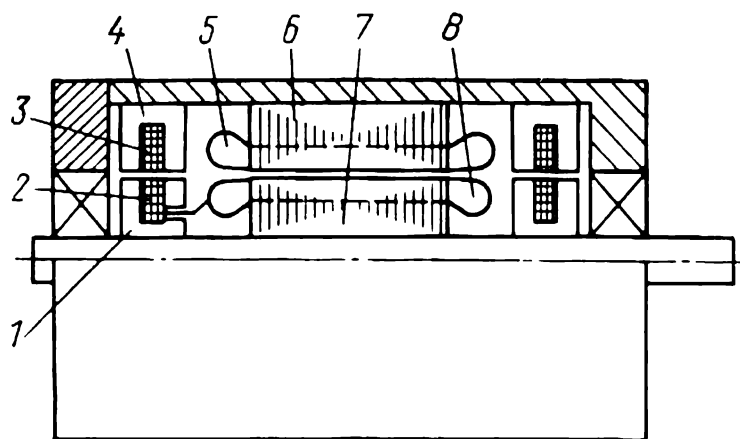


**Fig. 49-5** Brushless resolver:

1—rotating core of ring transformer; 2—rotating coil of ring transformer; 3—stationary coil of ring transformer; 4—stationary core of ring transformer; 5—synchro stator winding; 6—synchro stator core; 7—synchro rotor core; 8—synchro rotor winding

each other, and similar windings on the rotor. In fact, they are not unlike an induction motor with two-phase windings on the stator and rotor. Supply voltage is carried to the rotor by brushes and slip-rings or, if the rotation of the rotor is limited, by flexible conductors. In brushless resolvers, the rotor windings are energized by means of two intermediate ring transformers shown in Fig. 49-5.

For an induction resolver to perform its function, the mutual inductance between the stator and rotor windings must be varying with the angular displacement (shaft position)  $\propto$  sinusoidally or cosinusoidally. This requires that the magnetic fields set up by the windings be as close to sinusoidal as practicable. To this end, so-called “sinewave” windings are used, in which the number of turns is varied from slot to slot in an appropriate manner. Also, the laminations in the cores are stacked up so that every next layer

of punchings is displaced from the previous one by one or several tooth (or slot) pitches. The emfs that are likely to be generated by the higher harmonic fields are minimized by skewing the rotor slots one slot pitch. Furthermore, special care is taken to avoid inaccuracies in manufacture (the eccentricity between the stator and rotor on the sides facing the air gap, dissymmetry of the core, inaccuracy in slot skewing). As a net result of all these measures, high-accuracy resolvers generate the  $\sin \alpha$  and  $\cos \alpha$  functions accurate to within 0.01-0.02%.

In multipole resolvers, the output voltage undergoes a complete cycle of change as the rotor turns through  $2\pi/p$ , so for each revolution of the rotor the output voltage has  $p$  cycles of change. Therefore, the error in output voltage, referred to the mechanical angle of rotation, is  $1/p$  of the error referred to the electrical angle. In high-accuracy multipole resolvers, the output voltage goes through 60 to 120 cycles of change every revolution of the rotor. Such resolvers use concentrated windings. For a still better generation of  $\sin \alpha$  and  $\cos \alpha$  functions, an optimal tooth width is chosen and the slots are skewed one slot (or tooth) pitch.

The manner in which the windings of a resolver are connected in the associated circuit and fed with supply voltage(s) depends on the job it is intended to do.

**Sine-cosine induction resolver.** This device (Fig. 49-6) transforms an angular displacement (shaft position),  $\alpha$ , into two a.c. voltages,  $V_a$  and  $V_b$ , proportional in amplitude to  $\cos \alpha$  and  $\sin \alpha$ , respectively. A sine-cosine resolver has three windings,  $d$ ,  $a$ , and  $b$ . Winding  $d$  sets up the excitation field and is energized from an a.c. stabilized supply. The pulsating magnetic field set up by this winding induces an emf,  $E_a$ , proportional to  $\cos \alpha$  in winding  $a$ , and an emf,  $E_b$ , proportional to  $\sin \alpha$  in winding  $b$ . If we connect the rotor windings to loads with impe-

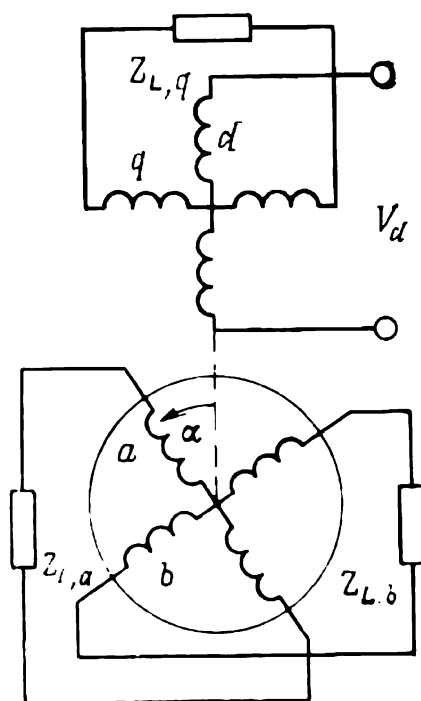


Fig. 49-6 Sine-cosine resolver

dances,  $Z_{L,a}$  and  $Z_{L,b}$ , currents will flow in them, giving rise to a secondary magnetic field.

So that the secondary field could not upset the cosine and sine relationship between the two emfs and the angular displacement, the resolver is subjected to secondary and primary balancing. For secondary balancing, the load impedances are chosen to be equal in value,  $Z_{L,a} = Z_{L,b}$ .

Primary balancing is effected by closing the quadrature ( $q$ -) winding of the stator across an impedance,  $Z_{L,q}$ , equal in magnitude to the internal impedance of the supply connected to the direct-axis ( $d$ -) winding. As a result, the currents induced in the  $q$ - and  $d$ -windings balance out the secondary fluxes to the same degree.

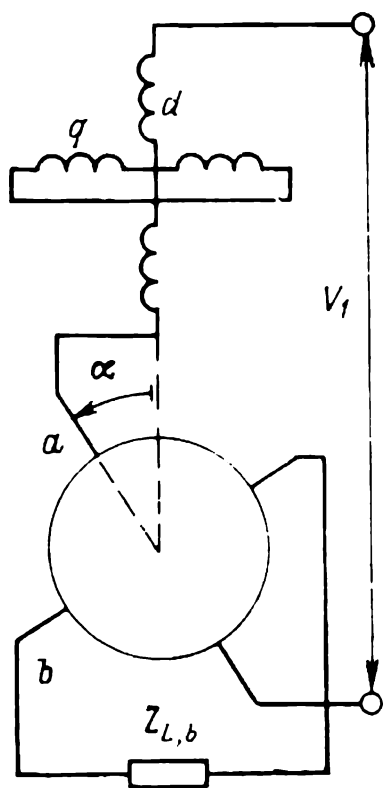


Fig. 49-7 Circuit of a linear induction resolver

**Linear resolver.** This device (Fig. 49-7) serves to convert angular displacement (shaft position),  $\alpha$ , into an alternating voltage,  $V_b$ , whose amplitude is proportional to the angle  $\alpha$ . In a linear resolver, the  $d$ -winding on the stator and

the cosine (or  $a$ -) winding on the rotor are connected in series and to an a.c. supply. The quadrature ( $q$ -) winding is short-circuited. The output voltage,  $V_b$ , is picked off the sine ( $b$ -) winding connected across a load impedance,  $Z_{L,b}$ .

In this connection, the  $q$ -component of the secondary flux is nearly completely damped out by the current induced in it. Therefore, in analyzing the operation of a linear resolver, we may neglect the flux along the  $q$ -axis and deem that all of the emf is induced by the direct-axis field (one along the  $d$ -axis) alone. Then, on assuming that the winding parameters are small, we may write the following voltage equation for the excitation circuit:

$$V_1 = E_d + E \cos \alpha = E_d (1 + n \cos \alpha)$$

and for the output circuit:

$$V_b = E \sin \alpha = nE_d \sin \alpha$$

where  $n = E/E_d$  is the transformation ratio. On eliminating  $E_d$  between the above equations, we get

$$V_b = nV_1 \sin \alpha / (1 + n \cos \alpha)$$

It is an easy matter to see that at  $n = 0.536$  the term  $\sin \alpha / (1 + n \cos \alpha)$  is equal to the angle  $\alpha$  accurate to within 0.06%, if the angle lies in the range from  $-60^\circ$  to  $+60^\circ$ . Hence, if we choose  $n = 0.536$ , the output voltage,  $V_b$ , will be proportional to the angular displacement,  $\alpha$ , that is

$$V_b = nV_1\alpha$$

**Coordinate transformation by induction resolvers.** The connection of an induction resolver for the transformation of Cartesian coordinates to account for the rotation of the coordinate axes is shown in Fig. 49-8. The  $d$ - and  $q$ -windings on the stator are energized with  $V_d$  and  $V_q$ , which are in phase. Their amplitudes are proportional to the coordinates being transformed,  $V_d \sim y$  and  $V_q \sim x$ . On applying primary and secondary balancing, the secondary voltages will be

$$V_a = m (V_d \cos \alpha + V_q \sin \alpha)$$

$$V_b = m (V_d \sin \alpha - V_q \cos \alpha)$$

That is, they are proportional, within the scale factor  $m$ , to the coordinate in the system turned through the angle  $\alpha$ .

For rectangular-to-polar coordinate transformation, an induction resolver is connected as shown in Fig. 49-9. As in the previous case, the  $d$ - and  $q$ -windings on the stator are supplied with voltages  $V_d$  and  $V_q$ , respectively. These voltages are in phase and have amplitudes proportional to the coordinates to be transformed, that is,  $V_d \sim y$  and  $V_q \sim x$ .

An appropriate servo system consisting of a servo motor  $M$  and a servo amplifier  $SA$  causes the rotor of the resolver to

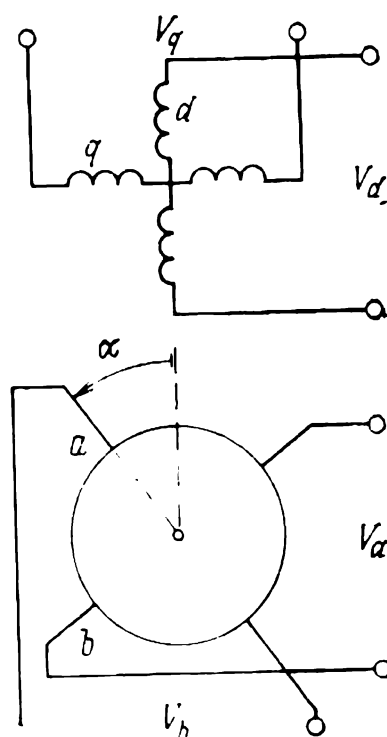


Fig. 49-8 Connection of an induction resolver for transformation of Cartesian coordinates upon rotation

take up an angular position in which the voltage across the sine winding is reduced to zero:

$$V_b = m (V_d \sin \alpha - V_q \cos \alpha) = 0$$

In this position, the voltage across the cosine winding is

$$V_a = m \sqrt{V_d^2 + V_q^2} \sim \sqrt{y^2 + x^2}$$

On an appropriately chosen scale, this gives a radial coordinate,  $r \sim V_a$ . At the same time, the angular position of the

rotor in electrical degrees,  $\alpha$ , is the same as the angle  $\theta$  in polar coordinates.

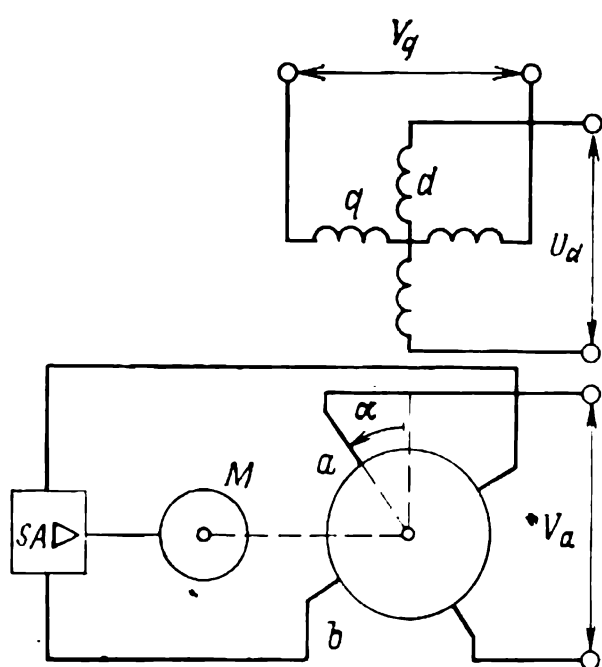


Fig. 49-9 Connection of an induction resolver for rectangular-to-polar coordinate transformation

**Inductosyn.** A refinement of the induction resolver discussed above is the *inductosyn* which can be made in a flat form, either circular or linear. A circular inductosyn consists essentially of two insulating (most often, glass) discs on which the coil conductors are printed. The two discs are mounted on a common shaft coaxially and separated from each other by an air gap. One of the discs, called the rotor, is free to rotate relative to the other, called the stator.

In performance, the inductosyn is similar to a concentrated-winding, multipolar induction resolver. However, it is more accurate owing to a large number of poles on the rotor and stator and the absence of conventional cores.

### 49-3 Synchros

The name “synchro” refers to a class of induction machines adapted for the remote measurement and/or transmission of angular position.

Synchros may be brush-type or brushless. In the former case, a salient-pole rotor carries a concentrated field winding,  $FW$ , which draws its current from an a.c. supply via slip-rings and brushes (not shown in Fig. 49-10). The stator slots accommodate three distributed synchronizing windings dis-

placed from one another by an electrical angle of  $2\pi/3$  and arranged similarly to the three-phase winding of a conventional induction machine. The stator and rotor cores are built up of insulated electrical-sheet steel laminations.

Three forms of synchro systems have found wide use in practice, namely: the direct (or data) transmission type

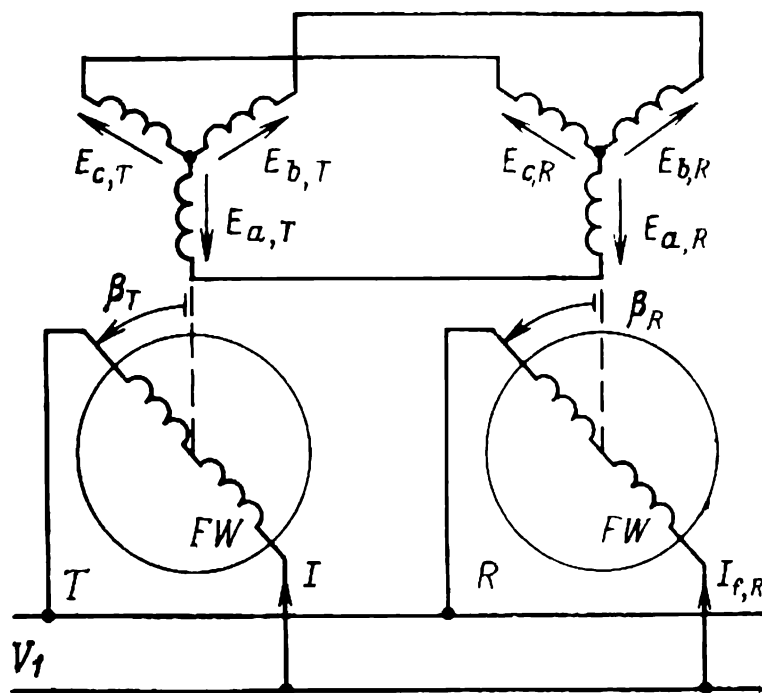


Fig. 49-10 Circuit of a direct transmission synchro system

(sometimes referred to also as the synchro repeater system), the differential-synchro type, and the control-transformer type.

In the direct transmission type, there is a synchro transmitter (or generator) and a synchro receiver (or motor), interconnected as shown in Fig. 49-10. The synchro receiver is usually of a size just sufficient to drive the pointer of an indicator. The field (rotor) windings,  $FW$ , of both the synchro transmitter and synchro receiver are supplied with  $V_1$  from a common supply, and the leads of the like phases in the synchronizing (stator) windings,  $SW$ , are interconnected as shown in Fig. 49-10.

When so energized, the rotor winding in the synchro receiver takes up an angular position that corresponds to the position of the rotor in the synchro transmitter,  $\beta_T = \beta_R$ . Because of this, the emfs induced by the pulsating rotor field in the like phases of the stator windings in both the transmitter and receiver are identical:

$$\dot{E}_{a,T} = \dot{E}_{a,R}, \quad \dot{E}_{b,T} = \dot{E}_{b,R}, \quad \dot{E}_{c,T} = \dot{E}_{c,R}$$

In the loops formed by the interconnected phases, these emfs are in opposition to one another. Therefore, no currents



are flowing in the stator windings, and the two synchros develop zero torques. Any change in the position of the transmitter rotor is not immediately followed by the receiver rotor, and their positions differ by what is called the *error angle*,

$$\Delta\beta = \beta_T - \beta_R$$

So long as the error angle is nonzero, the balance of emfs in the like phases is upset ( $E_{a,T} \neq E_{a,R}$ , and so on), currents begin to flow in the stator windings, and the currents in the rotor windings cease to be the same. The interaction of the stator and rotor currents produces torques,  $T_{em,T}$  and  $T_{em,R}$ , which act on the transmitter and receiver rotors, respectively. By a well-known rule, it can be found that these torques act in the opposite directions, so that the receiver rotor is constrained to take up the same position as the transmitter rotor, and the error angle reduces to zero,  $\Delta\beta = 0$ .

In actual systems, the receiver rotor is always acted upon by a small resistance torque due to friction in the bearings and at the slip-rings, and also the load torque due to the device coupled to the synchro shaft (this may be the pointer of an indicator, the wiper of a servo-operated potentiometer, and the like).

Because of this, when the two units are at rest, their positions will agree within a certain static error,  $\Delta\beta$ . An amount of inaccuracy (or uncertainty) may be added by manufacturing tolerances, the structure of the cores, etc. Depending on the accuracy class, synchros may be accurate to within 0.25 to 2.5 degrees of an arc.

Brushless synchros come in two basic modifications, namely nonsalient synchros with a ring transformer, and claw-pole synchros. In the former type, the single-phase rotor (field) winding, *FW*, is supplied from a ring transformer similar to that used in brushless induction resolvers (see Fig. 49-5). In the latter case (see Fig. 49-11), the field winding, 3, and the synchronizing winding, 4 are both wound on the stator, whereas the rotor carried in bearings 8 is made unwound. The synchronizing winding is placed in slots on the stator, 5. Both the winding and the stator core do not differ from their counterparts in a brush-type synchro.

In the synchro of Fig. 49-11, the heteropolar excitation field linking the synchronizing winding is established by the stationary field winding made up of two ring-shaped coils, 3.

The coils are supplied with a.c. and set up a pulsating flux which has its path completed around the coils as shown in the figure by the dashed line. This path runs through the stator frame 2, a nonmagnetic gap, the right-hand claw-pole 1, the nonmagnetic gap, the teeth and yoke of the stator core 5, the nonmagnetic gap, the left-hand claw-pole 1, the nonmagnetic gap, the teeth and yoke of the stator core 5, the nonmagnetic gap, the left-hand claw-pole 1, the nonmagnetic gap, the teeth and yoke of the stator core 5, the nonmagnetic gap, the right-hand claw-pole 1, the nonmagnetic gap, the stator frame 2, and so on.

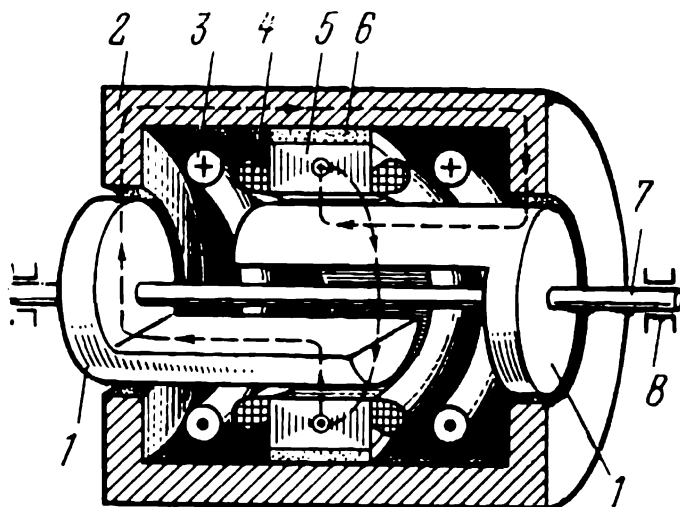


Fig. 49-11 Arrangement of a brushless synchro

and again the gap. In order to prevent the flux from “shorting” between the poles without threading the stator core and linking the synchronizing winding, the claw poles are separated by a nonmagnetic gap, and the shaft, 7, is made of a nonmagnetic material. Any other undesirable path for the flux is avoided by providing a broad gap 6 between the stator core and frame.

With the above arrangement, the field in the stator core varies with the rotation of the rotor in the same manner as in a conventional brush-type synchro.

Brushless synchros are more reliable and accurate, but their design is more elaborate and they have a larger size and mass.

## ☆ 50 Practical Induction Motors

### 50-1 General

In the Soviet Union, induction motors are fabricated in standard or unified ranges covering between them all the necessary power ratings and rpms.

General-purpose induction motors come in a fixed spectrum of power ratings at any rpm. Basic models are intended for a 50-Hz supply.

The more recent makes of induction motors are manufactured in compliance with relevant IEC recommendations as regards outline and mounting dimensions, so they are interchangeable with other makers' motors.

For the most part, the induction motors of Soviet manufacture are the squirrel-cage type, designed for the moderate climates.

The insulation is class E, class B, and class F, depending on motor size and axis height.

The terminal boxes on the motors are of enclosed construction, with a gland for attachment of a rigid or a flexible conduit or a cable.

**50-2      Modifications of the Basic Models**

Modifications involve tropicalization, enhanced resistance to chemicals, moisture, frost, etc. Some makes are adapted to a 60-Hz supply. In size, modified units are the same as their respective basic models.

As regards the type of enclosure, Soviet makers turn out splash-proof units (the enclosure will not permit entry of drops falling at 60° from the vertical, Fig. 50-1), and totally enclosed (the enclosure will keep out solid particles at least 1 mm in diameter and drops of water falling from any direction).

**Table 50-1    Electrical Modifications of Induction Motors**

Modification	Application
High starting torque	Heavy starting requirements (compressors, crushers, pug mills, etc.)
High-slip	High moments of inertia, pulsating load torque, frequent starting and reversals
High-performance (high efficiency and power factor)	Operation on a round-the-clock basis
Wound-rotor	Where the supply line does not have a sufficient power to start squirrel-cage units. In applications calling for continuous speed control downwards from the synchronous one
Low-noise	Where high noise level is prohibited
Multispeed	Drives for machine-tools, winches, etc.
Built-in	For machine-tools and other machinery

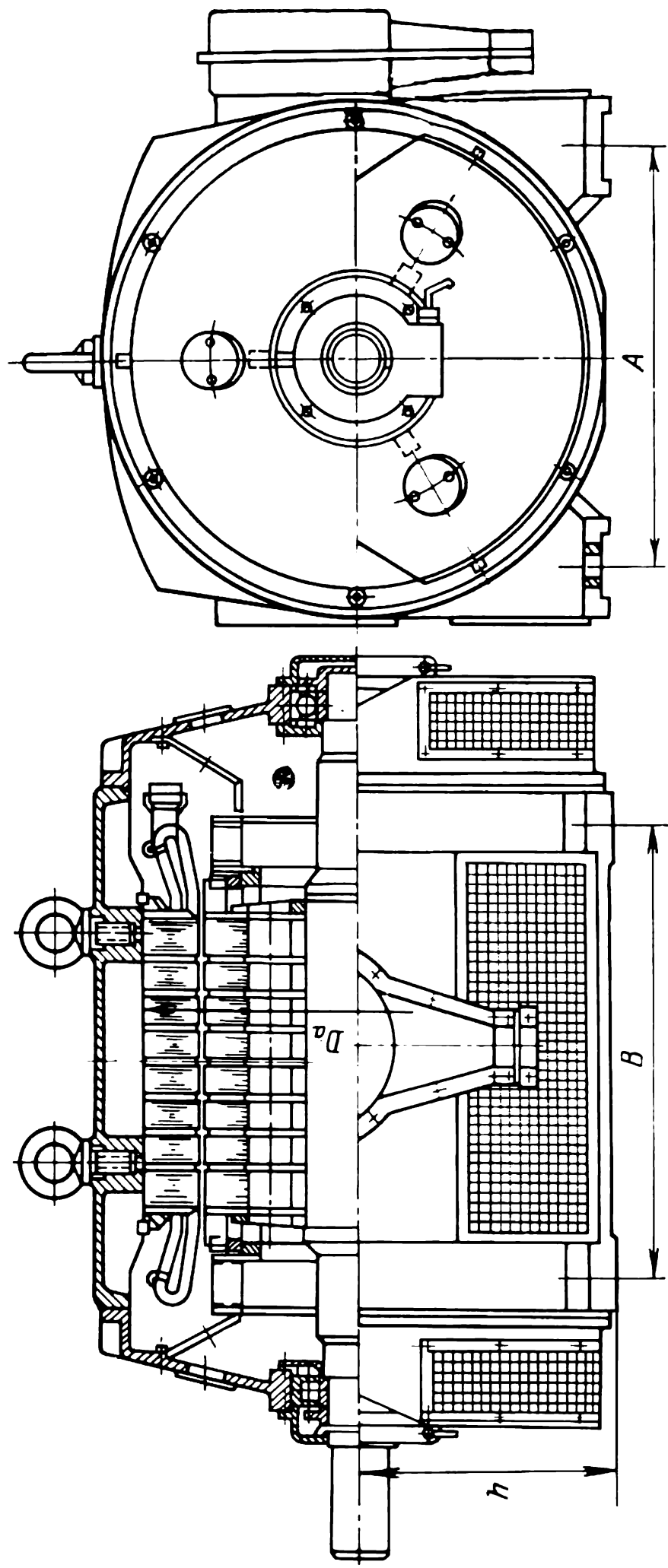


Fig. 50-1 Splash-proof induction motor

## 51 A General Outline of Synchronous Machines

### 51-1 Purpose and Field of Application

A synchronous machine is an a.c. two-winding machine in which one winding is connected to a supply line operating at a constant frequency  $\omega_1$ , and the other is excited by direct current ( $\omega_2 = 0$ )\*. It owes its name, “synchronous”, to the fact that the rotor must rotate at synchronous speed, that is, the speed corresponding to the frequency of the a.c. supply.

Most frequently, the stator carries a heteropolar, three-phase,  $2p$ -pole armature winding (see Chap. 22), and the rotor carries a heteropolar  $2p$ -pole field winding (Fig. 51-1a).

On small machines (2-5 kW), the armature is sometimes wound on the rotor; this is known as the *inverted arrangement* (Fig. 51-1b). The field winding is then wound on the stator. Whether the armature is wound on the stator or rotor does not affect the electromagnetic performance of the machine. However, for big machines, the normal arrangement with the armature on the stator is preferable. The point is that the sliding contacts on the rotor carry as little as 0.3% to 2% of the converted power, whereas in the inverted arrangement they have to transfer total power.

The part of the machine carrying the armature winding is called the *armature*, and the part carrying the field winding is sometimes called the *field structure*. So, in the normal arrangement, the stator is the armature, and in the inverted arrangement, the rotor is the armature.

---

\* In a wider sense, the term “synchronous” refers to two-winding a.c. machines in which both windings are excited from supply lines at fixed frequencies,  $\omega_1$  and  $\omega_2$  (see Sec. 21-2).

Frequently, the excitation field for synchronous machines is established by permanent magnets.

The primary use for synchronous machines is to convert mechanical energy to electricity. The bulk of the energy used in the Soviet Union is supplied by synchronous three-phase generators driven by steam, gas, or water turbines.

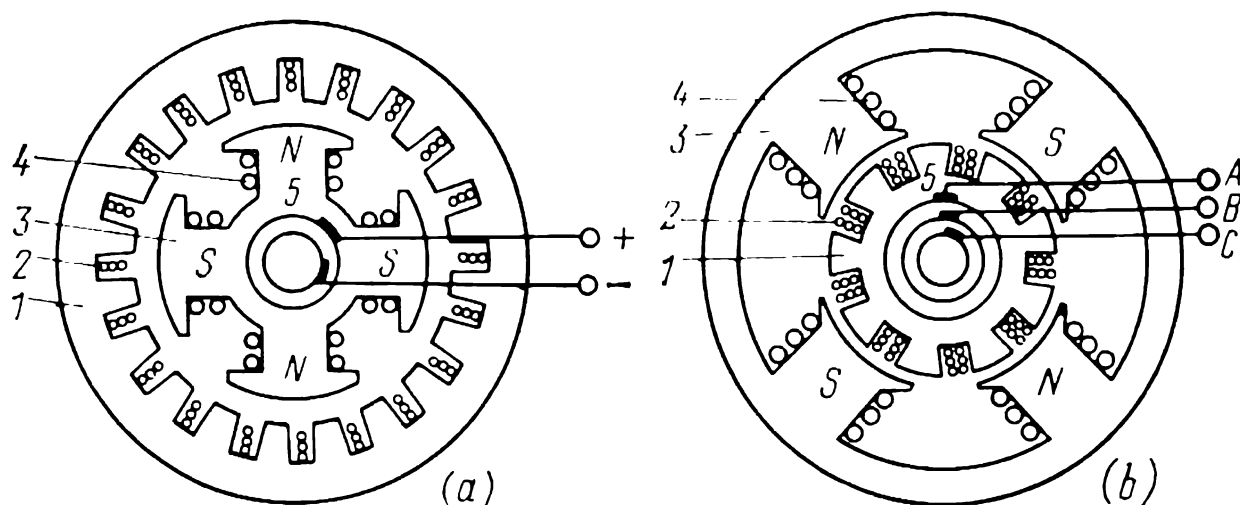


**Fig. 51-1** Synchronous machine: (a) normal (rotating-field) and (b) inverted (stationary-field) arrangement

1—armature core; 2—three-phase armature winding; 3—field-structure core; 4—field winding; 5—brushgear

There are also *engine-type* synchronous generators (those driven by Diesel, gasoline, or steam engines); they are built for small outputs and supply isolated loads.

The second important application for synchronous machines is as motors, especially for large units (reciprocating compressors, blowers, and hydraulic pumps). They compare favourable with induction motors in that they generate rather than expend reactive power. Small synchronous motors (notably those with permanent-magnet excitation) are very popular, too.

As a rule, synchronous machines are designed so that they can generate reactive power about equal to the active power (about 60% and 80% of the total power, respectively). Sometimes, it is advantageous to install near major industrial centres what are known as *synchronous condensers*—synchronous machines specifically built to generate reactive power only.

The data ordinarily stated on the nameplates of synchronous machines include the following:

- (a) Power rating (the total kVA for generators and synchronous condensers, and the shaft kW for motors).
- (b) The rated power factor (at overexcitation).

- (c) The rated efficiency (for motors only).
- (d) The stator phase connection.
- (e) The rated line voltage of the armature (stator) winding, V.
- (f) The rated rpm (and also the runaway rpm for hydro-electric generators).
- (g) The rated frequency of the armature current, Hz.
- (h) The rated line current of the armature, A.
- (i) The rated voltage and current of the field winding, V.

In the Soviet Union, all industrial synchronous machines are built for a 50-Hz supply. The requisite synchronous speed  $n$  (in rpm) or the requisite angular velocity  $\Omega$  (in radians per second) is obtained by securing the number of pole pairs as given by the following equation:

$$p = 60f/n = 2\pi f/\Omega$$

The numbers of pole pairs for some likely rpms are listed below.

$p$	. . . . .	1	2	3	4	8	16	32	64
$n$ , rpm	. .	3000	1500	1000	750	375	187.5	93.7	46.9

Depending on the turbine power rating and the water head available, the speed of hydro-electric generators ranges anywhere between 50 and 600 rpm. The higher speed hold for high-head dams with low-power turbines, and the lower speeds apply to low-head dams with large turbines.

In the Soviet Union, steam- and gas-turbine generators are built for 3 000 rpm and have two poles. Four-pole turbo-generators are built in the Soviet Union for nuclear power stations where the steam pressure and temperature are not high enough for the turbines to run faster than at 1 500 rpm.

The conditions under which hydro-electric and turbine-driven generators are operated affect their design. *Hydro-electric generators* (see Fig. 51-2) are predominantly built with their shaft in an upright position. The turbine is located under the generator, and its shaft carrying the impeller is coupled to the generator shaft by a flanged joint. Because the rpm is low, whereas the number of poles is high, the rotor of the generator has a large diameter and a relatively short active length. As a rule, the rotor is of salient-pole construction (see below). The active (electrical) parts take up a relatively small fraction of the total volume, the larger proportion being occupied by the structural (or me-

chanical) parts, such as the thrust bearing which supports all the rotating parts of the generator and turbine, the guide bearings to hold the rotor in its designated position, the top and bottom spiders giving support to the bearings, the stator frame, the rotor hub, air coolers, oil coolers, etc.

Generating units consisting each of a turbine and a hydro-electric generator are the biggest machines used in any industry. With a power output of 200 to 600 MVA apiece, they stand 20 to 30 m high. The world's largest hydro-electric generators are those built for the Sayano-Shushensk Station in the Soviet Union. They spin at 143 rpm and generate 715 MVA of power. The outside diameter of such a generator is about 15 m, and that of its rotor is about 12 m; the stator core is 2.75 m long.

In contrast to hydro-electric generators, *turbogenerators* are nearly always made with a horizontal shaft (see Fig. 51-5). The rotors of turbogenerators are usually of round (or cylindrical) construction, and their diameters are smaller than their active length. At 3 000 rpm, the limits (chosen from considerations of mechanical strength) are 1.2-1.25 m for the diameter and 6.0-6.5 m for the length. Because the structural parts are smaller in size, the active (electrical) parts account for a larger proportion of the total volume.

A recent trend in generator engineering has been to build units of ever increasing power ratings. As regards turbine-driven generators, this is achieved without an appreciable increase in physical size, through the use of better cooling methods and systems. Taking the Soviet Union as an example, the 800-MW to 1000-MW turbogenerators designed in the 1970s had practically the same overall dimensions as the 100-MW machines built in the 1940s. The only difference is that the newer machines use direct cooling for the windings by hydrogen at a pressure of  $5 \times 10^5$  Pa, distilled water, or mineral oil.

Synchronous motors of Soviet manufacture are commercially available in power ratings from 100 kW to tens of megawatts and with speeds from 3 000 to 100 rpm. 3000-rpm and 1500-rpm units have cylindrical rotors and are close in the general arrangement to turbogenerators. Units for 1 000 rpm and less have salient-pole rotors and are close in the general arrangement to hydro-electric generators when made with a vertical shaft, or to Diesel-driven generators when made with a horizontal shaft.



For pumped-storage stations, synchronous machines are designed for both motor and generator operation. When used as motors, they drive the pumps that move water to the upper reservoir. When the water released from the upper reservoir drives the associated turbine(s), the latter actuates the machine to operate as a generator. Such machines come in ratings of 200 to 300 MW.

*Synchronous condensers* of Soviet manufacture come in ratings from 15 to 160 MVA and for speeds from 750 to 1 000 rpm. They have salient-pole rotors and, usually, hydrogen cooling.

Depending on power rating and rpm, the rated armature voltages may be from 0.23 kV to 15.75 kV for generators and from 0.22 to 10 kV for motors. In large turbogenerators and hydro-electric generators, it is from 18 to 24 kV. The rated field voltage is from 24 to 400 V.

The efficiency of synchronous machines improves as their power rating and rpm are increased. For ratings from 100 to 4 000 kVA, it is 0.9-0.95. For large hydro-electric generators and turbogenerators, it is 0.97-0.99. For more detail, see Chap. 62.

## ☆ 51-2 A Brief Historical Outline of Synchronous Machines

The single-phase multipolar synchronous generator was invented in 1832, a year after Faraday had discovered electromagnetic induction. An anonymous inventor who signed his patent application by the letters P.M. proposed to use permanent magnets as the source of field excitation. The horse shoe-shaped magnets were mounted around the periphery of a rotating disc so that they formed a system of poles alternating in polarity. Opposite the permanent magnets were stationary, massive steel coil-carrying cores mounted on a steel ring acting as the yoke. The number of cores was the same as that of magnet poles. Further work on synchronous generators was delayed for a long time, because all practical applications in those days required direct current.

It was not until 1863 that Wilde implemented in the synchronous generator the idea advanced in 1851 to replace the permanent magnets by electromagnets energized from an auxiliary d.c. generator which later came to be known as the exciter.

In Wilde's single-phase synchronous generator, the stationary field structure was a U-shaped electromagnet whose pole-pieces enclosed a rotating armature. Instead of a bar-shaped armature, Wilde used an H-shaped armature proposed by Siemens in 1856 and now known as the salient-pole construction. Physically, it was the shape of a cylinder with slots on the outer surface for a winding whose terminal leads were brought out on slip rings.

Work on synchronous generators was stimulated by the invention of the electric lamp by Yablochkov in 1876. Immediately after the invention, Gramme's works began quantity production of single-phase synchronous generators. Earlier, they were made in units on the basis of d.c. machines. Already in 1876, Yablochkov designed, in cooperation with Gramme, several synchronous generators similar in overall design, each intended to power a different number of electric lamps (four, six, sixteen, or twenty). In fact, they were polyphase synchronous machines in which the phases were electrically isolated. A unit designed to supply 16 lamps had 16 coils on a stationary ring armature and 8 d.c.-excited salient poles on the rotor. The coils were interconnected so that two electrically independent phases were formed, with their emfs displaced by a quarter of a cycle from each other.

Until the end of the 1880s, the armatures of a.c. generators were made solid. To minimize heating by eddy currents, the armature core was made as small as practicable, or was omitted altogether. This naturally led to an increase in the reluctance of the magnetic circuit and a reduced efficiency. Still, this principle was embodied in fairly large a.c. machines. In 1882, Gordon built a two-phase synchronous generator with two electrically uncoupled phases, to feed electric lamps. The generator was driven by a steam engine at 146 rpm and produced 115 kW of power.

The subsequent period in the development of a.c. generators was associated with Dobrowolsky who proposed the use of a three-phase system of currents and came out with many ideas and embodiments, including three-phase synchronous generators. Among other things, he used a drum (or barrel) armature winding composed of three parts interconnected in a delta or a star. This led to a generator design capable of supplying an interconnected three-phase system which, in contrast to a system with independent phases,

required three instead of six line conductors. In 1890, he proposed a four-wire, three-phase system. The fourth “wire” was, as Dobrowolsky suggested, the ground.

The first three-phase generator was designed by Brown of the Erlikon company, in cooperation with Dobrowolsky, for the experimental Laufen-Frankfurt power transmission line whose commissioning was timed with an international electrical engineering exhibition in 1891. The 95-V, 40-Hz, 150-rpm, 230 kVA generator was driven by a hydraulic turbine. It embodied all the latest advances in the field of d.c. electrical machines of that time, notably a drum armature winding placed in the slots of a toothed core built up of laminations. The three-phase winding was wound on the stator, and the field windings on the rotor—an arrangement that is still in use in present-day synchronous machines.

Instead of a salient-pole rotor ordinarily used in single-phase synchronous generators, Brown employed a ring-shaped field winding (common to all the poles) put around the shaft and placed between two steel blocks with claw-shaped projections that set up a system of poles alternating in polarity. This rotor design did not prove its worth, and now it can only be found in special-purpose synchronous generators (see Chap. 63).

Emphasis on nonsalient-pole synchronous machines was stimulated by the advent of steam turbines having faster speeds and higher efficiency than reciprocating steam engines. For the first time, steam turbines were used to drive three-phase generators in 1899. In that same year, an electric station was put in service at Elberfeld, where the turbines were of the multistage reactive type invented by Parsons in 1884. They served as the prime movers for 1000-kW turbogenerators.

The early turbogenerators had salient-pole rotors with concentrated field windings. In the first decade of the 20th century, turbogenerators came to use nonsalient-pole rotors with a distributed field winding.

### 51-3 Construction of Salient-Pole Synchronous Machines

The construction of a synchronous machine and, above all, of its rotor substantially depends on the desired speed\*. At  $n < 1\,500$  rpm and  $p > 2$ , which applies to hydro-electric generators, synchronous condensers and low-speed motors, the rotor is of the salient-pole type, and a machine using it is referred to as a *salient-pole machine*. At  $n = 3\,000$  (or  $1\,500$ ) rpm and  $p = 1$  (or  $2$ ), which applies to turbo-generators and turbomotors, the rotor is a nonsalient-pole (round or cylindrical) type, and a machine using it is called a *nonsalient-pole, (round-rotor or cylindrical-rotor) machine*.

An example of a salient-pole synchronous machine is the vertical-shaft hydro-electric generator shown in a cut-away view in Fig. 51-2.

The stator of a synchronous machine does not differ from that of an induction machine. With an outside diameter of less than one metre, the stator core is built up of one-piece ring-shaped electrical-sheet steel laminations (see Chap. 39 and Figs. 39-1, 39-3, and 39-6). With an outside diameter of over one metre, which is true of most synchronous machines, each layer of the core is assembled of many segments (which is also true of induction machines).

The segments (Fig. 51-3) are punched in electrical-sheet steel 0.5 mm thick. On the outer surface, the yoke of each segment has recesses for attachment to structural parts of the machine. The circumferential dimensions of segments and the layout of recesses (usually, dove-tailed) are chosen so that each layer contains a whole number of segments, and the segments in the next layer are shifted relative to those in the previous layer (usually, by a half-width). In this way, the air gaps between segments in one layer can be shunted by those in the next adjacent layers in the same way as in a transformer core stacked up of individual laminations. Of the two likely segment designs shown in Fig. 51-3, preference is usually given to that in Fig. 51-3a where all

---

\* Only large synchronous machines will be discussed here. For more detail on fractional-hp synchronous machines, refer to Chap. 63.

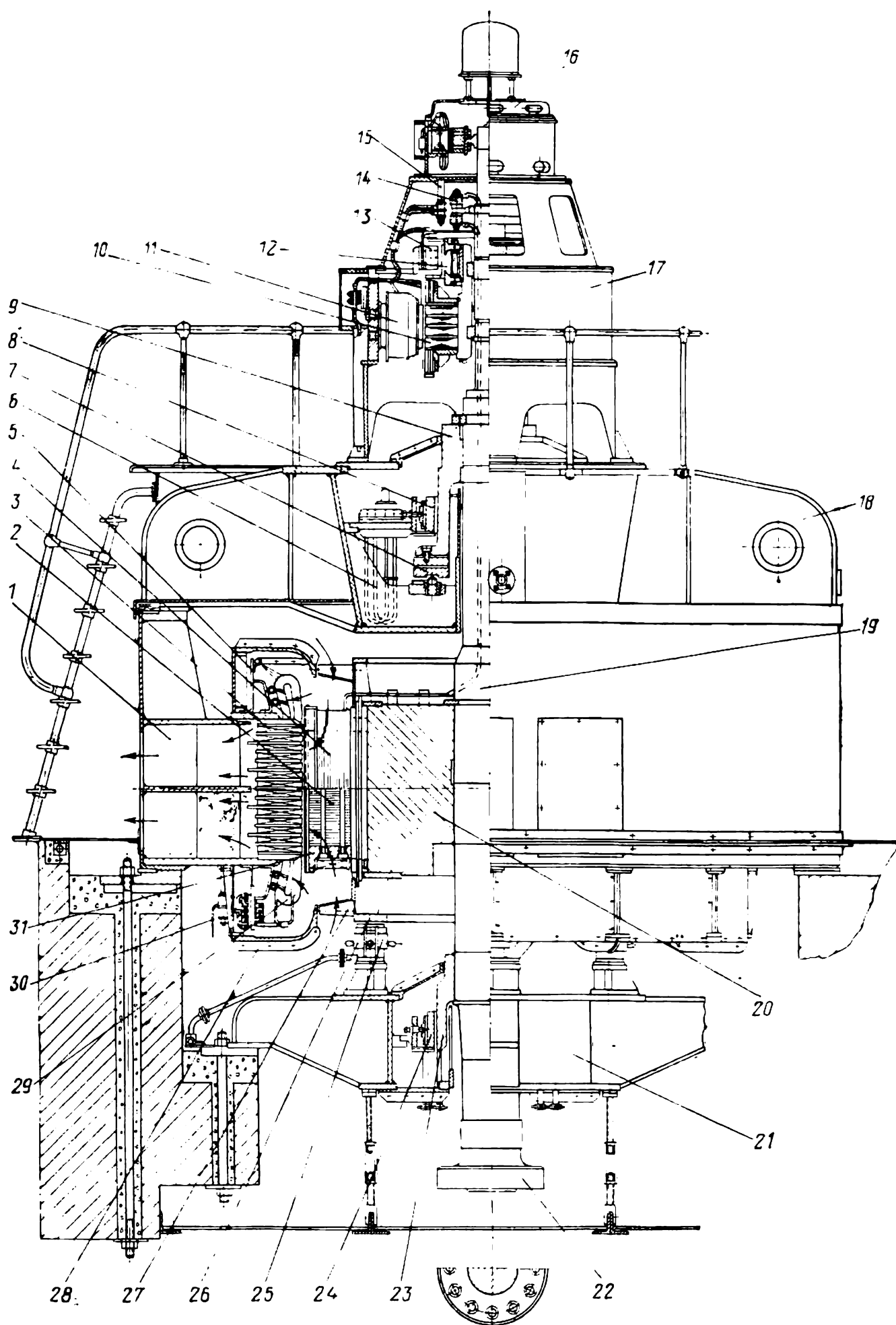


**Fig. 51-2 Indirectly air-cooled, salient-pole synchronous machine (hydro-electric generator):**

1—stator frame (yoke); 2—rotor pole; 3—stator core; 4—field coil; 5—winding bracket; 6—oil cooler; 7—thrust-bearing segment; 8—upper guide-bearing segment; 9—thrust and guide bearing sleeve; 10—exciter armature; 11—exciter pole and winding; 12—exciter commutator; 13—exciter brushgear; 14—generator slip rings; 15—slip-ring brushgear; 16—regulator generator; 17—exciter frame; 18—upper spider; 19—machine field to slip-ring connection; 20—rotor rim (yoke); 21—lower spider; 22—shaft; 23—lower guide bearing sleeve; 24—lower guide bearing segment; 25—brake; 26—rotor braking ring; 27—axial-flow fan; 28—air baffle; 29—stator coil; 30—coil winding terminal leads; 31—pole pressure plate

the teeth in a segment have the same strength and resistance to vibration.

A segment-type stator core (at 3 in Fig. 51-2) is stacked up on frame wedges 1 which enter the dove-tail recesses in the segments. Attachment of a wedge to the frame, 2, is shown in Fig. 51-4. An alternative form of attachment is shown in Fig. 51-5 where wedge 7 is made fast to frame 1

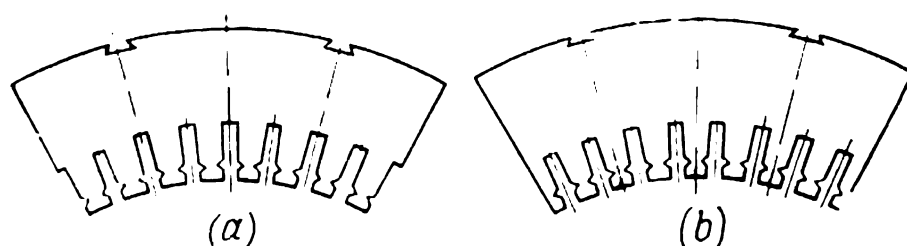


Fig. 51-3 Stator core segments: (a) with dove-tailed recesses on slot axis; (b) with dove-tailed recesses on tooth axis

by gussets 8. Axially, the core 6 is clamped by pressure segments 4, studs 3, and nuts 2. The studs are placed between the wedges, so in the sectional view they are seen at the background. A pressure segment, 4, and a vent segment, 5, which is included to form a radial ventilating duct in the core, are shown next to the sectional view of the stator in axonometric projection. Plates 9 fasten studs 3 to the frame and prevent them from vibration.

The slots in the stator core are usually of open design. They receive a heteropolar, three-phase winding (at 29 in Fig. 51-2).

Large salient-pole synchronous machines for 3 kV and higher use any one of two types of the two-layer winding, namely multiturn (from two to six turns) formed-coil lap windings, and bar-type (single-turn) wave windings. The insulation on a formed-coil and a bar-type winding is il-

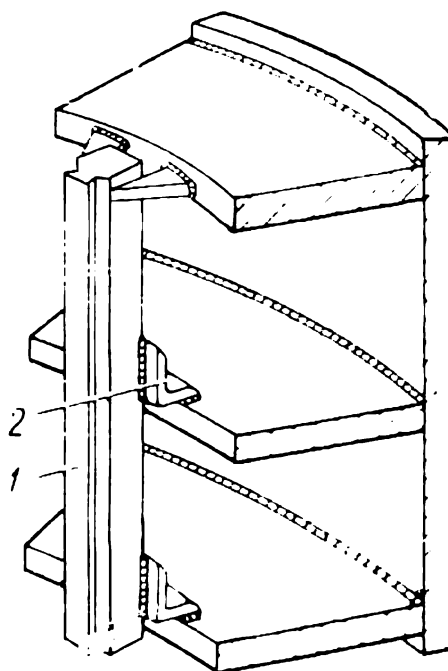


Fig. 51-4 Wedges welded to frame rings

illustrated in Fig. 51-6*a* and *b*, respectively. Each turn or bar of a winding consists of an even number of rectangular strands insulated from one another and arranged in two rows in the slot width. As a further remedy against the effect of eddy currents, it is usual to transpose the terminal

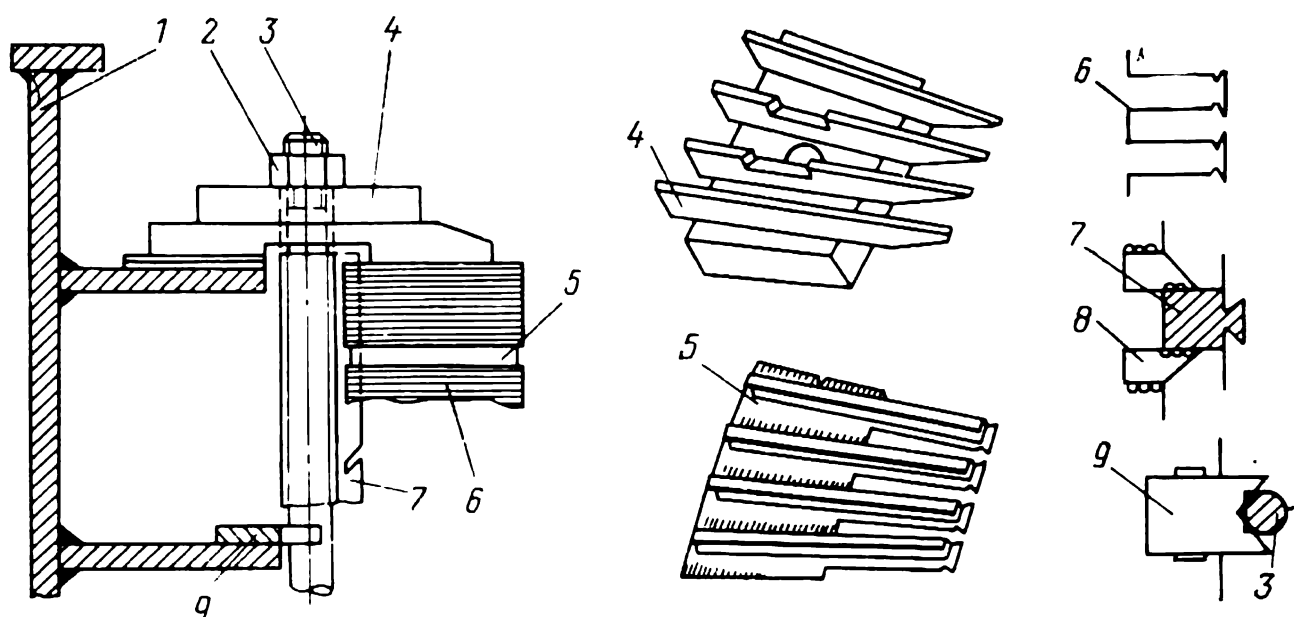


Fig. 51-5 Attachment of a segment-type core in the stator frame

leads and end connections (overhangs) of formed-coil windings and the strands within each slot in bar-type windings (see Sec. 31-2).

In a multi-turn formed-coil winding (see Fig. 51-6*a*), the turns consisting of one or several strands, 1, are insulated from one another by turn insulation, 2, and from the grounded parts by ground insulation, 3. In a bar-type winding (see Fig. 51-6*b*), the ground insulation, 3, also doubles as turn insulation. An insulating plate, 2, separates the adjacent rows of strands the voltage between which is very low (by two orders of magnitude lower than the turn voltage). As a way of reducing the electric field in the air gap between the ground insulation and the core, an outer wrapper of a semiconducting material, 4, is applied to the coil.

In large machines, the coil conductors, when energized, are subjected to appreciable electromagnetic forces. These forces are especially large at starting or in the case of a sudden short-circuit. To prevent damage to the coils or prohibitive vibration, the slot conductors, end connections and

overhangs must be reliably anchored in place. This is done with nonmagnetic built-up insulating wedges which are driven into recesses in the slot sides (at 7 in Fig. 51-6). As a further safety measure, insulating plates 6, 5 and 8 are placed under the wedges, between the layers, and at the slot bottom. Their thickness is chosen so as not to leave any clearance between the wedge and the coil.

The coil ends, or overhangs (at 5 in Fig. 51-7) are anchored by distance pieces 2 inserted between adjacent coil bars, and binding rings, 1, placed around the overhangs from the outside. Adjacent bar conductors between distance pieces are tied together by a strong cord, 3. A similar cord is used to tie the bar conductors (or formed coils) to the binding rings (in large machines, there may be several binding rings on either side of the stator). The connections between coils, 4, are tied by a cord to the overhangs (as shown in Fig. 51-7) or to brackets attached to the frame (as in Fig. 51-2).

The rotor core of a d.c.-excited salient-pole synchronous machine may be made solid or stacked up of individual punchings whose thickness is chosen from engineering and manufacturing considerations. In the generator of Fig. 51-2, the poles, 2, are built up of steel punchings 1.5 mm thick, the rotor rim (or yoke), 20, is made of a solid steel forging mounted on a shaft, 22. Sometimes, the poles may likewise

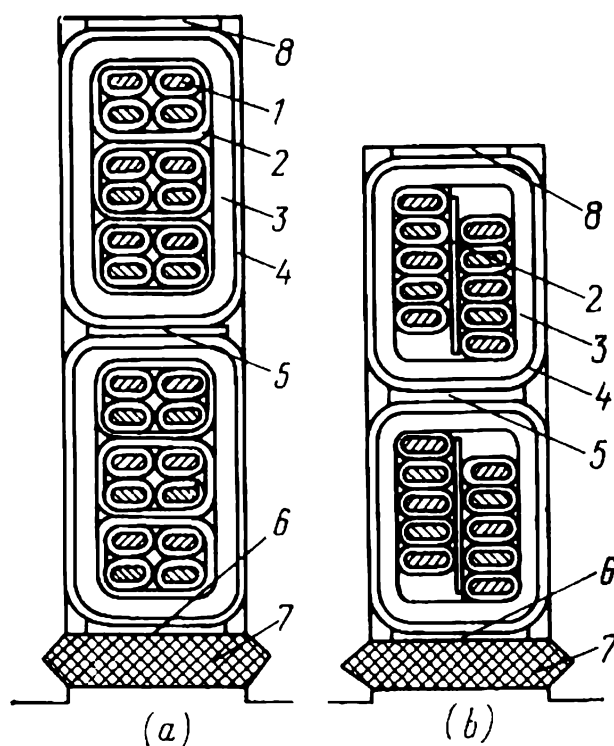


Fig. 51-6 Sectional views of slots with (a) two-layer formed-coil winding and (b) two-layer bar-type winding

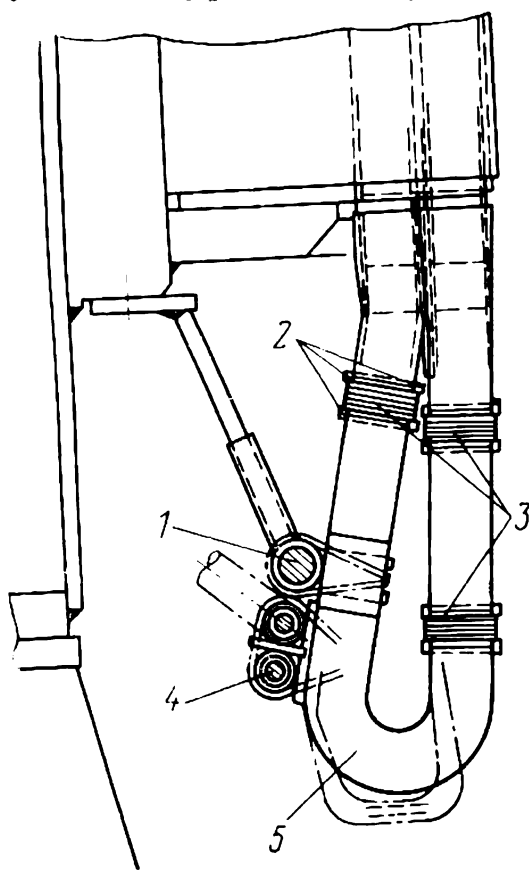
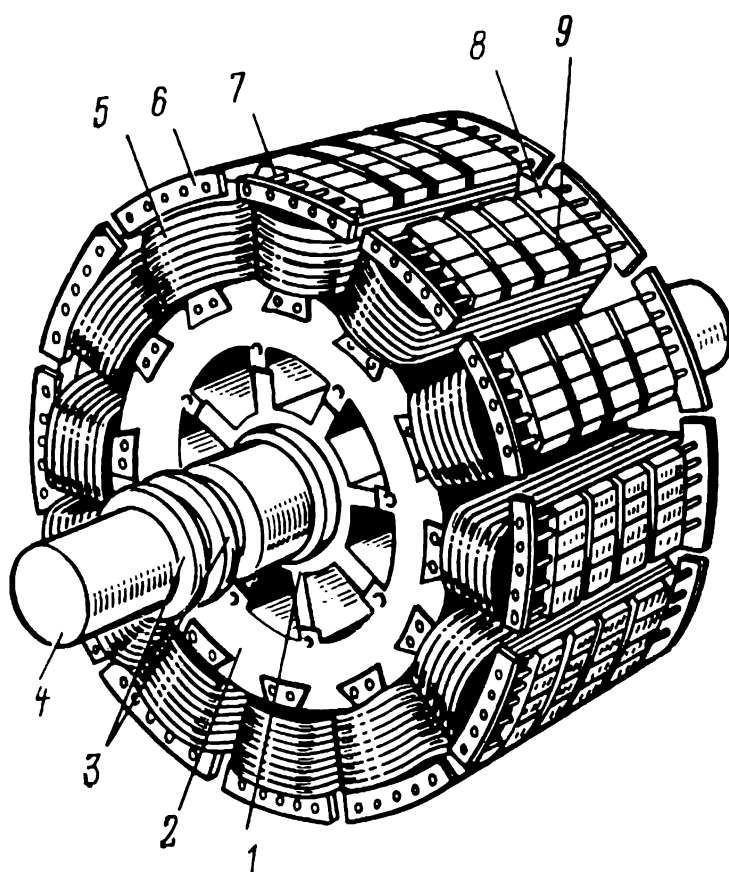


Fig. 51-7 Stator coil end (overhang) secured in place



be made solid. Most frequently, the rotor yoke is built up of steel plates 2 to 6 mm thick (if the plates are punched in a press) or to 100 mm (if they are gas-cut). The plates are clamped by studs. With an outside diameter of 2 to 4 m, the rotor yoke is made of one-piece ring-shaped plates and is mounted on a shaft directly. With a larger outside diameter, the yoke is assembled of individual segments held together by clamping studs and is mounted on a hub or



**Fig. 51-8** Salient-pole rotor:

1—rotor spider; 2—rotor rim (yoke); 3—slip rings; 4—shaft; 5—field coil; 6—damper winding segment; 7—damper winding bar; 8—pole core; 9—vent duct in pole

spider, 1, as in the case of the salient-pole rotor shown in Fig. 51-8. For better ventilation in the case of long machines, the yoke is divided into several blocks separated by vent ducts which give access for cooling air to the peripheral parts of the rotor. Sometimes (Fig. 51-8), radial vent ducts, 9, are also made in the poles.

The poles usually have a smaller width than their pole-pieces (or pole-shoes). Therefore, in order that preformed field coils, 4, could be put on the poles, the latter or their pole-pieces must be made detachable. Figure 51-9 shows the most commonly used design which employs detachable poles assembled of electrical-sheet steel punchings, 1-2 mm

thick, axially clamped by studs *10*. The poles are attached to the rotor core by means of T-shaped shanks, *11*, each of which terminates in two pairs of opposing rectangular steel wedges, *2*.

In laminated poles important elements are pressure, or end, plates having the same shape as the pole laminations.

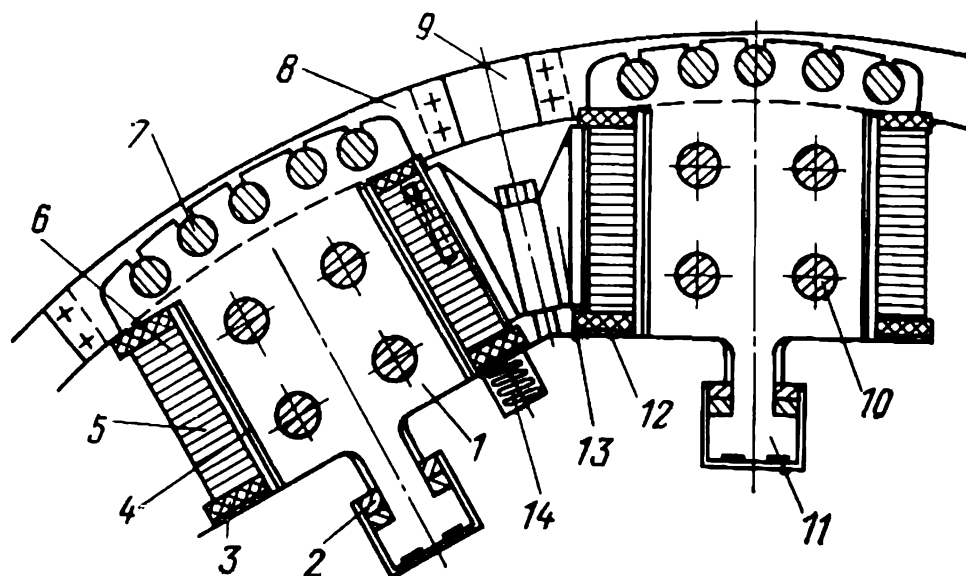


Fig. 51-9 Sectional view of a salient-pole rotor:

1—pole; 2—dove-tail joint wedges; 3—insulating washer; 4—pole ground insulation; 5—bare field coil conductor; 6—turn (or conductor) insulation; 7—damper-winding bar; 8—damper-winding segment; 9—pig-tail (flexible conductor) between segments; 10—clamping stud; 11—T-shaped pole shank; 12—steel washer; 13—interpole spacer; 14—spring

Their purpose is to distribute the force applied by the clamping studs evenly over the entire surface area of the pole lamination. The pressure plates (at *31* in Fig. 51-2) can be seen well in the sectional view of the generator.

The field coils are wound on edge with bare copper strip conductors of a large cross-sectional area (200 to 800 mm<sup>2</sup>). The conductors may be rectangular in cross-section (as at *5* in Fig. 51-9), or (such as for large hydroelectric generators) they may be given the shape of an axe for better cooling of the coil.

After conductor or turn insulation, *6*, impregnated in thermosetting resin, has been installed between adjacent turns, the coil is clamped and baked. Ground insulation, *4*, is applied to the poles before the coils are dropped in place. The manner in which coils are anchored on a pole can be seen from Fig. 51-9. The centrifugal force of the slot parts directed along the pole axis is resisted by the pole-piece tips insulated from the coil by a washer, *3*.

Recesses in the yoke hold springs *14* which act through a steel washer *12* and an insulating washer *3* and force the coil against the pole, thereby preventing any radial displacement of the coil at low speed. The normal component of the centrifugal force might deform the coil conductors. To avoid this, high-speed machines with a large active length may sometimes have one or (though seldom) several packing blocks *13* installed between the coils on adjacent poles.

The centrifugal force of the coil ends is taken up by the pole pressure tip (at *31* in Fig. 51-2). The field winding, *4*, is energized directly from the exciter armature, *10*. The ex-

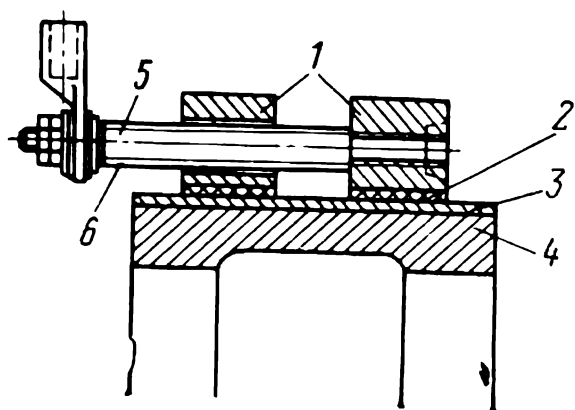


Fig. 51-10 Field slip-rings of a synchronous machine

citer brushes, *13*, held in contact with the exciter commutator, *12*, are connected by an automatic synchronizer (see Sec. 52-1) to the brushgear of the generator. The generator brushes are electrically connected by sliding contact to the field-winding slip rings *14* and, by cables *19* laid out in the shaft bore, to the field terminal leads.

A likely design of slip rings is shown in Fig. 51-10. The rotor shaft mounts a sleeve, *4*, moulded in an insulating material, *3*. The sleeve receives steel (or bronze) slip rings, *1*, which are mounted while hot. Prior to mounting, the spots on the sleeve to be in contact with the slip-rings are clad with sheet steel, *2*. Each slip ring has a stud, *5*, which points in the direction of the winding and to which one of the terminal leads is connected. From the other ring, the stud is insulated by a tube, *6*.

Riding the slip rings are brushes (at *6* in Fig. 51-11). Electrically, each brush is connected by a pig-tail (or flexible conductor), *3*, to a terminal on the brush yoke that carries the brush holders. One end of the pig-tail is embedded in a brush, and the other is terminated in a ring-shaped lug, *2*.

The necessary electric contact between the brushes and the slip-rings is maintained by brush-holders which orient the brushes as appropriate, apply the necessary pressure on the brushes, and permit them to move down as they wear.

One or several brushes can ride on the same slip ring. The brush boxes 7 are fastened by bolts 8 to a common steel yoke or bracket, 1, insulated from the machine frame and connected to one of the terminals in an external circuit. The force of spring 5 can be adjusted by moving a bracket, 4, up or down.

In the pole faces of synchronous motors and condensers and of most generators, it is usual to install heavy copper

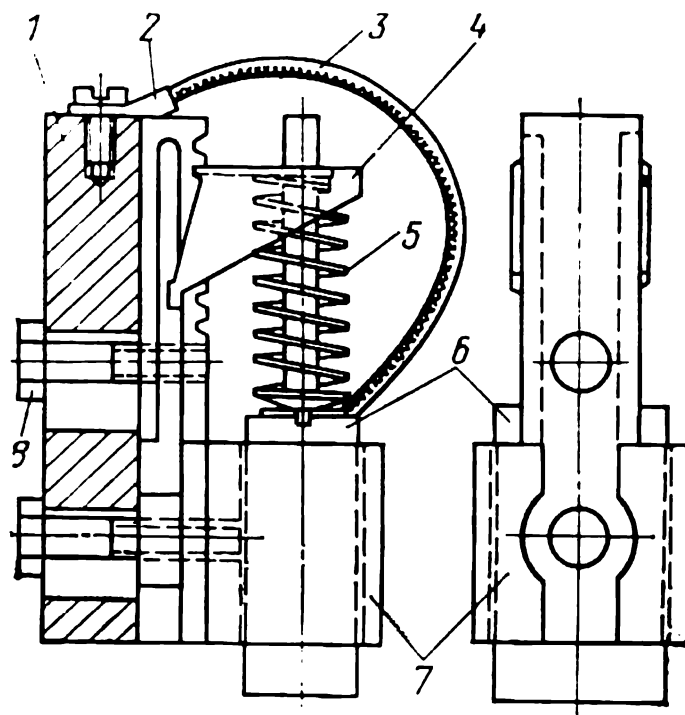


Fig. 51-11 Brushgear

bars (at 7 in Fig. 51-9) in semiclosed round slots. These bars are all shorted together at both ends of the rotor by segments 8 and jumpers 9, also made of copper. These short-circuited bars form what is known as a *damper* (or *amortisseur*) *winding*. It improves the transient stability, that is, the ability of the machine to withstand sudden changes in load without losing synchronism.

The damper winding serves an additional purpose at starting, doing the same job as the auxiliary winding in split-phase induction motors. For this reason, it is also called the *starting winding*. Good performance during transients and at starting is shown by a *double-axis damper winding* (see Fig. 51-9) in which the segments are combined into a single shorting ring by flexible jumpers. A *direct-axis damper winding* (see Fig. 51-8) without flexible jumpers is inferior in performance and is only used in small generators.

No damper winding is installed on machines with solid poles, because the eddy currents induced in such poles supply the necessary damping action during transients. As a way of enhancing the damping action, the faces of solid poles are electrically interconnected by flanged copper segments and flexible jumpers placed in between. With such an arrangement, the transient behaviour of the machine is the same as if it were fitted with a double-axis damper winding.

The functions of the structural parts in the vertical-shaft hydro-electric generator of Fig. 51-2 are explained in the accompanying legend. The arrows in the figure indicate the direction of air flow inside the machine (air is scooped from the outside, forced through the machine, and discharged into the generator hall). In more detail, the cooling systems and the structural parts of hydroelectric generators, synchronous condensers, and salient-pole synchronous motors will be discussed in Chap. 62.

#### **51-4 Construction of Nonsalient-Pole Synchronous Machines**

A nonsalient-pole rotor is typical of two- and four-pole synchronous machines running at 3 000 and 1 500 rpm. A salient-pole rotor cannot be used because of the difficulty in securing the concentrated field windings on the few poles (which is especially true of two-pole machines). So, two- and four-pole machines have nonsalient-pole rotors, although the salient-pole design would be less expensive to make.

The general arrangement of a typical nonsalient-pole synchronous machines—a low-rating two-pole turbogenerator with indirect air cooling—is shown in Fig. 51-12. The rotor core 2 is made integral with shaft extensions from a single steel forging. (Within the active zone, the core acts as the shaft.) More clearly, the core proper and a shaft extension of a nonsalient-pole rotor can be seen at 3 and 6 in Fig. 51-13.

To ensure a sufficient mechanical strength under the action of centrifugal forces, the core is fabricated from high-strength steels alloyed with chromium, nickel and molybdenum. As is shown in the sectional views in Fig. 51-14, rectangular slots are milled on the outer surface of the rotor to receive the coils 5 that make up the field winding whose circuit is shown in Fig. 22-12. The slots are uniformly dis-

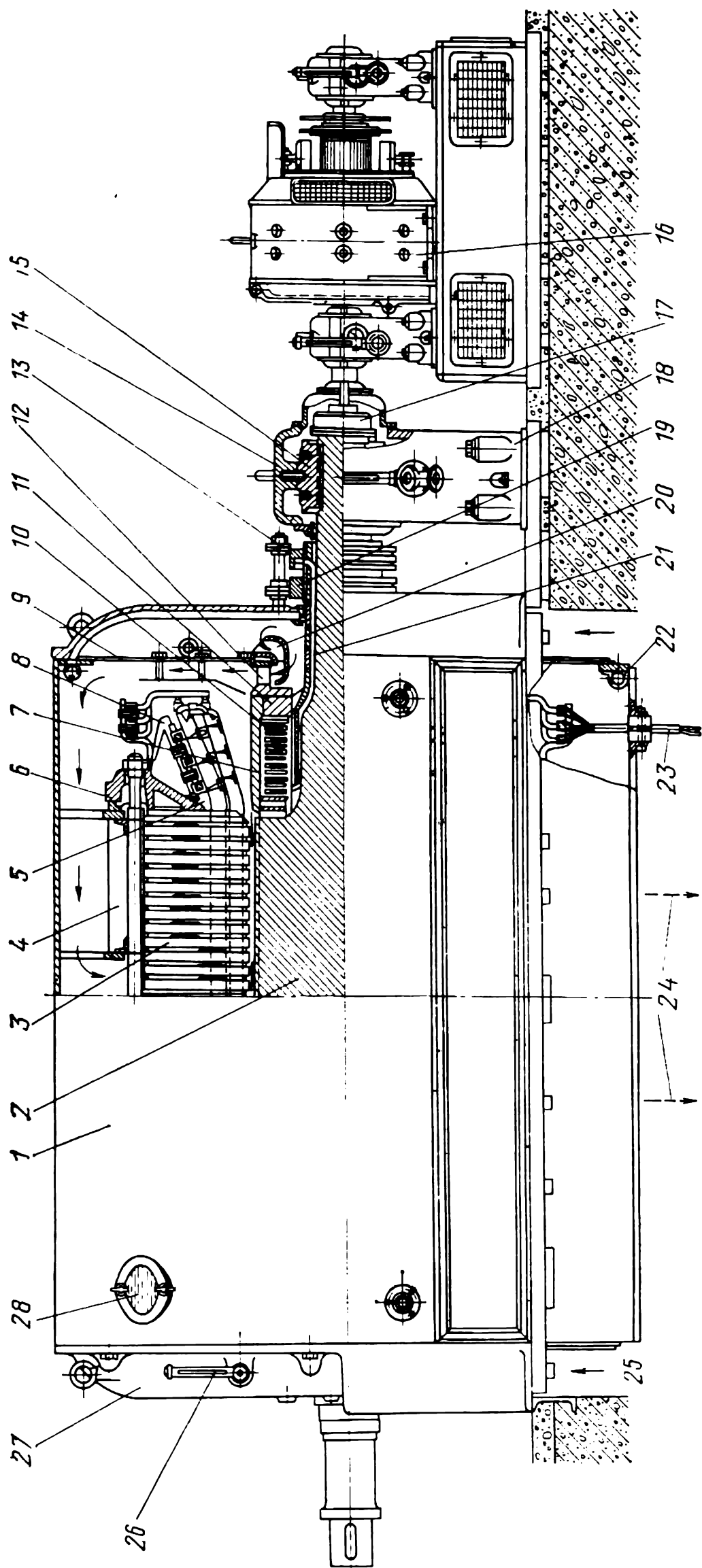


**Fig. 51-12 Indirectly air-cooled nonsalient-pole synchronous generator (turbogenerator):**

1--stator frame (yoke); 2--rotor core; 3--stator core; 4--clamping stud; 5--stator winding bar; 6--pressure ring; 7--rotor binding ring; 8--winding bracket; 9--air baffle and diffuser; 10--field coil; 11--centrifugal fan; 12--centring ring; 13--brush yoke and brushgear; 14--bearing end-shield; 15--exciter; 16--bearing pedestal; 17--flexible coupling; 18--bearing pedestal; 19--slip ring; 20--fan guide vanes; 21--slip-ring to field winding connection; 22--fire-extinguishing system line; 23--stator winding terminal leads; 24--direction of hot-air flow towards coolers; 25--direction of cooled-air flow; 26--cooled-air thermometer; 27--end shield; 28--inspection hole

tributed in two diametrically opposite belts each of which spans one-third of the circle. Within each belt, minor core teeth 3 are formed between the slots, and major teeth 2 are located between the two belts. In the centre, the rotor has a through opening, 4.

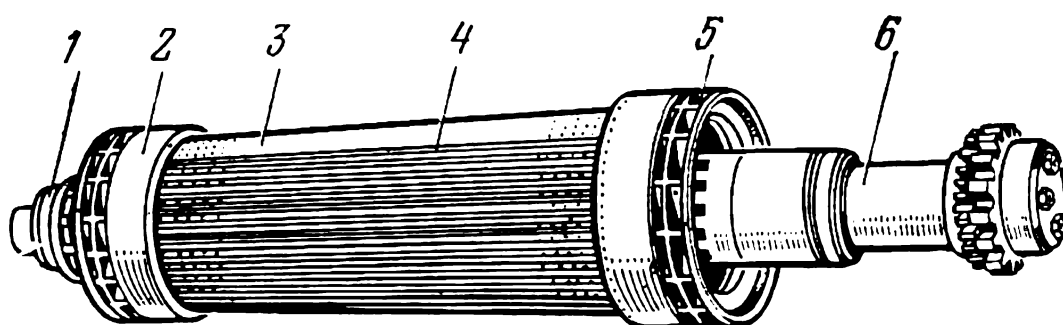


**Fig. 51-13** Nonsalient-pole rotor:

1—slip rings; 2—binding ring; 3—solid rotor; 4—nonmagnetic rotor slot wedge; 5—centrifugal fan; 6—rotor shaft extension

On high-speed nonsalient-pole machines, the conductors and insulation of the field winding are subjected to large centrifugal forces and appreciable thermal stresses. Because

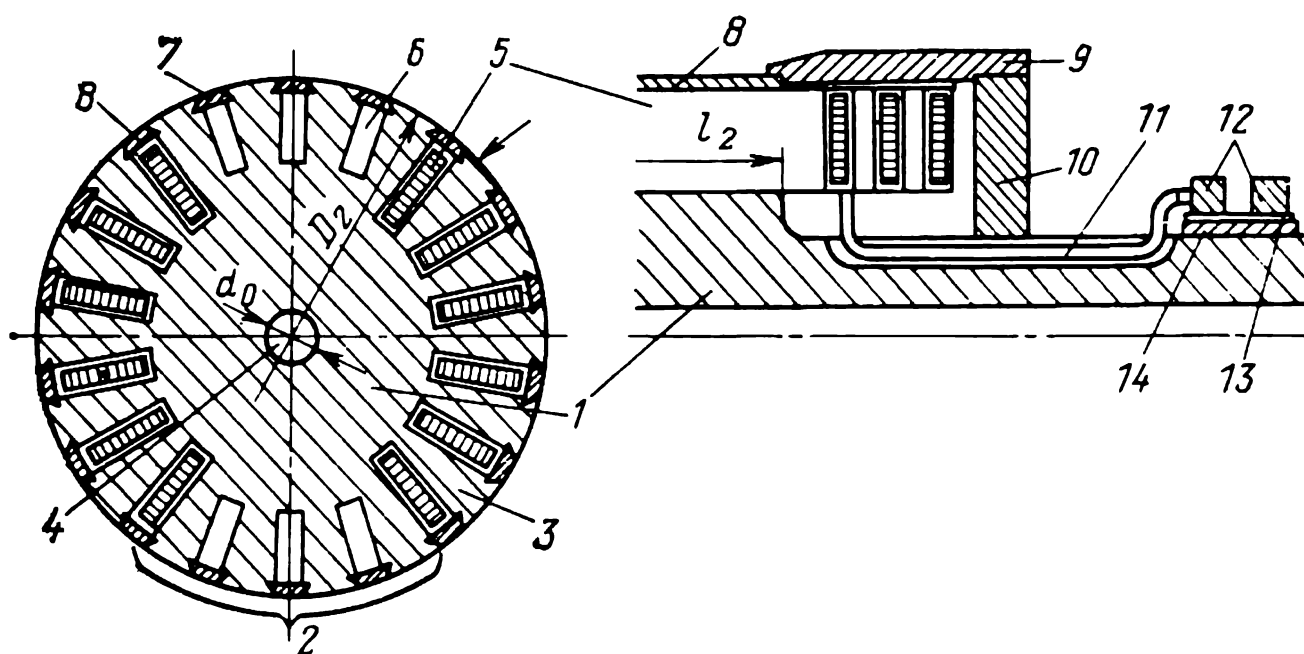


**Fig. 51-14** Sectional views across and along a nonsalient-pole rotor

1—rotor yoke; 2—major core tooth; 3—minor core tooth; 4—axial duct in core; 5—field coil; 6—axial duct in major tooth; 7—magnetic wedge in duct; 8—non-magnetic wedge; 9—binding ring; 10—centring ring; 11—field winding to slip ring connection; 12—slip rings; 13—sleeve insulation; 14—slip-ring sleeve

of this, the field conductors (at 1 in Fig. 51-15) are fabricated of silver-alloyed copper which has an increased mechanical strength. The type of insulation is chosen according to the type of cooling and ventilation used. With indirect cooling

(Fig. 51-15*a*), the turn insulation, 2, is made of micanite and glass-fibre tape. The ground insulation is in the form of slot cells fabricated from micanite or glass-fibre cloth, 3, by hot moulding. The slot cell has a protective wrapper 4 of steel. After the turns have been placed in a slot, the edges of the slot cell are heated and lap-folded. Before wedges 7 are to be driven in, a micanite plate 5 is placed over the cell, and this is topped by a steel plate, 6, which is in direct contact with the wedge. The wedges are made of duralumin, an aluminium alloy of high mechanical strength.

With direct hydrogen cooling (Fig. 51-15*b*), the turn insulation within a slot is in the form of glass-fibre cloth strips 2 pasted over the conductor, 1. The slot cell is made of glass-fibre cloth 3 with an outer wrapper 4 of steel. At the bottom of the slot cell is placed a profiled glass-fibre-cloth laminate plate 8 with ducts for cooling gas. The wedge 7 is driven over a glass-fibre-cloth laminate plate 5 which has slots to admit cooling gas to and from vent ducts on the sides of the coils within the slots.

The radial centrifugal forces acting on the field coils (at 5 in Fig. 51-14) within the slots are transferred via wedges 8 to teeth 2 and 3 and resisted by the rotor core yoke 1. The centrifugal forces acting on the coil ends (overhangs) are transferred through insulating plates to the solid, substantial binding rings. In small turbogenerators, the binding rings (at 7 in Fig. 51-12) made of high-strength alloy steel are separated from the core by an air gap so as to prevent the formation of a closed magnetic path around the coil-ends, and are solely supported by a centring ring, 11, mounted on the shaft extension of the rotor. In large turbogenerators, the binding rings (at 9 in Fig. 51-14) made of non-

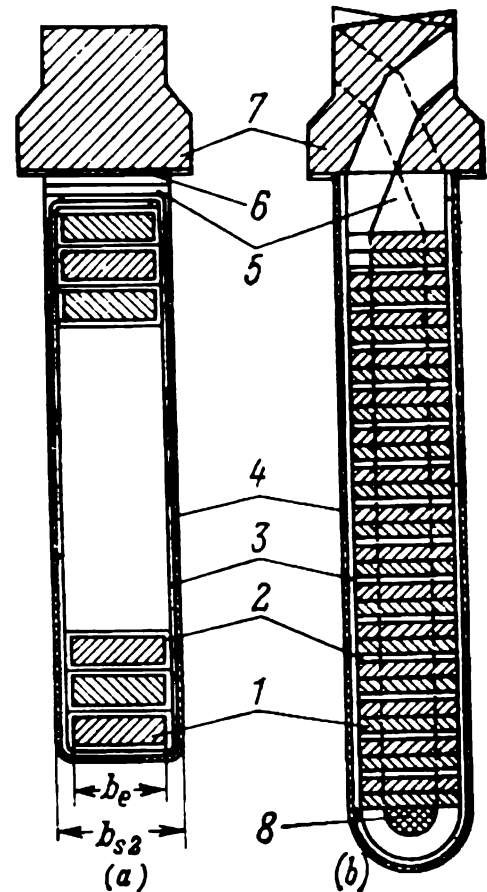


Fig. 51-15 Field-winding conductors in a slot of a nonsalient-pole synchronous machine: (a) indirect cooling; (b) direct cooling



magnetic steel are supported by the core teeth, 2 and 3, and a centring ring, 10.

Current from an exciter (at 16 in Fig. 51-12) is carried to the terminals of the field winding 10 over a circuit passing from the exciter brushes, via the automatic synchronizer, the brushes riding the slip-rings of the generator, the slip-rings of the field winding, to the conductors 21 that interconnect the slip-rings and the field winding.

The stator of a nonsalient-pole synchronous machine is built along the same lines as that of a salient-pole machine, and only differs in the relative magnitudes of the principal dimensions (see above). Small nonsalient-pole machines use lap windings assembled from multiturn (usually, two-turn) formed coils (at 5 in Fig. 51-12). Large turbogenerators only use lap windings with two bars per slot.

The construction of both formed-coil and bar-type windings has been described in Sec. 51-3 (see Fig. 51-6).

The turbogenerator shown in Fig. 51-12 uses indirect cooling, with the cooling air circulated in a closed-circuit system. The static pressure required to drive cooling air is supplied by centrifugal fans, 12. The direction of air flow is indicated by arrows. The air coolers, external to the machine, are not shown in the figure. In the cooling system of Fig. 51-12, the hot air is discharged as two streams. More advanced cooling systems for large turbogenerators are discussed in Chap. 62.

## 52 Excitation Systems for Synchronous Machines

### 52-1 Arrangement of and Requirements for an Excitation System

The direct current required to energize the field winding of a synchronous machine is taken from what is known as an *exciter*. Most frequently, this is a d.c. generator (see Sec. 64-12) whose shaft is mechanically coupled to that of the associated synchronous machine.

Several arrangements using a d.c. generator are shown in Fig. 52-1 and Fig. 52-2a. Apart from the main exciter, the system contains a pilot (or auxiliary) exciter to energize

the field winding of the separately excited main exciter, adjusting rheostats, contactors, remote-control facilities, automatic voltage regulators, and some other items.

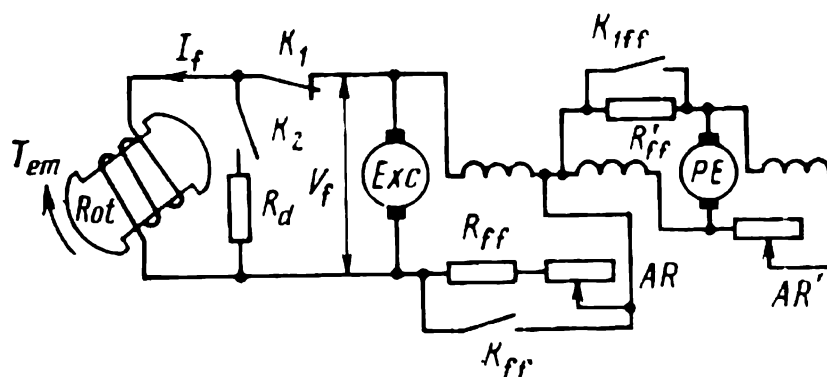


**Fig. 52-1** Rotating-machine excitation system of a large synchronous machine:

*Rot*—rotor; *Exc*—exciter (shunt-wound, separately excited d.c. generator); *PE*—pilot exciter (a separately excited d.c. generator); *AR* and *AR'*—adjusting resistors; *K<sub>ff</sub>* and *K<sub>1ff</sub>*—field-forcing contactors; *R<sub>ff</sub>* and *R'<sub>ff</sub>*—field-forcing resistors; *K<sub>1</sub>* and *K<sub>2</sub>*—contactors of an automatic synchronizer; *R<sub>d</sub>*—damping resistor

(1) **Field current control.** In large synchronous machines, the d.c. field current,  $I_f$ , runs into hundreds or even thousands of amperes. Therefore, it would be wasteful of

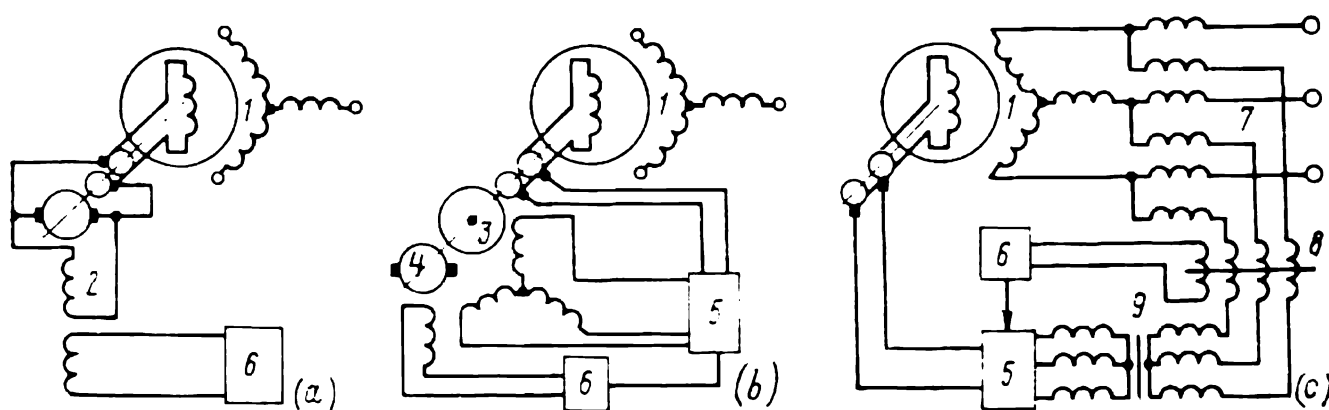


**Fig. 52-2** Excitation systems for synchronous machines:

(a) direct rotating-machine type; (b) direct rectifier-type; (c) self-excitation system; 1—synchronous generator; 2—d.c. exciter; 3—a.c. exciter; 4—a.c. pilot exciter; 5—gas-filled tube or crystal-diode rectifier; 6—field regulator; 7—transformer; 8—field-regulator controlled reactor; 9—transformer

power to adjust it with a rheostat connected in the field (armature) circuit of the exciter. The losses in the rheostat would markedly reduce the efficiency of the synchronous machine.

The field current is therefore adjusted solely by varying the exciter field voltage,  $V_f$ , because the field current varies

in proportion to  $V_f$ :

$$I_f = V_f/R_f$$

The level of field current and of field voltage that must be maintained depends on the mode of operation in which a given synchronous machine is used.

In the system of Fig. 52-1, the exciter field voltage is adjusted with rheostats ( $AR$  in the main exciter and  $AR'$  in the pilot exciter). The provision of a pilot exciter extends

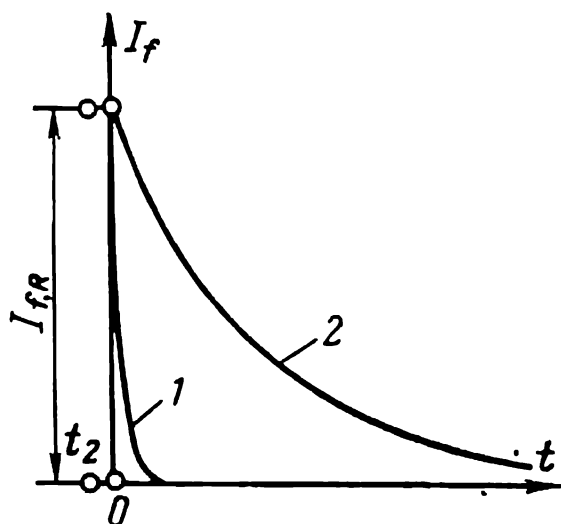


Fig. 52-3 Decay of field current on field killing: 1—with  $K_1$  open directly; 2—when using an automatic synchronizer

the range of exciter voltage adjustment appreciably. In smaller synchronous machines, a pilot exciter may be omitted (which is also true of cases where the range of exciter field voltage adjustment is extended by introducing nonlinear resistances).

### (2) Excitation field killing.

It is usual for an excitation system to include a device which would “kill” the field (reduce the field current to zero rapidly) when necessary.

The need for field killing may arise in both normal operation

and in an emergency (such as a short-circuit in the stator winding). This is done by an automatic synchronizer comprised of contactors  $K_1$  and  $K_2$  and a damping resistor,  $R_d$ . A direct break in the field circuit by contactor  $K_1$  would achieve the desired objective in the shortest time (curve 1 in Fig. 52-3). However, the resistance of the arc that would strike between the breaking contacts of  $K_1$  would dissipate all of the energy stored by the excitation field. In large machines, this energy is so large that upon a direct break the contacts would be destroyed. Also, the rapid fall in field current (owing to the high arc resistance brought in circuit) would give rise to a substantial emf of self-induction (back-emf)

$$e_k = -L_f dI_f/dt$$

It would be many times the rated voltage across the field winding and might damage its insulation.

To avoid this, the field is killed by the automatic synchronizer in the following sequence. With  $K_1$  closed,  $K_2$  is closed (at  $t = t_2$ ) and connects the field winding across the damping resistor,  $R_d \approx 5R_f$ . Then (at time  $t = 0$ ),  $K_1$  opens and disconnects the exciter from the field winding. Because the field energy in the synchronous machine proper remains unchanged, opening of  $K_1$  entails no complications. From that instant on, the field current decays at a time constant

$$T_{f,k} = L_f / (R_d + R_f) = T_f R_f / (R_d + R_f)$$

where  $T_f = L_f / R_f$  is the time constant of the field winding with all the other windings open-circuited (see Sec. 71-2), in accordance with the following equation

$$I_f = I_{f,R} \exp (-t/T_{f,k})$$

along curve 2 in Fig. 52-3.

The value of the damping resistor is chosen such that the field is killed at a sufficiently high rate, but without giving rise to voltages detrimental to the insulation:

$$\begin{aligned} v_d = R_d I_f &= -L_f dI_f/dt - R_f I_f \\ &= R_f I_f (R_d/R_f) = V_{f,R} (R_d/R_f) \end{aligned}$$

With the commonly used value of the damping resistor,  $R_d = 5R_f$ , the field-killing time constant is

$$T_{f,k} = T_f/6 \approx 1 \text{ s}$$

(for large machines). Then,  $v_d$  does not exceed five times the rated field voltage.

**(3) Excitation field forcing.** The need for excitation field forcing would arise when a remote short-circuit in the system might cause a fall in the system voltage (see Sec. 59-5), and the synchronous machines might otherwise drop out of synchronism. Field forcing is effected automatically by the relays of the machine from which a signal comes to close the contactors  $K_{ff}$  and  $K_{1ff}$  (see Fig. 52-1). On closing, the contactors short out the forcing resistors  $R_{ff}$  and  $R'_{ff}$  and the field adjusting resistor  $AR$ , and the exciter armature voltage rises at a high rate to its maximum value,  $V_{fm}$  (Fig. 52-4). With a delay decided by the time constant of the field winding in the synchronous machine, the field excitation current also rises to its limiting value:

$$I_{fm} = I_{f,R} (V_{fm}/V_{f,R})$$

The performance of a field forcing system is assessed in terms of the ratio of the maximum steady-state field excitation voltage,  $V_{fm}$ , to its rated value,  $V_{f,R} = R_f I_{f,R}$ , and also in terms of the rated rate of rise of the field voltage (from point 1 to point 2 on the curve in Fig. 52-4), given by

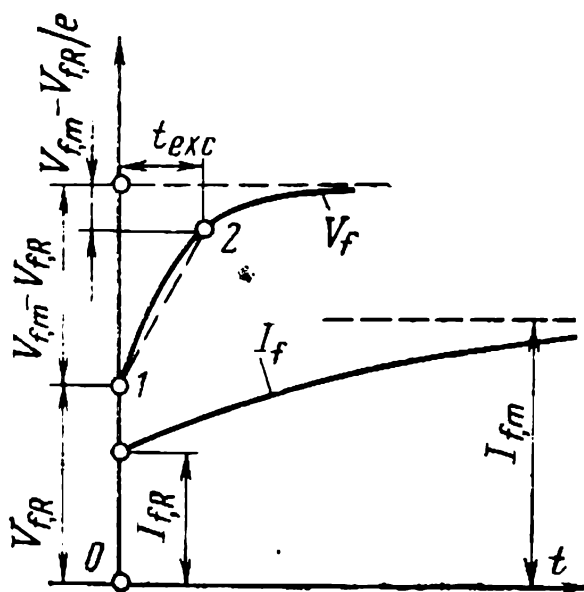


Fig. 52-4 Build-up of exciter voltage and field current upon field forcing

$$(1 - 1/e) \frac{V_{fm} - V_{f,R}}{V_{f,R} t_{exc}}$$

Under relevant Soviet standards, for large synchronous generators and condensers, the field voltage ratio must be anywhere between 1.8 : 1 and 2 : 1. The rated rate of field voltage rise must be from 1.5 to 2.0 times the rated slipping voltage per second. For other synchronous machines, the respective figures are at least 1.4 : 1 and at least 0.8 times the rated voltage per second.

## 52-2 Classification of Excitation Systems

Until the 1950s, the excitation systems for synchronous machines had solely been of what may be called the rotating-machine type described in Sec. 52-1. In such systems, the exciter is a d.c. commutator generator.

Rotating-machine excitation systems may be divided into *direct* and *indirect*. In a direct system, the exciter armature is directly coupled to the shaft of the synchronous machine (see Fig. 52-2a and b).

In an indirect excitation system, the exciter rotor may be driven by a synchronous or an induction motor energized from the station's auxiliary bus or from an auxiliary synchronous generator mounted on the shaft of the main generator, or from an auxiliary synchronous generator placed at the station specifically for that purpose in a more convenient location than on the shaft of the synchronous machine. Indirect excitation systems differ from those illustrated in Fig. 52-2a and b only in that the exciter rotor is coupled

to a separate motor rather than to the shaft of the main synchronous generator.

Under a relevant USSR standard, hydro-electric and turbine-driven generators must have direct excitation systems because they are more reliable (indirect excitation systems call for special care in coordination). The maximum power rating of rotary exciters, as dictated by commutation requirements (see Sec. 64-11), depends on their rpm which is, as a rule, the same as that of the main synchronous generator (not over 600 kW at 3 000 rpm). Therefore, rotating-machine excitation systems cannot be used on two-pole turbogenerators with ratings in excess of 100-150 MW.

In the 1960s, there was a growing use of rectifier-type excitation systems using silicon diodes and thyristors. In the 1970s, rectifier-type excitation systems almost completely ousted rotating-machine excitation systems. Today, they are used not only for synchronous motors and small synchronous generators, but also on large turbogenerators, hydro-electric generators, and synchronous condensers, including those of the highest power ratings.

Rectifier excitation systems may be classed into three broad groups, namely: self-excitation systems, separate-excitation systems, and brushless excitation systems.

In a *self-excitation system* (see Fig. 52-2c), the energy required to excite the synchronous machine is drawn from its armature winding as an alternating current which is then rectified by silicon controlled rectifiers (thyristors). The necessary energy is drawn via a transformer, 7, connected in parallel with the armature winding, and another transformer, 9, connected in series with the armature winding. The series-connected transformer permits the field forcing function in the case of a near short-circuit, when the voltage across the armature winding drops substantially.

In a *separate excitation system* (see Fig. 52-2b), the energy required to supply the field winding comes from an a.c. three-phase generator-exciter, 3, mounted on the shaft of the main generator with silicon-diode or thyristor rectifiers for a.c.-to-d.c. conversion. The diodes (or thyristors) are usually set up in a three-phase bridge circuit. Excitation control utilizes variations in both the rectified current and the exciter voltage.

In a *brushless excitation system*, the rectifiers are mounted on the rotating shaft, and the rectified output is fed directly

to the field winding, thus eliminating the sliding contact. This system differs from that in Fig. 52-2*b* in that the exciter armature is on the rotor, whereas the exciter field winding is on the stator and is supplied either from a pilot exciter, 4, or from an excitation regulator, 6.

## 53 Electromagnetic Processes in a Synchronous Machine

### 53-1 Voltage and Magnetic Field Waveforms on Open Circuit

On open circuit (at no load), the armature current is zero, whereas the field winding carries a direct current,  $I_f$ , which sets up an excitation field inducing an emf,  $E_f$ , in the armature winding. In an excited machine, this condition can be obtained in any one of two ways, namely:

(a) by opening the line leads of the armature winding (thereby introducing an infinite impedance in the armature circuit), or

(b) by injecting an emf in the armature winding to balance  $\dot{E}_f$ , that is,  $\dot{V}_s = -\dot{E}_f$ .

The procedure in (a) is simpler to implement and is nearly always used in measuring open-circuit characteristics. The procedure in (b), described in more detail in Sec. 58-2, calls for an additional source of  $V_s$ . Also the armature current will reduce to zero only if  $E_f$  and  $V_s$  are ideally sinusoidal in waveform.

In carrying out an open-circuit test by the second procedure, the armature winding always retains a small current associated with the harmonic emfs. Because of this current, the measurements are always in error, and the error is not always easy to estimate.

An excited machine on open circuit is subject to friction and windage losses,  $P_{f/w}$ , the armature core loss,  $P_c$ , and some additional (or stray) electromagnetic losses,  $P_{ad,oc}$ . The motor driving a synchronous machine must supply a power equal to the sum of the above losses,  $P_{f/w} + P_c + P_{ad,oc}$ , and accounting for about 0.3 to 3% of the total power of the machine.

The departure of voltage from a sinewave shape leads to additional losses (associated with harmonics) in all elements of an electrical system, including loads and power sources. This is the reason why the emf of a synchronous machine must be as close to sinusoidal as practicable.

The departure of a voltage or current waveform from a sinewave shape is stated in terms of the deviation factor (defined in Sec. 27-6). A relevant Soviet standard requires that the deviation factor for three-phase, 50-Hz generators (including synchronous units) should not exceed 5% at ratings in excess of 100 kVA, and 10% at ratings from 1 to 100 kVA, as measured at open-circuit rated voltage\*.

It has been shown in Sec. 27-6 that even when the excitation field is nonsinusoidal, the emf induced in the armature winding is nearly sinusoidal. The harmonic content of the emf waveform can be reduced by chording (short-pitching) the armature winding, distributing its coils on a sufficiently large number of slots, and connecting its phases into a star or a delta. As is seen from, say, Fig. 27-10, the excitation field with a deviation factor of 28% induces in a star-connected armature winding with  $y_c = 0.83\tau$  and  $q = 2$ , a linear emf with a deviation factor of 0.7%, which is appreciably lower than it is required by the standard. It would seem, therefore, that no further measures need be taken in order to improve the waveform of the excitation field, even though it would reduce the distortion of the emf still more.

However, the effort to improve the waveform of the excitation field is taken mainly to reduce the harmonic content in the field itself, because the harmonics entail additional losses as they do not contribute to energy conversion. In a star-connected armature winding, the  $v$ th harmonic of the excitation field causes the field magnetization to change cyclically at a frequency of  $50v$ , and this inevitably leads to stray losses. In a delta-connected armature winding, triplen harmonics give rise to a circulating current at a frequency of  $50v$ , and this, too, leads to increased copper losses. In a relevant Soviet standard it is required that the third-harmonic current in a delta connection should not exceed 20% of the rated current at the rated power. Also, one has to reckon with the likely effect of the harmonic fields on

---

\* On load, the deviation factor somewhat rises.



the saturation of the poles, armature teeth and other elements of the magnetic circuit.

As has been explained in Chap. 26, the waveform of the excitation field in salient-pole and nonsalient-pole machines is improved in different ways. In salient-pole machines this is achieved by a proper choice of the ratio of the maximum,  $\delta_m$ , and minimum,  $\delta$ , air gap (the air gap under a pole, see Fig. 26-1). In nonsalient-pole machines, this is done by the

choice of the relative wound length of the pole pitch,  $\rho$  (see Fig. 26-4).

The *waveform of the excitation field* on open circuit can be characterized in terms of a set of factors which depend on the relative (pole-pitch) dimensions (see Fig. 53-2).

The *field form factor* is the ratio

$$k_f = B_{\delta 1,m}/B_{\delta} \quad (53-1)$$

where  $B_{\delta 1,m}$  is the peak value of the fundamental flux density

(see Fig. 53-1), and  $B_{\delta} = B_{\delta f}$  is the radial component of the flux density at the pole axis. When the field is sinusoidal,  $k_f = 1$ .

The *excitation flux form factor* is the ratio

$$k_{\Phi} = \Phi_{fm}/\Phi_{f1,m} \quad (53.2)$$

where

$$\Phi_{fm} = \tau l_{\delta} B_{\delta, \text{mean}} = \alpha_{\delta} \tau l_{\delta} B_{\delta}$$

is the total mutual flux, and

$$\Phi_{f1,m} = \frac{2}{\pi} \tau l_{\delta} B_{\delta 1,m}$$

is the flux at the fundamental flux density. When the excitation field is sinusoidal,  $k_{\Phi} = 1$ .

The *pole span factor* is the ratio

$$\alpha_{\delta} = \Phi_{fm}/\tau l_{\delta} B_{\delta} = B_{\delta, \text{mean}}/B_{\delta} \quad (53.3)$$

where  $B_{\delta, \text{mean}}$  is the mean flux density in the air gap, and  $B_{\delta}$  is the flux density at the pole axis. Since

$$B_{\delta, \text{mean}} = \Phi_{fm}/\tau l_{\delta}$$

and

$$B_{\delta} = B_{\delta 1,m}/k_f = \pi \Phi_{fm}/2\tau l_{\delta} k_{\Phi} k_f$$

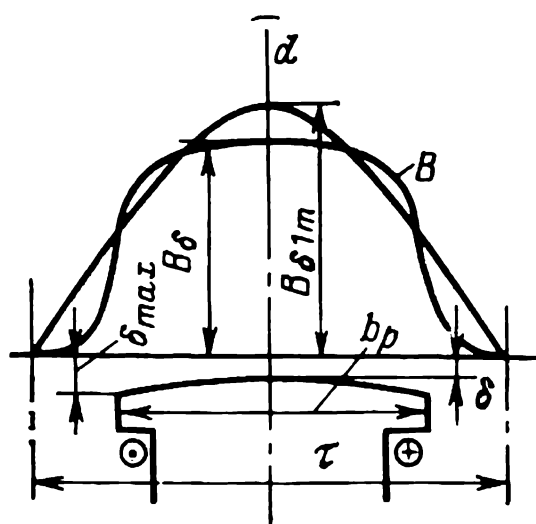


Fig. 53-1 Determination of the excitation field factors

The pole span factor may be expressed in terms of  $k_f$  and  $k_\Phi$  as

$$\alpha_\delta = B_{\delta, \text{mean}} / B_\delta = \frac{2}{\pi} k_\Phi k_f \quad (53.4)$$

When the excitation field is sinusoidal,  $\alpha_\delta = 2/\pi$ .

The *emf form factor*\* is the ratio

$$k_B = B_{\delta, \text{rms}, 1} / B_{\delta, \text{mean}} \quad (53.5)$$

where  $B_{\delta, \text{rms}, 1}$  is the rms value of the fundamental flux density, and  $B_{\delta, \text{mean}}$  is the mean air gap flux density. Since

$$B_{\delta, \text{rms}, 1} = B_{\delta 1, m} / \sqrt{2} = \pi \Phi_{fm} / 2 \sqrt{2} k_\Phi \tau l_\delta$$

the emf form factor can be expressed in terms of  $k_\Phi$  as:

$$k_B = B_{\delta, \text{rms}, 1} / B_{\delta, \text{mean}} = \pi / 2 \sqrt{2} k_\Phi \quad (53-6)$$

When the excitation field is sinusoidal,

$$k_B = \pi / 2 \sqrt{2} = 1.11$$

In a nonsalient-pole machine (without allowance for saturation), the factors  $k_\Phi$ ,  $k_f$ ,  $k_B$  and  $\alpha_\delta$  are functions of only the relative wound length of the rotor pole pitch,  $\rho$ . Recalling that in a nonsalient-pole machine the airgap is uniform and deeming that the flux density is proportional to mmf (see Sec. 26-2), the excitation field factors may be written analytically.

The excitation field form factor for a nonsalient-pole machine (neglecting saturation) will then be

$$k_f = B_{\delta 1, m} / B_\delta = F_{f1, m} / F_{fm} = \frac{4}{\pi} k_{df} = \frac{8 \sin(\rho\pi/2)}{\pi^2 \rho} \quad (53-7)$$

where

$$F_{fm} = I_f w_f = \text{mmf of the field winding (at the pole axis)}$$

$$F_{f1m} = (4/\pi) k_{df} F_{fm} = \text{peak value of the fundamental excitation mmf}$$

$$k_{df} \approx \sin(\rho\pi/2) / (\rho\pi/2) = \text{distribution factor for the fundamental mmf}$$

The pole span factor for a nonsalient-pole machine neglecting saturation is

$$\alpha_\delta = B_{\delta, \text{mean}} / B_\delta = F_{f, \text{mean}} / F_{fm} = 1 - 0.5\rho \quad (53.8)$$

---

\* This factor is so called because it enables the mutual emf,  $E_f$ , to be expressed in terms of the total mutual flux,  $\Phi_{fm}$  [see Eq. (53-11)].

where  $F_{f,\text{mean}} = (1 - 0.5\rho) F_f$  is the mean mmf at the pole axis, found upon replacing the stepped mmf waveform by a trapezoidal mmf waveform (see Fig. 26-2).

Graphically, plots of  $k_f$ ,  $\alpha_\delta$ ,  $k_\Phi$ , and  $k_B$  as functions of  $\rho$  are shown in Fig. 53-2. As is seen, the excitation field approaches a sinewave shape ( $k_\Phi$  and  $k_f$  are unity very nearly) at  $\rho \approx 0.65$  to  $0.75$ , when the winding of a nonsalient pole occupies about two-thirds of a pole pitch.

In a nonsalient-pole machine, the saturation of the teeth has the same effect on the shape of the excitation field and the values of  $k_B$  and  $\alpha_\delta$  as it does in an induction machine (see Sec. 40-2). This effect can be accounted for by applying the correction factors  $\xi_B$  and  $\xi_\alpha = f(k_z)$  in Fig. 40-2.

With saturation,

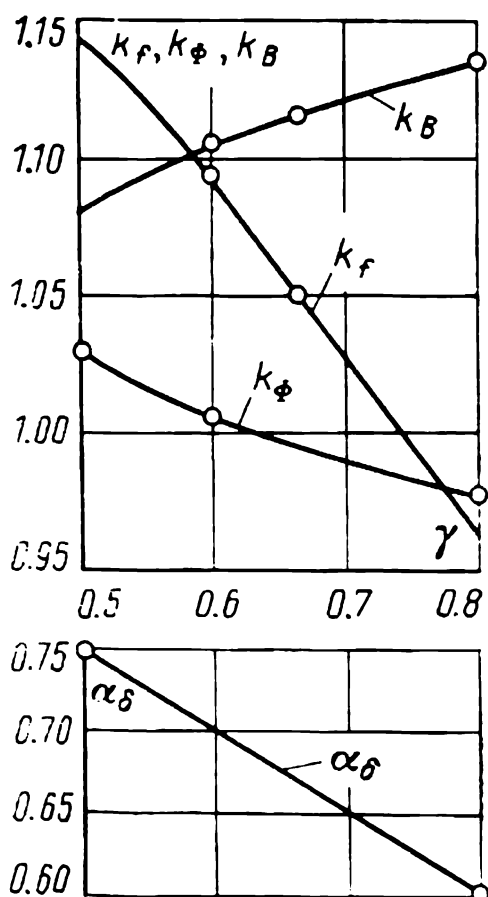


Fig. 53-2 Plots of  $\alpha_\delta$ ,  $k_B$ ,  $k_f$  and  $k_\Phi$  as functions of  $\rho$  for a nonsalient-pole synchronous machine

$$\left. \begin{aligned} k_B &= k_{B0} \xi_B \\ \alpha_\delta &= \alpha_{\delta 0} \xi_\alpha \end{aligned} \right\} \quad (53-9)$$

where  $k_{B0}$ ,  $\alpha_{\delta 0} = f(\rho)$  = values of  $k_B$  and  $\alpha_\delta$  neglecting saturation ( $k_z = 1$ , see Fig. 53-2)

$\xi_B$ ,  $\xi_\alpha = f(k_z)$  = correction factors from Fig. 40-2, with  $k_z = (F_\delta + F_{Z1})/F_\delta$  taken as appropriate

The value of  $k_z$  is found for each value of  $\Phi_{fm}$  in calculating the magnetic circuit (see below). In doing so, only  $F_\delta$ , the air gap mmf, and  $F_{Z1}$ , the stator tooth mmf, need be taken into account. To a first approximation,  $k_z = 1$ .

Once  $k_B$  and  $\alpha_\delta$  have been found, the next step is to determine  $k_\Phi$  and  $k_f$  from Eqs. (53-6) and (53-4). It will be seen that they, too, are functions of the saturation of the magnetic circuit (that is, functions of  $k_z$ ).

In a salient-pole machine,  $k_\Phi$ ,  $k_f$ ,  $k_B$  and  $\alpha_\delta$  are mainly dependent on the ratio of the maximum air gap,  $\delta_m$ , to the

air gap [at the pole axis,  $\delta$ , or the minimum air gap (see Fig. 53-1). Plots of  $k_\Phi$ ,  $k_f$ ,  $k_B$  and  $\alpha_\delta$  versus the ratio  $\delta_m/\delta'$ , as found from the field pattern of a smooth armature core and for the typical relative dimensions of salient-pole machines ( $\delta'/\tau = 0.03$  to  $0.05$ ,  $\alpha = b_p/\tau = 0.69$  to  $0.72$ ) are shown in Fig. 53-3. When the armature has a smooth surface,  $\delta'$  refers to the air gap between stator and rotor at the pole axis,  $\delta' = \delta$ .

The same set of form factors may be utilized in calculating the mmfs with saturation for real core designs having teeth and slots on the stator and the pole pieces. An analysis of the field in a real machine would show that the saliency of the air gap and the saturation of the stator teeth and yoke serve to bring down the flux density in the region of minimum air gap (at a given excitation mmf). At the tips of a pole-piece and between the poles, the effect of stator saliency and the saturation of the stator teeth and yoke is immaterial. Therefore, in the case of a saturated, toothed core with an air gap whose profile is shown in Fig. 53-4 by a full line, the flux density and mmf in the air gap may be determined, taking an equivalent, smooth, unsaturated core and an increased air gap,  $\delta'$ , whose profile is

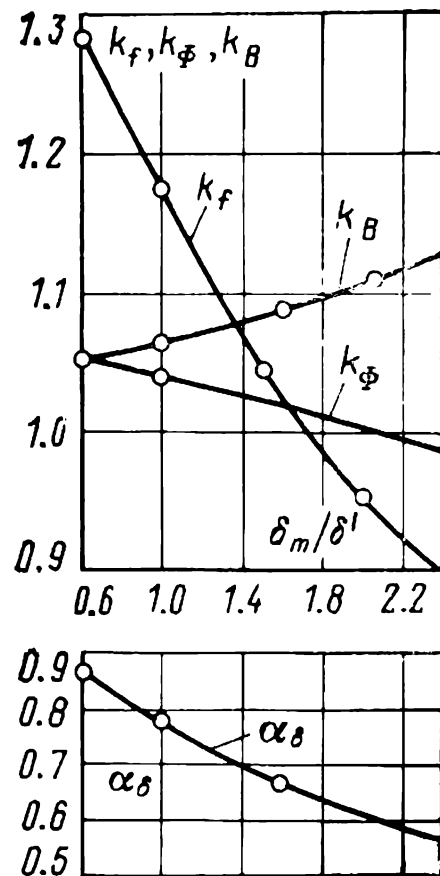


Fig. 53-3 Plots of  $\alpha_\delta$ ,  $k_B$ ,  $k'$  and  $k_\Phi$  as functions of  $\delta_m/\delta_f$  for a salient-pole synchronous machine

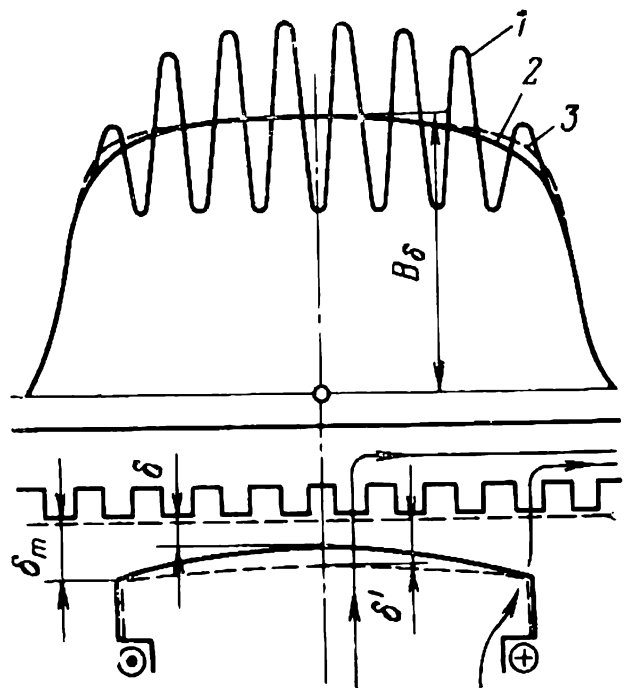


Fig. 53-4 Replacement of a toothed saturated core with air gap  $\delta$  by a smooth unsaturated core with air gap  $\delta'$ :

—— core surface; - - - - surface of equivalent core; 1—flux density with allowance for saturation and saliency; 2—averaged air gap flux density; 3—air gap flux density for an equivalent core with air gap  $\delta'$

shown in Fig. 53-4 by the dashed line. The best approximation is obtained when the air gap at the pole tip,  $\delta_m$ , is retained unchanged, and the air gap at the pole axis is taken equal to

$$\delta' = \delta k_\delta k_{za} \quad (53-10)$$

where  $k_\delta$  is the air gap factor (see below), and  $k_{za} = (F_\delta + F_{z1} + F_{a1})/F_\delta = 1.0$  to  $1.4$  is the saturation factor.

To begin with, a guessed value of  $k_{za}$  is taken, then it is refined by the method of successive approximation in the course of magnetic-circuit calculations (see below).

The various excitation field factors with allowance for saturation and saliency are found from the curves in Fig. 53-3 as functions of  $\delta_m/\delta'$ , where  $\delta'$  is the equivalent air gap from Eq. (53-10).

### 53-2 Calculation of the Magnetic Circuit of a Salient-Pole Machine on Open Circuit

The objective of magnetic-circuit calculation on open circuit is to determine the d.c. field current  $I_f$  or the excitation mmf  $F_{fm}$  that set up a mutual field with a flux  $\Phi_{fm} = \Phi_m$  inducing the desired  $E_f$  in the stator winding.

Recalling that the air-gap field is distributed nonsinusoidally (see above), the magnetic flux is calculated by the same equation as for an induction machine, Eq. (40-1):

$$\Phi_m = \Phi_{fm} = k_\Phi \Phi_{f1m} = E_f/4k_B f_1 w_1 k_{w1} \quad (53-11)$$

Here,  $k_\Phi$  accounts for the difference between the mutual flux and the fundamental flux given by

$$\Phi_{f1m} = \sqrt{2} E_{f1}/2\pi f_1 w_1 k_{w1}$$

The rms value of emf,

$$E_f = \sqrt{E_{f1}^2 + E_{f5}^2 + E_{f7}^2 + \dots}$$

is assumed to be the same as the rms value of the fundamental emf,  $E_f = E_{f1}$ , because the squares of the harmonic emfs,  $E_{f5}^2$ ,  $E_{f7}^2$ , are small in comparison with the square of the fundamental emf,  $E_{f1}^2$ . The emf form factor,  $k_B$ , in Eq. (53-11) can be expressed in terms of the flux form factor

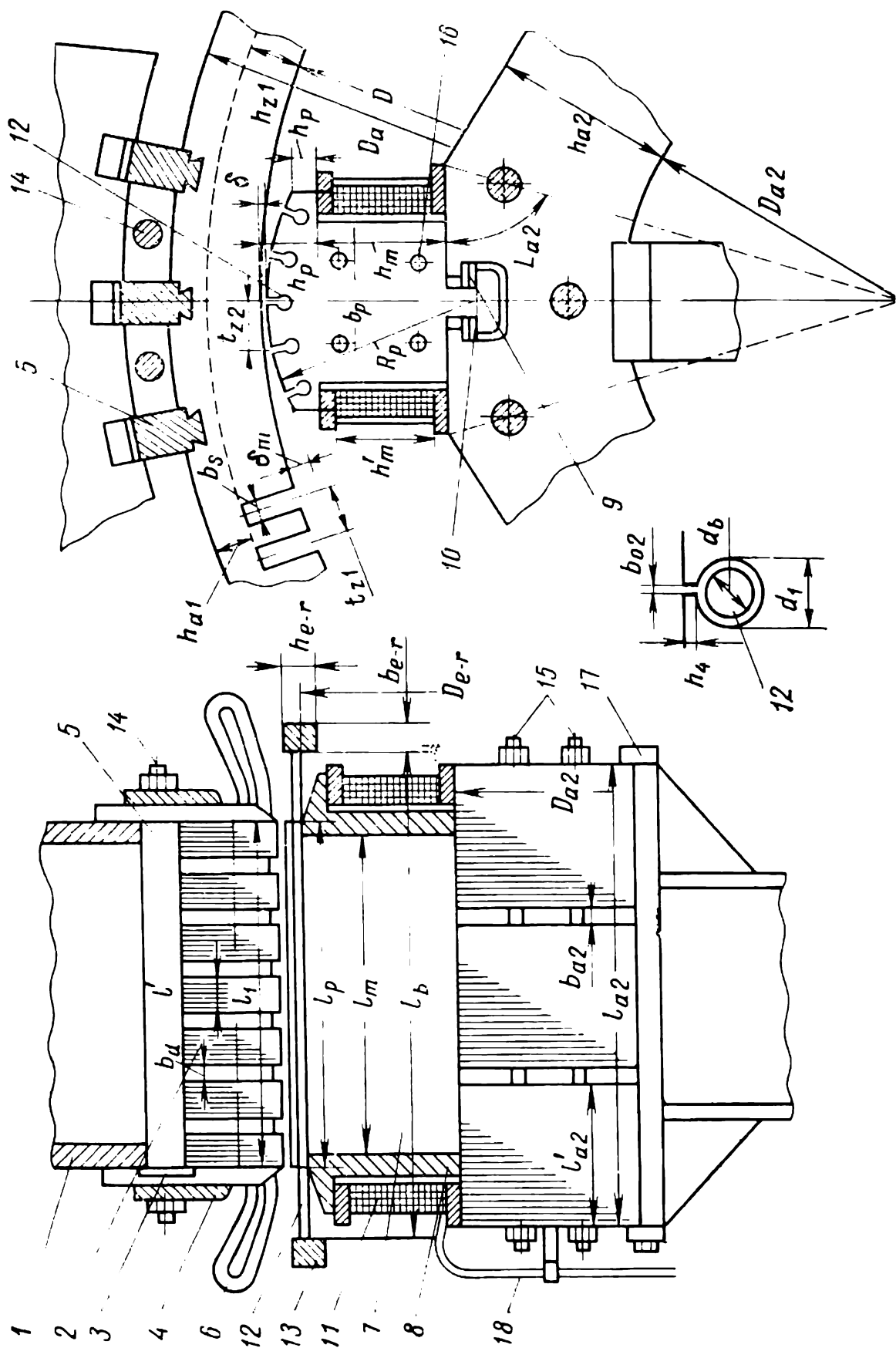


Fig. 53-5 Dimensions of the active parts in a salient-pole synchronous machine:

1—frame (stator yoke); 2—stator core; 3—pressure fingers; 4—pressure plates; 5—dove-tailed segment attachment blocks; 6—stator winding; 7—pole; 8—pole cheek; 9—opposing wedges; 10—T-shaped pole shank; 11—field coil; 12—damper-winding bar; 13—damper-winding short-circuiting segment (or ring); 14, 15, 16—stator-core, rotor-yoke and pole-core clamping studs; 17—rotor spider; 18—field winding terminal leads to slip rings

$k_\Phi$  as

$$k_B = \pi/2 \sqrt{2} k_\Phi$$

and is found with allowance for saturation, airgap shape, and mmf for each specified value of  $E_f$ . It is especially important to calculate the magnetic circuit for two characteristic values of flux, namely:

(1) The flux corresponding to the rated no-load voltage,  $E_f = V_R$ :

$$\Phi_{m,\text{no-load}} = V_R / 4k_B f_1 w_1 k_{w1} \quad (53-12)$$

and

(2) The flux,  $\Phi_{mR}$ , corresponding to the mutual emf at rated load,

$$E_f = k_E V_R$$

where  $k_E = E_{rR}/V_R$  is the mutual emf per-unit regulation accounting for the increase in mutual emf as the load is varied from no-load (open circuit) to full-load (for conventional generators and motors,  $k_E \approx 1.08$ ).

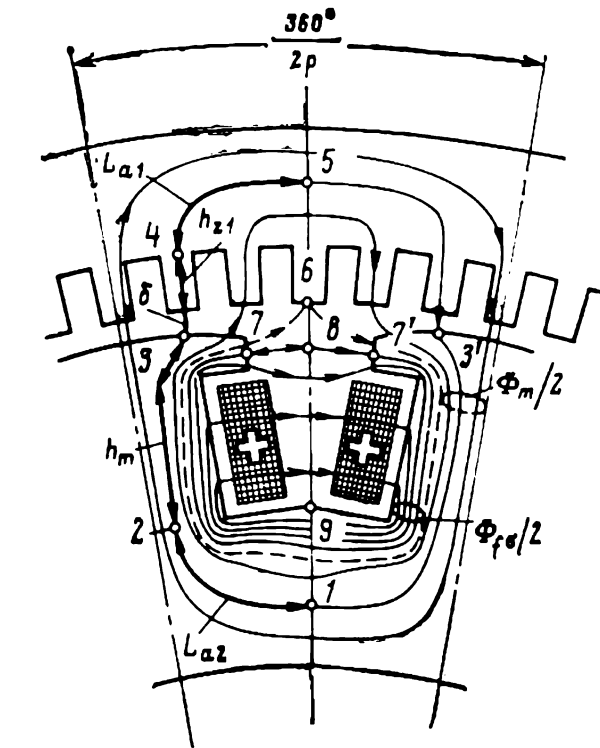


**Fig. 53-6** Magnetic field in a salient-pole synchronous machine at no load

To obtain a complete magnetization characteristic of a synchronous machine,  $\Phi_m = f(E_f)$ , it will suffice to carry out calculations for  $E_f = 0.5V_R$ ,  $V_R$ ,  $k_E V_R$ ,  $1.2V_R$ , and  $1.3V_R$ , with  $\Phi_m$  found from Eq. (53-11).

The magnetic circuit of a salient-pole synchronous machine is shown in Fig. 53-5, and the field pattern on open circuit (at no load), in Fig. 53-6.

The excitation mmf,  $F_{fm}$ , that gives rise to  $\Phi_m$ , is found by Ampere's circuital law for the mean magnetic line containing parts  $L_{a1}$  (the stator yoke),  $h_{z1}$  (the stator teeth),  $\delta$  (the air gap),  $h_m$  (the pole cores), and  $L_{a2}$  (the rotor yoke):

$$F_{fm} = F_\delta + F_{z1} + F_{a1} + F_m + F_{a2} \quad (53-13)$$

In calculating  $F_\delta$ , it is important to account for the effect produced by variations in the radial gap length owing to

saliency:

$$F_{\delta} = (1/\mu_0) B_{\delta} k_{\delta} \delta \quad (53-14)$$

where  $B_{\delta}$  is the flux density at the pole axis,  $\delta$  is the radial gap length at the pole axis, and  $k_{\delta}$  is the gap factor.

The value of  $B_{\delta}$  is found from

$$B_{\delta} = \Phi_m / \alpha_{\delta} \tau l_{\delta}$$

where  $\alpha_{\delta}$  is the design pole span factor (the pole arc ratio) with allowance for stator saliency and saturation, taken from Fig. 53-3 for  $\delta' = \delta k_{\delta} k_{za}$ . As has been explained in Sec. 51-1,  $k_{za}$  is first guessed, then refined after  $F_{\delta}$ ,  $F_{z1}$  and  $F_{a1}$  have been found to a first approximation. The value of  $k_{\delta} = k_{\delta 1} k_{\delta 2}$  is found via

$$k_{\delta 1} = t_{z1} / (t_{z1} - \gamma_1 \delta), \text{ where } \gamma_1 = \frac{(b_s/\delta)^2}{5 + b_s/\delta}$$

and the damper-winding slot factor

$$k_{\delta 2} = t_{z2} / (t_{z2} - \gamma_2 \delta), \text{ where } \gamma_2 = \frac{(b_{02}/\delta)^2}{5 + b_{02}/\delta}$$

The mmfs in the stator teeth and yoke,  $F_{z1}$  and  $F_{a1}$ , are found by the same equations as for an induction machine (see Sec. 40-2). Once  $F_{\delta}$ ,  $F_{z1}$  and  $F_{a1}$  are found, it is an easy matter to determine the stator and air gap mmf:

$$F_1 = F_{\delta} + F_{z1} + F_{a1} \quad (53-15)$$

and the saturation factor,  $k_{za} = F_1 / F_{\delta}$ . If the value of the saturation factor thus found markedly differs from the guessed value assumed in calculations for a given  $E_f$ , it is necessary to go through the same procedure, taking the refined values of the equivalent air gap at the centre of the pole,  $\delta' = \delta k_{\delta} k_{za}$  and of the factors  $k_B$  and  $\alpha_{\delta} = f(\delta_m / \delta')$ . In going from one approximation to the next,  $k_{za}$  goes up in value with an increase in  $E_f$  and in the saturation of the magnetic circuit.

In calculating the rotor mmfs it is important to remember that the rotor core is threaded not only by the mutual field which links both the stator and the rotor windings, but also by the leakage field linking only the field winding (Fig. 53-6).

The mean line of the mutual flux passes through points 1, 2, 3, 4, and 5. All lines of the mutual flux cut the air gap and take up positions outside the dashed line passing through point 6. The lines of the leakage field (say, the line



passing through points 7 and 8) encircle the field conductors, much as the mutual field lines do, but have their path completed through the gaps between the pole-pieces and between adjacent poles. The leakage-field lines take up position within the dashed line.

The pole leakage flux  $\Phi_{f\sigma}$  is the sum of two identical parts, one of which,  $\Phi_{f\sigma}/2$ , has its path completed through the next adjacent pole on the right, and the other part through the next adjacent pole on the left. Half the pole leakage flux,  $\Phi_{f\sigma}/2$ , is defined as the flux through the surface between points 6 and 9 along the design length of the machine (axial gap length)  $l_\delta$ . The total pole leakage flux is proportional to the permeance per unit length between adjacent poles,  $\lambda_s$ , and the mmf between adjacent pole-pieces,  $F_{77'}$  (between points 7 and 7'). Because the leakage-field line passing through points 7, 8, and 7' links the current in two coil sides,

$$2F_{fm} = 2\omega_f I_f$$

and includes, in addition to portion 7-8-7', also a pole-piece and the rotor yoke, we may write

$$F_{77'} = 2(F_{fm} - F_m - F_{a2})$$

From inspection of the loop 1-2-3-4-5 which coincides with the mean line of the mutual field, we may write in accord with Eq. (53-13)

$$F_1 = F_\delta + F_{z1} + F_{a1} = F_{fm} - F_m - F_{a2}$$

From a comparison of the last two equations it transpires that the mmf between two adjacent pole-pieces,  $F_{77'}$ , is equal to the mmf in the stator and air gap:

$$F_{77'} = 2F_1 = 2(F_\delta + F_{z1} + F_{a1})$$

The same result would be obtained, if we recalled that  $2F_1$  is equal to  $F_{33'}$ , the mmf between points 3 and 3' lying on adjacent pole-pieces, and that the magnetic potentials at points 3 and 7, 3' and 7' are respectively the same.

Now the pole leakage flux,  $\Phi_{f\sigma}$ , may be expressed in terms of  $F_1$  found earlier, and  $\lambda_s$ . Half of this flux is given by

$$\Phi_{f\sigma}/2 = \mu_0 \lambda_s l_\delta F_{77'} = \mu_0 \lambda_s l_\delta (2F_1)$$

Noting that  $\lambda_{f\Phi} = 4\lambda_s$  is the permeance seen by the pole leakage flux, we finally get:

$$\Phi_{f\sigma} = \mu_0 \lambda_{f\Phi} l_\delta F_1 \quad (53-16)$$

The permeance seen by the pole leakage flux, increases with an increase in pole-piece height  $h_p$  and pole-core height  $h_m$ , and with a decrease in the spacing between adjacent pole-pieces and adjacent poles (see Fig. 53-6). Equations giving  $\lambda_{f\Phi}$  can be found in [13] and [30].

To a first approximation,  $\lambda_{f\Phi}$  can be expressed as a fraction of  $\lambda_\delta$ , the air gap permeance seen by the mutual flux:

$$\lambda_{f\Phi} = k\lambda_\delta \quad (53-17)$$

The ratio of the two permeances,  $k = \lambda_{f\Phi}/\lambda_\delta$ , for salient-pole machines lies anywhere between 0.15 and 0.35. On the average, it may be taken as 0.25.

The air gap permeance per unit length [see Eq. (53-14)]

$$\lambda_\delta = \Phi_m/\mu_0 l_\delta F_\delta = \alpha_\delta \tau/\delta k_\delta \quad (53-18)$$

is expressed in terms of the principal dimensions of the machine,  $\delta$  and  $\tau$ .

On taking a particular value of  $k = \lambda_{f\Phi}/\lambda_\delta$ , we can express the pole leakage flux,  $\Phi_{f\sigma}$ , directly in terms of the mutual flux,  $\Phi_m$ . This can be done by considering together Eqs. (53-16) through (53-18):

$$\Phi_{f\sigma} = kk_{za}\Phi_m \quad (53-19)$$

where  $k = \lambda_{f\Phi}/\lambda_\delta \approx 0.25$ , and  $k_{za} = F_1/F_\delta$  is the saturation factor.

The total flux through a pole base,  $\Phi_2$ , is the sum of two terms (Fig. 53-6):

$$\Phi_2 = \Phi_m + \Phi_{f\sigma} = \sigma_f \Phi_m \quad (53-20)$$

where  $\sigma_f = \Phi_2/\Phi_m = 1 + \Phi_{f\sigma}/\Phi_m = 1 + kk_{za}$  is the pole leakage factor.

The mmf in a pole core is given by

$$F_m = h_m H_m + F_{\delta m} \quad (53-21)$$

where  $H_m$  is the field intensity at the pole base corresponding to the flux density at the same section [13]:

$$B_m = \Phi_2/k_{ms}l'_m b_m$$

where  $l'_m \approx l_\delta$  = design pole length with allowance for the end-plates

$k_{ms}$  = pole-core fill factor ( $k_{ms} = 0.95$  for a pole core built up of electrical-sheet

steel laminations 1-2 mm thick, and  $k_{ms} = 1.0$  for solid poles)  
 and  $F_{\delta m} = 225 B_m^2$  is the mmf at the joint between a pole and the yoke.

The mmf in the rotor yoke (see Fig. 53-6) is given by

$$F_{a2} \approx L_{a2} H_{a2} \quad (53-22)$$

where  $H_{a2}$  is the maximum field intensity in the yoke, corresponding to the flux density in the rotor yoke [13]:

$$B_{a2} = \frac{\Phi_2}{2k_{as} (l_{a2} - n_{d2} b_{a2}) h_{a2}}$$

where  $n_{d2}$  = number of ventilation ducts in the rim

$k_{as}$  = yoke fill factor ( $k_{as} = 0.95$  for a yoke built up of electrical-sheet steel laminations, and  $k_{as} = 1.0$  for a solid yoke)

The mmf in the rotor,  $F_2$ , is the sum of two terms:

$$F_2 = F_m + F_{a2} \quad (53-23)$$

The calculation of a magnetic circuit for each assumed (or specified) value of  $E_f$  is completed by determining the excitation mmf,  $F_{fm} = w_f I_f$ , which should balance the sum of mmfs in the stator, air gap and rotor:

$$F_{fm} = w_f I_f = F_1 + F_2 \quad (53-24)$$

The results of calculations for a range of values of  $E_f$  are plotted as no-load saturation (or open-circuit) and magnetization characteristics. A no-load saturation curve, or open-circuit characteristic, refers to the dependence of mutual emf,  $E_f$ , on d.c. field current,  $I_f$ , or excitation mmf,  $E_{fm}$ .

Magnetization curves include the basic magnetization characteristic which relates  $\Phi_m$  to  $F_{fm}$ ; the magnetization characteristic of the stator and air gap which relates  $\Phi_m$  to  $F_1$  (also called the transition magnetization curve); the air-gap line relating  $\Phi_m$  to  $F_\delta$ ; the leakage-flux magnetization curve relating  $\Phi_{f\sigma}$  to  $F_1$ ; and the rotor core magnetization curve, relating  $\Phi_2$  to  $F_2$ .

For a salient-pole synchronous machine, the open-circuit characteristics and magnetization curves are shown in Fig. 53-7. At low excitation,  $\Phi_m$  and  $E_f$  are proportional to  $F_{fm}$  which is practically the same as  $F_\delta$ . As saturation is increased, an increasingly larger fraction of the total mmf

comes from the iron portions of the magnetic circuit, that is,  $F_{fm} - F_\delta$ . The build-up is especially noticeable in  $F_2$ . This is because the rotor flux

$$\Phi_2 = \Phi_m + \Phi_{f\sigma}$$

depends more and more on  $\Phi_f$  which rises with increasing excitation at a faster rate than  $\Phi_m$ . (The ratio  $\Phi_{f\sigma}/\Phi_m$  by Eq. (53-19) gradually increases.) As a result,  $F_{fm} = F_1 + F_2$  differs more and more from  $F_\delta$ , and the  $\Phi_m = f(F_{fm})$  curve progressively departs from the air gap line,  $\Phi_m = f(F_\delta)$ .

The no-load saturation curve or open-circuit characteristic,  $E_f = f(F_{fm})$ , is similar in shape to the  $\Phi_m = f(F_{fm})$  curve. Both (see Fig. 53-7) may be plotted on a per-unit basis, taking as the base quantities the rated voltage  $V_R$ , the mutual flux on open circuit (at no load)

$$\Phi_{m,oc} = V_R / 4k_L f_1 w_1 k_{w1}$$

corresponding to the rated voltage on open circuit,  $E_f = V_R$ , and the excitation mmf,  $F_{fm} = F_{fm,oc} = w_f I_{f,oc}$ , also corresponding to the open-circuit rated voltage. The procedure is as follows. Going from point to point on the curves in Fig. 53-7, the quantities locating those points are written on a per-unit basis:

$$E_{*f} = E_f / V_R$$

$$\Phi_{*m} = \Phi_m / \Phi_{m,oc}$$

$$\Phi_{*f\sigma} = \Phi_{f\sigma} / \Phi_{m,oc}$$

$$\Phi_{*2} = \Phi_2 / \Phi_{m,oc}$$

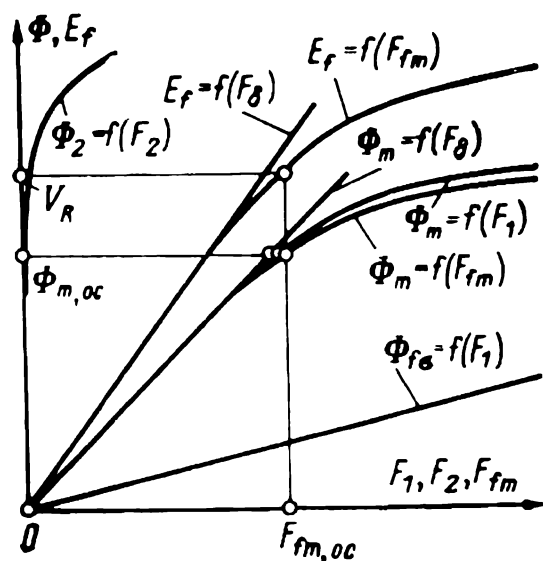


Fig. 53-7 Open-circuit and magnetization curves of a synchronous machine

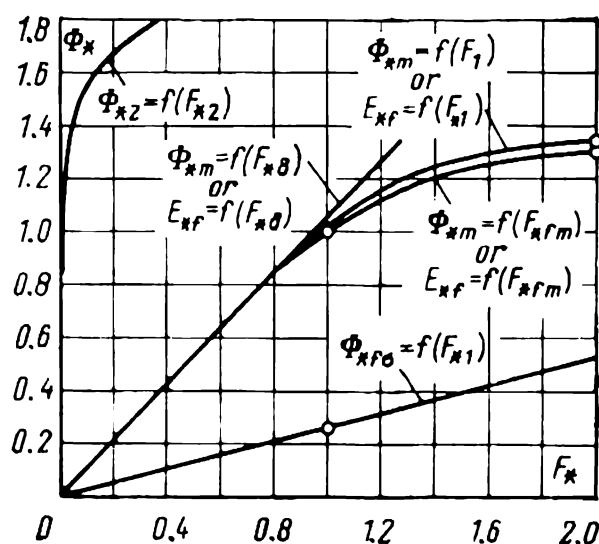


Fig. 53-8 Normalized open-circuit and magnetization curves of salient-pole synchronous machines

$$F_{*fm} = F_{fm}/F_{fm,oc}$$

$$F_{*1} = F_1/F_{fm,oc}$$

$$F_{*\delta} = F_{\delta}/F_{fm,oc}$$

$$F_{*2} = F_2/F_{fm,oc}$$

Now, the relationships between the per-unit quantities involved are plotted on a diagram. As is seen from Fig. 53-8, the open-circuit characteristics and basic magnetization curves drawn on a per-unit basis are identical. Also, a comparison of the per-unit magnetization curves for a range of different salient-pole machines will show that they too differ very little. The averaged per-unit open-circuit characteristics and magnetization curves, called the normal or normalized characteristics, are shown in Fig. 53-8.

### 53-3 Calculation of the Magnetic Circuit for a Nonsalient-Pole Machine on Open Circuit

The magnetic circuit of a nonsalient-pole machine differs from that of a salient-pole unit only in the rotor (Fig. 53-9). On open circuit (at no load), it is calculated in the same manner as explained in the previous section. The magnetic field pattern in a nonsalient-pole machine at no load is shown in Fig. 53-10. The resultant rotor field (Fig. 53-10) is shown as the sum of the mutual field (Fig. 53-10a) and the leakage field of the field winding (Fig. 53-10b).

The excitation mmf,  $F_f$ , which sets up the mutual flux  $\Phi_m$ , is found by applying Ampere's circuital law to the mean magnetic line, 1-2-3-4-5, which consists of several parts, namely:  $L_{a1}$  (the stator yoke),  $h_{z1}$  (the stator teeth),  $\delta$  (the air gap),  $h_{z2}$  (the rotor teeth), and  $L_{a2}$  (the rotor yoke):

$$F_{fm} = F_1 + F_2 \quad (53-25)$$

where  $F_1 = F_{\delta} + F_{z1} + F_{a1} = \text{mmf in the stator and air gap}$

$F_2 = F_{z2} + F_{a2} = \text{mmf in the rotor}$

The mmf in the stator and air gap,  $F_1$ , and its components  $F_{\delta}$ ,  $F_{z1}$  and  $F_{a1}$  are found by the same equations as for a salient-pole machine [see Eq. (53-14) and Sec. 40-2];  $k_B$ ,  $\alpha_{\delta}$  and  $k_{\delta}$  are found with allowance for the specific features of nonsalient-pole machines.

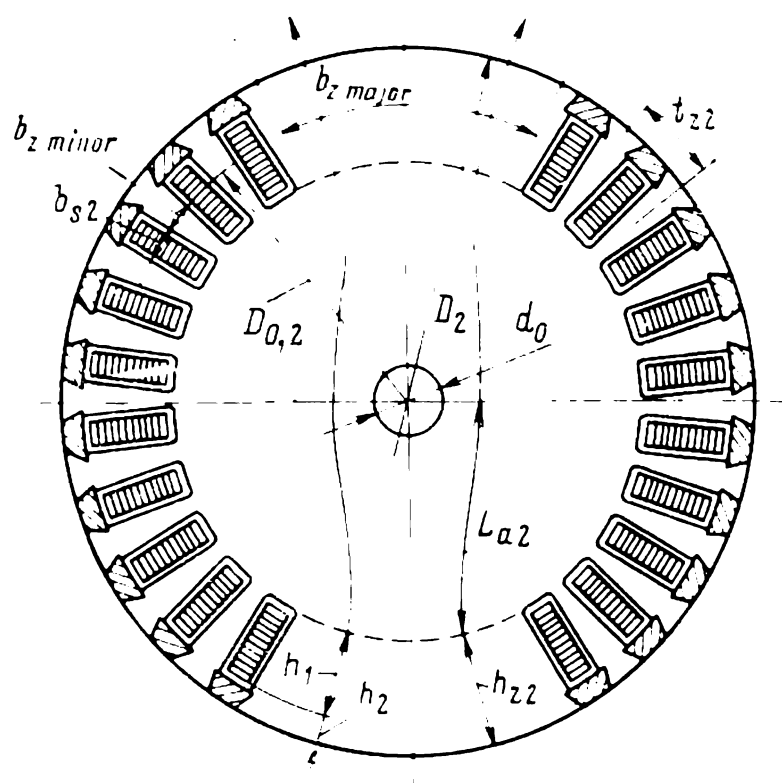


Fig. 53-9 Dimensions of the active zone in the rotor of a nonsalient-pole machine

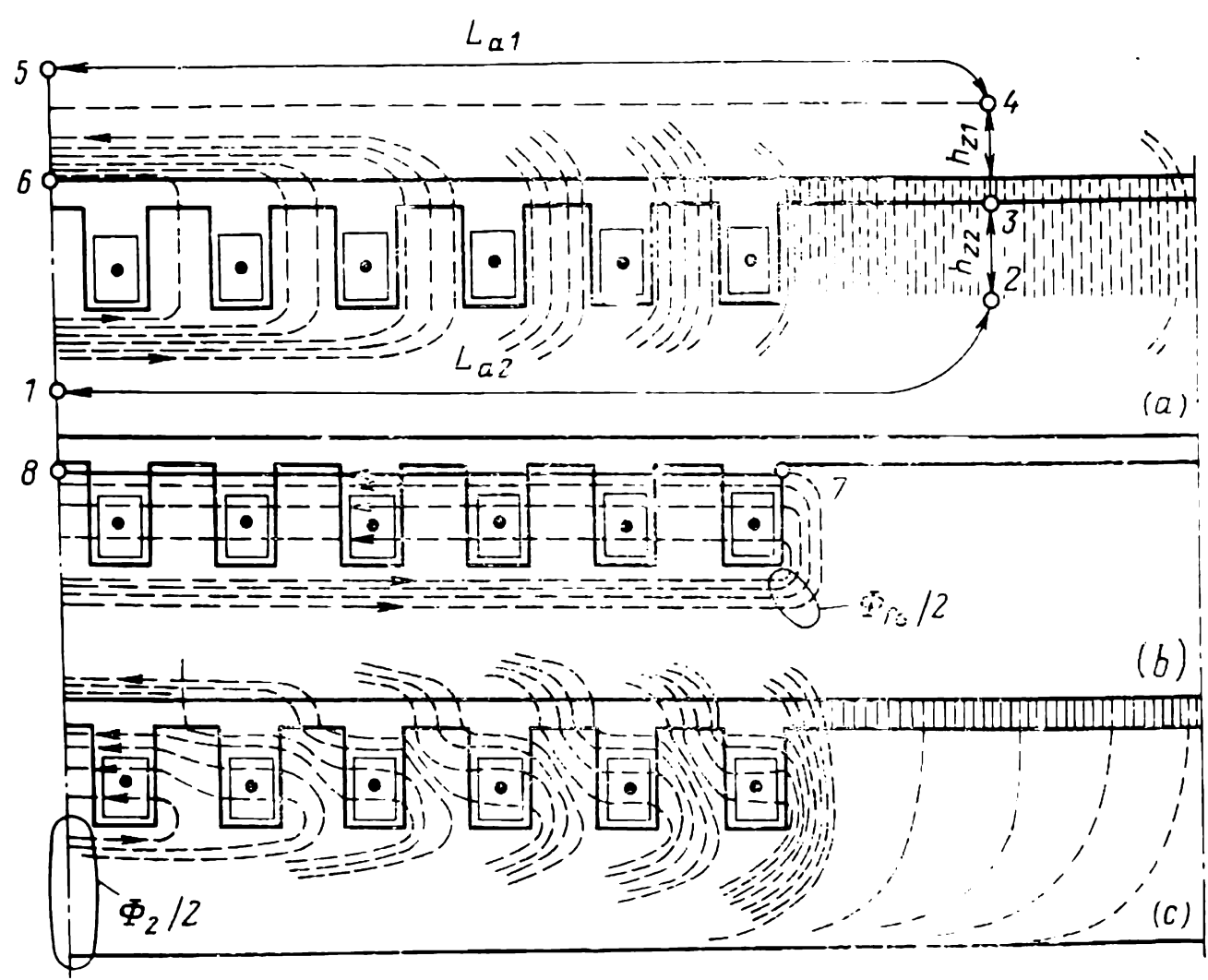


Fig. 53-10 Magnetic fields in a nonsalient-pole synchronous machine at no load: (a) mutual field; (b) leakage field; (c) resultant field

The values of  $k_B$  and  $\alpha_\delta$  with saturation are found as explained in Sec. 53-1, on taking a guessed value for  $k_z = (F_\delta + F_{z1})/F_\delta$ . The value of  $k_\delta$  is found by the equation

$$k_\delta = k_{\delta 1} k_{\delta 2} \rho + k_{\delta 1} (1 - \rho) \quad (53-26)$$

where  $k_{\delta 1}$  is found by Eq. (53-14),

$$k_{\delta 2} = t_{z2}/(t_{z2} - \gamma_2 \delta)$$

and

$$\gamma_2 = \frac{(b_{s2}/\delta)^2}{5 + b_{s2}/\delta}$$

In calculating  $F_2$  and its components  $F_{z2}$  and  $F_{a2}$ , it is important (as for a salient-pole machine) to take into account the effect of the leakage flux. To determine  $\Phi_2$  at the base of the rotor teeth,  $\Phi_m$  found from the field pattern in Fig. 53-10a should be augmented by  $\Phi_{f\phi}$  found from the field pattern in Fig. 53-10b. The leakage flux is found by the same equations (53-16) and (53-19) as were used for a salient-pole machine; it is likewise proportional to  $F_1$  between points 3 and 5, which is in turn equal to the mmf between points 7 and 8 (in Fig. 53-10, the characteristic points are numbered in the same sequence as in Fig. 53-6), and to  $\lambda_{f\phi}$ . The value of the latter varies with the shape and the number of rotor slots in the leakage-flux path 7-8-7' between adjacent heteropolar major teeth,  $Z_2/2p$  (in Fig. 53-10b, there are six slots in half this path), and can be found by the equation

$$\lambda_{f\phi} = (8p/Z_2) (\lambda_s + \lambda_t) \quad (53-27)$$

where  $\lambda_s = h_1/2b_{s2} + h_2/b_{s2}$  = rotor-slot permeance seen by the leakage flux

$\lambda_t = 0.2 + \delta/2t_{z2}$  = rotor tooth permeance seen by the leakage flux

$h_1$  = slot height taken up by conductors (Fig. 53-9)

$h_2$  = slot height free from conductors (in the same figure)

In nonsalient-pole machines,  $\lambda_{f\phi}$  is smaller than it is in salient-pole machines. Its ratio to the air gap permeance

$$\lambda_\delta = \alpha_\delta \tau / k_\delta \delta = \Phi_m / \mu_0 l_\delta F_\delta$$

ordinarily lies in the range 0.035-0.045, and may rise to 0.06-0.08 in directly cooled machines only. On the average, for indirectly cooled machines, this ratio may be taken as

$$k = \lambda_{f\phi} / \lambda_\delta = 0.04$$

so that the leakage flux may be calculated by Eq. (53-19) where  $\lambda_{f\Phi}$  does not enter.

The rotor-tooth flux density,  $B_{Z_2}$ , is calculated at the design tooth section corresponding to a surface whose diameter is assumed to be

$$D_{0.2} = D_2 - 2h_{Z_2} + 2 \times 0.2h_{Z_2}$$

and which lies within  $0.2h_{Z_2}$  of the tooth base. Also, it is important to remember that the design section (see Fig. 53-9)

$$S_{Z, \text{major}} = \frac{(1-\rho) \pi D_{0.2}}{2p} l_2 = b_{Z, \text{major}} l_2$$

of the major teeth lying within the region of high flux density is completely utilized by the flux. In contrast, the section of minor teeth,  $(Z_2/2p) l_2 b_{Z, \text{minor}}$ , distributed in the region of low flux density, is utilized incompletely. The fraction utilized is called their design section and given by

$$S_{Z, \text{minor}} = (Z_2/2p) l_2 b_{Z, \text{minor}} (0.715\rho)$$

where  $b_{Z, \text{minor}} = (\pi D_{0.2} \rho / Z_2) - b_{s2}$ , and  $Z_2$  is the number of slots on the rotor.

The mmf in the rotor teeth is given by

$$F_{Z_2} = h_{Z_2} H_{Z_2} \quad (53-28)$$

where  $H_{Z_2}$  is the field intensity at the design section of the rotor teeth,  $S_Z = S_{Z, \text{major}} + S_{Z, \text{minor}}$ , corresponding to the flux density at that section,  $B_{Z_2} = \Phi_2 / S_Z$  [13].

At  $B_{Z_2} > 1.8\text{T}$ , some of the flux is crowded from the teeth into slots, and this should be accounted for by applying a correction factor

$$k_{s, \text{oc}} = \frac{\pi D_{0.2} l_2 (1 - \rho + 0.715\rho^2)}{2p S_Z} - 1$$

Families of magnetization curves for rotors with several values of  $k_{s, \text{oc}}$  can be found in [13].

The mmf in the rotor yoke is given by

$$F_{a2} = L_{a2} H_{a2} \quad (53-29)$$

where  $L_{a2} = \frac{D_2 - 2h_{Z_2}}{2} \sin(\pi/2p)$ , or can be taken from Fig. 53-9, and  $H_{a2}$  is the maximum field intensity in the yoke, corresponding to the flux density given by [13]

$$B_{a2} = \frac{\Phi_2}{l_2 (D_2 - 2h_{Z_2} - d_0)}$$



The mmf in the rotor is given by

$$F_2 = F_{z2} + F_{a2} \tag{53-30}$$

The calculation of the magnetic circuit for each value of  $E_f$  terminates in finding the excitation mmf,  $F_{fm} = w_f I_f$ , required to balance the sum of mmfs in the stator and gap,  $F_1$ , and in the rotor,  $F_2$ :

$$F_{fm} = w_f I_f = F_1 + F_2 \tag{53-31}$$

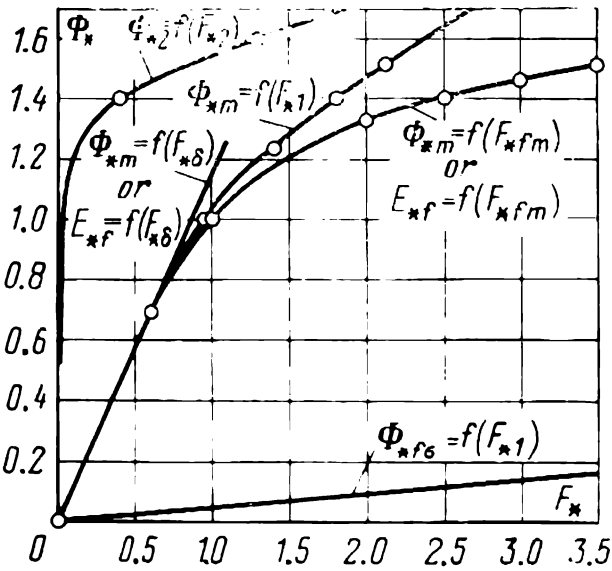


**Fig. 53-11** Normalized open-circuit and magnetization curves of nonsalient-pole synchronous machines

As for a salient-pole machine, the results are presented as open-circuit and magnetization curves which may be plotted in absolute units (as in Fig. 53-7) or on a per-unit basis (as in Fig. 53-8).

The per-unit characteristics of various nonsalient-pole machines differ very little, so when the characteristics of a particular machine are not available, calculations may be based on the averaged per-unit open-circuit and magnetization characteristics of nonsalient-pole machines, called the normal or normalized characteristics. Such characteristics are shown in Fig. 53-11.

# 54 MMF, Magnetic Field, EMF and Parameters of the Armature Winding

## 54-1 Armature MMF and Its Direct-Axis and Quadrature-Axis Components

In a loaded synchronous machine, the magnetic field is established by the current in the field winding and by a balanced set of currents in the polyphase (usually, three-phase) armature winding. The largest contribution to energy conversion in the machine comes from the mutual field cor-

responding to the fundamental component of the air gap flux density.

In turn, the mutual field is the result of the joint action of the mmf in the field winding, with a peak value  $F_{fm} = w_f I_f$ , and the fundamental mmf of the armature winding (see Sec. 25-4) with a peak value given by

$$F_{am} = (\sqrt{2}/\pi) m_1 I w_1 k_{w1} / p \quad (54-1)$$

To begin with, let us assume that the magnetic circuit is unsaturated and that the relative permeability of the

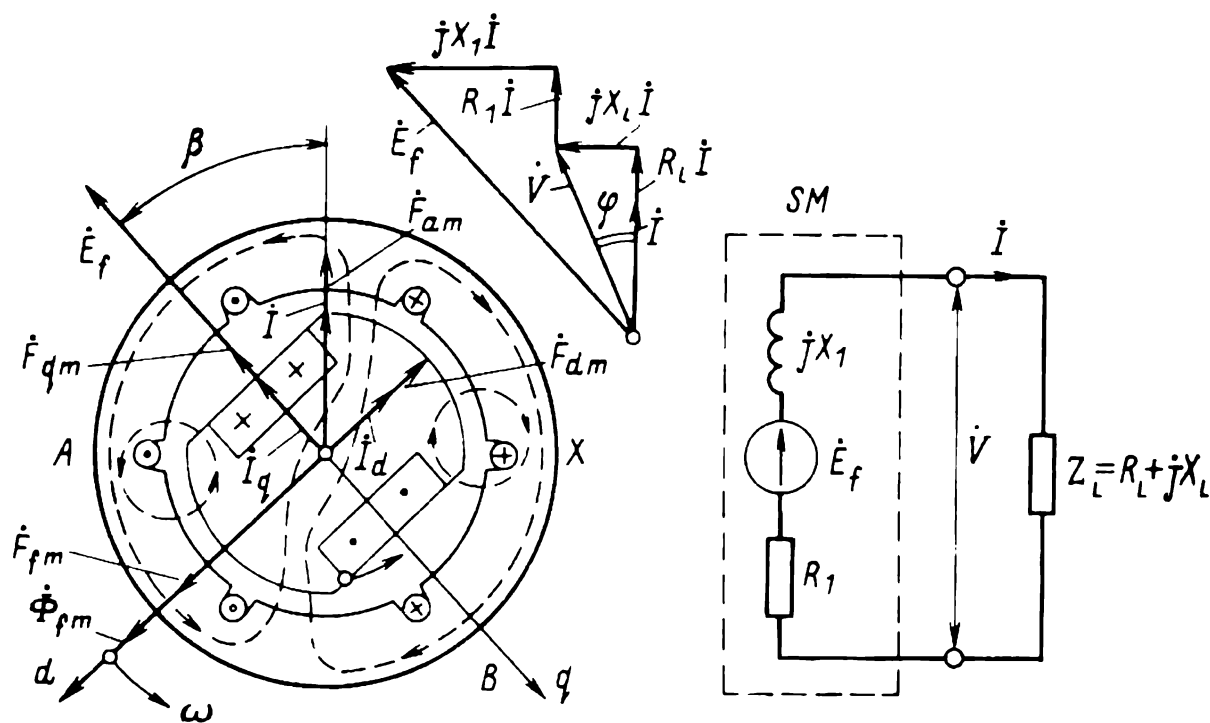


Fig. 54-1 Magnetic field due to the armature mmf on load

iron parts of the circuit is infinitely large,  $\mu_{rc} = \infty$ . On this assumption, the reluctance of the magnetic circuit has only one constant component, the reluctance of the air gap. The magnetic circuit may be deemed linear, and the mutual field in it may be represented by the sum of simpler fields, namely the field due to  $F_{fm}$  and the field due to  $F_a$ .

The field due to  $F_{fm}$  has already been investigated in connection with the no-load (open-circuit) condition (see Chap. 53). At  $\mu_{rc} = \infty$ , the mmfs in the iron parts of the circuit are zero ( $F_{a1} = F_{z1} = F_m = F_{z2} = F_{a2} = 0$ ), and the field mmf needs to balance only the gap mmf,  $F_{fm} = F_\delta$ . The excitation flux is equal to  $\Phi_m$ , and  $E_f$  may be found from the linear initial portions of the magnetization and no-load (open-circuit) characteristics (Fig. 53-7).

In the diagram of Fig. 54-1 plotted on the complex plane of a two-pole model of a three-phase synchronous machine, the directions of the  $\dot{F}_{fm}$  and  $\dot{\Phi}_{fm}$  phasors are determined by the field current phasor  $\dot{I}_f$ . The excitation mmf,  $\dot{E}_f$ , induced in the armature winding by the excitation field, lags behind  $\dot{\Phi}_{fm}$  by  $\pi/2$ .

The armature mmf,  $\dot{F}_{am}$ , is in line with the armature current,  $\dot{I}$  (see Sec. 25-4), whose magnitude and phase relative to  $\dot{E}_f$  vary with the load sustained by the machine. Depending on the mode of operation and the load in that mode, the phase angle  $\beta$  between  $\dot{E}_f$  and  $\dot{I}$  (or  $\dot{F}_{am}$ ) may lie anywhere between zero and  $2\pi$ .

In a nonsalient-pole machine, the magnetic field set up by an arbitrarily oriented  $F_{am}$  can be found with ease, because the air gap between the rotor and stator is the same everywhere (the field can be found in the same manner as in an induction machine). In a salient-pole machine, the field due to  $F_{am}$  taking up an arbitrary phase angle  $\beta$  is far more complex in pattern (see Fig. 54-1). However, its calculation can be substantially simplified, if it is represented as the sum of the fields due to two mutually perpendicular components of  $\dot{F}_{am}$ . One of these components is along the *direct* (or *d*-) *axis* of the rotor in the model, which is the axis of symmetry of poles, and is in line with  $\dot{F}_{fm}$ . The other component is along the *quadrature* (or *q*-) *axis* which is the axis of symmetry halfway between adjacent north and south poles and is in electrical quadrature leading with (90 electrical degrees or a quarter of a cycle from) the *d*-axis. Hence its name, the quadrature axis.

The resolution of  $\dot{F}_{am}$  into the *d*-axis component,  $\dot{F}_{dm}$ , and the *q*-axis component,  $\dot{F}_{qm}$ , is illustrated in Fig. 54-1. Their peak values are respectively given by:

$$\left. \begin{aligned} F_{dm} &= F_{am} |\sin \beta| \\ F_{qm} &= F_{am} |\cos \beta| \end{aligned} \right\} \quad (54-2)$$

From a comparison of Eqs. (54-1) and (54-2), it is readily seen that the components of  $F_{am}$  may be visualized as produced respectively by a set of direct-axis currents with an

rms value  $I_d = I |\sin \beta|$ , and by a set of quadrature-axis currents with a peak value  $I_q = I |\cos \beta|$

$$\left. \begin{aligned} \dot{F}_{dm} &= (\sqrt{2}/\pi) m_1 \dot{I}_d w_1 k_{w1}/p \\ \dot{F}_{qm} &= (\sqrt{2}/\pi) m_1 \dot{I}_q w_1 k_{w1}/p \end{aligned} \right\} \quad (54-3)$$

## 54-2 The Armature MMF at Various Loads in the Generator Mode

Let us consider the operation of a synchronous machine as a generator, with its armature winding connected to a balanced isolated load where all the phases have the same impedance equal to  $Z_L = R_L + jX_L$ . We set out to learn how the armature mmf,  $F_{am}$ , and its  $d$ - and  $q$ -axis components,  $F_{dm}$  and  $F_{qm}$ , vary with the magnitude of load.

An equivalent circuit for an unsaturated machine in this mode is shown in Fig. 54-1. The current  $\dot{I}$  produced in the armature winding by  $\dot{E}_f$  depends not only on the load impedance,  $Z_L$ , but on the own impedance of each armature phase,  $R_1 + jX_1$ ,

$$\begin{aligned} \dot{I} &= \frac{\dot{E}_f}{(R_1 + R_L) + j(X_1 + X_L)} \\ I &= \frac{E_f}{\sqrt{(R_1 + R_L)^2 + (X_1 + X_L)^2}} \end{aligned} \quad (54-4)$$

The phase angle  $\beta$  depends on the ratio of the reactive impedance to the resistance:

$$\beta = \arctan \frac{X_1 + X_L}{R_1 + R_L} \quad (54-5)$$

In the above equations, the inductive reactance of the armature winding,  $X_1$ , is the sum of the leakage inductive reactance,  $X_\sigma$ , and the mutual inductive reactance,  $X_a$ , associated with the mutual field in the armature. In a nonsalient-pole machine where the air gap is uniform,  $X_a$  is calculated in the same way as in an induction machine (see Sec. 28-5). In a salient-pole machine,  $X_a$  depends on the position of  $F_a$  relative to the pole axes (see Sec. 54-5).  $R_1$  is the resistance of an armature phase.

In a nonsalient-pole machine,  $R_1$  can be calculated in the same manner as in an induction machine (see Sec. 31-2); how it should be calculated for a salient-pole machine is explained in Sec. 54-5.

From the voltage diagram in Fig. 54-1, it is seen that the phase angle  $\beta$  is, in the general case, different from the phase

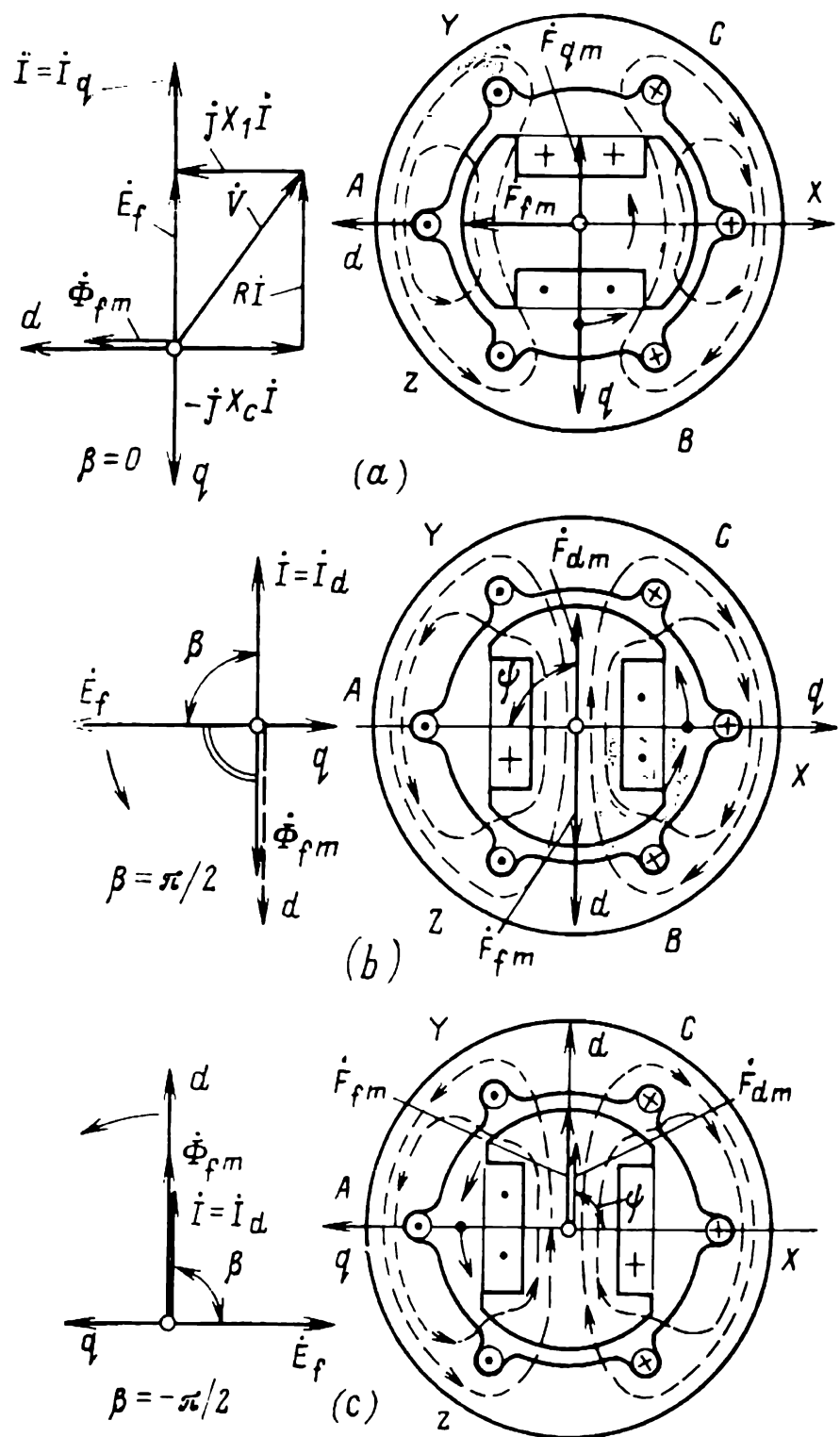


**Fig. 54-2** Armature magnetic field and mmf under characteristic loads:  
(a) field and mmf due to  $q$ -axis armature current; (b) field and mmf due to  $d$ -axis demagnetizing current; (c) field and mmf due to  $d$ -axis magnetizing current

angle between the current phasor  $\dot{I}$  and the terminal voltage phasor,  $\dot{V} = Z_L \dot{I}$ , solely dependent on the load impedance.  
**(1) Inductive load.** In the case of an inductive load (see Fig. 54-2b), when  $Z_L = jX_L$ ,  $R_L = 0$ ,  $X_L > 0$ , and

the own resistance of a phase,  $R_1$ , is small in comparison with  $X_1 + X_L$ , the current phasor  $\dot{I}$  lags behind the emf phasor  $\dot{E}_f$  by

$$\beta = \arctan \infty = +\pi/2$$

and is in line with the direct ( $d$ -) axis:

$$I_d = I \sin \beta = I$$

$$I_q = I \cos \beta = 0$$

As is seen, the armature mmf,  $F_{am} = F_{dm}$ , and the magnetic field established by the set of direct-axis currents,  $I = I_d$ , oppose the excitation mmf,  $F_{fm}$ , thereby weakening the excitation field. Thus, in the case of an inductive load, the armature winding carries a set of direct-axis demagnetizing currents,  $\dot{I}_d$ .

**(2) Capacitive load.** A capacitive load (with respect to  $E_f$ ) exists when the armature winding is connected across a set of balanced capacitances  $C$  with an impedance  $Z_L = jX_L$  chosen such that  $X_L = -X_C = -1/\omega C < 0$  exceeds in absolute value the own inductive reactance of the armature, that is,

$$X_C = |X_L| > X_1$$

and

$$X_1 + X_L = X_1 - X_C < 0$$

If, in the case of a capacitive load, the own phase resistance  $R_1$  is small in comparison with the inductive reactance,  $|X_L + X_1|$  (Fig. 54-2c), the phase angle between  $\dot{I}$  and  $\dot{E}_f$  is

$$\beta = \arctan \frac{X_L + X_1}{R_1} = \arctan (-\infty) = -\pi/2$$

This means that the armature current,  $\dot{I}$ , leads  $\dot{E}_f$  by an angle  $\beta$  and is therefore in line with the  $d$ -axis:

$$I_d = I |\sin \beta| = I$$

$$I_q = I |\cos \beta| = 0$$

Now the armature mmf,  $F_{am} = F_{dm}$ , and the magnetic field established by the set of  $d$ -axis currents,  $I = I_d$ , are in line with the excitation mmf,  $F_{fm}$ , and boost the excitation field. Thus, in the case of a capacitive load, the armature winding carries a set of  $d$ -axis magnetizing currents,  $I_d$ .

(3) **Resistive load.** A resistive load (with respect to  $\dot{E}_f$ ) is that load at which the armature current,  $\dot{I}$ , is in phase with  $\dot{E}_f$  or, which is the same,  $\beta = 0$  (Fig. 54-2a). This condition can be achieved in practice, if we connect the armature winding to a set of balanced  $RC$  impedances,

$$Z_L = R_L + jX_L$$

where  $X_L = -X_C = -1/\omega C$ , so adjusted in value that  $X_1 = X_C$  and the total reactance of the loop,  $X_1 + X_L = X_1 - X_C$ , vanishes (see the voltage diagram in Fig. 54-2a, plotted on neglecting  $R_1$ ). With such a load, the phase angle between  $\dot{I}$  and  $\dot{E}_f$  is

$$\beta = \arctan \frac{X_L + X_1}{R_L} = \arctan 0 = 0$$

and the armature current is directed along the  $q$ -axis:

$$I_q = I \cos \beta = I$$

$$I_d = I \sin \beta = 0$$

Now, the armature field established by the armature mmf,  $F_a = F_q$  is acting along the  $q$ -axis. Its path is across a much longer air gap, than that of the  $d$ -axis field. Combined with the excitation field, the  $q$ -axis field somewhat boosts the resultant field, but causes it to depart from the  $d$ -axis.

### 54-3 Mutual Field and EMF due to the Armature Currents

Neglecting saturation (on assuming that  $\mu_{rc} = \infty$ ), the magnetic field established by the armature currents  $I$  may be investigated independently of the excitation field.

In a nonsalient-pole machine with a uniform air gap  $\delta$ , the armature field in the air gap has the same waveshape as the fundamental component of the armature mmf,  $F_{am}$ . The flux is distributed in the air gap sinusoidally (see Sec. 25-5), and its peak value is

$$B_{\delta 1m} = \mu_0 F_{am} / \delta k_\delta$$

The armature winding is linked by a mutual flux

$$\Phi_m = \frac{2}{\pi} \tau l_\delta B_{\delta 1m} \quad (54-6)$$

which produces with an armature phase a flux linkage given by

$$\Psi_{am} = w_1 k_{w1} \Phi_m \quad (54-7)$$

The emf induced by the mutual field in the armature winding is

$$\dot{E}_a = -j\omega \dot{\Psi}_{am} / \sqrt{2} \quad (54-8)$$

lagging by  $\pi/2$  behind  $\dot{\Psi}_{am}$ ,  $\dot{\Phi}_m$ ,  $\dot{B}_\delta$ ,  $\dot{F}_a$ , and  $\dot{I}$ , which are all in phase.

In a salient-pole machine, the mutual field established by the armature current,  $\dot{I}$ , taking up an arbitrary phase angle  $\beta$ , has a very complex pattern (see Fig. 54-1). To simplify calculations, it is customary to treat it as a sum of simpler fields, namely, the mutual field due to  $I_d$ , and the mutual field due to  $I_q$ .

**(1) Mutual field and emf due to  $I_d$ .** Referring to Fig. 54-2b or c, the  $d$ -axis currents in the armature winding,  $I_d$ , establish a sinusoidally distributed mmf with a peak value  $F_{dm}$ . The mutual field due to this mmf can be found by numerical methods or by mathematical modelling. As is shown in Fig. 54-3a, the radial component of air gap flux density is distributed nonsinusoidally.

The ratio of the fundamental flux density set up by the  $d$ -axis armature mmf,  $B_{ad1m}$ , to the peak flux density,  $B_{adm}$ , due to the same mmf (as found for a uniform air gap and shown by a dashed line in Fig. 54-3) is the direct-field form factor

$$k_d = B_{ad1m} / B_{adm} \quad (54-9)$$

where  $B_{adm} = \mu_0 F_{dm} / \delta$ .

Once  $B_{adm}$  is known, it is an easy matter to calculate  $B_{ad1m}$ , using  $k_d$  which is mainly dependent on the ratio of the maximum air gap,  $\delta_m$ , to the minimum air gap,  $\delta$  (Fig. 54-3a). Plots of  $k_d = f(\delta_m/\delta')$  and  $k_d = f(\delta'/\tau)$ , as found from the magnetic field patterns for a smooth armature core and for the pole-piece dimensions typical of salient-pole machines ( $\alpha = b_p/\tau = 0.69$  to  $0.72$ ), are given in Fig. 54-4. For a smooth round armature,  $\delta'$  is taken to be the air gap between the stator and rotor at the pole axis,  $\delta' = \delta$ .

Where it is important to account for the effect of slots on the armature core and in the pole pieces,  $\delta'$  must be taken



equal to  $\delta k_\delta$  and  $\delta_m/\delta'$  to  $\delta_m/k_\delta\delta$ . (For the calculation of  $k_f$ ,  $k_\Phi$ , and other factors see Sec. 53-1.)

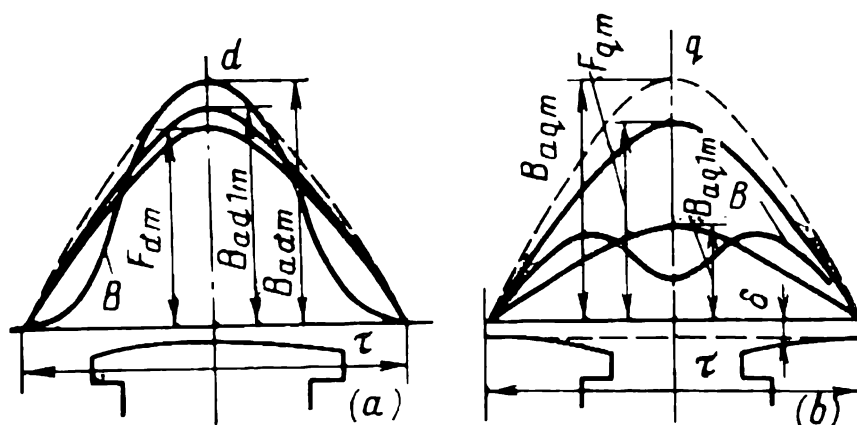


Fig. 54-3 Magnetic fields due to (a)  $d$ -axis and (b)  $q$ -axis set of armature currents

Once the value of  $k_d$  is found from the curves in Fig. 54-4 it is an easy matter to calculate the mutual flux corresponding to  $I_d$ :

$$\Phi_{adm} = \frac{2}{\pi} \tau l_\delta B_{ad1m} = \frac{2}{\pi} \tau l_\delta k_d B_{adm} \quad (54-10)$$

where  $B_{adm} = \mu_0 F_{dm}/\delta k_\delta$ .

With an armature phase, this flux produces a flux linkage given by

$$\Psi_{adm} = w_1 k_{w1} \Phi_{adm} \quad (54-11)$$

and induces in it a mutual emf defined as

$$\dot{E}_{ad} = -j\omega \dot{\Psi}_{adm}/\sqrt{2} \quad (54-12)$$

(2) **Mutual flux density and emf due to  $I_{qm}$ .** The mutual field established by the set of  $q$ -axis currents in the armature winding,  $I_{qm}$  (see Fig. 54-2a) is likewise nonsinusoidal in waveshape. As is seen from Fig. 54-3b, the radial component of  $B$  between pole-pieces is substantially weakened in comparison with the flux density that would exist if the air gap were uniform (shown by a dashed line in the figure).

The mutual flux due to the  $q$ -axis mmf is calculated by

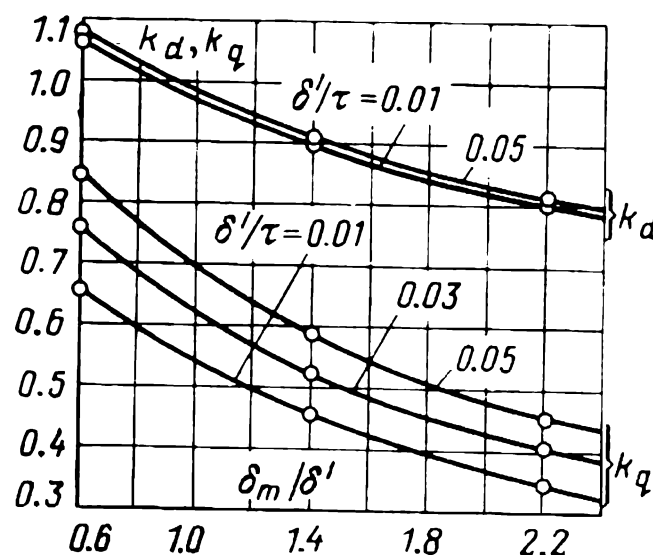


Fig. 54-4 Plots of  $k_d$  and  $k_q$ , the direct- and quadrature-axis field form factors

applying the  $q$ -axis field form factor,  $k_q$ , defined as the ratio of the fundamental flux density due to the armature  $q$ -axis mmf,  $B_{aq1m}$ , to the peak flux density due to the same mmf,  $B_{aqm}$ , as found for a uniform air gap and shown by the dashed line:

$$k_q = B_{aq1m}/B_{aqm} \quad (54-13)$$

where  $B_{aqm} = \mu_0 F_{qm}/\delta$ .

Plots of  $k_q$  as a function of  $\delta_m/\delta'$  and  $\delta'/\tau$ , deduced from the magnetic field patterns applicable to a round (nonsalient) armature core, appear in Fig. 54-4. As already explained, in the case of a smooth-surface armature,  $\delta' = \delta$ . So, when it is important to account for the effect of slots, one should take  $\delta' = \delta k_\delta$ . Once  $k_q$  has been found from the curves in Fig. 54-4, it is easy to calculate the mutual flux corresponding to  $I_q$ ,

$$\Phi_{aqm} = \frac{2}{\pi} \tau l_\delta B_{aq1m} = \frac{2}{\pi} \tau l_\delta k_q B_{aqm} \quad (54-14)$$

where  $B_{aqm} = \mu_0 F_{qm}/\delta k_\delta$ .

Linking the armature phase, this flux is

$$\Psi_{aqm} = w_1 k_{w1} \Phi_{aqm} \quad (54-15)$$

where it induces a mutual emf

$$\dot{E}_{aq} = -j\omega \dot{\Psi}_{aqm}/\sqrt{2} \quad (54-16)$$

#### 54-4 Equivalent Armature MMF in an Unsaturated Machine

The armature mmf,  $F_{am}$ , and its  $d$ - and  $q$ -axis components,  $F_{dm}$  and  $F_{qm}$ , differ in waveshape from the field mmf,  $F_f$ . The armature mmf is distributed over the surface sinusoidally; the field mmf is distributed in a manner substantially differing from sinusoidal. This stands in the way of combining the two mmfs. To simplify calculations, the sinusoidal armature mmfs are therefore replaced by equivalent field mmfs chosen so as to retain the fundamental flux density in the air gap and the fundamental emf induced in the armature winding.

The  $d$ -axis armature mmf,  $F_{dm}$ , which gives rise to a field whose fundamental flux density is

$$B_{ad1m} = k_d B_{adm} = k_d \mu_0 F_{dm}/\delta k_\delta$$

is replaced by the field mmf,  $F_{fm} = F_{adm}$ , which sets up a field with the same fundamental flux density

$$B_{\delta 1m} = k_f \mu_0 F_{adm} / \delta k_\delta = B_{ad1m}$$

(see Sec. 53-1). Hence, the field mmf equivalent to the  $d$ -axis armature mmf is given by

$$F_{adm} = k_{ad} F_{dm} \quad (54-17)$$

where  $k_{ad} = k_d/k_f$  is the  $d$ -axis armature reaction factor, with  $k_d$  found from the curves in Fig. 54-4, and  $k_f$  from the curves in Fig. 53-3.

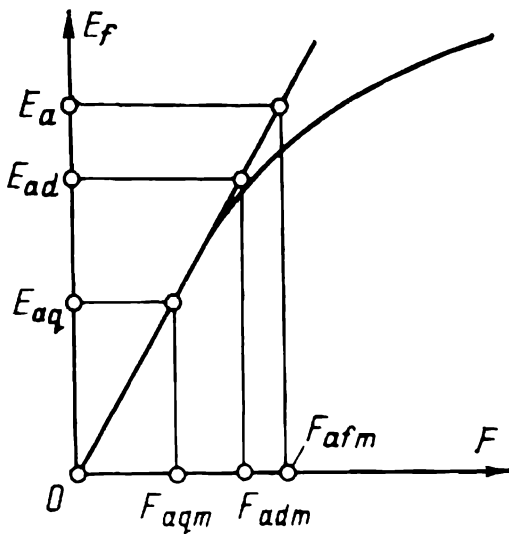


Fig. 54-5 Determination of emf due to armature currents by means of equivalent field mmfs

Similarly, the field mmf equivalent to the  $q$ -axis armature mmf is

$$F_{aqm} = k_{aq} F_{qm} \quad (54-18)$$

where  $k_{aq} = k_q/k_f$  is the  $q$ -axis armature reaction factor, with  $k_q$  found from Fig. 54-4, and  $k_f$  from Fig. 53-3.

In a nonsalient-pole machine, the armature mmf,  $F_{am}$ , establishing a field with a fundamental flux density

$$B_{a1m} = \mu_0 F_{am} / \delta k_\delta$$

is replaced by a field mmf,  $F_{fm} = F_{afm}$ , which establishes a field with the same fundamental flux density

$$B_{\delta f1m} = k_f \mu_0 F_{afm} / \delta k_\delta = B_{a1m}$$

Hence, in a nonsalient-pole machine, the field mmf equivalent to the armature mmf is

$$F_{afm} = k_a F_{am} = F_{am} / k_f \quad (54-19)$$

where  $k_a = 1/k_f$  is the armature reaction factor found from the curves in Fig. 53-3.

When replacing  $F_{dm}$ ,  $F_{qm}$ , and  $F_{am}$  with  $F_{adm}$ ,  $F_{aqm}$ , and  $F_{afm}$ , it is important to remember that on a phasor vector diagram their axes retain their original directions.

The use of equivalent field mmfs ( $F_{adm}$  and  $F_{aqm}$  in a salient-pole machine and  $F_{afm}$  in a nonsalient-pole machine) enables the analyst or designer to find the mutual emfs  $E_{ad}$ ,  $E_{aq}$  and  $E_a$  due to the currents  $I_d$ ,  $I_q$ , and  $I$  in the

armature winding from the no-load characteristic,  $E_f = f(F_{fm})$ , without having to use Eqs. (54-8), (54-12), and (54-16).

In an unsaturated machine, where  $F_{fm} = F_\delta$ , this can be done by using the linearized no-load characteristics,  $E_f = f(F_\delta)$ , as illustrated in Fig. 54-5.

### 54-5 Parameters of the Armature Winding (for Positive Sequence Currents)

Each phase of the armature winding in a synchronous machine has a resistance and an inductive reactance associated with the mutual and leakage fields set up by the armature currents.

In steady-state balanced operation, the armature winding carries a set of currents,  $I$ , that give rise to the fundamental mmf,  $F_{am}$ , and the mutual field. These currents are rotating at the same speed as the rotor does, and take up a certain definite position relative to the  $d$ - and  $q$ -axes of the rotor. They are positive-sequence currents.

The field established by such currents is stationary relative to the rotor, and it does not induce any currents in the rotor, field or damper windings that might lead to additional losses or weaken the field set up by the armature currents. Therefore, in calculating the impedances of armature phases to positive-sequence currents, one needs only to take into account the magnetic field and losses due to the currents in the armature winding itself.

(1) **Resistance of the armature conductors.** It can be found from the copper losses as calculated with allowance for current crowding (see Sec. 31-2). To minimize the copper loss

$$P_{Cu1} = m_1 R I^2 \quad (54-20)$$

and the resistance,  $R$ , of the armature phase conductors, it is usual in large synchronous machines to strand and transpose the conductors. Stranding and transposition reduces the per-unit resistance in large machines to

$$R_* = R I_R / V_R = 0.006 \text{ to } 0.002 \text{ (or even less)}$$

(2) **Leakage inductive reactance of the armature winding.** The leakage inductive reactance of an armature phase,  $X_\sigma$ , is associated with the leakage fields and the leakage induct-

ance of the armature phase,  $L_{\sigma 1}$ , (see Sec. 28-7):

$$X_{\sigma} = 2\pi f L_{\sigma 1} = 4\pi\mu_0 f w_1^2 (l_{\delta}/pq_1) \lambda_{\sigma 1} \quad (54-21)$$

Since leakage fields depend little, if at all, on the air gap shape, the equations given in Sec. 28-7 are equally applicable to nonsalient- and salient-pole machines. The reluctance to the armature leakage fields mainly comes from the various nonmagnetic gaps (in the slots, air gap, and overhangs) with permeability  $\mu_0$ . Therefore, it is legitimate to neglect the reluctance presented by the iron parts to the leakage fields and deem the leakage reluctance constant under any operating conditions (even when the magnetic circuit of the mutual field is saturated).

Since the leakage fields alternate at frequency  $f$ , a leakage emf is induced in the armature winding

$$\dot{E}_{\sigma} = -jX_{\sigma}\dot{I} = -j\omega\dot{\Psi}_{\sigma m}/\sqrt{2} \quad (54-22)$$

where  $\dot{\Psi}_{\sigma m} = L_{\sigma 1} (\sqrt{2}\dot{I})$  is the leakage flux linkage of an armature phase.

**(3) Mutual inductive reactance of the armature (in a nonsalient-pole machine).** In an unsaturated, nonsalient-pole machine with a uniform air gap, the mutual inductive reactance of the armature,  $X_a$ , is calculated from  $L_{11}$ :

$$X_a = 2\pi f L_{11} = 4\mu_0 m_1 f_1 (w_1 k_{w1})^2 \lambda_{\delta} / \pi p \quad (54-23)$$

where  $\lambda_{\delta} = \tau l_{\delta} / k_{\delta} \delta$  is the permeance of a uniform air gap per pole.

The emf induced by the rotating mutual armature field, Eq. (54-8), is

$$\dot{E}_a = -j\omega\dot{\Psi}_{am}/\sqrt{2} = -jX_a\dot{I} \quad (54-24)$$

where  $\dot{\Psi}_{am} = L_{11} (\sqrt{2}\dot{I})$  is the mutual flux linkage per phase due to the armature currents  $\dot{I}$ .

**(4) Direct- and quadrature-axis mutual inductive reactances of the armature (in a salient-pole machine).** It has been shown in Sec. 54-3 that in a salient-pole machine identical sets of  $d$ - and  $q$ -axis currents produce fields differing in the fundamental flux density because of the difference in the radial gap length (see Fig. 54-3a and b). Accordingly, the  $d$ - and  $q$ -axis mutual armature inductances,  $L_{ad}$  and  $L_{aq}$ , respectively associated with the  $d$ - and  $q$ -axis currents,  $I_d$  and  $I_q$ , are different. From Eqs. (54-10), (54-11), and

(54-3) it follows that the  $d$ -axis mutual inductive reactance of the armature is

$$\begin{aligned} X_{ad} &= 2\pi f L_{ad} = 2\pi f \Psi_{adm} / \sqrt{2} I_d \\ &= \frac{4\mu_0}{\pi p} m_1 f_1 (w_1 k_{w1})^2 \lambda_{ad} \end{aligned} \quad (54-25)$$

where  $\lambda_{ad} = k_d \tau l_\delta / k_\delta \delta = k_d \lambda_\delta = d$ -axis permeance of the air gap

$k_d = d$ -axis field form factor  
(see Fig. 54-4).

From Eqs. (54-3), (54-14) and (54-15), it follows that the  $q$ -axis mutual inductive reactance of the armature is

$$\begin{aligned} X_{aq} &= 2\pi f L_{aq} = 2\pi f \Psi_{aqm} / \sqrt{2} I_q \\ &= \frac{4\mu_0}{\pi p} m_1 f_1 (w_1 k_{w1})^2 \lambda_{aq} \end{aligned} \quad (54-26)$$

where  $\lambda_{aq} = k_q \tau l_\delta / k_\delta \delta = k_q \lambda_\delta = q$ -axis permeance of the air gap

$k_q = q$ -axis field form factor  
(see Fig. 54-4)

The  $d$ - and  $q$ -axis mutual inductive reactances of the armature are proportional to the respective permeances. As the radial gap length increases, the permeances decrease. Because, however, the  $q$ -axis permeance is smaller, the  $q$ -axis mutual reactance is always smaller than the  $d$ -axis mutual reactance,  $X_{aq} < X_{ad}$ .

The mutual emfs induced in each phase by the direct- and quadrature-axis sets of currents [see Eqs. (54-12) and (54-16)] can be expressed in terms of the  $d$ - and  $q$ -axis mutual inductive reactances as follows:

$$\begin{aligned} \dot{E}_{ad} &= -j\omega \dot{\Psi}_{adm} / \sqrt{2} = -jX_{ad} \dot{I}_d \\ \dot{E}_{aq} &= -j\omega \dot{\Psi}_{aqm} / \sqrt{2} = -jX_{aq} \dot{I}_q \end{aligned} \quad (54-27)$$

where  $\dot{\Psi}_{adm} = L_{ad} (\sqrt{2} I_d) =$  mutual flux linkage due to  $\dot{I}_d$

$\dot{\Psi}_{aqm} = L_{aq} (\sqrt{2} I_q) =$  mutual flux linkage due to  $\dot{I}_q$

**(5) Inductive reactance of the armature (in a nonsalient-pole machine).** This is the total inductive reactance of the armature winding for a balanced set of positive-sequence currents. The inductive reactance of the armature,  $X_1$ , in a nonsalient-pole machine is the sum of the leakage arma-

ture inductive reactance,  $X_\sigma$ , and the mutual armature inductive reactance,  $X_a$ :

$$X_1 = X_\sigma + X_a \quad (54-28)$$

**(6) Direct- and quadrature-axis inductive reactances of the armature (in a salient-pole machine).** These reactances are each the sum of the leakage and mutual reactances for  $I_d$  and  $I_q$ , respectively. Because the leakage inductive reactance for the components of the armature current does not differ from that for the armature current itself,  $X_\sigma$ , the  $d$ -axis inductive reactance of the armature may be written

$$X_d = X_\sigma + X_{ad} \quad (54-29)$$

and the  $q$ -axis inductive reactance of the armature may be written

$$X_q = X_\sigma + X_{aq} \quad (54-30)$$

**(7) Direct- and quadrature-axis inductive reactances of the armature (in a nonsalient-pole machine).** In a nonsalient-pole machine, the inductive reactance of the armature does not depend on the position of the mmf relative to the rotor axes. Therefore, for both the  $d$ - and  $q$ -axis sets of currents, it does not differ from the total inductive reactance of the armature given by Eq. (54-28):

$$X_d = X_q = X_1 \quad (54-31)$$

The same goes for the  $d$ - and  $q$ -axis mutual inductive reactances. In a nonsalient-pole machine, they do not differ from the mutual inductive reactance of the armature:

$$X_{ad} = X_{aq} = X_a \quad (54-32)$$

**(8) Armature impedance.** Visualize the total emf,  $\dot{E}_a$ , induced by the armature field due to  $\dot{I}$  as the sum of  $\dot{E}_{ad}$  and  $\dot{E}_{aq}$ , induced respectively by  $\dot{I}_d$  and  $\dot{I}_q$ ,

$$\dot{E}_a = \dot{E}_{ad} + \dot{E}_{aq} \quad (54-33)$$

and express the mutual impedance of the armature,  $Z_a$ , as the ratio of the mutual emf,  $-\dot{E}_a$ , to  $\dot{I}$ :

$$Z_a = R_a + jX_a = -\dot{E}_a/\dot{I} \quad (54-34)$$

It can be shown that the resistive component,  $R_a$ , and the reactive component,  $X_a$ , of the armature mutual impe-

dance  $Z_a$ , depend on the  $d$ - and  $q$ -axis mutual inductive reactances of the armature,  $X_{ad}$  and  $X_{aq}$ , and on the position of the armature mmf,  $\dot{F}_a$  (or the armature current  $\dot{I}$ ) relative to the rotor, as given by the phase angle  $\beta$  (see Fig. 54-1). To this end,  $\dot{I}$  and  $\dot{E}_a$  must be plotted on the complex plane shown in Fig. 54-6. Deeming the angle  $\beta$  positive when  $\dot{I}$  lags behind the negative direction of the  $q$ -axis or  $\dot{E}_f$ , the armature current phasor may be written

$$\dot{I} = \dot{I}_d + \dot{I}_q \quad (54-35)$$

where

$$\dot{I}_d = I \sin \beta = I_d$$

$$\dot{I}_q = jI \cos \beta = jI_q$$

and the emf may be written as

$$\dot{E}_a = \dot{E}_{ad} + \dot{E}_{aq} \quad (54-36)$$

where

$$\dot{E}_{ad} = -jX_{ad}\dot{I}_d = -jX_{ad}I \sin \beta$$

$$\dot{E}_{aq} = -jX_{aq}\dot{I}_q = +X_{aq}I \cos \beta$$

Taking the above equations together and equating the respective coefficients of the real and imaginary terms on the right- and left-hand sides of Eq. (54-34), we get

$$\begin{aligned} X_a &= \frac{X_{ad} + X_{aq}}{2} - \frac{X_{ad} - X_{aq}}{2} \cos 2\beta \\ R_a &= \frac{X_{ad} - X_{aq}}{2} \sin 2\beta \end{aligned} \quad (54-37)$$

Plots of  $X_a$  and  $R_a$  as functions of  $\beta$  appear in Fig. 54-7. The same figure gives plots of  $I_d$  and  $I_q$  as functions of  $\beta$  (as  $\beta$  varies,  $I$  remains unchanged).

At  $\beta$  equal to zero or  $\pi$ , when the current is directed along the quadrature axis,  $\dot{I} = \dot{I}_q$ , the inductive component of the mutual impedance is equal to the  $q$ -axis mutual inductive reactance of the armature,  $X_a = X_{aq}$ , whereas the

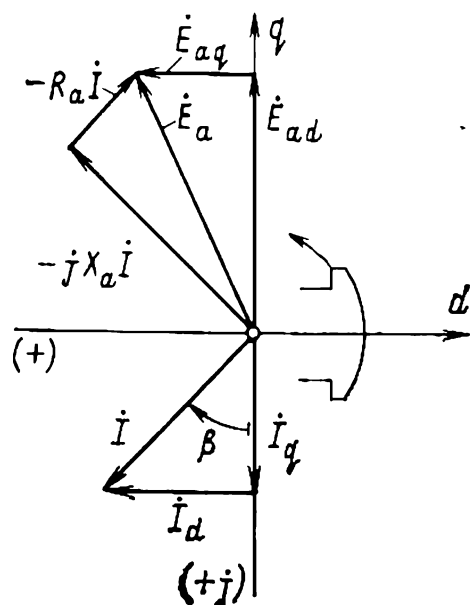


Fig. 54-6 Determination of the mutual impedance of the armature in a salient-pole synchronous machine



resistive component of the mutual impedance vanishes,  $R_a = 0$ .

At  $\beta = \pm\pi/2$ , when the current is along the  $d$ -axis,  $\dot{I} = \dot{I}_d$ , the inductive component is equal to the  $d$ -axis mutual inductive reactance of the armature,  $X_a = X_{ad}$ , whereas the resistive component vanishes,  $R_a = 0$ .

The physical meaning of  $R_a$  in a salient-pole machine will be explained in Sec. 56-2, in connection with energy

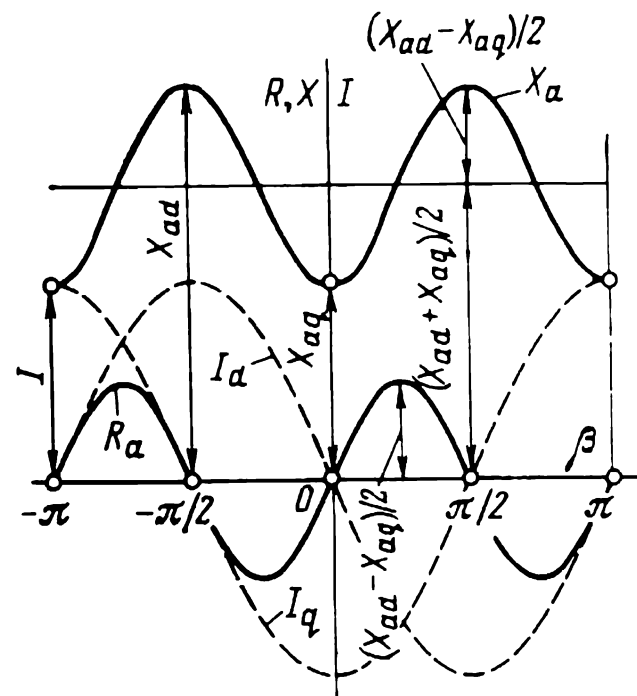


**Fig. 54-7** Components of the mutual armature impedance in a salient-pole machine, plotted as functions of the angle  $\beta$  between the armature current and the  $q$ -axis

conversion in synchronous machines. As will be shown, the term  $m_1 R_a I^2$  is the electric power converted to mechanical power when the rotor is of the salient-pole design (at  $R_a < 0$ , the direction of energy conversion is reversed). The resistive component

$$|R_a| = (X_{ad} - X_{aq})/2$$

at  $\beta = \pm\pi/4 + k\pi$ , where  $k$  is an integer.

The maximum value of resistance, coinciding with the peak value of oscillations in inductive reactance about its mean value,  $(X_{ad} + X_{aq})/2$ , is equal to half the difference between  $X_{ad}$  and  $X_{aq}$ . Therefore in a nonsalient-pole machine where  $X_{ad} = X_{aq}$ , the

resistive component is zero,  $R_a = 0$ , and the inductive component is the same at any value of  $\beta$ ,  $X_a = X_{ad} = X_{aq}$ .

In finding the armature winding impedance,  $Z_1$ , it is important to take into account the armature conductor resistance  $R$  and the armature leakage inductive reactance,  $X_\sigma$

$$Z_1 = R_1 + jX_1 \quad (54-38)$$

where

$$R_1 = R + R_a = R + \frac{X_d - X_q}{2} \sin 2\beta$$

is the resistive component of the armature impedance, and

$$X_1 = X_\sigma + X_a = \frac{X_d + X_q}{2} - \frac{X_d - X_q}{2} \cos 2\beta$$

is the inductive component of the armature impedance. In a salient-pole machine they are functions of the angle  $\beta$ . Therefore, when  $\beta = \pm\pi/2$  (the  $d$ -axis set of currents)

$$R_1 = R, X_1 = X_d = X_\sigma + X_{ad}$$

whereas at  $\beta$  equal to zero or  $\pi$  (the  $q$ -axis set of currents)

$$R_1 = R, X_1 = X_q = X_\sigma + X_{aq}$$

In a nonsalient-pole machine, the armature impedance and its components are independent of the current phase angle,  $\beta$ :

$$R_1 = R, R_a = 0, X_1 = X_\delta + X_a$$

## 55 Electromagnetic Processes in a Synchronous Machine on Load

### 55-1 Electromagnetic Processes in a Nonsalient-Pole Machine (Neglecting Saturation)

A study into the electromagnetic processes that take place in a synchronous machine is undertaken in order to develop a mathematical model in the form of equations relating the quantities in its electric and magnetic circuits.

To begin with, we shall turn to an unsaturated machine, assuming that the relative permeability of the iron parts in its magnetic circuit is infinitely large,  $\mu_{rc} = \infty$ . Neglecting the reluctance of the iron, we may treat the “magnetic” circuit as linear, and apply the principle of superposition, that is, determine the magnetic field as the sum of the fields established independently by the d.c. field current,  $I_f$ , and the armature currents,  $I$ . Then, the per-phase voltage equation for the armature of a nonsalient-pole synchronous machine may be written as

$$\dot{E}_f + \dot{E}_\sigma + \dot{E}_a = \dot{V} + R\dot{I} \quad (55-1)$$

where  $\dot{E}_f$  = field emf induced by the mutual field due to the field mmf,  $F_{fm}$

$\dot{E}_a$  = armature mutual emf induced by the mutual field due to the armature set of currents,  $\dot{I}$

$\dot{E}_\sigma$  = leakage emf induced by the leakage field set up by the armature currents,  $\dot{I}$

$\dot{V}$  = phase voltage at the armature terminals

$R$  = per-phase resistance of the armature

The value of  $E_f$  is found from the linearized no-load curve,  $E_f = f(F_\delta)$ . The value of  $E_a$  (Fig. 55-1) is proportional to the armature current,  $I$ . It can be found in one of two ways.

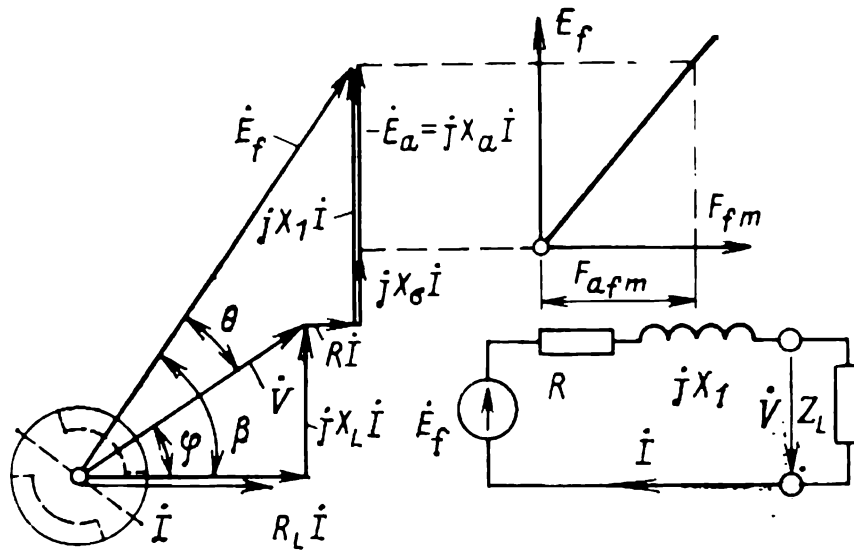


Fig. 55-1 Voltage phasor diagram and equivalent circuit of a non-salient-pole synchronous machine (neglecting saturation)

1. Using Eq. (54-1), find the armature mmf,  $F_{am}$ . Referring to Fig. 53-2, determine the armature reaction factor,  $k_a = 1/k_f = f(\rho)$ . Replace  $F_{am}$  by an equivalent field mmf,  $F_{afm} = k_a F_{am}$ . Recalling that for a uniform air gap the magnetization characteristic is independent of the direction of mmf, find  $E_a$  as an emf corresponding to  $F_{afm}$  on the linearized  $E_f = f(F_\delta)$  curve in Fig. 55-1.

2. Express  $\dot{E}_a$  in terms of the mutual inductive reactance of the armature:

$$\dot{E}_a = -jX_a \dot{I}$$

The leakage emf may be expressed in terms of the leakage inductive reactance of the armature from Eq. (54-22)

$$\dot{E}_\sigma = -jX_\sigma \dot{I}$$

Now the armature voltage equation may be re-written as

$$\dot{E}_f = \dot{V} + R\dot{I} + jX_1 \dot{I} \quad (55-2)$$

where  $X_1 = X_\sigma + X_a$  is the total inductive reactance of the armature.

Graphically, Eqs. (55-1) and (55-2) can be represented by a voltage phasor diagram. In Fig. 55-1, the voltage phasor diagram is constructed for a machine operating as a generator supplying an isolated resistive-inductive load,  $Z_L = R_L + jX_L$ . In the circumstances,  $\dot{V}$  can be expressed as

$$\dot{V} = \dot{V}_a + \dot{V}_r \quad (55-3)$$

where  $\dot{V}_a = R_L \dot{I}$  and  $\dot{V}_r = jX_L \dot{I}$  are the active and reactive components of the voltage, respectively.

In an arbitrary mode of operation, the phase of  $V$  is decided by the phase angle  $\varphi$  between  $V$  and  $I$ . If  $V$  is leading  $I$ , the angle  $\varphi$  is taken to be positive.

When the active current component,  $I_a = I \cos \varphi$  is in phase with the voltage,  $I_a = I \cos \varphi > 0$ , the machine is operating as a generator and delivers active power to the load,

$$P = m_1 VI \cos \varphi > 0$$

When  $I_a = I \cos \varphi < 0$ , it is operating as a motor and draws active power from the supply line

$$P = m_1 VI \cos \varphi < 0$$

The reactive power generated by the machine is taken to be positive

$$Q = m_1 VI \sin \varphi > 0$$

when the reactive current component,  $I_r = I \sin \varphi > 0$ , lags behind  $V$  by 90 electrical degrees (it is said to be in electrical quadrature lagging). This will happen if the load is inductive,  $X_L > 0$ , and  $0 < \varphi \leq \pi/2$ , as in Fig. 55-1.

The reactive power generated by a synchronous machine is taken to be negative

$$Q = m_1 VI \sin \varphi < 0$$

when the reactive current component,  $I_r = I \sin \varphi < 0$ , leads  $V$  by 90 electrical degrees (it is said to be in electrical quadrature leading). This will happen if the load is capacitive,  $X_L = -X_C < 0$  and  $-\pi/2 \leq \varphi < 0$ , as in Fig. 55-1.

When a synchronous machine is operating as a motor, positive reactive power is generated at  $\pi > \varphi \geq \pi/2$ , and negative reactive power, at  $-\pi/2 \geq \varphi > -\pi$ .

Formally, Eq. (55-3) may be extended to the motor mode of operation as well. Let us write the resistive and inductive components of the load in terms of its impedance:

$$\left. \begin{aligned} R_L &= Z_L \cos \varphi = (V/I) \cos \varphi \\ X_L &= Z_L \sin \varphi = (V/I) \sin \varphi \end{aligned} \right\} \quad (55-4)$$

its voltage in terms of the active and reactive components:

$$\dot{V} = \dot{V}_a + \dot{V}_r \quad (55-5)$$

where

$$\begin{aligned} V_a &= R_L I = V \cos \varphi \\ V_r &= X_L I = V \sin \varphi \end{aligned}$$

and its active and reactive powers in terms of the load resistance and reactance:

$$\left. \begin{aligned} P &= m_1 I (V \cos \varphi) = m_1 R_L I^2 \\ Q &= m_1 I (V \sin \varphi) = m_1 X_L I^2 \end{aligned} \right\} \quad (55-6)$$

It is seen from Eq. (55-6) that  $P$  is positive and the machine is operating as a generator at  $R_L > 0$ . In contrast,  $P$  is negative and the machine is operating as a motor at  $R_L < 0$ , when it is loaded into a fictitious negative resistance,  $R_L$ . Physically, this means that the machine is not delivering any active power to the load; rather, the load is supplying active power to the machine at  $V$ .

From the same equations it also follows that in both the generator and the motor mode of operation,  $Q$  is positive at  $X_L > 0$  and negative at  $X_L < 0$ . Therefore, whatever the mode of operation defined by  $V$ ,  $I$  and the phase angle  $\varphi$  between them,  $\dot{V}$  can be expressed as the sum of  $\dot{V}_a$  and  $\dot{V}_r$  in accord with Eq. (55-3) or in terms of  $R_L$  and  $X_L$ , as given by Eqs. (55-4) and (55-5).

The mode in which a machine is running is characterized by four defining quantities, namely the armature voltage  $V$ , the armature current  $I$ , the phase angle  $\varphi$  between them, and the d.c. field current  $I_f$ . Instead of  $V$  and  $\varphi$ , we may take  $R_L$  and  $X_L$ , in which case the mode of operation will be characterized by another set of four defining quantities, namely  $R_L$ ,  $X_L$ ,  $I$ , and  $I_f$ .

A particular mode of operation can be specified by giving any three of the four defining quantities. The fourth can then be found either graphically (from a voltage pha-

sor diagram), or analytically, using Eq. (55-2) to which Eq. (55-3) should be added, if and where necessary. Most naturally, a particular mode of operation can be specified by giving (1)  $V$ ,  $I$ , and  $\varphi$ , or  $R_L$ ,  $X_L$ , and  $I$ , in which case  $I_f$  needs to be found. Alternative sets of defining quantities are (2)  $V$ ,  $\varphi$ , and  $I_f$ ; (3)  $\varphi$ ,  $I$  and  $I_f$ ; and (4)  $V$ ,  $I$ , and  $I_f$ .

In an unsaturated machine, the d.c. field current  $I_f$  is replaced in the design equation by  $E_f$  as found from the linearized no-load curve. The unknown  $E_f$  (for the 1st set of defining quantities) can be found from Eq. (55-2) written in terms of the projections of the complex quantities on the current direction and on a direction at right angles to it:

$$E_f = \sqrt{(V \cos \varphi + RI)^2 + (V \sin \varphi + X_1 I)^2} \quad (55-7)$$

or, subject to Eq. (55-5),

$$E_f = I \sqrt{(R + R_L)^2 + (X_1 + X_L)^2} \quad (55-8)$$

where  $I = V/Z_L$ .

Solving Eq. (55-7) for  $I$ ,  $V$ , or  $\varphi$  will give the unknown  $I$  (if the 2nd set of defining quantities is used):

$$I = [-2V(X_1 \sin \varphi + R \cos \varphi) \pm \sqrt{4V^2(X_1 \sin \varphi + R \cos \varphi)^2 + 4(X_1^2 + R^2)(E_f^2 - V^2)}] / 2(X_1^2 + R^2) \quad (55-9)$$

or the unknown  $V$  (if the 3rd set of defining quantities is used):

$$V = -I(X_1 \sin \varphi + R \cos \varphi) \pm \sqrt{I^2(X_1 \sin \varphi + R \cos \varphi)^2 + E_f^2 - (X_1^2 + R^2)I^2} \quad (55-10)$$

or the unknown  $\varphi$  (if the 4th set of defining quantities is used):

$$\varphi = \arcsin(X_1/Z_1) \pm \arccos \frac{E_f^2 - V^2 - (X_1^2 + R^2)I^2}{2VIZ_1} \quad (55-11)$$

## 55-2 Electromagnetic Processes in a Salient-Pole Synchronous Machine (Neglecting Saturation)

Neglecting saturation, a salient-pole synchronous machine may likewise be treated as having a linear magnetic circuit. Now, however, it is convenient to represent the mutual field established by the armature current as a sum

of two independent fields, one set up by  $I_d$  and the other by  $I_q$ . Then the mutual emf may be written

$$\dot{E}_a = \dot{E}_{ad} + \dot{E}_{aq} \quad (55-12)$$

Accordingly, the armature emf will be

$$\dot{E}_f + \dot{E}_\sigma + \dot{E}_{ad} + \dot{E}_{aq} = \dot{V} + R\dot{I} \quad (55-13)$$

As in an unsaturated nonsalient-pole machine,  $E_f$  in the above equation (see Fig. 55-2) can be found from the linearized no-load characteristic,  $E_f = f(F_\delta)$ . The armature leakage emf is, in accord with Eq. (54-22), given by  $\dot{E}_\sigma = -jX_\sigma \dot{I}$ . The mutual emfs of the armature,  $E_{ad}$  and

$E_{aq}$ , respectively proportional to  $I_d$  and  $I_q$ , can be found in one of two ways, as follows.

(1) Using  $I_d = I \sin \beta$  and  $I_q = I \cos \beta$ , found earlier (see Sec. 54-1), determine  $F_{adm}$  and  $F_{qgm}$  from Eq. (54-3). Referring to Fig. 53-3 and Fig. 54-4, find the excitation field form factor,  $k_f$ , and the armature field form factors,  $k_d$  and  $k_q$ . (In an unsaturated machine, the design air gap, or the axial gap length, is  $\delta' = k_\delta \delta$ .) Calculate the armature reaction factors,  $k_{ad} = k_d/k_f$  and  $k_{aq} = k_q/k_f$ , and replace (see Sec. 54-3) the direct- and quadrature-axis mmfs,

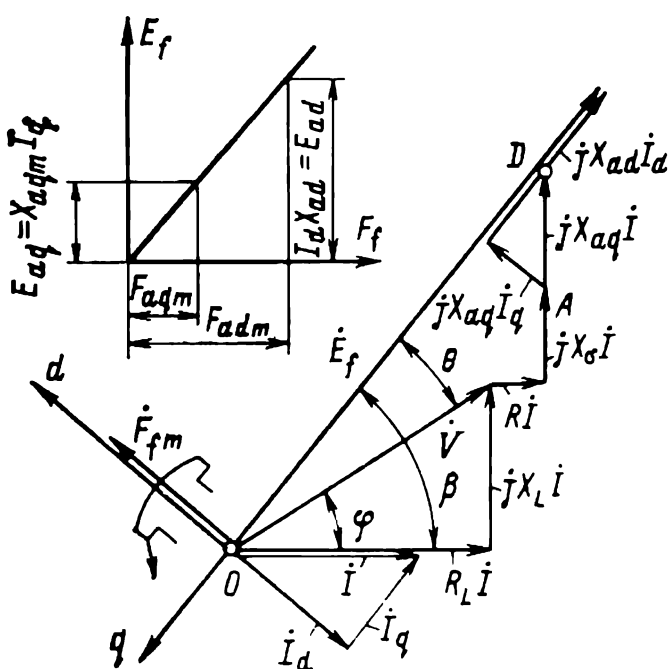


Fig. 55-2 Voltage phasor diagram of a salient-pole synchronous machine in the generator mode of operation (neglecting saturation)

$F_{adm}$  and  $F_{qgm}$ , by equivalent field mmfs,  $F_{adm} = k_{ad}F_{adm}$  and  $F_{aqm} = k_{aq}F_{qgm}$ . Determine  $E_{ad}$  and  $E_{aq}$  as the emfs corresponding to  $F_{adm}$  and  $F_{aqm}$  from the linearized no-load characteristic,  $E_f = f(F_\delta)$  in Figs. 54-5 and 55-2. This method can be used, if we know  $\delta$ ,  $\delta_m$ , and  $k_\delta$  (to a first approximation, it may be taken that  $\delta_m/\delta' = 1.5$ ), and the winding data of the machine.

(2) Express  $E_{ad}$  and  $E_{aq}$  in terms of the mutual inductive reactances  $X_{ad}$  and  $X_{aq}$  (see Sec. 54-5):

$$\dot{E}_{ad} = -jX_{ad}\dot{I}_d$$

$$\dot{E}_{aq} = -jX_{aq}\dot{I}_q$$

This method is more convenient, because one only needs to know the parameters of the armature winding.<sup>¶</sup>

On expressing  $E_\sigma$ ,  $E_{ad}$  and  $E_{aq}$  in Eq. (55-13) in terms of the respective inductive reactances and currents, the armature voltage equation may be re-written as

$$\dot{E}_f = \dot{V} + R\dot{I} + jX_\sigma\dot{I} + jX_{aq}\dot{I}_q + jX_{ad}\dot{I}_d \quad (55-14)$$

or

$$\dot{E}_f = \dot{V} + R\dot{I} + jX_q\dot{I}_q + jX_d\dot{I}_d$$

where  $X_d = X_\sigma + X_{ad}$  and  $X_q = X_\sigma + X_{aq}$  are the total  $d$ - and  $q$ -axis inductive reactances, respectively.

A voltage phasor diagram for a salient-pole synchronous machine answering the above equation is shown in Fig. 55-2. It has been plotted for a machine in the generator mode of operation, supplying an isolated resistive-inductive load for which  $V \sin \varphi > 0$  and  $V \cos \varphi > 0$ . The simplest approach is to construct a phasor diagram from which to find  $E_f$  (or  $I_f$ ). When the operating conditions are specified by giving  $V$ ,  $I$  and  $\varphi$ , its construction poses no difficulty. As is seen from Fig. 55-2, the angle  $\beta$  that defines the direction of  $E_f$  (or the negative direction of the  $q$ -axis) may be found graphically before the  $\dot{E}_f$  itself is found. To this end, it will suffice to locate the point  $D$  which is the tip of the phasor

$$OD = \dot{V} + R\dot{I} + jX_\sigma\dot{I} + jX_{aq}\dot{I} = \dot{V} + R\dot{I} + jX_q\dot{I}$$

and draw the  $q$ -axis in the direction opposite to the phasor. The  $d$ -axis must lag behind the  $q$ -axis by  $90^\circ$ . The phasor diagram can be constructed for any mode of operation of a synchronous machine, as specified by giving  $V$ ,  $I$ , and  $\varphi$ . (See the explanation for the equations of a nonsalient-pole machine.)

As has already been explained, the operating mode of a synchronous machine may alternatively be specified by giving any one of three more sets of defining quantities.



In such cases, however, the fourth (unknown) quantity is difficult to find graphically, so it should preferably be found analytically, using Eq. (55-14). Prior to that, it is necessary to set up equations leading to the angle  $\beta$  or its basic trigonometric functions by reference to Fig. 55-2. Projecting the phasor  $OD$  on the direction of the current  $I$  and on a direction at right angles to it and referring the projections thus obtained to its magnitude, we get

$$\begin{aligned}\cos \beta &= \frac{V \cos \varphi + RI}{\sqrt{(V \sin \varphi + X_q I)^2 + (V \cos \varphi + RI)^2}} \\ &= \frac{R_L + R}{\sqrt{(X_L + X_q)^2 + (R_L + R)^2}} \\ \sin \beta &= \frac{V \sin \varphi + X_q I}{\sqrt{(V \sin \varphi + X_q I)^2 + (V \cos \varphi + RI)^2}} \\ &= \frac{X_L + X_q}{\sqrt{(X_L + X_q)^2 + (R_L + R)^2}}\end{aligned}\quad (55-15)$$

On finding the trigonometric functions of  $\beta$  from Eq. (55-15) for the operating mode specified in terms of  $V$ ,  $I$  and  $\varphi$  or in terms of  $X_L$  and  $R_L$ , we can determine  $E_f$ . As is seen from Fig. 55-2, it is

$$E_f = V \cos \theta + X_d I_d + R I_q \quad (55-16)$$

where  $\theta = \beta - \varphi$ ,  $\cos \theta = \cos \beta \cos \varphi + \sin \beta \sin \varphi$ .

On substituting for  $\sin \beta$  and  $\cos \beta$  from Eq. (55-15), we get

$$E_f = \frac{V^2 + IV(X_d + X_q) \sin \varphi + 2VIR \cos \varphi + I^2(R^2 + X_d X_q)}{\sqrt{V^2 + 2VI(X_q \sin \varphi + R \cos \varphi) + I^2(R^2 + X_q^2)}} \quad (55-17)$$

$$E_f = I \frac{Z_L^2 + X_L(X_d + X_q) + 2RR_L + X_d X_q + R^2}{\sqrt{Z_L^2 + 2(X_L X_q + R_L R) + X_q^2 + R^2}} \quad (55-18)$$

where  $Z_L = \sqrt{R_L^2 + X_L^2}$  is the load impedance, and  $I = V/Z_L$ .

The same result might be obtained, if we used the equivalent circuit of a synchronous machine or the phasor diagram in Fig. 54-1 which are applicable to both nonsalient-pole and salient-pole machines. By inspection of the equivalent circuit,

$$E_f = I \sqrt{(R_L + R_1)^2 + (X_L + X_1)^2} \quad (55-19)$$

where  $R_1$  = resistance of the armature

$X_1$  = inductive reactance of the armature as defined by Eq. (54-38)

On re-arranging, Eq. (55-19) reduces to the same form as Eq. (55-18). Depending on the manner in which the operating mode of a machine is specified, the unknown quantity may be found from Eq. (55-17) or from Eq. (55-18). If the operating mode is specified in terms of  $V$ ,  $I$  and  $\phi$ , the unknown  $I_f$  (or  $E_f$ ) can conveniently be found from Eq. (55-17). If the operating mode is specified in terms of  $Z_L$ ,  $I$ , and  $\phi$ , then  $V = Z_L I$ , and  $I_f$  can be found from Eq. (55-18). If, on the other hand, the defining quantities are  $Z_L$ ,  $V$ , and  $\phi$ , then  $I = V/Z_L$ , and  $I_f$  can be found from Eq. (55-18). Finally, if the operating mode is specified in terms of  $Z_L$ ,  $I_f$ , and  $\phi$ , then  $E_f$  can be found from the linearized no-load characteristic,  $I$  can be found from Eq. (55-19), and  $V = Z_L I$ .

### 55-3 Electromagnetic Processes in a Nonsalient-Pole Synchronous Machine (with Saturation)

As has been shown in calculating the magnetic circuit at no load (see Sec. 53-3), the magnetization characteristics of a saturated machine plotted for the mutual field are nonlinear. Because of this, we cannot investigate the mutual field due to  $F_f$  independently of the mutual field due to  $F_a$ , and then superimpose the two fields so as to obtain the resultant field.

Instead, we have to consider the resultant field with the flux  $\Phi_{rm} = \Phi_m$ , set up by  $F_{fm}$  and  $F_{am}$  jointly. Prior to that,  $F_{am}$  must be replaced by an equivalent field mmf,  $F_{afm}$ . If we know the mutual inductive reactance of the armature,  $X_a = X_1 - X_\sigma$ , found neglecting saturation, then  $E_{afm}$  can be found from  $E_a = X_a I$  by reference to the linearized no-load characteristic (see Figs. 55-1 and 54-5).

Recalling that  $\dot{F}_{fm}$  acts along the  $d$ -axis of the poles, and  $\dot{F}_{afm}$  is in line with  $\dot{I}$  (see Fig. 55-3), the resultant mmf,  $\dot{F}_{rm}$ , can be written in complex notation as:

$$\dot{F}_{rm} = \dot{F}_{fm} + \dot{F}_{afm} \quad (55-20)$$

It should be remarked in passing that equivalent trapezoidal mmfs are combined in the same manner as the fundamental mmfs.

Because  $F_r$  has the same waveshape as the field mmf, it sets up nearly the same mutual field and gives rise to nearly

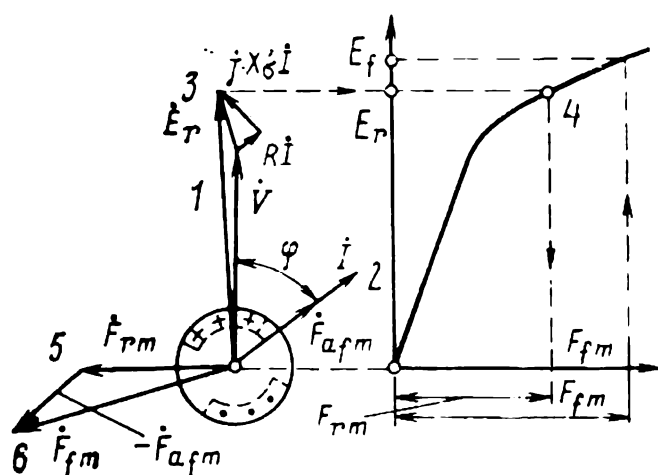


Fig. 55-3 Voltage and mmf phasor diagram of a nonsalient-pole synchronous machine (with allowance for saturation)

the same mutual emf as the no-load field emf equal to it. Owing to this, we are in a position to determine the resultant mutual flux  $\Phi_{rm}$  and the resultant mutual emf  $E_r$  from the basic magnetization curve,  $\Phi_m = f(F_{fm})$  and from the no-load characteristic,  $E_f = f(F_{fm})$ , on deeming  $F_f = F_r$ ,  $\Phi_{rm} = \Phi_m$ , and  $E_r = E_f$  (see Sec. 53-3).

To make the description of electromagnetic processes in a nonsalient-pole machine more complete, we should add to the mmf equation (55-20) and the no-load characteristic  $E_f = f(F_{fm})$  also the armature voltage equation

$$\dot{E}_r + \dot{E}_\sigma = \dot{V} + R\dot{I} \quad (55-21)$$

or

$$\dot{E}_r = \dot{V} + R\dot{I} + jX_\sigma\dot{I}$$

The voltage equation is written on a fairly plausible assumption that the mutual field and the leakage field of the armature do not affect each other and exist independently.

**(1) Finding the field current neglecting variations in the leakage flux of the field winding on load.** This approach can be used to determine  $I_f$  in operation on load, as specified by giving the armature voltage  $V$ , the armature current  $I$ , and their phase difference  $\phi$ . Figure 55-3 illustrates how  $I_f$  can be found graphically, using a phasor diagram plotted in accord with Eqs. (55-20) and (55-21), and from the no-load curve in Fig. 53-11. The construction can be carried out in absolute or per-unit terms. For the no-load curve to be plotted on a per unit basis, we need to know  $I_{fm,oc}$   $F_{fm,oc}$  at rated voltage. The steps involved in determin-

ing  $I_{fm}$  for the generator mode of operation specified in terms of  $V$ ,  $I$  and  $\varphi$  and for a resistive-inductive load are illustrated in Fig. 55-3, where they are numbered from 1 through 6. On load, however, the no-load characteristic and Eqs. (55-20) and (55-21) fail to give an accurate value of the field current, because the effect of  $\Phi_{f\sigma}$  on  $\Phi_2$  and  $F_2$ , the rotor flux and mmf, respectively, is not taken into account properly. The point is that at no load the mutual flux  $\Phi_m = \Phi_{fm}$  and the leakage flux  $\Phi_{f\sigma}$  are functions of  $F_{fm}$ . On load,  $\Phi_{rm}$  depends on the resultant mmf,  $\dot{F}_{rm} = \dot{F}_{fm} + \dot{F}_{am}$ , whereas the leakage flux is solely decided by  $F_{fm}$ , as at no load. Therefore, when we use the no-load curve to determine  $E_r$  from  $F_{rm}$  on load, we base our calculations on the leakage flux  $\Phi_{f\sigma}$  corresponding to the resultant mmf,  $F_{rm}$ , whereas actually the leakage flux on load corresponds to  $F_{fm}$  substantially different from  $F_{rm}$ .

In the generator mode of operation into a resistive-inductive load, the above approach leads to an underestimated leakage flux and to an underestimated field mmf,  $F_{fm}$ . As a way out, it has been proposed to replace the leakage inductive reactance  $X_\sigma$  by a fictitious quantity  $X_P$  known as the *Potier reactance* (after the investigator who has proposed it), which is somewhat larger than  $X_\sigma$ . The value of  $I_f$  can be obtained still more accurately, if we properly account for the effect of the field leakage flux on load, as this is done in the paragraph that follows.

**(2) Finding the field current with allowance for variations in the leakage flux of the field winding on load.** This involves the use of the magnetization characteristics

$$\begin{aligned}\Phi_m &= f(F_1), \quad \Phi_{f\sigma} = f(F_1), \\ \Phi_2 &= f(F_2)\end{aligned}$$

found in calculating the magnetic circuit (see Sec. 53-3). If they are not available for the machine in question, it may be assumed that on a per-unit basis they are the same the normalized magnetization characteristics of a non-salient pole machine, shown in Fig. 53-11. In Fig. 55-4, they are drawn to a more convenient scale. The “per-unit” subscript, (\*), has been dropped. To present the characteristics in absolute units (which is necessary sometimes),

we need to know  $V_R$ ,  $\Phi_{fm,oc}$  and  $F_{fm,oc}$  (or  $I_{fm,oc}$ ). Then,

$$E = E_* V_R$$

$$\Phi = \Phi_* \Phi_{fm,oc}$$

$$F = F_* F_{fm,oc}$$

$$I_f = F_* I_{fm,oc}$$

Now,  $I_f$  (or  $F_{fm}$ ) in the on-load condition, specified in terms of  $V$ ,  $I$  and  $\phi$ , can be determined as illustrated in

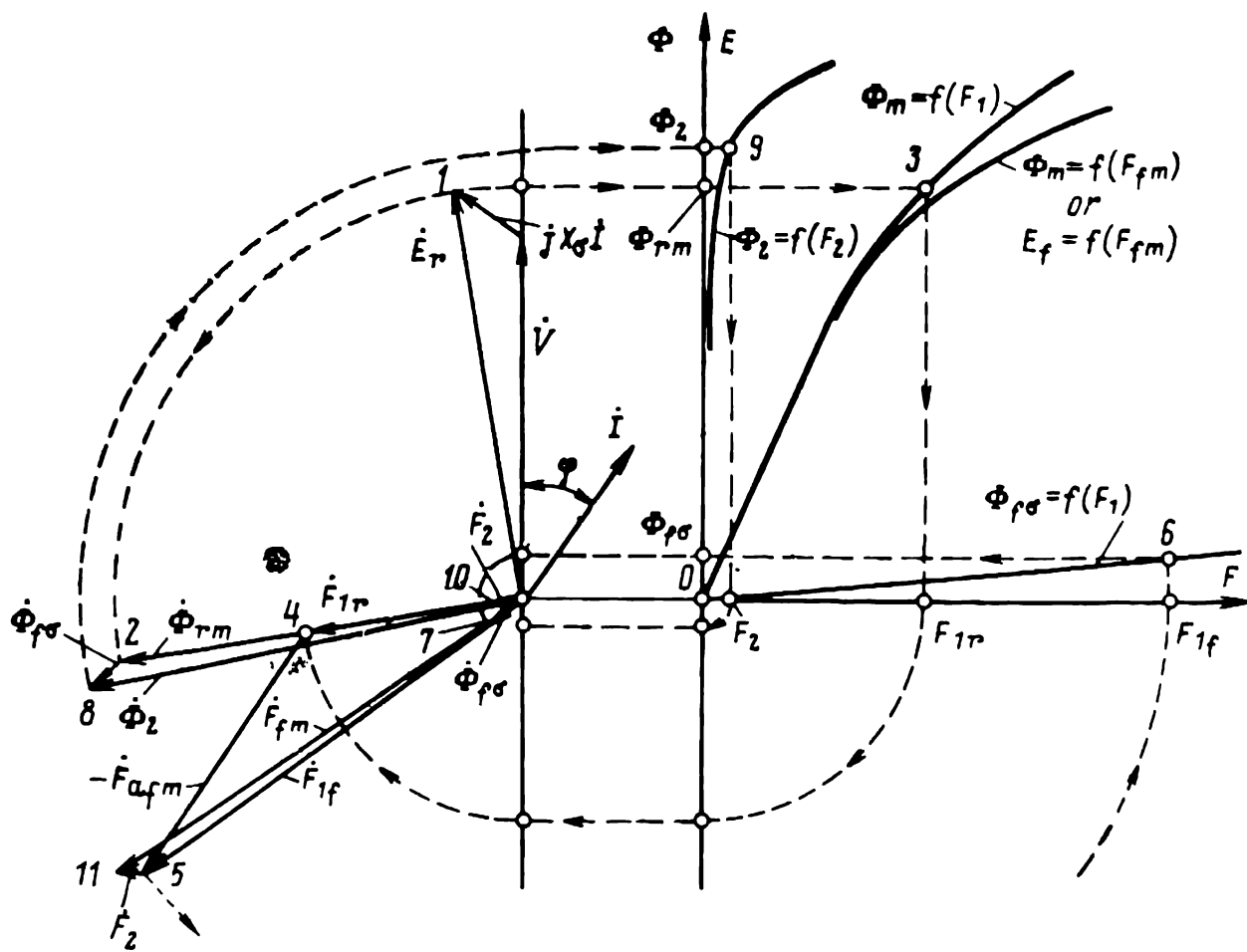


**Fig. 55-4** Voltage phasor diagram of a nonsalient-pole synchronous machine (with allowance for saturation and variations in the leakage flux)

Fig. 55-4. The steps involved are numbered from 1 through 11. The first step is to draw a phasor diagram of the voltages defined by Eqs. (55-21) and to determine the resultant mutual emf,  $\dot{E}_r$  (1), and the resultant mutual flux,  $\Phi_{rm}$ , equal to it when drawn on a per-unit basis, (2). The next step (3) is to determine the resultant mmf,  $F_{1r}$ , corresponding to the stator and air-gap mmf, at  $\Phi_m = \Phi_{rm}$ , by reference to the magnetization curve,  $\Phi_m = f(F_1)$ , where  $F_1$  is taken as the stator and air-gap mmf. In doing so, we still neglect the effect of the rotor mmf,  $F_2$ , and the value

of  $F_{1r}$  thus found differs from  $F_{rm}$  by the value of  $F_2$ :

$$\dot{F}_{1r} = \dot{F}_{rm} - \dot{F}_2 \quad (55-22)$$

The phasor  $\dot{F}_{1r}$  (4) is in phase with  $\dot{\Phi}_{rm}$ . Now we find  $\dot{F}_{1f}$  (5) neglecting  $\dot{F}_2$ . It differs from the total excitation mmf by  $\dot{F}_2$ :

$$\dot{F}_{1f} = \dot{F}_{fm} - \dot{F}_2 \quad (55-23)$$

On subtracting  $F_2$  from the right- and left-hand sides of Eq. (55-20),

$$\dot{F}_{rm} - \dot{F}_2 = \dot{F}_f - \dot{F}_2 + \dot{F}_{afm}$$

we may write

$$\dot{F}_{1r} = \dot{F}_{1f} + \dot{F}_{afm} \quad (55-24)$$

Hence,

$$\dot{F}_{1f} = \dot{F}_{1r} - \dot{F}_{afm}$$

Using the  $\Phi_{f\sigma} = f(F_1)$  curve and recalling that  $\dot{F}_1 = \dot{F}_{fm} - \dot{F}_2$ , we may write the on-load leakage flux,  $\dot{\Phi}_{f\sigma}$  (step 6), as a flux corresponding to  $\dot{F}_{1f} = \dot{F}_{fm} - \dot{F}_2$ .

In the phasor diagram,  $\dot{\Phi}_{f\sigma}$  (step 7) is in line with  $\dot{F}_{1f}$  which produces it. Combining  $\dot{\Phi}_{rm}$  and  $\dot{\Phi}_{f\sigma}$  gives the total rotor flux

$$\dot{\Phi}_2 = \dot{\Phi}_{rm} + \dot{\Phi}_{f\sigma} \text{ (step 8)} \quad (55-25)$$

Next, using the rotor magnetization curve,  $\Phi_2 = f(F_2)$ , we find (step 9) the rotor mmf,  $F_2$ , which is in the same direction as  $\Phi_2$  (step 10). Finally, using Eq. (55-23), we obtain the total field mmf (step 11):

$$\dot{F}_{fm} = \dot{F}_{1f} + \dot{F}_2$$

and, if necessary, also the resultant mmf from Eq. (55-22):

$$\dot{F}_{rm} = \dot{F}_{1r} + \dot{F}_2$$

With a resistive-inductive load and the generator mode of operation, the field mmf thus found is somewhat greater than

the field mmf found from the no-load curve (see Fig. 55-3); if the resistive-inductive load is sufficiently large, it may be somewhat smaller than that mmf.

In Figs. 55-3 and 55-4,  $I_f$  (or  $E_f$ ) is found for the generator mode of operation and a resistive-inductive load. A similar procedure may be used to determine  $I_f$  in any other operating mode specified in terms of the first set of defining quantities ( $V$ ,  $I$  and  $\varphi$ ). If the mode of operation is specified in terms of any other set of three defining quantities, namely: (2)  $V$ ,  $\varphi$ ,  $I_f$  (3)  $\varphi$ ,  $I$ ,  $I_f$  and (4)  $V$ ,  $I$ ,  $I_f$ , the fourth unknown quantity will have to be found in a more complicated manner.

Taking the second set as an example, several values of  $I$  are taken arbitrarily, and for each (with  $V$  and  $\varphi$  fixed in advance) the d.c. field current,  $I_f$ , is found. Then an  $I_f = f(I)$  curve is plotted, and the value of  $I$  corresponding to the assumed value of  $I_f$  found from that curve. With the third set of defining quantities, several values of  $V$  are taken arbitrarily, and with the fourth set, several values of  $\varphi$ . The remainder of the procedure is the same as has been just explained.

#### **55-4 Electromagnetic Processes in a Salient-Pole Synchronous Machine with Allowance for Saturation**

**(1) The effect of the armature mmf on the mutual field and emf.** In a saturated, salient-pole machine, the fields set up by different mmfs cannot be treated independently of one another.

The effect of the armature field on the excitation field can be accounted for as proposed by Richter. According to him, the actual sinusoidally distributed direct- and quadrature-axis mmfs,  $F_{dm}$  and  $F_{qm}$ , which have a certain definite effect on the fundamental mutual field and the associated mmf, are replaced by equivalent field mmfs,  $F_{adm}$ ,  $F_{aqm}$ , and  $F_{qdm}$ , found with allowance for saturation.

The equivalent field mmfs are found as follows.

Assuming several values of load, differing in the values of  $F_{fm}$ ,  $F_{dm}$  and  $F_{qm}$ , the air-gap field is found with allowance for iron (teeth and stator yoke) saturation. The rotor mmf is assumed to be zero,  $F_2 = 0$ . The results are

presented as three air-gap flux density distribution curves shown in Fig. 55-5. One curve represents the distribution of  $B_I$  due to  $F_{fm}$ , the second curve represents the distribution of  $B_{II}$  due to the joint action of  $F_{fm}$  and  $F_{dm}$ , and the third curve gives the distribution of  $B_{III}$  due to the joint action of  $F_{fm}$ ,  $F_{dm}$ , and  $F_{qm}$ .

From each curve, the  $d$ - and  $q$ -axis fundamental components of flux density are then found. The fundamental component of  $B_I$  due to  $F_{fm}$  is along the  $d$ -axis and its peak value is  $B_{IIIdm}$ ; in the armature winding it induces  $E_{IIId} = E_f$ . The fundamental component of  $B_{II}$  due to  $F_{fm}$  and  $F_{dm}$  is likewise along the  $d$ -axis and has a peak value  $B_{IIIdm}$ ; in the armature winding it induces  $E_{IIId}$ . The fundamental component of  $B_{III}$  due to  $F_f$ ,  $F_d$  and  $F_q$  has a  $d$ -axis and a  $q$ -axis component, with a peak value  $B_{IIIdm}$  and  $B_{III1qm}$ , respectively; in the armature winding they induce  $E_{IIId} = E_{rd}$  and  $E_{III1q} = E_{rq} = E_{aq}$ . The former is the resultant mutual emf due to the  $d$ -axis field, and the latter is the resultant mutual emf due to the  $q$ -axis field. When combined, the two emfs give the resultant mutual emf

$$\dot{E}_r = \dot{E}_{rd} + \dot{E}_{rq} \quad (55-26)$$

The effect of the demagnetizing  $d$ -axis armature mmf,  $F_{dm}$ , on the excitation field consists in that the fundamental flux density and emf are somewhat reduced ( $B_{IIIdm} < B_{IIIdm}$ ,  $E_{IIId} < E_{IIId} = E_f$ ). By reference to a partial no-load characteristic  $E_f = f(F_1)$ , where  $F_1 = F_{fm} - F_2$ , the  $d$ -axis mmf,  $F_{dm}$ , may be replaced by a field mmf,  $F_{adm}$  (see Fig. 55-6), equivalent to it in terms of its effect on the fundamental emf.

The effect of  $F_{qm}$  can be assessed by comparing  $B_{II}$  and  $B_{III}$ . As is seen, in addition to setting up a  $q$ -axis

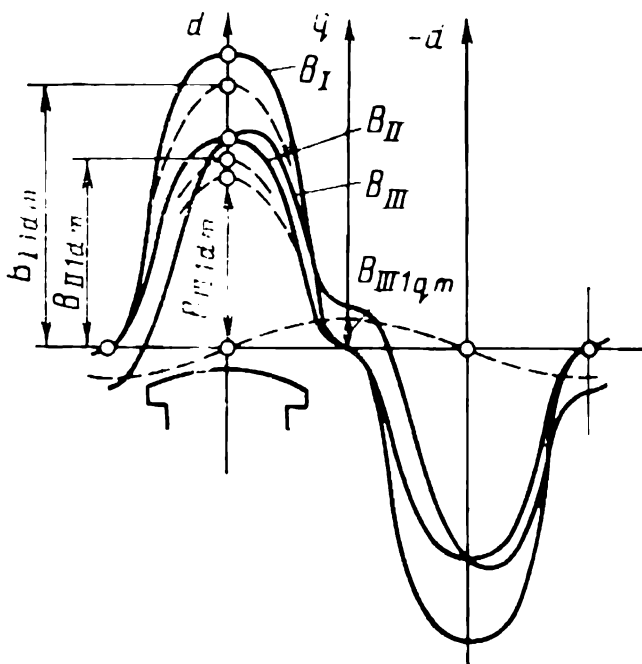


Fig. 55-5 Effect of the  $d$ - and  $q$ -axis armature mmfs,  $F_{dm}$  and  $F_{qm}$ , on the excitation field



field with a fundamental flux density  $B_{IIIIqm}$ , the  $q$ -axis mmf  $F_{qm}$  has a certain demagnetizing effect on the  $d$ -axis field ( $B_{IIII1dm} < B_{IIII1dm}$ ).

Using the partial no-load characteristic,  $E_f = f(F_1)$ , we may replace  $F_{qm}$  by  $F_{aqm}$  and  $F_{qdm}$  (see Fig. 55-6).  $F_{aqm}$

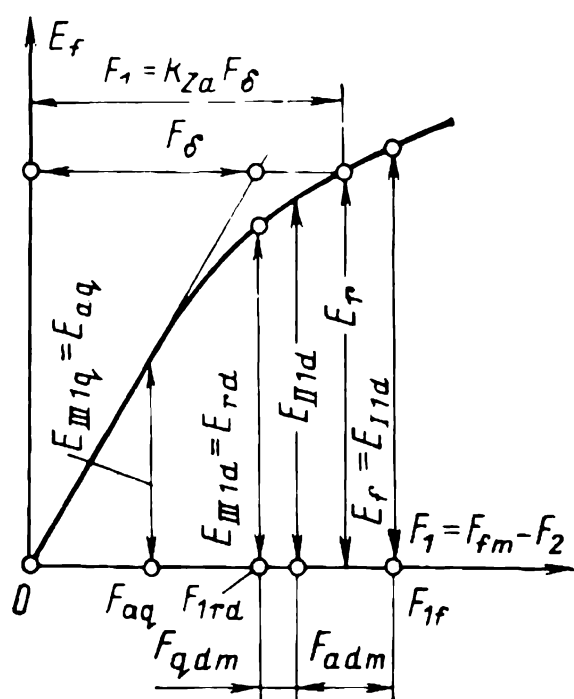


Fig. 55-6 Determination of  $F_{adm}$ ,  $F_{qdm}$ , and  $F_{aqm}$  equivalent to  $F_{dm}$  and  $F_{qm}$  in a saturated salient-pole machine

is equivalent to  $F_{qm}$  as regards the production of the  $q$ -axis field on load;  $F_{aqm}$  gives rise to the same emf,  $E_{II1q} = E_{aq}$ , as the  $q$ -axis field with a flux density  $B_{IIII1qm}$ .

$F_{qdm}$  is equivalent to  $F_{qm}$  in terms of its effect on the  $d$ -axis field—it brings down the peak value of the  $d$ -axis flux density from  $B_{IIII1dm}$  to  $B_{IIII1dm}$  and the corresponding emf from  $E_{II1d}$  to  $E_{IIII1d}$ , in the same way as  $F_{qm}$  does.

$F_{qm}$  has a demagnetizing effect on the  $d$ -axis field only in a saturated machine. This is because the increase in the flux density due to  $F_{qm}$ , appearing within that part

of the pole pitch where the  $d$ - and  $q$ -axis mmfs are combined due to saturation, is not completely balanced out by its decrease within that part of the pole pitch where the  $q$ -axis mmf is subtracted from the  $d$ -axis mmf (compare the  $B_{IIII}$  and  $B_{II}$  curves).

The above procedure can be repeated for a range of salient-pole machines differing in the air gap geometry (that is, in the value of the ratios  $\delta_m/\delta'$ , and  $\delta'/\tau$ ).

An analysis of such calculations will show that the equivalent mmfs  $F_{adm}$ ,  $F_{aqm}$  and  $F_{qdm}$  depend not only on  $F_{dm}$ ,  $F_{qm}$ , and the air gap shape, but also on the degree of saturation of the magnetic circuit by the resultant mutual field which corresponds to  $E_r$ . The field mmf  $F_{adm}$  equivalent in its effect to  $F_{dm}$  is found to be dependent not only on the  $d$ -axis mmf of the armature and the value of  $k_{ad}$ , as in a nonsalient-pole machine, Eq. (54-17), but also on the factor  $\xi_d$ :

$$F_{adm} = \xi_d k_{ad} F_{dm} \quad (55-27)$$

$F_{aqm}$ , equivalent to  $F_{qm}$  as regards the production of the  $q$ -axis field, is found to be dependent not only on the  $q$ -axis mmf of the armature and the value of  $k_{aq}$ , as in a non-salient-pole machine, Eq. (54-18), but also on the factor  $\xi_q$ :

$$F_{aqm} = \xi_q k_{aq} F_{qm} \quad (55-28)$$

$F_{qdm}$  equivalent to  $F_{qm}$  in terms of the demagnetizing effect on the  $d$ -axis field can be expressed in terms of  $\delta'/\tau$ ,  $k_{qd}$ , and  $F_{qm}$  itself:

$$F_{qdm} = k_{qd} (\tau/\delta') F_{qm} \quad (55-29)$$

The dimensionless factors  $\xi_d$ ,  $\xi_q$ , and  $k_{qd}$  in Eqs. (55-27) and (55-29) depend on the saturation factor  $k_{za} = F_1/F_\delta$  (see Sec. 53-1), characterizing the degree of saturation of the core by the resultant mutual flux  $\Phi_{rm}$ , and on the ration  $\delta_m/\delta' = \delta_m/\delta k_\delta$ , which characterizes the air gap shape with allowance for the effect of saliency (Fig. 55-7). The value of  $k_{za}$  can be found from the partial no-load characteristic,  $E_f = f(F_1)$ , as the ratio of  $F_1 = F_{fm} - F_2 = F_\delta + F_{z1} + F_{a1}$ , corresponding to the resultant mutual emf  $E_r$ , to the air gap mmf,  $F_\delta$  (see Fig. 55-6).

As is seen from Fig. 55-7, in an unsaturated machine (at  $k_{za} = 1$ ),  $\xi_d$  and  $\xi_q$  are equal to unity, whereas  $k_{qd} = 0$ .

In the circumstances, Eqs. (55-27) and (55-28) for the equivalent mmfs are the same as Eqs. (54-17) and (54-18) for the equivalent mmfs in an unsaturated machine.

Using  $\xi_d$  and  $\xi_q$ , we are in a position to find the saturated values of the  $d$ - and  $q$ -axis mutual inductive reactances of the armature

$$\begin{aligned} X_{ad,s} &= \xi_d X_{ad} \\ X_{aq,s} &= \xi_q X_{aq} \end{aligned} \quad (55-30)$$

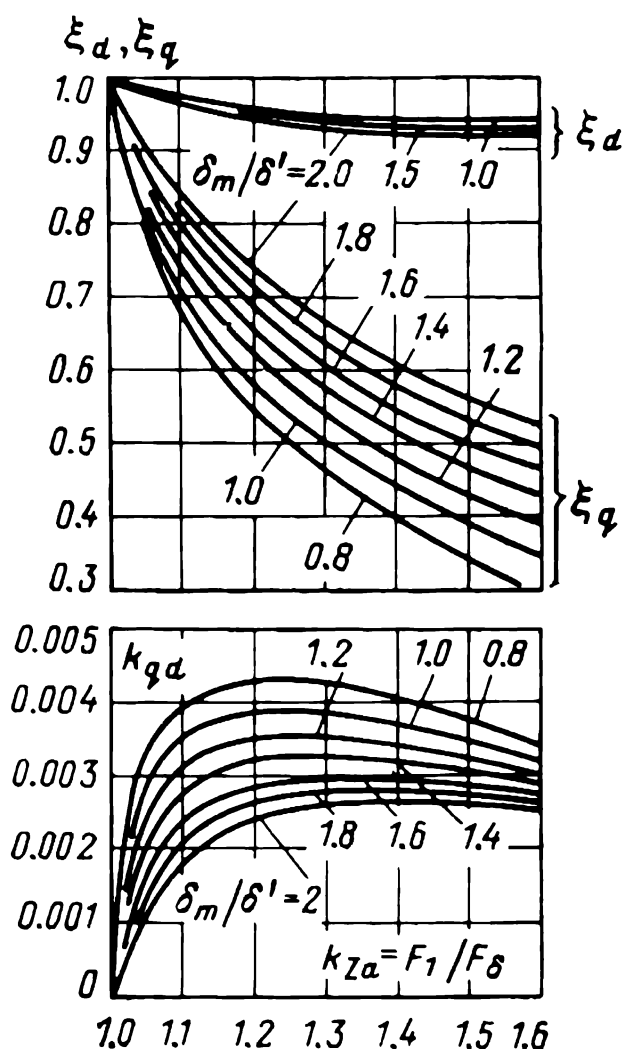


Fig. 55-7 Plots of  $\xi_d$ ,  $\xi_q$ , and  $k_{qd}$  as functions of  $k_{za}$ , and  $\delta_m/\delta'$



where  $X_{ad,s}$  and  $X_{aq,s}$  are the saturated inductive reactances, and  $X_{ad}$  and  $X_{aq}$  are their values obtained neglecting saturation.

Using  $X_{ad,s}$  and  $X_{aq,s}$ , we may write the respective mutual emfs

$$\dot{E}_{ad} = -jX_{ad,s}\dot{I}_d$$

and

$$\dot{E}_{aq} = -jX_{aq,s}\dot{I}_q$$

induced by  $\dot{I}_d$  and  $\dot{I}_q$  in a saturated machine. Using  $E_{ad}$  and  $E_{aq}$  and also the linearized no-load characteristic,  $E_f = f(F_\delta)$ , we can readily determine the equivalent mmf,  $F_{adm}$  and  $F_{aqm}$ , with allowance for saturation (Fig. 55-8 and 55-9). Now, we need not calculate  $F_{dm}$ ,  $F_{qm}$ ,  $k_{ad}$ , and  $k_{aq}$ .

If the magnetization characteristics and the radial gap length of a machine are not known, then the values of  $\xi_d$  and  $\xi_q$  can be found by reference to the normalized no-load and magnetization curves of a salient-pole machine in Fig. 53-8. Assuming also that the machine has the relative air-gap dimensions typical of salient-pole machines, namely  $\delta_m/\delta = 1.5$ ,  $\delta_m/\delta' = 1.4$ , and  $\delta'/\tau = 0.03$ , we can write  $\xi_d$  and  $\xi_q$  as functions of the resultant mutual emf,  $E_r$  (on a per-unit basis). The plots of  $\xi_d$  and  $\xi_q$  as functions of  $E_r$  shown in Fig. 55-10 have been constructed, using the plots of  $\xi_d$  and  $\xi_q$  as functions of  $k_{za}$  (see Fig. 55-7) and the normalized no-load characteristic (see Fig. 53-8) from which  $k_{za} = f(E_r)$  has been determined. Considering Eqs. (55-28) and (55-29) together,  $F_{qdm}$  can be expressed in terms of  $F_{aqm}$ :

$$F_{qdm} = \xi_{qd}F_{aqm} \quad (55-31)$$

where  $\xi_{qd} = k_{qd}\tau/k_{aq}\delta'\xi_q$  is a dimensionless factor. For a salient-pole machine having a normal no-load curve and typical air-gap dimensions,  $\xi_{qd}$  depends solely on  $E_r$ . A plot of this dependence is shown in Fig. 55-10.

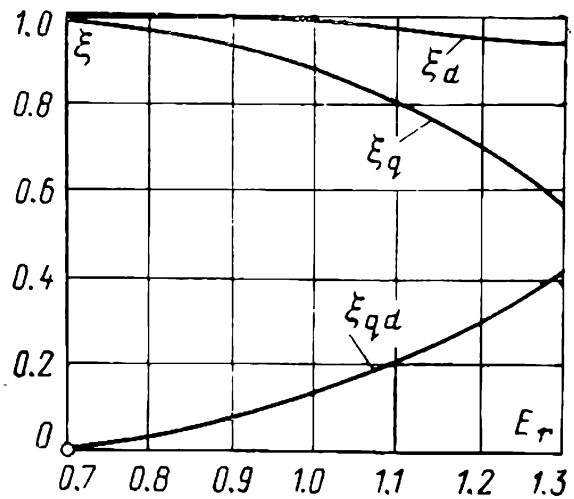


Fig. 55-10 Plots of  $\xi_d$ ,  $\xi_q$  and  $\xi_{qd}$  as functions of  $E_r$

**(2) Voltage and mmf equations.** Assuming that the armature leakage field is independent of the mutual field and neglecting the effect of saturation on the leakage inductive reactance,  $X_\sigma$ , we may write the armature voltage equation as

$$\dot{E}_r = \dot{V} + R\dot{I} + jX_\sigma\dot{I} \quad (55-32)$$

where

$\dot{E}_r = \dot{E}_{rd} + \dot{E}_{aq} =$  emf induced by the resultant mutual field

$\dot{E}_{rd} =$  emf induced by the resultant  $d$ -axis mutual field with  $\Phi_{rdm}$ . It corresponds to  $\dot{F}_{1rd} = \dot{F}_{rdm} - \dot{F}_2$  found neglecting the rotor mmf, from the partial no-load curve

$\dot{E}_{aq} = -jX_{aq,s}\dot{I}_q =$  emf induced by the resultant  $q$ -axis field set up by  $\dot{I}_q$

$X_{aq,s} =$  saturated value of the  $q$ -axis mutual inductive reactance of the armature, as defined in Eq. (55-30)

The resultant  $d$ -axis mmf,  $\dot{F}_{1rd}$ , corresponding to  $\dot{E}_{rd}$  and leading the latter by  $90^\circ$ , is the sum of all mmfs acting along the  $d$ -axis:

$$\dot{F}_{1rd} = \dot{F}_{1f} + \dot{F}_{adm} + \dot{F}_{qdm} \quad (55-33)$$

Equation (55-33), which is the  $d$ -axis mmf equation, contains the mmfs found neglecting the rotor mmf:

$\dot{F}_{1f}$ , which is always acting in the same direction as  $\dot{F}_{1rd}$

$\dot{F}_{adm}$ , which is in line with  $\dot{I}_d$ , and

$\dot{F}_{qdm}$ , which is always in electrical quadrature lagging with  $\dot{E}_{rd}$  and in opposition to  $\dot{F}_{1f}$ .

The on-load leakage flux,  $\Phi_{f\sigma}$ , corresponds to the field mmf,  $\dot{F}_{1f} = \dot{F}_{fm} - \dot{F}_2$ , on the  $\Phi_{f\sigma} = f(F_1)$  curve. The rotor mmf,  $F_2$ , is found with reference to the  $\Phi_2 = f(F_2)$  curve, from the flux at a rotor pole

$$\dot{\Phi}_2 = \dot{\Phi}_{rdm} + \dot{\Phi}_{f\sigma} \quad (55-34)$$

The total on-load field mmf is given by

$$\dot{F}_{fm} = \dot{F}_{1f} + \dot{F}_2 \quad (55-35)$$

where  $\dot{F}_{1f} = \dot{F}_{1rd} - \dot{F}_{adm} - \dot{F}_{aqm}$  in accord with Eq. (55-33).

**(3) Finding the on-load field current (with allowance for variations in the field leakage flux).** The field current  $I_f$  (or the excitation mmf  $F_f$ ) in the loaded mode of operation, specified by giving  $V$ ,  $I$  and  $\varphi$ , can be found graphically, as illustrated in Fig. 55-8. The steps involved are numbered from 1 through 17. The field mmf is found for a salient-pole machine with normal no-load curves,  $E_f = f(F_{fm})$  and  $E_f = f(F_1)$  and normal magnetization curves,  $\Phi_m = f(F_f)$ ,  $\Phi_m = f(F_1)$ ,  $\Phi_{f\sigma} = f(F_1)$  and  $\Phi_2 = f(F_2)$  plotted in Fig. 55-8 on a per-unit basis. The per-unit inductive reactances of the machine (neglecting saturation) are as follows:  $X_d = 1.0$ ,  $X_q = 0.627$ ,  $X_\sigma = 0.2$ ,  $X_{ad} = 0.8$ , and  $X_{aq} = 0.427$ . The armature winding resistance is neglected ( $R = 0$ ).

We shall consider the operation of the machine as a generator into a resistive-inductive load with  $V = 1.0$ ,  $I = 1.0$ , and  $\cos \varphi = 0.8$ .

The first step is to plot a voltage phasor diagram in accord with Eq. (55-32) and locate point 3 which represents the per-unit resultant mutual emf,  $E_r = 1.13$ . (The voltage and mmf diagrams should be plotted on scales adopted for performance characteristics.)

Using  $E_r$  thus found and referring to the curves in Fig. 55-10, the next step is to determine  $\xi_d = 0.967$ ,  $\xi_q = 0.77$  and  $\xi_{qd} = 0.23$ . Then using Eq. (55-30), calculate the mutual inductive reactances with allowance for saturation:

$$X_{ad,s} = \xi_d X_{ad} = 0.967 \times 0.8 = 0.772$$

$$X_{aq,s} = \xi_q X_{aq} = 0.77 \times 0.427 = 0.329$$

As for an unsaturated, salient-pole machine (see Fig. 55-2), plot the phasor  $\dot{E}_r + jX_{aq,s}\dot{I}$  whose tip locates point 4 and the negative direction of the  $q$ -axis. The  $d$ -axis lags behind the  $q$ -axis by  $90^\circ$ . Resolving  $\dot{I}$  (step 5) into the  $q$ - and  $d$ -axis components, find  $I_d = 0.805$  and  $I_q = 0.595$  and the corresponding emf, namely

$$E_{ad} = X_{ad,s}I_d = 0.772 \times 0.805 = 0.622$$

$$E_{aq} = X_{aq,s}I_q = 0.329 \times 0.595 = 0.196$$

Using the above emfs and referring to the linearized no-load characteristics, determine the equivalent field mmfs,  $F_{adm} = 0.583$  (steps 6 and 7), and  $F_{aqm} = 0.18$  (steps 8 and 9), and plot them on the diagram in phase with the corresponding currents.  $F_{qdm}$  (step 10) is found from Eq. (55-31):

$$F_{qdm} = \xi_{qd} F_{aqm} = 0.23 \times 0.18 = 0.042$$

It is directed in opposition to the  $d$ -axis and lags behind  $E_{rd}$  by  $90^\circ$ .

To find  $\dot{E}_{rd}$  (step 11) induced by the resultant  $d$ -axis mmf,  $\dot{E}_r$  must be projected on the  $q$ -axis (or one must add  $-\dot{E}_{aq} = jX_{aq,s}\dot{I}_q$  to it). Using  $E_{rd}$  and referring to the partial no-load characteristic,  $E_f = f(F_1)$ , find (step 12) the resultant  $d$ -axis mmf (neglecting the rotor mmf),  $F_{1rd} = 1.1$ , and plot it on the diagram as the phasor  $\dot{F}_{1rd}$  (step 13) which leads  $\dot{E}_{rd}$  by  $90^\circ$ .

Now using Eq. (55-33), determine graphically (step 14) the field mmf,  $\dot{F}_{1f} = 1.725$ , neglecting the rotor mmf.

The leakage flux,  $\Phi_{f\sigma} = 0.45$ , is found (step 15) as a flux corresponding to  $F_{1f}$  on the  $\Phi_{f\sigma} = f(F_1)$  curve. Adding  $\Phi_{f\sigma}$  to the resultant  $d$ -axis mutual flux,  $\Phi_{rdm} = E_{rd} = 1.1$ , we can find from Eq. (55-34) the pole flux

$$\Phi_2 = \Phi_{rdm} + \Phi_{f\sigma} = 1.1 + 0.45 = 1.55$$

The next steps are to determine from the  $\Phi_2 = f(F_2)$  curve the corresponding rotor mmf,  $F_2 = 0.107$ , and calculate from Eq. (55-35) the total field mmf

$$F_{fm} = F_{1f} + F_2 = 1.725 + 0.107 = 1.83$$

plotted on the diagram as the  $\dot{F}_{fm}$  phasor (step 17).

**(4) Finding the d.c. field current (neglecting variations in the field leakage flux).** If the d.c. field current need not be found very accurately, we may neglect variations in the field leakage flux on load and determine the field current from the basic no-load characteristic,  $E_f = f(F_f)$ , without resort to the partial no-load characteristic,  $E_f = f(F_1)$ , and other magnetization curves. The necessary constructions are illustrated in Fig. 55-9 (where somewhat different parameters have been adopted). The steps involved are numbered from 1 through 12. The

sequence of graphical constructions is the same as it was in the previous case. It differs from the sequence shown in Fig. 55-8 only in that  $E_{rd}$  is used to find directly the resultant  $d$ -axis mmf,  $F_{rdm}$ , which approximately allows for the rotor mmf as well and is then used to determine the total field mmf

$$\dot{F}_{fm} = \dot{F}_{rdm} - \dot{F}_{adm} - \dot{F}_{qdm}$$

With  $\dot{F}_{fm}$  found in the above manner, we obtain underestimated values of the leakage flux and the rotor mmf in the case of a resistive-inductive load. As is seen from Fig. 55-8, instead of  $\Phi_{f\sigma} = 0.45$ , we use  $\Phi_{f\sigma,oc} = 0.29$ , and instead of  $F_2 = 0.107$ , we use  $F_{2,oc} = 0.052$ . Because of this, the field mmf found in this manner is smaller than that found in Fig. 55-8 by  $F_2 - F_{2,oc} = 0.107 - 0.052 = 0.055$ . With the parameters used in Fig. 55-8, it is

$$F_{fm} = 1.83 - 0.055 = 1.78$$

whereas its true value is 1.83.

Fortunately, because  $F_2$  is very small, the error in  $F_{fm}$  as found from Fig. 55-9 is not very large (in the case on hand, it is 3%). Therefore, it would be a good plan to determine  $F_{fm}$  from the basic no-load characteristic in some cases.

If the mode of operation is specified by giving other sets of defining quantities and the unknown quantity is not the field current, but  $V$ ,  $I$ , or  $\phi$ , the procedure must be the same as is used for a saturated, nonsalient-pole machine (see above).

## 56 Energy Conversion by a Synchronous Machine

### 56-1 Energy Conversion in the Generator Mode of Operation. Losses and Efficiency

Energy conversion by a.c. electric machines has been examined in Chap. 30. In this chapter, we shall be concerned with energy conversion by synchronous machines, with special reference to the generator mode of operation.



In the generator mode of operation (Fig. 56-1), a prime mover supplies the generator with an amount of mechanical power given by

$$P_2 = T_2 \Omega$$

where  $T_2$  is the input torque acting in the direction of rotation. A fraction of this input power, equal to  $P_f/\eta_f$ , is expended to drive an exciter with efficiency  $\eta_f$ . Some of this power,  $P_f/\eta_f - P_f$ , is dissipated as heat in the exciter.

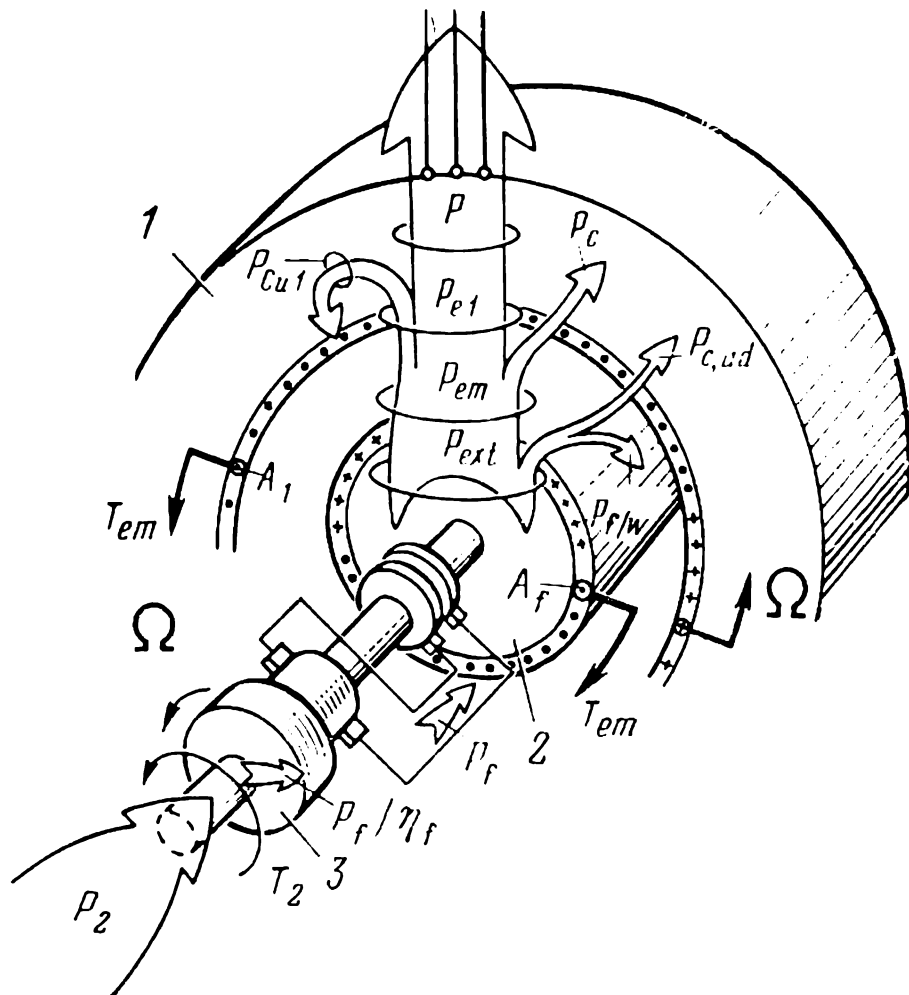


**Fig. 56-1** Energy conversion in a synchronous machine (in the generator mode of operation):

1—armature (stator); 2—field structure (rotor); 3—exciter (d.c. generator)

Here,  $P_f = R_f I_f^2$  is the power picked off the exciter commutator and delivered via its brushes and slip-rings to the field winding of the generator where it is likewise dissipated as heat. Owing to the torque  $P_f/\eta_f \Omega$  required to drive the exciter, the torque supplied by the prime mover is somewhat reduced, and the torque acting on the rotor, 2, of the synchronous machine proper is

$$T_{\text{ext}} = T_2 - P_f/\eta_f \Omega$$

As a result, the mechanically stressed shaft applies to the rotor an amount of mechanical power given by

$$P_{\text{ext}} = P_2 - P_f/\eta_f = T_{\text{ext}}\Omega \quad (56-1)$$

The mechanical power,  $P_m$ , converted electromagnetically, is smaller than the power applied to the rotor by an amount equal to the friction and windage losses,  $P_{f/w}$ , and the stray core losses,  $P_{c,ad}$ , associated with the harmonics of the air gap field:

$$P_m = T_{\text{em}}\Omega = P_{\text{ext}} - P_{f/w} - P_{c,ad} \quad (56-2)$$

Accordingly, the mechanical torque which balances the electromagnetic torque,  $T_{\text{em}}$ , acting on the rotor is smaller than  $T_{\text{ext}}$  applied to the rotor, by the brake torque due to the above listed factors:

$$T_{\text{em}} = T_{\text{ext}} - (P_{f/w} + P_{c,ad})/\Omega$$

In a synchronous machine, the field winding is excited by a direct current,  $I_f$ . Therefore, in contrast to induction machines, the power required for excitation,  $P_f$ , is taken from an exciter.

The direct current in the field winding,  $I_f$ , may be replaced by an equivalent surface current of density  $A_f$  (see Fig. 56-2) which sets up an equivalent fundamental field (stationary relative to the rotor). The surface current of density  $A_f$ , stationary relative to the rotor, travels in space at the same angular velocity,  $\Omega$ , as the rotor does. Therefore, the electromagnetic power generated by the rotating surface current  $A_f$  does not differ from the mechanical power supplied by the shaft

$$P_m - P_{\text{em}} = T_{\text{em}}\Omega \quad (56-3)$$

The rotating magnetic field transfers  $P_{\text{em}}$  to the stator. Some of this power, representing the core loss,  $P_c$ , is dissipated as heat in the stator core. The remainder

$$P_{e1} = P_{\text{em}} - P_c \quad (56-4)$$

is converted to electric power transferred to the armature winding

$$P_{e1} = P + P_{\text{Cu1}} \quad (56-5)$$

where  $P_{\text{Cu1}} = m_1 RI^2 =$  armature copper loss including stray losses.



and noting that

$$V \cos \varphi + I_r = E_r \cos \beta_r$$

and

$$I \cos \beta_r + I_c = I' \cos \beta'_r$$

we get

$$P_{em} = m_1 E_r I' \cos \beta'_r \quad (56-8)$$

Using Eq. (56-8), we can write  $P_{em}$  transferred across the air gap to the stator, in terms of the armature quantities, namely the resultant mutual emf  $E_r$ , the armature current  $I'$  adjusted for the additional current  $I_c$  associated with the core losses,  $P_c$ :

$$I' = \sqrt{(I_c + I \cos \beta_r)^2 + (I \sin \beta_r)^2}$$

and the cosine of the angle  $\beta'_r$  between  $E_r$  and  $I'$ :

$$\cos \beta'_r = (I \cos \beta_r + I_c) / I'$$

As is seen, using Eq. (56-8), we can find the electromagnetic power in a saturated or an unsaturated synchronous machine, once  $E_r$ ,  $I$ ,  $\cos \beta_r$  and  $P_c$  have been determined for the specified mode of operation as explained in Chap. 55. It may be added that, given  $E_r$  or  $\Phi_r$ , the armature (stator) core loss  $P_c$  can be found from the same equations as for an induction machine (see Sec. 40-3).

As already noted, the electromagnetic power transferred to the stator is the sum of two terms, namely

$$P_{el} = P + P_{Cu1} = m_1 E_r I \cos \beta_r$$

and

$$P_c = m_1 E_r I_c$$

We may treat  $P_{el}$  as the power expended to move the surface current  $A_1$  equivalent to the armature current  $I$ , at an angular velocity  $\Omega$ . Likewise,  $P_c$  may be treated as the power expended to move the surface current  $A_{1c}$  equivalent to  $I_c$ , at an angular velocity  $\Omega$ .

The electromagnetic torque,  $T_{em}$ , acting on the stator (see Fig. 56-1) is produced by the interaction of the resultant mutual field having a flux  $\Phi_{rm}$ , with the surface current  $A'_1$  equivalent to the armature current

$$\dot{i}' = \dot{i} + \dot{i}_c$$

The equation of electromagnetic torque can be derived from the expression for electromagnetic power

$$T_{em} = P_{em}/\Omega = m_1 p \Psi_{rm} I' \cos \beta'_r / \sqrt{2} \quad (56-9)$$

where

$$\Psi_{rm} = \sqrt{2} E_r / p \Omega = w_1 k_{w1} \Phi_{rm}$$

is the flux linkage of the resultant mutual field with the armature winding\*.

The equation of electromagnetic torque

$$T_{em} = (m_1 p / \sqrt{2}) \Psi_{rm} I' \sin (\pi/2 + \beta'_r) \quad (56-10)$$

can likewise be derived from Eq. (29-2) which includes the sine of the angle between  $\Psi_{rm}$  and  $I'$  (see Fig. 56-2) equal to  $\pi/2 + \beta'_r$ . Because  $\sin (\pi/2 + \beta'_r) = \cos \beta'_r$ , Eq. (56-10) reduces to Eq. (56-9).

If we neglect the core loss and set  $P_c = 0$ ,  $I_c = 0$ , and  $R_c = 0$ , the torque acting on the stator will be given by

$$T_{em} = P_{em}/\Omega = (m_1 p / \sqrt{2}) \Psi_{rm} I \cos \beta_r \quad (56-11)$$

where

$$P_{em} = m_1 I E_r \cos \beta_r$$

Assuming that the armature is free from both core and copper losses,  $P_c = 0$  and  $P_{Cu1} = 0$ , the electromagnetic power is equal to the active power

$$P_{em} = m_1 E_r I \cos \beta_r = m_1 V I \cos \varphi = P$$

Also,

$$E_r \cos \beta_r = V \cos \varphi$$

(see the phasor diagram in Fig. 56-2), and the electromagnetic torque can be expressed in terms of  $\Psi_{vm}$ , the total flux linkage with the armature winding, corresponding to  $V$ :

$$T_{em} = P/\Omega = (m_1 p / \sqrt{2}) \Psi_{vm} I \cos \varphi \quad (56-12)$$

where

$$\Psi_{vm} = \sqrt{2} V / p \Omega$$

In the generator mode of operation, the electromagnetic torque is positive when  $-\pi/2 < \beta'_r < \pi/2$ ,  $-\pi/2 < \beta_r < \pi/2$ , and  $-\pi/2 < \varphi < \pi/2$ . On the stator, the positive

---

\*  $\Psi_{rm}$  and  $\Phi_{rm}$  are found from the fundamental component of the air gap field.

torque acts in the direction of rotation, and on the rotor, in the opposite direction.

At  $3\pi/2 > \beta'_r > \pi/2$ ,  $3\pi/2 > \beta_r > \pi/2$ , and  $3\pi/2 > \varphi > \pi/2$ , the electromagnetic torque is negative, which corresponds to the motor mode of operation.

In an unsaturated salient-pole machine, the electromagnetic torque may be visualized as a sum of two components.

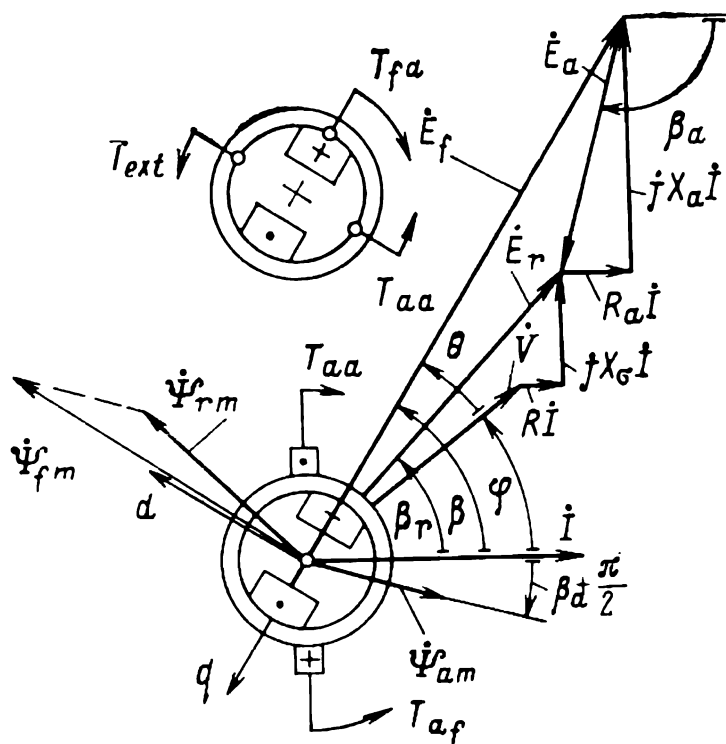


Fig. 56-3 Determining the electromagnetic torque components for a salient-pole saturated machine operating into a resistive-inductive load ( $\beta > 0$ )

Neglecting the core losses ( $P_c = 0$ ) so as to simplify calculations, the resultant mutual emf,  $\dot{E}_r$ , can be written as the sum of  $\dot{E}_f$  and  $\dot{E}_a = -R_a \dot{I} - jX_a \dot{I}$  induced by the armature field in accord with Eq. (54-34), where,  $R_a$  and  $X_a$  are the components of the mutual impedance of the armature given by Eq. (54-37), that is,

$$\dot{E}_r = \dot{E}_f + \dot{E}_a$$

and replace in Eq. (56-11) the projection of  $\dot{E}_r$  on the direction of  $\dot{I}$  by the sum of the projections of  $\dot{E}_f$  and  $\dot{E}_a$  on that direction (see Fig. 56-3)

$$E_r \cos \beta_r = E_f \cos \beta + E_a \cos \beta_a$$

where  $E_a \cos \beta_a = -R_a I$ .

The same can be done for the flux linkages

$$\Psi_{rm} \cos \beta_r = \Psi_{fm} \cos \beta + \Psi_{am} \cos \beta_a$$

Then, proceeding from Eq. (56-11), we get

$$T_{em} = P_{em}/\Omega = T_{af} + T_{aa} \quad (56-13)$$

where

$$T_{af} = m_1 E_f I_q / \Omega = (m_1 p / \sqrt{2}) \Psi_{fm} I \cos \beta$$

is the torque produced by the interaction of the armature current  $I$  with the excitation field which gives rise to the flux linkage  $\Psi_{fm}$ ; and

$$T_{aa} = -m_1 R_a I^2 / \Omega = (m_1 p / \sqrt{2}) \Psi_{am} I \cos \beta_a$$

is the torque produced by the interaction of the armature current with the own field displaced because of the rotor saliency through a certain angle,  $\beta_a + \pi/2$ , from the current and giving rise to the flux linkage  $\Psi_{am}$ .

The torque  $T_{af}$  exists only in an excited machine. The torque  $T_{aa}$  can appear only in a salient-pole machine ( $X_d \neq X_q$ ) at  $\beta$  not equal to 0,  $\pi/2$ ,  $\pi$ , or  $3\pi/2$ , when  $\beta_a \neq -\pi/2$  and  $R_a \neq 0$ . This torque is produced when the flux linkage  $\Psi_{am}$  (or the armature field) is displaced through a certain angle,  $\beta_a + \pi/2$ , from the current. This occurs when  $\dot{I}$  is not directed along the  $d$ - or the  $q$ -axis of the rotor.

The torques  $T_{af}$  and  $T_{aa}$  acting on the stator in the generator mode of operation into a resistive-inductive load ( $\varphi > 0$ , and  $\beta > 0$ ) are shown in Fig. 56-3. Their directions can be determined by the left-hand rule applied to the stator current, or formally from Eq. (56-13). As is seen, in this mode of operation  $T_{aa}$  is negative ( $R_a > 0$ ).

Similar torques, but directed in opposition to the stator torques, act on the rotor as well. The direction of  $T_{af}$  acting on the rotor can be found by the left-hand rule applied to the electromagnetic force produced by the interaction of the excitation field and the armature field. The torque  $T_{aa}$  acting on a salient-pole rotor in the armature field always tends to turn the rotor so that its pole axis (the  $d$ -axis) runs with the armature field. To demonstrate, as

follows from

$$T_{aa} \equiv i^2 dL_{11}/d\gamma$$

(at fixed armature current) the torque  $T_{aa}$  acts in the direction of displacements  $d\gamma$  such that the armature inductance  $L_{11}$  increases and  $dL_{11} > 0$ . As a result, the  $d$ -axis of the rotor is forced to align itself with the axis of the armature field.

Figure 56-4 shows a phasor diagram for a synchronous machine operating as a generator into a resistive-capacitive load ( $\varphi < 0$ ) at  $\beta < 0$ .

Irrespective of the field current,  $T_{af}$  in the generator mode is always positive and acts on the rotor in a direction opposite to the direction of rotation. The torque  $T_{aa}$  in the case of a resistive-inductive load ( $\varphi > 0$ ,  $\beta > 0$ ) is negative, whereas in the case of a resistive-capacitive load ( $\varphi < 0$ ) at  $\beta < 0$  it is positive. Formally, this is associated with the change of sign by the resistive component,  $R_a$ , of the mutual impedance, which is positive at  $\beta > 0$  and negative at  $\beta < 0$ .

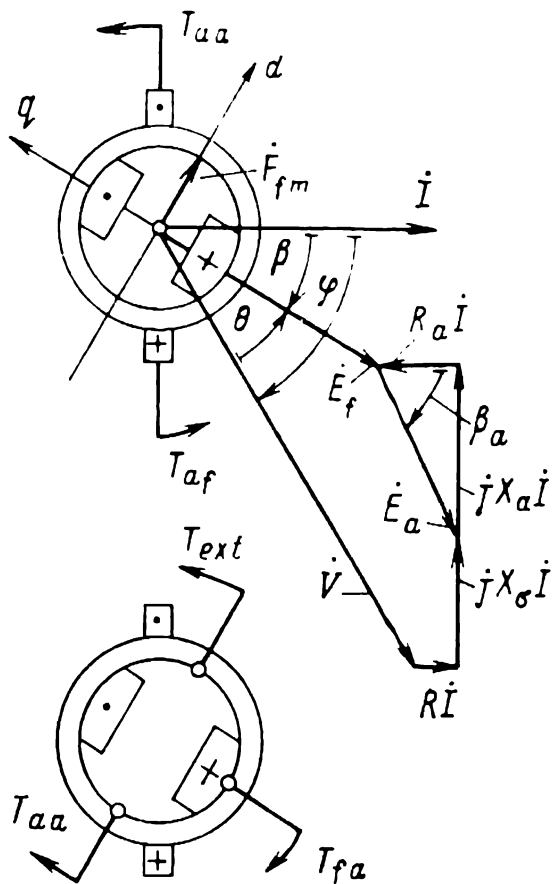


Fig. 56-4 Determining the electromagnetic torque components for a salient-pole unsaturated machine operating into a resistive-capacitive load ( $\beta < 0$ )

## 57 Characteristics of a Synchronous Generator Supplying an Isolated Load

### 57-1 Operation of a Synchronous Generator into an Isolated Load

The operating conditions of a synchronous generator supplying an isolated load vary according to the nature of that load.



Under normal service conditions when the power drawn by the load does not exceed its rated value, the amplitude and frequency of the voltage across the terminals of the generator must be as close to their rated values as practicable. In present-day plant, this objective is achieved by controlling the field and rpm of the prime mover automatically.

Under abnormal conditions, such as a balanced, steady-state short circuit across the generator terminals (or in the associated electric system), the armature current of the generator may rise to dangerous proportions\*. To avoid this, safety features are built into both the generator and the electric system, such as overcurrent and undervoltage relays. Together with the excitation and field controls, they keep the generator running under abnormal conditions as well as they do under normal conditions.

## 57-2 Excitation Characteristic of a Synchronous Generator

The excitation characteristic of a synchronous generator is a plot of its field current as a function of its armature current

$$I_f = f(I)$$

with the terminal voltage  $V$ , angular velocity  $\Omega$  and load angle  $\phi$  held constant.

The excitation characteristic shows how the field current must be varied for the terminal voltage  $V$  to remain constant in spite of any changes in the load impedance,  $Z_L$ . Ordinarily, such characteristics are plotted for the rated voltage and the rated velocity, assuming several per-unit values of armature current ( $I = 0, 0.2, 0.4, 0.6, 0.8$  and  $1.0$ ), and finding the respective field current,  $I_f$ , as explained in Chap. 55.

Neglecting saturation, the field current can be found analytically from Eq. (55-7) or Eq. (55-17). With allowance for saturation, this is done graphically, using the magnetization curves and the voltage and mmf phasor diagram in Fig. 55-4 (for a nonsalient-pole machine) and Fig. 55-8 (for a salient-pole machine).

---

\* Unbalanced load and unbalanced short circuits are examined in Chap. 61, and the transients accompanying a balanced short circuit, in Chap. 73.

A family of excitation characteristics for a synchronous generator at various load angles is shown in Fig. 57-1.

With a resistive-inductive load ( $\varphi > 0$ ), the armature mmf has a demagnetizing effect, and the field current must be raised so as to maintain the desired terminal voltage. The largest increase in field current occurs in the case of a purely inductive load ( $\varphi = 90^\circ$ ), and the least, in the case of a purely resistive load ( $\varphi = 0$ ).

This can be borne out qualitatively by reference to the simple voltage phasor diagram in Fig. 57-2a (neglecting saturation and saliency, as explained in Sec. 55-1), at  $\varphi = 37^\circ$ . The locus of  $I$  is the line  $1'-2'-3'$ , the locus of  $E_f$  is the line  $1-2-3$ . As is seen, at  $\varphi > 0$ , an increase in  $I$  is accompanied by a continuous rise in  $E_f$  or  $I_f$  (on the excitation characteristic in Fig. 57-1 for  $\varphi = 37^\circ$ , the numerals 1, 2 and 3 label the same points as in Fig. 57-2a).

The effect of load on field current grows in proportion to the inductive reactance

$$X_1 = X_\sigma + X_a$$

of the armature winding.

Point 3 ( $\cos \varphi_R = 0.8$ ,  $I_R = 1.0$ ) marks the rated field current,  $I_{f,R}$ . It differs from the open-circuit field current in proportion to the per-unit value of  $X_1$ .

Accurate values of the field current could be found from diagrams constructed with allowance for saturation and saliency. However, the excitation characteristics constructed with allowance for saturation (in Fig. 57-1, they are shown as dashed lines) would differ but little from those plotted neglecting saturation.

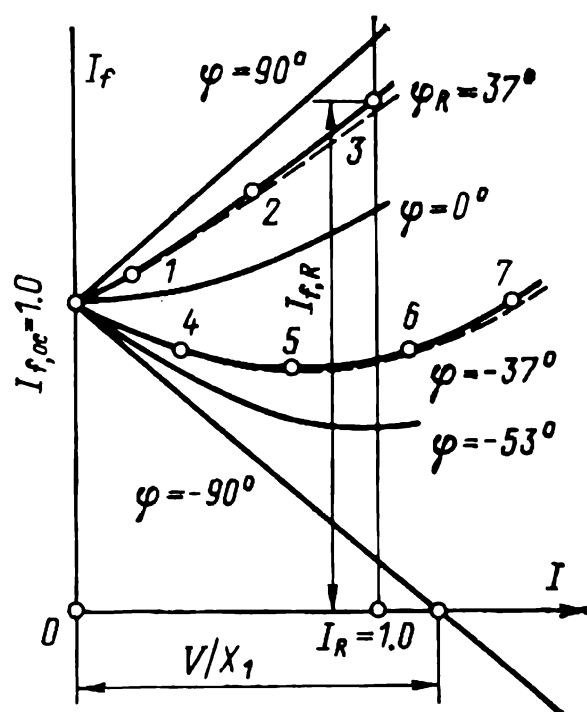


Fig. 57-1 Control characteristics,  $I_f = f(I)$ , of a synchronous generator at  $V_R$ ,  $\Omega_R$  and  $\varphi$  held constant:

— neglecting saturation;  
 - - - with allowance for saturation

When the load is resistive-capacitive ( $\varphi < 0$ , see Fig. 57-2b), the field current at small armature currents is lower than it is on open circuit (say, at point 4), drops to a minimum value (at point 5), and rises again.

This behaviour can be explained by reference to the family of voltage diagrams in Fig. 57-2b. As is seen,  $E_f$  for which the locus is the line 4-5-6-7 varies with the increase

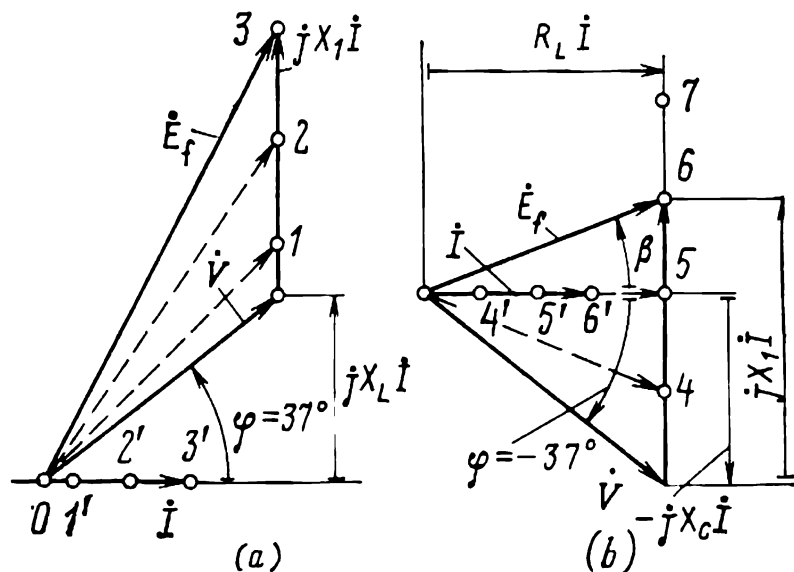


Fig. 57-2 Construction of excitation characteristics

in armature current from point 4' to point 6' in the same manner as the field current, as already explained. At low armature currents (points 4 and 4')

$$I = V |\sin \varphi| / X_C$$

which flow at  $X_C > X_1$ ,

$$\beta = \arctan \frac{X_1 - X_C}{R_L} < 0$$

and  $\dot{E}_f$  lags behind  $\dot{I}$ . At the above points, the  $d$ -axis current and the  $d$ -axis mmf of the armature are magnetizing in their effect.  $E_f < V$ , and  $I_f$  is smaller than  $I_{f,oc}$ , the field current on open circuit.

At points 5 and 5', where  $X_C = X_1$ , a voltage resonance takes place—the equivalent-circuit reactance to  $E_f$  vanishes,  $X_1 - X_C = 0$ , and the armature current

$$I = V |\sin \varphi| / X_1 = V |\cos \varphi| / R_L$$

is now in phase with  $E_f$  ( $\varphi = 0$ ). In the circumstances, the field current takes the least possible value,  $I_{f,min}$ , corresponding to  $E_{f,min} = V \cos \varphi$  (point 5 in Fig. 57-1).

At  $I = V |\sin \varphi| / X_C > V |\sin \varphi| / X_1$ , that is, at

$X_C < X_1$ , the phase angle  $\beta$  is nonzero positive, and  $\dot{E}_f$  leads  $\dot{I}$  (for example, at points 6 and 6'). Now the  $d$ -axis current and mmf of the armature are demagnetizing in their effect,  $E_f > E_{f,\min}$ , and  $I_f$  exceeds  $I_{f,\min}$  which exists at point 5 when the armature current has only the  $q$ -axis component,  $I_q$ , whereas the  $d$ -axis component vanishes.

Finally, at the armature current

$$I = \tilde{V} |\sin \varphi| / X_C = 2V |\sin \varphi| / X_1$$

that is, at  $X_C = X_1/2$ , we again see that  $E_f = V$ , and  $I_f = I_{f,oc}$  (point 7 in Fig. 57-1).

When saturation and saliency are allowed for, the quantitative relationships are somewhat different, but the qualitative picture remains unchanged, the effect of saturation alone being insignificant (compare with the curves for  $\varphi = -37^\circ$  in Fig. 57-1).

When the load is purely capacitive, the field current falls off with an increase in the armature current at an especially high rate, although in a linear fashion. At the armature current given by

$$I = V |\sin \varphi| / X_C = V/X_C = V/X_1$$

which corresponds to voltage resonance, the field current reduces to zero. Therefore, when the machine is connected across a capacitive reactance, a voltage may exist across its terminals even when no excitation is applied. This is what is called the *self-excitation* of a synchronous machine (in more detail, this will be explained later in this chapter).

If we reduce the capacitive reactance still more so that  $X_C < X_1$ , which corresponds to  $I > V/X_1$ , we will be able to maintain the desired terminal voltage by exciting the machine with a negative current,  $I_f < 0$ , whose mmf will be in opposition to the armature mmf. A detailed analysis of operation at negative excitation would show that this is an unstable condition. Should the rotor depart by any change from a position where its mmf,  $F_{fm}$ , opposes the armature mmf,  $F_{am}$ , there would appear an electromagnetic torque that would tend to increase the departure. As a result, the rotor and its mmf would turn relative to  $F_{am}$  through  $180^\circ$  (electrical), so that  $F_{fm}$  would be in line with  $F_{am}$ .

Negative excitation can be effected only in machine fitted with suitable fast-acting automatic field and rpm control circuits.

### 57-3 External Characteristics

An external characteristic is a plot of the terminal voltage of a generator as a function of its armature current,  $V = f(I)$ , with the field current, rpm and load angle held constant.

An external characteristic shows how the terminal voltage of a generator varies as the load current increases, if the field current and the nature of load remain unchanged.

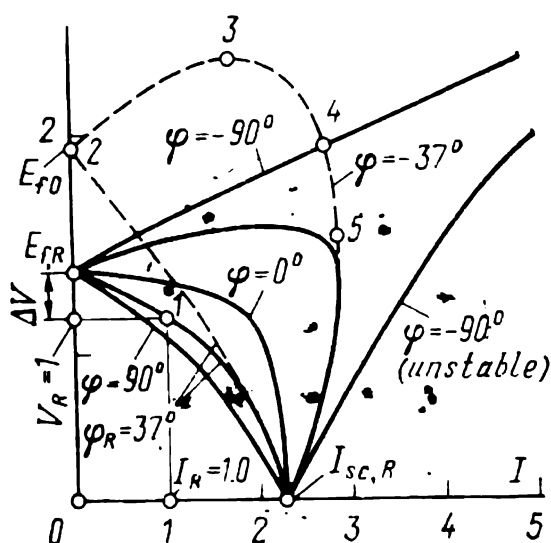


**Fig. 57-3** External characteristics,  $V = f(I)$ , of a synchronous generator at  $I_f = I_{f,R}$ ,  $\Omega_R$  and  $\phi$  held constant:

———— with allowance for saturation; — — — — neglecting saturation

As a rule, external characteristics are plotted for two characteristic values of field current, namely  $I_{f,oc}$  corresponding to  $V_R$  on open circuit, and  $I_{f,R}$  corresponding to the rated operating conditions ( $V_R$ ,  $I_R$ , and  $\phi_R$ ).

A family of external characteristics for a synchronous generator ( $X_1 = 0.86$ ,  $X_\sigma = 0.16$ , and  $X_a = 0.70$ ) plotted at  $V = V_R$ ,  $I_f = I_{f,oc}$ , and various load angles  $\phi$ , is shown in Fig. 57-3. In plotting external characteristics, it is essential to allow for the effect of saturation.

From a comparison of the external characteristics for  $\phi = \pm 37^\circ$  ( $\cos \phi = 0.8$ ), plotted at the same field current with allowance for saturation (full curves) and neglecting saturation (dashed curves), it is seen that the curves drawn neglecting saturation are the same as the exact curves only at low terminal voltages and give, in the general case, only a qualitative idea about variations in terminal voltage. In constructing external characteristics,  $V$  needs to be determined under various sets of operating conditions as specified in terms of  $I_f$ ,  $I$  and  $\phi$  (see Chap. 55).

The characteristics shown as full curves in Fig. 57-3 have been constructed by reference to the phasor diagram of a nonsalient-pole synchronous machine and using the normalized open-circuit characteristic of a nonsalient-pole machine from Fig. 53-11.

The basic external characteristic at the rated load angle,  $\varphi_R = 37^\circ$ , passes through point  $I$  where the terminal voltage and current are at their rated values (on a per-unit basis,  $V_R = 1$  and  $I_R = 1$ ). A decrease in the current through a resistive-inductive load (at  $\varphi = \varphi_R$ ), with the field current held constant, is accompanied by an increase in the terminal voltage due to a decrease in the demagnetizing effect of the armature mmf,  $F_a$ . On open circuit, when  $Z_L = \infty$ ,  $I = 0$  and  $F_a = 0$ , the terminal voltage becomes equal to  $E_{f,R}$ , where  $E_{f,R}$  is a function of  $I_{f,R}$ , as follows from the open-circuit characteristic. Using  $E_{f,R}$ , we can determine the inherent voltage regulation in the case of load shedding:

$$\Delta V_* = \Delta V/V_R = (E_{f,R} - V_R)/V_R \quad (57-1)$$

For the machine in question,

$$\Delta V_* = (1.26 - 1.0) \div 1.0 = 0.26$$

This gives a percentage voltage regulation of 26%.

An increase in the current through a resistive-inductive load (at  $\varphi = \varphi_R$ ) is accompanied by a fall in the terminal voltage. When  $Z_L = 0$ , that is, when the terminal leads of the armature are shorted together, a balanced, steady-state short circuit occurs, with  $I_f = I_{f,R}$ . The terminal voltage of the generator is then equal to zero, and the current becomes equal to the short-circuit current at normal excitation:

$$I = I_{sc,R} (E_{f,R0}/X_1) = 1.93 \div 0.86 = 2.25$$

where  $E_{f,R0} = f(I_{f,R})$  is found from the air-gap line — the linearized open-circuit characteristic,  $E_f = f(F_\delta)$ .

External characteristics plotted for the same value of  $I_{f,R} = 1.68$ , but for other value of  $\varphi \neq \varphi_R$ , have a common open-circuit point ( $V = E_{f,R}$  and  $I = 0$ ) and a common short-circuit point ( $V = 0$  and  $I = I_{sc,R}$ ) with the basic external characteristic.

With a resistive-inductive load, when  $90^\circ > \varphi > 0$ , an increase in current from zero to  $I_{sc,R}$  is accompanied by a monotone decrease in the terminal voltage from  $E_{f,R}$  to zero. The rate of fall is especially pronounced in the case of a purely inductive load ( $\varphi = 90^\circ$ ,  $\cos \varphi = 0$ ), and is

very slow in the case of a purely resistive load ( $\varphi = 0$ ,  $\cos \varphi = 1.0$ ).

With a resistive-capacitive load, when  $0 > \varphi > -90^\circ$ , the terminal voltage varies in a more elaborate manner (see the full curve for  $\varphi = -37^\circ$  in Fig. 57-3). At low armature currents, when  $X_C$  is high,  $V > E_{f,R}$ . At a certain armature current corresponding to a voltage resonance ( $X_C = X_{1,R}$ , where  $X_{1,R}$  is the armature inductive reactance with allowance for saturation),  $V = V_{\max}$ . As  $Z_L$  keeps decreasing, the terminal voltage goes down too, but the armature current keeps rising until it attains its maximum value,  $I_{\max} > I_{sc,R}$ . From that instant on, it again falls to  $I_{sc,R}$ .

With a purely capacitive load, when  $\varphi = -90^\circ$ , the characteristic has two non-intersecting portions, one of which passes through the open-circuit point ( $V = E_{f,R}$  and  $I = 0$ ), and the other passes through the short-circuit point ( $V = 0$ ,  $I = I_{sc,R}$ ). The second portion corresponds to unstable operation, because it involves negative field currents (see the analysis of field control characteristics).

Neglecting saturation, external characteristics can be described analytically by Eq. (55-18) for salient-pole machines, or by Eq. (55-8) for nonsalient-pole machines. As already noted, they are identical with the exact characteristics at low terminal voltages and may be used to advantage in a qualitative analysis of external characteristics.

As will be recalled, external characteristics are measured for constant power factor ( $\sin \varphi$ ), and constant  $E_f = E_{f,R0}$ , the only variable being  $Z_L$ . Then, differentiating Eq. (55-8) and putting  $dV/dZ_L = 0$ , we find that

$$V = V_{\max} = E_{f,R0}/\cos \varphi \text{ (point 3)}$$

at  $|X_L| = X_1$  and  $Z_L = X_1/|\sin \varphi|$ . At this point, a voltage resonance takes place, and the current

$$I = V/Z_L = (E_{f,R0}/X_1) |\tan \varphi| = I_{sc,R} |\tan \varphi|$$

Accordingly, taking the derivative Eq. (55-8) and equating it to zero, we will see that the current is a maximum

$$I_{\max} = E_{f,R0}/X_1 \cos \varphi = I_{sc,R}/\cos \varphi$$

at  $Z_L = X_1 \sin \varphi$  (point 5), where

$$V = Z_L I_{\max} = E_{f,R0} \tan \varphi$$

Using Eq. (55-8), it is as easy to find the current at which the voltage first falls off, then becomes equal to that on open circuit,  $V = E_{f,R}$  (point 4). This current is

$$I = 2E_{f,R0} |\sin \varphi| / X_1 = 2 |\sin \varphi| I_{sc,R}$$

and corresponds to  $Z_L = X_1/2 |\sin \varphi|$ .

#### 57-4 Short-Circuit Characteristic

A short-circuit characteristic relates the armature current to the field current on a balanced, steady-state short circuit at the armature terminals:

$$I_{sc} = f(I_f)$$

Experimentally, a short-circuit characteristic is measured as follows. With the machine stopped, three ammeters or current transformers are connected in a star to its terminals. The generator is brought up to rated speed  $\Omega_R$  at  $I_f = 0$ , then the field current is gradually raised, and the armature current is measured for each value of  $I_f$ . The results are plotted as an  $I_{sc} = f(I_f)$  curve shown in Fig. 57-4. Experiments have shown that this relation remains linear even when the short-circuit current is three or four times the rated armature current.

On a short-circuit, the excitation field is substantially weakened by the demagnetizing action of the  $d$ -axis component of armature mmf. The magnetic circuit of the machine is only slightly saturated, and the short-circuit current may well be found from the equivalent circuit drawn for an unsaturated salient-pole synchronous machine in Fig. 54-1 or the voltage equation, (55-19). On a short circuit,  $Z_L = 0$ ,  $R_L = 0$ , and  $X_L = 0$ , so the short-circuit current is solely limited by the resistance,  $R$ , and inductive reactance,  $X_1$ , of the armature winding.

The armature conductors have a negligible resistance in comparison with their  $q$ -axis inductive reactance (in per-unit,  $R = 0.01$  to  $0.001$ ,  $X_q = 0.3$  to  $1.5$  for salient-pole machines, and  $X_q = X_d = 1.0$  to  $2.5$  for nonsalient-pole machines). Therefore, at  $Z_L = 0$ ,  $\cos \beta$ , Eq. (55-15), is zero very nearly:

$$\cos \beta = R / \sqrt{X_q^2 + R^2} \approx 0$$





where  $E_{f0}$  is the emf corresponding to the specified field current and found from the linearized open-circuit characteristic,  $E_f = f(F_{fm})$ .

At the rated angular velocity,  $\Omega = \Omega_R$  (or  $\omega = \omega_R$ ), the resistance of the armature winding is small in comparison with its inductive reactance. Therefore, it is safe to calculate the short-circuit current by the equation

$$I_{sc} = E_{f0}/X_d \quad (57-3)$$

It is to be noted that at a constant field current the short-circuit current is nearly independent of the angular velocity of the rotor, because both  $E_{f0}$  and  $X_d$  are proportional to that velocity:

$$E_{f0} = E_{f,R0}\Omega_*$$

$$X_d = X_{d,R}\Omega_*$$

where  $X_{d,R}$  and  $E_{f,R0}$  are the inductive reactance and emf at the rated angular velocity (neglecting saturation), and  $\Omega_*$  is the per-unit angular velocity of the rotor.

From the approximate equation (57-3) it follows that under the above conditions the short-circuit current is independent of angular velocity:

$$\begin{aligned} I_{sc} &= E_{f0}/X_d = E_{f,R0}/X_{d,R} \\ &= I_{sc,R} = \text{constant} \end{aligned}$$

If we allow for the effect of the resistance in accord with Eq. (57-2), it can be shown that the short-circuit current is practically constant at sufficiently high angular velocities and that it begins to fall off at very low velocities and decreases gradually to zero. This is illustrated in Fig. 57-5 which is a plot of  $I_{sc}/I_{sc,R} = f(\Omega_*)$ , constructed at a constant field current for a machine with  $R = 0.01$ , and  $X_d = 1.0$ . Figure 57-4 shows how  $I_f$  (or  $F_f$ ) can be found for a salient-pole machine at a specified short-circuit current graphically. This is done by using the phasor-vector diagram for a saturated salient-pole machine (Fig. 55-9) and the open-circuit

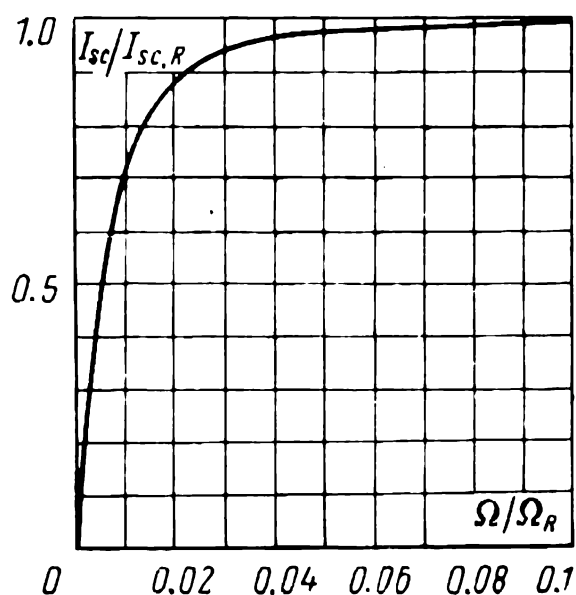


Fig. 57-5 Short-circuit current as a function of the relative rotor velocity at constant field current

characteristic so as to see how large the currents may be for the magnetic circuit of the machine to remain still unsaturated.

As is seen,  $F_{fm}$  is the sum of  $F_{rm}$  corresponding to  $E_r = X_\sigma I$ , and  $F_{adm}$  equivalent to the  $d$ -axis mmf of the armature. At  $E_{*r} = X_{*\sigma} I_* < 0.7$ , when the  $E_f = f(F_{fm})$  open-circuit characteristic is practically linear and is the same as the  $F_f = f(F_\delta)$  curve,  $F_{rm}$  is proportional to  $E_r = X_\sigma I$  and to the short-circuit current. Also,  $k_{za} = F_1/F_\delta = 1.0$ ,  $\xi_d = 1.0$ ,  $k_{qd} = 0$ , and, in accord with Eq. (55-30),

$$\begin{aligned} X_{ad,s} &= X_{ad} \\ E_{ad} &= X_{ad} I \end{aligned}$$

By the same token,  $F_{adm}$  corresponding to  $E_{ad}$  from the  $E_f = f(F_\delta)$  curve is likewise proportional to the short-circuit current, and this implies that both  $F_{fm} = F_{rm} + F_{adm}$  and  $F_f/w_f$  are proportional to the short-circuit current so long as  $E_{*r}$  remains less than 0.7, and the short-circuit current itself is

$$I_{*sc} < 0.7/X_{*\sigma} \approx 4 \text{ to } 7.0^*$$

On a per-unit basis, the short-circuit characteristic,  $I_{sc} = f(I_f)$ , can readily be plotted, using the so-called short-circuit triangle ( $\triangle ABC$  in Fig. 57-4). The vertical side of this triangle,  $AB$ , represents the leakage emf,  $X_\sigma I$ , and the horizontal side  $BC$  represents the  $d$ -axis armature mmf. The dimensions of the triangle or of its sides  $AB$  and  $BC$  are proportional to the armature current.

Using the short-circuit triangle, it is an easy matter to find  $I_f$  or  $F_{fm}$  corresponding to the specified short-circuit current. If we position corner  $A$  on the open-circuit characteristic and align the side  $BC$  with the axis of abscissae, corner  $C$  will locate  $I_f$ . By varying the dimensions of triangle  $ABC$  in proportion to the short-circuit current, we will see that within the limits stated the short-circuit remains linear.

The performance of a synchronous generator can to a certain extent be described in terms of the short-circuit current which corresponds to the open-circuit mmf,  $F_{fm,oc}$ , producing rated voltage on open circuit. The ratio of this current,  $I_{sc,oc}$ , to the rated current,  $I_R$ , is called the *short-*

---

\* It is assumed that  $X_{*\sigma}$  is independent of the current in the armature winding.

*circuit ratio* of a synchronous machine\*:

$$\text{SCR} = I_{\text{sc,oc}}/I_{\text{R}} = I_{\text{sc,oc}} \quad (57-4)$$

The SCR may be expressed in terms of the  $d$ -axis inductive reactance of the armature [see Fig. 57-4 and Eq. (57-3)]:

$$\begin{aligned} \text{SCR} &= E_{f,\text{oc}}/X_d I_{\text{R}} \approx (1.06 \text{ to } 1.15) V_{\text{R}}/X_d I_{\text{R}} \\ &= 1.06 X_{*d} \text{ to } 1.15 X_{*d} \end{aligned} \quad (57-5)$$

where  $X_{*d}$  is the per-unit  $d$ -axis armature inductive reactance (neglecting saturation). The factor 1.06 applies to salient-pole machines, and 1.15 to nonsalient-pole units with normal open-circuit characteristics.

The steady-state short-circuit current,  $I_{\text{sc,R}}$ , at rated excitation,  $F_{fm,\text{R}}$ , is 1.5 to 3 times the current at  $F_{fm,\text{oc}}$

$$\begin{aligned} I_{* \text{sc,R}} &= I_{*,\text{sc,oc}} (F_{fm,\text{R}}/F_{fm,\text{oc}}) \\ &= I_{*,\text{sc,oc}} F_{*f,\text{oc}} \end{aligned} \quad (57-6)$$

### 57-5 Load Characteristics

A load characteristic relates the terminal voltage of a generator to its field current, with the armature current, angular velocity and load angle held constant.

$$V = f(I_f)$$

A load characteristic shows how the terminal voltage varies with changes in the field current, if the armature current is held constant in amplitude ( $I = \text{constant}$ ) and in phase ( $\varphi = \text{constant}$ ) by adjusting  $Z_{\text{L}}$ , the load impedance.

A special case of the load characteristic is the open-circuit characteristic which may be treated as a load characteristic

$$V = E_f = f(I_f)$$

measured at an armature current equal to zero ( $I = 0$  and  $Z_{\text{L}} = \infty$ ).

Of all other load characteristics, use is practically made of only the inductive load characteristic applicable to an inductive load ( $\varphi = 90^\circ$ ).

---

\* Some authors define the SCR as the ratio of the field current producing rated voltage on open circuit to the field current producing rated short-circuit current.—*Translator's note.*



Accordingly, in constructing the characteristic, we may put  $I = I_d$ ,  $I_q = 0$ ,  $I_{qm} = 0$ , and  $E_{rd} = E_r = V + X_\sigma I$ . Most accurately, the construction is carried out as illustrated in Fig. 55-8, using the magnetization curves (see Fig. 53-8), because it takes into account variations in the leakage flux on load, and the excitation mmf is found as

$$F_{fm} = F_{1rd} + F_{adm,s} + F_2$$

where  $F_{1rd}$  = mmf corresponding to  $E_{rd} = E_r$ , as found from the  $E_f = f(F_1)$

$F_{adm,s}$  = mmf found with allowance for saturation and corresponding to  $X_{ad,s}I = \xi_d X_{ad}I$  on the  $E_f = f(F_\delta)$  curve, and  $\xi_d = f(E_r)$  in Fig. 55-10

$F_2$  = rotor mmf on the  $\Phi_2 = f(F_2)$  curve

Curve 1 in Fig. 57-6 has been plotted in the manner explained just above. Curve 2 in the same figure has been plotted in accord with Fig. 55-9, using the open-circuit characteristic in Fig. 53-8. It neglects variations in the leakage flux on load, and the excitation mmf is given by

$$F_{fm} = F_{rdm} + F_{adm,s}$$

where  $F_{rdm}$  is the mmf corresponding to  $E_{rd} = E_r$  on the  $E_f = f(F_{fm})$  curve.

Load curve 3 has likewise been constructed as illustrated in Fig. 55-9, using the open-circuit characteristic, but neglecting variations in the leakage flux on load and the effect of saturation on  $F_{adm}$ . Accordingly, the field mmf can be found as

$$F_{fm} = F_{rdm} + F_{adm}$$

where  $F_{adm}$  is the mmf found neglecting saturation (at  $\xi_d = 1.0$ ) and corresponding to  $X_{ad}I$  on the  $E_f = f(F_\delta)$  curve.

The simplest way to construct load curve 3 is illustrated in sufficient detail in Fig. 57-6. On the assumptions used,  $F_{adm}$  at a constant  $I$  is likewise constant and equal to that on a steady-state circuit with  $I_{sc} = I$ , when the magnetic circuit of the machine is unsaturated (see above in this section). Therefore, curve 3 can be constructed, using the short-circuit triangle,  $\triangle ABC$ , with the side  $AB$  equal to  $X_\sigma I$ , and the side  $BC$  to  $F_{adm}$ . From the construction in Fig. 57-6 it follows that at  $V$  point  $C$  on load curve 3 can be located with the aid of the short-circuit triangle, when the side

$BC$  is aligned with the line of constant  $V$  and the corner  $A$  is positioned on the open-circuit characteristic. As point  $A$  is moved along the open-circuit characteristic, point  $C$  will trace out the load characteristic,  $V = f(F_{fm})$  or  $V = f(I_f)$ . At  $V = 0$ , when the triangle takes up the position labelled  $A_1B_1C_1$ , point  $C_1$  will give the field mmf on a short circuit with  $I = I_{sc}$ .

At  $V < 0.7$ , curve 3 is the same as curves 2 and 1 constructed on more rigorous assumptions. At high voltages, curve 3 substantially differs from curve 1 which is practically the same as the experimental load curve.

The open-circuit characteristic,  $E_f = f(F_{fm})$ , and the inductive load characteristic,  $V = f(F_{fm})$ , obtained by experiment, may well be used to determine the leakage inductive reactance. The procedure is as follows. Choose point  $C$  within the nonlinear part of the  $V = f(F_{fm})$  curve, lay off  $OC = O_1C_1$  as shown in Fig. 57-6, and draw through point  $O$  a line parallel to the initial part of the open-circuit characteristic. Point  $A$  at the intersection with the open-circuit characteristic will give the side  $AB$  of the triangle on a voltage scale. Now the armature leakage inductive reactance may be written

$$X_\sigma = AB/I$$

where  $I$  is the current at which the load characteristic is measured.

The error in the value of  $X_\sigma$  thus found is proportional to the discrepancy between curves 3 and 1, and  $X_\sigma$  is being somewhat overestimated.

### 57-6 Self-Excitation of a Synchronous Generator Operating into a Capacitive Load

From analysis of the field control characteristics for a synchronous generator at a constant  $\dot{V}$ , it can be seen that a decrease in the capacitive reactance of the load entails an increase in the armature current,  $I$ , with the result that the field current gradually falls off until, at a certain value of  $X_C$ , it disappears altogether, although the terminal voltage of the generator remains the same as before, that is, equal to  $V$ .

In a nonsalient-pole machine, this happens when  $X_C$  is equal to  $X_1$ , the inductive reactance of the armature. Now  $R + R_L = 0$ , a voltage resonance takes place, and

$E_f$  given by Eq. (55-8) vanishes:

$$E_f = I \sqrt{(X_1 - X_c)^2} = 0$$

In the circumstances, the field is excited by the  $d$ -axis magnetizing current in the armature winding, and no excitation is needed from the rotor's side ( $I_f = 0$ ).

If we connect an unexcited synchronous machine, with its rotor spinning, across a capacitive reactance,  $X_c = X_1$ ,

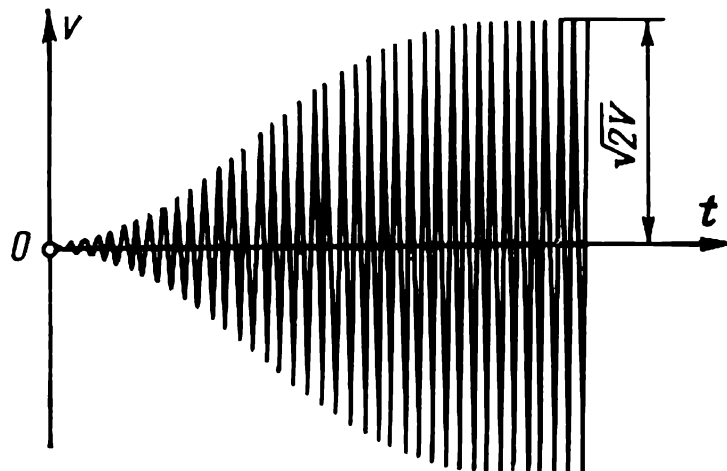


Fig. 57-7 Variations in terminal voltage due to self-excitation of a synchronous generator

what is known as *self-excitation* will take place. The small emf always existing across the armature terminals due to the remanence of the poles gives rise to a magnetizing current in the armature winding, and the current boosts the field. In turn, the field induces a larger emf which boosts the field still more, and so on. The transient thus initiated (see Fig. 57-7) causes the terminal voltage to build up until it attains a steady-state amplitude,  $\sqrt{2}V$ . This value corresponds to the onset of saturation in the magnetic circuit and the associated insignificant decrease in  $X_1$ .

When a salient-pole machine is operating into a capacitive load ( $X_L = -X_c$ ,  $R + R_L = 0$ ), the resultant current acts along the  $d$ -axis, see Eq. 55-15:

$$I_d = I |\sin \beta| = I$$

$$I_q = I \cos \beta = 0$$

$$\sin \beta = (X_q - X_c) / \sqrt{(X_q - X_c)^2} = \pm 1$$

At  $X_c \geq X_q$ , it has a magnetizing effect, because

$$\sin \beta = -1$$





resultant emf is proportional to the armature current

$$\begin{aligned}\dot{E}_r &= \dot{E}_{rd} + \dot{E}_{aq} = \dot{E}_{rd} \\ &= \dot{V} + jX_\sigma I \\ &= -j(X_C - X_\sigma) \dot{I}\end{aligned}$$

The emf induced by the  $d$ -axis armature field,  $E_{ad}$ , can be found, using the open-circuit characteristic  $E_f = f(E_{fm})$ , from the mmf

$$F_{adm} = \xi_d k_{ad} F_{dm} \approx k_{ad} (\sqrt{2}/\pi) m_1 (w_1 k_{w1}/p) I$$

proportional to  $I$  (with a sufficient accuracy it may be taken that  $\xi_d$  is equal to unity). Therefore, the  $E_{ad} = f(I)$  curve shown in Fig. 57-8 is in effect an open-circuit characteristic re-drawn as a function of the armature current which replaces  $F_{fm} = F_{adm}$ . At  $I = 1.0$  and neglecting saturation, the per-unit  $E_{ad}$  is given by

$$E_{ad} = X_{ad} I = X_{ad}$$

Therefore, as is shown in Fig. 57-8,

$$E_f = E_{ad} = X_{ad}$$

corresponds on the open-circuit characteristic to  $I_R = 1.0$ . Thus, the condition arising at the end of self-excitation corresponds to point  $A$  where the  $E_{rd} = (X_C - X_\sigma) I$  and  $E_{ad} = f(I)$  curves intersect and where  $E_{rd} = E_{ad}$ . The corresponding armature voltage

$$V = E_{rd} + X_\sigma I$$

is represented by the corner  $C$  of the short-circuit triangle with its side  $BC$  drawn on the armature current scale. On expressing  $E_{ad}$  at point  $A$  in terms of the current and saturated  $d$ -axis inductive reactance

$$E_{ad} = X_{ad,s} I$$

where  $X_{ad,s} < X_{ad}$ , it can be seen that

$$\begin{aligned}E_{ad} + X_\sigma I &= X_C I \\ X_{ad,s} + X_\sigma &= X_C \\ X_{d,s} &= X_C\end{aligned}$$

This implies that in a steady state a voltage resonance occurs as an outcome of saturation in the magnetic circuit. The linear part of the  $E_{ad} = f(I)$  curve is described by the equation  $E_{ad} = X_{ad}I$ . Therefore, the  $E_{rd} = (X_c - X_\sigma)I$  and  $E_{ad} = f(I)$  curves can intersect at point  $A$  only when  $X_{ad} \geq X_c - X_\sigma$  or  $X_d \geq X_c$ , which checks with Eq. (57-7). When  $X_d < X_c$ , the two curves can intersect only at point  $O$  where  $I = 0$ ,  $V = 0$ , and no self-excitation can take place. If  $X_c \geq X_q$ , the armature voltage that exists after self-excitation will rise as  $X_c$  is decreased.

The risk of self-excitation in the case of synchronous generators supplying capacitive loads complicates the operation of electrical systems and impairs the strength of the insulation in the generators and the machines or devices they feed. In practice, self-excitation may take place, if a synchronous generator is connected via a transformer to a sufficiently long, open-circuited transmission line whose reactance is capacitive in its behaviour,  $X_L = -X_c$ .

In designing an electric station and a transmission line, care is always taken to make the  $d$ -axis inductive reactance of the generator smaller than the capacitive reactance of the line, with allowance for a transformer,

$$X_d < X_c$$

This will ordinarily rule out the likelihood of self-excitation due to a rise in the line voltage.

Self-excitation may as well take place in the case of a resistive-capacitive load,

$$Z_L = R_L - jX_c$$

if the total resistance of the armature circuit

$$R_\Sigma = R + R_L$$

is sufficiently small. In order to see how large this resistance should be, let us turn to the equations (55-14) and the diagram, Fig. 57-9, of an unsaturated, salient-pole machine. It is assumed that  $R = 0$  and  $X_d > X_c > X_q$ . Obviously, self-excitation will lead to  $\dot{V} = (R_L - jX_c)\dot{I}$  only if the armature current,  $\dot{I} = \dot{I}_d + \dot{I}_q$ , gives rise to an emf

$$\dot{E}_a = \dot{E}_{ad} + \dot{E}_{aq} = -jX_{ad}\dot{I}_d - jX_{aq}\dot{I}_q$$

which is equal to the required mutual emf

$$\dot{E}_r = \dot{V} + jX_\sigma \dot{I} = [R_L - j(X_C - X_\sigma)] \dot{I}$$

that is, if  $\dot{E}_a = \dot{E}_r$ .

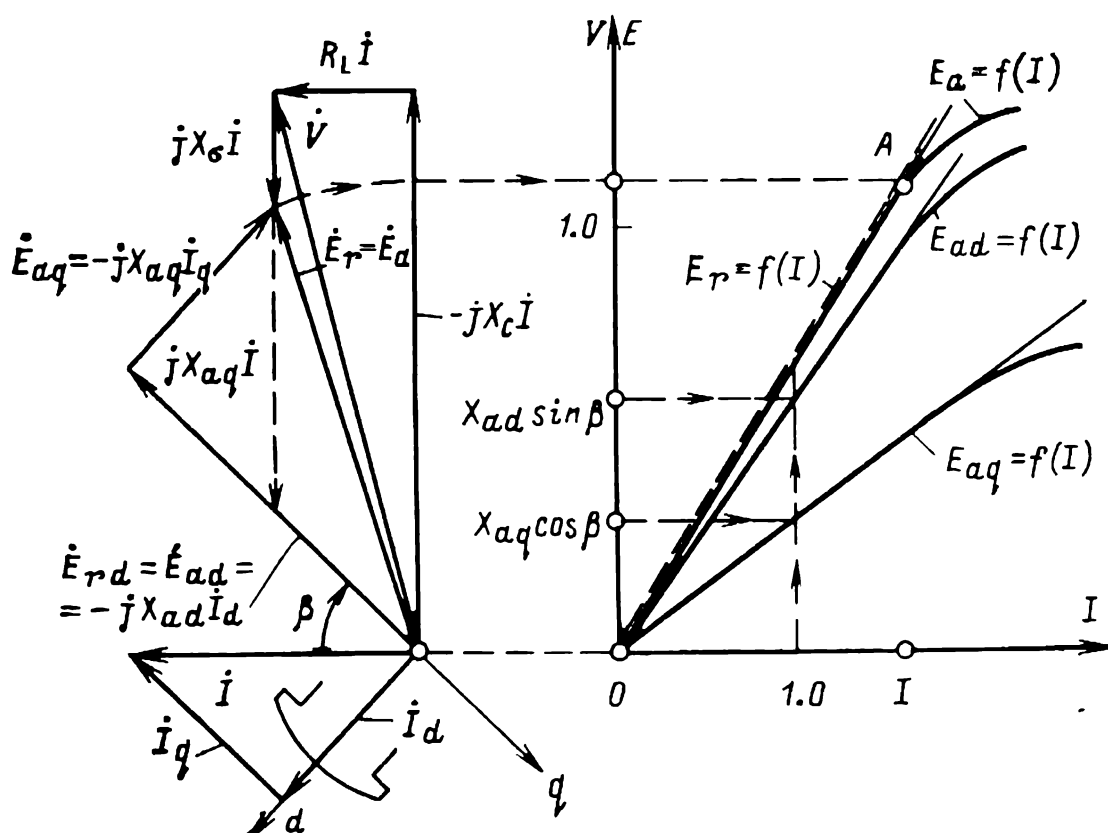


Fig. 57-9 Conditions for self-excitation in the case of a resistive-capacitive load

Using Eq. (55-15) and finding  $\cos \beta$  and  $\sin \beta$  from the specified load resistance and reactance:

$$\cos \beta = \frac{R_L}{\sqrt{(X_C - X_q)^2 + R_L^2}}$$

$$\sin \beta = \frac{X_q - X_C}{\sqrt{(X_C - X_q)^2 + R_L^2}} < 0$$

the equality  $\dot{E}_r = \dot{E}_a$  may be re-written in scalar form as  $E_r = E_a$ , where

$$E_r = I \sqrt{(X_C - X_\sigma)^2 + R_L^2}$$

$$E_a = \sqrt{E_{ad}^2 + E_{aq}^2} = I \sqrt{X_{ad}^2 \sin^2 \beta + X_{aq}^2 \cos^2 \beta}$$

or

$$(X_C - X_\sigma)^2 + R_L^2 = \frac{X_{ad}^2 (X_C - X_q)^2 + X_{aq}^2 R_L^2}{(X_C - X_q)^2 + R_L^2}$$

On solving the last equation for  $R_L$ , we find that self-excitation can occur at

$$R_L = \sqrt{(X_d - X_C)(X_C - X_q)} \quad (57-8)$$

From an analysis of Eq. (57-8) it follows that at  $X_C = X_d$  or  $X_C = X_q$ , self-excitation can take place only in the case of a purely capacitive load, that is, when  $R_L = 0$ . At  $X_C > X_d$  and  $X_C < X_q$ , a real resistance at which self-excitation could occur simply does not exist. At  $X_C = (X_d + X_q)/2$ , self-excitation will occur at the highest value of resistance equal to  $R_L = (X_d - X_q)/2$ .

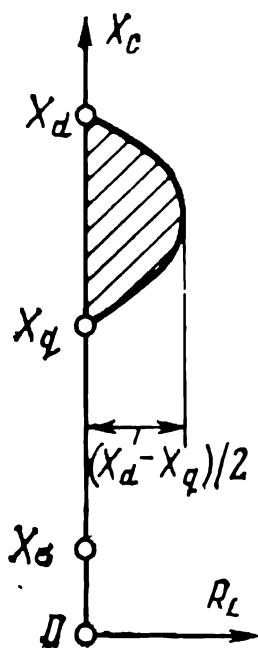


**Fig. 57-10** Conditions for capacitive self-excitation (the shaded area of  $X_C$  and  $R_L$  indicates where self-excitation is possible)

A plot of  $R_L$  as a function of  $X_C$  appears in Fig. 57-10. The values of voltage that exist at the value of  $R_L$  and  $X_C$  lying on the  $R_L = f(X_C)$  curve may be found graphically. For each combination of  $R_L$  and  $X_C$  corresponding to a particular value of  $\beta$ , the  $E_a = f(I)$  and  $E_r = f(I)$  curves

coincide over the entire length of the linear part of the  $E_a$  curve (see Fig. 57-9). Therefore, self-excitation results in  $E_a$  and  $E_r$  at point A corresponding to the onset of saturation. Obviously, at  $X_d > X_C > X_q$ , self-excitation can take place not only at the value of  $R_L$  given by Eq. (57-8), but also at  $R_L = 0$  and any values of  $R_L \leq \sqrt{(X_d - X_C)(X_C - X_q)}$ , that is, at values of  $R_L$  falling within the shaded area in Fig. 57-10. The values of armature voltage that exist when self-excitation occurs at such values of  $R_L$  lie between the voltage found from Fig. 57-8 for  $R_L = 0$  and the voltage found from Fig. 57-9 at  $R_L = f(X_C)$ .

## 58 Parallel Operation of Synchronous Machines

### 58-1 Parallel Operation of Synchronous Generators in an Electric System

Mechanical energy is converted to electricity predominantly by synchronous machines. In the Soviet Union, about 85% of the total comes from the steam-turbine generators installed at fuel-fired stations, about 15% by hydro-electric

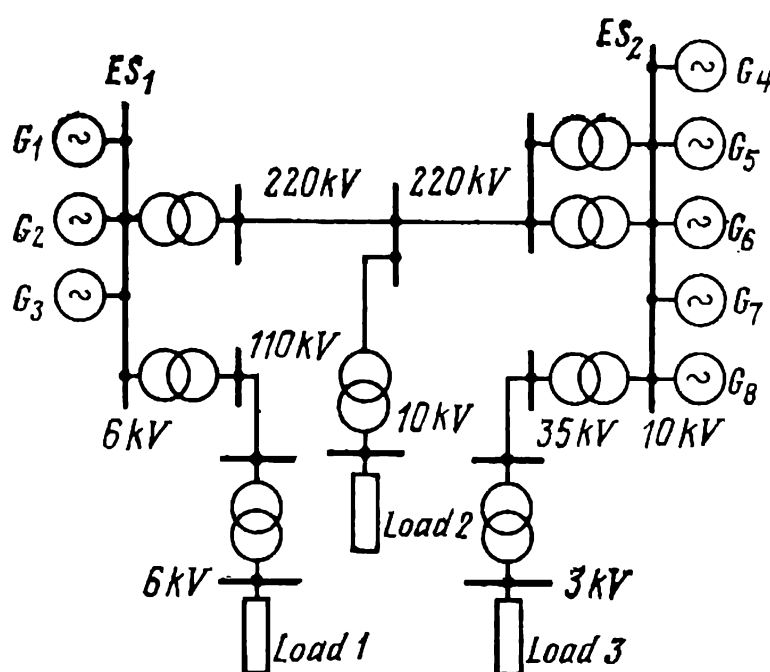


**Fig. 58-1** Single-line diagram of a simple electric system

generators, and a few per cent by the steam-turbine generators operating at nuclear power stations.

The bulk of the electric supply is produced by synchronous generators connected in parallel and feeding a common load.

A single-line diagram of a three-phase electrical system containing paralleled synchronous generators and paralleled loads is shown in Fig. 58-1. As is seen, the system has several electric stations ( $ES_1$ ,  $ES_2$ , . . .) with several generators installed at each ( $G_1$ ,  $G_2$ , . . .). The three-phase stator windings of the generators are connected in parallel to common buses. Remote stations are interconnected for parallel operation by means of transmission lines and three-phase transformers with which the voltage level can be

varied at will. The transmission lines on tappings from them supply power to the loads ( $L_1, L_2, \dots$ ) connected in the system.

Most often, the loads are various a.c. motors, heating appliances, lighting fixtures, and a.c./d.c. converters supplying systems that operate on d. c. All the loads are connected in parallel and add up to resistive-inductive impedances inserted at various nodes of the electric system. Because the paralleled generators are interconnected electrically or via transformers, their voltages alternate at the same frequency

$$f_1 = f_2 = f_3 = \dots = f$$

Their rotors, too, rotate at the same electrical angular velocity

$$\omega_1 = \omega_2 = \omega_3 = \dots = \omega = 2\pi f$$

whereas their mechanical angular velocities are inversely proportional to the number of pair poles in the generators

$$\Omega_1 = \omega/p_1, \quad \Omega_2 = \omega/p_2, \quad \Omega_3 = \omega/p_3 \dots$$

For this reason, the paralleled generators are said to be operating *in step* or *synchronism* with one another, and the procedure of bringing the machines into parallel operation (putting them on line) is called *synchronizing* or *synchronization* (see Chap. 59).

To secure reliable and economic operation of power systems, it is usual to group individual stations into what are usually referred to as power pools or interconnections, each with up to several hundred large generators totalling between them 10 million kW or even more. In the Soviet Union, there are tens of power interconnections of such caliber. Most frequently, power pools are grouped into still larger entities, known as interconnected power systems or grids (or grid systems). This is true of most industrially developed countries of the world, and the tendency has of late been to scale up the interconnections and grids still more.

As already noted, power service from interconnections and grids is more reliable than it would be from individual generators each supplying an isolated load. With the generators connected in parallel, an electric station can remove any one generator from service for maintenance without interrupting power supply to its loads. Another advantage

of interconnections is that they can pool power from stations using different sources of energy—fossil fuel, falling water, fissile or fissionable elements. A third advantage is that the installed capacity at any one station can be reduced to a reasonable and more manageable size, and the demand, however fluctuating it may be (from day to day, from season to season, and over a year), can be met more flexibly, because the peak loads on the constituent stations will be staggered in time.

The running of power pools and, even more so, power grids or supergrids, each incorporating a large number of stations, substations, power transmission lines, and loads, is a formidable task. No matter how the load may vary, the system frequency and voltage level must be maintained at their optimal values. Each pool, grid and, even supergrid is run from a control centre operated by a team of dispatchers who send out commands to put a generator (or generators) on line, or to remove them from service, as the case may be, to increase or decrease the generation of active and reactive power, etc.

As is seen, control of a power system reduces essentially to the control of the individual synchronous generators operating into (or, rather, in parallel with) an electric system. Therefore, a major topic in a course on electric machines is the behaviour of an individual synchronous machine when it is operating in parallel with an electric system.

If a system has a sufficiently large capacity in comparison with the machine of interest, the system power can be deemed infinitely large and treated as what is known as an infinite bus. This implies that, whatever variations in the operating conditions of the machine (changes in the armature current and output power), the system frequency,  $f_s$ , and the peak value of the system voltage,  $V_s$ , will remain constant, because they will be maintained by the other units. By the same token, when  $f_s$  or  $V_s$  is controlled via the remaining generators, the effect of a given generator may safely be neglected. Any change in performance of the generator can be assessed from changes in system voltage at its terminals.



## 58-2 Bringing in a Generator for Parallel Operation

The connection of a three-phase synchronous generator,  $G$ , for parallel operation with a system is shown in Fig. 58-2. For simplicity, the system is shown to contain one equivalent 2-pole synchronous generator of an infinitely large capacity,  $G_s$ , supplying a system load and the incoming generator is represented by its 2-pole model.

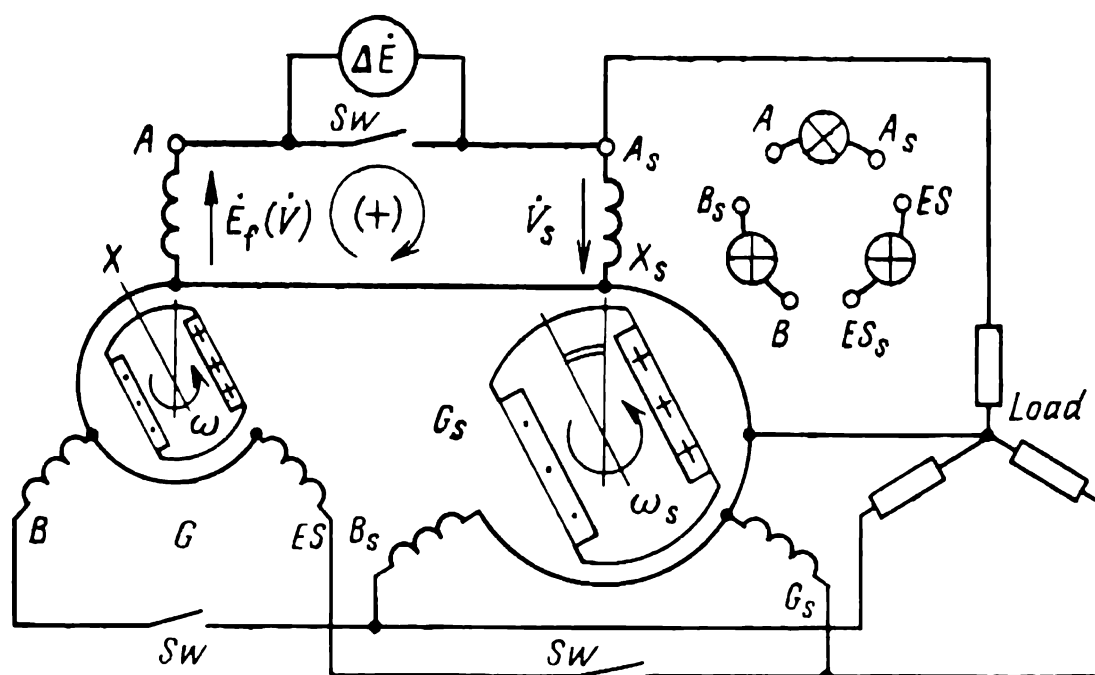


Fig. 58-2 Connection of a synchronous generator for parallel operation with a system containing  $G_s$  and  $Load$

Let the positive direction of  $\dot{V}_s$  in the generator-system loop be from the start  $A_s$  to the finish  $X_s$  of its phase. The positive direction of the emf and current in the  $A_s$ - $X_s$ - $X$ - $A$  loop formed by the like phases of  $G_s$  and  $G$  is chosen to be the same as the direction of  $\dot{V}_s$  and is shown in the figure by an arrow. Then  $\dot{E}_f$  (or  $\dot{V}$ ) supplied by  $G$  will be positive, when it is directed from  $X$  to  $A$ , as shown in Fig. 58-2. With the switch (usually a circuit-breaker)  $Sw$  open,  $G$  is running on an open circuit, and the emf existing between the phase contacts of the switch is

$$\Delta \dot{E} = \dot{E}_f + \dot{V}_s \quad (58-1)$$

which is a function of  $\dot{E}_f$  and of its phase relative to  $\dot{V}_s$ , given by the angle  $\alpha$  in Fig. 58-3. If, before the generator  $G$

is to be put on line, its angular velocity  $\Omega$  and its field current  $I_f$  are chosen such that

$$\omega = 2\pi f = \Omega/p = \omega_s = 2\pi f_s$$

or, in words, the generator frequency is the same as the system frequency, and the generator emf  $E_f$  is equal to the

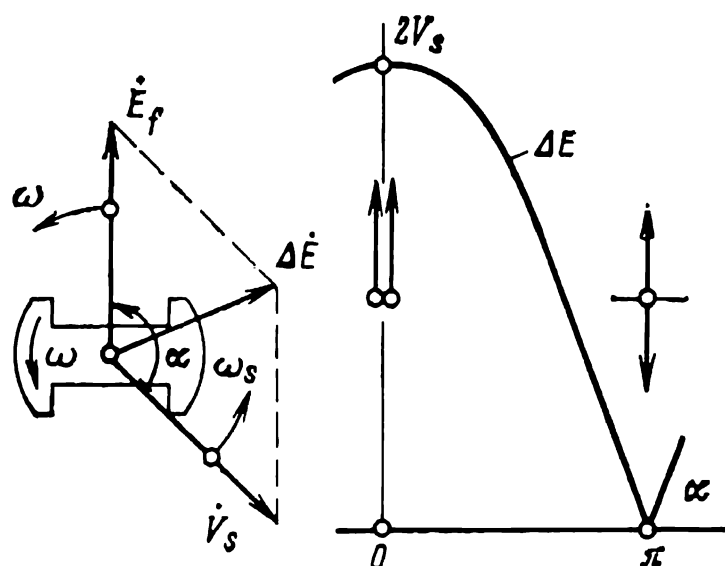


Fig. 58-3 Exact synchronization

system voltage  $V_s$ , the emf across the switch contacts can be found from an equation of the form

$$\Delta E = 2V_s | \cos \alpha/2 |$$

As  $\alpha$  is varied,  $\Delta E$  may take on any values from zero to  $2V_s$  (see Fig. 58-3).

The conditions most favourable for the generator to be put on line are when  $\alpha = \pi$ , because then  $\Delta \dot{E} = 0$ ,  $\dot{E}_f = -\dot{V}_s$ , and no transient (or circulating) currents are flowing in the armature winding. After the generator has been put on line, its armature current will remain zero, and the generator will keep running on an open circuit ( $I = 0$ ). This manner of putting a generator on line is called *exact synchronization* (for more detail, refer to Chap. 59).

Now let us see what will happen if we fail to satisfy the conditions for exact synchronization

$$f = f_s, E_f = V_s, \dot{E}_f = -\dot{V}_s, \alpha = \pi \quad (58-2)$$

with regard to the angle  $\alpha$ .

Neglecting iron saturation and saliency, the armature current,  $\dot{I}$ , can be found by Eq. (55-2) and the equivalent

circuit in Fig. 55-1 re-drawn for parallel operation in Fig. 58-4. The value of  $\dot{I}$  is limited by  $X_1$ , the armature inductive reactance, and lags behind the resultant emf,  $\Delta\dot{E} = \dot{E}_f + \dot{V}_s$ , existing in the generator-system loop, by an angle  $\pi/2$ :

$$\dot{I} = \Delta\dot{E}/jX_1 = (\dot{E}_f + \dot{V}_s)/jX_1 \quad (58-3)$$

The emf,  $-jX_1\dot{I}$ , induced by this current affects the terminal voltage, so that instead of  $E_f$  we have

$$\dot{V} = \dot{E}_f - jX_1\dot{I} = -\dot{V}_s \quad (58-4)$$

As is seen,  $\dot{I}$  acts to equalize the generator voltage and the system voltage,  $V = V_s$ , and causes the generator voltage to be directed in opposition to the system voltage.

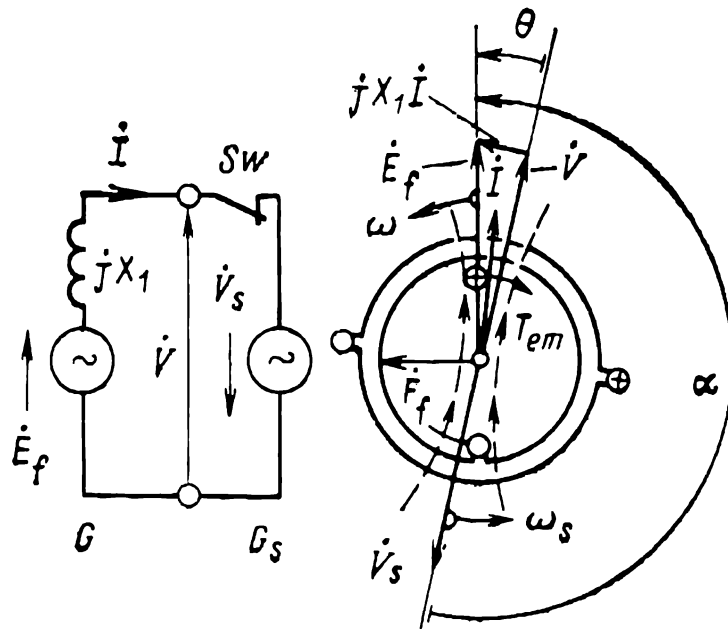


Fig. 58-4 Production of a synchronizing torque

A voltage phasor diagram for values of  $\alpha$  appreciably larger than  $\pi$  is constructed in Fig. 58-4. The diagram also shows the angle  $\theta$  between  $\dot{V}$  and  $\dot{E}_f$ , which is related to the angle  $\alpha$ ,  $\theta = \alpha - \pi$  and is taken to be positive, if  $\dot{E}_f$  leads  $\dot{V}$ . At small positive value of  $\theta$ , that is, when  $\pi \gg \theta > 0$ , the armature current given by Eq. (58-3) is practically in line with  $E_f$ . Its magnitude is proportional to the angle  $\theta$ :

$$I = \frac{|\dot{E}_f + \dot{V}_s|}{X_1} \approx \frac{2E_f \sin \theta/2}{X_1} \approx (E_f/X_1) \theta$$

Figure 58-4 shows (by dashed curves) the field set up by  $I$ . The interaction of this field with the rotor field current  $I_f$  giving rise to  $F_f$ , produces an electromagnetic torque,  $T_{em}$ , which acts on the rotor in opposition to its direction of rotation. Because  $T_{ext}$  is balanced by the friction and windage torque and the core loss torque,  $T_{em}$  is left unbalanced, and it causes the rotor to slow down

$$d\Omega/dt = - |T_{em}| / J$$

As a result, the electrical angular velocity of the rotor,  $\omega = \Omega p$ , becomes smaller than  $\omega_s$ , and this leads to a decrease in  $\theta$ ,  $I$ , and  $T_{em}$ , and to the recovery of open-circuit conditions. At  $\theta < 0$ , the current phase is reversed, the torque changes sign, the angular velocity of the rotor goes up, and open-circuit conditions are again restored at  $\theta = 0$ ,  $I = 0$ , and  $T_{em} = 0$ . Any departure from synchronism ( $\omega \neq \omega_s$ ) likewise leads to a mismatch between the phasors  $\dot{E}_f$  and  $\dot{V}$  (or  $\dot{V}_s$ ), the angle  $\theta$  is no longer equal to zero, and there appears an electromagnetic torque,  $T_{em}$ , which restores synchronism. This is the reason why it is called the *synchronizing torque* in parallel operation. It keeps the rotor in synchronism after the generator has been put on line. As will be shown, this torque maintains synchronism in operation on load as well.

### 58-3 Control of Load on a Synchronous Generator Connected to an Infinite Bus

The operating conditions of a synchronous generator connected to an infinite bus, that is, a large-capacity system for which a constant  $f_s$ , and a constant  $V_s$  may be assumed, depend on its total power  $S$  in comparison with the total power,  $S + S_s$ , of all the paralleled generators supplying a common load ( $S_s$  is the total power of the remaining generators in the system). As its per-unit power,  $S_* = S / (S + S_s)$ , increases, variations in its operating conditions have a progressively stronger effect on the system frequency,  $f_s$ , and the system voltage,  $V_s$ .

Connections of a generator to load for two limiting values of its per-unit total power are shown in Figs. 58-5 and 58-6. In Fig. 58-5, the synchronous generator is the only system generator ( $S_s = 0$ ), and its per-unit total power is  $S_* = S/S = 1$ . Now, it is in effect supplying an isolated load,

$Z_L = R_L + jX_L$ , so the frequency

$$f = p\Omega/2\pi$$

and the voltage (at a given load impedance) are solely decided by the power supplied by the prime mover (a turbine),

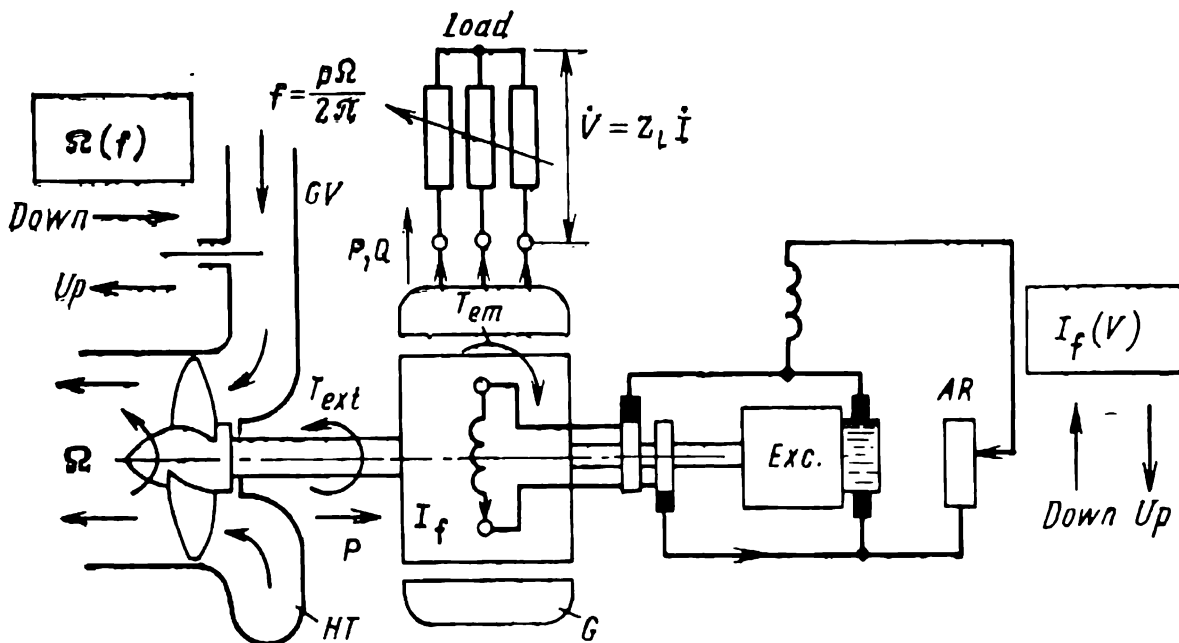


Fig. 58-5 Control of a hydro-electric generating unit serving an isolated load:

*HT*—hydraulic turbine; *G*—generator; *Exc*—exciter; *AR*—adjusting rheostat in the excitation system; *GV*—guide vanes of the turbine

in turn dependent on the opening of the guide vanes, *GV*, and the field current dependent on the setting of the adjusting rheostat, *AR*.

In Fig. 58-6, the generator in question has a power output which is negligibly small in comparison with the infinitely large power of the remaining generators in the system. Therefore, changes in the operating conditions of the generator have no effect on the system frequency,  $f_s$ , and the system voltage,  $V_s$ . The angular velocity of its rotor in all forms of synchronous operation remains the same:

$$\Omega = 2\pi f_s/p$$

In the circumstances, any change in the settings of the controls of the turbine and the generator will result in a change in the active and reactive power delivered to the system. An increase in the opening of the guide vanes, *GV*, will lead to an increase in the prime mover's torque,  $T_{ext}$ , in the active power of the synchronous machine,  $P = T_{ext} \Omega$ , and in the active component of armature current,  $I_a = P/3V_s$ . An

increase in  $I_f$  will be accompanied by an increase in the reactive component of armature current,  $I_r$ , and in the reactive power delivered to the system,  $Q = 3V_s I_r$ .

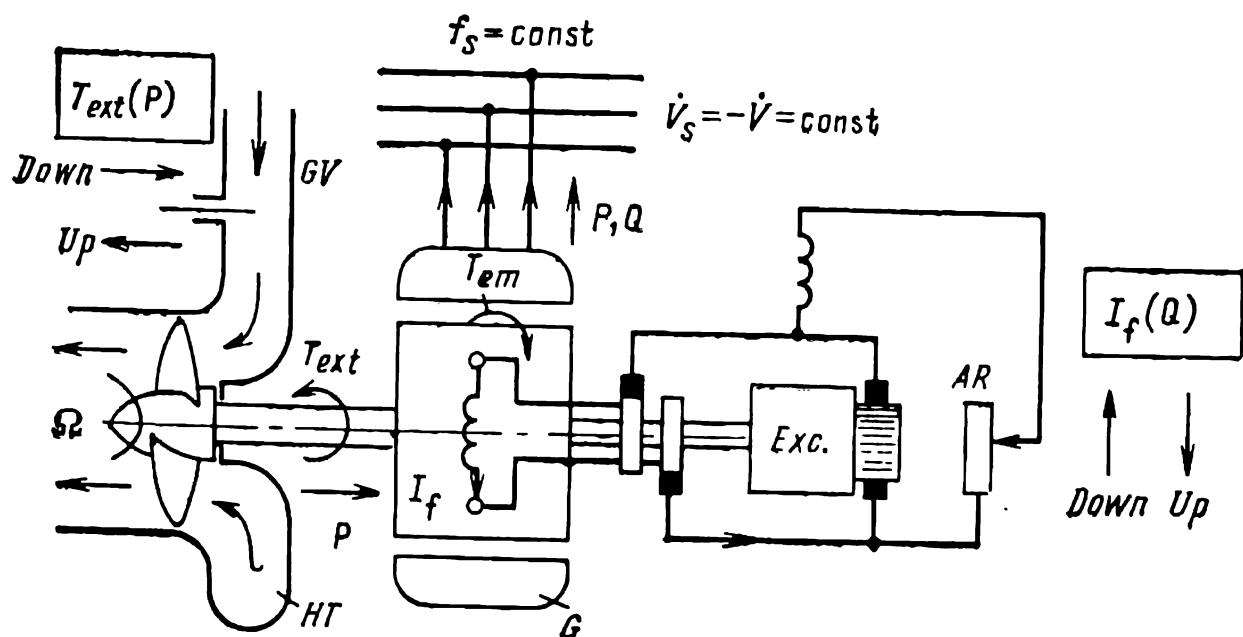


Fig. 58-6 Control of load on a hydro-electric generating unit operating in parallel with an electric system (see the legend to Fig. 58-5)

In the intermediate cases, where the per-unit total power of the generating unit ranges between zero and unity, changes in the settings of the controls (the guide vanes and the adjusting rheostat) will lead to simultaneous changes not only in the active and reactive power, but also in  $f_s$  and  $V_s$ .

**58-4 Active and Reactive Power of a Synchronous Machine Connected to an Infinite Bus**

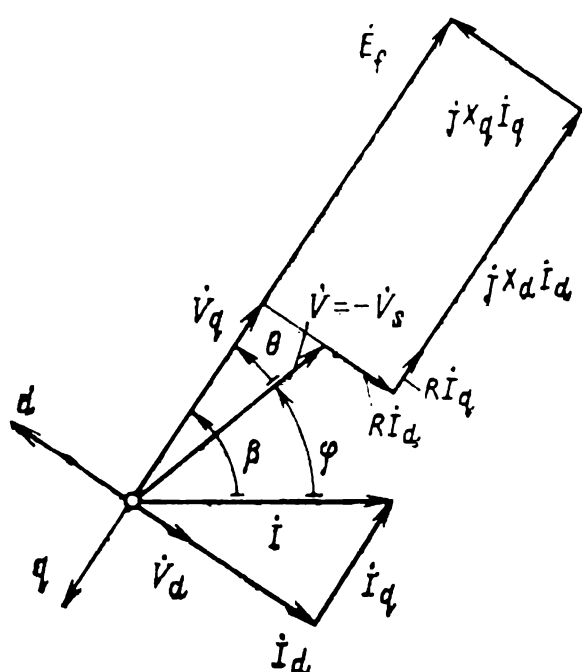
Let us take a closer look at the factors that affect the active and reactive power of a salient-pole synchronous machine connected to an infinite bus, that is, as before, a large-capacity system for which constant frequency,  $f_s$ , and constant voltage,  $V_s$ , may be assumed.

The two powers are functions of the armature current  $I$ , and the phase angle between  $I$  and the generator voltage,  $\dot{V} = -\dot{V}_s$ ,

$$\begin{aligned} P &= m_1 V I \cos \varphi \\ Q &= m_1 V I \sin \varphi \end{aligned} \tag{58-5}$$

In turn,  $\dot{I}$  is a function of  $\dot{I}_f$  and the spatial position of the rotor relative to  $V_s$ , defined by the angle  $\theta$  between the  $\dot{V}_s$  phasor and the  $q$ -axis.

In an unsaturated synchronous machine,  $\dot{I}$  is determined by  $\dot{V} = -\dot{V}_s$ ,  $\dot{E}_f$ , and the phase angle  $\theta$  between them (with  $E_f$  aligned with the negative direction of the  $q$ -axis). On



open circuit,  $\theta = 0$ . Under the action of an external torque,  $T_{\text{ext}}$ , the rotor takes up a position, or angle  $\theta$ , at which  $T_{\text{em}}$  balances  $T_{\text{ext}}$ . Therefore, a study into the transients associated with parallel operation can markedly be simplified, if we express the active and reactive powers as functions of  $V = V_s$ ,  $E_f$ , and  $\theta$ :

$$P = f(V, E_f, \theta)$$

$$Q = f(V, E_f, \theta)$$

Fig. 58-7 Active and reactive powers expressed in terms of  $V$ ,  $E_f$ , and  $\theta$

To begin with, let us consider the active power. Noting that  $\varphi = \beta - \theta$ , we can write  $P$  defined by Eq. (58-5) as a function of  $\theta$ ,  $I_d$  and  $I_q$  as

$$P = m_1 V I \cos(\beta - \theta) = m_1 V (I_q \cos \theta + I_d \sin \theta) \quad (58-6)$$

Expressions for  $I_d$  and  $I_q$  in terms of  $V$ ,  $E_f$  and  $\theta$  can be derived from the phasor diagram drawn in Fig. 58-7 for an unsaturated, salient-pole synchronous generator connected to an infinite bus ( $\dot{V}_s = -\dot{V} = \text{constant}$ ). The diagram has been plotted for a current lagging behind the voltage by an angle  $\pi/2$ . Assuming the positive directions of  $I_d$  and  $I_q$  along the  $d$ - and  $q$ -axis, respectively, the projections of  $V$  on these directions can be written

$$V \sin \theta = X_q I_q - R I_d$$

$$V \cos \theta = E_f - X_d I_d - R I_q$$

Solving the above equations simultaneously, we get

$$I_q = \frac{V [\varepsilon R + (X_d \sin \theta - R \cos \theta)]}{X_d X_q + R^2} \quad (58-7)$$

$$I_d = \frac{V [\varepsilon X_q - (X_q \cos \theta + R \sin \theta)]}{X_d X_q + R^2} \quad (58-8)$$

where  $\varepsilon = E_f/V$  is the excitation ratio.

Substituting Eq. (58-7) and Eq. (58-8) into Eq. (58-6) gives a general expression for active power

$$P = P' + P'' \quad (58-9)$$

where

$$P' = \frac{m_1 V^2 \varepsilon (X_q \sin \theta + R \cos \theta)}{(X_d X_q + R^2)}$$

$$P'' = \frac{m_1 V^2 (X_d - X_q)}{2 (X_d X_q + R^2)} \sin 2\theta$$

The component  $P'$  arises when the saturation factor,  $\varepsilon$ , is nonzero. So it is the power that would additionally be delivered to the line at  $V$  at a nonzero  $\varepsilon$ .

The component  $P''$  arises from the interaction of an unexcited salient-pole rotor with the currents that are produced in the armature winding due to  $V$ . These currents can be found from Eqs. (58-7) and (58-8) at  $\varepsilon = 0$ . So it would be developed owing to saliency ( $X_d \neq X_q$ ) by a synchronous machine connected to a line with  $V$  at a given angle  $\theta$ , if it were unexcited ( $\varepsilon = 0$ ), because then  $P'$  would be zero. In a nonsalient-pole machine,  $X_d = X_q = X_1$ , and  $P''$  is nonexistent.

It is worth while noting that  $R$  needs to be accounted for only in the design of fractional-hp machines where it plays an important role. In large machines, it is legitimate to put  $R = 0$ , because the armature winding has a negligibly small resistance ( $R \ll X_q < X_d$ ). Then,

$$P = P' + P'' = P_{em} = T_{em} \Omega \quad (58-10)$$

where

$$P' = \frac{m_1 V^2 \varepsilon \sin \theta}{X_d}$$

$$P'' = \frac{m_1 V^2}{2} (1/X_q - 1/X_d) \sin 2\theta$$



in a salient-pole machine, and

$$P = P' = \frac{m_1 V^2 \epsilon \sin \theta}{X_1}$$

in a nonsalient-pole machine.

Taking  $S_R$  as the base quantity, we may re-write the equation of active power on a per-unit basis. For example, at  $R = 0$ ,

$$P_* = \frac{V_* E_{*f} \sin \theta}{X_{*d}} + \frac{V_*^2}{2} (1/X_{*q} - 1/X_{*d}) \sin 2\theta$$

The reactive power defined by Eq. (58-5) can be re-written in a similar manner. Since  $\varphi = \beta - \theta$ , it may likewise be presented as a function of  $\theta$ ,  $I_d$  and  $I_q$

$$Q = m_1 V I \sin (\beta - \theta) = m_1 V (I_d \cos \theta - I_q \sin \theta)$$

Then, using Eqs. (58-7) and (58-8), we can write it in a form more convenient for a study into parallel operation

$$Q = \frac{m_1 V^2}{X_d X_q + R^2} [\epsilon (X_q \cos \theta - R \sin \theta) - X_q \cos^2 \theta - X_d \sin^2 \theta] \quad (58-11)$$

At  $R = 0$ , the components of the reactive power,

$$Q = Q_d + Q_q \quad (58-12)$$

can be written in a simpler form, namely

$$Q_d = Q'_d + Q''_d = m_1 I_d (V \cos \theta)$$

where

$$Q'_d = (m_1 E_f / X_d) V \cos \theta$$

$$Q''_d = -m_1 (V \cos \theta)^2 / X_d$$

and

$$Q_q = -m_1 I_q V \sin \theta = -m_1 (V \sin \theta)^2 / X_q$$

The  $d$ -axis reactive power,  $Q_d$ , is associated with the  $d$ -axis current

$$I_d = (E_f - V \cos \theta) / X_d$$

and the  $q$ -axis voltage,

$$V_q = V \sin \theta$$

It is the sum of two terms, namely:

(1) reactive power

$$Q''_d = m_1 (-V \cos \theta / X_d) V \cos \theta < 0$$

drawn by an unexcited synchronous machine in order to set up the  $d$ -axis armature field at  $V_q = V \cos \theta$  and  $I_{d(V)} = -V \cos \theta / X_d$  which leads  $\dot{V}_q$  by  $90^\circ$ ; and

(2) reactive power

$$Q'_d = m_1 (E_f / X_d) V \cos \theta > 0$$

generated owing to the excitation supplied by the additional  $d$ -axis current,  $I_{d(sc)} = E_f / X_d$ , equal to the short-circuit current at  $\dot{E}_f$  and lagging behind  $\dot{V}_q$  (and  $\dot{E}_f$ ) by  $90^\circ$ .

The  $q$ -axis reactive power,  $Q_q$ , is drawn by a machine to set up the  $q$ -axis field at  $V_d = V \sin \theta$  and  $I_q = -V \sin \theta / X_q$ , which leads  $\dot{V}_d$  by  $90^\circ$ .

$Q_d$  is positive at a level of excitation such that

$$\begin{aligned} E_f - V \cos \theta &> 0 \\ \beta &> 0 \end{aligned}$$

and  $I_d$  is in quadrature lagging with  $V_q = V \cos \theta$ . In contrast,  $Q_d$  is negative at a level of excitation such that

$$\begin{aligned} E_f - V \cos \theta &< 0 \\ \beta &< 0 \end{aligned}$$

and  $I_d$  is in quadrature leading with  $V_q$ .

The  $q$ -axis reactive power is negative always.

On a per-unit basis and at  $R = 0$ , the reactive power may be written

$$Q_* = \frac{V_* E_{*f} \cos \theta}{X_{*d}} - \frac{(V_* \cos \theta)^2}{X_{*d}} - \frac{(V_* \sin \theta)^2}{X_{*q}}$$

### 58-5 Electromagnetic Power and Electromagnetic Torque of a Synchronous Machine Connected to an Infinite Bus

In accord with Eq. (56-13), the electromagnetic torque and electromagnetic power of a salient-pole synchronous machine may be written each as a sum of two terms

$$T_{em} = T_{af} + T_{aa} \tag{58-13}$$

$$P_{em} = T_{em} \Omega = P_{af} + P_{aa}$$

where  $P_{af} = \Omega T_{af}$  and  $P_{aa} = \Omega T_{aa}$ .

As has been explained in Sec. 56-2,  $T_{af}$  results from the interaction of the armature field with the excitation field,

and  $T_{aa}$  is acting on an unexcited, salient-pole rotor in the field set up by the armature current. Using Eqs. (56-13), (54-35), (54-37), (58-7) and (58-8), the components  $P_{af}$  and  $P_{aa}$  can be expressed in terms of  $E_f$ ,  $V$  and  $\theta$  as:

$$P_{af} = T_{af}\Omega = m_1 E_f I_q = \frac{m_1 V^2 \varepsilon}{(X_d X_q + R^2)} [\varepsilon R + (X_d \sin \theta - R \cos \theta)] \quad (58-14)$$

$$\begin{aligned} P_{aa} &= T_{aa}\Omega = -m_1 I^2 R_a = m_1 I^2 \frac{X_q - X_d}{2} \sin 2\beta \\ &= m_1 (X_q - X_d) I_d I_q \\ &= \frac{m_1 V^2 (X_q - X_d)}{(X_d X_q + R^2)^2} [\varepsilon X_q - (X_q \cos \theta + R \sin \theta) \\ &\quad \times [\varepsilon R + (X_d \sin \theta - R \cos \theta)]] \end{aligned} \quad (58-15)$$

In the above equations, both  $P_{af}$  and  $P_{aa}$  are functions of the excitation factor,  $\varepsilon = E_f/V$ . In investigating parallel operation, it is convenient to write the electromagnetic power and the electromagnetic torque each as a sum of two terms, one of which ( $T'_{em}$  or  $P'_{em} = \Omega T'_{em}$ ) depends on  $\varepsilon$ , and the other ( $T''_{em}$  or  $P''_{em} = \Omega T''_{em}$ ) is independent of  $\varepsilon$ . Then,

$$P_{em} = P_{af} + P_{aa} = P'_{em} + P''_{em} \quad (58-16)$$

where

$$\begin{aligned} P''_{em} &= \Omega T''_{em} = P_{aa(\varepsilon=0)} \\ &= \frac{m_1 V^2 (X_d - X_q)}{(X_d X_q + R^2)^2} (X_d \sin \theta - R \cos \theta) (X_q \cos \theta + R \sin \theta) \end{aligned} \quad (58-17)$$

$$\begin{aligned} P'_{em} &= \Omega T'_{em} = P_{af} + P_{aa} - P_{aa(\varepsilon=0)} \\ &= \frac{m_1 V^2 \varepsilon}{(X_d X_q + R^2)^2} [(X_q^2 X_d + 2R^2 X_d - X_q R^2) \sin \theta \\ &\quad + R (X_q X_d - 2X_q^2 - R^2) \cos \theta + \varepsilon R (X_q^2 - R^2)] \end{aligned} \quad (58-18)$$

In Eq. (58-18),  $T'' = P''_{em}/\Omega$  is the electromagnetic torque that would be developed owing to saliency by an unexcited synchronous machine connected to a system with  $V = V_s$  at a power angle  $\theta$  corresponding to the excited state. In the same equation,  $T'_{em}$  is the additional electromagnetic torque that would be developed by an excited machine.

Where the winding resistance may be neglected, the electromagnetic power does not differ from the active power in Eq. (58-10), and its components do not differ from those of the active power

$$P_{em} = P, P'_{em} = P', P''_{em} = P''$$

### 58-6 Control of Active Power at Constant $V$ and $I_f$ . Power Angle Characteristic

The active power generated by a synchronous machine connected to an infinite bus is governed by  $T_{ext}$ , the external torque applied to the machine shaft, and its direction. In the steady state (with the rotor spinning at synchronous speed), the external torque is always balanced by an equal electromagnetic torque,  $T_{em} = f(V, E_f, \theta)$ , as given by Eq. (58-13) or (58-16), so that

$$T_{em} = T_{ext}$$

and the active power is

$$P = T_{em}\Omega$$

If  $P$  or  $T_{em}$  is varied so that  $I_f$  remains constant, then (neglecting saturation),  $E_f$  will likewise remain constant, and of all the quantities governing the operating conditions, only the power angle  $\theta$  will be varying.

The plot of  $P$  or  $T_{em}$  as a function of the power angle  $\theta$  for constant  $V_s$ ,  $f_s$ , and  $I_f$  (in an unsaturated machine,  $E_f$  is constant) is called the power versus power angle or torque versus power angle characteristic or curve of a synchronous machine.

The active power versus power-angle characteristic of a synchronous machine (with  $R = 0$  and neglecting saturation) appears in Fig. 58-8. When drawn to a different scale, it is

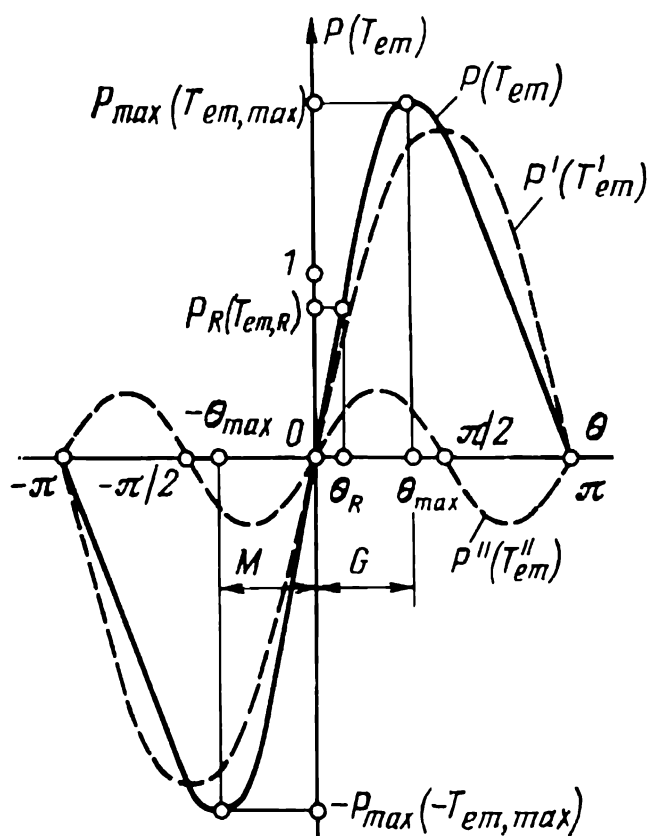


Fig. 58-8 Power/angle and torque/angle curves of a salient-pole synchronous machine ( $V_R = 1.0$ ,  $E_{f,R} = 1.77$ ,  $X_d = 1.0$ ,  $X_q = 0.6$ ,  $P_R = \cos \varphi_R = 0.8$ )

at the same time the torque versus power angle characteristic (an electromagnetic torque is meant). The characteristic is constructed, using Eq. (58-10), in which one of the components with a peak value

$$P' = (m_1 V E_f / X_d) = \text{constant}$$

is proportional to  $\sin \theta$ , and the other, with a peak value

$$P'' = (m_1 V^2 / 2) (1/X_q - 1/X_d) = \text{constant}$$

is proportional to  $\sin 2\theta$ . The second component exists only in a salient-pole machine, when  $X_d \neq X_q$ . The first component exists only in an excited machine, when  $E_f \neq 0$ . In a salient-pole machine, the first component gains in importance with an increase in the ratio of its peak value to the peak value of the second component:

$$n = P'/P'' = \frac{2E_f X_q}{V(X_d - X_q)} \quad (58-19)$$

The total active power is the sum of the above two components:

$$P = P' \sin \theta + P'' \sin 2\theta \quad (58-20)$$

On taking the derivative with respect to  $\theta$  and equating it to zero,

$$dP/d\theta = P' \cos \theta + 2P'' \cos 2\theta = 0$$

we can see that the power takes on an extremal value when

$$\theta_{\max} = \pm \arccos \frac{\sqrt{n^2 + 32} - n}{8} \quad (58-21)$$

where  $n$  is as defined by Eq. (58-19).

At  $\theta_{\max} > 0$ , the power is a positive maximum,  $P_{\max} > 0$ . At  $\theta_{\max} < 0$ , it is a negative maximum,  $P_{\max} < 0$ . In the former case, the machine is delivering active power to the system. In the latter, it is absorbing active power from the system.

The maximum power that a synchronous machine can deliver to, or absorb from, the system before it drops out of synchronism is called the *pull-out power*.

The pull-out power of a synchronous machine is given by

$$\begin{aligned} P_{\max} &= P' \sin \theta_{\max} + P'' \sin 2\theta_{\max} \\ &= P' \sin \theta_{\max} (1 + 2n \cos \theta_{\max}) \end{aligned} \quad (58-22)$$

For a nonsalient-pole machine,  $n = \infty$ ,  $\cos \theta_{\max} = 0$ ,  $\theta_{\max} = \pi/2$ ,  $\sin \theta_{\max} = 1$ , and

$$P_{\max} = P' = m_1 E_f V / X_d \quad (58-23)$$

In a salient-pole machine at  $I_{f,R}$ , the pull-out power is a few per cent higher than  $P'$ .

It follows from Eq. (58-23) that  $P_{\max}$  increases with an increase in  $I_f$  and with a decrease in  $X_d$  (see Sec. 54-5). Therefore, in designing a synchronous machine, its dimensions are chosen such that the pull-out power is substantially higher than the rated active power

$$P_R = S_R \cos \varphi_R = m_1 V_R (\cos \varphi_R) I_R$$

so that the generator could, if and when necessary, to operate on an overload.

The ratio of the pull-out power at rated terminal voltage and rated field current to the rated power gives what we shall call the steady-state power stability ratio (that is, one for a slowly rising external torque)

$$k_{\text{sspc}} = P_{\max,R} / P_R$$

It can be found (exactly for a nonsalient-pole generator and approximately for a salient-pole generator) by the equation

$$\begin{aligned} k_{\text{sspc}} &= P_{\max,R} / P_R = P'_R / P_R \\ &= E_{*f,R} / X_{*d} \cos \varphi_R \end{aligned} \quad (58-24)$$

where  $E_{*f,R} = E_{f,R} / V_R$  and  $X_{*d}$  are in per-unit.

Under a relevant USSR standard, the steady-state power stability ratio for turbogenerators is set at 1.7 as a minimum.

As with maximum power, the maximum torque that a synchronous machine can develop before it drops out of synchronism is called the pull-out torque.

The pull-out torque of a synchronous machine is proportional to the pull-out power

$$T_{\text{em,max}} = m_1 E_f V / \Omega X_d = P_{\max} / \Omega \quad (58-25)$$

At rated excitation, the pull-out torque is

$$T_{\max,R} = m_1 V_R E_{f,R} / \Omega X_d \quad (58-26)$$

For synchronous motors, it is convenient to use the concept of the *torque stability ratio* (identical to the steady-state

power stability ratio)

$$\begin{aligned} T_{em,max,R} / T_{em,R} &= P_{max,R} / P_R \\ &= E_{*f,R} / X_{*d} \cos \varphi_R \end{aligned}$$

Under a relevant USSR standard, the torque stability ratio for synchronous motors at a power factor of 0.9 must be at least 1.65.

**58-7      Stability in Parallel Operation**

The power angle  $\theta$  (also called as the torque angle or the displacement angle) is solely a function of  $T_{ext}$ , the external torque (see Fig. 58-8).

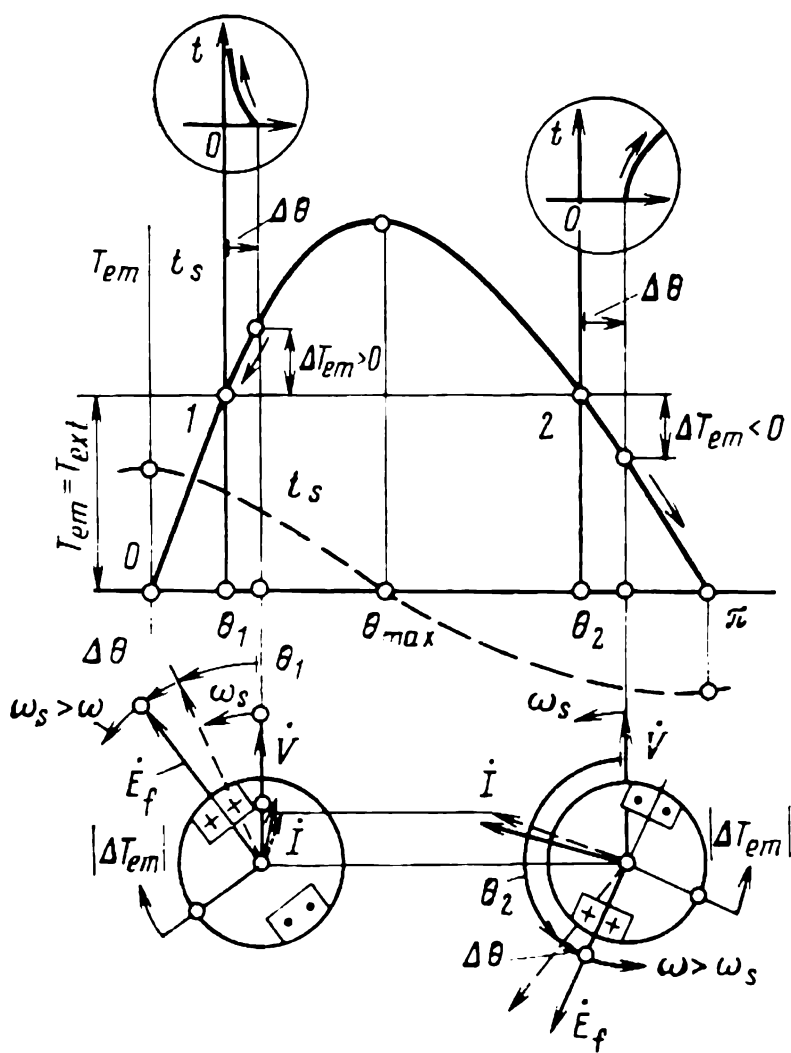


Fig. 58-9 Conditions for stability in parallel operation

As is seen from Fig. 58-9, the external torque may be balanced by the electromagnetic torque,  $T_{em}$ , at two values of  $\theta$ , namely  $\theta_1$  and  $\theta_2$ , which correspond to the intersections of the constant  $T_{ext}$  line with the torque-vs-power angle characteristic,  $T_{em} = f(\theta)$ , within one cycle of change (in the

range —  $\pi < \theta < \pi$ ). In Fig. 58-9, only the part of the characteristic corresponding to the generator mode of operation is shown.

At first glance, it may appear that the conditions at points 1 and 2 are identical. However, although  $T_{em}$  and  $P = T_{em}\Omega = m_1 VI \cos \varphi$  are the same in either case, there is a lot of difference in other respects. Because  $\theta$  at points 1 and 2 takes on different values (see Fig. 58-9), the armature current  $I$  at those points will have a different magnitude and a different phase angle, but its projections on  $I \cos \varphi$  will be the same. What is more important is that the departure of  $\theta$  from its value at points 1 and 2 produces opposite effects. An increase in  $\theta_1$  by  $\Delta\theta$  results in an increase in the electromagnetic torque, whereas an increase in  $\theta_2$  by  $\Delta\theta$  results in a decrease in the electromagnetic torque. Also, an increase in  $\theta_1$  leads to an increase, whereas an increase in  $\theta_2$ , to a decrease in the active component of current. At  $\theta_1$  and  $\theta_2$ , the emf  $E_f$  and the current  $I$  are shown by dashed lines; at the angles  $\theta + \Delta\theta$ , by full lines.

Because of the above differences, the operation at point 1 is stable, because the machine is capable of going back to a stable running (that is, in synchronism with the system) in spite of chance departures in the associated operating variables. In contrast, the operation at point 2 is unstable, because the machine is no longer capable of counteracting the departures in its operating variables.

Let us demonstrate that the operation at point 1 is stable. Suppose that some chance factors have caused  $\theta_1$  to increase by  $\Delta\theta$ , whereas  $T_{ext}$ ,  $V$ ,  $f_s$ , and  $I_f$  have all remained unchanged. Then the electromagnetic torque will be  $T_{em} + \Delta T_{em}$ , where

$$\Delta T_{em} = (\partial T_{em} / \partial \theta) \Delta \theta$$

is the positive change in the electromagnetic torque,  $\Delta T_{em} > 0$ . Obviously, this upsets the balance of torques that existed in the steady state and, as follows from the equation of motion for the rotor,

$$\begin{aligned} T_{ext} - (T_{em} + \Delta T_{em}) &= J d\Omega / dt \\ - \Delta T_{em} &= J d\Omega / dt \end{aligned} \quad (58-27)$$

the excess torque,  $\Delta T_{em}$ , which acts against the direction of rotation, gives rise to a negative acceleration, or deceleration.



ration, given by

$$d\Omega/dt = - \Delta T_{em}/J$$

As a result, the angular velocity of the rotor decreases

$$\Omega = \Omega_s + \int_0^t (d\Omega/dt) dt < \Omega_s$$

The angular velocity of the rotor, with  $\dot{E}_f$  acting along its  $q$ -axis, will likewise decrease, so that

$$\omega < \omega_s$$

Because  $\dot{V} = - \dot{V}_s$  rotates at  $\omega_s$ , a decrease in the angular velocity of  $\dot{E}_f$  leads to a gradual decrease in  $\theta = \theta_1 + \Delta\theta$ , until  $\theta$  becomes again equal to  $\theta_1$  and the machine settles to the previous synchronous condition at point 1 (a plot of  $\theta$  as a function of time is shown in Fig. 58-9).

Should  $\theta_1$ , by some chance, decrease by  $\Delta\theta$ , then  $\Delta T_{em}$  will be negative and, in accord with Eq. (58-27),  $d\Omega/dt$  will be positive. This implies that the angular velocity of the rotor in the model and  $\dot{E}_f$  will increase, and the angle  $\theta = \theta_1 - \Delta\theta$  will keep rising until it is again equal to  $\theta$ . Thus, the operation at point 1 and at all other points on the torque-vs-power angle characteristic in the range  $0 < \theta < \theta_{max}$  will be stable.

In contrast, the operation at point 2 and at all other points on the torque versus-power angle curve in the range  $\theta_{max} < \theta < \pi$  will be unstable. This can be demonstrated by considering the behaviour of the generator when, by some chance factor,  $\theta_2$  is incremented by  $\Delta\theta$ . Then,

$$\Delta T_{em} = (\partial T_{em}/\partial\theta) \Delta\theta < 0$$

because  $\partial T_{em}/\partial\theta < 0$ , and, in accord with Eq. (58-27),  $d\Omega/dt > 0$ . This implies that the angular velocity of the rotor in the model and  $\dot{E}_f$  will rise, and the angle  $\theta = \theta_2 + \Delta\theta$  will keep rising and departing from the original angle  $\theta_2$  more and more. Graphically, this is shown as a plot of  $\theta$  versus time in Fig. 58-9.

As follows from the above analysis, the operation of the machine is stable if at  $\Delta\theta > 0$  the rotor slows down, that is,  $d\Omega/dt < 0$ , and if at  $\Delta\theta < 0$ , the rotor picks up speed, that is,  $d\Omega/dt > 0$ .

On expressing in Eq. (58-27) the change in electromagnetic torque,  $\Delta T_{em}$ , in terms of the change in power angle,  $\Delta\theta$ ,

$$d\Omega/dt = - \Delta T_{em}/J = (\partial T_{em}/\partial\theta) \Delta\theta/J$$

we can see that  $d\Omega/dt$  and  $\Delta\theta$  take opposite signs, and the operation is stable at those points on the torque-versus-power-angle characteristic where the partial derivative of torque with respect to power angle is positive,

$$t_s = \partial T_{em}/\partial\theta > 0$$

Conversely, the operation will be unstable at those points where

$$t_s = \partial T_{em}/\partial\theta < 0$$

The partial derivative of electromagnetic torque with respect to power angle for constant  $V_s$ ,  $\omega_s$ , and  $I_f$  or  $E_f$  is called the *specific synchronizing torque*.

Referring to Eq. (58-10) and taking the partial derivative with respect to  $\theta$ , we find that the specific synchronizing torque is given by

$$\begin{aligned} t_s &= \partial T_{em}/\partial\theta = \partial P/\Omega \partial\theta \\ &= \frac{m_1 V E_f}{\Omega X_d} \cos \theta + m_1 V^2 (1/X_q - 1/X_d) \cos 2\theta \end{aligned} \quad (58-28)$$

The corresponding *specific synchronizing power* is given by

$$p_s = \partial P/\partial\theta = \Omega t_s \quad (58-29)$$

A plot of  $t_s$  as a function of  $\theta$  for the generator mode of operation appears in Fig. 58-9. As is seen, at  $0 < \theta < \theta_{max}$   $t_s > 0$ , and the operation is stable. In contrast, at  $\theta_{max} < \theta < \pi$ ,  $t_s < 0$ , and the operation is unstable. Sustained operation in the generator mode can only take place between  $\theta = 0$  and  $\theta = \theta_{max}$ . The higher the synchronizing torque, the more stable is the operation, and it is increasingly more difficult for the machine to slip out of synchronism with the system (or bus) voltage. The best stability exists when the machine is floating on line, that is, neither delivers nor absorbs power; then  $t_s = t_{s,max}$ . As the electromagnetic torque or active power increases, the synchronizing torque decreases. At  $T_{em} = T_{em,max}$  and  $P = P_{max}$ , the synchronizing torque is zero, and the machine is no longer capable to go back to stable operation of its own accord.

The torque-versus-power angle characteristic of a synchronous machine is a periodic curve in which we can isolate stable regions ( $t_s > 0$ ) and unstable regions ( $t_s < 0$ ) for operation as a generator or a motor (Fig. 58-10). The period of the curve,  $\theta = 2\pi$ , corresponds to the rotation of the rotor in space (relative to the stator voltage) by an angle  $2\pi/p$ .

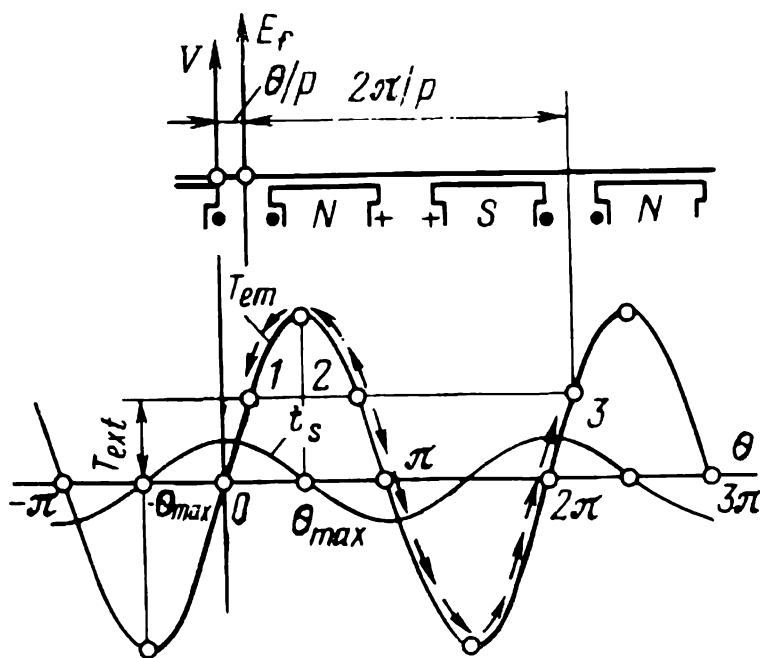


Fig. 58-10 Regions of stable operation on the torque/angle characteristic

The operation in the generator mode is stable at  $0 < \theta < \theta_{\max}$ , and also at  $\theta \pm 2\pi k$ , where  $k$  is an integer. The operation in the motor mode is stable at  $-\theta_{\max} < \theta < 0$ , and also at  $\theta \pm 2\pi k$ .

As we have seen, sustained operation in the unstable region of the characteristic (say, at point 2) is impossible. Even a slight, inadvertent change in  $\theta$  will cause it to decrease progressively until (as the rotor slows down) the machine moves in the stable region at point 1. Conversely, a chance increase in  $\theta$  at point 2 will cause it to rise until (as the rotor picks up speed) the machine moves in the stable region at point 3. As is seen,  $\theta_3$  differs from  $\theta_1$  by  $2\pi$  which corresponds to the rotation of the rotor relative to the stator voltage by  $2\pi/p$  (or by two poles, see Fig. 58-10).

The active power of a synchronous machine can be controlled by varying  $T_{\text{ext}}$ . At  $T_{\text{ext}} = 0$ , the machine is operating at no load,  $\theta = 0$ , and  $T_{\text{em}} = f(\theta) = 0$ . An increase in  $T_{\text{ext}}$  in the direction of rotation of the rotor upsets the balance of torques ( $T_{\text{ext}} \neq T_{\text{em}}$ ), so that an acceleration is

produced in accord with Eq. (58-27), the angular velocity of the rotor exceeds the synchronous angular velocity,  $\dot{E}_f$  begins to rotate faster than  $\dot{V}$ , the power angle  $\theta$  begins to grow and keeps doing so until a synchronous operation in the generator mode is again obtained at an angle  $\theta > 0$  such that  $T_{em} = f(\theta)$  in Fig. 58-8 becomes equal to  $T_{ext}$ . When  $T_{ext}$  is negative, an angle  $\theta < 0$  is finally reached where  $T_{ext} = T_{em}$ , and the machine goes motoring. Thus, control of active power at constant  $V_s$ ,  $f_s$  and  $I_f$  (or  $E_f$ ) is accompanied by a change in the power angle,  $\theta$ .

### 58-8 Reactive Power- $\theta$ Characteristic of a Synchronous Machine

This refers to a plot of  $Q$  as a function of  $\theta$ , with  $V_s$ ,  $f_s$  and  $I_f$  (or, in an unsaturated machine,  $E_f$ ) held constant, that is under the same conditions as are assumed in plotting the active power-vs-power angle characteristic.

An example of the reactive power-vs-power angle characteristic is shown in Fig. 58-11. It spans the region of stable parallel operation (that is in synchronism with the system voltage). Apart from the total reactive power,  $Q$ , it shows its components,  $Q'_d$ ,  $Q''_d$ , and  $Q_q$ , explained earlier.

The power angle  $\theta$  is a function of  $T_{ext}$ . Considering together the curves in Fig. 58-8 and Fig. 58-11, we can see how the reactive power changes whenever the active power is changed.

At no load (with the machine floating on line),  $\theta = 0$ , and the reactive power is a maximum,  $Q_{max}$  (in Figs. 58-8 and 58-11, the field current and voltage are at their rated values),

$$Q_{(\theta=0)} = Q_{max} = Q'_d + Q''_d + Q_q = \frac{m_1 V (E_f - V)}{X_d}$$

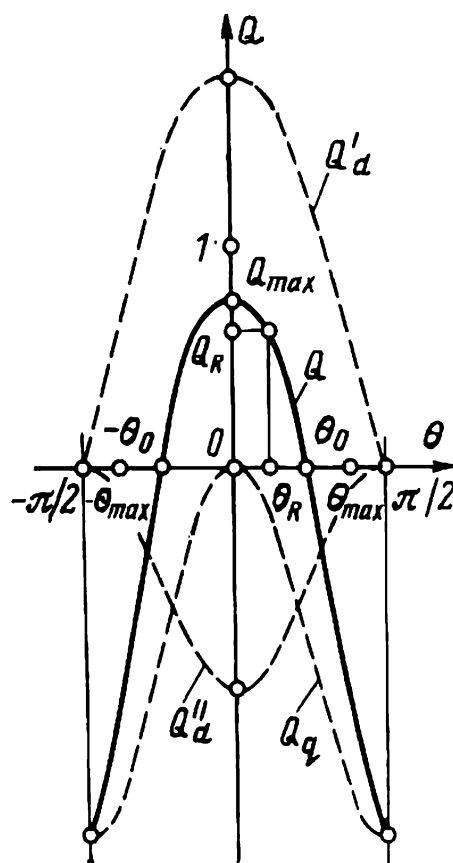


Fig. 58-11 Reactive power/angle curve of a synchronous machine ( $V_R = 1.0$ ,  $E_{f,R} = 1.77$ ,  $X_d = 1.0$ ,  $X_q = 0.6$ ,  $P_R = \cos \varphi_R = 0.8$ )

When  $E_f > V$ ,  $Q_{\max} > 0$ , and reactive power is delivered to the system. When  $E_f < V$ , reactive power is drawn from the system. When  $I_f = I_{f,R}$  or  $E_f = E_{f,R}$  and the voltage is at its rated value,  $E_{f,R} > V_R$ , and the maximum reactive power is always positive:

$$Q_{\max} = \frac{m_1 V_R (E_{f,R} - V_R)}{X_d} > 0$$

Or, in per-unit, as in Fig. 58-11,

$$Q_{*\max} = Q_{\max}/S_R = \frac{V_* (E_{*f} - V_*)}{X_{*d}}$$

When  $T_{\text{ext}} > 0$ , the machine is delivering active power to the system. When  $T_{\text{ext}} < 0$ , it is absorbing active power from the system. Positive values of  $P$  correspond to positive values of  $\theta$ ; negative values of  $P$  correspond to negative values of  $\theta$ . As is seen from Figs. 58-8 and 58-11, an increase in active load and  $\theta$  leads to a decrease in reactive power. This decrease solely depends on the absolute value of active power and  $\theta$  and is the same in both the generator and motor modes of operation:

$$Q(\theta) = Q(-\theta), \quad P(\theta) = -P(-\theta)$$

Under rated operating conditions, when  $P = P_R$ ,  $\cos\varphi = \cos\varphi_R (= 0.8)$  and  $\theta = \theta_R$ , the machine delivers rated reactive power,  $Q_R = \sin\varphi_R = 0.6$ . At  $\theta_0 (-\theta_0)$ , the reactive power is zero. As active power keeps rising (in absolute value), the reactive power becomes negative, that is, the machine absorbs it from the system.

### 58-9 Control of Reactive Power in Parallel Operation. "V" Curves

At constant active power reactive power,  $Q$ , can be controlled by varying  $I_f$ . To obtain more reactive power at a constant system (or bus) voltage, the field current must be raised; to reduce the amount of reactive power,  $I_f$  must be brought down. As a proof, consider what happens when the field current is, say, reduced.

Suppose that initially the machine is operating as a generator at point 1 on the power angle curve, with  $T_{\text{em}} = T_{\text{ext}}$ ,  $I_f = I_{f1}$ , and  $\theta = \theta_1$  (Fig. 58-12). When  $I_{f1}$  is reduced to  $I_{f3}$ , and  $E_{f1}$  to  $E_{f3}$ , the torque-versus-power angle and reac-

tive power-versus-power angle curves become different, but  $\theta$  retains its original value for some time owing to the inertia of the rotor. The electromagnetic torque acting on the rotor goes down by  $\Delta T_{em}$  to its value at point 2 on the power-angle curve at  $I_f = I_{f3}$ . Now the rotor is subjected to an unbalanced torque

$$|\Delta T_{em}| = T_{ext} - [T_{em} - |\Delta T_{em}|]$$

which accelerates the rotor, so that its angular speed,  $\omega$ , exceeds  $\omega_s$ , which is the velocity of the  $\dot{V}$  phasor, and the power angle begins to increase until, augmented by  $\Delta\theta$ ,

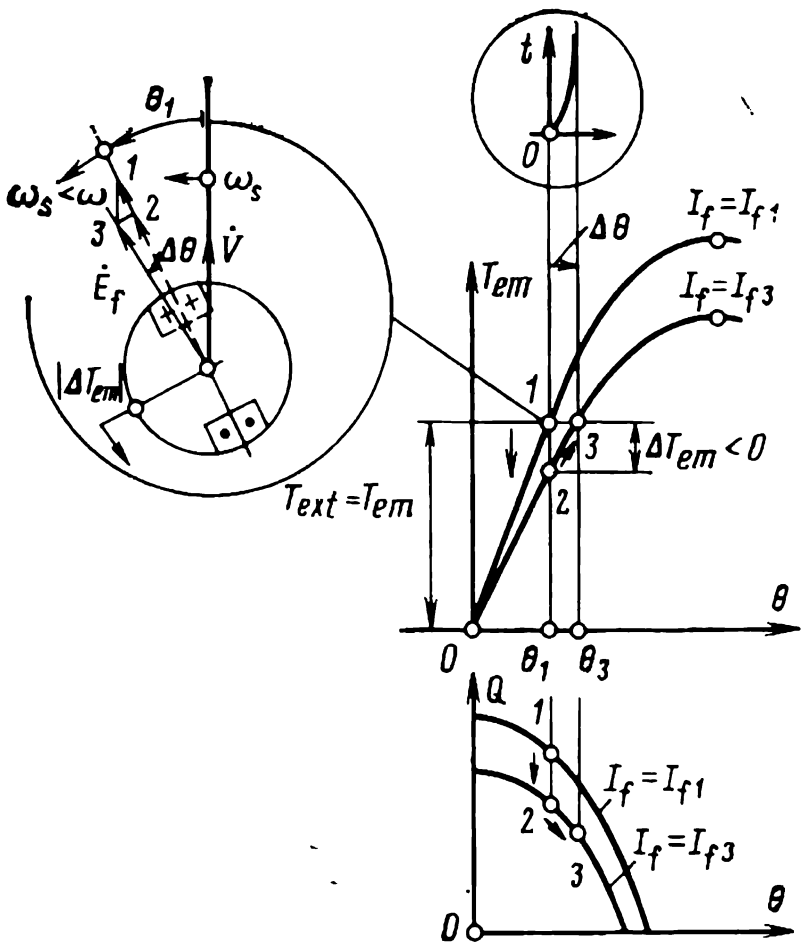


Fig. 58-12 Onset of new operating conditions upon a decrease in field current (at a constant external torque)

it takes on the value  $\theta_3$  such that the electromagnetic torque and the applied torque strike a balance again,  $T_{em} = T_{ext}$  (a plot of  $\theta$  as a function of time appears in the same figure). The reactive power at point 3 on the power/angle curve at  $\theta = \theta_1 + \Delta\theta = \theta_3 > \theta_1$  and at  $I_{f3} < I_{f1}$  will always be smaller than it is at point 1 with  $\theta = \theta_1$  and  $I_f = I_{f1}$ . As is seen from Fig. 58-12, the reactive power versus power angle characteristic at  $I_{f3} < I_{f1}$  runs below the characteristic at  $I_{f1}$ .

When  $Q$  is controlled by varying  $I_f$  and/or  $E_f$ , with  $V_s$  and  $T_{\text{ext}}$  held constant, the active component of current corresponding to a given torque remains unchanged

$$I_a = I \cos \varphi = P/m_1V = T_{\text{em}}\Omega/m_1V = \text{constant}$$

and the armature current

$$\dot{I} = \dot{I}_a + \dot{I}_r$$

changes only owing to the change in its reactive component

$$I_r = I \sin \varphi = Q/m_1V = \text{variable}$$

The plots of armature current as a function of  $I_f$  for constant power and for constant system (bus) voltage  $V_s$  are

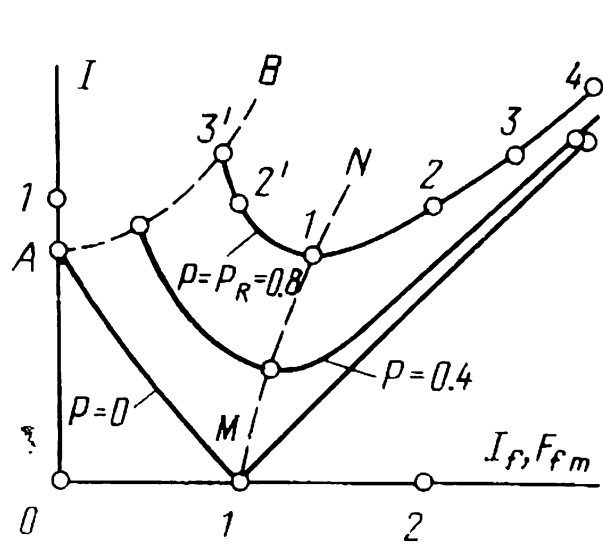


Fig. 58-13 “V”-curves of a synchronous machine ( $X_d = X_q = 1.2$ ,  $X_\sigma = 0.2$ ,  $\cos \varphi_R = 0.8$ )

called the “V”-curves of the machine. A family of “V”-curves for several levels of active power ( $P = 0, 0.4$  and  $0.8$ ) appear in Fig. 58-13.

“V”-curves are constructed by means of phasor/vector diagrams with allowance for saturation. Figure 58-14 shows the phasor/vector diagrams used in constructing the “V”-curve of the nonsalient-pole machine in Fig. 58-13 for  $P_R = \cos \varphi_R = 0.8$  per unit. Detailed steps are shown for point 2

on the curve where  $I_a = I_{aR} = \cos \varphi_R = 0.8$ ,  $I_r = I_{aR} \sin \varphi_R = 0.6$ . At other points on the curve (1, 3, 4, 2', and 3'), the active component of current remains unchanged,  $I_a = I_{aR}$ . The reactive component is allowed to take on several values, namely a value of zero at point 1; at points 2, 3 and 4 it is lagging behind  $V$  and assumed to be positive,  $I_r = I \sin \varphi > 0$ ; at points 2' and 3' it is leading  $V$ , and is assumed to be negative,  $I_r = I \sin \varphi < 0$ . The locus of armature current on the complex plane is the armature current line which is at right angles to the voltage line.

From the construction thus obtained, we can readily find  $F_{fm}$  and  $I_f = F_{fm}/w_f$  corresponding to the armature current existing at the points of interest. The positions that the tip of the  $\dot{F}_{fm}$  vector takes up on the locus are labelled by appro-

appropriate numerals. Between points 3' and 2, where the magnetic circuit is not saturated, the locus of  $F_{fm}$  is a straight line. As the magnetic circuit saturates (between points 2 and 4), the locus progressively departs from a straight line.

The “V”-curves for  $P = 0.4$  and  $P = 0$  are constructed in a similar manner, with  $I_a = 0.4$  and  $I_a = 0$  (in per unit).

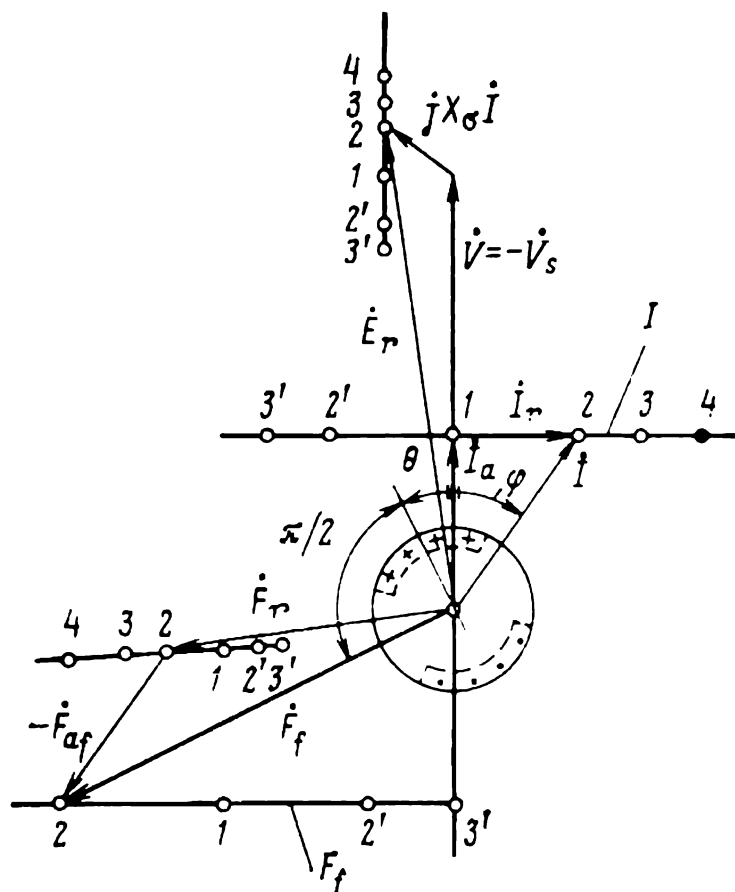


**Fig. 58-14 Construction of a "V"-curve ( $X_d = X_q = 1.2$ ,  $X_\sigma = 0.2$ ,  $\cos \varphi_R = 0.8$ )**

The minimum value of current on the “V”-curve (at point  $I$ ) occurs at a field current ( $\cos \varphi = 1$ ) such that  $I_r = 0$  and there is only the active component remaining,  $I_a = I \cos \varphi = I$ ,  $\cos \varphi = 1$ .

The curve connecting the minima of the curves for various power levels is called the *compounding curve* (curve  $MN$  in Fig. 58-13). Observe that minimum current always corresponds to unity power factor,  $\cos \phi = 1$ . At points on the "V"-curves lying to the right of the minima (say, points 2, 3, and 4), the machine is *overexcited* as compared with the conditions existing at point 1 where  $I = I_a$ . Its field current is  $I_f > I_{f(\cos \phi = 1)}$ , and, as is seen from Fig. 58-14, its reactive current is positive,  $I_r > 0$ , that is, it is lagging behind the voltage. Conversely, at points lying to the left of the minima (say, at points 2' and 3'), the machine is *underexcited*. Its



field current is  $I_f < I_{f(\cos\phi=1)}$ , and its reactive current is negative,  $I_r < 0$ , that is, it is leading the voltage.

At overexcitation, the system acts as an inductive load for the machine (the reactive current in the armature bucks the excitation field). At underexcitation, the system acts as a capacitive load for the machine (the reactive current in the armature boosts the excitation field). If we look at the things the other way around, relative to the system with  $V_s = -V$  which is in antiphase with the machine voltage, an overexcited machine acts as a capacitive load delivering reactive power, whereas an underexcited machine acts as an inductive load which absorbs reactive power (see Fig. 58-13).

A decrease in excitation leads to a decrease in the *steady-state stability limit* which for a nonsalient-pole machine is given by  $P_{\max} = m_1 E_f V / X_d$ . The underexcitation region is bounded by line  $AB$  to the left of which a synchronous machine is unstable. On line  $AB$  (say, at point  $3'$ ),  $P_{\max}$  becomes equal to the constant  $P$  level for which a given "V"-curve has been constructed.

For the motor mode of operation, "V"-curves are plotted in a similar manner, except that the active component of current is drawn in the opposite direction from the voltage,  $I_a < 0$ .

## 58-10 Synchronous Motors

Any synchronous machine is reversible — it can be operated as a generator and a motor. Nearly always, however, the makers slate their machines for one particular mode of operation only, and the nameplate gives the particulars (rated torque, efficiency, etc.) for that duty.

A synchronous machine intended for operation in both modes is called a *reversible synchronous machine*. Such machines are employed at pumped-storage hydro-electric stations usually built to equalize the load on fuel-fired stations. A pumped-storage station has two water reservoirs, upper and lower. At peak load, water is allowed to flow from the upper to the lower reservoir, and the reversible synchronous machines driven by hydraulic (or water-wheel) turbines are running as generators. When the load on the system is low, the synchronous machines are operating as motors driving

the pumps which transfer water from the lower to the upper reservoir.

Three-phase synchronous motors in the Soviet Union come in ratings from 20 kW to several tens of megawatts. At speeds from 100 to 1 000 rpm, motors usually have a salient-pole rotor. At higher speeds (1 500 and 3 000 rpm), the rotor is of nonsalient-pole construction. Depending on their ratings, synchronous motors can be built for voltages from 220 V to 10 kV. The rotational speed of a synchronous motor depends on the supply-line frequency and is independent of the load applied to the motor shaft.

Given the same power rating and rpm, synchronous motors are identical in construction to synchronous generators. The only exception is the design of their damper (starting) windings with which synchronous motors can be started as induction units where necessary.

The electromagnetic processes occurring in synchronous motors are described by the same equations, phasor and vector diagrams as in synchronous generators (see Chap. 55). As an example, Fig. 58-15 shows the phasor and vector diagram of an overexcited, salient-pole synchronous motor (neglecting saturation). It differs from the phasor and vector diagram of a synchronous generator (see Fig. 55-2) only in that the active component of armature current is drawn in the opposite direction from  $\dot{V}$ , and is in line with  $\dot{V}_s = -\dot{V}$ . As in an overexcited generator,  $I_r$  lags behind  $\dot{V}$  by  $\pi/2$  and leads  $\dot{V}_s$  by  $\pi/2$ .

The torque, active and reactive power of a synchronous motor are calculated by the equations derived for a synchro-

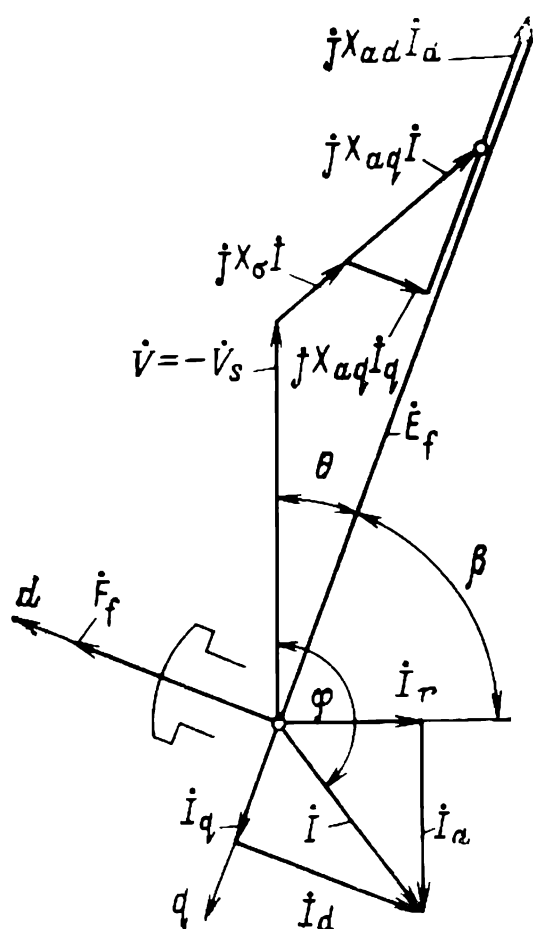


Fig. 58-15 Voltage phasor diagram of a salient-pole synchronous machine operating as a motor (neglecting saturation)

nous machine connected to an infinite bus (see Chap. 58). At constant excitation, variations in the above quantities with changes in the power angle are assessed from the power-angle curves for active and reactive power (see Figs. 58-8 and 58-11), which also cover the region of motor operation ( $-\theta_{\max} < \theta < 0$ ). The effect of field current on reactive power in the motor mode of operation can be judged from

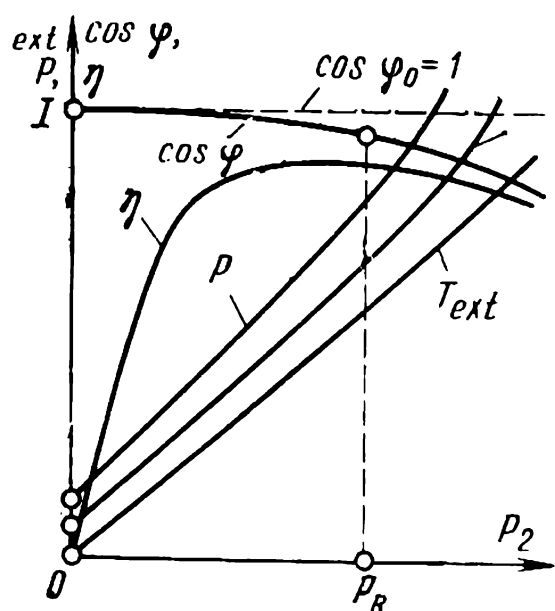


Fig. 58-16 Operating characteristics of a synchronous motor

the "V"-curves plotted for the motor mode of operation. They are in effect exact copies of the "V"-curves for a generator (see Fig. 58-13).

The operating characteristics of a synchronous motor for constant field current chosen so that on open circuit the power factor is unity are shown in Fig. 58-16. As the load is increased, the power factor falls off, and the current becomes lagging. If the field current is chosen so that the motor has the rated power factor at rated load and leading current,

then a reduction in load will cause it to deliver to the line still more reactive power than at rated load ( $\cos \phi < \cos \phi_R$ ). Conversely, as the load increases, the power factor first increases owing to a decrease in the leading reactive current, then becomes equal to unity, and finally drops again owing to the appearance of a lagging reactive current.

Automatic control of voltage as a function of armature current can produce any desired reactive power or power factor.

Synchronous motors are either direct rotating-machine excitation systems (d.c. exciters) or self-excitation systems incorporating static rectifiers (a.c. exciters with static rectification), described in detail in Chap. 52.

Synchronous motors can be started as induction motors (see Sec. 59-4) by means of a short-circuited damper (or starting) winding embedded in the pole-face slots.

In nonsalient-pole synchronous motors with a solid rotor and in salient-pole synchronous motors with solid poles, induction-motor action at starting occurs due to the interac-

tion of the eddy currents in the solid iron parts with the rotating magnetic field.

The performance of a synchronous motor started as an induction motor can be stated in terms of the starting torque,  $T_s$ , at  $s = 1$ , and the *pull-in torque* which is defined as the torque at  $s = 0.05$  and designated as  $T_{0.05}$ . Sometimes, these torques and current are given as fractions of the rated torque and current in synchronous running (see below).

As has been noted in Sec. 37-2, the principal dimensions, weight and cost of a synchronous motor depend on its total (or apparent) power

$$S_R = P_R/\eta_R \cos \varphi_R$$

and increase with decreasing power factor. As is seen from Table 58-1, a synchronous motor operating at unity power factor is by a mere 17% more expensive than a comparable squirrel-cage induction motor, whereas at  $\cos \varphi = 0.8$ , it is 44% more expensive. On the other hand, a synchronous motor operating at unity power factor does not generate reactive power, that with  $\cos \varphi = 0.8$  leading does generate a sizeable amount of reactive power equal to about 75% of the active power. Unfortunately, at  $\cos \varphi = 0.8$ , the efficiency is lower. Synchronous motors capable of supplying reactive power make it possible to reduce the reactive power of unit synchronous generators (those installed at electric stations) and of synchronous condensers.

Table 58-1 Comparison of Synchronous and Induction Motors, 1 000 kW, 1 000 rpm

Motor type	Rated power factor	Efficiency, %	Relative cost, %
Synchronous	1.0	96.4	117
	0.8 leading	95.3	144
	0.6 leading	93.7	166
Phase-wound, induction	0.9 lagging	94.9	127
Squirrel-cage, induction	0.9 lagging	95.1	100

The choice of power factor for synchronous generators and motors is a multifaceted optimization problem in which the objective is to minimize the manufacturing cost of the machines and the operating cost of the system. Because the efficiency increases with the size of a machine, it is advant-

ageous to obtain the bulk of reactive power from large synchronous generators, and the remainder from synchronous motors having relatively lower ratings. Synchronous generators are usually designed for operation at  $\cos \varphi = 0.8$ , and synchronous motors, at  $\cos \varphi = 0.9$  (at overexcitation).

Whereas they are superior to induction motors in that they can deliver reactive power to the system, synchronous motors are inferior in some other respects. For one thing, they are more elaborate in design, especially as compared with squirrel-cage induction motors. For another, they are more expensive, mainly because they need excitation systems for their operation. Also, synchronous motors need skilled attendance and are less reliable in service. The decision on which of the two varieties of motor is preferable is made in each particular case from a comparison of the likely alternatives in terms of manufacturing and operating costs.

At ratings over 100-200 kW, synchronous motors are more attractive than induction units. At lower ratings, they are used more seldom, and then mainly in cases where it is important to maintain their speed at a constant value close to synchronous.

A special variety of synchronous motors (rated at not over 2 kW), known as *reluctance-torque* (or simply, *reluctance*) *motors* have no field winding and are excited by reactive current drawn from the line. Still smaller synchronous motors draw their excitation from permanent magnets (see Sec. 63-6).

Still another variety of synchronous motors are *synchronous induction* (or *auto-synchronous*) *motors*, similar to induction motors with a wound rotor. From the latter, they differ in that they have a larger air gap and a larger three-phase secondary winding. At starting, the rotor winding of a synchronous induction motor is closed through a starting rheostat, then d.c. is applied to its field structure from an exciter or a rectifier, and the rotor pulls into synchronism. Thereafter, it is running as a synchronous motor with its power-factor control features.

Synchronous induction motors have about the same starting performance as comparable wound-rotor induction motors. They are intended for use where a constant rpm is essential and the starting requirements are heavy and call for a high power factor (large compressors, pumps, and the like).

### 58-11 Synchronous Condensers

*Synchronous condensers* (also called synchronous compensators or synchronous capacitors) are synchronous machines intended to supply reactive power.

At fuel-fired and hydro-electric stations, this function is performed by synchronous generators. Synchronous condensers are connected across power transmission lines at the receiving ends, that is, at load points (Fig. 58-17), so the reactive power they supply need not be transmitted over long

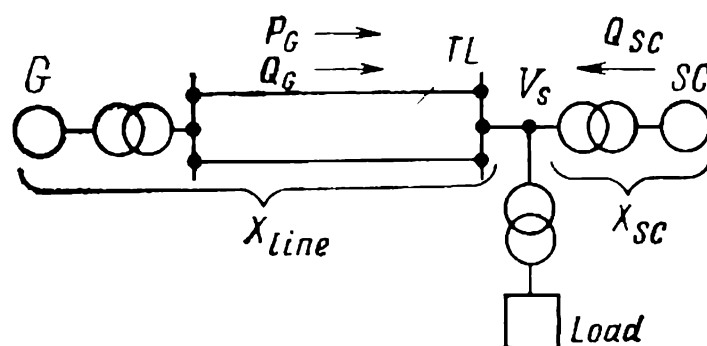


**Fig. 58-17** Connection of synchronous condensers in an electric system:

*SC*—synchronous condenser; *G*—unit (station) generator; *TL*—power transmission line

distances. Owing to reduced energy losses in transmission lines and at intervening transformer substations, the reactive power supplied by synchronous condensers is markedly less expensive than when it comes from synchronous generators.

The money put into the installation and running of synchronous condensers is well spent, if their output accounts for 20 to 30% of the total power handled by a given transmission line. Then, the synchronous generators set up at stations need to supply only 60% of the total line power, and also active power accounting for 80% of the total. With an output breakdown like that, the total power that the generators are called upon to supply exceeds their active power by a mere 25%. Therefore, the need to generate both active and reactive power does not lead to a prohibitive increase in their size, weight and cost. (This also goes for the transmission line, transformers and other equipment at the intervening substations linking the generators to their loads.)

The reactive power generated by a synchronous condenser connected to an infinite system is a function of its field cur-

rent,  $I_f$ . An overexcited synchronous condenser, that is one with  $I_f > I_{f,oc}$  (or  $E_f > V_s$ ), is operating with  $I_r$  leading  $V_s$ , and delivers reactive power to the system,

$$Q = VI_r > 0$$

An underexcited synchronous condenser, that is, one with  $I_f < I_{f,oc}$  (or  $E_f < V_s$ ), is operating with  $I_r$  lagging behind  $V_s$  (Fig. 58-18) and is absorbing reactive power from the system,

$$Q = VI_r < 0$$

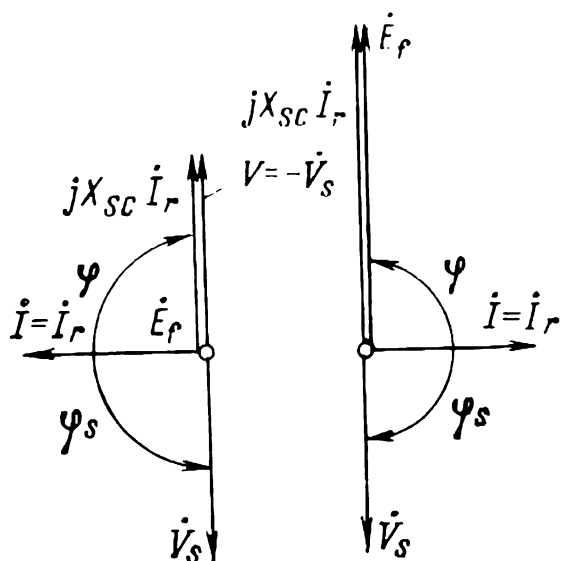


Fig. 58-18 Voltage phasor diagrams of a synchronous condenser at underexcitation ( $E_f < V_s$ ) and overexcitation ( $E_f > V_s$ )

The rated conditions are assumed to be those when a synchronous condenser is delivering its rated power at overexcitation and is absorbing from the system a small amount of active power needed to sustain the losses in the machine (core loss, copper loss, and friction and windage loss). Therefore, the armature current of a synchronous condenser contains both a reactive component,  $I_r$ , and an active component,

$I_a$ , which is in phase with the system voltage,  $V_s$ . However, the active component is so small that the total armature current does not practically differ from the reactive component,

$$I = \sqrt{I_a^2 + I_r^2} \approx I_r$$

In Fig. 58-18, the active component is not even shown as being very small.

As follows from the foregoing, a synchronous condenser connected to an infinite system operates as a synchronous motor on no load, that is, with a zero external torque,  $T_{ext} = 0$ .

The operating costs of a synchronous condenser are directly proportional to its total active power loss,  $\Sigma P$ . In present-day large synchronous condensers, the per-unit total active

power loss (with  $S_R = Q_R$  taken as the base quantity) does not exceed 0.013 to 0.016 with hydrogen cooling, and 0.02-0.24 with air cooling.

Synchronous condensers come in units rated from 10 to 160 mVA at 6.6-15.75 kV, usually with a horizontal shaft. The choice of speed is a matter of engineering and economic consideration. As Soviet experience shows, for large synchronous condensers used in electrical systems, the optimal speed at 50 Hz is anywhere between 750 and 1 000 rpm. Although the size and weight of two-pole, 3 000-rpm synchronous condensers are minimal, their cost is by 20% to 25% higher because their nonsalient-pole rotors are far more expensive to manufacture. Also, at 3 000 rpm there is an appreciable increase in the friction and windage loss, and this leads to an increase in operating costs.

As a rule, synchronous condensers are started as induction motors (see Sec. 59-4). Since there is no load torque acting on the shaft, synchronous condensers are relatively easier to start than loaded synchronous motors.

The shaft of a synchronous condenser need not to transfer any torque, so it is designed only to resist bending due to the self-weight of the rotor and the forces of magnetic attraction (see Sec. 34-3). Given the same total power, the shaft of a synchronous condenser may be smaller in diameter than the shaft of a synchronous generator or motor. This leads to a reduction in the bearing and overall size of condensers. The shaft of a synchronous condenser is not carried outside, and its casing is relatively easy to seal. This was the reason why hydrogen cooling was first applied to synchronous condensers, first at a pressure of  $0.05 \times 10^5$  Pa (gauge), later at  $1 \times 10^5$  to  $2 \times 10^5$  Pa (gauge). Owing to hydrogen cooling, electric loading has been raised to an impressive level: from  $580 \times 10^4$  to  $620 \times 10^4$  A m<sup>-1</sup> with indirect air cooling, to  $800 \times 10^4$  to  $1000 \times 10^4$  A/m with indirect hydrogen cooling.

The electromagnetic processes in synchronous condensers are described by the same equations and diagrams as in synchronous generators (see Chap. 55). Notably, this applies to the diagrams of a synchronous condenser plotted in Fig. 58-18, neglecting saturation. The synchronous condenser is connected to the system with  $V_s$  via a transformer as shown in Fig. 58-17. In the diagram,  $V_s$  is referred to the transformer winding connected to the synchronous condenser.



The inductive reactance is the sum of the inductive reactance of the synchronous condenser and that of the transformer

$$X_{sc} = X_T + X_d$$

where  $X_T$  is the short-circuit reactance of the transformer, and  $X_d$  is total  $d$ -axis armature inductive reactance of the synchronous condenser.

The most important characteristic of a synchronous condenser is its “V”-curve,  $I = f(I_f)$ , plotted for constant  $V_s$ . It does not differ from the “V”-curve of a synchronous generator plotted for  $P = 0$ . For a synchronous condenser, it is useful to construct a family of “V”-curves at several system voltage levels ( $V_s = V_R = \text{constant}$ ,  $V_s = 0.95V_R$ ,  $V_s = 1.05V_R$ , and so on). From such a family of V-curves, one can readily form an idea about the response of the synchronous condenser to changes in  $V$  at constant  $I_f$ : as  $V$  goes down, more reactive power is delivered to the system, and vice versa. In fact, a synchronous condenser operates as a voltage regulator. In automatic voltage control, the performance of a synchronous condenser as a voltage regulator improves still more.

In choosing the parameters of a synchronous condenser, one need not strive for a high steady-state power capability (see Sec. 58-7), as for synchronous generators or motors. The fact is that a synchronous condenser operates at active power and power angle equal to zero very nearly,  $P \approx 0$ , and  $\theta \approx 0$ . Hence, the  $d$ -axis armature inductive reactance is chosen so as to supply the required reactive power at under-excitation. At  $I_f = 0$ , the reactive power a synchronous condenser absorbs from the system is

$$Q_* = Q/S_R = 1/X_{*d}$$

Hence, its per-unit induction reactance is  $X_{*d} = 1/Q$ . As a rule, the desired  $Q_*$  is set at 0.4 to 0.6, so  $X_{*d}$  must be 2.5 to 1.65.

## 59 Synchronization Methods

### 59-1 Exact Synchronization

In order to connect any synchronous machine in parallel with another machine or a system, it must be synchronized, that is, the speed of its rotor must be brought up to synchro-

nous, the field current must be chosen such that  $E_f$  corresponds to  $V_s$ , and the machine must be connected in such a way that, immediately following closure of the switch, it will be floating on the line, with  $\theta = 0$ .

The simplest method is exact synchronization described in brief in Sec. 58-2. It is equally applicable to any synchronous generator driven by a prime mover, and also to synchronous motors and condensers if they are fitted with an auxiliary motor which can accelerate them to the synchronous speed.

The procedure in exact synchronization is as follows (see Fig. 58-2).

(1) The prime mover or an auxiliary motor raises the angular velocity  $\Omega$  of the incoming generator,  $G$ , to synchronous (or nearly so)

$$\Omega \cong \omega_s/p = \Omega_s$$

(2) An automatic synchronizer connects the generator field winding (Fig. 59-1) to the armature brushes of the exciter ( $K_1$  closes and  $K_2$  opens).  $I_f$  is adjusted so that  $E_f$  (or  $V = E_f$ ) at the terminals of the disconnected generator is equal to  $V_s$  ( $K$  is open).

(3) The speed  $\omega$  of the prime mover is increased or decreased a little in comparison with  $\omega_s$  (say, by varying the setting of the guide vanes in the turbine as in Fig. 58-6). As a consequence, the angle  $\alpha$  between  $E_f$  and  $V_s$  (see Fig. 58-3) slowly changes

$$\alpha = \alpha_0 + (\omega - \omega_s) t$$

The difference emf,  $\Delta E = 2V |\cos \alpha/2|$ , also changes with a period

$$T_\alpha = 2\pi / |\omega - \omega_s|$$

(4) The rate of change of  $\alpha$  is slowed down so that the operator has time to close the contactor (or circuit-breaker)  $K$  at the instant when  $\Delta E \approx 0$ . This can be done if  $T_\alpha$  is

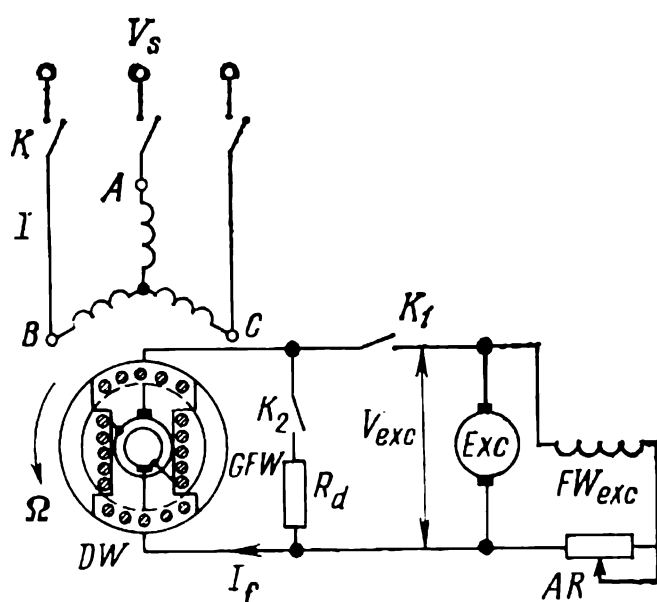


Fig. 59-1 Connection of a generator to a system for parallel operation

anywhere from 20 to 40 s, and the relative slip of the rotor is small

$$s = |\omega - \omega_s| / \omega_s = 2\pi / \omega_s T_\alpha = T_s / T_\alpha \\ = \text{from } 0.001 \text{ to } 0.0005$$

Here,  $T_s = 2\pi / \omega_s = 1 / f_s$  is the period of change in system voltage, equal to 0.02 s at  $f_s = 50$  Hz.

(5) Keeping watch on variations in  $\Delta E$  as indicated by the voltmeter shown in Fig. 58-2, or by a synchronoscope, the operator closes the contactor when  $\Delta E = 0$  and the condition required for exact synchronization, namely

$$\dot{E}_f = \dot{V} = -\dot{V}_s$$

is satisfied.

If  $K$  is closed at exactly such an instant, no current will be flowing in the armature winding ( $I = 0$ ), and the machine will be floating on the line. This is however, an idealization. In practice the incoming generator is put on line a split second too early or too late, and  $\Delta E$  somewhat differs from zero. This gives rise to small transient currents, and a condition arises in which the armature current  $I$  differs from zero. If, at the instant when the circuit-breaker is closed  $\omega > \omega_s$ , the machine will run as a generator with a small current  $I \ll I_R$ . If  $\omega < \omega_s$ , it will run as a motor.

When a generator is to be put on line for the first time and also after any changes in connections, the above procedure is extended to include a check on the phase sequence in the generator and the system. It must be the same, because it is only then that  $\Delta \dot{E} = 0$  will be in each phase,

$$\Delta \dot{E}_A = \dot{E}_{fA} + \dot{V}_{sA} = 0$$

$$\Delta \dot{E}_B = \dot{E}_{fB} + \dot{V}_{sB} = 0$$

$$\Delta \dot{E}_C = \dot{E}_{fC} + \dot{V}_{sC} = 0$$

and the incoming generator will be connected to the line without any damage to either.

Exact synchronization is carried out with the aid of suitable instruments, such as lamp synchronizers, synchronoscopes, or synchronoscopes. They are described in detail in books on electrical instruments and measurements. The simplest of them is the *lamp synchronizer* which is in effect a combination of three incandescent lamps (see Fig. 58-2) connected for the

voltage  $\Delta E$  across the pairs of contacts ( $A$  and  $A_s$ ,  $B$  and  $B_s$ ,  $C$  and  $C_s$ ) of the contactor (or circuit-breaker). The lamps must be either designed for twice the phase voltage,  $2V_s$ , or connected via step-down transformers. As  $\Delta E$  varies with a period  $T_\alpha$ , the lamp voltage varies between zero and  $2V_s$ , and the three lamps go dark or bright at the same time.

For exact synchronization, the contactor must be closed at the instance when the three lamps are dark\*. As an aid,  $\Delta E$  can be monitored by a voltmeter (see Fig. 58-2).

A lamp synchronizer will also indicate the phase sequence. If the phase sequence of the machine differs from that of the system, the lamps will "flicker", one going completely dark, and the other two being half-bright.

### 59-2 Self-Synchronization. Conditions for Pulling into Synchronization

Putting an incoming generator on line by exact synchronization takes from five to ten minutes, as the contactor (or circuit breaker) may only be closed at a certain definite angular position of the rotor.

A faster procedure is *self-synchronization* which does not call for an exact adjustment of speed and angular position of the rotor. It can be applied to both synchronous generators and synchronous motors fitted with an auxiliary accelerating motor.

The procedure for self-synchronization is as follows (see Fig. 59-1).

(1) The prime mover or an auxiliary motor accelerates the incoming generator to synchronous (or nearly so) speed. For large machines, the relative slip ought not to exceed

$$s_0 = |\Omega_s - \Omega| / \Omega_s \leq 0.01 \text{ to } 0.04$$

During acceleration, the field winding is disconnected from the exciter (the field killer is "OFF",  $K_1$  is open, and  $K_2$  is closed), and the armature winding is disconnected from the system (circuit-breaker  $K$  is open).

(2) At  $\Omega$  close to synchronous, the voltage existing across the armature brushes of the exciter,  $V_{exc}$ , is sufficient to induce (after the automatic synchronizer has been turned on)

---

\* This is true only of the connection shown in the figure. If the secondary of one transformer is reverse, the lamps will be brightest at synchronism and dark at  $180^\circ$  of phase difference.—*Translator's note.*

in the generator field winding, GFW, a field current,

$$I_{f,oc} = V_{exc}/R_f$$

corresponding to  $E_f = V_s$ . The value of  $V_{exc}$  is found by experiment in advance, with the machine running on no load.

(3) The automatic synchronizer is activated ( $K_1$  is closed, and  $K_2$  is opened), and the generator field winding is connected to the running exciter. Immediately after that, circuit-breaker  $K$  is closed, and the armature winding is connected to the system with voltage  $V_s$ .

(4) This initiates a transient process associated with a build-up of  $i_f$  in the field winding, and of  $i$  in the armature winding. The interaction of the two currents gives rise to a periodically varying electromagnetic torque which causes (under certain conditions) the rotor to pull into synchronism—now it is spinning at synchronous speed, and the power angle  $\theta$  between  $\dot{V} = -\dot{V}_s$  and  $\dot{E}_f$  reduces to zero. (It is assumed that the torque supplied by the prime mover,  $T_{ext}$ , is balanced by the friction/windage torque and the no-load torque.)

The transient process terminating in synchronism is the superposition of two simpler transient processes. One of them occurs after the armature winding has been connected to the line; the other takes place after the field winding has been connected to the exciter.

The armature current attains its maximum value about a half-cycle after connection to the line, that is, in time

$$t = T_s/2 = \pi/\omega_s$$

It is several times the rated current. In the worst case, it is given (on a per-unit basis) by

$$i_{*max} = i_{max}/\sqrt{2} I_R = 2V_{*s}/(X''_d + X_*) = 8 \text{ to } 3$$

where  $X''_d$  is the per-unit supertransient inductive reactance of the armature winding (usually anywhere from 0.15 to 0.3; for more detail, refer to Sec. 73-3),  $X_*$  is the inductive reactance of the step-down transformer and other system elements interposed between the synchronous machine and the buses, the bus voltage  $V_s$  may be deemed constant ( $X_*$  ranges between 0.1 and 0.3, depending on the system arrangement).

The field current is the sum of the current produced by the exciter voltage (see Sec. 72-5), and several components induced in the field winding by variations in its flux linkage with the armature winding.

Some time after the onset of the transient process (usually within one to three seconds), the transient currents arising when the armature winding is connected to the line die out nearly completely, and the synchronous electromagnetic torque may be expressed in terms of the rms armature current,  $I_s = V_s/X_1$ , produced by  $V_s$ , and the armature flux linkage,  $\Psi_{fm} = V \sqrt{2} E_f / \omega$ , due to the steady-state excitation field set up by  $I_f = V_{\text{ext}}/R_f$ .

Neglecting saturation and deeming the slip sufficiently small ( $s_0 \ll 1$ ), the synchronous electromagnetic torque applied to a nonsalient-pole rotor can be found from Eq. (58-13) deduced for synchronous operation. Now, however, it should be noted that at nonsynchronous speed,  $\omega \neq \omega_s$ ,  $X_1 = \omega_s L_1$  (because  $I_s = V_s / X_1$  depends on the system frequency), and  $E_f = \omega \Psi_f / 2$  (because the angular velocity of the field emf,  $\omega = p\Omega$ , is proportional to the angular velocity of the rotor,  $\Omega$ ). Thus, the synchronous electromagnetic torque may be written

$$T_s = \frac{mV_s E_f}{X_1 \Omega} \sin \theta = (pm / \sqrt{2}) I_s \Psi_{fm} \sin \theta \quad (59-1)$$

The angle  $\theta$  in Eq. (59-1) may be taken as the angle between  $\dot{I}_s = \dot{V}_s / jX_1$  and  $\dot{\Psi}_f$ . As is seen from the phasor-vector diagram of the model in Fig. 59-2, this angle does not differ from the angle between  $\dot{V} = -\dot{V}_s$  and  $\dot{E}_f$ .

Should the rotor slip out of synchronism, such as when  $\omega = \omega_s/(1 - s) < \omega_s$ , the angle  $\theta$  will be varying continually. With the origin of time chosen as shown in

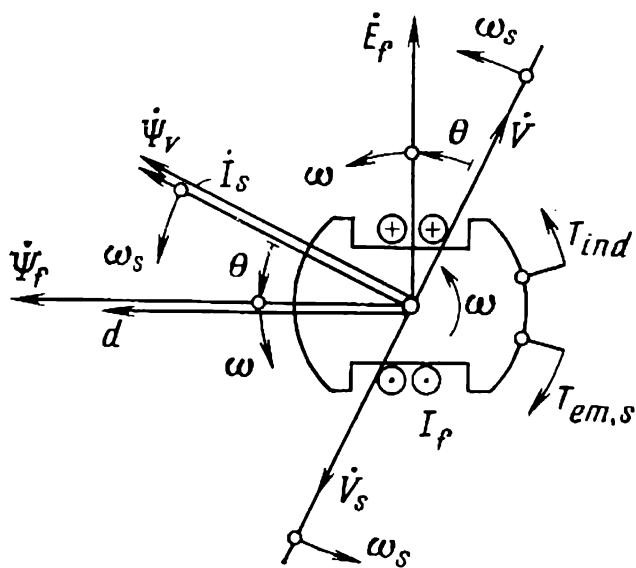


**Fig. 59-2** Electromagnetic torques with the incoming machine running at asynchronous velocity,  $\omega_s > \omega$ ,  $T_{em, s}$ —synchronous electromagnetic torque;  $T_{ind}$ —induction (asynchronous) electromagnetic torque

Fig. 59-3, the angle  $\theta$  will be defined as

$$\theta = \int_0^t (\omega - \omega_s) dt$$

and will be negative. As  $\theta$  varies,  $T_s$  will also vary periodically. A plot of  $T_s$  as a function of both  $\theta$  and  $t$  appears in Fig. 59-3.

The negative electromagnetic torque is acting in the direction of rotation, so the rotor picks up speed. In contrast,

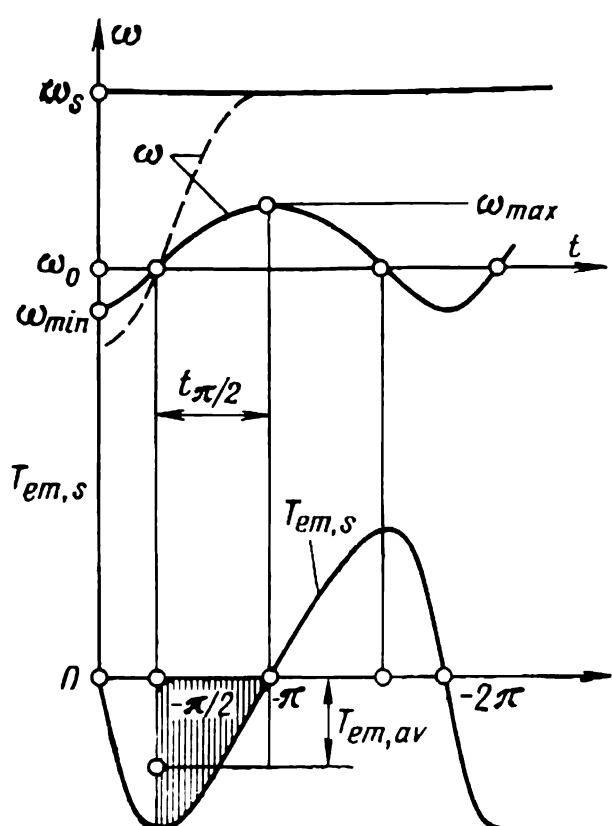


Fig. 59-3 Pulling into synchronism

the positive electromagnetic torque tends to slow down it. As is seen from the plot, the angular velocity of the rotor oscillates about the initial angular velocity,  $\omega_0 = \omega_s(1 - s_0)$ , going from its maximum,  $\omega_{\max} = \omega_s(1 - s_{\max})$ , to its minimum,  $\omega_{\min}$  and back. Because at  $\omega > \omega_0$ , the angle  $\theta$  varies at a lower rate than it does at  $\omega < \omega_0$ , the scale of  $\theta$  on the plots appears non-uniform (whereas the time scale is uniform).

Let us take a closer look at what happens over the interval of  $\theta$  from  $-\pi/2$  to  $-\pi$ , at the end of which the rotor velocity,  $\omega = \omega_{\max}$ , comes closest to synchronous. This change in  $\theta$  by  $90^\circ$ , occurs in a time  $t_{\pi/2}$  approximately equal to

$$t_{\pi/2} = \frac{\pi}{2(\omega_s - \omega_{av})} = \pi/2s_{av}\omega_s \quad (59-2)$$

where

$$\omega_{av} = \omega_0 + \frac{2}{\pi}(\omega_{\max} - \omega_0) = \omega_s(1 - s_{av})$$

is the average angular velocity over the interval, and

$$s_{av} = s_0 + \frac{2}{\pi}(s_{\max} - s_0)$$

is the relative slip corresponding to  $\omega_{av}$ .

The average angular acceleration of the rotor,  $|d\omega/dt|_{av}$ , depends on the average electromagnetic torque over the same interval, as given by Eq. (59-1)

$$T_{em, av} = \frac{2}{\pi} T_{em, max} = (2pm/\pi \sqrt{2}) I_s \Psi_{fm}$$

The average angular acceleration over the interval (as found from the equation of motion for the rotor) is

$$|d\omega/dt|_{av} = p |d\Omega/dt|_{av} = p T_{em, av} / J \quad (59-3)$$

where  $J$  is the moment of inertia of the rotor and associated rotating parts.

Over the time interval  $t_{\pi/2}$ , the above angular acceleration causes the electrical angular velocity of the rotor to increase by  $(\omega_{max} - \omega_0)$ , so that we may write

$$t_{\pi/2} |d\omega/dt|_{av} = |\omega_{max} - \omega_0| = |s_0 - s_{max}| \omega_s \quad (59-4)$$

Using Eqs. (59-2), (59-3), and (59-4), we can find  $s_{max}$  and  $\omega_{max} = \omega_s (1 - s_{max})$  for the values of  $s_0$  and  $\omega_0 = \omega_s (1 - s_0)$  that should exist at the instant when the incoming generator is put on line. Obviously, the incoming generator will pull into synchronism if, as the rotor oscillates, its frequency becomes equal to synchronous, so that  $\omega_{max} = \omega_s$  and  $s_{max} = 0$  (the dashed  $\omega$ -curve in Fig. 59-3).

On substituting for  $t_{\pi/2}$  and  $|d\omega/dt|_{av}$  from Eqs. (59-2) and (59-3) into Eq. (59-4), and solving it for  $s_0$ , we will see that the rotor will pull into synchronism (at  $\omega_s = \omega_{max}$  and  $s_{max} = 0$ ), if the initial slip at the instant of putting on line is such that

$$s_0 \leq \frac{p}{0.6\omega_s} \sqrt{\frac{S_R I_{*s} \Psi_{*fm}}{\omega_R J}} = (p/0.6\omega_s) \sqrt{T_{em, max}/pJ} \quad (59-5)$$

where

$$I_{*s} = I_s / I_R = V_s / X_1 I_R$$

is the per-unit armature current component due to  $V_s$

$$\Psi_{*fm} = \Psi_{fm} / \Psi_{R, m} = \Psi_{fm} \omega_R / \sqrt{2} V_R$$

is the per-unit flux linkage of the field winding, and

$$\omega_R = 2\pi f_R$$

is the rated angular velocity of the machine.



**Example.** Self-synchronization is applied to a hydrogenerator for which  $S_R = 25 \times 10^6$  VA,  $\omega_s = \omega_R = 2\pi f_R = 314$  rad/s,  $f_R = 50$  Hz,  $p = 24$ ,  $V_{*s} = 1$ ,  $X_1 = 1$ ,  $I_{*s} = 1.0$ ,  $\Psi_{*f} = 1.0$ , and  $J = 9 \times 10^5$  kg m<sup>2</sup>. The rotor will pull into synchronism, if the slip at the instant of putting on line does not exceed (in absolute terms) the value given by

$$|s_0| = 24 \div 0.6 \times 314 \sqrt{\frac{25 \times 10^6}{314 \times 9 \times 10^5}} = 0.0373$$

We have derived Eq. (59-5), defining the conditions for an incoming generator to pull into synchronism when it is put on line off-synchronism, without allowing for the induction electromagnetic torque,  $T_{em,ind}$ , which appears when the machine is running off-synchronism with a slip  $s = (\omega_s - \omega)/\omega_s$ . At  $\omega > \omega_s$  and  $s < 0$ , the induction torque retards the rotor. At  $\omega < \omega_s$  and  $s > 0$  (as in Fig. 59-2), it accelerates the rotor. In either case, it tends to close the gap in speed between the rotor and the field, that is, forces the rotor to pull into synchronism.

If we allow for the effect of the induction torque, we shall see that, with self-synchronization, the incoming machine pulls into synchronism at a somewhat higher initial slip,  $s_0$ , than that given by Eq. (59-5). In more detail the effect of induction torque will be examined in Sec. 59-4.

A major limitation of self-synchronization is that it is accompanied by heavy transient currents and, as a corollary, strong electromagnetic forces which may work loose or even damage the armature winding. It is safe to use only where transient currents are not dangerous to the machine. In other cases, its use is warranted only if a machine must be brought into the system with a minimum delay.

### 59-3 Synchronizing by Frequency Control

As we have learned, for the incoming machine to pull into synchronism, it is required that at the instant of coming on line the difference,  $s_0\Omega_s$ , between the angular velocities of the rotor  $\Omega = \Omega_s(1 - s_0)$ , and the rotating field,  $\Omega_s = \omega_s/p$ , be sufficiently small.

As follows from Eq. (59-5), the difference, or slip, velocity must be such that

$$\Omega_s - \Omega = s_0 \Omega_s = s_0 (\omega_s / p) \leq (1/0.6) \sqrt{\frac{S_R I_{*s} \Psi_{*f}}{\omega_R J}} \quad (59-6)$$

With self-synchronization, the difference in speed is kept small by bringing the rotor up to synchronous speed, which is done by a synchronizing (accelerating) servo-motor. In the course of synchronization, the field velocity and the system frequency do not change and remain at their rated values.

With frequency control, no accelerating motor is required, because the same effect is achieved in a different way. At the beginning of synchronization, the rotor of the incoming machine is stationary,

$$\Omega = 0, s_0 = (\Omega_{s0} - \Omega) / \Omega_{s0} = 1$$

To obtain the desired small difference velocity, the system frequency should be reduced from its rated value to a value  $f_{s0} \ll f_R$  necessary for Eq. (59-6) to be satisfied

$$\Omega_{s0} = \frac{2\pi f_{s0}}{p} \leq (1/0.6) \sqrt{\frac{S_R I_{*s} \Psi_{*f}}{\omega_R J}}$$

For this to happen, the per-unit system frequency must be

$$f_{*s0} = f_{s0} / f_R \leq (p/0.6\omega_R) \sqrt{\frac{S_R I_{*s} \Psi_{*f}}{\omega_R J}}$$

**Example.** Given the same generator as in the previous example, find the frequency at which the incoming machine will pull into synchronism.

$$f_{*s0} \leq (24 \div 0.6 \times 314) \sqrt{\frac{25 \times 10^6}{314 \times 9 \times 10^5}} = 0.0373$$

Then,

$$f_{s0} = f_{*s0} f_R = 0.0373 \times 50 = 1.86 \text{ Hz}$$

After the incoming machine has pulled into synchronism, the system frequency is gradually raised to its rated value,  $f_R$ . Owing to the synchronizing torque, the rotor speed is likewise brought up to its rated value (with synchronous operation maintained at all intermediate frequencies).

Synchronization by frequency control may be used for large synchronous motors and also during tests.

Synchronization by frequency control calls for a voltage source whose frequency,  $f_s$ , can be varied between broad limits (from nearly zero to  $f_R$ ). To maintain the armature current component

$$I_s = V_s/X_1 = V_s/\omega_s L_1$$

due to  $V_s$ , at the value it has at the rated frequency,

$$I_{s,R} = V_{R}/\omega_R L_1$$

the system voltage must be varied in proportion to the system frequency,

$$V_s = (\omega_s/\omega_R) V_R$$

This can be achieved, using a servo synchronous generator accelerated by its prime mover from rest to rated angular velocity while keeping its field current unchanged. Alternatively, this purpose can be served by a thyristor converter with an ample output.

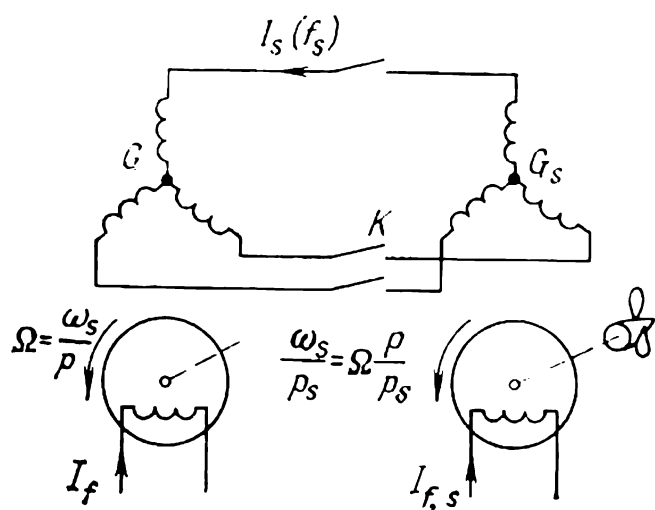


Fig. 59-4 Synchronization by frequency control:

$G$ —incoming synchronous machine;  
 $G_s$ —servo synchronous generator

$I_f$  maintained at a constant value throughout the starting period. The circuit-breaker  $K$  interconnecting the armature windings of the two machines is then closed, and the servo generator is accelerated by its prime mover. When the angular velocity of the field in the incoming generator,  $\Omega_{s0} = 2\pi f_{s0}/p$ , rises to a value sufficient to give rise to the required armature current,  $I_s$  (with allowance for the ohmic resistances of the armatures), and for the incoming generator to pull into synchronism, the incoming generator sets in motion, and does so in step with the system. If the servo generator and the incoming generator differ in the num-

The arrangement using synchronous generator is shown in Fig. 59-4. The procedure involves two steps as follows.

(1) The servo generator,  $G_s$ , and the incoming generator,  $G$ , are first excited each from an external source of its own, with  $I_{f,s}$  and

ber of pole pairs, the incoming generator will set in motion at the velocity of the servo generator equal to  $\Omega_{s0}p/p_s$ .

(2) After  $G_s$  comes up to its rated angular velocity,  $\Omega_{s,R} = \omega_R/p_s$ , and to its rated frequency,  $f_s = f_R = \Omega_{s,R}p_s/2\pi$ , the incoming generator, held in synchronism by electrical coupling between the rotors, comes up to its rated velocity,  $\Omega_R = \omega_R/p$ .

### 59-4 Induction Starting

Induction starting of a synchronous machine does not call for a servo motor to bring up the incoming machine to a velocity close to synchronous. This is done owing to the induction torque,  $T_{ind}$ , that is developed when the armature winding of the incoming machine is connected to the system (Fig. 59-1).

When the incoming machine is connected to the system with  $V_s$  and  $f_s$ , the currents traversing the armature winding set up a magnetic field which rotates at  $\Omega_s$ . Relative to the rotor, this field travels at  $\Omega_s - \Omega = s\Omega_s$  (where  $\Omega$  is the mechanical angular velocity of the rotor and  $s$  is the relative slip) and induces currents at frequency  $sf_s$  in the field winding closed through a damping resistor,  $R_d$ , and in the damper winding. It is the interaction of these currents with the rotating field that produces  $T_{ind}$ .

The greater proportion of  $T_{ind}$  is produced by the currents induced in the damper winding. Therefore, its resistance and reactance are chosen so as to supply a sufficient induction torque at any stage of starting. In turn, the resistance and reactance of the damper winding depend on the number, dimensions and material of the damper bar.

In a synchronous motor, the dimensions of the damper winding motor are governed by the external (load) torque,  $T_{ext}$ , that must be overcome at starting. In any case, the damper winding must be proportioned so that its temperature at the end of starting does not rise above 250°C.

A sufficiently large  $T_{ind}$  is best supplied by series-shunt damper winding in which all the bars are connected to short-circuiting rings at the pole faces (see Fig. 51-9). The rings are formed by the conducting segments interconnecting the bars of each pole, and the flexible jumpers interconnecting the segments of adjacent poles.

The induction torque varies with slip in about the same manner as in a squirrel-cage induction motor (see Sec. 43-3).

The theory of the induction machine may be extended to the induction running of a synchronous machine on replacing the two short-circuited windings on its rotor (field and damper) with one short-circuited winding with an equivalent resistance  $R'_2$  and an equivalent reactance  $X'_2$  (for more detail, refer to Sec. 73-3). Then the induction torque in a synchronous machine may approximately be found, neglecting the single-axis effect (see Sec. 43-3):

$$T_{\text{ind}} = \frac{m_1 R'_2 V_1^2}{s \Omega_1 [(R_1 + R'_2/s)^2 + X_{\text{sc}}^2]} \quad (59-7)$$

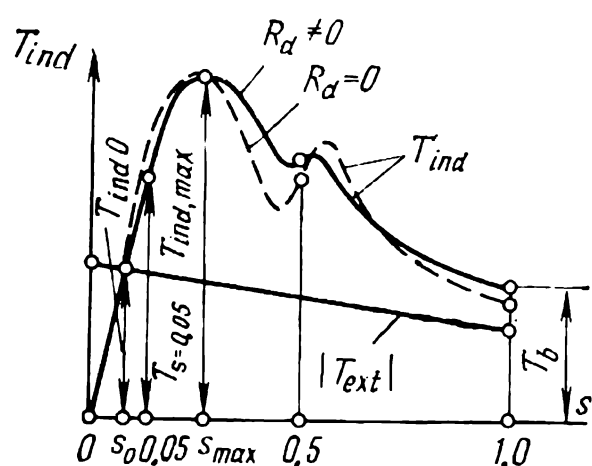


Fig. 59-5 Torques at induction (asynchronous) starting

As applied to the induction running of a synchronous machine, the notation used is as follows:  $m_1 = m$  is the number of armature phases,  $V_1 = V_s$  is the system (bus) voltage,  $\Omega_1 = \Omega_s$  is the mechanical angular velocity of the field,

$R_1$  is the resistance per armature phase,  $R'_2$  is the equivalent resistance of the damper and field windings referred to the armature winding,  $X_{\text{sc}} = X_1 + X'_2$  is the inductive reactance of the armature winding at  $s = 1$ , where  $X_1 = X_0$  is the leakage inductive reactance of the armature winding, and  $X'_2$  is the equivalent inductive reactance of the field and damper windings referred to the armature winding.

An approximate plot of the induction torque of a synchronous machine as a function of slip,  $T_{\text{ind}} = f(s)$ , appears in Fig. 59-5.

As the motor just changes from rest to rotation, when  $s = 1$ , the rotor is acted upon by what is known as the *breakaway torque*,  $T_b$ . At full speed, when the slip is a maximum,  $s_{\text{max}}$ , there appears the maximum induction torque,  $T_{\text{ind,max}}$ . As a rule, the nameplate of a synchronous motor also gives the torque at  $s = 0.05$ , referred to as the *pull-in torque*. Since  $T_{\text{ind}} = V_s^2$ , it is usual to state the voltage at which  $T_b$ ,  $T_{\text{ind,max}}$ , and  $T_{0.05}$  were determined.

Ordinarily, the characteristic induction torques of a synchronous machine are stated as fractions of the rated synchronous torque, namely

$$T_b/T_{em,R}, \quad T_{ind,max}/T_{em,R}, \quad T_{0,05}/T_{em,R}$$

where

$$T_{em,R} = S_R \eta_R \cos \varphi_R / \Omega_R$$

The single-phase field winding also contributes to the induction torque. The currents induced in it set up a pulsating ("breathing") field acting along the  $d$ -axis, rather than a rotating field like that established by the polyphase damper winding. Because of this, the induction torque has a "dip" at  $s = 0.5$  which might have an adverse effect on the starting performance of the motor. This effect is minimized by inserting a damping resistor,  $R_d$ , in the field circuit. As is seen from Fig. 59-5, the starting characteristic at  $R_d \approx \approx 5R_f \neq 0$  is substantially better than at  $R_d = 0$  (see Sec. 46-2).

At starting, the field winding must be closed through an exciter or a damping resistor. The reason for this is as follows.

When the machine is just changing from rest to rotation,  $s \approx 1$  and  $s\Omega_s = \Omega_s$ , the voltage existing across the open-circuited field winding is

$$V_{\sim} = (w_f / qu_s) V_{ph}$$

where  $V_{ph}$  is the phase voltage of the armature winding,  $w_f$  is the number of turns per pole in the field winding,  $q$  is the number of armature slots per pole, and  $u_s$  is the number of winding conductors per slot. The voltage existing across the open-circuited field may be three to five times the phase voltage, rising to 20-50 kV which is about a hundred times the rated voltage for which the winding insulation is designed. This would damage field insulation and even knock the machine out of operation. By short-circuiting the field winding, the induced voltage is reduced to zero. When the field winding is closed through  $R_d \approx 5R_f$ , it vanishes almost completely or does not exceed the rated voltage of the field winding.

Induction starting of a synchronous motor proceeds in the same manner as the starting of an induction motor discussed in Part 4. At starting, the load (external) torque,  $T_{ext}$ , on the motor shaft (see Fig. 59-5) must be smaller than  $T_{ind}$ . Then, as follows from the equation of motion, the motor

will come up to speed with an acceleration given by

$$d\Omega/dt = (T_{\text{ind}} - T_{\text{ext}})/J$$

where  $J$  is the moment of inertia of the rotating parts, and the mechanical angular velocity can be brought up to

$$\Omega_0 = \Omega_s (1 - s_0)$$

corresponding to a balance between  $T_{\text{ind}}$  and  $|T_{\text{ext}}|$ . If the pull-in torque of the motor is sufficiently high, and  $s_0$  at  $T_{\text{ind}} = |T_{\text{ext}}|$  satisfies Eq. (59-5), then, upon closure of the automatic synchronizer and the appearance of current in the field winding, the motor will pull into synchronism. (In starting on load, when  $T_{\text{ext}} \neq 0$ ,  $s_0$  must be somewhat smaller than is given by Eq. (59-5).) If the load torque is high, starting must be done at  $V_s = V_R$ . The initial starting current (that is, the steady-state armature current at  $s = 1$ ) in the circumstances is fairly heavy, so that its ratio to rated armature current,  $I_{\text{start}}/I_R$ , ranges from 3:1 to 5:1. Here,  $I_R = S_R/3V_s$  is the rated armature current at synchronism.

The currents in the damper (starting) winding are as heavy. If the starting conditions are especially severe, the temperature of the damper winding might rise to above 250°C. To keep its temperature within safe limits,  $V_s$  must be held below  $V_R$ . This is done by switching in a reactor or an auto-transformer. Unfortunately, this also reduces the induction torque as it is proportional to the system (bus) voltage squared, so the motor takes more time to start.

At rated voltage, a synchronous motor is induction-started, using the arrangement in Fig. 59-1. The procedure is as follows.

(1) Before the armature winding is connected to the supply line, the field winding is disconnected from the exciter ( $K_1$  is opened) and connected across the damping resistor,  $R_d$  ( $K_2$  is closed). As already explained, this is done by opening the automatic synchronizer which combines  $K_1$  and  $K_2$ .

(2) Contactor (or circuit-breaker)  $K$  is closed to connect the armature winding to the supply line with  $V_s$ . The resultant induction torque brings the motor up to  $s_0$ . Depending on the power rating and angular velocity of the motor, this may take from a few seconds to several minutes. At  $\Omega_0 = \Omega_s (1 - s_0)$ , the exciter is self-excited, and  $V_{\text{exc}}$  appears across its

terminals. (Prior to starting, the adjusting rheostat  $AR$  is set so that  $V_{\text{exc}}$  is sufficient for the desired  $I_f = V_{\text{exc}}/R_f$  to be obtained.)

(3) At  $\Omega_0$ , the automatic synchronizer operates and connects the field winding to the exciter,  $Exc$ , supplying  $V_{\text{exc}}$ . In doing so,  $K_1$  closes first and  $K_2$  opens second. Otherwise, the field winding would be left open-circuited (even though for an instant) and damaged. As with self-synchronization, the field current builds up and the motor pulls into synchronism (if  $s_0$  is sufficiently small). In this, the motor is aided by induction torque.

(4) In starting at load,  $V_{\text{exc}}$  is pre-adjusted so that the motor will be brought up to synchronism at the desired power factor. In starting at no load ( $T_{\text{ext}} \approx 0$ ), the motor is first brought up to synchronism, then the desired  $T_{\text{ext}}$  is set, and the field current is adjusted so that the machine will generate the required reactive power.

### 59-5 Induction Running of Synchronous Machines. Resynchronization

As we have learned, except salient-pole machines with solid-iron poles, nearly all synchronous machines (motors, condensers and, especially, large generators) have damper windings (see Sec. 51-3).

Damper windings give the synchronous machines quite a number of valuable properties. Most important among them is that the damper winding enables the machine to keep running even if it “swings” out of synchronism. Also, any transients caused by a change in voltage, field current or external torque give a more favourable response owing to the transient currents that are induced in the damper bars.

Importantly, induction torque in a synchronous machine is also produced due to a short-duration departure of the angular velocity of the rotor from synchronous. This may, for example, occur when there is a change in the operating conditions and, as a result, a change in the power (or torque) angle. In the circumstances, induction torque enables the machine to slip back to synchronism (see Sec. 60-1) more gradually.

A swing out of synchronism may be caused by a sudden fall in the system voltage or field current, or by a sudden increase in the load torque beyond the pull-out torque,



$T_{s,\max}$ . When this happens, the angular speed of the machine exceeds synchronous if it has been running as a generator, or falls below synchronous, if it has been running as a motor.

As the difference in speed between the rotor and the field increases, the relative slip increases too. This leads to a gradual build-up in induction torque until it balances the external (load) torque at a certain definite value of slip.

How a synchronous machine will run upon a fall out of synchronism depends on its induction torque characteristic which can approximately be found from Eq. (59-7). In per-unit, the maximum induction torque (see Sec. 43-3) is given by

$$\begin{aligned} T_{*ind,\max} &= T_{ind,\max}/T_B \\ &\approx V_{*s}^2/2X_{*sc} \approx \text{from 1.5 to 3.0} \end{aligned}$$

where  $T_B = S_R/\Omega_s$  is the synchronous torque taken as the base quantity, and  $X_{*sc}$  is the short-circuit reactance at  $s = 1$ :

$$X_{*sc} \approx (X_{*d}'' + X_{*q}'')/2 = \text{from 0.15 to 0.3}$$

The maximum induction torque is 2 to 3.5 times the external torque under rated synchronous conditions

$$\begin{aligned} T_{*ext} &= T_{ext}/T_B = P_{*,R} \approx \cos \varphi_R \\ &= \text{from 0.8 to 0.9} \end{aligned}$$

Because of this, it often happens that

$$T_{*ind,\max} > T_{*ext}$$

even when the system (bus) voltage is reduced by a sizeable amount ( $V_{*s} < 1$ ), so, upon a fall out of synchronism, the machine keeps running on induction torque at a small slip,  $0 < s < s_{\max}$ , where

$$s_{\max} = R_{*2}'/X_{*sc}$$

is the slip corresponding to  $T_{ind,\max}$  (see Fig. 59-5). At  $s < s_{\max} \ll 1$ , the induction torque equation (59-7) can markedly be simplified

$$T_{ind} = t_{ind}s \quad (59-8)$$

where  $t_{ind} = mV_s^2/\Omega_s R_2'$  is a constant, and induction torque is proportional to slip. On setting  $T_{ind} = T_{ext}$ , it is an easy matter to find from Eq. (59-8) the slip required for asynchro-

nous running to take place

$$s = T_{\text{ext}}/t_{\text{ind}} = R'_{*2} \cos \varphi_R / V_{*s}^2$$

This slip is very small, being a few thousandths in large machines.

As we have seen, after it has dropped out of synchronism, a synchronous machine will in many cases keep running as an induction machine. Obviously, this is an abnormal condition which requires appropriate steps to be taken.

To avoid likely damage, the first thing to do is to turn off excitation. This is done by disabling the automatic synchronizer and closing the field winding through a damping resistor. This will cancel the alternating synchronous torque that causes oscillations in the angular velocity and armature current. Upon removal of excitation, the machine will run on induction torque at a slip  $s$ , delivering the same active power as before. However, instead of delivering reactive power to the system, the machine will draw it from the system (because the reactive component of current lags behind the system voltage as in an induction machine).

For how long induction running may be tolerated depends on the losses dissipated in the short-circuited field and damper windings:

$$P_{\text{Cu2}} = sP_{\text{em}} \approx sP$$

It must be found in advance by thermal calculations. As a rule, sustained induction running can be permitted at reduced power output (for turbogenerators, at 50 to 70% of rated power).

After the cause of falling out of synchronism has been cleared, the machine must again be synchronized. This procedure is called *resynchronization*. In a way, it is not unlike self-synchronization. If the slip in induction running is substantially smaller than the value of  $s_0$  given by Eq. (59-5) and required for a machine to pull into synchronism, resynchronization can be effected without removing load from the machine that is, without reducing  $T_{\text{ext}}$ . It will suffice to connect the field winding to an exciter. This will cause the field current to rise, and the machine will pull into synchronism. If the slip in induction running exceeds  $s_0$ , the load on the machine should first be somewhat reduced by bringing down  $T_{\text{ext}}$ . This done, the automatic synchronizer may be activated for resynchronization as already explained.

## 60 Instability of Synchronous Machines in Parallel Operation

### 60-1 Free Oscillations of the Rotor Following a Sudden Change in External Torque

When a machine is operating in parallel with another machine or a system, for each synchronous steady state there is a certain definite angular position that the rotor takes up relative to the rotating field. This position is described in terms of the load (torque or displacement) angle,  $\theta$ , which is the same as the angle between  $\dot{\Psi}_{fm}$  and  $\dot{\Psi}_{vm}$  (see Fig. 59-2).

At constant  $V_s$  and  $I_f$ , each value of  $T_{\text{ext}}$  corresponds to a certain definite value of  $\theta$  on the power-angle characteristic of the machine (see Sec. 58-6). Any change in the quantities that govern the power angle inevitably leads to a change in the position of the rotor relative to the rotating field. The response of  $\theta$  to such changes is usually oscillatory. Oscillations of  $\theta$  about its new value are accompanied by oscillations in the angular velocity of the rotor, armature current, electromagnetic torque, and active and reactive power.

We shall limit our discussion to small oscillations of the rotor. Then  $\Delta\theta$ , the deviations of  $\theta$  from its initial value,  $\theta_0$ , will be so small that

$$\sin \alpha \approx \alpha = \theta - \theta_0$$

where  $\alpha$  designates the deviation,  $\Delta\theta$ .

Suppose that initially (at  $t < 0$ ), the machine is operating as a generator at  $V_s$ ,  $T_{\text{ext},0}$  balanced by  $T_{\text{em},0}$ , synchronous velocity  $\omega_s$ , and  $\theta = \theta_0$ . Then the armature current\* will be

$$\dot{I}_0 = \dot{E}_f - \dot{V}/jX_1$$

In Fig. 60-1, the positions of the rotor and all the phasors and vectors involved are shown at  $t \geq 0$  by full lines, and on the power-angle characteristic the initial operating conditions correspond to point *I*. At  $t = 0$ , the external torque suddenly increases by  $\Delta T_{\text{ext}}$  to become

$$T_{\text{ext}} = T_{\text{ext},0} + \Delta T_{\text{ext}}$$

---

\* The current equation is written for a nonsalient-pole machine.

This upsets the balance of torques

$$T_{\text{ext}} - T_{\text{em},0} = \Delta T_{\text{ext}}$$

and the rotor picks up speed with an acceleration

$$(d\Omega/dt)_0 = \Delta T_{\text{ext}}/J$$

where  $J$  is the moment of inertia of the rotating parts of the machine.

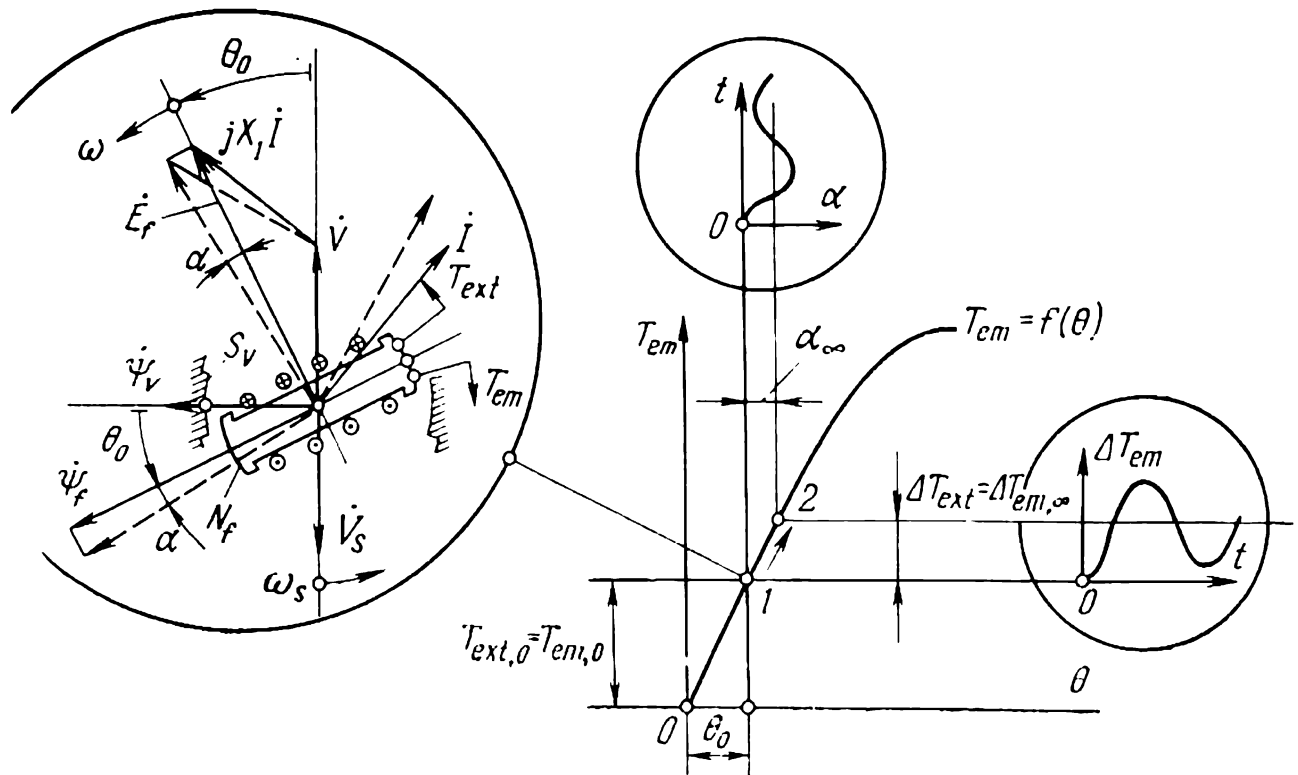


Fig. 60-1 Transient response to a small change in  $T_{\text{ext}}$

The rotor will keep picking up speed (with a gradually decreasing acceleration) and the power angle,  $\theta = \theta_0 + \alpha$  will increase until the increasing electromagnetic torque,  $T_{\text{em}} = T_{\text{em},0} + \Delta T_{\text{em}}$ , balances the external torque

$$T_{\text{em}} = T_{\text{ext},0} + \Delta T_{\text{ext}},$$

at point 2 on the power-angle curve (see Fig. 60-1).

Despite the equality of torques, however, the conditions at point 2 corresponding to  $\theta = \theta_0 + \alpha_\infty$  (where  $\alpha_\infty$  is the steady-state change of angle) will not settle to their steady-state values at once, because the rotor velocity  $\omega$  exceeds the synchronous velocity,  $\omega_s$ , at which  $\dot{V} = -\dot{V}_s$  and  $\dot{\Psi}_v$  rotate (Fig. 60-2). The angle  $\theta = \theta_0 + \alpha$  will keep increasing ( $\alpha > \alpha_\infty$ ), but with  $\Delta T_{\text{em}}$  exceeding  $\Delta T_{\text{ext}}$ . Because of this an electromagnetic counter torque,  $\Delta T_{\text{em}} - \Delta T_{\text{ext}}$ , will

be acting on the rotor giving rise to a deceleration

$$d\Omega/dt = (\Delta T_{ext} - \Delta T_{em})/J$$

The rotor will slow down until it slips back to synchronous velocity,  $\omega = \omega_s$ . But again, this will not be a steady state, because  $\alpha > \alpha_\infty$ , that is, the electromagnetic torque will exceed the external torque, and the machine will be decelerated still more (see Fig. 60-2). As is seen from Figs. 60-1

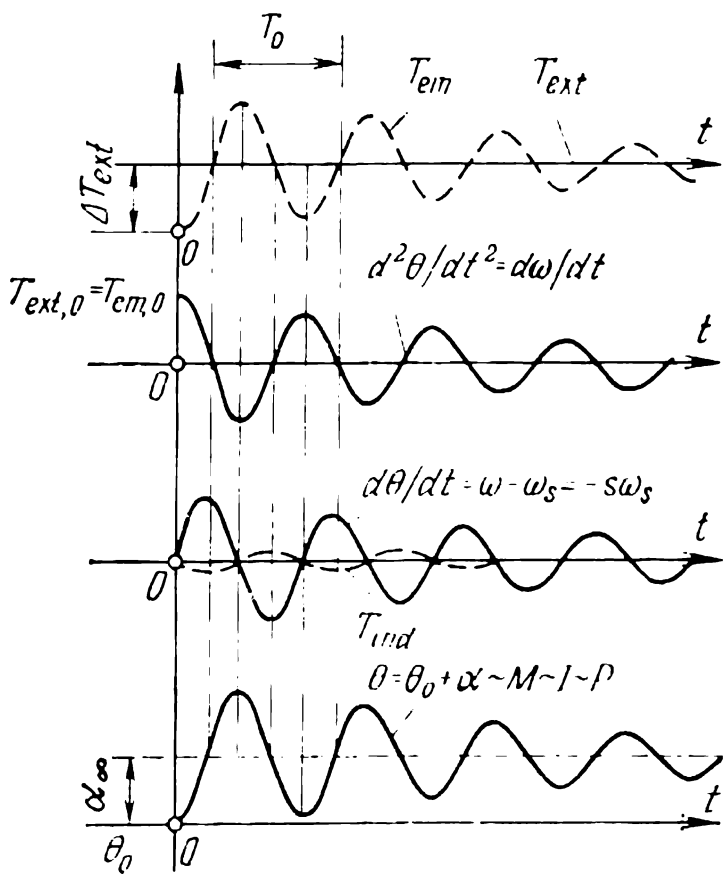


**Fig. 60-2** Oscillatory transient response of  $\theta$ ,  $s$ ,  $d\omega/dt$ ,  $T_{em}$ ,  $I$ , and  $P$  to a small change in  $T_{ext}$

and 60-2, this causes oscillations in  $\theta = \theta_0 + \alpha$ , in  $T_{em}$ ,  $d\omega/dt$ , and in  $\omega$ . (Plots of  $\alpha$  and  $\Delta T_{em}$  as functions of time are shown in circles in Fig. 60-1.) This is accompanied by an interchange of energy between the rotating rotor and the magnetic field. If there were no losses of energy, the oscillations would go on undamped. However, some energy is inevitably lost as heat in the rotor circuits as they cut the magnetic field. Because of this, the oscillations gradually decay as shown in Fig. 60-2.

For a mathematical description of rotor oscillations, all the necessary quantities must be expressed in terms of the initial power angle  $\theta_0$  and its small deviation,  $\Delta\theta = \alpha$ .

(1) The angle  $\theta$  between  $\dot{E}_f$ , rotating in the model at  $\omega$ , and  $\dot{V} = -\dot{V}_s$ , rotating at  $\omega_s = 2\pi f_s$ , is the same (see Fig. 60-1) as the angle between the  $d$ -axis of the rotor (or  $\dot{\Psi}_{fm}$ ) and the axis of the resultant field (or  $\dot{\Psi}_{vm}$ ),

$$0 = \theta_0 + \Delta\theta = \theta_0 + \alpha$$

Alternatively, the angle  $\theta$  may be interpreted as the angle between the unlike magnetic poles,  $S_v$  and  $N_f$  (see Fig. 60-1), respectively representing  $\dot{\Psi}_{vm}$  and  $\dot{\Psi}_{fm}$ .

(2) The electrical angular velocity of the rotor (or the mechanical angular velocity of the rotor in a two-pole model) is the sum of the synchronous angular velocity  $\omega_s$  and an additional angular velocity associated with the deviation of the power angle from its initial value,  $\theta_0$ :

$$\omega = \omega_s + d\theta/dt = \omega_s + d\alpha/dt$$

The mechanical angular velocity of the rotor is

$$\Omega = \omega/p = \Omega_s + (d\alpha/dt)/p$$

(3) The slip of the rotor relative to the resultant field is

$$s = (\Omega_s - \Omega)/\Omega_s = - (d\alpha/dt)/\omega_s$$

(4) The acceleration of the rotor is

$$d\Omega/dt = (d^2\alpha/dt^2)/p$$

(5) The synchronous electromagnetic torque acting on the rotor at  $\theta = \theta_0 + \alpha$  (see Fig. 60-1) is

$$T_{em} = T_{em,0} + \Delta T_{em} = T_{em,0} + t_s \alpha$$

where  $T_{em,0} = f(\theta_0)$  = electromagnetic torque at  $\theta = \theta_0$   
on the power-angle characteristic  
 $t_s = (\partial T_{em}/\partial \theta)_{\theta=\theta_0}$  = specific synchronizing torque at  
 $\theta = \theta_0$  (see Sec. 58-7).

For a nonsalient-pole machine

$$T_{em,0} = mVE_f \sin \theta_0 / X_1 \Omega_s$$

$$t_s = mVE_f \cos \theta_0 / X_1 \Omega_s$$

(6) The induction torque produced by the interaction of the currents in the damper and field windings with the resultant field can be found at small values of slip from Eq. (59-8)

$$T_{ind} = t_{ind}s = -D d\alpha/dt$$

where  $t_{\text{ind}} = mV^2/\Omega_s R'_2$ , and  $D = t_{\text{ind}}/\omega_s$  is the damping factor which is inversely proportional to the referred resistance of the damper and field windings,  $R'_2$ . The induction electromagnetic torque is assumed to be positive when it is acting with the direction of rotation.

Now we can write the equation of motion for small oscillations of the rotor caused by a sudden change in external torque,  $\Delta T_{\text{ext}}$ ,

$$T_{\text{ext}} - T_{\text{em}} + T_{\text{ind}} = J d\Omega/dt$$

On expressing the torques in terms of  $\alpha$  and its derivatives,  $d\alpha/dt$  and  $d^2\alpha/dt^2$ , we get a linear inhomogeneous second-order differential equation with constant coefficients

$$d^2\alpha/dt^2 + (Dp/J) (d\alpha/dt) + (t_s p/J) \alpha = (p/J) \Delta T_{\text{ext}} \quad (60-1)$$

from which we can readily find the angle  $\alpha$ . The solution of Eq. (60-1) is the sum of a complementary and a particular solution. The complementary solution of

$$d^2\alpha/dt^2 + (Dp/J) (d\alpha/dt) + (t_s p/J) \alpha = 0$$

is a force-free or transient term. The particular solution is a steady-state term, that is, one at  $t = \infty$ .

The complementary part may be written

$$\alpha = C_1 \exp(r_1 t) + C_2 \exp(r_2 t)$$

where  $C_1$  and  $C_2$  are constants definable from the initial conditions, and  $r_1$  and  $r_2$  are the roots

$$r_{1,2} = -(Dp/2J) \pm \sqrt{(Dp/2J)^2 - t_s p/J}$$

of the characteristic equation

$$r^2 + (Dp/J)r + t_s p/J = 0$$

In the underdamped case, when

$$(Dp/2J)^2 \ll t_s p/J$$

and the induction torque is a small fraction of the synchronous torque, the roots of the characteristic equation are complex conjugates

$$r_{1,2} = -\beta_D \pm j\omega_0$$

the real part of which

$$\beta_D = Dp/2J$$

is the decay factor, and the coefficient of the imaginary part

$$\omega_0 = \sqrt{t_s p / J}$$

is the angular frequency of free oscillations of the rotor in the magnetic field.

With such roots, the complementary solution may be simplified still more

$$\alpha = C_0 \exp(-\beta_D t) \cos(\omega_0 t + \varphi_0)$$

where  $C_0$  and  $\varphi_0$  are constants to be found.

The particular solution of Eq. (60-1), or the steady-state part (at  $t = \infty$ ), when  $d\alpha/dt = 0$  and  $d^2\alpha/dt^2 = 0$ , is the steady-state change of angle

$$\alpha_{(t=\infty)} = \alpha_\infty = \Delta T_{\text{ext}} / t_s$$

The complete solution of Eq. (60-1) is the sum of the two above solutions

$$\alpha = C_0 \exp(-\beta_D t) \cos(\omega_0 t + \varphi_0) + \alpha_\infty$$

The constants  $C_0$  and  $\varphi_0$  in the complete solution are found from the initial conditions:

(1) at  $t = 0$ ,  $\omega = \omega_s$  and  $s = 0$ , so  $d\alpha/dt = 0$ . Also in the underdamped case,  $\beta_D \ll \omega_0$ , and

$$(d\alpha/dt)_{t=0} \approx [-C_0 \omega_0 \exp(-\beta_D t) \sin(\omega_0 t + \varphi_0)]_{t=0} = 0$$

Hence,  $\varphi_0 = 0$ ;

(2) at  $t = 0$ ,  $\theta = \theta_0$  and  $\alpha = 0$ . Recalling that  $\varphi_0 = 0$ , we get

$$\alpha = C_0 \cos \varphi_0 + \alpha_\infty = C_0 + \alpha_\infty = 0$$

Hence,  $C_0 = -\alpha_\infty$

Finally, the deviation of the power angle  $\theta$  in the case of force-free, or transient, oscillations can be written

$$\alpha = \alpha_\infty [1 - \exp(-\beta_D t) \cos \omega_0 t]$$

The waveform of oscillation in the angle  $\theta = \theta_0 + \alpha$  is shown in Fig. 60-2 which also gives the  $d\theta/dt$  and  $d^2\theta/dt^2$  curves.

As follows from the equation for  $\alpha$ , the rotor is oscillating in the resultant magnetic field about its steady-state position,  $\theta = \theta_0 + \alpha_\infty$ . In the underdamped case, force-free or transient oscillations occur at the frequency given by

$$\omega = 2\pi/T_0 = \sqrt{t_s p / J} \quad (60-2)$$



As follows from Eq. (60-2), the frequency is inversely proportional to the square root of the moment of inertia and directly proportional to the square root of the specific synchronizing torque. For large machines,  $T_0$  is anywhere from a split second to several seconds. The frequency of oscillation is a maximum at no load, when  $\theta_0 = 0$  and  $t_s = t_{s,\max}$ . As the load is increased, the frequency of oscillation decreases. In approaching the steady-state stability limit,  $\theta_0$  tends to  $\theta_{\max}$ ,  $t_s$  tends to zero, and so does the frequency of oscillation.

At the onset of the transient response, the amplitude of angle oscillations is  $\alpha_\infty = \Delta T_{\text{ext}}/t_s$ . With time the oscillations gradually collapse with a decay factor  $\beta_D = Dp/2J$  and with a decay (or transient) time constant

$$T_D = 1/\beta_D = 2J/Dp$$

At time  $T_D$ , it reduces to  $1/e$  of its original value. At time  $2T_D$ , it decays to  $1/e^2$  of its original value, and so on.

The oscillations of  $\theta$  are accompanied by torque oscillations with an initial peak value  $\Delta T_{\text{em},0} = t_s \alpha_\infty$ , and active-power oscillations with an initial peak value  $\Delta P_0 = \Omega_s \Delta T_{\text{em},0} = \Omega_s t_s \alpha_\infty$ .

As is seen from Fig. 60-1, changes in the angular position of the rotor are accompanied by oscillations in the rms value and phase of current. Using the voltage ( $\dot{E}_f$ ,  $\dot{V}$ ,  $jX_1\dot{I}$ ) triangle, we can readily express  $X_1 I$  in terms of  $E_f$ ,  $V$ , and  $\theta$ , and find the rms value of current

$$I = \sqrt{\frac{E_f^2 + V^2 - 2VE_f \cos \theta}{X_1}}$$

the change in the rms current

$$\Delta I = (\partial I / \partial \theta)_{\theta=\theta_0}, \quad \Delta \theta = (\partial I / \partial \theta)_{\theta=\theta_0}$$

$$\alpha = \frac{E_f V \sin \theta_0}{X_1 \sqrt{E_f^2 + V^2 - 2VE_f \cos \theta_0}} \alpha_\infty$$

and the initial amplitude of oscillation of the rms current

$$\Delta I_0 = (\partial I / \partial \theta)_{\theta=\theta_0} \alpha_\infty$$

In the overdamped case,

$$(Dp/2J)^2 > t_s p/J$$

the characteristic equation has real roots, and the machine goes to a new steady state at  $\theta_\infty = \theta_0 + \alpha_\infty$  aperiodically.

## 60-2 Forced Oscillations of the Rotor

If the prime mover of a synchronous generator is a reciprocating engine, the external torque will contain a constant (zero-frequency) terms and several harmonics

$$T_{\text{ext}} = T_{\text{ext},0} + \sum_{v=1}^{\infty} T_{\text{ext},v} \cos \omega_v t$$

where  $T_{\text{ext},v}$  is the amplitude of the  $v$ th-harmonic external torque, and  $\omega_v$  is its angular frequency.

Suppose that  $T_{\text{ext},0}$  corresponds to  $\theta_0$  on the torque-angle characteristic (see Fig. 60-1). Then, the  $v$ th-harmonic torque will cause  $\theta$  to oscillate about its mean value,  $\theta_0$ . If  $T_{\text{ext},v} \ll T_{\text{ext},0}$ , we may write  $\theta$  as

$$\theta = \theta_0 + \alpha$$

where  $\alpha$  is a small change in  $\theta$  due to the  $v$ th-harmonic torque. This small change can be found from the equation of motion for the rotor, written by analogy with Eq. (60-1):

$$d^2\alpha/dt^2 + (Dp/J)(d\alpha/dt) + (t_s p/J)\alpha = (p/J) T_{\text{ext},v} \cos \omega_v t$$

The particular solution of the above equation for  $\alpha$ , assuming a steady state ( $t = \infty$ ), may be written

$$\alpha = \alpha_{\text{max}} \cos (\omega_v t - \varphi_v) \quad (60-3)$$

where

$$\alpha_{\text{max}} = \frac{T_{\text{ext},v}}{\omega_v \sqrt{D^2 + (\omega_v J/p - t_s/\omega_v)^2}}$$

is the amplitude of the  $v$ th-harmonic oscillation of  $\theta$ , and

$$\varphi_v = \arctan \frac{\omega_v J/p - t_s/\omega_v}{D}$$

is its phase.

To begin with, let us investigate the oscillations of the rotor when a synchronous generator is serving an isolated load (as shown in the diagram of Fig. 58-5). The  $v$ th-harmonic torque causes the rotor to oscillate about its mean electrical angular synchronous velocity  $\omega_s = \Omega_s p$ . Because the load voltage,  $\dot{V}$ , has the same electrical frequency  $\omega$  as

$\dot{E}_f$ , the angle  $\theta$  between them and the synchronous electromagnetic torque,  $T_{em}$ , remain unchanged.  $T_{em}$  balances the constant term of the external torque,  $T_{em} = T_{ext,0}$ . As the rotor departs by an angle  $\alpha$  from the axis rotating at synchronous velocity, no change occurs in the electromagnetic torque,

$$\Delta T_{em} = f(\alpha) = 0$$

Formally, this enables us to deem the specific synchronizing torque in the general expression for the change of torque equal to zero,  $t_s = 0$ .

Assuming at the same time (for simplicity) that the amount of damping is small (the underdamped case),  $D = 0$ , and using Eq. (60-3), we find that the deviation in the power angle of a synchronous generator serving an isolated load, caused by the  $v$ th-harmonic torque is

$$\alpha = \alpha_{0,\max} \cos(\omega_v t - \varphi_v) \quad (60-4)$$

where

$$\alpha_{0,\max} = T_{ext,v} p / \omega_v^2 J$$

is the amplitude of the  $v$ th harmonic of oscillation of the power angle in operation into an isolated load, and

$$\varphi_v = \pm \pi/2$$

is its phase.

Recalling that the electrical angular velocity of the rotor is

$$\omega = \omega_s + d\alpha/dt$$

it is an easy matter to find the speed regulation

$$\begin{aligned} \xi &= \frac{\omega_{\max} - \omega_{\min}}{\omega_s} = 2 (d\alpha/dt)_{\max} / \omega_s \\ &= 2 T_{ext,v} p / \omega_v \omega_s J \end{aligned}$$

where  $\omega_{\max} = \omega_s + (d\alpha/dt)_{\max}$   
 $\omega_{\min} = \omega_s - (d\alpha/dt)_{\max}$

When a synchronous generator is supplying a lighting load, the moment of inertia for its rotor must be chosen such that  $\xi < 0.01$  to  $0.005$ . Failure to meet this requirement will cause flicker unpleasant and tiring to the eye.

When a synchronous generator is connected to an infinite bus or system (as in Fig. 58-6), which implies constant  $V_s$  and constant  $f_s$ , the amplitude of the  $v$ th-harmonic oscilla-

tion of the power angle is a function of the synchronizing torque,  $t_s \neq 0$ . In the underdamped case, when  $D = 0$ , Eq. (60-3) may be re-written as

$$\alpha_{\max} = \left| \frac{\alpha_{0, \max}}{1 - (\omega_0 / \omega_v)^2} \right| \quad (60-5)$$

where  $\omega_0$  is the angular velocity of free oscillations of the rotor in parallel operation at  $\theta = \theta_0$  from Eq. (60-2), and  $\alpha_{0, \max}$  is the amplitude of the  $v$ th-harmonic oscillation of the power angle in supplying an isolated load under the same conditions.

As is seen from Eqs. (60-5) and (60-4), the ratio between the amplitude of the  $v$ th-harmonic oscillation of the power angle when the machine is connected to an infinite bus to the same amplitude when the machine is serving an isolated load, called the resonance modulus of the  $v$ th harmonic

$$\begin{aligned} \zeta_v &= \alpha_{\max} / \alpha_{0, \max} \\ &= \left| \frac{1}{1 - (\omega_0 / \omega_v)^2} \right| \end{aligned} \quad (60-6)$$

strongly depends on the ratio of  $\omega_0$ , the natural frequency of rotor oscillation, to  $\omega_v$ , the frequency of oscillation of the  $v$ th-harmonic of external torque (Fig. 60-3).

At  $\omega_0 / \omega_v \ll 1$ , the amplitude of oscillations of the power angle in operation into an infinite system,

$$\alpha_{\max} = \zeta_v \alpha_{0, \max} \approx \alpha_{0, \max}$$

is the same as with the machine serving an isolated load. In this case, the motion of the rotor is mainly governed by its inertia, and the synchronizing torque plays a minor role

$$t_s \alpha \ll (J/p) (d^2 \alpha / dt^2)$$

In contrast, at  $\omega_0 / \omega_v \gg 1$ , the amplitude of oscillation of the power angle with the machine connected to an infinite bus,

$$\alpha_{\max} = (\omega_v / \omega_0)^2 \alpha_{0, \max}$$

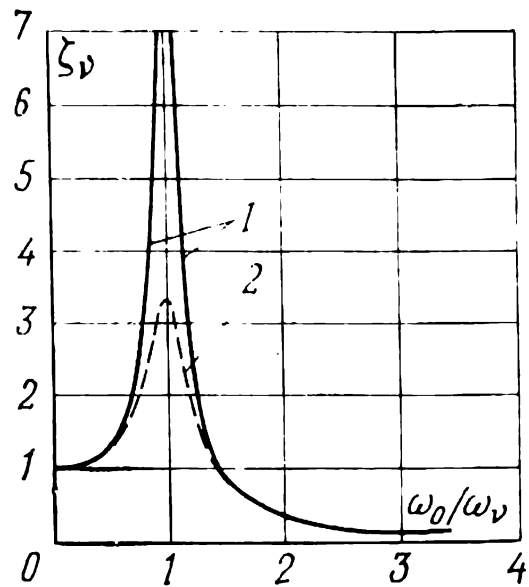


Fig. 60-3 Plot of  $\zeta_v = \alpha_{\max} / \alpha_{0, \max}$  as a function of  $\omega_0 / \omega_v$ :  
1 — at  $D = 0$ ; 2 — at  $D = \frac{1}{3} \sqrt{J t_s / p} > 0$

is a small fraction of the amplitude in the case of an isolated load. In this case, the inertia of the rotor is unimportant,

$$(J/p) (d^2\alpha/dt^2) \ll t_s\alpha$$

and the amplitude of oscillation of the power angle, as can readily be checked, is solely dependent on the amplitude of oscillation of the external torque, that is

$$\alpha_{\max} = (\omega_v^2/\omega_0^2) \alpha_{0,\max} = (T_{\text{ext},v}/t_s) = \alpha_{\infty,v}$$

Finally, at  $\omega_v = \omega_0$ , that is, when the torque oscillates at the same frequency as the rotor does, there occurs a resonance of forced and free oscillations,  $\alpha_{\max} = \infty$ . As a result, if no damping action were supplied,  $D=0$ , the machine would not be able to operate into an infinite system. Fortunately, the rotor circuits do supply some damping action, so that  $D > 0$ , the amplitude of oscillation of the power angle decreases to a finite value even within the resonance range (see Fig. 60-3).

When a synchronous generator is connected to an infinite system, the forced oscillations of the power angle are accompanied by oscillations of armature current (see above); oscillations of the rotor give rise to currents in its field and damper windings. The net result is an increase in losses, an impairment in efficiency, and a higher temperature rise. These drawbacks can be minimized by reducing the amplitude of oscillations of the power angle as much as practicable. Because the value of  $\omega_v$  is fixed for each particular reciprocating prime mover, a shift outside the resonance region can be secured by changing  $\omega_0$ , the natural frequency of oscillations, through an increase or a decrease in the moment of inertia. If  $\omega_0 \geq 1.15\omega_v$  or  $\omega_0 \leq 0.82\omega_v$ , then  $\zeta_v \leq 3$ . A further decrease in the amplitude of oscillations can be obtained by bringing down the resistance of the damper winding—this leads to a higher damping factor.

Similar forced oscillations arise in synchronous motors which drive reciprocating pumps. Their amplitude can be minimized in the same manner as explained above.

## 61 Unbalanced Operation of Synchronous Machines

### 61-1 An Outline of Unbalanced Operation

Unbalanced operation is a frequent occurrence in the use of synchronous machines. It may arise from internal causes, such as damage which upsets the symmetry of the armature winding, and from external causes, such as lack of symmetry and balance in the load or the system to which a given synchronous machine is connected.

In this section, we shall limit ourselves to steady-state unbalanced conditions arising solely from the dissymmetry or unbalance of the system to which the machine is connected. In all cases, it will be assumed that the three-phase armature winding of the machine is well balanced and symmetric. If not otherwise qualified, it will be assumed that the winding is star-connected.

In the case of an isolated load, current unbalance can arise from a difference in load impedance between the generator phases. This form of unbalance also includes various external unbalanced short-circuits (a two- or a single-phase fault to ground, etc.), when the resistance between the shorted points falls to zero.

In operation into an infinite system, current unbalance between the generator phases may occur owing to voltage unbalance in the system (in turn caused by an unequal sharing of load among the phases), or owing to various unbalanced faults in the system's parts (transmission lines, transformers, etc.).

The unbalanced conditions arising in a synchronous machine can conveniently be analysed by the method of symmetric components. In the general case, when the armature winding is star-connected with the neutral point brought out, the armature carries all the three sets of symmetric current components, namely positive, negative, and zero.

### 61-2 Positive-Sequence Impedance of the Armature Winding

The positive-sequence set of currents in the armature phases ( $\dot{I}_1 = \dot{I}_{A1}$ ,  $\dot{I}_{B1} = \dot{I}_{A1}a^2$ , and  $\dot{I}_{C1} = \dot{I}_{A1}a$ ) produces a fun-

damental mmf,  $\dot{F}_{am} = \dot{F}_{1m}$ , rotating at  $\Omega_1 = 2\pi f/p$  in the direction of positive phase sequence (from phase *A* to phase *B* to phase *C*).

Under synchronous steady-state conditions, this mmf is stationary relative to the rotor (see Sec.54-1) and can be resolved into a *d*-axis and a *q*-axis component:

$$F_{1dm} = F_{1m} \sin \beta$$

$$F_{1qm} = F_{1m} \cos \beta$$

where  $\beta$  is the angle between  $F_{1m}$  and the negative direction of the *q*-axis.

The *d*-axis mmf is produced by the positive-sequence set of *d*-axis currents

$$\dot{I}_{A1d} = I_{A1} \sin \beta \exp [-j(\pi/2 - \beta)]$$

$$\dot{I}_{B1d} = \dot{I}_{A1d} a^2$$

$$\dot{I}_{C1d} = \dot{I}_{A1d} a$$

The *q*-axis mmf is produced by the positive-sequence set of *q*-axis currents

$$\dot{I}_{A1q} = \dot{I}_{A1} \cos \beta \exp (j\beta)$$

$$\dot{I}_{B1q} = \dot{I}_{A1q} a^2$$

$$\dot{I}_{C1q} = \dot{I}_{A1q} a$$

As has been explained earlier, the synchronous field established by positive-sequence currents depends solely on the dimensions of the stator and rotor cores and the angle  $\beta$  (see Fig. 54-2).

The armature impedance seen by the positive-sequence set of *d*-axis currents is the sum of the phase-conductor resistance and the *d*-axis inductive reactance

$$Z_{1d} = R + jX_d$$

where

$$X_d = X_\sigma + X_{ad}$$

Accordingly, the impedance seen by the positive-sequence set of *q*-axis currents is

$$Z_{1q} = R + jX_q$$

where

$$X_q = X_\sigma + X_{aq}$$

In the general case, the positive-sequence impedance of the armature (see Sec. 54-5) is a function of  $\beta$ :

$$Z_1 = R_1 + jX_1 \quad (61-1)$$

where

$$R_1 = R + R_a$$

$$X_1 = X_\sigma + X_a$$

$$X_a = X_{aq} \cos^2 \beta + X_{ad} \sin^2 \beta$$

$$R_a = 0.5 (X_{ad} - X_{aq}) \sin^2 \beta$$

For a nonsalient-pole machine where  $X_{ad} = X_{aq} = X_a$  and  $R_a = 0$ , the impedance is

$$Z_1 = R + jX_1$$

where

$$X_1 = X_\sigma + X_a$$

### 61-3 Negative-Sequence Impedance of the Armature Winding

The negative-sequence set of currents in the armature phases ( $\dot{I}_2 = \dot{I}_{A2}$ ,  $\dot{I}_{B2} = \dot{I}_{A2} a$ ,  $\dot{I}_{C2} = \dot{I}_{A2} a^2$ ) produces a fundamental mmf,  $\dot{F}_{2m}$ , rotating at  $\Omega_2 = 2\pi f/p = -\Omega_1$  in the direction of negative phase sequence (from phase  $A$  to phase  $C$  to phase  $B$ ).

If the rotor of a synchronous machine is magnetically and electrically symmetrical and balanced, which is true, for example, of the polyphase ( $m_2 \geq 2$ ), squirrel-cage rotor of an induction machine, the negative-sequence impedance of the armature winding can be determined by reference to the equivalent circuit of an induction machine in Fig. 42-3. As will be recalled, at synchronous speed the rotor slip,  $s_1$ , relative to the positive-sequence currents is zero. Therefore, in calculating the negative-sequence impedance, the rotor slip relative to the negative-sequence field must be taken as

$$s_2 = 2 - s = 2$$

This can readily be proved, because

$$s_2 = (\Omega_2 - \Omega_1)/\Omega_2 = (\Omega_2 + \Omega_2)/\Omega_2 = 2$$

Assume that the rotor is of the nonsalient-pole design, the field winding is open-circuited, and the damper is an electrically symmetric, equal-pitch, short-circuited winding. Let us adopt for the equivalent circuit in Fig. 42-3 the nota-



tion used for synchronous machines, namely: the resistance of the armature-phase conductors is  $R_1 = R$ , the armature leakage inductive reactance is  $X_1 = X_\sigma$ , the mutual armature reactance is  $Z_0 = R_0 + jX_0 \approx jX_a$ , the damper-winding resistance referred to the armature winding is  $R'_2 = R'_{sc}$ , and the leakage inductive reactance of the damper winding referred to the armature winding is  $X'_2 = X'_{sc}$ . Then the negative-sequence impedance of the armature winding may be written

$$Z_2 = R_2 + jX_2 = R + jX_\sigma + \frac{1}{1/jX_a + 1/(0.5R'_{sc} + jX'_{sc})}$$

If  $X_a \gg X'_{sc} > 0.5R'_{sc}$ , then approximately we may write

$$\begin{aligned} R_2 &= R + 0.5R'_{sc} > R \\ X_2 &= X_\sigma + X'_{sc} \ll X_1 \end{aligned}$$

As is seen from the above equations, the negative-sequence reactance of the armature is substantially smaller than the positive-sequence reactance. This is because the negative-sequence field is bucked by the currents induced in the damper winding. The currents in the damper winding hinder the penetration of the magnetic field into the rotor core which has a low reluctance, and crowd it outside the damper-winding loop where it sees the high reluctance presented by the nonmagnetic gaps and clearances. These same gaps and clearances complete the path for the damper-winding leakage flux defined in terms of  $X'_{sc}$ . Because of this, the negative-sequence impedance is equal to the sum of  $X_\sigma$  and  $X'_{sc}$ .

In contrast, the negative-sequence resistance is higher than the positive-sequence resistance, because it is associated not only with the copper losses in the armature winding,

$$P_{Cu} = mRI_2^2$$

but also with the electromagnetic power transferred across the gap to the rotor

$$P_{em} \approx (mR'_{sc}/s) I_2^2$$

which should be found for the braking mode of operation. The rotor copper losses,  $P_{Cu_2} = mR'_{sc}I_2^2$  are made up for by the  $P_{em}$  supplied from the stator side and by an equal mechanical power input

$$|P_m| = mR'_{sc}I_2^2 | (1 - s)/s | = P_{em}$$

coming from the rotor's side.

Now we assume that the rotor is of the salient-pole design with a short-circuited, single-axis field winding and a variable-pitch damper winding. Then there will be both electrical and magnetic dissymmetry owing to which the  $d$ - and  $q$ -axis quantities will be different.

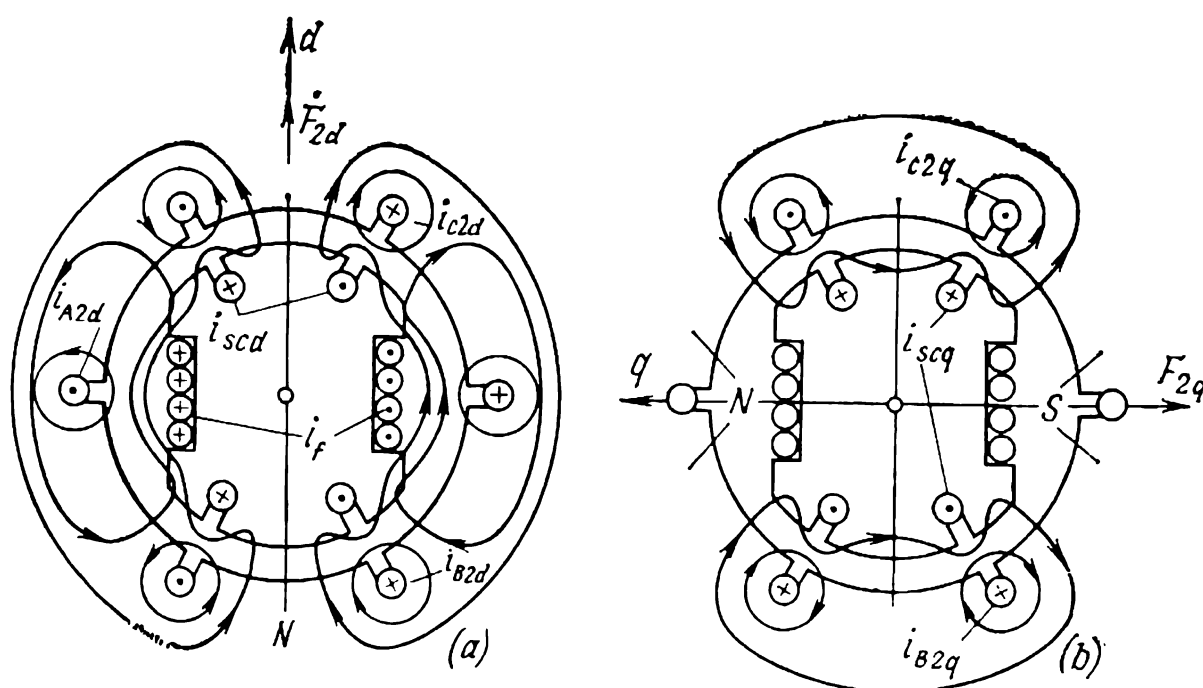


**Fig. 61-1** Magnetic fields set up by negative-sequence currents along (a)  $d$ -axis and (b)  $q$ -axis

Among other things, the magnetic unbalance of a salient-pole rotor is responsible for the difference between the  $d$ - and  $q$ -axis mutual reactances of the armature,

$$X_{ad} \neq X_{aq}$$

Electrical unbalance is responsible for the difference between the  $d$ - and  $q$ -axis leakage reactances and resistances of the damper winding,

$$X'_{sc,d} \neq X'_{sc,q}$$

$$R'_{sc,d} \neq R'_{sc,q}$$

Electrical unbalance is aggravated by the fact that the field winding can only affect the  $d$ -axis field (its effect increases with decreasing  $X'_{f\sigma}$  and decreasing  $R'_f$ )\*.

To determine the negative-sequence field and impedance of the armature winding, we may, as in a balanced induction

---

\* The manner in which the rotor quantities are referred to the armature winding is discussed in Sec. 71-3.

machine, replace the rotor travelling with a slip  $s_2 = 2$  by an equivalent, standstill rotor and divide the resistance by  $s_2$ .

As the negative-sequence mmf travels relative to the rotor at standstill, it aligns itself now with the  $d$ -axis,  $\dot{F}_{2dm}$ , now with the  $q$ -axis,  $\dot{F}_{2qm}$ . The  $d$ -axis field set up by  $\dot{F}_{2dm}$  (which corresponds to the rms current  $\dot{I}_{2d}$  or the instantaneous currents  $i_{A2d}$ ,  $i_{B2d}$  and  $i_{C2d}$ ) is bucked by the currents induced in the  $d$ -axis loop of the damper winding,  $i_{sc,d}$ , and in the field winding,  $i_f$  (see Fig. 61-1a). When the rotor resistances are small, the field is crowded nearly completely out of the field and damper windings. The impedance

$$Z_{2d} = R_{2d} + jX_{2d}$$

that the armature presents to the negative-sequence currents  $\dot{I}_{2d}$  establishing the  $d$ -axis field can be found from the equivalent circuit at the top of Fig. 61-2:

$$Z_{2d} = R + jX_\sigma + [(jX_{ad})^{-1} + (0.5R'_{sc,d} + jX'_{sc,d})^{-1} + (0.5R'_f + jX'_{f\sigma})^{-1}]^{-1} \quad (61-2)$$

The  $q$ -axis field set up by  $\dot{F}_{2qm}$  corresponding to the rms current  $\dot{I}_{2q}$  or the instantaneous currents  $i_{A2q}$ ,  $i_{B2q}$  and  $i_{C2q}$  (in the figure,  $i_{A2q} = 0$ ), is solely bucked by the current induced in the  $q$ -axis loop of the damper winding,  $i_{sc,q}$ , and is nearly completely crowded out of that loop (see Fig. 61-1b). The impedance  $Z_{2q} = R_{2q} + jX_{2q}$  that the armature presents to the negative-sequence currents  $\dot{I}_{2q}$  that set up the  $q$ -axis field can be found from the equivalent circuit at the bottom of Fig. 61-2.

$$Z_{2q} = R + jX_\sigma + [(jX_{aq})^{-1} + (0.5R'_{sc,q} + jX'_{sc,q})^{-1}]^{-1} \quad (61-3)$$

In a salient-pole machine, the  $d$ - and  $q$ -axis negative-sequence impedances and their resistive and inductive components differ from the positive-sequence quantities:

$$\begin{aligned} |Z_{2d}| &\neq |Z_{2q}| \\ R_{2d} &\neq R_{2q} \\ X_{2d} &\neq X_{2q} \end{aligned}$$

A more detailed analysis would show that the magnetic and electric dissymmetry of the rotor in a salient-pole machine

manifests itself under asynchronous conditions in the same manner as the unbalance of phase impedances in the rotor of an induction machine (see Sec. 46-2). The negative-sequence field at the fundamental frequency,  $f = f_1$ , rotates at an electrical angular velocity  $\omega_1$ , the rotor travels in the opposite direction at  $\omega = -\omega_1$ , and its slip relative to the negative-sequence field is

$$s = (\omega_1 - \omega)/\omega_1 = 2$$

As a result, currents are induced in the rotor circuits at frequency

$$f_2 = sf = 2f$$

Because the rotor is unbalanced, the field set up by the currents in the rotor circuits can be visualized as the sum of two rotating fields. One is the forward field travelling at  $s\omega_1 = 2\omega_1$  relative to the rotor and at  $s\omega_1 + \omega = 2\omega_1 - \omega_1 = \omega_1$  relative to the stator. The other is the backward field travelling at  $-s\omega_1 = -2\omega_1$  relative to the rotor and at  $-s\omega_1 + \omega = -2\omega_1 - \omega_1 = -3\omega_1$  relative to the stator.

In the stator winding, the forward field of the rotor induces an emf at  $f_1 = \omega_1/2\pi$ , and, travelling at the same velocity as the fundamental negative-sequence field, combines, with the latter. In the same winding, the backward field of the rotor induces a third-harmonic emf,  $\dot{E}_3$ , at a triple frequency,  $f_3 = 3\omega_1/2\pi = 3f$ . The effect it produces depends on the impedances in the stator circuits. When the stator winding is connected to a negative-sequence set of voltages via large external impedances, the third-harmonic currents flowing in those impedances are negligible in comparison with the fundamental current, and their effect may be neglected. The armature winding is traversed solely by the negative-sequence currents at the fundamental frequency. Because  $Z_{2d}$  and  $Z_{2q}$  are small in comparison with the external impedances, the negative-sequence currents are independent of the position that the rotor takes up relative to the field,

$$\dot{I}_2 = \dot{I}_{2d} = \dot{I}_{2q}$$

Combining with the fundamental voltage,  $\dot{V}_2$ , the third-harmonic emf,  $\dot{E}_3 = \dot{V}_3$ , distorts the waveform of the terminal voltage in such a way that when the rotor is aligned with

the field along the  $d$ -axis, the voltage is

$$\dot{V}_2 + \dot{V}_3 = \dot{V}_{2d} = -Z_{2d}\dot{I}_2$$

and when the rotor is aligned with the field along the  $q$ -axis, the voltage is

$$\dot{V}_2 - \dot{V}_3 = \dot{V}_{2q} = -Z_{2q}\dot{I}_2$$

In an analysis of unbalanced operation, only the fundamental negative-sequence current and voltage are considered, namely the current  $\dot{I}_2$ , and the voltage given by

$$\dot{V}_2 = (\dot{V}_{2d} + \dot{V}_{2q})/2 = -\dot{I}_2 (Z_{2d} + Z_{2q})/2$$

which is found from the set of equations given earlier. The negative-sequence impedance is equal to the ratio of the negative-sequence voltage to the negative-sequence current

$$Z_2 = R_2 + jX_2 = -\dot{V}_2/\dot{I}_2 = (Z_{2d} + Z_{2q})/2 \quad (61-4)$$

Using Eqs. (61-2), (61-3) and (61-4), we can readily determine the resistive and reactive components of the negative sequence impedance in the case of large external impedances in the armature phases.

Conversely, when the stator winding is connected to a negative-sequence set of voltages through small external impedances (as compared with  $Z_{2d}$  or  $Z_{2q}$ ), the stator terminal voltage is the same as those voltages and remains unchanged, whatever the position of the rotor relative to the field,

$$\dot{V}_2 = \dot{V}_{2d} = \dot{V}_{2q}$$

With respect to the third-harmonic emf,  $\dot{E}_3$ , the armature winding is short-circuited (the system and external impedances are small). Therefore, in the armature winding  $\dot{E}_3$  gives rise to third-harmonic currents  $\dot{I}_3$  which reduce the third-harmonic terminal voltage to zero,  $\dot{V}_3 = 0$ . Combining with the fundamental currents,  $\dot{I}_2$ , the third-harmonic currents distort the waveform of the armature current in such a way that when the rotor is aligned with the field along the  $d$ -axis the current is

$$\dot{I}_2 + \dot{I}_3 = \dot{I}_{2d} = -\dot{V}_2/Z_{2d}$$

and when the rotor is aligned with the field along the  $q$ -axis, the current is

$$\dot{I}_2 - \dot{I}_3 = \dot{I}_{2q} = -\dot{V}_2/Z_{2q}$$

Using the above equations, the fundamental current may be written as

$$\dot{I}_2 = (\dot{I}_{2d} + \dot{I}_{2q})/2 = -(\dot{V}_2/2) (1/Z_{2d} + 1/Z_{2q})$$

and the negative-sequence impedance may be defined as

$$Z_2 = R_2 + jX_2 = -\dot{V}_2/\dot{I}_2 = \frac{2Z_{2d}Z_{2q}}{Z_{2d} + Z_{2q}} \quad (61-5)$$

Using Eqs. (61-2), (61-3) and (61-5), we can find the resistive and inductive components of the negative-sequence impedance when the armature phases contain small external impedances, such as when a machine is connected to an unbalanced, infinite system.

When the rotor is balanced and  $Z_{2d} \approx Z_{2q}$ , the negative-sequence impedance will be the same in either of the two above cases,

$$Z_2 = R_2 + jX_2 = Z_{2d} = Z_{2q}$$

In per unit,  $X_2$  is 0.12 to 0.18 for nonsalient-pole machines and 0.2 to 0.4 for salient-pole machines (with indirect cooling used in either case).

In calculating negative-sequence impedance,  $R_f$  refers to the total resistance of the field winding (that is, including the resistance of the exciter armature or the damping resistor). All the resistances and reactances involved in Eqs. (61-2) and (61-3) and in the diagram of Fig. 61-2 must be found with allowance for current crowding which occurs at  $2f$ .

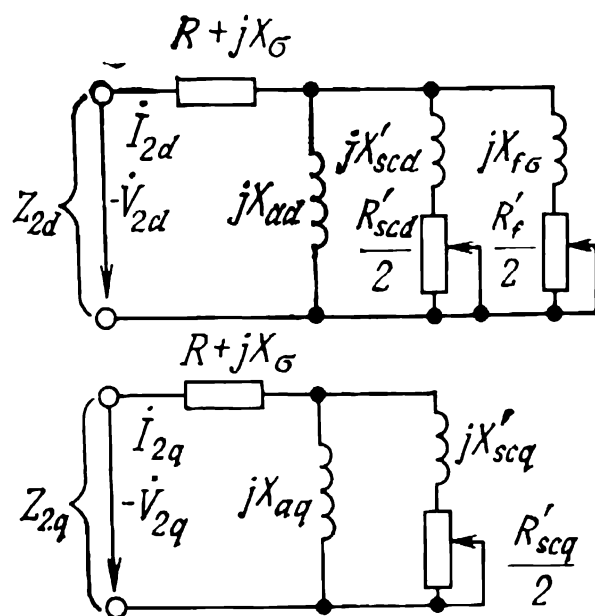


Fig. 61-2 Direct- and quadrature-axis equivalent circuits of a synchronous machine for negative-sequence currents

### 61-4 Zero-Sequence Impedance of the Armature Winding

The zero-sequence currents are the same in all the phases, that is,  $\dot{I}_0 = \dot{I}_{A0} = \dot{I}_{B0} = \dot{I}_{C0}$ . The fundamental pulsating fields (those with the fundamental number of pole pairs,  $p$ ) produced by the zero-sequence phase currents are displaced from one another through  $120^\circ$  (electrical) and cancel out. This leaves only the mutual field with a number of pole

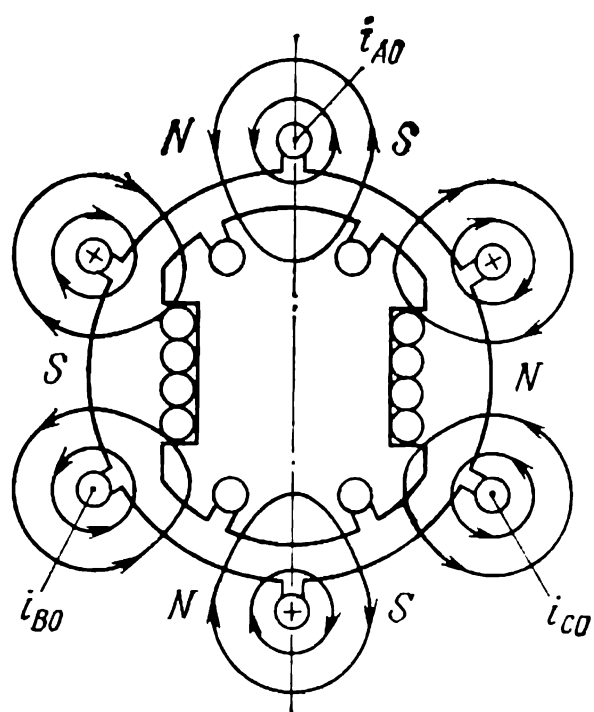


Fig. 61-3 Magnetic field set up by zero-sequence currents

pairs equal to  $3p$ ,  $9p$ ,  $15p$ , etc., associated with the odd spatial harmonics of the phase mmfs with a number of pole pairs equal to  $\nu p$  and with a harmonic order which is a multiple of three,  $\nu = 3$  (triplen harmonics). The largest contribution comes from the mutual field with  $3p$  pole pairs. Its lines for  $p = 1$  are shown in Fig. 61-3 (as is seen, this is a six-pole field).

The zero-sequence mutual inductive reactance,  $X_{a(0)}$ , owes its existence solely to the field set up by triplen mmfs. Because these mmfs and the associated flux linkages are

small,  $X_{a(0)}$  is a small fraction of,  $X_a$ , the positive-sequence mutual reactance. The zero-sequence leakage reactance,  $X_{\sigma(0)}$ , is likewise smaller than  $X_\sigma$ , the positive-sequence leakage reactance. The point is that, because of short-pitching (chording), the other phases buck the leakage flux linkage of a given phase in the case of zero-sequence currents and boost it in the case of positive-sequence currents. The total zero-sequence phase reactance is the sum of the two terms defined above,

$$X_0 = X_{a(0)} + X_{\sigma(0)}$$

In two-layer, short-pitched windings,  $X_0$  is ordinarily a little smaller than the positive-sequence leakage reactance,  $X_0 \approx X_\sigma$ . In per-unit,  $X_0$  is 0.05 to 0.08 in indirectly cooled, nonsalient-pole machines, 0.08 to 0.16 in

directly cooled, nonsalient-pole machines, and 0.07 to 0.10 in indirectly cooled salient-pole machines.

The zero-sequence field only links the damper winding (its linkage with the field winding is negligible). The currents induced in the damper winding by the zero-sequence field somewhat reduce  $X_0$ . The zero-sequence phase resistance differs very little from the positive-sequence resistance  $R_0 \approx R_a$ . This is because the additional losses in the damper winding owing to the currents induced in it by the zero-sequence field are small in comparison with the ohmic losses in the armature winding.

The total zero-sequence impedance per phase is

$$Z_0 = R_0 + jX_0 \quad (61-6)$$

### 61-5 Unbalanced Operation of a Synchronous Machine

Under unbalanced operating conditions, the phase voltages are defined as the sum of PS, NS and ZS voltages associated with currents of the corresponding phase sequences:

$$\left. \begin{aligned} \dot{V}_A &= \dot{V}_{A1} + \dot{V}_{A2} + \dot{V}_{A0} \\ \dot{V}_B &= \dot{V}_{B1} + \dot{V}_{B2} + \dot{V}_{B0} \\ \dot{V}_C &= \dot{V}_{C1} + \dot{V}_{C2} + \dot{V}_{C0} \end{aligned} \right\} \quad (61-7)$$

where

$$\begin{aligned} \dot{V}_{B1} &= \dot{V}_{A1}a^2 \\ \dot{V}_{C1} &= \dot{V}_{A1}a \\ \dot{V}_{B2} &= \dot{V}_{A2}a \\ \dot{V}_{C2} &= \dot{V}_{A2}a^2 \\ \dot{V}_{B0} &= \dot{V}_{C0} = \dot{V}_{A0} \end{aligned}$$

Contributions to the positive-sequence voltage come from the field set up by the field (excitation) current and the field set up by the positive-sequence armature currents rotating at synchronous velocity. The equation for the positive-sequence voltage is written in the same manner as for balanced synchronous operation (see Chap. 55). It can be written with and without iron saturation. If the magnetic circuit is unsaturated, the phase  $A$  positive-sequence voltage



will be given by

$$\dot{V}_{A1} = \dot{E}_{Af} - Z_1 \dot{I}_{A1} \quad (61-8)$$

where

$$\dot{E}_{Af} = \dot{E}_f$$

is the excitation voltage of phase  $A$ , and

$$Z_1 = R_1 + jX_1$$

is the positive-sequence impedance from Eq. (61-1).

The phase  $A$  negative- and zero-sequence voltages are produced only by currents of the corresponding phase sequences:

$$\dot{V}_{A2} = -Z_2 \dot{I}_{A2} \quad (61-9)$$

$$\dot{V}_{A0} = -Z_0 \dot{I}_{A0} \quad (61-10)$$

The PS, NS and ZS voltages of the other phases can be found from the relations explaining Eq. (61-7).

Using Eqs. (61-7), we can write the total phase voltages in terms of  $E_f$ , the phase  $A$  excitation emf, and symmetrical current components:

$$\left. \begin{aligned} \dot{V}_A &= \dot{E}_f - Z_1 \dot{I}_{A1} - Z_2 \dot{I}_{A2} - Z_0 \dot{I}_{A0} \\ \dot{V}_B &= (\dot{E}_f - Z_1 \dot{I}_{A1}) a^2 - Z_2 \dot{I}_{B2} - Z_0 \dot{I}_{B0} \\ \dot{V}_C &= (\dot{E}_f - Z_1 \dot{I}_{A1}) a - Z_2 \dot{I}_{C2} - Z_0 \dot{I}_{C0} \end{aligned} \right\} \quad (61-11)$$

where

$$\dot{E}_f - Z_1 \dot{I}_{A1} = \dot{V}_{A1}$$

Equations (61-11) could be used to construct a voltage phasor diagram for unbalanced load. Unfortunately, it would be rather cumbersome. It is simpler to construct a combined voltage phasor diagram for unbalanced load (as shown in Fig. 61-4) which corresponds to Eqs. (61-12) deduced from Eqs. (61-11) upon multiplying the second line by  $a$  and the third line by  $a^2$ :

$$\left. \begin{aligned} \dot{V}_A &= \dot{E}_f - Z_1 \dot{I}_{A1} - Z_2 \dot{I}_{A2} - Z_0 \dot{I}_{A0} \\ a \dot{V}_B &= \dot{E}_f - Z_1 \dot{I}_{A1} - Z_2 a \dot{I}_{B2} - Z_0 a \dot{I}_{B0} \\ a^2 \dot{V}_C &= \dot{E}_f - Z_1 \dot{I}_{A1} - Z_2 a^2 \dot{I}_{C2} - Z_0 a^2 \dot{I}_{C0} \end{aligned} \right\} \quad (61-12)$$

where

$$\dot{E}_f - Z_1 \dot{I}_{A1} = \dot{V}_{A1}$$

In the case of a balanced load,

$$\dot{V}_A = a \dot{V}_B = a^2 \dot{V}_C = \dot{V}_{A1}$$

The combined diagram shows how much  $\dot{V}_A$ ,  $a \dot{V}_B$  and

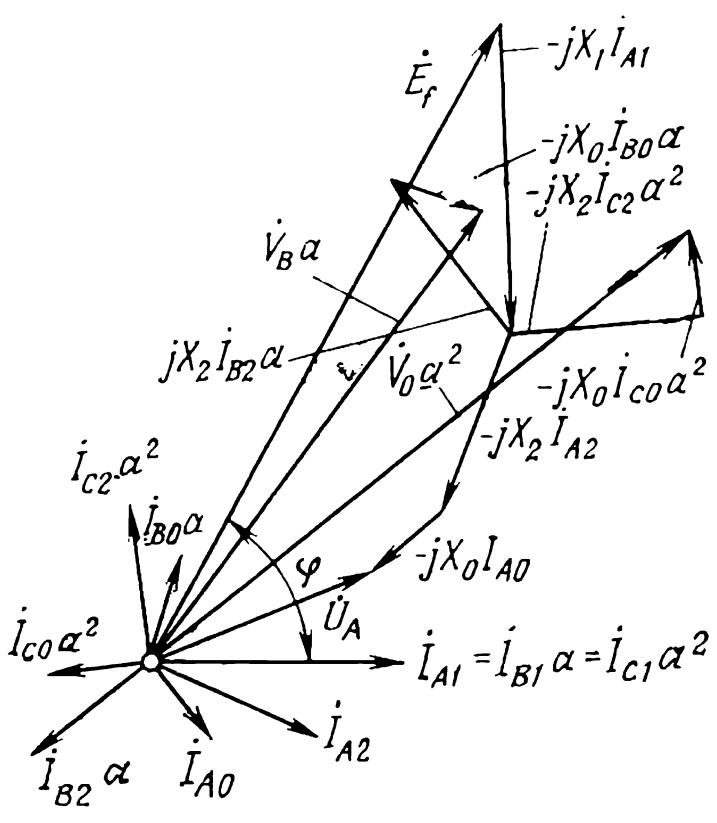


**Fig. 61-4** Combined voltage phasor diagram of a nonsalient-pole synchronous generator operating into an unbalanced load (neglecting saturation,  $R = R_2 = R_0 = 0$ )

$a^2 \dot{V}_C$  differ in the case of an unbalanced load and which currents are responsible for this difference.

**61-6 Parallel Operation with an Unbalanced System**

When a synchronous machine is connected to an infinite system, the operating conditions can be specified by giving the unbalanced system voltages

$$\begin{aligned} \dot{V}_{As} &= -\dot{V}_A \\ \dot{V}_{Bs} &= -\dot{V}_B \\ \dot{V}_{Cs} &= -\dot{V}_C \end{aligned}$$

From them, it is an easy matter to find the symmetric components of the terminal voltage. Also, the magnitude and phase of the positive-sequence current in one of the phases, say,  $\dot{I}_{A1}$ , and the angle  $\varphi$  between  $\dot{V}_{A1}$  and  $\dot{I}_{A1}$  must be specified. The magnitude and phase of  $\dot{I}_{A1}$  depend on the duty in which the machine is running, and the active and reactive power it delivers or absorbs. The above data are sufficient for the analyst (or the designer) to determine the required  $E_f$  and  $I_f$ , and also the negative- and zero-sequence currents.

The phase  $A$  field emf is given by

$$\dot{E}_f = \dot{V}_{A1} + Z_1 \dot{I}_{A1}$$

where

$$Z_1 = R_1 + jX_1$$

is the armature impedance whose components in a nonsalient-pole machine are

$$R_1 = R$$

and

$$X_1 = X_\sigma + X_a$$

whereas for a salient-pole machine they can be found from the specified  $V_{A1}$ ,  $I_{A1}$  and  $\varphi$ , as explained in Chap. 55.

The negative- and zero-sequence currents are

$$\dot{I}_{A2} = -\dot{V}_{A2}/Z_2$$

and

$$\dot{I}_{A0} = -\dot{V}_{A0}/Z_0$$

In the rotor circuits, the negative-sequence field induces appreciable second-harmonic currents which may lead to a prohibitive temperature rise of the rotor. Therefore, whether or not a machine can safely be operated at a given voltage unbalance depends on the magnitude of negative-sequence currents. For long-term operation of large machines, the per-unit negative-sequence current should be less than 0.1 or 0.2, that is,  $I_{*2} = I_2/I_R < 0.1$  to 0.2.

A still lower limit is set for the negative-sequence voltage

$$\begin{aligned} V_{*2} &= |Z_{*2}| I_{*2} < 0.1 |Z_{*2}| \quad \text{to} \quad 0.2 |Z_{*2}| \\ &= \text{from } 0.015 \text{ to } 0.05 \end{aligned}$$

because usually

$$|Z_{*2}| \approx X_{*2} = 0.15 \text{ to } 0.25$$

This implies that a synchronous machine can operate in parallel with a system for a long time only at practically balanced voltages, when the negative-sequence voltage is such that

$$V_{*2}/V_{*1} = 0.015 \text{ to } 0.05$$

The positive-sequence voltage is always very close to its rated value, that is

$$V_{*1} = 1.0$$

### 61-7 Operation of a Synchronous Generator into an Isolated Unbalanced Load

In this case, unbalanced operating conditions can be specified by giving an unbalanced set of load impedances

$$Z_A \neq Z_B \neq Z_C$$

and their connection diagram.

Suppose that the load impedances are connected in a star whose neutral point is brought out to the neutral point of

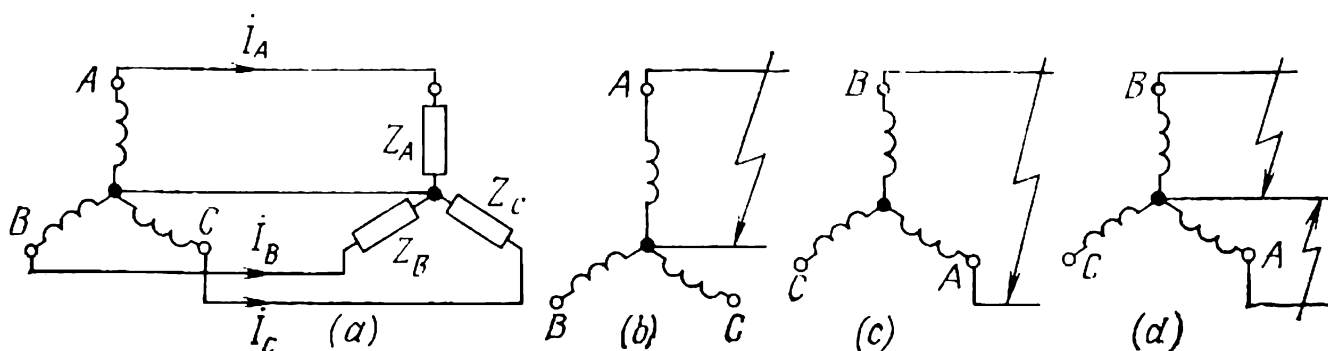


**Fig. 61-5** Connection to an unbalanced load:

(a) general case; (b) single-phase fault to ground; (c) two-phase short-circuit; (d) double single-phase fault to ground

the armature winding in the generator (Fig. 61-5a). Then the phase voltages of the armature winding may be written in terms of the load impedances and phase currents as

$$\left. \begin{aligned} \dot{V}_A &= \dot{I}_A Z_A \\ \dot{V}_B &= \dot{I}_B Z_B \\ \dot{V}_C &= \dot{I}_C Z_C \end{aligned} \right\} \quad (61-13)$$

Considering Eqs. (61-11) and (61-13) together, expressing the currents in Eq. (61-13) in terms of symmetrical components, and deeming  $\dot{E}_f = E_f$  fixed in advance, the set of equations thus obtained can be solved for the symmetric components of currents.

The equations for symmetric components of currents are the simplest to write and solve for an unsaturated, non-salient-pole machine, where  $Z_1 = R_1 + jX_1$  is fixed in advance and independent of the angle  $\beta$ .

$$\left. \begin{aligned} E_f &= (Z_1 + Z_A) \dot{I}_{A1} + (Z_2 + Z_A) \dot{I}_{A2} + (Z_0 + Z_A) \dot{I}_{A0} \\ E_f a^2 &= (Z_1 + Z_B) a^2 \dot{I}_{A1} + (Z_2 + Z_B) a \dot{I}_{A2} + (Z_0 + Z_B) \dot{I}_{A0} \\ E_f a &= (Z_1 + Z_C) a \dot{I}_{A1} + (Z_2 + Z_C) a^2 \dot{I}_{A2} + (Z_0 + Z_C) \dot{I}_{A0} \end{aligned} \right\} \quad (61-14)$$

Hence,

$$\dot{I}_{A1} = D_1/D, \quad \dot{I}_{A2} = D_2/D, \quad \dot{I}_{A0} = D_0/D \quad (61-15)$$

where

$$D = \begin{vmatrix} Z_1 + Z_A & Z_2 + Z_A & Z_0 + Z_A \\ (Z_1 + Z_B) a^2 & (Z_2 + Z_B) a & Z_0 + Z_B \\ (Z_1 + Z_C) a & (Z_2 + Z_C) a^2 & Z_0 + Z_C \end{vmatrix}$$

is the determinant of Eqs. (61-14).

The determinants  $D_1$ ,  $D_2$  and  $D_0$  are derived from the determinant  $D$  upon replacing the column of the coefficients of the unknown current by the column of the free terms  $E_f$ ,  $E_f a^2$  and  $E_f a$ . For example,  $D_1$  is derived from  $D$  by replacing the column  $(Z_1 + Z_A)$  with  $E_f$ , the column  $(Z_1 + Z_B) a^2$  with  $E_f a^2$ , and the column  $(Z_1 + Z_C) a$  with  $E_f a$ .

Once the currents are found, the corresponding voltages and their symmetric components can be obtained from Eqs. (61-11).

## 61-8 Unbalanced Steady-State Short-Circuits

(1) **Single Phase-to-Ground Fault (Fig. 61-5b).** This is a special case of unbalanced load, where  $Z_A = 0$  and  $Z_B = Z_C = \infty$ . However, in order to find the fault (or short-circuit) current, it is simpler to use Eq. (61-11) and not

Eq. (61-14), because  $\dot{V}_A = 0$ ,  $\dot{I}_B = \dot{I}_C = 0$ , and  $\dot{E}_f = E_f$ .

The first step is to write the symmetric components of currents in terms of the unknown fault current for phase  $A$

$$\begin{aligned}\dot{I}_{A0} &= (\dot{I}_A + \dot{I}_B + \dot{I}_C)/3 = \dot{I}_A/3 \\ \dot{I}_{A1} &= (\dot{I}_A + \dot{I}_B a + \dot{I}_C a^2)/3 = \dot{I}_A/3 \\ \dot{I}_{A2} &= (\dot{I}_A + \dot{I}_B a^2 + \dot{I}_C a)/3 = \dot{I}_A/3\end{aligned}$$

Now, using Eq. (61-11) for phase  $A$ , it is easy to find the single-phase fault current:

$$\begin{aligned}\dot{I}_A &= \frac{3\dot{E}_f}{Z_1 + Z_2 + Z_0} \\ I_A &\approx \frac{3E_f}{X_1 + X_2 + X_0}\end{aligned}\tag{61-16}$$

**(2) Phase-to-Phase Fault (Fig. 61-5c).** In this form of fault (also known as two-phase fault) the line voltage turns to zero

$$\dot{V}_{AB} = \dot{V}_B - \dot{V}_A = 0$$

Also, the fault current in phases  $A$  and  $B$  is the same, whereas phase  $C$  remains unaffected:

$$\begin{aligned}\dot{I}_B &= -\dot{I}_A \\ \dot{I}_C &= 0\end{aligned}$$

The symmetric components of currents may be written in terms of fault current as

$$\begin{aligned}\dot{I}_{A0} &= \frac{1}{3}(\dot{I}_A + \dot{I}_B) = 0 \\ \dot{I}_{A1} &= \frac{\dot{I}_A}{3}(1 - a) = (\dot{I}_A/\sqrt{3})\exp(-j30^\circ) \\ \dot{I}_{A2} &= \frac{\dot{I}_A}{3}(1 - a^2) = (\dot{I}_A/\sqrt{3})\exp(j30^\circ) \\ \dot{I}_{B1} &= \dot{I}_{A1}a^2 = -\dot{I}_{A2} \\ \dot{I}_{B2} &= \dot{I}_{A2}a = -\dot{I}_{A1}\end{aligned}$$

Now, using Eqs. (61-11), we can write an equation for the line voltage,  $\dot{V}_{AB}$

$$\dot{V}_{AB} = \dot{V}_B - \dot{V}_A = E_f (a^2 - 1) - Z_1 (\dot{I}_{B1} - \dot{I}_{A1}) - Z_2 (\dot{I}_{B2} - \dot{I}_{A2}) = 0$$

where

$$\begin{aligned}\dot{I}_{B1} - \dot{I}_{A1} &= -\dot{I}_{A2} - \dot{I}_{A1} = -\dot{I}_A \\ \dot{I}_{B2} - \dot{I}_{A2} &= -\dot{I}_{A1} - \dot{I}_{A2} = -\dot{I}_A \\ 1 - a^2 &= \sqrt{3} \exp(j30^\circ)\end{aligned}$$

On solving the above equation, we get the phase-to-phase fault current

$$\begin{aligned}\dot{I}_A &= \frac{\sqrt{3} E_f \exp(j30^\circ)}{Z_1 + Z_2} \\ I_A &\approx \sqrt{3} E_f / (X_1 + X_2)\end{aligned}\quad (61-17)$$

**(3) Double Phase-to-Ground Fault (Fig. 61-5d).** In this form of fault, two phases are faulted to ground, so that

$$\dot{V}_A = 0 \quad \text{and} \quad \dot{V}_B = 0$$

The phase  $C$  current is zero,  $I_C = 0$ . The symmetric components of currents can be expressed in terms of an equal fault current in phases  $A$  and  $B$ :

$$\begin{aligned}\dot{I}_{A0} &= (\dot{I}_A + \dot{I}_B)/3 \\ \dot{I}_{A1} &= (\dot{I}_A + a\dot{I}_B)/3 \\ \dot{I}_{A2} &= (\dot{I}_A + a^2\dot{I}_B)/3\end{aligned}$$

Solving the equations for  $\dot{V}_A = 0$  and  $\dot{V}_B = 0$ , derived from Eqs. (61-11) and neglecting the resistive components of  $Z_1$ ,  $Z_2$  and  $Z_0$ , the double phase-to-ground fault current is found to be

$$\begin{aligned}\dot{I}_A &= -\frac{jE_f \sqrt{3} (X_2 e^{-j30^\circ} + X_0 e^{j30^\circ})}{X_1 X_2 + X_0 X_1 + X_2 X_0} \\ I_A &= \frac{\sqrt{3} E_f \sqrt{X_2^2 + X_0^2 + X_2 X_0}}{X_1 X_2 + X_0 X_1 + X_2 X_0}\end{aligned}\quad (61-18)$$

## ☆ 62 Synchronous Machines of Soviet Manufacture

### 62-1 Turbogenerators

These are nearly always two-pole, 3000-rpm, horizontal-shaft, nonsalient-pole machines. Turbogenerators with ratings under 30 MVA use indirect air cooling. Air is circulated in a closed-circuit ventilation system, absorbing heat from the active parts and giving it up in water-cooled heat exchangers. A sectional view of an air-cooled turbogenerator is shown in Fig. 51-12 (see Sec. 51-12 for more detail).

A closed-circuit ventilation system (see Sec. 33-3) may use not only air, but also hydrogen which compares favourably with other gaseous coolant. With a machine, it is maintained 97% pure, the remaining 3% being water vapour and air. At a pressure of  $0.05 \times 10^5$  Pa (gauge), this mixture has a density which is one-eighth of that of air. The heat transfer coefficient from the cooling surface to hydrogen is 1.35 times the figure for air, and the thermal conductivity is about five times that of air. Because of this, indirect hydrogen cooling offers the following advantages.

1. Friction and windage losses are reduced to about one-eighth. In turbogenerators rated at 25 to 100 MW, these losses account for 25% to 50% of the total losses, so the efficiency is improved by 0.9 to 1.0%.

2. The temperature gradients due to gas layers in the insulation and also between the insulation and the slot sides are practically non-existent. The heat transfer coefficient of the insulation is improved by about 30%. Coupled with the improved heat transfer, this permits the rating of turbogenerators to be raised by about 20% for the same temperature rise and the same dimensions of the stator and rotor windings.

3. The insulation is more reliable and durable, because there is no oxidation, dirt or dampness, and also because a corona discharge in a hydrogen atmosphere is less detrimental to the insulation than in air.

4. Since hydrogen will not sustain combustion, there is no risk of a fire breaking out in the windings.

5. Hydrogen cooling systems require smaller coolers than for air.



Unfortunately, a mixture of 7% to 70% hydrogen and air presents an explosive hazard. Therefore, to avoid any explosion risk, the hydrogen inside the machine must be maintained extremely pure and at a slightly excessive (positive) pressure (the minimum figure is  $0.05 \times 10^5$  Pa (gauge)). This will eliminate ingress of air through the unavoidable clearances and the shaft seals (Fig. 62-1).

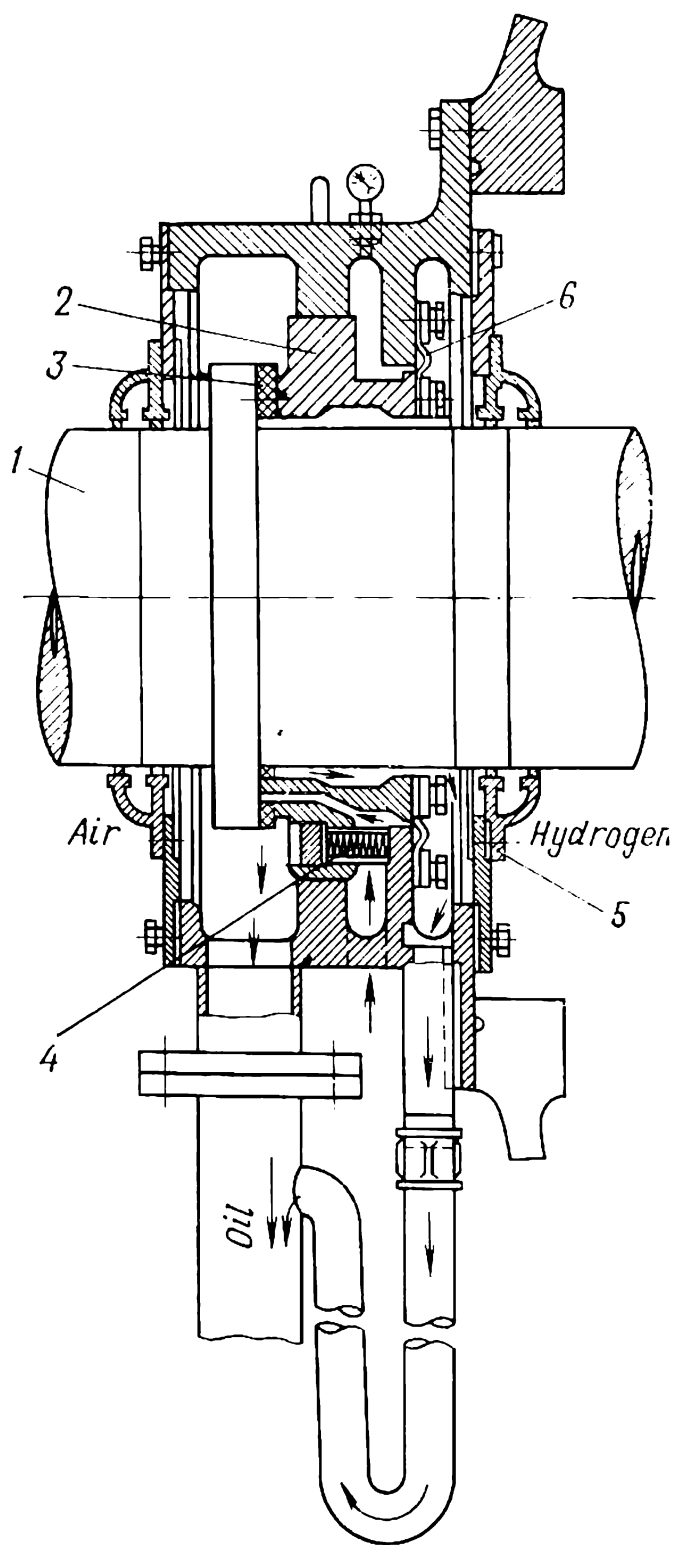


**Fig. 62-1** Hydrogen shaft seal:  
1—rotor shaft; 2—gland; 3—bab-  
bitt; 4—pressure springs; 5—laby-  
rinth; 6—gasket

multiplicity of inlets. Figure 62-5 shows a six-inlet hydrogen cooling system.

In indirectly cooled turbogenerators, the rotor is cooled by hydrogen from the outside. Because of this, there exist

The frames of hydrogen-cooled machines are built sufficiently robust to withstand the pressure of an explosion, if any should occur. With a margin of safety, the frames and end-shields are built for a pressure of  $8 \times 10^5$  Pa.

Common practice in the USSR is to supply hydrogen in cylinders where it is held compressed to a pressure of about  $150 \times 10^5$  Pa. Water-cooled heat exchangers are built either into the stator frame (as in Figs. 62-2 and 62-3) or into the stator end-shields (as in Fig. 62-9).

The manner in which hydrogen is circulated inside a machine will be clear from reference to Figs. 62-5. Hydrogen is admitted into the machine through a

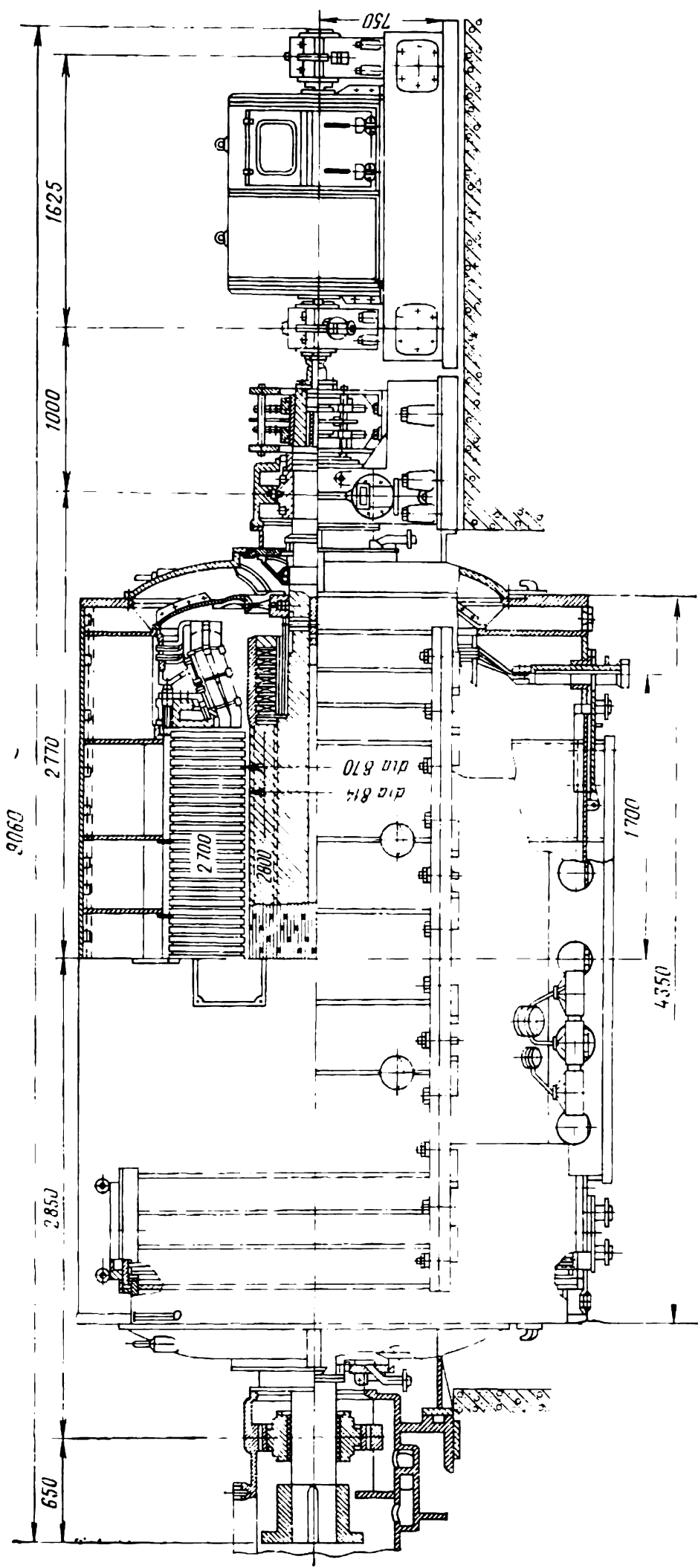
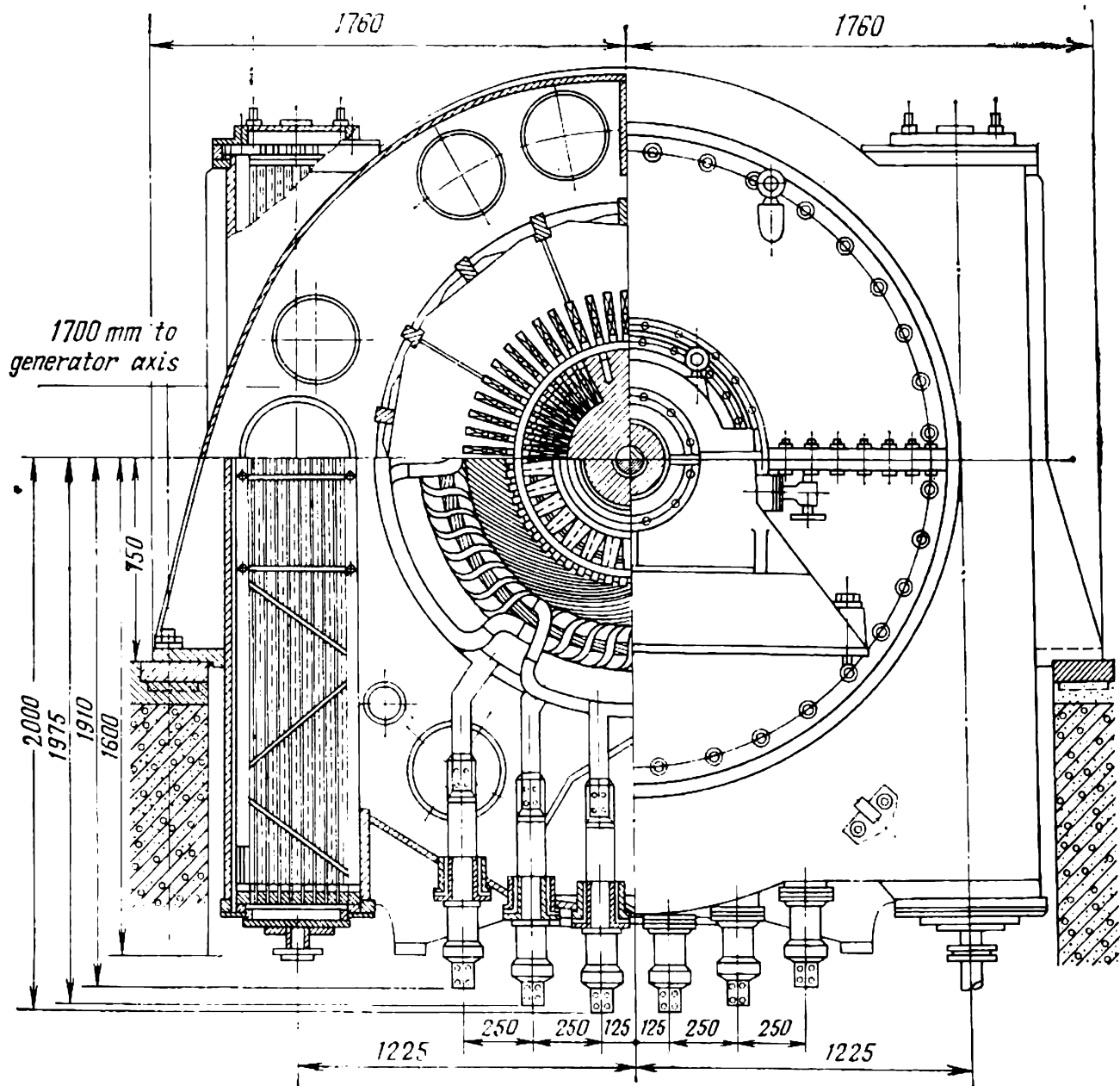


Fig. 62-2 Sectional view of a 30-MW, 3000-rpm, turbogenerator using indirect hydrogen cooling (all dimensions in mm)

marked temperature gradients in the slot insulation. It would seem that the temperature rise of the windings could be lowered and, as a result, the power rating of machines for the same size could be improved by using hydrogen at



**Fig. 62-3** Cross-section through a 30-MW, 3000-rpm turbogenerator using indirect hydrogen cooling (all dimensions in mm)

a high pressure. This however only leads to a lower temperature gradient from surface to coolant and a lower temperature of the coolant (roughly in inverse proportion to pressure), but leaves unaffected the temperature gradients at the other places, as is the case with indirect cooling. The likely increase in power rating for indirectly cooled machines using hydrogen at an elevated pressure can be assessed from Table 62-1.

Table 62-1

Hydrogen pressure, $\times 10^5$ Pa	0.035	0.5	1.05	2.1
Load ratio (load at $0.035 \times 10^5$ Pa taken as reference)	1	1.07	1.15	1.25

In turbogenerators using indirect hydrogen cooling, the electric loading may be raised to a higher value,  $A = 7.3 \times 10^4$  to  $8.0 \times 10^4$  Am<sup>-1</sup>.

For turbogenerators indirectly cooled by hydrogen at a pressure of  $0.05 \times 10^5$  Pa (gauge) and using rotors of maximum permissible dimensions (1.1-1.15 m in diameter and 6.5 m long) the limit of power rating is set at 150 MW.

An increase in hydrogen pressure used for indirect cooling does not lead to a decrease in temperature gradient between slot insulation and core iron. Therefore, the rise in pressure to about  $2 \times 10^5$  Pa (gauge) can raise the limit of power rating for turbogenerators to only 200 MW.

Any further decrease in temperature gradient from the winding to the coolant at constant power output or an increase in power output at constant temperature rise is only possible with direct cooling. This eliminates the temperature gradient in the insulation, and even at a pressure of  $0.05 \times 10^5$  Pa (gauge) the temperature rise of the winding is not over 50% of the figure with indirect cooling. At a pressure of  $2 \times 10^5$  Pa (gauge), the temperature gradient is as low as 20% of the figure with indirect cooling.

If the temperature rise be maintained unchanged, the power rating can be raised by a factor of  $\sqrt{100/20} \approx 2.4$ , that is, to about 350-500 MW.

As is seen from Table 62-2, the limit of power rating as fixed from considerations of temperature rise varies with hydrogen pressure in a greater proportion than in the case of surface cooling.

Table 62-2

Hydrogen pressure, $\times 10^5$ Pa (gauge)	0.035	0.7	1.4	2.1	2.8	4.2
Total power, % of power at $2.1 \times 10^5$ Pa	40	62	83	100	112	123

Liquids, such as water and transformer oil, abstract heat better than hydrogen. Given the same temperature gradients and the practically acceptable flow rates of the coolant in ducts, transformer oil can withdraw 5.5 times and water, 41.7 times the amount that can be abstracted by hydrogen at a pressure of  $2.0 \times 10^5$  Pa (gauge). When applied to the stator winding, liquid cooling makes it possible to reduce the cross-sectional area of ducts, to raise the current density in the winding (if this is warranted by economic considerations), or to reduce (to a half or even to a third) the temperature rise of the winding, if the current density is held at the previous level. In the latter case, a reduction in winding temperature leads to a marked decrease in the resistivity and major losses of the winding.

However, the use of liquid cooling for the stator winding only does not permit any further rise in the power rating of a machine, because it is limited by the rotor. One way to raise the power rating to 1000 MW and more is to cool both the stator and rotor windings by distilled water.

Another advantage of direct cooling in turbogenerators is a substantial increase in electric loading (Table 62-3).

Table 62-3 Electric Loading in Directly Cooled Turbogenerators

$P_R$ , MW	100	200	300	500	800
$A$ , kA m <sup>-1</sup>	110	135	150	175	200

At the time of writing, four basic types of indirect cooling systems for turbogenerators were in use in the Soviet Union.

(1) Axial systems for the stator and rotor windings and the stator core, using hydrogen at elevated pressure (Fig. 62-4).

(2) Multiple-inlet radial systems using hydrogen at elevated pressure, with the rotor winding directly cooled and the stator winding indirectly cooled.

(3) Multiple-inlet radial systems using hydrogen for the stator core and the rotor winding, combined with a water cooling system for the stator winding (Fig. 62-5).

(4) Liquid (oil or water) cooling systems for the stator and rotor windings combined with air or hydrogen cooling for the stator and rotor cores and the inner space of the

machine. Sometimes, the stator core is liquid-cooled as well.

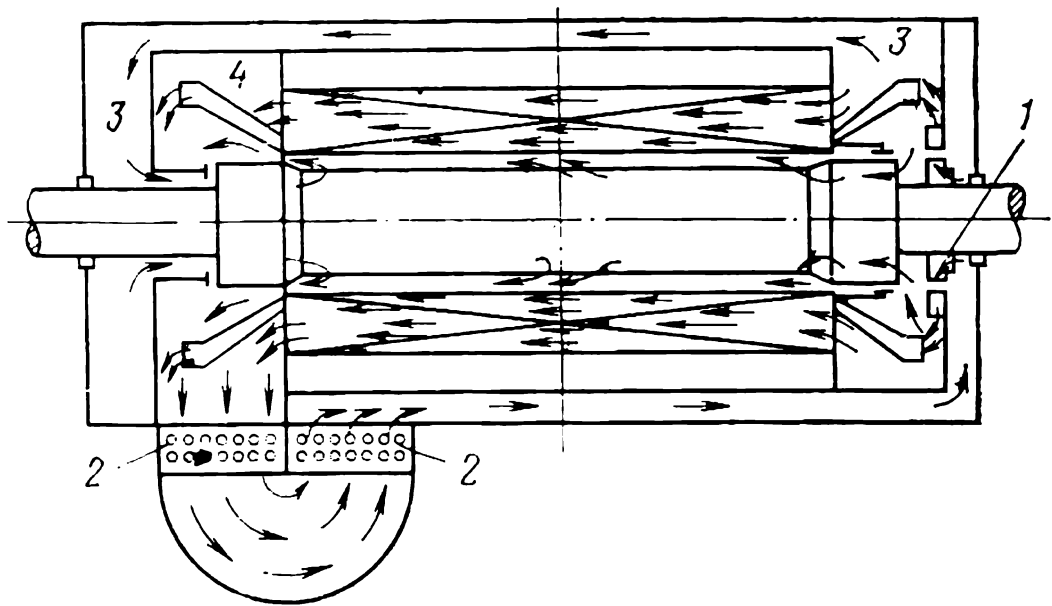


Fig. 62-4 Axial system of direct ventilation for a turbogenerator

In the first type of systems (see Fig. 62-4), hydrogen is made to circulate inside the machine by a centrifugal com-

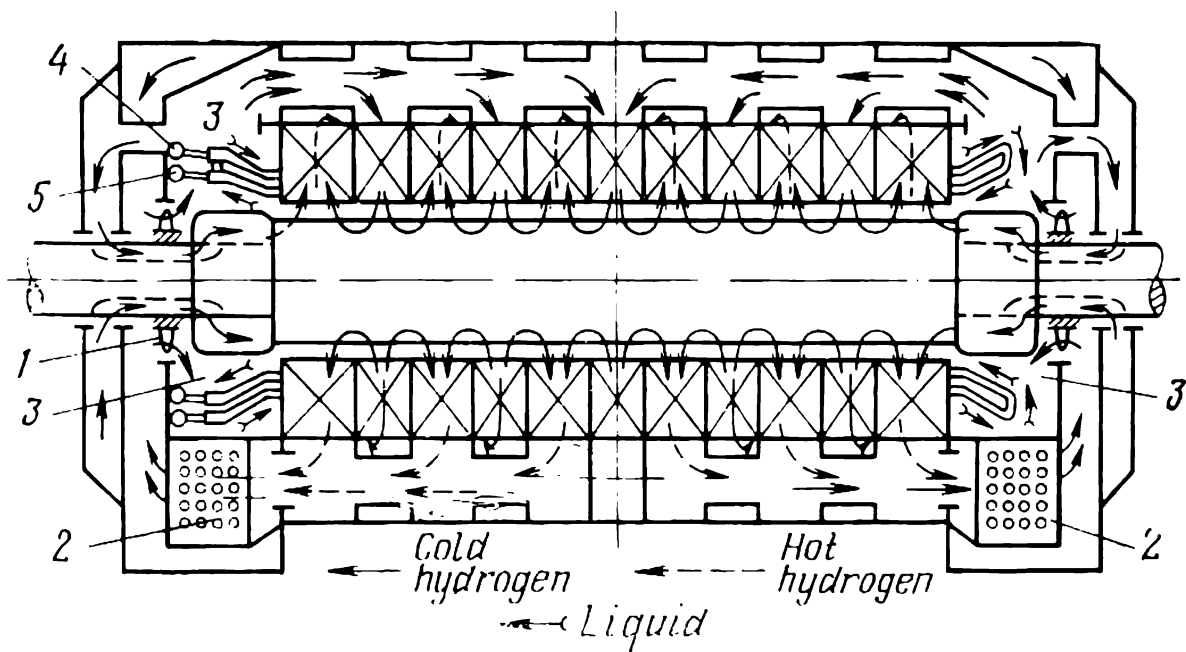


Fig. 62-5 Multiple-inlet radial system of direct hydrogen cooling for the stator core and rotor winding combined with direct liquid cooling for the stator winding:

1—axial flow fan; 2—water-cooled heat-exchanger; 3—high-pressure compartment; 4—cold-liquid header; 5—hot-liquid header

pressor, 1, mounted on the rotor shaft. From the high-pressure compartment, 3, hydrogen is distributed in the following pattern:

(a) Some hydrogen enters inlets in vent tubes embedded in the stator bars (see Fig. 62-6), cools them, and enters a hot-gas compartment, 4 (see Fig. 62-4).

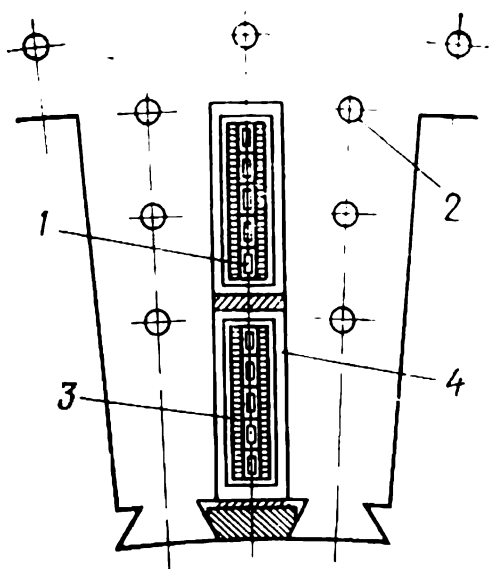


Fig. 62-6 Section through the stator of a turbogenerator using axial direct hydrogen cooling: 1—hydrogen line; 2—axial vent ducts in core; 3—copper conductors; 4—slot insulation

(b) Some hydrogen enters the axial ducts in the stator core, cools it, and enters compartment 4 (see Fig. 62-4).

(c) Some hydrogen finds its way under the binding rings on the rotor from both ends of the machine, enters the rotor conductors (see Fig. 62-7), cools them, and is discharged through radial openings into the gap whence it goes to compartment 4 (see Fig. 62-4). From compartment 4, the hydrogen passes through cool-

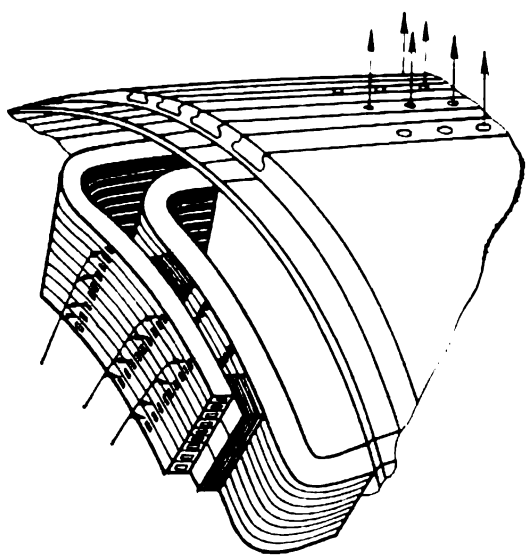


Fig. 62-7 Circulation of hydrogen in the rotor-winding ducts of a turbogenerator using axial direct cooling

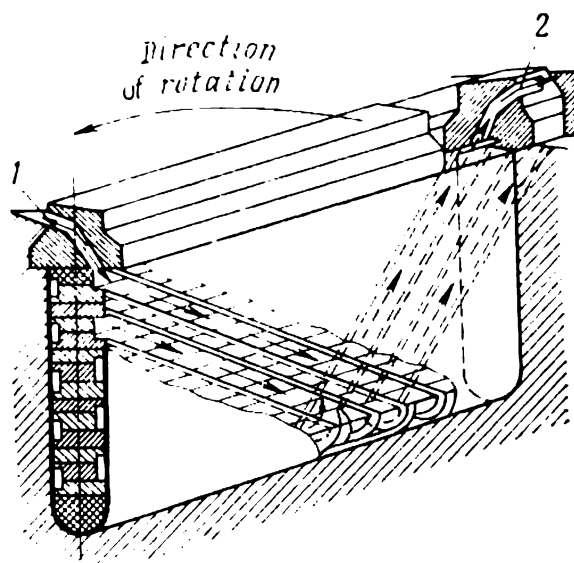


Fig. 62-8 Rotor winding in a turbogenerator directly cooled by hydrogen drawn from the gap

1—hydrogen inlet to winding ducts;  
2—hydrogen outlets from winding ducts

ler 2 and is conveyed by ducts to compartment 5 at the inlet to the compressor.

In the second and third types (see Fig. 62-5), hydrogen circulates inside a machine in about the same manner as in indirectly cooled machines (see above). The only difference

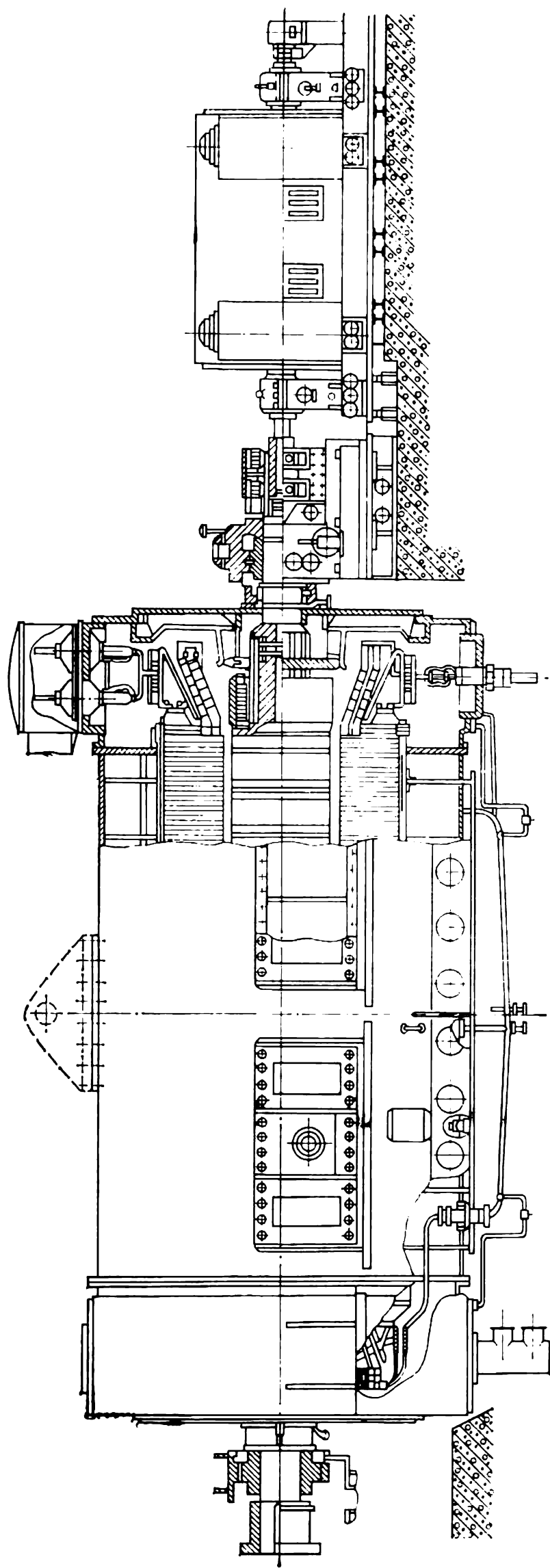


Fig. 62-9 Turbogenerator with the stator windings directly cooled by water and the rotor winding cooled by hydro-  
gen at a pressure of  $3.5 \times 10^6$  Pa (gauge)



is that the hydrogen entering the gap through radial ducts in the stator not only cools the rotor from the outside, but is scooped and conveyed inside the rotor (Fig. 62-8). Then, on passing through a multiplicity of inclined ducts on the rotor coil surface, it cools the coil from both sides and is discharged into the gap.

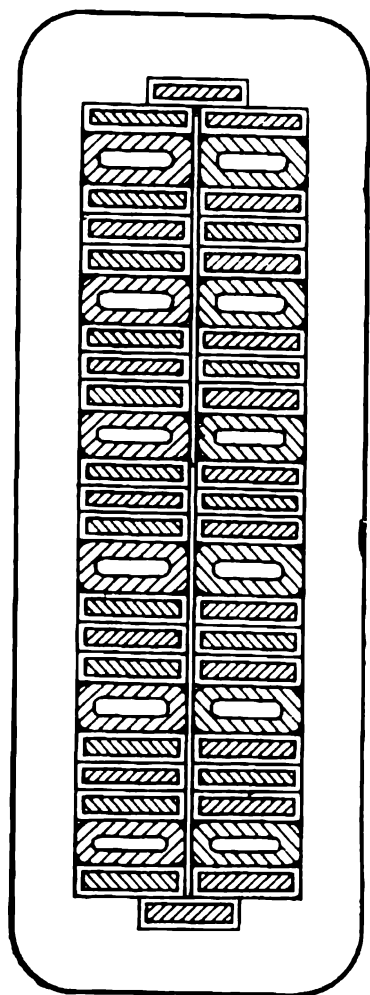


Fig. 62-10 Stator slot with water-cooled conductor

The area where hydrogen is admitted inside the rotor coincides with the area where hydrogen emerges from the radial vent ducts in the stator. The area where hydrogen is discharged into the gap coincides with the area where hydrogen enters the stator ducts. The stator winding is liquid-cooled.

The only difference between the second and third types is that in the former case the stator winding is indirectly cooled by hydrogen, whereas in the latter case the stator winding is cooled by water flowing in the hollow stator conductors (Fig. 62-10) which communicate via insulating-material tubes with a cold-liquid header, 4, and a hot-

liquid header, 5 (see Fig. 62-5). From header 5, the liquid passes through a cooler and enters header 4 again. In Fig. 62-11, the arrangement of water inlets and outlets is shown in more detail.

The fourth type has two modifications as explained above. In some turbogenerators, the stator and rotor windings are water-cooled, whereas the stator core and the inner space of the machine are cooled by hydrogen at a pressure of  $3 \times 10^5$  Pa. In some other turbogenerators, the stator space is filled with oil, the rotor is separated from the stator by an insulating cylinder, and the space around the rotor is filled by rarefied air. In this arrangement, the stator winding and core are cooled by oil, and the rotor winding by water.

## 62-2 Hydrogenerators and Engine-Driven Synchronous Generators

**Hydrogenerators.** As has already been explained, these electric machines are driven by hydraulic (or water-wheel) turbines.

As a rule, they have from 8 to 120 poles, and rotor is always of salient-pole design (see Sec. 51-3). Both horizontal and vertical-shaft arrangements are used, the former for high-speed machines and the latter for low-speed machines. In the vertical-shaft arrangement, the dead weight of the rotating parts of the generator and turbine and also the pressure of water on the water wheel of the turbine are carried by a thrust (or axial) bearing. The thrust bearing is built into a pad which transfers the vertical force to the foundation. If the rotor is mounted below the thrust bearing, this is the 'suspension' form of rotor construction (see Fig. 51-2). If the thrust bearing is located below the generator, this is the "umbrella" form of rotor construction (see Figs. 62-12 and 62-15).

Hydro-electric generators mostly use indirect air cooling. For small hydrogenerators with ratings not over 4 MVA, open-circuit self-ventilation may be used (see Fig. 51-2). Larger hydro-electric generators are built with closed-circuit self-ventilation systems, with air cooled in heat exchangers (see Fig. 62-12).

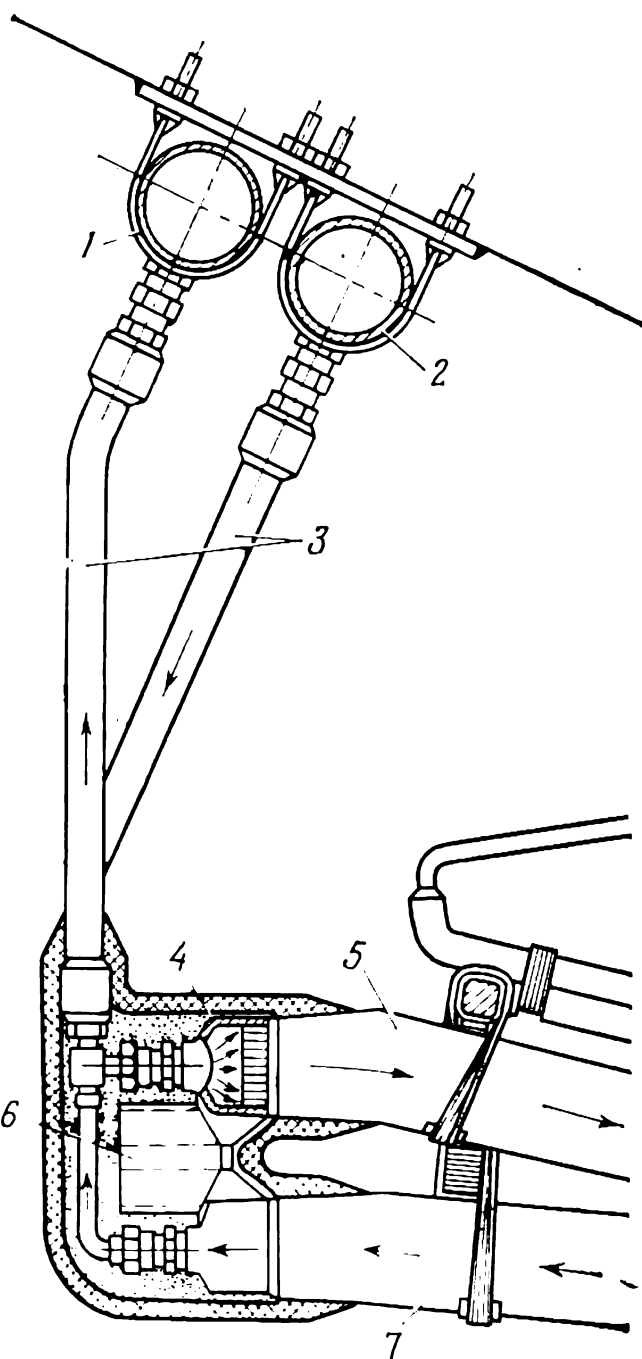


**Fig. 62-11** Connection of stator bars to cold- and hot-water distribution tubes:

1—hot-water distribution tube; 2—cold-water distribution tube; 3—flexible insulating hoses; 4—copper water-distributing bar nozzle; 5—bar conveying water to winding; 6—electrical connection between bar nozzles; 7—bar conveying water from winding

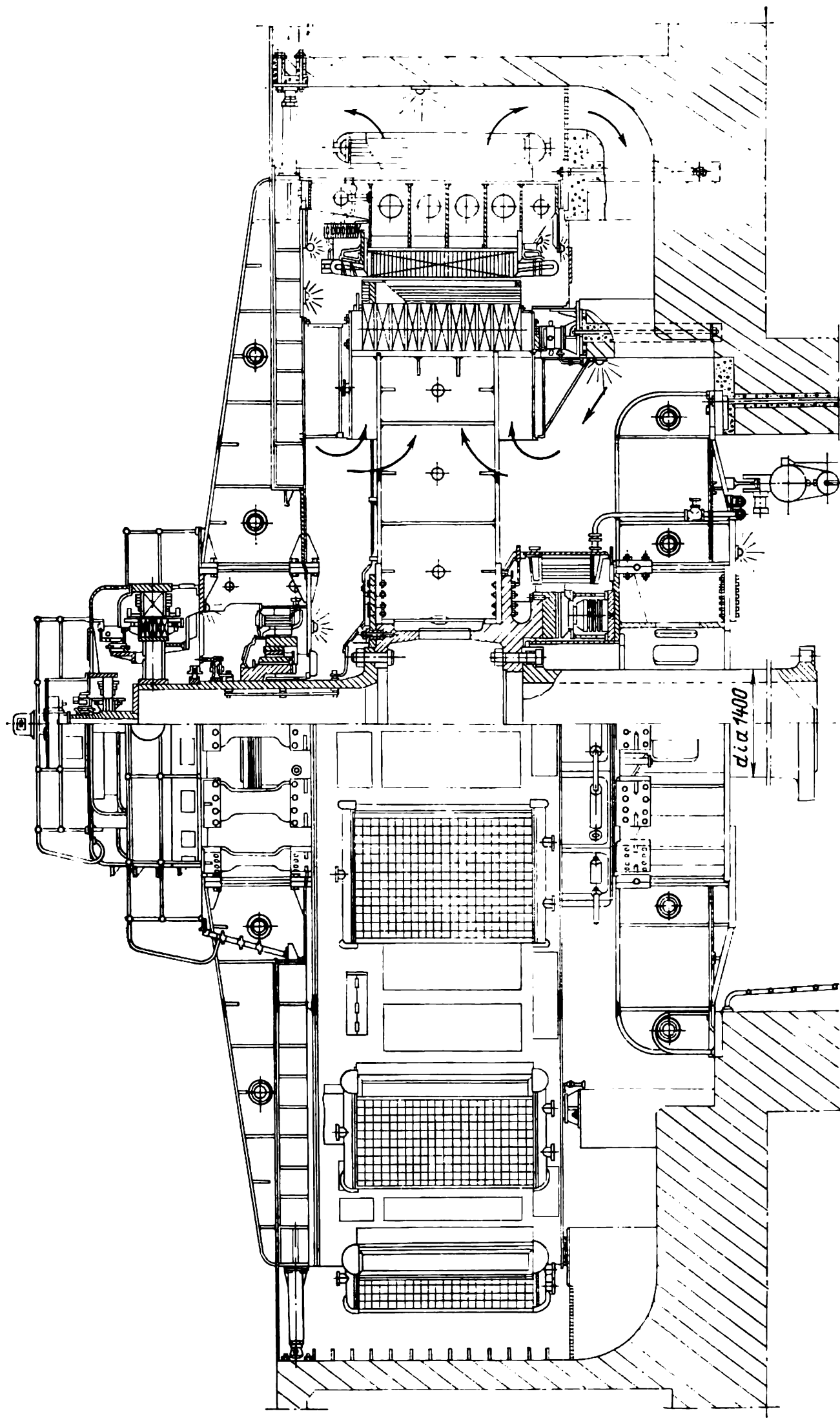


Fig. 62-12 Umbrella-type 150-MW, 15.75-kV, 100-rpm hydro-electric generator

Table 62-4 Electric Loading of Indirectly Air-Cooled Salient-Pole Hydrogenerators

$S_R/2p$ , kVA	10	50	200	1000	2000	5000 and more
Electric loading, kA/m:						
$p \geq 10$	38	45	50	61	67	70
$p = 4$	32	40	45	49	50	—
$p = 2$	28	32	36	41	45	—

In more detail the construction of indirectly air-cooled hydro-electric generators is described in Sec. 51-3. Power ratings per pole and electric loading (linear current density) are listed in Table 62-4.

A more recent trend has been to use direct cooling for hydrogenerators, especially for machines in the top power output bracket. Hydrogen is used because the machines cannot be properly sealed against leaks. The best coolant for hydrogenerators is distilled water. Given the same principal dimensions, the power rating of a hydrogenerator totally water-cooled can be more than doubled in comparison with indirect cooling. The maximum power rating may be increased in the same proportion. The direct water cooling system for the stator winding is built along the same lines as for turbogenerators (see above).

A sectional view of a pole in a hydrogenerator with a water-cooled stator winding is shown in Fig. 62-13. The distilled water that is used to cool the rotor is allowed to

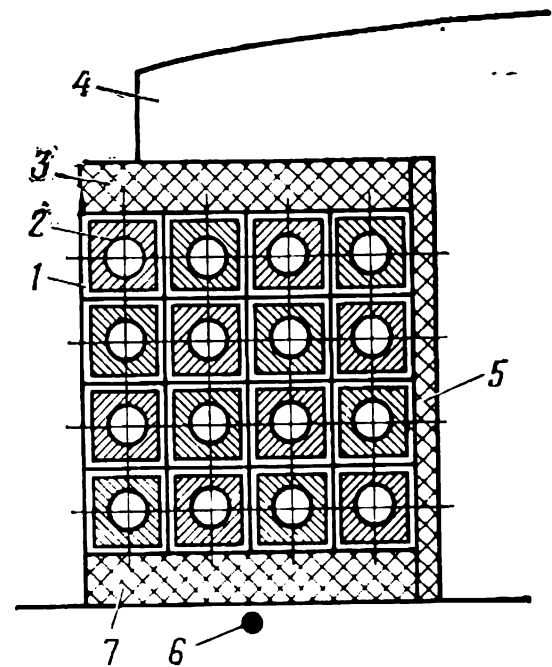


Fig. 62-13 Pole of a hydro-electric generator directly cooled by water:

1—conductor insulation; 2—hollow field-winding conductor; 3,5— pole insulation; 4—rotor pole; 6—rotor rim (yoke); 7—rotor-rim insulation

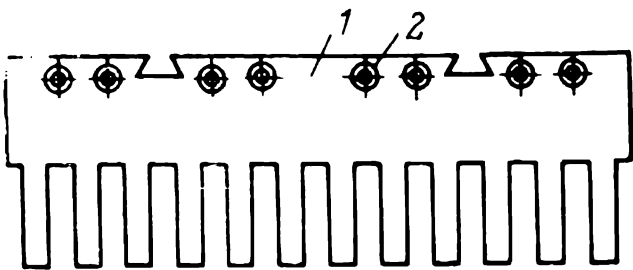
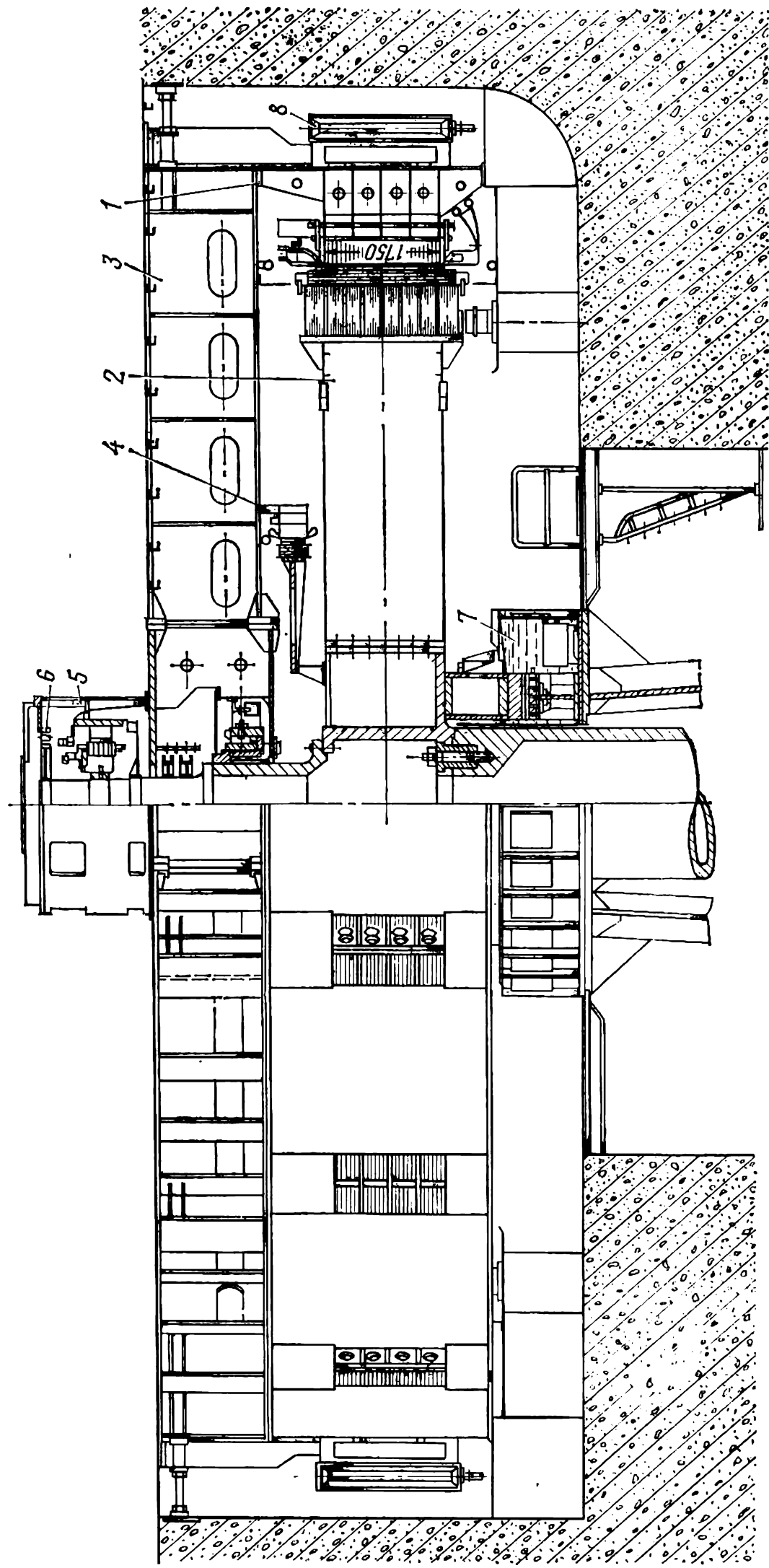


Fig. 62-14 Water cooling of the stator core



**Fig. 62-15 Umbrella-type, 500-MW, 15.75-kV, 93.8-rpm hydro-electric generator installed at Krasnoyarsk Hydro (USSR):**

**1—stator; 2—rotor; 3—upper spider; 4—air cooler; 5—auxiliary generator; 6—exciter; 7—regulator generator; 8—thrust bearing; 8—air cooler**

flow in the ducts provided within the field conductors. For the flow of water, the coil turns are connected in series.

In hydrogenerators with water-cooled stator and rotor windings, the stator core may likewise be cooled by water (Fig. 62-14). For this purpose, openings are punched in core laminations, 1, to accommodate tubes 2 which carry cooling water. To avoid currents that might be induced by the pulsating field, the water-carrying tubes must be located within the shortest distance of the core surface. As a way of minimizing the thermal resistance, the tubes are press-fitted in a fully assembled core. For the flow of water, the tubes are connected in series-parallel. Some of the heat dissipated in the machine is abstracted by the air in the gap and by the water that cools the stator winding through the insulation. This somewhat reduces the tooth temperature.

Apart from cooling systems which use only water, there are mixed direct cooling systems. In them, the stator is directly cooled by water, and the stator winding, directly by air. In such cases, the stator core is likewise cooled by air. The most popular arrangement for the field winding is one in which the cooling-air ducts, 3 (Fig. 62-16) run across the field winding.

To form these ducts, each conductor is made up of two strands one of which, 2, has a groove that forms a duct, and the other, 1, is constant in cross-section. Air entering the transverse ducts comes from ducts, 8, in the rotor rim, located opposite a hollow, 6, in the pole, 5. There is a circular duct, 4, which serves to distribute cooling air uniformly among the transverse ducts. The pressure required to circulate air is supplied by the centrifugal force of the air column between distance pieces 7 in the rotor rim ducts, 8, and

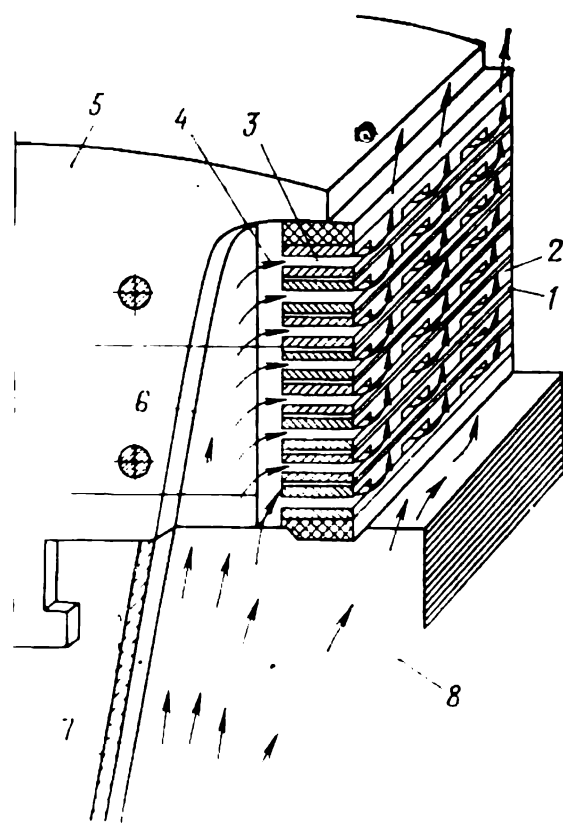


Fig. 62-16 Direct air cooling of the rotor winding in a hydroelectric generator

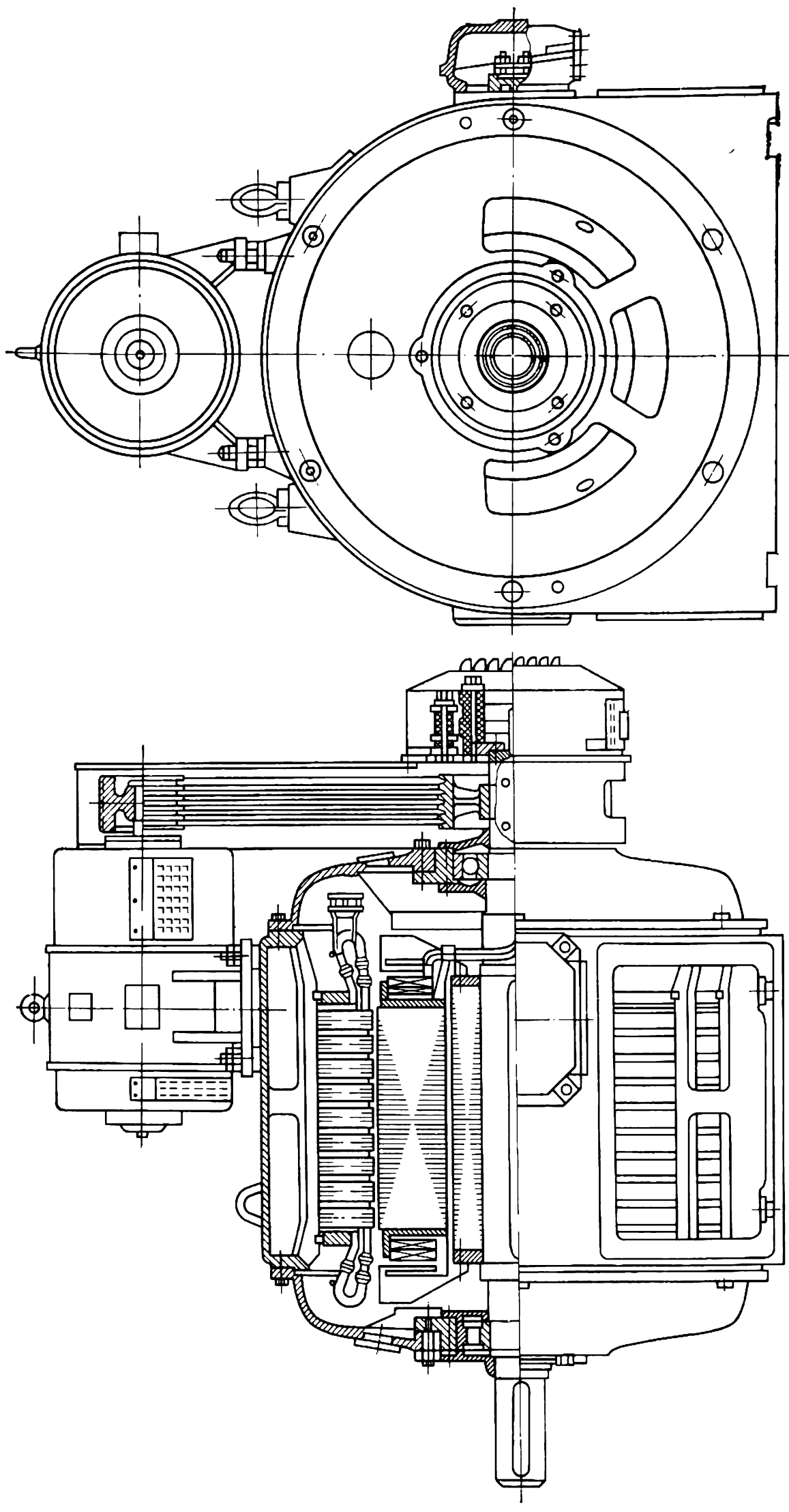


Fig. 62-17 Totally-enclosed synchronous machine

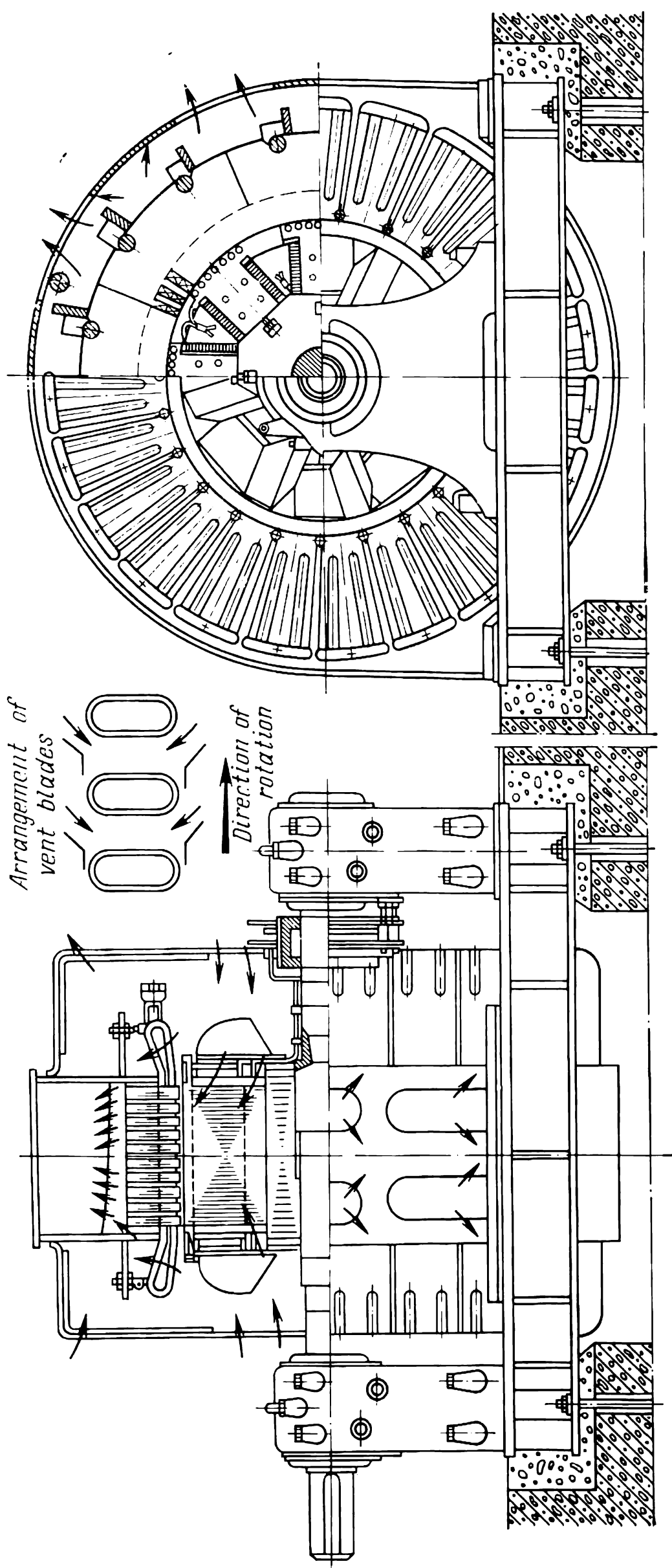


Fig. 62-18 Open synchronous machine



in ducts 6 and 4. A fraction of the cooling air comes from the rotor-rim ducts into the inter-pole space where it is mixed with hot air from the transverse ducts and serves to cool the stator. Transverse ducts increase the cooling surface area of the rotor winding by a factor of 8 to 12.

**Engine-driven synchronous generators.** These are medium-sized generators direct-connected to reciprocating or internal-combustion (Diesel) engines, intended for industrial use and small isolated power systems.

Most frequently, they are salient-pole, horizontal-shaft units with two end-shield or pedestal bearings, with a totally enclosed (Fig. 62-17) or an open (Fig. 62-18) enclosure cooled by self-ventilation. The excitation system is usually of the direct type, with the exciter either driven by a V-belt or coupled to the generator shaft. Some engine-driven synchronous generators use a.c. exciters with static rectification (the voltage regulator unit is mounted on the generator frame).

### **62-3 Synchronous Motors and Synchronous Condensers**

General-purpose synchronous motors of Soviet manufacture are available in several ranges and modifications. Some of them have a salient-pole, horizontal rotor carried in two end-shield (see Fig. 62-17) or two pedestal bearings (see Fig. 62-18). They may be enclosed or open with self-ventilation. Some motors use direct excitation systems, with the exciter either driven by a V-belt or coupled directly to the generator shaft.

Some of the Soviet-made synchronous condensers are protected units with indirect air cooling and are intended for indoor installation. The cooling system is of a closed-circuit type, with the air cooled in water coolers installed in a pit beneath the machine. There are also synchronous condensers of totally enclosed construction (Fig. 62-19). They are cooled by hydrogen at a pressure of  $10^5$  to  $2 \times 10^5$  Pa (gauge). Hydrogen is cooled in coolers built into the end bells of the stator.

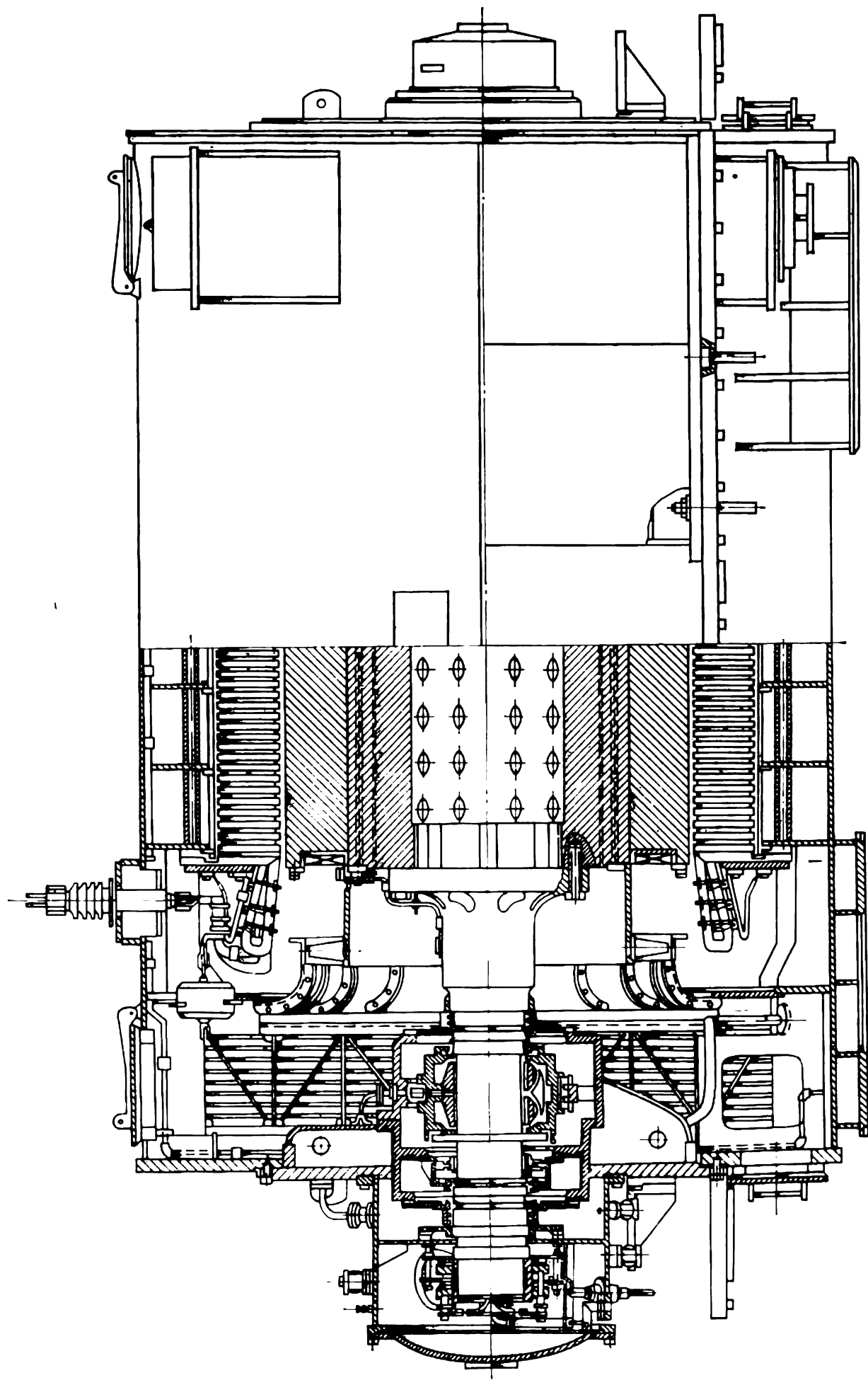


**Fig. 62-19 Synchronous condenser using indirect hydrogen cooling**

## 63 Special-Purpose Synchronous Machines

### 63-1 Electromagnetically Excited Single-Phase Synchronous Generators

These machines have a single-phase armature winding (Fig. 63-1), its conductor spanning about two-thirds of a pole pitch. Such a winding may be visualized as formed by two phases of an ordinary three-phase winding connected in a star. Then, the operation of a single-phase machine may be regarded as the unbalanced operation of a conventional synchronous machine

in which two phases carry a line voltage,

$$\dot{V} = \dot{V}_{AB}$$

and a common current,

$$\dot{I} = \dot{I}_A = -\dot{I}_B$$

whereas the third phase is dead,

$$\dot{I}_C = 0$$

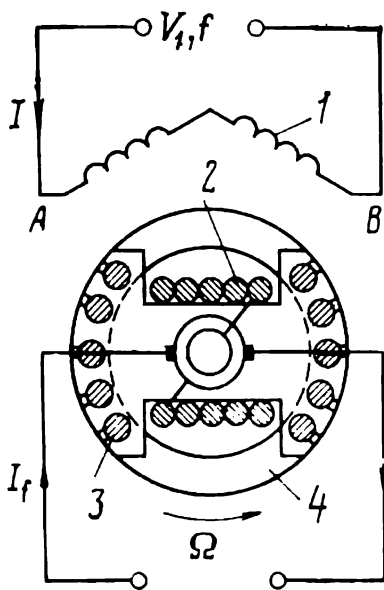


**Fig. 63-1** Single-phase synchronous generator:

1—armature winding; 2—field winding; 3—damper bar; 4—damper-winding end ring

Let us analyze the events taking place in a single-phase synchronous machine, using the theory of unbalanced operation as applied to a three-phase machines (see Chap. 61).

By this theory, the pulsating mmf is resolved into two equal-amplitude rotating mmfs, one of which is travelling at  $\Omega$  (in synchronism with the rotor), and the other at  $-\Omega$ , that is, in the opposite direction. The forward synchronous component of the armature mmf affects the excitation field as it does in a conventional synchronous machine. The backward synchronous component travels relative to the rotor at twice the synchronous speed,  $2\Omega$ . Relative to the backward mmf, the rotor slip is equal to 2, so the emfs and currents induced in its damper and field windings are like-

wise at double frequency,  $2f$ . The useful synchronous electromagnetic torque is produced only by the interaction of the synchronous field with the armature current. The backward synchronous field is detrimental. To minimize it, the rotor of a single-phase synchronous machine carries a series-shunt damper winding in which the bars and the short-circuiting end rings have a larger cross-section than they have in a three-phase synchronous machine. This type of damper winding has a reduced resistance and leakage reactance. The reduction in resistance leads to reduced losses in the damper winding, lower temperature, and improved efficiency of the machine.

Because of low efficiency, higher cost, and inferior vibration characteristics, single-phase synchronous machines are solely used to supply isolated loads. As a rule, their rating does not exceed a few tens of kilowatts, although there are units with ratings up to 50 MW for use on a.c. electric-traction railways.

### 63-2 Reluctance Synchronous Motors

A reluctance synchronous motor is a device with a salient-pole rotor without a winding and an excited winding on the stator which may be salient or non-salient.

**Polyphase reluctance motors.** In a polyphase (three- or two-phase) reluctance motor, the stator is similar to that in conventional synchronous machines (Fig. 63-2). The events taking place in a polyphase reluctance motor can be analyzed, using the theory of salient-pole synchronous machines, assuming that the field current is zero,

$$I_f = 0, \quad E_f = 0$$

When a polyphase reluctance machine is connected to an infinite system (which implies a constant terminal voltage,  $V$ ), the electromagnetic torque is given by Eq. (58-16) for  $\varepsilon = E_f/V = 0$ . The torque is a function of the angle  $\theta$

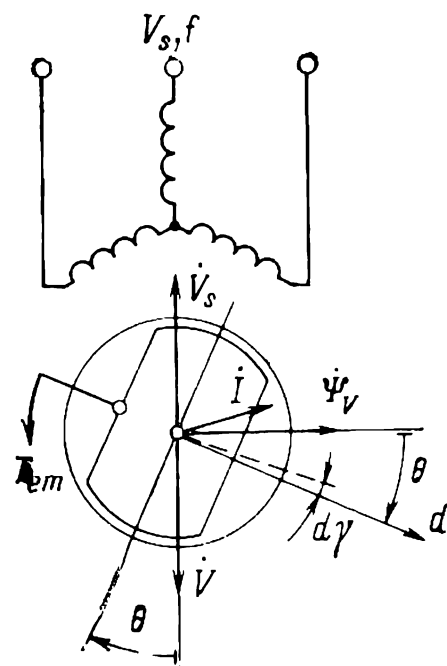


Fig. 63-2 Reluctance synchronous machine (motor mode of operation,  $\theta < 0$ ,  $T_{em} < 0$ )

between the  $d$ -axis of the rotor and the axis of the resultant field,  $\dot{\Psi}_v$ , which in this case is solely set up by the armature current,  $\dot{I}$ .

For its operation, a reluctance motor depends on the difference in permeance along the  $d$ - and  $q$ -axis of the rotor,

$$X_d > X_q$$

The electromagnetic torque acting on the rotor of a reluctance motor always tends to align its  $d$ -axis with the field. This can be proved by reference to the basic equation of energy conversion by electric machines

$$T_{em} = (dW/d\gamma)_{i=\text{constant}}$$

In a reluctance machine,

$$W \sim i^2 L$$

where  $L$  is the inductance of the armature winding and  $i$  is the armature phase current. As the  $d$ -axis of the rotor moves through an angle  $d\gamma > 0$ , tending to line up with the axis of the armature mmf (or towards the field axis), the armature inductance goes up

$$dL > 0$$

because  $L_d > L_q$ , and the energy stored by the magnetic field is incremented by

$$dW = i^2 dL$$

As a consequence,

$$T_{em} = (dW/d\gamma) > 0$$

and this implies that the electromagnetic torque is acting in the direction of  $d\gamma$  and tends to line up the  $d$ -axis of the rotor with the field axis. In the motor mode of operation (Fig. 63-2), when the  $d$ -axis of the torque lags behind the field axis,  $\theta < 0$ , the electromagnetic torque operating on the rotor acts in the direction of rotation,  $T_{em} < 0$ . At  $R = 0$  and  $|\theta| = \pi/4$ , the electromagnetic torque is a maximum,

$$T_{em, \max} = \frac{m_1 V^2}{2\Omega} (1/X_q - 1/X_d)$$

In analyzing fractional-horsepower reluctance motors (especially, those with ratings of a few watts or less), it

is important to consider the effect of the stator resistance (see Sec. 58-5). It consists in a reduction of the maximum torque and the value of  $\theta$  at which it is observed,  $|\theta| < \pi/4$ .

A major advantage of reluctance synchronous motors is a very simple construction (they have neither a field winding nor an excitation system). Unfortunately, they suffer from a vital shortcoming—they draw reactive power from the system to which they are connected. This can be seen from

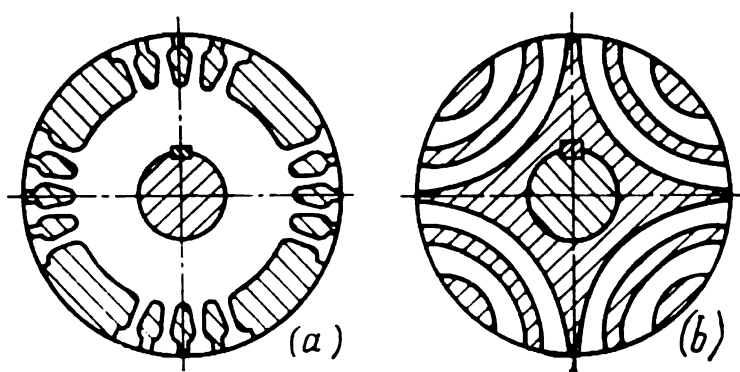


**Fig. 63-3** Sectional views of the rotor cores used in four-pole reluctance synchronous motors:

(a) conventional core carrying a cast-aluminium damper winding; (b) sectionalized core carrying a cast-aluminium damper winding whose shaped bars form non-magnetic gaps

Eq. (58-11), if we put  $\varepsilon = 0$ . Because of this, three-phase reluctance motors are mainly used in low-power drives (a few tens of watts).

Reluctance motors are started as induction motors, for which purpose their rotors carry an aluminium-cast, unequal-pitch, short-circuited auxiliary winding (Fig. 63-3a).

As follows from the equation given earlier, the maximum torque could be increased by reducing  $X_d$  and  $X_q$ . This could in turn be done by increasing the radial gap length. This would, however, lead to an increased consumption of reactive power and impairs the power factor.

A better way to improve the performance of reluctance motors is to sectionalize the rotor core by providing several nonmagnetic gaps in the path of the  $q$ -axis field, with no such gaps made in the path of the  $d$ -axis field. Whereas in the conventional design,  $X_d/X_q \approx 2$ , in a sectionalized rotor with its nonmagnetic gaps filled by aluminium bars (Fig. 63-3b), the ratio  $X_d/X_q$  rises to four or five. This markedly improves  $T_{em, \max}$ , with the reactive power drawn

from the system held at its previous value. In terms of power factor and efficiency, three-phase reluctance motors using sectionalized rotors are comparable with induction motors. As a result, they can be used even where the required power output must be as high as several kilowatts. At its ends, a sectionalized rotor carries short-circuiting rings cast of aluminium integral with the shaped bars filling the non-magnetic gaps. The bars and rings form the starting winding of the machine.

Fractional-hp, single-phase reluctance motors are widely used in automatic control systems, recording instruments, video and sound tape recorders. At starting and in running, the rotating magnetic field is obtained by the same methods as in single-phase induction motors. The most commonly used types are shaded-pole and capacitor-type reluctance motors in which the stator is built exactly as it is in similar induction fractional-hp motors (see Secs. 47-4 and 47-5).

The rotor of a single-phase reluctance motor may be built similarly to that of a polyphase reluctance motor. Here, too, a sectionalized rotor core (see Fig. 63-3*b*) can markedly improve the starting and running performance of the machine. In contrast to induction single-phase motors, the auxiliary winding of a reluctance motor under operating conditions only affects the backward field and has no effect on the forward field. Conversely, the saliency has a marked effect on the forward field because it depends on the position of the rotor relative to the mmf. Its effect on the backward field can be accounted for in averaged terms.

Another important factor is that the starting torque of a reluctance single-phase motor (especially, that of the capacitor type) at  $\Omega = 0$  depends on the initial position of the rotor axes relative to the axes of the main and auxiliary windings. This is because the auxiliary winding has different values for the permeance and leakage inductances along the  $d$ - and  $q$ -axis. Given certain conditions, this factor may be the cause of cogging in capacitor-type motors.

The difference in permeance and reactances along the  $d$ - and  $q$ -axis in the auxiliary winding adds a good measure of complexity to the electromagnetic processes that take place in a single-phase reluctance motor as compared with single-phase induction motors. Moreover, it makes the pattern of the rotating field still more dependent on the rotor speed at starting and the angular position of the rotor under

running conditions. Therefore, in a capacitor-type motor a nearly circular field can be obtained only under one particular set of operating conditions, namely, at a certain definite rpm at starting or at a certain load in operation. In all other cases, the ellipticity of the field will be more pronounced than in similar single-phase induction motors. At starting and in running, a circular field can be obtained by varying the capacitance of the capacitors connected in the auxiliary-winding circuit, after the motor has pulled into synchronism.

In shaded-pole single-phase reluctance motors, the field remains elliptical always, both at starting and in running. Therefore, shaded-pole, single-phase reluctance motors are inferior to capacitor-type reluctance motors in all respects — efficiency, power factor, and initial (static) torque.

### 63-3 Claw-Pole Synchronous Machines

Claw-pole synchronous machines differ from conventional synchronous motors by the construction of the field (rotor) core and the field winding.

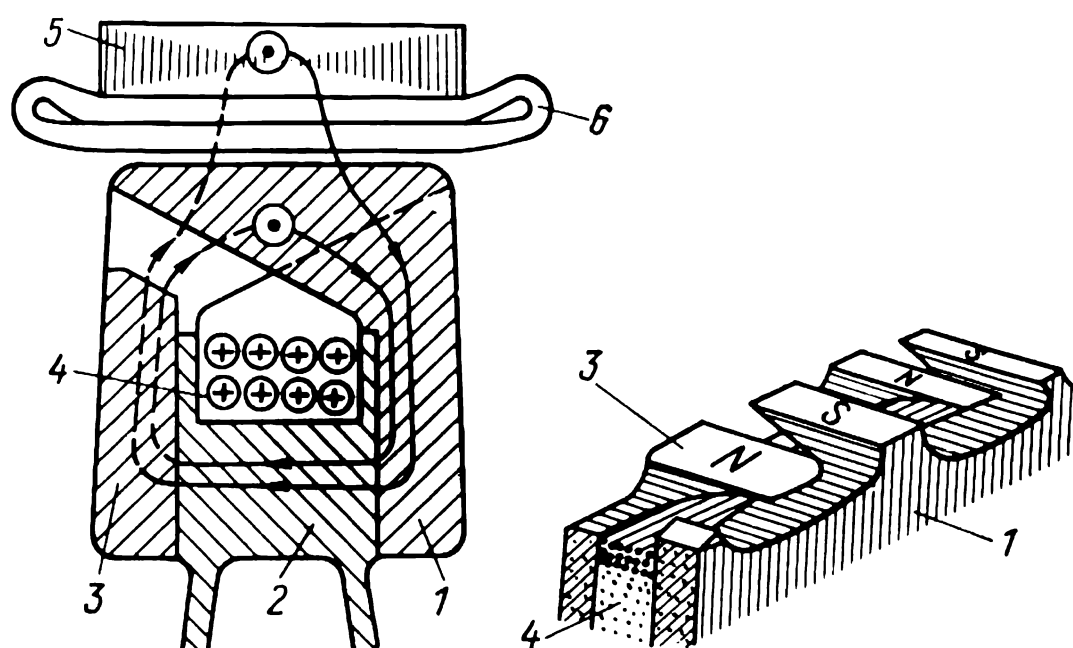


**Fig. 63-4** Claw-pole synchronous machine:

1—N-pole disc; 2—field yoke; 3—S-pole disc; 4—field winding; 5—armature core; 6—armature winding

The rotor core consists of three parts (Fig. 63-4), namely a yoke 2, a disc 1 with claw-shaped projections which serve as north (N) poles, and a disc 3 with claw-shaped projections



which serve as south (S) poles. The ring-shaped field winding, 4, is placed between the claw-pole discs 1 and 3, and energized from an exciter via slip-rings. Excitation gives rise to a magnetic flux which encircles the field conductors as shown by arrows in the figure. The larger proportion of the flux emerging from the N poles crosses the gap, links the armature winding, threads the yoke, and goes back to the field structure across the gap between the armature

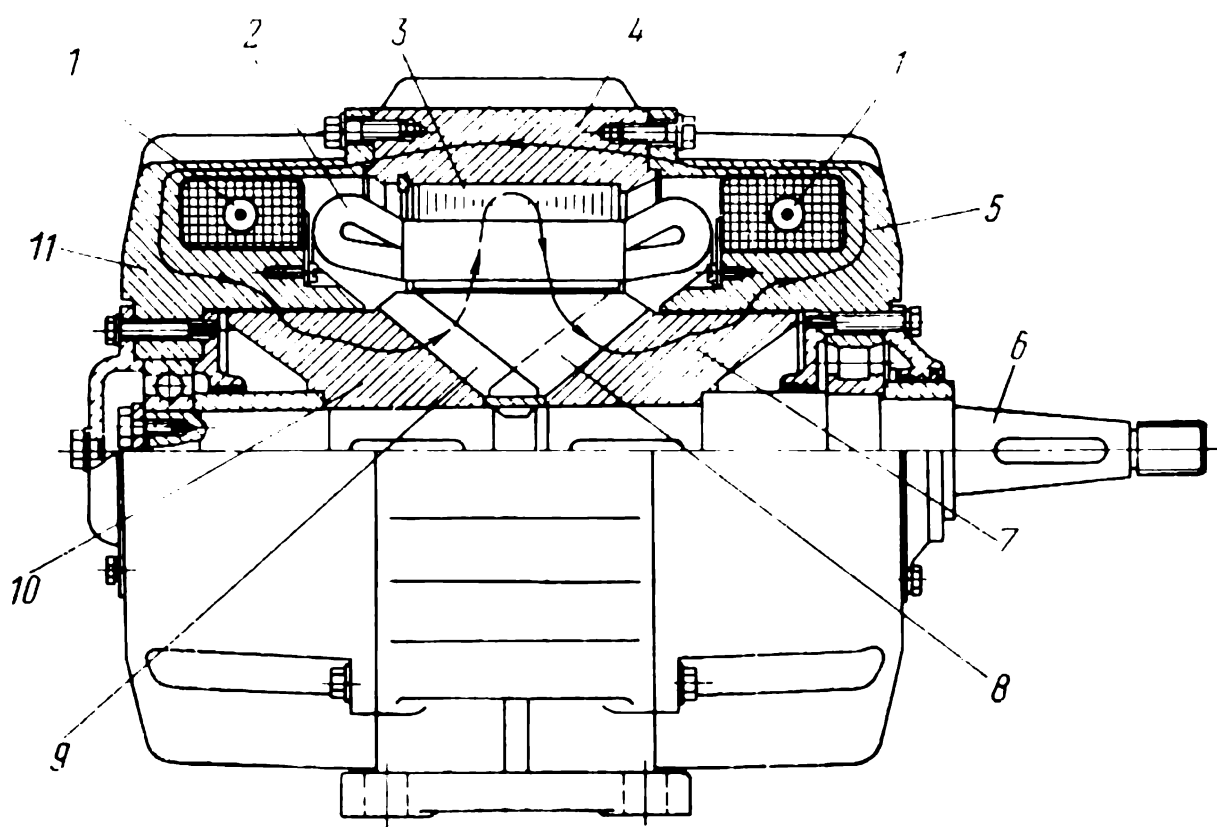


**Fig. 63-5** Brushless, claw-pole synchronous machine:

1—ring-shaped field windings; 2—armature winding; 3—armature core; 4—frame; 5—end-shield; 6—shaft; 7—S-pole yoke; 8—S poles; 9—N poles; 10—N-pole yoke; 11—end-shield

teeth and the S poles. This is the mutual flux. The smaller proportion of the total flux goes directly from the N to the S poles without linking the armature winding. This is the leakage flux of the field winding.

The best performance is shown by claw-pole machines in which the ring-shaped winding is stationary. Because such a design needs neither a sliding contact nor brushgear to supply the field winding, it is called the brushless type. A sectional view of a brushless synchronous generator with claw-shaped poles on the rotor is shown in Fig. 63-5, and its rotor in Fig. 63-6. Its field winding consists of two stationary ring-shaped coils, 1, installed in recesses of the end shields, 5 and 11. The flux set up by the coil currents has

its path basically as shown in the figure, that is, from the N poles 9, across the gap, to the teeth of the armature core 3 along the yoke and armature teeth, again across the gap to the S poles 8, through the S pole yoke 7, across the gap between yoke 7 and end-shield 5, through the end-shield, the frame 4, the other end-shield 11, across the gap between

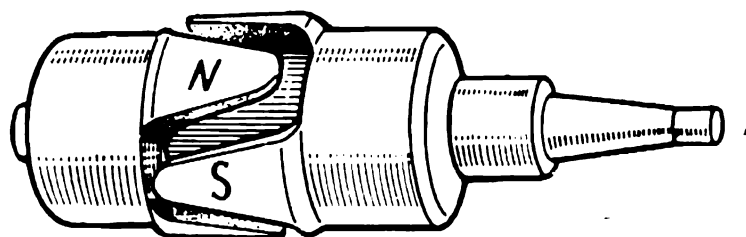


Fig. 63-6 Rotor of a brushless, claw-pole synchronous generator

end-shield 11 and the N pole yoke 10, and from yoke 10 again to the N poles. The greater proportion of the field-winding flux links the armature winding and produces the mutual flux, and the remainder acts as the leakage flux. As the shaft 6, the pole yokes 7 and 10, and the poles 8 and 9 rotate, the flux linkage with the armature winding (that is, the mutual flux) varies periodically and induces an emf in the armature.

Brushless synchronous generators and motors are employed in cases where brushgear would be hard of access or maintenance and where the machine must operate with high reliability for a long time under adverse service conditions. For example, such generators are used as sources of electricity for railways cars. They come in ratings of 10 kW and higher.

#### 63-4 Inductor Machines

**General.** In an inductor machine, the armature and field windings are stationary, and the rotor is made of laminated steel and has a large number of teeth, or, rather, notches but no winding.

Energy conversion in an inductor machine is based on variations in the mutual inductance between the armature and field windings as the rotor notches pass the stator teeth (see Sec. 20-4).

In fact, any electric machine with a toothed rotor and with two windings of a suitable type wound on the stator

can be used as an inductor synchronous machine. Its mutual inductance (see Eq. (20-8)) is proportional to the number of rotor notches,  $Z$ :

$$f = Z\Omega/2\pi$$

With the field winding excited by d.c., the emf induced in the armature has the same frequency. The armature winding can be connected to an isolated load or to a system operating at the same frequency. When connected to a system, an inductor machine can operate as a generator or a motor, according to the direction of the external torque applied to the shaft.

In performance, inductor alternators (as they are usually called) and inductor-type synchronous motors do not differ from conventional synchronous machines. Their theory is based on the general mathematical description of energy conversion by electric machines, as outlined in brief in Sec. 18-2.

As compared with a conventional synchronous machine, an inductor machine has a substantially larger size and weight. The point is that the flux in the toothed layer of the stator in an inductor machine varies only in magnitude, whereas in a conventional synchronous machine it varies in both magnitude and direction. Given the same size and the same maximum tooth flux density, the peak value of the fundamental flux in an inductor machine is one-third to one-fourth of its value in a conventional machine. Therefore, the use of inductor machines is warranted only in cases where the desired frequency is difficult to obtain with a conventional multipole or claw-pole synchronous machine.

According to the construction of the field winding, there may be heteropolar and homopolar inductor machines. In polyphase machines, the armature winding is always heteropolar; in single-phase machines, it is more frequently heteropolar, although the homopolar design is also used. In either case, the stator may be salient or nonsalient. Within each design class, there may be a multiplicity of modifications (with reference to a single-phase machine, they are described in Sec. 20-4). As an example of a heteropolar design, we shall take up a machine with a salient-pole stator.

In this design (Fig. 63-7), the field winding,  $FW$ , is held in the major slots of the stator and sets up a two-pole

flux ( $p = 1$ ) whose lines emerge from the N pole of the stator in zones *II* and *III*, cross the gap, enter the rotor core, and cross the gap in the reverse direction to enter the S pole of the stator in zones *I* and *IV*. The armature winding *AW*, is wound for the same number of poles as the field winding

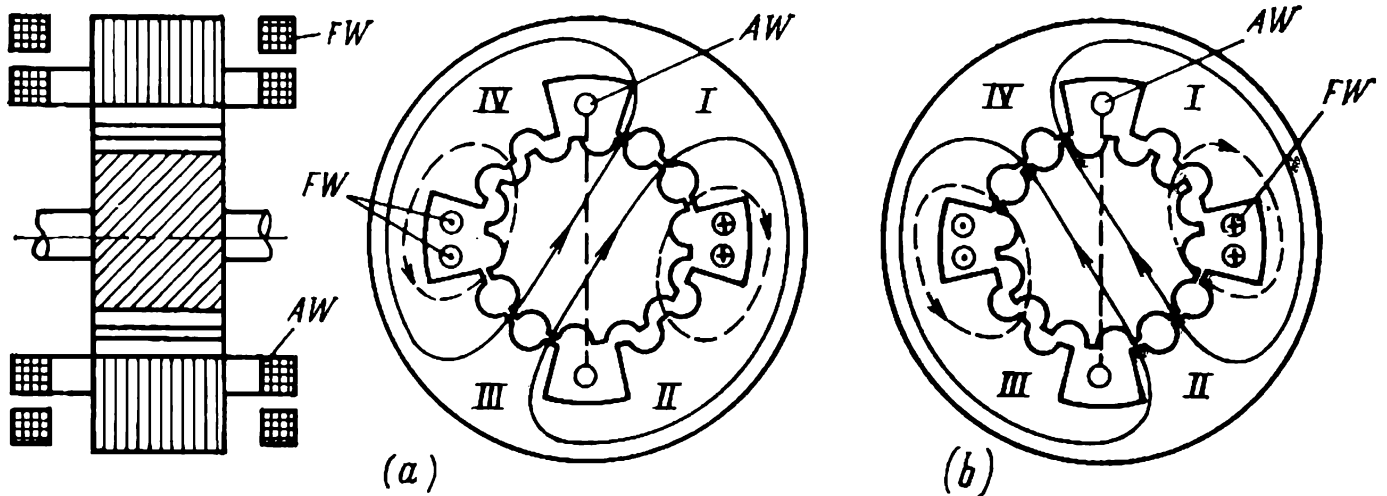


Fig. 63-7 Heteropolar inductor-type synchronous machine

and is held in the major slots of the stator, displaced from the field-winding slots by a quarter of a cycle. The number of rotor teeth is set at

$$Z = 2pk$$

where  $k$  is an odd integer (in Fig. 63-7,  $Z = 2 \times 1 \times 7 = 14$ ). On their surface, the major teeth (in zones *I-IV*) have recesses between which minor stator teeth are formed, with an angular pitch equal to the rotor tooth pitch,

$$\alpha_z = 2\pi/Z$$

In all the zones, the same number of minor teeth is made (in Fig. 63-7, there are three minor teeth in each zone).

As the rotor turns, the relative position of the teeth on the stator and rotor varies periodically. When the rotor takes up the position shown in Fig. 63-7*a*, the rotor teeth line up with the minor teeth on the stator in zones *I* and *III*, the gap permeance in those zones reaches a maximum value, and the excitation flux is oriented basically as shown by the full lines (the dashed lines show the flux whose path runs through low-permeance zones *II* and *IV* where the rotor teeth line up with the stator slots). When the rotor turns through a half of a tooth pitch,

$$\alpha_z/2 = \pi/Z$$

and takes up the position shown in Fig. 64-7*b*, the rotor teeth line up with the stator teeth in zones *II* and *IV*, and the excitation flux is oriented basically as shown by the full lines. From a comparison of Fig. 63-7*a* and *b*, it is seen that the direction in which the flux cuts the plane of the armature coil is reversed.

When the rotor turns through another half of a tooth pitch, that is, an angle  $\alpha_z/2$ , the flux pattern will be the

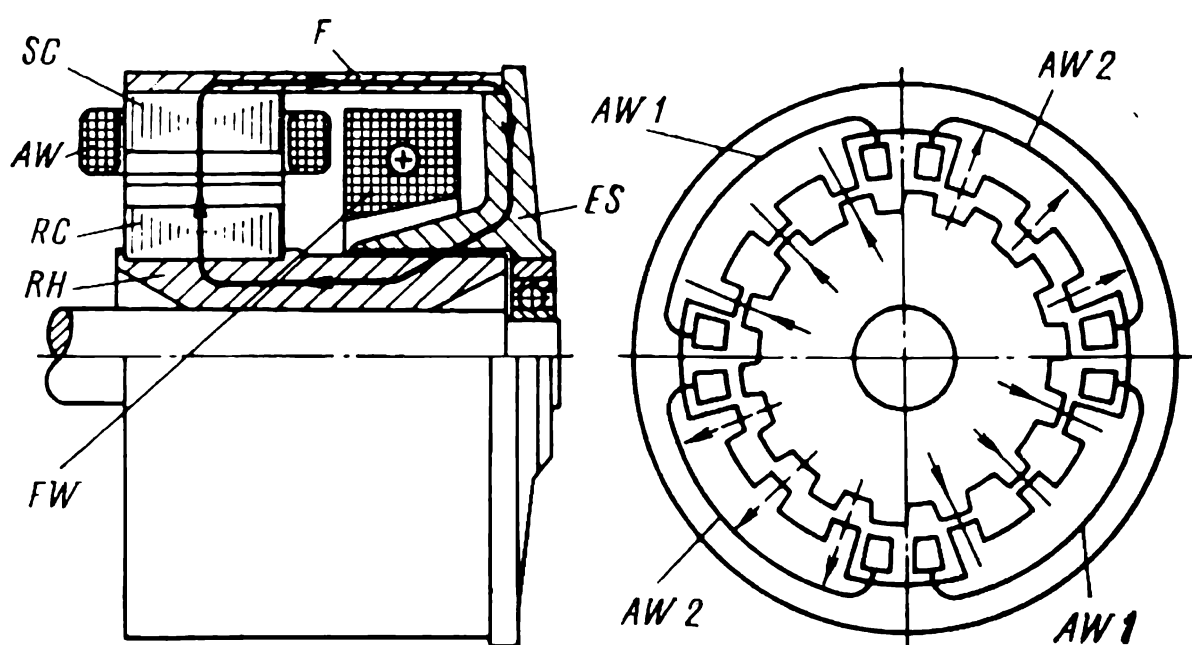


Fig. 63-8 Homopolar inductor-type synchronous machine

same as it was in the initial position shown in Fig. 63-7*a*. Thus, the flux linking the armature winding varies with a period

$$T = \alpha_z / \Omega$$

which corresponds to the rotation of the rotor through an angle  $\alpha_z$ .

As an example of the homopolar design, we shall take up a machine with a toothed stator, which differs from the machine in Fig. 20-9 only in that its armature winding is located in the major slots.

In this homopolar machine (Fig. 63-8), the ring-shaped field winding, *FW*, encircles the rotor shaft and is located between the end-shield and the stator and rotor cores. This winding sets up an axi-symmetric excitation flux. All of the flux (one of its lines is shown in the sectional view) links the field winding. From the rotor magnetized in north polarity, the flux goes back across the gap to the stator

magnetized in south polarity. The magnetic circuit of the mutual flux linking the two sections of the armature winding,  $AW1$  and  $AW2$ , and the field winding, consists of the following parts: the rotor core  $RC$ , the main toothed gap, the stator core  $SC$ , the frame  $F$ , the end-shield  $ES$ , an auxiliary annular gap  $AG$ , and the rotor hub  $RH$ . The coils of the sectionalized armature winding are placed, as already noted, in the major parts of the stator core. The rotor core does not differ from that in the heteropolar machine shown in Fig. 63-7. It has  $Z = (Z_{major}/2)k$  teeth, where  $Z_{major}$  is the number of major teeth on the stator core, and  $k$  is an odd integer. In Fig. 63-8,  $Z = (4 \div 2) \times 7 = 14$ .

On their surface, the major stator teeth carrying the coils  $AW1$  and  $AW2$  have recesses between which minor stator teeth are formed, with an angular pitch equal to the tooth pitch of the rotor,  $\alpha_z = 2\pi/Z$ . (In Fig. 63-8, there are three minor teeth in each zone between major teeth.) As the rotor turns, the relative position of the stator and rotor teeth varies periodically. When the rotor takes up the position shown in Fig. 63-8, the rotor teeth line up with the minor teeth in the zones encircled by the coils  $AW1$ . The gap permeance in those zones reaches a maximum value; the flux is basically oriented as shown by the full lines, and links the coils  $AW1$ . The flux shown by the dashed lines produces a markedly smaller linkage with the coils  $AW2$ , because in the zones encircled by these coils the rotor teeth line up with the stator slots, and the gap permeance is a minimum.

When the rotor turns through a half of a tooth pitch, that is, an angle  $\alpha_z/2 = \pi/Z$ , the rotor teeth line up with the stator teeth in the zones encircled by the coils  $AW2$ , and the flux linkage produced by these coils is a maximum, whereas the flux linkage produced by the coils  $AW1$  is a minimum. The armature flux linkage varies with a period  $T$  corresponding to the rotation of the rotor through an angle  $\alpha_z$ . Therefore, as with the heteropolar design,

$$T = \alpha_z/\Omega$$

Because variations in the flux linkages with  $AW1$  and  $AW2$  are displaced in time by  $T/2$ , that is, are in antiphase, the two armature sections must be connected in series opposition. In each section,  $AW1$  and  $AW2$ , the coils must however be connected in series aiding.

**Inductor-type alternators.** Originally, the inductor machine went into use as a generator. In 1854, Knight took out a British patent for a machine which operated by the inductor principle. In 1877, Yablochkov invented a cylindrical-rotor inductor generator which bore a close resemblance to the machine as we know it today.

With the advent of radio in 1895, inductor alternators came to be used as sources of current at 50 kHz and higher for the antenna resonant circuit. Known today as constant-flux inductor alternators (see Sec. 20-4, “*b*” and “*d*”), they remained in this capacity for a long time (until about the 1920s), although already in 1901 Guy had proposed his toothed-stator inductor alternator, now more commonly known as the pulsating tooth-flux inductor generator (see Sec. 20-4, “*c*” and “*e*”).

For the generation of frequencies at the values given above the heteropolar armature winding of cylindrical-rotor inductor alternators was made with a minimum attainable number of pole pairs, and their rotor was made to spin at the maximum permissible speed (as high as 20 000 rpm). The difficulties in the manufacture of inductor alternators for such frequencies were circumvented by the pulsating tooth-flux inductor alternator where the desired high frequency is obtained owing to an increased number of rotor and stator teeth.

At present, inductor alternators are no longer used in radio engineering where other sources of high-frequency supply have been found. Instead, they are widely used in a multiplicity of industrial processes such as induction melting, induction welding and brazing, induction heat treatment, induction drying, and so on, which need power sources operating at 1 000 to 10 000 Hz. Among their other uses are high-speed drives and radar.

**Inductor-type synchronous motors.** Although they do not differ from inductor-type synchronous generators in construction and operation, they found practical application much later and did not see a growing interest until the 1960-70s.

In an inductor-type synchronous motor, the synchronous speed at a given supply frequency,  $f$ , is solely a function of  $Z = Z_4$ , the number of rotor teeth,

$$n = \Omega/2\pi = f/Z_4$$

With a sufficiently large number of rotor teeth, very low synchronous speeds can be obtained. For example, at  $f = 50$  Hz and  $Z_4 = 100$ ,

$$n = 0.5 \text{ rps} = 30 \text{ rpm}$$

If the number of rotor teeth is limited and the heteropolar armature winding can be made with a number of pole pairs close to that of rotor teeth, two modifications of the smooth stator core design can be used, namely:

(1) with heteropolar (or radial) excitation (see Sec. 20-4, "b", Fig. 20-6);

(2) with homopolar (or axial) excitation (see Sec. 20-4, "d", Fig. 20-8).

If the rotor has so many teeth that a smooth stator design is out of the question, resort can be made to a toothed stator in any one of the two modifications discussed above, namely:

(1) with heteropolar (radial) excitation (see Fig. 63-7 and also Sec. 20-4, "c", and Fig. 20-7);

(2) with homopolar (axial) excitation (see Fig. 63-8, Sec. 20-4, "e", and Fig. 20-9).

The field motor draws its power from an a.c. supply line via a rectifier. In self-excited motors, the field winding is energized from the armature winding by transformer action. In this arrangement, the field circuit is closed through a rectifier, and transformer coupling is provided by using the heteropolar arrangement with a pole ratio,  $p_2/p_1$ , equal to an odd number. With both heteropolar and homopolar excitation, the excitation field can be produced by suitably magnetized permanent magnets. The armature winding can be single-, two-, or three-phase. Starting is by direct connection to the line.

In addition to a main (or run) winding, single-phase inductor-type motors have an auxiliary (or starting) winding connected to the supply line via a capacitor. To facilitate starting in which the currents interact with the armature field rotating at  $\Omega_2 = 2\pi f/p_2$  which is many times the rated synchronous velocity of the motor,  $\Omega = 2\pi f/Z_4$ . The variables of the short-circuited winding must be matched so that the starting torque exceeds the load (external) torque, but is smaller than the maximum synchronous (or pull-out) torque. If this requirement is not met, the rotor may "skip" the rated rotational speed. If the moment of inertia of the rotor is not very high, and the synchronous speed is suffi-



ciently low, the motor can be started even without a short-circuited auxiliary winding, solely owing to synchronous torque. In the circumstances, the rotor has time to come up to synchronous speed and pull into synchronism during a half-cycle of the synchronous torque, when its direction remains constant.

**Inductor-type reluctance motors.** In contrast to conventional reluctance motors, inductor-type reluctance units are nonexcited single- or three-phase synchronous motors with a number of rotor teeth in excess of the number of poles on the armature winding, that is

$$Z > 2p_2$$

In a conventional reluctance synchronous machine,  $Z = 2p$  (see Sec. 63-2 and also Sec. 20-3).

This type of machine with one winding and toothed stator and rotor cores is described in Sec. 20-3. The stator must always be salient, and the number of stator tooth pitches along the gap circle,  $Z'_s$ , must be either the same as the number of rotor teeth,  $Z_r$  (see Fig. 20-2), or differ from it by the number of armature poles,  $Z_r - Z'_s = 2p_1$  (see Fig. 20-3).

In a reluctance synchronous machine, the armature inductance alternates at

$$\omega = 2\pi f = Z\Omega$$

On the other hand, as is shown in Sec. 21-1, for electro-mechanical energy conversion it is essential that the armature winding be connected to a line with  $\omega_1 = 2\pi f_1 = \omega/2$ . Hence, in synchronous operation a reluctance motor is running at

$$\Omega = 2\omega_1/Z = 4\pi f_1/Z$$

which is twice the speed of an inductor motor having the same number of teeth on the rotor.

### 63-5 Rolling-Rotor and Flexible Wave-Rotor Motors

Like the motors described in the previous section, these motors serve to produce low rotational speeds. Instead of electromagnetic effects, however, they do so with the aid of mechanical speed reduction.

**Rolling-rotor motors.** Proposed by Moskvitin in 1944, it differs from all other motors in two respects. Firstly, the rotor core has neither a winding nor any projections or notches on its surface. Secondly, a rotating field causes the rotor to roll on guides so that it remains eccentrically positioned inside the stator.

The construction of a rolling-rotor motor is shown in Fig. 63-9. Its stator carries two windings, namely a heteropolar armature winding, 1, and a homopolar field winding, 2.

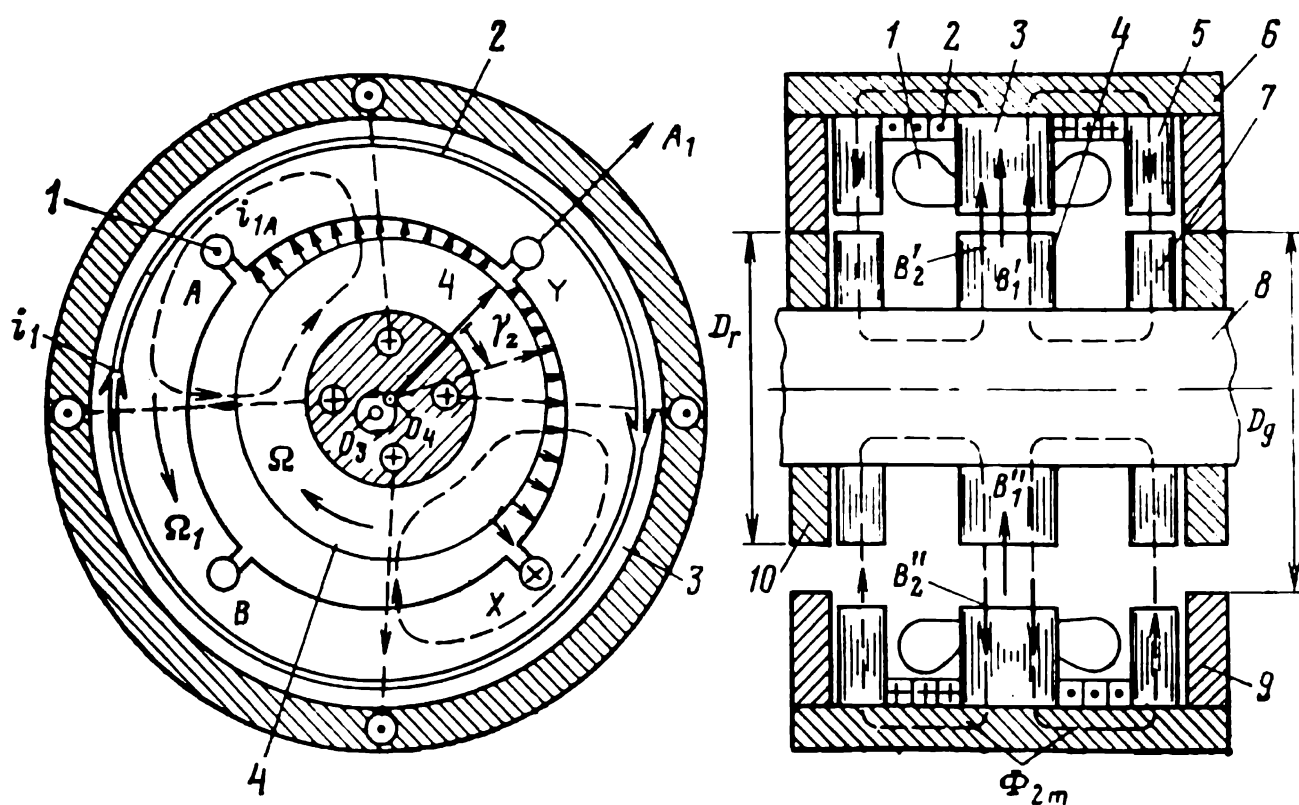


**Fig. 63-9** Rolling-rotor motor ( $p_1 = 1$ ,  $m_1 = 2$ )

Figure 63-9 shows a two-phase armature winding, but it can be made three- or poly-phase as well. In any case, however, it must be a two-pole winding ( $p_1 = 1$ ). The field winding consists of two symmetrically disposed coils encircling the shaft. The two-pole field set up by the armature winding has its path in the main stator (3) and rotor (4) cores. The two cores are smooth and built up of electrical-sheet steel laminations. The openings of the stator slots are so small that the effect of stator saliency on the performance of the motor may be neglected.

The paths for the excitation flux are provided by auxiliary stator (5) and rotor (7) cores which are likewise cylindrical and built up of electrical-sheet steel laminations. Thus, the magnetic circuit for the excitation flux has the following parts: the main gap, core 3, stator frame 6, core 5,

auxiliary gap, core 7, shaft 8, and core 4. The rotor shaft mounts rollers 10. When driven by the rotating field, the rollers carry the rotor on cylindrical guides 9.

The diameters of the rollers and guides,  $D_r$  and  $D_g$ , are chosen so as to produce a sufficiently large gap eccentricity

$$e = (\delta_{\max} - \delta_{\min})/2 = \delta_{\max} - \delta$$

and so that the rotor core does not touch the stator core. That is,  $\delta_{\min} > \delta_{\text{safe}}$ . Here,  $\delta_{\max}$ ,  $\delta_{\min}$ ,  $\delta$  and  $\delta_{\text{safe}}$  are the maximum, minimum, average (mean) and safe radial gap lengths, respectively. As is easily seen, the above requirement is satisfied when  $D_g - D_r = 2e$ .

The rollers and guides are made either toothed or smooth, of special wear-resistance materials having a sufficiently high coefficient of friction.

A rolling-rotor motor is started by exciting the field winding with a direct current  $i_2$  and by connecting its armature winding to a supply line at  $f_1$ . When excited, the field winding sets up a unipolar field in the gap, and the armature winding establishes a two-pole rotating field which travels at  $\Omega_1 = \omega_1 = 2\pi f_1$ . Because within one pole pitch the two field are combined,

$$B' = B'_1 + B'_2$$

and within the other they are subtracted,

$$B'' = B''_1 - B''_2$$

the rotor is attracted towards the pole pitch with the larger rms flux density,  $B'_{\text{rms}} > B''_{\text{rms}}$ . Figure 63-9 shows the position that the rotor takes up at  $i_{1A} = I_{1m}$  and  $i_{1B} = 0$ , when the axis of the rotating armature field is aligned with the axis of phase  $A_1$ . The gap is a minimum,  $\delta_{\min}$ , on axis  $A_1$ , and a maximum at the diametrically opposite point,  $\delta_{\max}$ . As a result, the force of magnetic attraction proportional to  $(B''_{\text{rms}})^2 - (B'_{\text{rms}})^2$  holds the rollers down to the guides. In travelling, the field tends to pull the rotor along. Since, however, the force of sliding friction exceeds the force of rolling friction, the rotor is moving down the guides on the rollers. After a time  $T_1$ , which is the period of change of current, the field axis turns through an angle  $2\pi$  counter-clockwise, where it is again aligned with axis  $A_1$ , the point on rotor 4 that was originally on axis  $A_1$  will have turned through an angle  $\gamma_z$  to take up the position

marked by a dashed line. The angle  $\gamma_z$  is the difference between the angles through which the minimum-gap point moves on the surface of the rotor and stator, respectively, that is,

$$\gamma_z = (D_g/D_r) 2\pi - 2\pi$$

As a result, the rotor turns at a speed which is a small fraction of the field velocity (and in the opposite direction). As the rollers travel on the guides, they reduce the angular velocity of the rotor mechanically by a factor of  $D_r/(D_g - D_r)$  in comparison with the field velocity

$$\Omega = \gamma_z/T_1 = \frac{D_g - D_r}{D_r} \Omega_1$$

The torque of a rolling-rotor motor can be found in an easier way, if we observe that electromagnetically it is in effect an inductor-type synchronous motor with a smooth stator and homopolar (axial) excitation (see Sec. 20-4, "b", Fig. 20-6).

On this assumption and with a two-pole armature winding ( $p_1 = 1$ ), the rotor would have only one tooth, because according to Eq. (20-12),

$$Z_4 = p_1 = 1$$

and its eccentrically displaced cylindrical rotor would, as regards the permeance distribution, be analogous to a single-tooth rotor. If the cylindrical rotor were eccentrically mounted on the shaft carried by bearings, it would rotate at

$$\Omega = 2\pi f_1/Z_4 = 2\pi f_1 = \Omega_1$$

Mechanical speed reduction brings it down to the value given above. Therefore, assuming fixed currents in the winding, the torque of a rolling-rotor motor can be expressed, as for any electromechanical device, in terms of the change in magnetic-field energy,  $dW$ , due to rolling through an angle  $d\gamma$ , that is,

$$T_{em} = dW/d\gamma$$

—Noting that

$$\gamma = \frac{D_g - D_r}{D_r} \gamma_1$$

where  $\gamma$  is the angle through which the rotor rolls and  $\gamma_1$  is the angle through which the rotor moves in simple rota-

tion, it is seen that the rolling torque  $T_{em}$  exceeds the torque

$$T_{em,1} = dW/d\gamma_1$$

developed when an eccentric rotor is carried by bearings by a factor of  $D_r/(D_g - D_r)$ , that is

$$T_{em} = [D_r/(D_g - D_r)] T_{em,1}$$

The ratio  $D_r/(D_g - D_r)$ , called the mechanical speed reduction ratio, can be as high as 100 or even more. Owing to this, rolling-rotor motors can give very low rotational speeds—from several rpm to tens of rpm, and large torques.

A major disadvantage of rolling-rotor motors is that the centre of gravity of the rotor,  $O_4$ , moves round a circle with a radius  $O_4O_3$  at a very high angular velocity,  $\Omega_1$ . This circular motion of the centre of gravity necessitates the use of suitably designed couplings to transmit rotation from the rotor to the output shaft, and also leads to vibration and noise in operation.

**Flexible wave-rotor motors.** Their distinction is that their hollow, thin-walled rotor, 4, made of a ferromagnetic

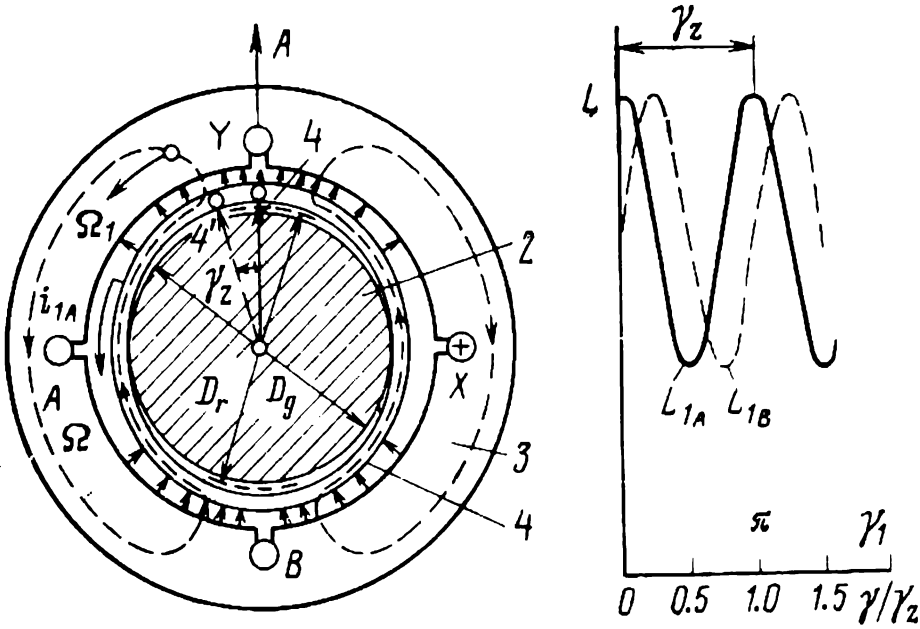


Fig. 63-10 Flexible wave-rotor machine ( $p_1 = 1$ ,  $m_1 = 2$ )

material, can be deformed by forces of magnetic attraction (Fig. 63-10). Attracted to the stator at points where the flux density of the rotating field is a maximum, the rotor is shaped into a polygon with rounded apexes acting as rotor teeth whose number,  $Z_4$ , is the same as that of field poles,  $2p_1$ . With a two-pole field,  $2p_1 = 2$ , as in Fig. 63-10, the rotor takes the shape of an ellipse with two high points

or “teeth”,  $Z_4 = 2$ , where the radial gap length is a minimum, and two low points, or “slots” at the centre of which the radial gap length is a maximum. The deformation of the rotor is limited by cylindrical guides, 2, which support the rotor directly (as in Fig. 63-10) or via flexible rollers. To avoid slippage, the contacting surfaces of the rotor rollers and guides should preferably be made toothed. Alternatively the guides can be placed externally to the rotor rollers, as in the rolling-rotor motor in Fig. 63-9. The value of  $D_r$  for the undeformed rotor and that of  $D_g$  are chosen such that

$$D_r - D_g = \delta_{\max} - \delta_{\min}$$

The stator core, 3, is cylindrical, and its slots hold a two (or three)-phase winding (usually with two poles), 1, which is energized from an a.c. line at  $f_1$ .

Figure 63-10 shows the position of the rotor at  $i_{1A} = I_{1\max}$  and  $i_{1B} = 0$ , when the flux density of the rotating field is a maximum on the axis of phase  $A$  and at the diametrically opposite point. The force of magnetic attraction holds the deformed rotor against the guides at two points lying in zones with a maximum radial gap length. In moving, the field pulls along at the field velocity both the wave of deformation and the points of contact between the flexible rotor and guides. As the rotor rollers move on the guides, they reduce the angular velocity of the flexible rotor by a factor of  $D_g/(D_r - D_g)$  in comparison with the field velocity,

$$\Omega = \gamma_z/T_1 = \frac{D_r - D_g}{D_g} \Omega_1$$

where

$$\gamma_z = \frac{D_r - D_g}{D_g} 2\pi$$

is the angle through which the rotor turns over a period of change,  $T_1$ , of current. When  $D_r > D_g$ , the rotor will rotate with the field; when  $D_r < D_g$ , it will rotate against the field.

In determining the torque of a wave-rotor motor, it should be remembered that, electromagnetically, it is in effect a reluctance synchronous motor (see Sec. 63-2). On this assumption, the deformed rotor has the same number of “teeth”,  $Z_4 = 2p_1$ , as a salient-pole rotor. If the deformed rotor were able to rotate at the field velocity, the electro-

magnetic torque,  $T_{em,1}$ , acting on it, could be found from Eq. (58-16), on putting  $\varepsilon = 0$ . Owing to mechanical speed reduction, the actual speed is brought down by a factor of  $D_g/(D_r - D_g)$ , and the actual torque is increased in the same proportion to the value given by

$$T_{em} = \frac{m_1 V^2}{2\Omega_1} (1/X_q - 1/X_d) \frac{D_g}{D_r - D_g} \sin 2\theta$$

where  $V$  is the phase voltage,  $X_d$  is the  $d$ -axis reactance,  $X_q$  is the  $q$ -axis reactance, and  $\theta$  is the angle between the field axis and the axis of the deformed rotor (the power or torque angle).

As compared with the rolling rotor, the flexible wave rotor offers two unquestionable advantages: it has a low moment of inertia and a stationary centre of gravity, so that its operation does not produce vibration or noise.

### 63-6 Permanent-Magnet Synchronous Machines

In this type of synchronous machines, the excitation field constant in direction is set up by permanent magnets. Therefore, there is no need for an exciter and there are no losses associated with excitation and the sliding contact. As a result, permanent-magnet synchronous machines have a better efficiency and reliability than conventional synchronous machines where damage to the rotating field structure and the brush system is a frequent occurrence. Also, they need practically no maintenance throughout their service life.

Permanent magnets can replace the field winding in both general-purpose polyphase synchronous machines and all special-purpose machines (single-phase, claw-pole, and inductor-type units).

Naturally, the field structure of permanent-magnet synchronous machine differs in construction from that of conventional designs. The counterpart of the rotor of a conventional nonsalient-pole machine is a ring-shaped non-salient magnet magnetized in a radial direction (Fig. 63-11*b*). The counterpart of the rotor of a **salient**-pole synchronous machine is a star-shaped magnet as in Fig. 63-11*a*, where the magnet, 1, is made fast to a shaft, 3, by means of a cast-aluminium hub, 2.

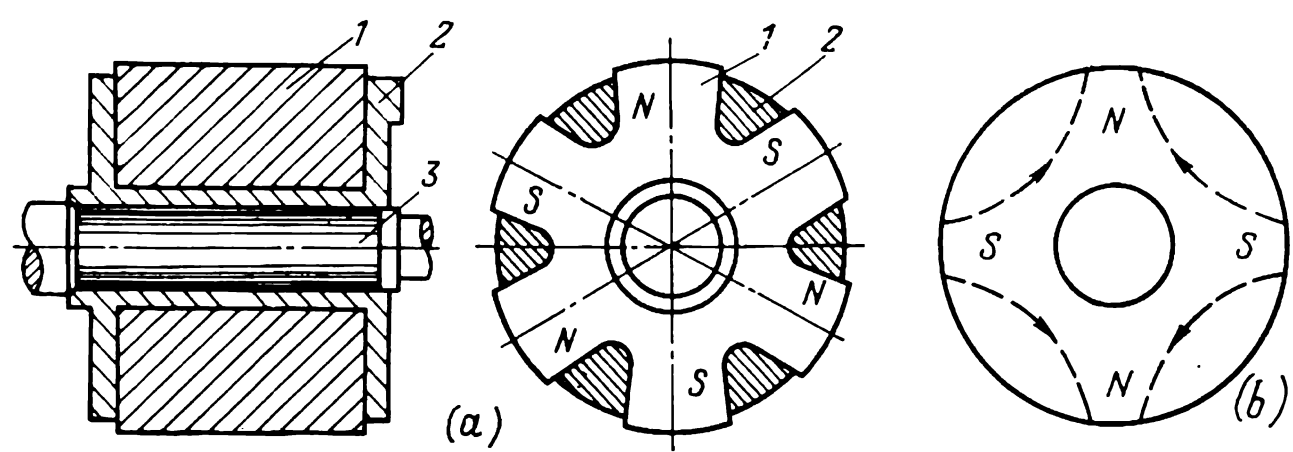


Fig. 63-11 Permanent-magnet field structures for inductor-type machines: (a) star-type magnet without pole-pieces; (b) four-pole cylindrical magnet

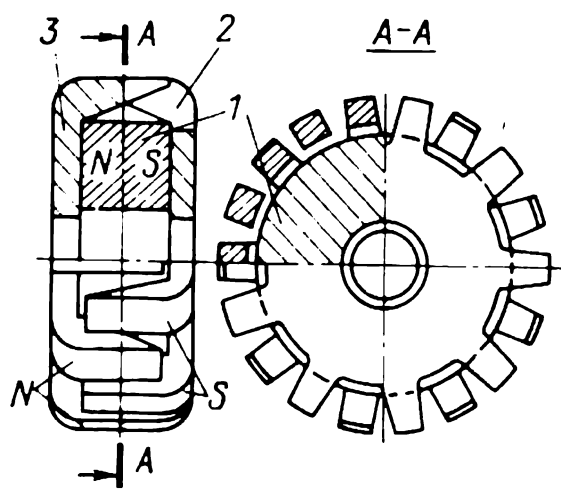


Fig. 63-12 Permanent-magnet-excited claw-pole rotor: 1—ring-shaped permanent magnet; 2—S-pole disc; 3—N-pole disc

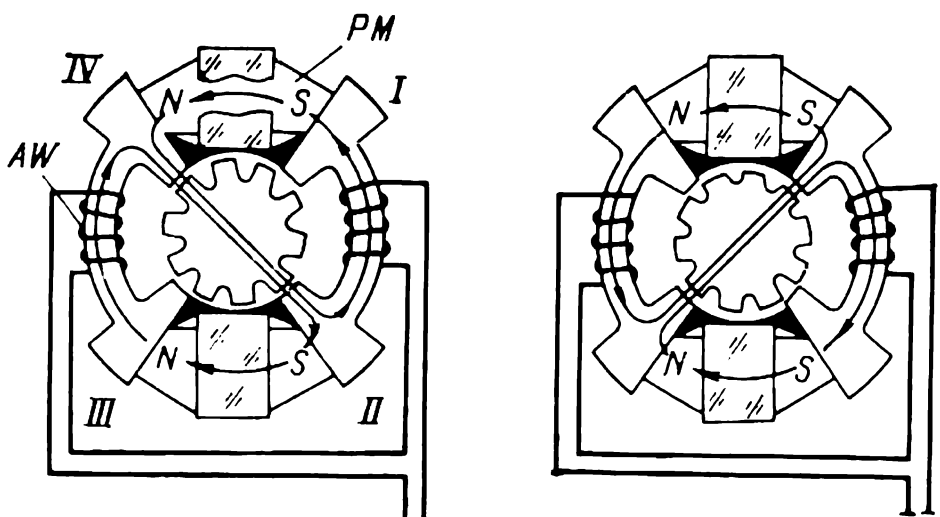


Fig. 63-13 Heteropolar inductor-type generator using permanent-magnet excitation:  
AW—armature winding; PM—permanent magnet



In a claw-pole machine (Fig. 63-12), a ring-shaped magnet magnetized in an axial direction serves as a ring-shaped field winding (compare with Fig. 63-4). In the heteropolar inductor machine shown in Fig. 63-7, electromagnetic excitation can be replaced by permanent magnets as shown in Fig. 63-13 (instead of three minor teeth in each zone, *I* through *IV*, as in Fig. 63-7, this design has only one). The homopolar machine of Fig. 63-8 likewise can have a permanent-magnet counterpart. In this case, the permanent magnet can be made in the form of an axially magnetized ring inserted between the frame and end-shield.

The electromagnetic processes taking place in permanent-magnet synchronous machines may well be described by the theory of electromagnetically excited synchronous machines. Before it can be applied, however, it is necessary to determine the no-load emf  $E_f$  or the excitation ratio  $\varepsilon = E_f/V$  from the demagnetization curve of the permanent magnet, and to calculate  $X_{ad}$  and  $X_{aq}$  with allowance for the reluctance of the magnet, which may be so large that  $X_{ad} < X_{aq}$ .

Permanent-magnet synchronous machines were invented in the early days of electrical engineering. However, they did not come into wide use until quite recently following the advent of better materials for permanent magnets (such as Magnico, and samarium- and cobalt-base alloys). Within a certain power and rpm range, permanent-magnet synchronous machines can now compete with electromagnetically excited synchronous machines as regards size, weight, power output, and torque.

High-speed permanent-magnet synchronous generators with ratings of tens of kilowatts are widely used as power supplied on aircraft. Low-power permanent-magnet synchronous generators and motors are mainly used on aircraft, automobiles and tractors where reliability is of paramount importance. Fractional-hp permanent-magnet machines have found a very broad field of application in many industries. As compared with reluctance machines, they have a more stable rpm, and better performance in terms of power output and torque. Unfortunately, they are more expensive to make and have a poorer starting performance.

Permanent-magnet, fractional-hp synchronous motors can be self-starting and induction-started.

Self-starting permanent-magnet fractional-hp motors serve as drives in clocks, relays, timing devices, and the like.

For ease of starting, they usually have more than eight pole pairs and are energized from a single-phase supply at commercial (power) frequency.

Such motors are started by the synchronous torque that is developed by the interaction of a pulsating field with the permanent magnets of the rotor. For the start to be successful and in the desired direction, such machines are fitted with suitable mechanical devices that permit the rotor to turn in one direction only and decouple it from the shaft during synchronization.

Induction-started fractional-hp permanent-magnet synchronous motors come in two modifications namely with a radial permanent magnet and short-circuited auxiliary (starting) winding, and with an axial permanent magnet and auxiliary winding. As regards the stator construction, they do not differ from electromagnetically excited machines. In either case, the stator winding has two or three phases.

In motors with a radial permanent magnet and auxiliary winding, the latter is arranged in the slots of the laminated pole-pieces of the permanent magnets. The leakage fluxes between the pole-pieces of adjacent poles are kept to an acceptable value by nonmagnetic gaps. Sometimes, the pole-pieces are interconnected by saturable jumpers into an integral ring-shaped core to make the rotor more robust mechanically.

In motors with an axial permanent magnet and auxiliary winding, some of the active length is taken up by the permanent magnet, and the remainder is occupied by the laminated auxiliary-winding core located next to the magnet. Both are mounted on the same shaft. Because at starting permanent-magnet motors are excited, their starting performance is inferior to conventional synchronous motors where the excitation is removed. The point is that, at starting, the positive induction torque produced by the interaction of the rotating field with the currents induced in the auxiliary winding co-exists with the negative induction torque due to the interaction of the permanent magnets with the currents induced in the stator winding by the permanent field.



tern shown in the figure, the lines of flux in the core and in the gap are directed radially, and the flux density  $B$  does not differ from the gap flux density.

Consider the magnetization of the rotor core rotating at  $\Omega$  which is smaller than  $\Omega_1$ , the angular velocity of the stator mmf,  $F_{1m}$ , that is, with a slip given by

$$s = (\Omega_1 - \Omega)/\Omega_1 > 0$$

The rotating stator mmf

$$F_{1m} = (m_1 \sqrt{2}/\pi) I_1 w_1 k_{w1}/p$$

magnetizes the parts of the magnetic circuit cyclically in a sinusoidal manner. This gives rise to a field such that the sum of the partial mmfs balances  $\dot{F}_1$ ,

$$\dot{F}_{1m} = \dot{F}_{0m} + \dot{F}_m$$

where

$$\dot{F}_{0m} = c \dot{B}_{1m} \approx \dot{B}_{1m} \delta / \mu_0$$

is the peak value of mmf existing in all the parts of the magnetic circuit where the hysteresis effect may be neglected, except the rotor core proper.  $\dot{F}_m$  is the peak value of mmf within the rotor core, equal to  $\dot{H}_m \Delta$ .

Suppose that an element of the rotor core is cyclically magnetized in a sinusoidal manner at the slip frequency  $s\omega_1$ . Then the magnetic field intensity in that element will vary likewise sinusoidally,

$$H = H_m \sin (s\omega_1) t$$

The flux density in the element under consideration varies periodically by tracing out the hysteresis loop corresponding to the peak field intensity,  $H_m$ . From knowledge of  $H_m$  at each instant of time,  $t$ , we can readily determine  $B = f(t)$  (Fig. 63-15). As is seen, the flux density varies with time nonsinusoidally. Applying a Fourier expansion, we can isolate the fundamental component (varying at the slip frequency  $s\omega_1$ ) and determine its peak value,  $B_{1m}$ , and the phase shift  $\alpha$  relative to  $H_m$ . Then, we can calculate the mutual flux

$$\dot{\Phi}_m = 2l\tau \dot{B}_{1m}/\pi$$

its linkage with the stator winding

$$\dot{\Psi}_{10m} = w_1 k_{w1} \dot{\Phi}_m$$

the mutual emf of the stator

$$\dot{E}_1 = -j\omega_1 \dot{\Psi}_{10m} / \sqrt{2}$$

and the stator voltage,

$$\dot{V}_1 = -\dot{V}_{1s} = \dot{E}_1 - jX_\sigma \dot{I}_1$$

A phasor-vector diagram of a hysteresis motor, constructed in accord with the above equations and the mmf equations, is shown in Fig. 63-14.

The electromagnetic torque developed by a hysteresis motor can be found from the general equation for the electromagnetic torque of an a.c. machine (29-4). It is more convenient to find the torque acting on the stator (it is equal to the torque acting on the rotor, but is acting in the opposite direction):

$$T_{em} = (m_1 p / \sqrt{2}) \Psi_{10m} I_1 \sin \alpha_{10}$$

On expressing  $\Psi_{10m}$  in terms of  $\Phi_m$  and  $I_1$  in terms of  $F_{1m}$ , we get:

$$T_{em} = (p^2 \pi / 2) \Phi_m F_{1m} \sin \alpha_{10}$$

As is seen from the phasor-vector diagram, however,

$$F_{1m} \sin \alpha_{10} = F_m \sin \alpha = H_m \Delta \sin \alpha$$

Also, the mutual flux is expressed in terms of  $B_{1m}$  and the dimensions of the rotor core proper. Therefore, finally,

$$T_{em} = (p/2\pi) V W_h$$

where  $V = 2p\tau l\Delta$  is the volume of the rotor core proper,  $W_h = \pi B_{1m} H_m \sin \alpha$  is the specific hysteresis loss dissipated per cycle per unit volume, and  $\tau = \pi R/p$  is the pole pitch.

This, on the assumptions made, the electromagnetic torque of a hysteresis machine is independent of slip and is proportional to the hysteresis loss per cycle of magnetization. (The area of the ellipse corresponding to cyclic magnetization at the fundamental  $H$  and  $B$  is always equal to the area of the hysteresis loop, see Fig. 63-15.)

At starting, a hysteresis motor develops the same electromagnetic torque, whatever the slip,  $s > 0$ . If this torque exceeds the load (retarding) torque even by a small amount, the motor will come up to synchronous speed. At synchronous speed, it can develop the same maximum torque at an angle  $\alpha$  between  $H_m$  and  $B_{m1}$ . Now, however, it will be running as a permanent-magnet synchronous motor, because its rotor is no longer subjected to cyclic magnetization, and

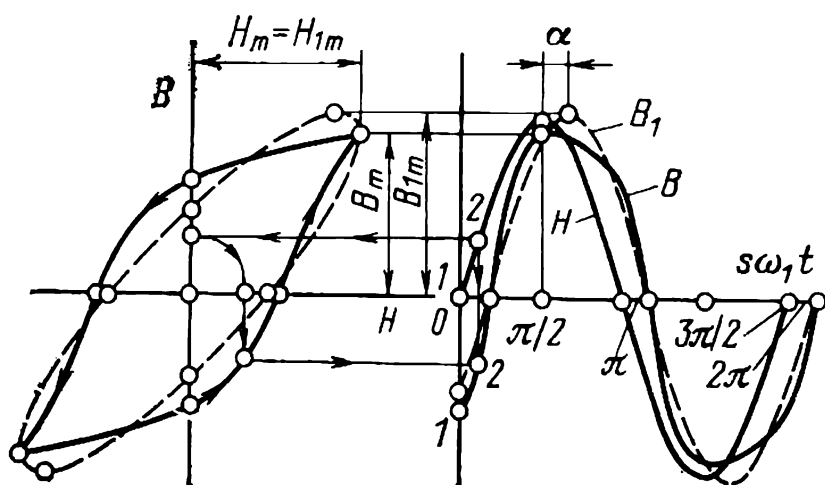


Fig. 63-15 Cyclic magnetization of the rotor core in a hysteresis motor

no hysteresis effect takes place. Should the load torque go down, the machine will keep running under synchronous conditions, but the angle between the primary current and the flux linkage will decrease. At  $T_{em} = 0$ , it is equal to zero. Should the load torque change sign, the machine will keep running under synchronous conditions, but it will now be operating as a motor. Finally, should the load torque exceed the maximum electromagnetic torque and act in the direction of rotation, the machine will drop out of synchronism and begin rotating at a speed exceeding synchronous. Now, it will be delivering energy to the system.

Hysteresis motors of low power ratings (a few tens of watts) are widely used in various fields. They are especially advantageous in cases where they are used to drive bodies having high moments of inertia (such as gyroscopes).

Most frequently, hysteresis motors are made with a rotor hub fabricated from a nonmagnetic material. Then the rotor core proper acts as a yoke, and the flux in it is predominantly tangential. In other respects, a hysteresis motor with a nonmagnetic rotor hub behaves in the same manner as explained above and obeys all the relevant relations.

63-8 Stepper Motors

These motors are important in automatic control systems, computers, numerically controlled machine-tools, and other position-control applications. Instead of a continuous rotation, their rotors move in steps in response to control pulses. Thus, over a rotor-slot pitch, the rotor can take up several stable positions.

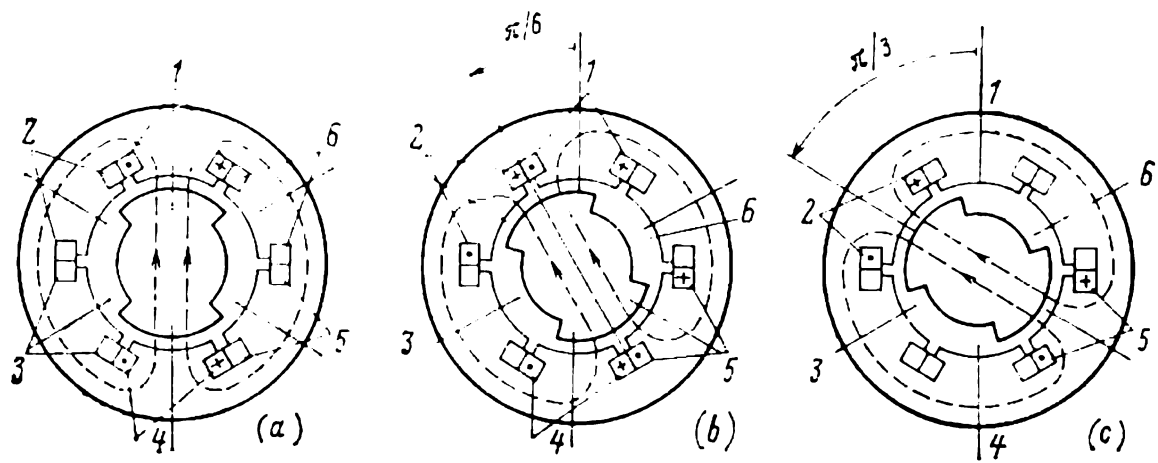


Fig. 63-16 Explaining operation of a four-phase stepper motor

Figure 63-16 shows the simplest 6-phase, 2-pole reluctance stepper motor. Its phase coils are divided into three groups (1 and 4, 2 and 5, 3 and 6). In each group, the phase coils are connected in parallel

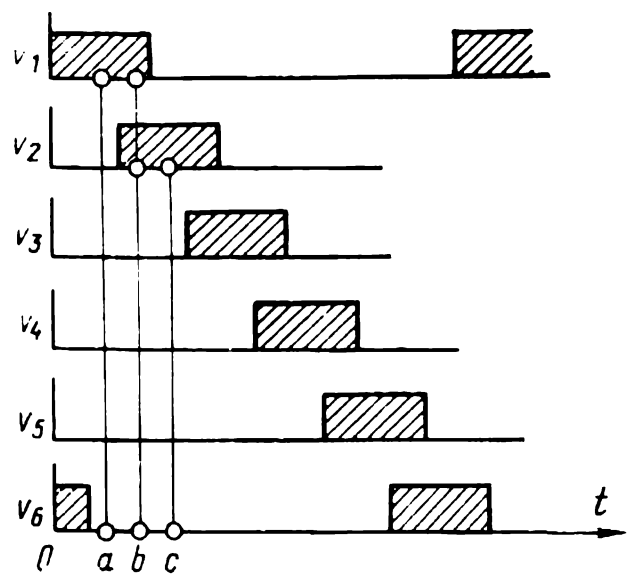


Fig. 63-17 Commutation sequence in the stepper motor of Fig. 63-16

opposition. Therefore, when a positive pulse is applied to one of the phases in a group, a negative pulse is applied at the same time to the other phase in that group. When phase 1 is excited, the salient-pole rotor takes up the position shown in Fig. 63-16a. If, with phase 1 still excited, voltage is applied to phase 2, the rotor will move to the position shown in Fig. 63-16b, that is, through a step  $\alpha_0 = \pi/6$ . Upon removal of voltage from phase 1, the rotor will move by an angle of  $\pi/6$  once more, thereby advancing another step (c), and so on.

If we apply control pulses in the sequence shown in

Fig. 63-17, the rotor will move counter-clockwise by an angle  $\alpha = N\alpha_0$ , proportional to the number  $N$  of control pulses. If we apply control pulses in a reversed sequence, the rotor will move clockwise.

Control pulses of an appropriate waveform and frequency are generated by electronic (tube-type or semiconductor) switching circuits. They are steered by a control circuit which also locks the rotor in position between pulses.

The performance of a stepper motor is described in terms of its step size, torque-angle characteristic, and maximum pulse repetition frequency sufficient for all transients to die out between steps. The starting performance of a stepper motor is characterized in terms of the pull-in frequency, that is, the maximum pulse repetition frequency at which the motor can still be started without missing some steps (that is, without falling out of synchronism). Depending on type of motor, this frequency may extend from 10 to 10 000 Hz.

A stepper motor can be based on any one of known modifications of the synchronous motor. The best choice is offered by polyphase, multiple-pole reluctance synchronous motors, reluctance inductor-type synchronous motor, and polyphase inductor-type motors.

For better control accuracy, the step size is usually kept to a minimum. This is achieved by increasing the number of phases and poles, and also the number of rotor teeth in the case of inductor-type motors. According to the desired level of accuracy, the step size can range from  $180^\circ$  to  $1^\circ$  or even less.

### 63-9 Doubly-Fed Synchronous Machines

**Doubly-fed synchronous motors.** In construction, they are similar to a wound-rotor induction machine. The stator and rotor carry each a three-phase winding, 1 and 2, with the same effective turns. The two windings are connected in parallel (or in series) to a common a.c. supply line operating at  $V_1$  and  $f_1$  (Fig. 63-18). Therefore, they carry equal currents,  $I_1$  and  $I_2$ . As has been shown in Sec. 21-1, this type of machine will be capable of energy conversion, if its rotor is spinning at an electrical angular velocity

$$\omega = \omega_1 \pm \omega_2 = \omega_1 \pm \omega_1 = 2\omega_1$$



or a mechanical angular velocity

$$\Omega = \omega/p = 2\omega_1/p = 2\Omega_1,$$

that is, at twice the mechanical angular velocity as compared with a conventional synchronous machine having the same number of pole pairs,  $p$ .

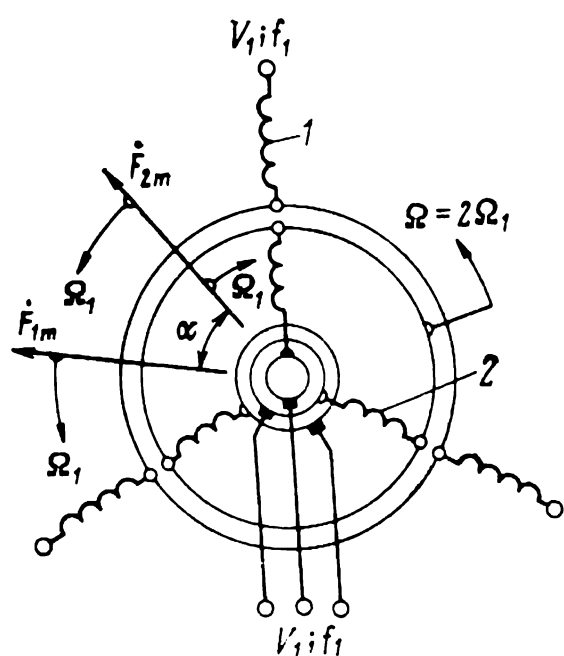


Fig. 63-18 Circuit of a doubly excited synchronous motor

To meet this requirement, the stator winding, 1, must be connected to a positive-sequence supply, and the rotor winding, 2, to a negative-sequence supply. Then,  $F_{1m}$  will rotate at  $\Omega_1$  in the positive direction, and  $F_{2m}$  will do so in the opposite direction, and they will move in synchronism, if the rotor is travelling at  $2\Omega_1$  in the positive direction.

As a result of the interaction between the synchronously rotating stator and rotor fields set up by  $F_{1m}$  and  $F_{2m}$ , the rotor is acted upon by an electromagnetic torque,  $T_{em}$ , which can be found by the same equation as for induction or conventional synchronous machines (see Sec. 29-2). Numerically, this torque is equal to the torque acting on the stator,

$$T_{em} = (m_1 p / \sqrt{2}) \Psi_{10m} I_1 \sin (\alpha / 2)$$

Here,  $\Psi_{10m}$  is the flux linkage of the mutual field with the stator winding,  $I_1$  is the stator current, and  $\alpha/2$  is a half of the angle between  $\dot{F}_{1m}$  and  $\dot{F}_{2m}$ , or the angle between  $\dot{\Psi}_{10m}$  and  $I_1$  (see Fig. 63-19).

The electromagnetic torque balances the load torque applied to the shaft, thereby keeping the rotor at synchronous speed. A change in the load torque brings about a change only in the angle  $\alpha$ . In the motor mode of operation,  $\dot{F}_{1m}$  leads  $\dot{F}_{2m}$ , so  $\alpha > 0$  and  $T_{em} > 0$ . In the generator mode of operation, the situation is reversed, so  $\alpha < 0$  and  $T_{em} < 0$ .

Neglecting losses, the active power of the motor, equally shared between the stator and rotor windings, can be written



to be brought up to synchronous speed by an auxiliary (servo) motor, which is a decisive limitation. Also, doubly-fed motors tend to hunting, because the damping torque appearing upon a departure from synchronous rotation is too small (see Sec. 60-1).

**Synchronous induction machine.** This machine (also known as the auto-synchronous motor) is similar to an induction motor with a wound secondary.

It has a two-phase rotor (field) winding excited with a.c. at  $f_2$  from a thyristor frequency converter. Its stator does not differ from the conventional design and is connected to a supply at  $f_1$ . In a way, a synchronous induction machine may be looked upon as a doubly-fed machine in which the stator and rotor are energized with currents differing in frequency,  $f_1 \neq f_2$  (ordinarily,  $f_2 \ll f_1$ ).

In this type of machine, energy conversion will take place only if

$$\omega_2 = \omega_1 - \omega = s\omega_1$$

or

$$\Omega_2 = \Omega_1 - \Omega = s\Omega_1$$

This condition can be satisfied both when the rotor is travelling at synchronous speed,  $\Omega_1 = \Omega$ , and at synchronous speed, with some slip,

$$s = (\Omega_1 - \Omega)/\Omega_1$$

At synchronous speed, the rotor phases are excited with d.c.:

$$\Omega_2 = \Omega_1 - \Omega = 0$$

At asynchronous speed, the rotor phases are excited with a.c. at the slip frequency,  $f_2 = sf_1$ , shifted in time phase by  $\pi/2$ . As a result, the excitation field is rotating relative to the rotor at the desired angular velocity,  $\Omega_2 = s\Omega_1$ .

The frequency of field current,  $f_2$ , is controlled continuously and automatically in such a way that the stator field and the rotor field are travelling at a constant velocity such that

$$\Omega_1 = \Omega + \Omega_2$$

and produce an electromagnetic torque which maintains synchronous rotation.

A synchronous induction machine can be used as a generator and as a motor.

To minimize the active power drawn by the frequency converter

$$P_2 = sT_{em}\Omega$$

variations in the slip and the frequency of field current are usually held within very narrow limits:

$$s = \pm 0.01, \quad f_2 = 0 \text{ to } 0.5 \text{ Hz}$$

Even with this tight tolerance on likely departures from synchronous speed, synchronous induction machines stand

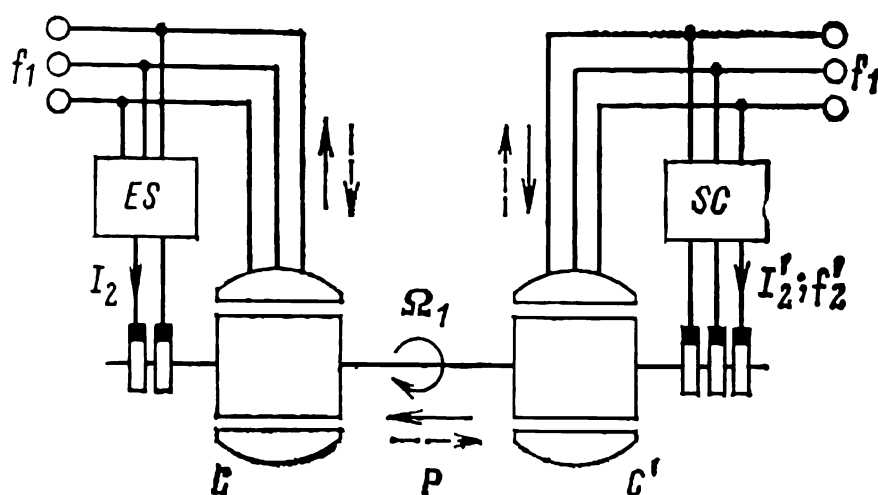


**Fig. 63-20** Variable-ratio connection giving “flexible tie” between two electric systems

up to abnormal and fault conditions (such as short-circuits in the system, hunting provoked by load shedding, and the like) and retains stability far better than conventional synchronous machine. In this lies their most valuable advantage. Unfortunately, synchronous induction machines are more expensive to make and operate, so they are only warranted in large installations where their advantage is decisive.

Recently, synchronous induction machines have come to be used as a “flexible tie” (known as the variable-ratio connection) between two electrical systems slightly differing in frequency ( $f_1 - f_1' \leq 0.5\% - 1\%$ ). The need for a “flexible tie” arises when the interconnected systems belong to different owners (states or utilities, as the case may be), and the power exchanged between them ought not to depend on the operating conditions of either system.

The arrangement ordinarily used for a flexible tie is shown in Fig. 63-20. As is seen, it uses two machines with the same number of pole pairs. One is a conventional syn-

chronous machine,  $S$ . The other is a synchronous induction machine,  $S'$ . Their rotors are coupled by a common shaft. The stator of  $S$  is connected to a system operating at  $f_1$ , and the stator of  $S'$  to a system operating at  $f'_1$ . The rotor of  $S$  is excited with direct current  $I_2$  from an excitation system,  $ES$ . The two-phase rotor winding of  $S'$  is excited with alternating current  $I'_2$  at  $f'_1$  from a static frequency converter.

For unidirectional energy conversion, the static frequency converter maintains the field current at a constant frequency

$$f'_2 = s'f'_1$$

where  $s' = (f'_1 - f_1)/f'_1$ . The magnitude and direction of power transfer is controlled by varying the phase of  $I'_2$  and the angle  $\alpha$  between the stator and rotor mmfs,  $F'_{1m}$  and  $F'_{2m}$ , rotating in synchronism in the synchronous induction machine. If  $F'_{2m}$  lags behind  $F'_{1m}$ , the synchronous induction machine will operate as a motor, and the synchronous machine as a generator. As a result, power will be transferred from the system at  $f'_1$  to the system at  $f_1$  (the direction of power transfer is shown by full arrows). If  $F'_{2m}$  leads  $F'_{1m}$ , power will be transferred the other way around (the direction of power transfer in this case is shown by dashed arrows).

# Bibliography

1. Петров Г. Н. *Электрические машины*. ч. 1, Энергия, Москва, 1974; ч. 2, Энергия, Москва, 1963; ч. 3, Энергия, Москва, 1968.
2. Костенко М. П. и Плотровский Л. М. *Электрические машины. Часть специальная*. Госэнергоиздат, Москва — Ленинград, 1949.
3. Kostenko M. P., Piotrovsky L. M. *Electrical Machines*. Mir Publishers, Moscow, 1973.
4. Вольдек А. И. *Электрические машины*. Энергия, Ленинград, 1974.
5. Важнов А. И. *Электрические машины*. Энергия, Ленинград, 1974.
6. Сергеев П. С. *Электрические машины*. Госэнергоиздат, Ленинград, 1962.
7. Алексеев А. Е. *Конструкция электрических машин*. Госэнергоиздат, Москва — Ленинград, 1958.
8. Виноградов Н. В. *Производство электрических машин*. Энергия, Москва, 1970.
9. Бертинов А. И. *Электрические машины авиационной автоматики*. Оборонгиз, Москва, 1961.
10. Хрущев В. В. *Электрические микромашины автоматических устройств*. Энергия, Ленинград, 1976.
11. Юферов Ф. М. *Электрические машины автоматических устройств*. Высшая школа, Москва, 1976.
12. Брускин Д. Э., Зорохович А. Е., Хвостов В. С. *Электрические машины и микромашины*. Высшая школа, Москва, 1971.
13. *Электротехнический справочник*. т. I. Под общей ред. П. Г. Грудинского и др. Изд. 5, исправл. Энергия, Москва, 1974.
14. Korn G. A., Korn T. M. *Mathematical Handbook for Scientists and Engineers*. McGraw-Hill Book Co., N. Y., 1968.
15. Петров Г. Н. *Трансформаторы*. ОНТИ, Москва, 1934.
16. Тихомиров П. М. *Расчет трансформаторов*. Энергия, Москва, 1976.
17. Сапожников А. В. *Конструирование трансформаторов*. Госэнергоиздат, Москва — Ленинград, 1959.
18. Алексеенко Г. В., Ашрятов А. К., Аеремей Е. В., Фрид Е. С. *Испытания мощных трансформаторов и реакторов*. Энергия, Москва, 1978.
19. Каганович Е. А., *Испытание трансформаторов малой и средней мощности на напряжение до 35 кВ включительно*. Энергия, Москва, 1969.
20. Фарбман С. А., Бун А. Ю., Райхлин И. М. *Ремонт и модернизация трансформаторов*. Энергия, Москва, 1974.
21. Васютинский С. Б. *Вопросы теории и расчета трансформаторов*. Энергия, Ленинград, 1970.
22. Поливапов К. М. *Теоретические основы электротехники*. ч. I. *Линейные электрические цепи с сосредоточенными постоянными*. Энергия, Ленинград, 1972.

23. Жуховицкий Б. Я., Негцевицкий П. Б. *Теоретические основы электротехники*. ч. 2. Москва, 1972.
24. Поливанов К. М. *Теоретические основы электротехники*. ч. 3. Энергия, Москва, 1975.
25. Adkins B. *The General Theory of Electrical Machines*. Chapman and Hall, London, 1959.
26. White C., Woodson H. *Electromechanical Energy Conversion*. J. Wiley and Son, Inc., New York, 1959.
27. Копылов И. П. *Электромеханическое преобразование энергии*. Энергия, Москва, 1973.
28. Иванов-Смоленский А. В. *Электромагнитные поля и процессы в электрических машинах и их физическое моделирование*. Энергия, Москва, 1969.
29. Schuisky W. *Berechnung elektrischer Maschinen*. Wien, Springer, 1960.
30. Сергеев П. С., Виноградов Н. В., Горяинов Ф. И. *Проектирование электрических машин*. Энергия, Москва, 1969.
31. Постников И. М. *Проектирование электрических машин*. Гостехиздат УССР, Киев, 1960.
32. Liwschitz-Garik M. *Winding Alternating-Current Machines*.
33. Кучера Я., Гапл И. *Обмотки электрических машин*. Пер. с чешск. Изд-во Академии наук, Прага, 1963.
34. Зимин В. И., Каплан М. Я., Палей А. М. и др. *Обмотки электрических машин*. Энергия. Ленинград, 1970.
35. Данилевич Я. Б., Капарский Э. Г. *Добавочные потери в электрических машинах*. Госэнергоиздат, Москва — Ленинград, 1963.
36. Данилевич Я. Б., Кулик Ю. А. *Теория и расчет демпферных обмоток синхронных машин*. Изд-во АН СССР, Москва, 1962.
37. Данилевич Я. Б., Домбровский В. В., Казарновский Е. Я., *Параметры электрических машин переменного тока*. Наука, Москва, 1965.
38. Талалов И. И. *Параметры и характеристики явнополюсных синхронных машин*. Энергия, Москва, 1978.
39. Детишко Ф. М., Загородная Г. А., Фастовский В. М. *Прочность и колебания электрических машин*. Энергия, Ленинград, 1969.
40. Шлыгин В. В. *Прочностные и размерные расчеты электрических машин*. Госэнергоиздат, Москва — Ленинград, 1963.
41. Филиппов И. Ф. *Основы теплообмена в электрических машинах*. Энергия, Ленинград, 1974.
42. Борисенко А. И., Данько В. Г., Яковлев А. И., *Аэродинамика и теплопередача в электрических машинах*. Энергия, Москва, 1974.
43. Бернштейн Л. М. *Изоляция электрических машин общепромышленного применения*. Энергия, Москва, 1971.
44. Геллер Б., Гамата В. *Дополнительные поля, моменты и потери мощности в асинхронных машинах*. Пер. с чешск., Энергия, Москва, 1964.
45. Сыромятников И. А., *Режимы работы асинхронных и синхронных электродвигателей*. Госэнергоиздат, Москва — Ленинград, 1953.

46. Харитонов А. М. *Многоскоростные электродвигатели*. Госэнергиздат, Москва — Ленинград, 1954.
47. Лопухина Е. М., Сомихина Г. С. *Расчет асинхронных микродвигателей однофазного и трехфазного тока*. Госэнергиздат, Москва — Ленинград, 1961.
48. Свечарник Д. Б. *Дистанционные передачи*. Энергия. Москва, 1974.
49. *Микродвигатели для систем автоматики* (технический справочник). Под ред. Э. А. Подочникова и Ф. М. Юферова. Энергия, Москва, 1969.
50. Лопухина Е. М., Сомихина Г. С., *Асинхронные микромашины с полым ротором*. Энергия, Москва, 1967.
51. Гурин Я. С., Кузнецов Б. И. *Проектирование серий электрических машин*. Энергия, Москва, 1978.
52. Каасик П. Ю., Несговорова Е. Д. *Управляемые асинхронные двигатели*. Энергия, Ленинград, 1965.
53. Домбровский В. В., Еремеев А. С., Иванов П. И. и др., *Проектирование гидрогенераторов*. Т. 1, Энергия, Ленинград, 1965.
54. Гольденберг С. И., Мо Л. С., Нейман З. Б., Пекне В. З., *Синхронные компенсаторы*. Энергия, Москва, 1959.
55. Титов В. В. и др. *Турбогенераторы*. Энергия, Ленинград, 1967.
56. Абрамов А. И., Иванов-Смоленский А. В. *Расчет и конструкция гидрогенераторов*. Высшая школа, Москва, 1964.
57. Блюменкранц и др. *Технология крупного энергомашиностроения*. Т. 1. Турбогенераторы. Т. 2. Гидрогенераторы. Энергия, Ленинград, 1966.
58. Осип И. Л., Колесников В. П., Юферов Ф. М. *Синхронные микродвигатели с постоянными магнитами*. Энергия, Москва, 1976.
59. Балагуров В. А., Галтеев Ф. Ф., Ларионов А. Н. *Электрические машины с постоянными магнитами*. Энергия, Москва, 1964.
60. Постников И. М., Ралле В. В. *Синхронные реактивные двигатели*. Техника, Киев, 1970.
61. Альпер Н. Я., Терзян А. А. *Индукторные генераторы*. Энергия, Москва, 1970.
62. Ахметжанов А. А. *Синхронно-следящие системы повышенной точности*. Оборонгиз, Москва, 1962.



# Index

- Air gap factor, 67
- Air gap mmf, 67
- Angular slip velocity, 78
- Armature electric loading, 49
- Armature winding, 265
  - impedance, 268
  - inductive reactance, 267
  - leakage inductive resistance, 265
  - mutual inductive reactance, 266
  - parameters, 265
  - resistance of conductors, 265
- Automatic synchronizer, 224, 230, 232
- Auto-synchronous motors, 354
  
- Block fill factor, 68
- Breakaway torque, 370
  
- Capacitor motor, 174
- Circle diagram of induction machine, 125
- Claw-pole synchronous machines, 429
- Compounding torque, 349
- Condition for stable operation, 140
- Crawling, 116, 118, 120
- Critical angular velocity of shaft, 31
- Cooling arrangements, 21
  
- Damper (amortisseur) winding, 225
  - direct axis, 225
  - double axis, 225
- Decay factor, 382
- Deviation factor, 237
- Direct cooling of windings, 42
- Doubly-fed synchronous motors, 453
  
- Efficiency of induction motor, 91
- Electrical machines
  - cooling system of, 22
    - closed-circuit, 22
    - direct, 22
    - indirect, 22
    - open-circuit, 22
  - drip-proof, 19
  - forced air-cooled, 21
  - guarded, 18
  - mechanical analysis and design, 25
  - naturally air-cooled, 21
  - noise-level classification of, 24
  - open, 18
  - sea-proof, 21
  - self-ventilated, 21
  - separately ventilated, 22
  - short-time submersible, 21
  - Soviet standards for, 24
  - splash-proof, 19
  - water-proof, 21
- Electromagnetic dampers, 198
- Electromagnetically excited single-phase synchronous generators, 424
- Electromagnetic induction pump, 189
  - annular linear, 192
  - flat linear, 191
  - helical, 189
- Electromagnetic power, defined, 89
  - of synchronous machine, 296
- Electromagnetic torque,
  - defined, 110
  - inherent (static) starting, 113, 132
  - maximum, 112
  - of synchronous machine, 336
  - stray, 115-125
    - eddy-current, 123
    - hysteresis, 123
    - induction, 115
    - reactive, 122
    - synchronous, 118
- Elliptical revolving field, 165
- EMF form factor, 239
- Equivalent armature mmf in unsaturated machine, 263
- Excitation field forcing, 233
- Excitation field form factor, 238
- Excitation flux form factor, 238
- Excitation field killing, 232
- Excitation ratio of synchronous machine, 333
- Excitation systems for
  - field current control, 231
  - synchronous machine, 230
- Exciter, 230
  
- Field voltage ratio, 234
- Flexible wave-rotor motors, 442
- Flux density waveform shape factor, 49, 66
- Forced oscillation of rotor, 383
  
- Hydrogenerators, 212, 415
- Hysteresis motors, 448
  
- Indirect cooling, 42
- Induction control motor, 195
- Induction frequency converter, 180
- Induction generator, 179
- Induction generator with self-excitation, 180
- Induction machine,
  - breaking, 106, 107
  - circle diagram of, 125
  - defined, 53
  - equivalent circuit of, 98, 99
  - generator, 104, 105
  - magnetizing current of, 84
  - mechanical power of, 114
  - mmf's and currents of, 84
  - modes of operation of, 103, 108
  - stator leakage inductive reactance of, 77
  - voltage and current diagrams of, 86
- Induction machine at no load, 64
- Induction machine on load, 73
- Induction motors,
  - efficiency of, 91, 103, 104, 134
  - limited rotation, 192
  - linear, 192
  - loading conditions of, 139
  - multispeed, 144
  - phase-wound, 54
  - single-phase, 163
  - slip-ring, 61

- Induction motors,
  - solid rotor, 186
  - speed control, 143
    - by line frequency change, 144
    - by pole changing, 144
    - by primary voltage change, 149
    - by rotor circuit resistance, 150
    - without slip power recovery, 148
    - with slip power recovery, 148
  - split-phase, 170
  - squirrel cage, 57
- Induction resolver, 200
  - coordinate transformation by, 203
  - linear, 202
  - sine-cosine, 201
- Induction starting, 369
- Induction tachogenerator, 199
- Inductor machines, 431
- Inductor-type alternators, 436
- Inductor-type synchronous motors, 436
- Inductosyn, 204
- Instability of synchronous machines in parallel operation, 376
- Insulation classes, 16
- Lamp synchronizer, 360
- Limited-rotation induction motor, 192
- Linear induction motor, 192
- Local hydraulic resistance, 44
- Machine constant, 49
- Magnetizing curve of a machine, 72
- Main stator winding impedance, 72
- MMF,
  - armature, 254
  - in generator mode, 257
- Multispeed induction motor, 144
- Negative sequence impedance of armature winding, 389
- Noise level classification, 23
- No-load characteristic of a machine, 72
- No-load current, 71
- No-load (open-circuit) mode of operation, 73
- Nominal service conditions, 15
- Nonmagnetic drag-cup motor, 188
- Nonsalient-pole synchronous machine, 217, 226
  - electromagnetic processes in, 271, 279
  - voltage diagram of, 272, 280
- Operation of synchronous generator into
  - isolated load, 301
  - isolated unbalanced load, 401
- Performance characteristics, 141, 142, 143
- Permanent-magnet synchronous machines
- Phase regulator, 182
- Phase-to-phase fault, 403
- Phase-wound induction motor, 54
- Pole enclosure, 50
- Pole span factor, 238
- Polyphase reluctance motors, 425
- Positive sequence impedance of armature winding, 387
- Pull-in torque, 353, 370
- Pulling into synchronization, 361
- Pull-out power, 338
- Potier reactance, 281
- Power angle characteristic, 337
- Processes in induction machines on load, 73
- Radial force of magnetic attraction, 30
- Rectifier type excitation systems,
  - brushless, 235
  - self-excitation, 235
  - separate, 235
- Referred quantities, 95
- Reluctance synchronous motors, 425
  - polyphase, 425
  - single-phase, 428
- Reluctance-torque motors, 354
- Resonance modulus of  $v$ th harmonic, 385
- Resynchronization, 372, 375
- Reversible synchronous machine, 350
- Rolling-rotor motors, 438
- Rotating field transformer, 184
- Rotating-machine excitation system,
  - direct, 234
  - indirect, 234
- Rotor teeth mmf, 69
- Rotor yoke mmf, 70
- Salient-pole synchronous machine, 217
  - electromagnetic processes in, 275, 284
  - voltage diagram of, 276
- Self-synchronization, 361
- Shaded-pole motor, 177
- Short-circuit ratio (SCR) of synchronous machine, 313
- Short-circuit triangle, 312
- Single phase induction motor, 163
  - basic equations, 167
  - equivalent circuit, 167
- Single phase-to-ground fault, 402
- Skewed slots, 118, 122
- Slip-ring induction motor, 61
- Solid-rotor induction motor, 186
- Soviet turbogenerators, 405
- Special-purpose induction machines, 179
- Specific magnetic tensile force, 30
- Specific synchronizing power, 343
- Specific synchronizing torque, 343
- Split-phase induction motor, 170
- Squirrel-cage induction motor, 57
- Squirrel-cage winding analysis, 81
- Stability in parallel operation, 340
- Starting of induction motors, 131
  - improved starting performance, 135
    - bell-shaped bar design, 138, 139
    - deep-bar design, 136
    - double cage design, 137
    - torque-slip characteristic, 138
    - trapezoidal-bar design, 138

- Starting of induction motors
  - inherent starting torque, 132
  - starting time, 132
  - torque-speed characteristic, 131
- Starting of phase-wound induction motors, 133
- Starting of squirrel-cage induction motors, 131
- Stator phase mutual emmf, 77
- Stator teeth mmf, 68
- Stator yoke mmf, 70, 75
- Steady-state power stability ratio, 339
- Steady-state stability limit, 350
- Steady-state temperatures, 39
- Stepper motors, 452
- Stray torques, 115
  - eddy current and hysteresis, 123
  - induction, 115
  - reactive, 122
  - synchronous, 118
- Synchronization, 324, 358
  - exact, 327, 358
  - methods of, 358
- Synchronizing by frequency control, 366
- Synchronizing torque, 329
- Synchronous compensators (capacitors), 355
- Synchronous condenser, 211, 214, 355
- Synchronous generator(s),
  - control of load for infinite bus, 329
  - excitation characteristics of, 302
  - external characteristics of, 306
  - load characteristics of, 313
  - operation into isolated load, 301
  - parallel operation of, 323
  - self excitation of, 305, 316
  - short-circuit characteristics of, 309
- Synchronous induction motors, 354
- Synchronous machine,
  - armature of, 210
  - claw-pole, 429
  - compounding curve of, 349
  - electromagnetic power of, 296
  - electromagnetic processes in, 236
  - electromagnetic torque, 298
  - energy conversion in generator mode by, 293
  - engine type, 24
  - field structure of, 210
  - historical outline, 214
  - induction running of, 373
  - inductor-type, 436
  - in generator mode, 293
  - inverted arrangement of, 210
  - of Soviet manufacture, 405
  - permanent magnet, 444
  - reactive power -0 characteristic, 345
    - overexcited, 349
    - underexcited, 349
  - reversible, 350
- Synchronous machine on load,
  - electromagnetic processes in, 271
  - nonsalient-pole machine, 279
  - salient-pole machine, 275
  - unbalanced operation of, 397
- Synchronous motors, 350
  - doubly fed, 453
- Synchros, 204
- Thermal analysis of cooling system, 32
- Thermal resistance, 34
  - network, 39, 40
- Three-phase induction regulator, 183
- Time constant of heating, 37
- Torque motors, 198
- Torque-slip characteristics, 111, 113
  - of flat induction motor, 143
- Torque-speed characteristics, 131
- Torque stability ratio, 339
- Transformer theory for induction machines, 91
- Transient oscillations, 381
- Turbogenerator, 213
- Unbalanced operation of synchronous machines, 397
- Unbalanced steady-state short circuits, 402
- V-curves, 346
- Zero-sequence impedance of armature winding, 396